

WL-TR-91-4032
DOT/FAA/CT-91/23
VOL II, Part 2

AD-A249 130



COMPOSITE FAILURE ANALYSIS HANDBOOK
VOL II - TECHNICAL HANDBOOK
PART 2 - ATLAS OF FRACTOGRAPHS

R.J. Kar
Northrop Corporation
One Northrop Avenue
Hawthorne, California 90250-3277



February 1992

Final Report for Period January 1987 - October 1990



U.S. Department
of Transportation
Federal Aviation
Administration

Approved for public release; distribution unlimited.

MATERIALS DIRECTORATE
WRIGHT LABORATORY
AIR FORCE SYSTEMS COMMAND
WRIGHT-PATTERSON AIR FORCE BASE, OH 45433-6533

and

FEDERAL AVIATION ADMINISTRATION TECHNICAL CENTER
U.S. DEPARTMENT OF TRANSPORTATION
ATLANTIC CITY, NEW JERSEY 08405

DTIC
ELECTE
APR 17 1992
S B D

92-09217



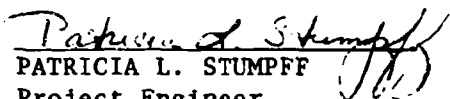
92 4 09 03t

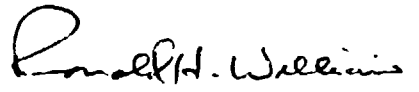
NOTICE

When Government drawings, specifications, or other data are used for any purpose other than in connection with a definitely Government-related procurement, the United States Government incurs no responsibility or any obligation whatsoever. The fact that the Government may have formulated or in any way supplied the said drawings, specifications, or other data, is not to be regarded by implication, or otherwise in any manner construed, as licensing the holder, or any other person or corporation; or as conveying any rights or permission to manufacture, use, or sell any patented invention that may in any way be related thereto.


This report is releasable to the National Technical Information Service (NTIS). At NTIS, it will be available to the general public, including foreign nations.

This technical report has been reviewed and is approved for publication.


PATRICIA L. STUMPP
Project Engineer
Materials Integrity Branch


RONALD H. WILLIAMS
Technical Manager
Structural and Electronic
Failure Analysis

FOR THE COMMANDER


GARY E. STEVENSON, Actg Br Chf
Materials Integrity Branch
Systems Support Division

If your address has changed, if you wish to be removed from our mailing list, or if the addressee is no longer employed by your organization please notify WL/MLSA, WPAFB, OH 45433-6533 to help us maintain a current mailing list.

Copies of this report should not be returned unless return is required by security considerations, contractual obligations, or notice on a specific document.

REPORT DOCUMENTATION PAGEForm Approved
OMB No. 0704-0188

Public reporting burden for this collection of information is estimated to average 1 hour per response, including the time for reviewing instructions, searching existing data sources, gathering and maintaining the data needed, and completing and reviewing the collection of information. Send comments regarding this burden estimate or any other aspect of this collection of information, including suggestions for reducing this burden, to Washington Headquarters Services, Directorate for Information Operations and Reports, 1215 Jefferson Davis Highway, Suite 1204, Arlington, VA 22202-4302, and to the Office of Management and Budget, Paperwork Reduction Project (0704-0188), Washington, DC 20503.

1. AGENCY USE ONLY (Leave blank)		2. REPORT DATE February 1992	3. REPORT TYPE AND DATES COVERED Final for 1 Jan 1987 to 31 Oct 1990	
4. TITLE AND SUBTITLE Composite Failure Analysis Handbook Volume II: Technical Handbook Part 2 - Atlas of Fractographs			5. FUNDING NUMBERS Contract Number F33616-87-C-5212	
6. AUTHOR(S) R.J. Kar				
7. PERFORMING ORGANIZATION NAME(S) AND ADDRESS(ES) Northrop Corporation Aircraft Division One Northrop Avenue Hawthorne, California 90250-3277			8. PERFORMING ORGANIZATION REPORT NUMBER	
9. SPONSORING/MONITORING AGENCY NAME(S) AND ADDRESS(ES) Wright Laboratory (WL/MLSA) Materials Directorate Wright-Patterson AFB, Ohio 45433-6533			10. SPONSORING/MONITORING AGENCY REPORT NUMBER WL-TR-91-4032, DOT/FAA/CT-91-23 Volume II - Part 2	
11. SUPPLEMENTARY NOTES Additional Funding/Sponsorship Provided By: FEDERAL AVIATION ADMINISTRATION TECHNICAL CENTER U. S. DEPARTMENT OF TRANSPORTATION ATLANTIC CITY, NEW JERSEY 08405				
12a. DISTRIBUTION /AVAILABILITY STATEMENT Approved for public release; distribution is unlimited			12b. DISTRIBUTION CODE	
13. ABSTRACT (Maximum 200 words) The objective of this program was to create a comprehensive handbook for use in conducting failure analysis investigations on failed composite structure. This program builds upon previous efforts as documented in the "Compendium of Post-Failure Analysis Techniques for Composite Materials," AFWAL-TR-86-4137. The purpose of creating this handbook was to document the techniques, the fractographic and material property data and case history studies currently being utilized in the analysis of failed composite structure. The major tasks on this program included: (1) procedural guidelines for field investigation techniques; (2) an expanded fractographic data base for carbon/epoxy materials tested under known conditions, (3) a fractographic data base for resin based composite materials other than carbon/epoxy; (4) fractographic documentation of composite material and processing defects; (5) documentation of fracture characteristics in adhesive and mechanical joint failures; (6) compilation of material property data for composite materials; and (7) documentation of case histories recently conducted on failed composite structure.				
14. SUBJECT TERMS Composites; Composite Structures; Failure Analysis; Fractography; Adhesive Joints; Mechanical Joints; Case History Studies			15. NUMBER OF PAGES 488	
			16. PRICE CODE	
17. SECURITY CLASSIFICATION OF REPORT UNCLASSIFIED	18. SECURITY CLASSIFICATION OF THIS PAGE UNCLASSIFIED	19. SECURITY CLASSIFICATION OF ABSTRACT UNCLASSIFIED	20. LIMITATION OF ABSTRACT	

SUMMARY

The objective of this program was to develop a comprehensive handbook for failure analyses of fiber-reinforced composites. The program objectives were accomplished through technical tasks that resulted in the compilation of a reference manual for evaluating failed composite structures.

A field handling logic network was prepared for on-site handling of composites during accident investigations. Procedural guidelines were developed from inputs provided by key field personnel from several government agencies, and from the results of tests performed in-house at Northrop. Several current and new fractographic techniques were evaluated to identify methods for initiation site determination and failure sequence identification in failed composite specimens. Macrophotography, ply-sectioning, and photographic methods were determined to be valuable supplemental techniques but could not directly provide initiation site/fracture propagation direction when used alone. The microchemical analysis technique of Fourier Transform Infrared Spectroscopy was determined to be useful in contaminant failure investigations but will require development of a database of chemical "signatures."

Northrop expanded the fractographic database originally developed by the Boeing Company for AS4/3501-6 graphite/epoxy (Gr/Ep) under Air Force Contract No. F33615-84-C-5010 to include the effects of load, manufacturing, processing, and environmental variables on simple interlaminar and translaminar test coupons. It was determined that applied load was the principal parameter that altered the fracture surface characteristics in Gr/Ep. Material form and processing variables indirectly affected the fracture characteristics in that these caused localized variations in applied load, thereby altering fractographic features. No significant effects of environment on fracture surface features were determined. The fractographic database also included documentation of manufacturing and processing defects that occur in Gr/Ep. The flaws were characterized using optical microscopy, and macrophotography techniques.

Failure modes in adhesively bonded Gr/Ep and graphite/bismaleimide (Gr/BMI) specimens were also characterized. Variations in ply thickness, orientation, and loading were carried out to develop mixed cohesive-adhesive, and singular cohesive or adhesive failures. It was determined that specimen geometry, lap/strap ratios, and test load played roles in controlling fracture surface characteristics. Fracture characteristics in the failed adherends served as indicators of fracture direction in mixed and total adhesive failure modes. The crack directions could not be readily determined in pure cohesive joint failures.

A test matrix was developed for characterizing the six different failure modes in mechanically joined composite structures. A computer code entitled SAMCJ (Strength Analysis of Multifastened Composite Joints), previously developed by Northrop for the USAF was run to develop the matrix for quasi-isotropic AS4/3501-6 Gr/Ep joined with titanium "Hi-Lok" tension or

shear-type flush head fasteners. Failure tests and fractographic evaluation were carried out on the specimens. It was determined that the failure modes were a function of applied load, specimen, and fastener geometries.

Detailed in-plane shear tests were also carried out for Gr/Ep. This failure mode was characterized by the occurrence of hackles on fractured resin and tension fracture characteristics on fractured fiber ends. Processing variables did not significantly alter the fracture surface characteristics for Gr/Ep tested under in-plane shear. The information gained from the Northrop and Boeing Gr/Ep studies was used in initiating a fractographic database for other material systems. The material systems chosen were kevlar 49/3501-6 epoxy (K/Ep), AS4 graphite/5250-3 bismaleimide (Gr/BMI), and AS4 graphite/APC-2 PEEK thermoplastic (Gr/PEEK). Testing and fractographic evaluation were carried out for baseline and several variable conditions. The results for these systems indicated that the type of resin and fiber played strong roles in controlling the resulting fracture surface characteristics. As for Gr/Ep, environment and processing variables did not significantly alter fracture characteristics.

Northrop reviewed formats previously used for reporting metallic and composite fractography and failure analysis data. Based on an assessment of existing report schemes, Northrop proposed three data formats for 1) reporting fractographic data, 2) failure analysis information, and 3) organization of the Composite Failure Analysis Handbook. These were subsequently approved by the Air Force with minor modifications.

Northrop compiled material properties on current and near-term composite structural materials. Literature searches were carried out on government and commercial databases for product information and properties. Properties obtained were incorporated into database files using a personal computer. The data were organized into tabular formats for reporting in the Handbook. The properties for several classes of fiber, prepreg, and laminates were compiled and organized into the Handbook.

Under an engineering services agreement between Northrop and the University of Utah, Professor Willard Bascom of the University of Utah performed a literature search and made on-site visits to several government agencies to gather information on composite fractography and failure analysis that may have been performed at these agencies. No other information was found other than that previously reported by Boeing. Dr. Bascom also reviewed stress analysis methods and failure micromechanisms for use in failure analysis investigations. A new failure criterion developed by Dr. Richard Christensen of Lawrence Livermore Laboratories was determined to be of utility in composite failure investigations.

Verification of the composite failure analysis logic system was performed through evaluation of several failed structural items provided by the Air Force. The structural items represented "real-world" configurations and included 1) a vertical stabilizer, 2) a horizontal torque box assembly, 3) a canopy support fitting, and 4) two simple components. All the results are presented as case histories in the Handbook.

As part of the verification process, two simple Gr/Ep structures containing intentional defects were fabricated and tested to failure under controlled laboratory conditions. The failed

specimens and related test documentation were shipped to the Air Force for subsequent evaluation by the Boeing Company.

The Composite Failure Analysis Handbook is divided into two volumes. Volume I is the Program Overview. Volume II comprises the Technical Handbook, and is divided into three parts. Part 1 describes all the techniques and procedures for performing composite failure analysis. Part 2 represents an atlas of fractographs. Part 3 is a compilation of case histories of investigations performed by Northrop, Boeing, and General Electric.

In summary, Northrop has achieved the objective of producing a Handbook containing all the known techniques, procedures, sample data, and reference supporting data for performing post-failure analysis of fiber-reinforced composite structures.

Accession For	
NTIS GRA&I	<input checked="checked" type="checkbox"/>
DTIC TAB	<input type="checkbox"/>
Unannounced	<input type="checkbox"/>
Justification _____	
By _____	
Distribution/ _____	
Availability Codes	
Dist	Avail and/or Special
A-1	

FOREWORD

The final report documents work performed under Contract F33615-87-C-5212 from January, 1987 through October, 1990 by the Northrop Corporation, Aircraft Division, Hawthorne, California for the United States Air Force Systems Command. The program was administered under the technical direction of Ms Patricia Stumpff, Materials Directorate, Wright Laboratory, Wright-Patterson Air Force Base, Ohio 45433-6533. The majority of funding for this program was provided by the Federal Aviation Administration Technical Center, Aviation Safety Division, Atlantic City, New Jersey 08405. Mr Lawrence Neri, ACD-210, acted as the Federal Aviation Administration technical manager. Mr Joseph Soderquist, National Resource Specialist, Advanced Materials, Federal Aviation Administration, AIR-103, 800 Independence Avenue, S.W., Washington, D. C. 20591, also provided technical direction for this program.

The work was performed by Northrop's Materials Analysis Laboratory. Dr R. J. Kar was the Program Manager and Principal Investigator. The contributions of the following members of the Materials Analysis Laboratory are gratefully acknowledged: Ms L. M. Concepcion (Co-Principal Investigator), Mr O. P. DeCastro (SEM and materialography), Mr J. M. Dobson (case histories), Mr T. N. Gindraux (materialography and SEM) Mr L. J. Havemann (SEM), Mr M. D. Ensminger (FTIR), Mr L. S. Dhillon (materialography) and Mr E. E. Ramirez (materialography). Mr P. J. Dager of Northrop's Mechanical Testing Laboratory and Mr R. J. Isberner of Northrop's Structures Test Laboratory performed the mechanical testing of laminate coupons and real-world elements. Mr R. B. Deo, and Mr T. A. Dyer of Northrop's Structures Research Department participated in the selection of test laminates.

Professor W. D. Bascom, Department of Materials Science and Engineering at the University of Utah, also made significant contributions by conduction of literature survey on composite fractography and identifying new composite failure criteria.

The results of additional work in composites failure analysis by the Boeing Military Airplane Company under Air Force Contracts F33615-84-C-5010 and F33615-86-C-5071 from 1984 through 1988 have been included in this report for the purpose of providing the most complete Composite Failure Analysis Handbook. Mr R. A. Grove, Mr B. W. Smith, and Ms C. T. Hua were Principal Investigators, and Mr D. F. Sekits was the Program Manager of these programs. The author wishes to thank Boeing and the numerous publishing houses and authors who granted permission to include their works in this document.

TABLE OF CONTENTS

Section		Page
1	INTRODUCTION AND PURPOSE	1-1
1.1	FRACTOGRAPHIC APPLICATIONS, EXAMPLES AND INTERPRETIVE METHODS	1-4
1.1.1	Fracture Types	1-5
1.1.2	Fracture Modes, Features, and Growth Directions.....	1-9
1.1.2.1	Interlaminar and Intralaminar	1-9
1.1.2.2	Translaminar	1-31
1.1.3	Interlaminar Fracture Mapping.....	1-42
1.1.4	Crack Origin Analysis	1-46
1.1.5	Environmental Effects	1-46
1.1.5.1	Translaminar Fractures	1-46
1.1.5.2	Delamination Fractures.....	1-48
1.1.6	Summary of Composite Materials Fractography	1-48
1.1.6.1	Brittle Resin Composite Crack Growth	1-52
1.1.6.2	Ductile Resin Composite Crack Growth	1-52
1.1.6.3	Fracture Mode Determination (Tension, Shear and Compression)	1-52
1.1.6.4	Mixed Mode Loading Effects	1-53
1.1.6.5	Temperature and Absorbed Moisture Effects	1-53
1.1.6.6	Processing Defects Effects	1-53
1.1.6.7	Material Forms Effects	1-54
1.1.6.8	Post-Failure Environment Effects.....	1-54
1.1.6.9	Fatigue Effects	1-55
1.2	ORGANIZATION OF THE ATLAS OF FRACTOGRAPHS	1-55
2	GRAPHITE EPOXY	2-1
2.1	INTERLAMINAR TENSION (MODE I DCB)	2-1
2.2	INTERLAMINAR SHEAR (MODE II ENF)	2-65
2.3	INTERLAMINAR MIXED MODE FLEXURAL	2-119
2.4	IN-PLANE SHEAR	2-145
2.5	TRANSLAMINAR TENSION.....	2-153
2.6	TRANSLAMINAR COMPRESSION	2-188
2.7	TRANSLAMINAR SHEAR	2-218
2.8	TRANSLAMINAR FLEXURE	2-229
2.9	FATIGUE.....	2-231
2.10	CREEP	2-245
2.10.1	Interlaminar Mode I Tension, RT/Dry	2-245
2.10.2	Interlaminar Mode I Tension, 270 F/Dry	2-245
2.10.3	Interlaminar Mode II Shear, RT/Dry	2-245
2.10.4	Interlaminar Mode II Shear, 270 F/Dry	2-245
2.11	HIGH RATE	2-259

TABLE OF CONTENTS (Concluded)

Section	Page
2.11.1 Mode I Tension, RT/Dry	2-259
2.11.2 Mode II Shear, RT/Dry	2-259
2.12 COMPRESSION-AFTER-IMPACT	2-266
2.13 DEFECTS	2-271
2.13.1 ..Contaminants	2-271
2.13.2 ..Voids	2-274
3 KEVLAR/EPOXY	3-1
4 BORON/EPOXY	4-1
4.1 INTERLAMINAR MODE I TENSION, RT/DRY	4-1
4.2 INTERLAMINAR MODE I TENSION, 270 F/WET	4-1
4.3 INTERLAMINAR MODE II SHEAR, RT/DRY	4-2
4.4 INTERLAMINAR MODE II SHEAR, 270 F/WET	4-2
4.5 TRANSLAMINAR TENSION, RT/DRY	4-2
4.6 TRANSLAMINAR TENSION, 270 F/WET	4-2
4.7 TRANSLAMINAR COMPRESSION, RT/DRY	4-3
4.8 TRANSLAMINAR COMPRESSION, 270 F/WET	4-3
5 FIBERGLASS/EPOXY	5-1
5.1 INTERLAMINAR MODE I TENSION, RT/DRY	5-1
5.2 INTERLAMINAR MODE I TENSION, 200 F/WET	5-1
5.3 INTERLAMINAR MODE II SHEAR, RT/DRY	5-1
5.4 INTERLAMINAR MODE II SHEAR, 200 F/WET	5-2
5.5 TRANSLAMINAR TENSION, RT/DRY	5-2
5.6 TRANSLAMINAR COMPRESSION, RT/DRY	5-2
5.7 TRANSLAMINAR COMPRESSION, 200 F/WET	5-2
6 GRAPHITE/BISMALEIMIDE	6-1
7 GRAPHITE/THERMOPLASTIC	7-1
8 CARBON/POLYIMIDE	8-1
8.1 INTERLAMINAR FRACTURE	8-1
8.1.1 Mode I DCB Tension	8-1
8.1.2 Mode II ENF Shear	8-1
8.2 TRANSLAMINAR FRACTURE	8-2
8.2.1 Tension	8-2
8.2.2 Compression	8-2
9 BOLTED JOINTS	9-1
10 ADHESIVELY BONDED COMPOSITES	10-1

LIST OF FIGURES

Figure		Page
1-1	Laminate Flexure Specimens	1-6
1-2	Tensile and Compression Translaminar Fractures	1-7
1-3	The Basic Fracture Modes	1-8
1-4	Visual Macroscopic Fracture Surface Features	1-10
1-5	V-22 Osprey Wing Box Failure	1-10
1-6	Basic Modes of Loading Involving Different Crack Types and Surface Displacements (Interlaminar and Translaminar)	1-11
1-7	Fracture Surface of 4340 M Steel Illustrating Cleavage Fracture Features Indicative of Crack Growth Direction	1-13
1-8	Fracture of Unreinforced Neat Epoxy Resin	1-14
1-9	Mode I Tension Fracture	1-15
1-10	Beach Marks Found in a Delamination Surface Indicative of Crack Front Shape and Crack Growth Direction During Fracture	1-16
1-11	Optical Photomicrographs of Intended Fracture Plane Between 0/0 Degree Plies, DCB 21C (70F) Specimen	1-18
1-12	SEM Fractographs of Mode I Delamination Between 0/0 Degree Plies	1-19
1-13	Photomicrograph Illustrating Adhesive Fracture Areas of Textured Microflow ...	1-20
1-14	TEM Image of Resin Microplane With River Marks and Resin Microflow	1-20
1-15	SEM Photomicrographs of Mode I Delamination Between 0/90 Degree Plies	1-22
1-16	SEM Photomicrographs of Mode I Delamination Between 0/+45 Degree Plies	1-23
1-17	SEM Fractographs of Mode I Delamination Between +45/+45 Degree Plies	1-24
1-18	Optical Photomicrographs of Intended Fracture Plane Between 0/0 Degree Plies, ENF 21C (70F) Specimen	1-25
1-19	SEM Photomicrographs of Mode II Delamination Between 0/0 Degree Plies	1-27
1-20	Free Body Diagram of Resolved Tensile Stresses and Inclined Microcracks	1-28
1-21	Microstructure of Cracks Found in Short Beam Shear Specimen Tested at 132C (270 F)	1-28

LIST OF FIGURES (Continued)

Figure		Page
1-22	Scalloped Resin Fracture Areas and Their Development	1-29
1-23	Possible Hackle Separation Mechanisms	1-30
1-24	Orthogonally Shaped Symmetrical Hackles	1-30
1-25	Triangular Asymmetric Hackles, With River Marks and Fiber-Matrix Separation	1-50
1-26	Interlaminar Mixed Mode (Tension and Shear) Fracture Morphology	1-32
1-27	Interlaminar Mixed Mode Flexural (MMF, Tension and Shear) Specimen Fracture Morphology	1-32
1-28	Macroscopic View of a Translaminar Tension Fracture From a Unidirectional Laminate	1-34
1-29	Translaminar Fracture Morphology	1-35
1-30	Typical Tensile Fiber Fracture Characteristics	1-35
1-31	SEM Photomicrograph Showing Direction of Crack Propagation	1-37
1-32	Compression Buckling Failure Damage of Stringer Stiffened Laminate	1-38
1-33	End-View of Translaminar Compression Fracture	1-39
1-34	SEM Micrograph of Compression-Generated Fracture Surface Showing Severe Fracture Surface Damage	1-39
1-35	Cross Section of Compressively Loaded Laminate With Microbuckling or Kinking of the Fiber Bundles Oriented Parallel to the Axial Compressive Load .	1-40
1-36	Typical Flexural Fracture Morphology Found on the Fiber Ends From a Compression Failure	1-41
1-37	Fiber End Fracture Morphology From Compression Buckling Failure	1-41
1-38	Slant or Shear-Type Fracture From Compression-Induced Translaminar Failure	1-43
1-39	SEM Photographic Montage Showing Crack Propagation Direction Mapping	1-45
1-40	Damage Defect Checklist	1-47
1-41	SEM Micrographs of Translaminar Fracture Conditions at Different Temperatures	1-49

LIST OF FIGURES (Continued)

Figure		Page
1-42	Low Magnification Series of Characteristic 0/0 Degree Interface Mode I Fractures at Each Environmental Condition	1-50
1-43	High Magnification Series of 0/0 Degree Interface Mode II (Shear) Fractures Showing Features of Fiber-Matrix Separation	1-51
2-1	Double-Cantilever Beam Test Type	2-2
2-2	Overall Crack-Growth Direction by River Markings	2-2
2-3	Overall Crack-Growth Direction by Resin Microflow	2-2
2-4	Photographs of Interlaminar Mode I Tension, 0/0 Fracture, 70 F/Dry	2-6
2-5	SEM Photographs of Interlaminar Mode I Tension Fracture, 0/0, 70 F/Dry	2-7
2-6	Photographs of Interlaminar Mode I Tension, 0/0 Fracture, -65, 70, and 270 F/Dry	2-8
2-7	SEM Photographs of Interlaminar Mode I Tension, 0/0 Fracture, -65, 70 and 270 F/Dry (50X)	2-8
2-8	SEM Photographs of Interlaminar Mode I Tension, 0/0 Fracture, -65, 70, and 270 F/Dry (200X)	2-10
2-9	SEM Photographs of Interlaminar Mode I Tension, 0/0 Fracture, -65 and 70 F/Dry	2-11
2-10	Photographs of Interlaminar Mode I Tension, 0/0 Fracture, 70 and 180 F/Wet	2-12
2-11	SEM Photographs of Interlaminar Mode I Tension, 0/0 Fracture, 70 and 180 F/Wet	2-13
2-12	SEM Photographs of Interlaminar Mode I Tension, 0/0 Fracture, 70 F/Wet, 180 F/Dry, and 180 F/Wet	2-14
2-13	Photographs of Interlaminar Mode I Tension, +45/-45 Fracture, 70 F/Dry	2-15
2-14	SEM Photographs of Interlaminar Mode I Tension, +45/-45 Fracture, 70 F/Dry ..	2-16
2-15	Photographs of Interlaminar Mode I Tension, +45/-45 Fracture, -65, 70, and 270 F/Dry	2-17
2-16	SEM Photographs of Interlaminar Mode I Tension, +45/-45 Fracture, -65, 70, and 270 F/Dry (50X)	2-18
2-17	SEM Photographs of Interlaminar Mode I Tension, +45/-45 Fracture, -65, 70, and 270 F/Dry (200X)	2-19

LIST OF FIGURES (Continued)

Figure		Page
2-18	Photographs of Interlaminar Mode I Tension, +45/-45 Fracture, 70 and 180 F/Wet	2-20
2-19	SEM Photographs of Interlaminar Mode I Tension, +45/-45 Fracture, 70 and 180 F/Wet	2-21
2-20	Photographs of Interlaminar Mode I Tension, 0/45 Fracture, 70 F/Dry	2-22
2-21	Photographs of Interlaminar Mode I Tension, 0/45 Fracture, -65, 70 and 270 F/Dry (400X)	2-23
2-22	SEM Photographs of Interlaminar Mode I Tension, 0/45 Fracture, 70 F/Wet	2-24
2-23	Photographs of Interlaminar Mode I Tension, 0/90 Fracture, 70 F/Dry	2-25
2-24	SEM Photographs of Interlaminar Mode I Tension, 0/90 Fracture, 70 F/Dry	2-26
2-25	Photographs of Interlaminar Mode I Tension, 0/90 Fracture, -65 and 70 F/Dry ..	2-27
2-26	Photographs of Interlaminar Mode I Tension, 90/90 Fracture, 70 F/Dry	2-28
2-27	SEM Photographs of Interlaminar Mode I Tension, 90/90 Fracture, 70 F/Dry	2-29
2-28	Optical and SEM Photographs of Mode I DCB Interlaminar Fracture in Filament Wound Gr/Ep - [+45/-45] _{gs} , Room Temperature Ambient	2-30
2-29	Optical and SEM Photographs of Mode I DCB Interlaminar Fracture in Filament Wound Gr/Ep - [+45/0/-45] _{gs} , Room Temperature Ambient	2-31
2-30	Optical and SEM Photographs of Mode I DCB Interlaminar Fracture in Filament Wound Gr/Ep - [0/90] _{gs} , Room Temperature Ambient	2-32
2-31	Optical Photomicrographs of Interlaminar Mode I Tension, Room Temperature, Fabric Fracture, [0/90] _{gs}	2-34
2-32	SEM Fractographs of Interlaminar Mode I Tension, Room Temperature, Fabric Fracture, [0/90] _{gs}	2-35
2-33	Macrograph of 3-D Weave Mode I DCB Gr/Ep Coupons	2-36
2-34	SEM Photographs of Mode I DCB Interlaminar Fracture in 3-D Weave Gr/Ep - [+45/-45] _{gs}	2-37
2-35	SEM Photographs of Mode I DCB Interlaminar Fracture in 3-D Weave Gr/Ep - [+45/0/-45] _{gs}	2-38
2-36	SEM Photographs of Mode I DCB Interlaminar Fracture in 3-D Weave Gr/Ep ...	2-39

LIST OF FIGURES (Continued)

Figure		Page
2-37	SEM Photographs of Mode I DCB Fracture in 3-D Weave Gr/Ep - [0/90] _{6S} in Crack-Growth Region	2-40
2-38	Optical and SEM Photographs of Mode I DCB Interlaminar Fracture in Gr/Ep - [0] _{24T} , Impact Damaged Before Test	2-41
2-39	Optical and SEM Photographs of Mode I DCB Interlaminar Fracture in Gr/Ep - [+45/0/-45] _{4S} , Impact Damaged Before Test	2-43
2-40	SEM Photographs of Mode I DCB Interlaminar Fracture in Gr/Ep - [0] _{24T} , Water Immersed Before Test	2-45
2-41	Optical Photomicrographs of Interlaminar Mode I Tension, 0/90 Fracture, Water Immersed (160 F) After Test	2-46
2-42	SEM Fractographs of Interlaminar Mode I Tension, 0/90 Fracture, Water Immersed (160 F) After Test	2-47
2-43	Optical Photomicrographs of Interlaminar Mode I Tension, 0/90 Fracture, Exposure to Humidity (160 F) After Test	2-48
2-44	SEM Fractographs of Interlaminar Mode I Tension, 0/90 Fracture, Exposure to Humidity (160 F) After Test	2-49
2-45	Optical and SEM Photographs of Mode I DCB Interlaminar Fracture in Undercured Gr/Ep - [0] _{24T}	2-50
2-46	Optical and SEM Photographs of Mode I DCB Interlaminar Fracture in Undercured Gr/Ep - [+45/0/-45] _{4S}	2-52
2-47	Optical and SEM Photographs of Mode I DCB Interlaminar Fracture in Undercured Gr/Ep - [0/90] _{6S}	2-54
2-48	Optical and SEM Photographs of Mode I DCB Interlaminar Fracture in Overcured Gr/Ep - [0] _{24T}	2-55
2-49	Optical and SEM Photographs of Mode I DCB Interlaminar Fracture in Overcured Gr/Ep - [+45/0/-45] _{4S}	2-56
2-50	Optical Photomicrographs of Interlaminar Mode I Tension, 0/90 Fracture of Low Resin Content Specimen	2-57
2-51	SEM Fractographs of Interlaminar Mode I Tension, 0/90 Fracture of Low Resin Content Specimen	2-58
2-52	Optical and SEM Photographs of Mode I DCB Interlaminar Fracture in High Resin Content Gr/Ep - [0] _{24T}	2-59

LIST OF FIGURES (Continued)

Figure		Page
2-53	SEM Photographs of Mode I DCB Interlaminar Fracture in High Resin Content Gr/Ep, Conditioned 180 F/Dry	2-60
2-54	SEM Photographs of Mode I DCB Interlaminar Fracture Details in High Resin Content Gr/Ep, Conditioned 180 F/Dry After Test	2-61
2-55	SEM Photographs of Mode I DCB Interlaminar Fracture in Overcured Gr/Ep, Conditioned 180 F/Wet After Test	2-62
2-56	Optical Photomicrographs of Interlaminar Mode I Tension, 0/90 Fracture, 2000 F Exposure for 5 Minutes After Test	2-63
2-57	SEM Fractographs of Interlaminar Mode I Tension, 0/90 Fracture, 2000 F Exposure for 5 Minutes After Test	2-64
2-58	End-Notched Flexural Test Type	2-67
2-59	Photographs of Interlaminar Mode II Shear, 0/0 Fracture, 70 F/Dry	2-67
2-60	SEM Photographs of Interlaminar Mode II Shear, 0/0 Fracture, 70 F/Dry	2-68
2-61	Photographs of Interlaminar Mode II Shear, 0/0 Fracture, -65, 70, and 270 F/Dry (400X)	2-69
2-62	SEM Photographs of Interlaminar Mode II Shear, 0/0 Fracture, -65, 70, and 270 F/Dry (400X)	2-70
2-63	SEM Photographs of Interlaminar Mode II Shear, 0/0 Fracture, -65, 70, and 270 F/Dry (2000X)	2-71
2-64	Photographs of Interlaminar Mode II Shear, 0/0 Fracture, 70 F/Wet, 180 F/Dry, and 180 F/Wet (400X)	2-72
2-65	SEM Photographs of Interlaminar Mode II Shear, 0/0 Fracture, 70 and 180 F/Wet	2-73
2-66	Photographs of Interlaminar Mode II Shear, +45/-45 Fracture, 70 F/Dry	2-74
2-67	SEM Photographs of Interlaminar Mode II Shear, +45/-45 Fracture, 70 F/Dry ...	2-75
2-68	Photographs of Interlaminar Mode II Shear, +45/-45 Fracture, -65, 70 and 270 F/Dry	2-76
2-69	SEM Photographs of Interlaminar Mode II Shear, +45/-45 Fracture, -65, 70 and 270 F/Dry (400X)	2-77
2-70	SEM Photographs of Interlaminar Mode II Shear, +45/-45 Fracture, -65, 70 and 270 F/Dry (2000X)	2-78

LIST OF FIGURES (Continued)

Figure		Page
2-71	Photographs of Interlaminar Mode II Shear, 0/45 Fracture, 70 F/Dry	2-79
2-72	SEM Photographs of Interlaminar Mode II Shear, 0/45 Fracture, 70 F/Dry	2-80
2-73	Photographs of Interlaminar Mode II Shear, 0/90 Fracture, 70 F/Dry	2-81
2-74	Photographs of Interlaminar Mode II Shear, 90/90 Fracture, 70 F/Dry	2-82
2-75	SEM Photographs of Interlaminar Mode II Shear, 90/90 Fracture, 70 F/Dry	2-83
2-76	Optical and SEM Photographs of Mode II ENF Interlaminar Shear Fracture in Filament Wound Gr/Ep - $[0]_{24T}$, Room Temperature Ambient	2-84
2-77	Optical and SEM Photographs of Mode II ENF Interlaminar Shear Fracture in Filament Wound Gr/Ep - $[+45/0/-45]_{4S}$, Room Temperature Ambient	2-86
2-78	Optical Photomicrographs of Interlaminar Mode II Shear, Room Temperature, 0/90 Fabric Fracture	2-88
2-79	SEM Fractographs of Interlaminar Mode II Shear, Room Temperature, 0/90 Fabric Fracture	2-89
2-80	SEM Photograph of Mode II ENF Interlaminar Shear Fracture in 3-D Weave Gr/Ep - $[+45/0/-45]_{4S}$ in Crack-Growth Region	2-90
2-81	Optical and SEM Photographs of Mode II ENF Interlaminar Shear Fracture in Gr/Ep - $[0/90]_{6S}$, Impact Damaged Before Test	2-91
2-82	Optical and SEM Photographs of Mode II ENF Interlaminar Shear Fracture in Gr/Ep - $[0]_{24T}$, Water Immersed Before Test	2-94
2-83	Optical and SEM Photographs of Mode II ENF Interlaminar Shear Fracture in Gr/Ep - $[0/90]_{6S}$, Water Immersed Before Test	2-96
2-84	Optical Photomicrographs of Interlaminar Mode II Shear, 0/90 Fracture, Water Immersion (160 F) After Test	2-98
2-85	SEM Fractographs of Interlaminar Mode II Shear, 0/90 Fracture, Water Immersion (160 F) After Test	2-99
2-86	Optical Photomicrographs of Interlaminar Mode II Shear, 0/90 Fracture, Exposure to Humidity (160 F) After Test	2-100
2-87	SEM Fractographs of Interlaminar Mode II Shear, 0/90 Fracture, Exposure to Humidity (160 F) After Test	2-101
2-88	Optical and SEM Photographs of Mode II ENF Shear Interlaminar Fracture in Undercured Gr/Ep - $[0]_{24T}$	2-102

LIST OF FIGURES (Continued)

Figure		Page
2-89	Optical and SEM Photographs of Mode II ENF Shear Interlaminar Fracture in Undercured Gr/Ep - [+45/0/-45] ₄₅	2-104
2-90	Optical and SEM Photographs of Mode II ENF Shear Interlaminar Fracture in Overcured Gr/Ep - [0] _{24T}	2-106
2-91	Optical and SEM Photographs of Mode II ENF Shear Interlaminar Fracture in Overcured Gr/Ep - [+45/0/-45] ₄₅	2-108
2-92	Optical Photomicrographs of Interlaminar Mode II Shear, 0/90 Fracture of Low Resin Content Specimen	2-109
2-93	SEM Fractographs of Interlaminar Mode II Shear, 0/90 Fracture of Low Resin Content Specimen	2-110
2-94	Optical and SEM Photographs of Mode II ENF Shear Interlaminar Fracture in High Resin Content Gr/Ep - [0] _{24T}	2-111
2-95	Optical and SEM Photographs of Mode II ENF Interlaminar Shear Fracture in High Resin Content Gr/Ep - [0/90] ₆₅	2-113
2-96	SEM Photographs of Mode II ENF Interlaminar Shear Fracture in High Resin Content Gr/Ep, Conditioned 180 F/Dry After Test	2-115
2-97	SEM Photographs of Mode II ENF Interlaminar Shear Fracture in Overcured Gr/Ep, Conditioned 180 F/Wet After Test	2-116
2-98	Optical Photomicrographs of Interlaminar Mode II Shear, 0/90 Fracture, 2000 F Exposure for 5 Minutes After Test	2-117
2-99	SEM Fractographs of Interlaminar Mode II Shear, 0/90 Fracture, 2000 F Exposure for 5 Minutes After Test	2-118
2-100	Mixed Mode Flexural Test Type	2-119
2-101	SEM Photograph of Interlaminar Mode I and Mode II, 0/0 Fracture, 70 F/Dry ...	2-121
2-102	SEM Photographs of Interlaminar Mode I and Mode II, +45/-45 Fracture, 70 F/Dry	2-122
2-103	SEM Photographs of Interlaminar Mode I and Mode II, 0/45 Fracture, 70 F/Dry	2-123
2-104	SEM Photographs of Interlaminar Mode I and Mode II, 0/90 Fracture, 70 F/Dry	2-124
2-105	SEM Photographs of Mode I and Mode II MMF Interlaminar Fracture in Filament Wound Gr/Ep - [0] _{24T}	2-125
2-106	SEM Photograph of Mode I and Mode II MMF Interlaminar Fracture in Crack-Growth Region of Filament Wound Gr/Ep - [+45/0/-45] ₄₅	2-126

LIST OF FIGURES (Continued)

Figure		Page
2-107	SEM Photographs of Mode I and Mode II MMF Interlaminar Fracture in 3-D Weave Gr/Ep - [+45/0/-45] _{4S}	2-127
2-108	SEM Photographs of Mode I and Mode II MMF Interlaminar Fracture in Impact Damaged Gr/Ep - [0] _{24T}	2-128
2-109	Optical and SEM Photographs of Mode I and Mode II MMF Impact Damaged Gr/Ep - [+45/0/-45] _{4S}	2-129
2-110	SEM Photograph of Mode I and Mode II MMF Interlaminar Fracture in Gr/Ep - [0] _{24T} , Water Immersion Before Test	2-131
2-111	Optical and SEM Photographs of Mode I and Mode II MMF Interlaminar Fracture in Undercured Gr/Ep - [0] _{24T}	2-132
2-112	Optical and SEM Photographs of Mode I and Mode II MMF Interlaminar Fracture in Undercured Gr/Ep - [+45/0/-45] _{4S}	2-135
2-113	Optical and SEM Photographs of Mode I and Mode II MMF Interlaminar Fracture in Overcured Gr/Ep - [0] _{24T}	2-137
2-114	Optical and SEM Photographs of Mode I and Mode II MMF Interlaminar Fracture in Overcured Gr/Ep - [+45/0/-45] _{4S}	2-139
2-115	Optical and SEM Photographs of Mode I and Mode II MMF Interlaminar Fracture in High Resin Content Gr/Ep - [0] _{24T}	2-141
2-116	SEM Photographs of Mode I and Mode II MMF Interlaminar Fracture in High Resin Gr/Ep - [0] _{24T} , Conditioned 180 F/Dry After Test	2-143
2-117	SEM Photographs of Mode I and Mode II MMF Interlaminar Fracture in Overcured Gr/Ep - [+45/0/-45] _{4S} , Conditioned 180 F/Wet After Test	2-144
2-118	Rail-Shear Specimen	1-146
2-119	Optical and SEM Photographs of AS4/3501-6 Gr/Ep - [0/90] _{6S} , In-Plane Shear-Tested (Baseline)	2-147
2-120	Optical and SEM Photographs of AS4/3501-6 Gr/Ep - [+45/-45] _{6S} , In-Plane Shear Tested (Baseline)	2-149
2-121	Optical and SEM Photographs of AS4/3501-6 Undercured Gr/Ep - [+45/-45] _{6S} , In-Plane Shear Tested	2-151
2-122	Optical and SEM Photographs of AS4/3501-6 Overcured Gr/Ep - [+45/-45] _{6S} , In-Plane Shear Tested	2-152
2-123	Four-Point Bend Tension Test Specimen	1-154

LIST OF FIGURES (Continued)

Figure		Page
2-124	Fracture of Adjacent Fibers	1-154
2-125	SEM Photographs of Translaminar Mode I Tension, +45/-45 Fracture, -65, 180, and 270 F/Dry (Fiber Pullout)	2-156
2-126	SEM Photographs of Translaminar Mode I Tension, +45/-45 Fracture, -65, 180, and 270 F/Dry (Fiber Breakage)	2-157
2-127	SEM Photographs of Translaminar Mode I Tension, +45/-45 Fracture, 70, 180, and 270 F/Wet (50X)	2-158
2-128	SEM Photographs of Translaminar Mode I Tension, +45/-45 Fracture, 70, 180, and 270 F/Wet (2000X)	2-159
2-129	SEM Photographs of Translaminar Mode I Tension, 0/90 Fracture, 180 F/Dry (Various Magnifications)	2-160
2-130	SEM Photographs of Translaminar Mode I Tension, 0/90 Fracture, -65, 180, and 270 F/Dry (Low Magnification)	2-161
2-131	SEM Photographs of Translaminar Mode I Tension, 0/90 Fracture, -65, 180, 270 F/Dry (High Magnification)	2-162
2-132	SEM Photographs of Translaminar Mode I Tension, 0/90 Fracture, 70, 180, 270 F/Wet (50X)	2-163
2-133	SEM Photographs of Translaminar Mode I Tension, 0/90 Fracture, 70, 180, 270 F/Wet (2000X)	2-164
2-134	SEM Photographs of Translaminar Mode I Tension, 0/45/90 Fracture, -65, 180, 270 F/Dry (50X)	2-165
2-135	SEM Photographs of Translaminar Mode I Tension, 0/45/90 Fracture, -65, 180, 270 F/Dry (2000X)	2-166
2-136	SEM Photographs of Translaminar Mode I Tension, 0/45/90 Fracture, 70, 180, 270 F/Wet (50X)	2-167
2-137	SEM Photographs of Translaminar Mode I Tension, 0/45/90 Fracture, 70, 180, 270 F/Wet (2000X)	2-168
2-138	Optical and SEM Photographs of Translaminar Tension Fracture in Filament Wound Gr/Ep - 32 Ply/Quasi-Isotropic	2-169
2-139	SEM Fractographs of Translaminar Tension, Room Temperature, 0/90 Fabric Fracture	2-171
2-140	Optical and SEM Photographs of Translaminar Tension Fracture in Impact Damaged Gr/Ep -32 Ply/Quasi-Isotropic	2-173

LIST OF FIGURES (Continued)

Figure		Page
2-141	Optical and SEM Photographs of Translaminar Tension Fracture in Gr/Ep -32 Ply/Quasi-Isotropic, Water Immersed Before Test	2-175
2-142	SEM Fractographs of Translaminar Tension, 0/90 Fracture, Water Immersion (160 F) After Test	2-177
2-143	SEM Fractographs of Translaminar Tension, 0/90 Fracture, 100% Relative Humidity (160 F) Exposure After Test	2-179
2-144	Optical and SEM Photographs of Translaminar Tension Fracture in Undercured Gr/Ep -32 Ply/Quasi-Isotropic	2-181
2-145	SEM Fractographs of Translaminar Tension, 0/90 Fracture, Low Resin Content	2-183
2-146	SEM Photographs of Translaminar Tension Fracture in High Resin Content Gr/Ep - 32 Ply Quasi-Isotropic	2-185
2-147	SEM Fractographs of Translaminar Tension, 0/90 Fracture, 2000 F Exposure for 5 Minutes After Test	2-187
2-148	Four-Point Bend Test Type	2-188
2-149	Translaminar Compression Fracture	2-189
2-150	SEM Photographs of Translaminar Mode I Compression, 0/0 Fracture, 70 F/Dry	2-190
2-151	SEM Photographs of Translaminar Mode I Compression, 0/0 Fracture, -65, 180, 270 F/Dry (20X)	2-191
2-152	SEM Photographs of Translaminar Mode I Compression, 0/0 Fracture, -65, 180, 270 F/Dry (400X)	2-192
2-153	SEM Photographs of Translaminar Mode I Compression, 0/0 Fracture, 70, 180, 270 F/Wet (20X)	2-193
2-154	SEM Photographs of Translaminar Mode I Compression, 0/0 Fracture, 70, 180, 270 F/Wet (400X)	2-194
2-155	SEM Photographs of Translaminar Mode I Compression, +45/-45 Fracture, 70 F/Dry	2-195
2-156	SEM Photographs of Translaminar Mode I Compression, +45/-45 Fracture, -65, 180, 270 F/Dry (20X)	2-196
2-157	SEM Photographs of Translaminar Mode I Compression, +45/-45 Fracture, -65, 180, 270 F/Dry (400X)	2-197

LIST OF FIGURES (Continued)

Figure		Page
2-158	SEM Photographs of Translaminar Mode I Compression, +45/-45 Fracture, 70, 180, 270 F/Wet (20X)	2-198
2-159	SEM Photographs of Translaminar Mode I Compression, +45/-45 Fracture, 70, 180, 270 F/Wet (400X)	2-199
2-160	SEM Photographs of Translaminar Mode I Compression, 0/90 Fracture, 70 F/Dry	2-200
2-161	SEM Photographs of Translaminar Mode I Compression, 0/90 Fracture, -65, 180, 270 F/Dry (20X)	2-201
2-162	SEM Photographs of Translaminar Mode I Compression, 0/90 Fracture, -65, 180, 270 F/Dry (400X)	2-202
2-163	SEM Photographs of Translaminar Mode I Compression, 0/90 Fracture, 70, 180, 270 F/Wet (20X)	2-203
2-164	SEM Photographs of Translaminar Mode I Compression, 0/90 Fracture, 70, 180, 270 F/Wet (400X)	2-204
2-165	SEM Photographs of Translaminar Mode I Compression, 0/45/90 Fracture, 70 F/Dry	2-205
2-166	SEM Photographs of Translaminar Mode I Compression, 0/45/90 Fracture, -65, 180, 270 F/Dry (20X)	2-206
2-167	SEM Photographs of Translaminar Mode I Compression, 0/45/90 Fracture, -65, 180, 270 F/Dry (400X)	2-207
2-168	SEM Photographs of Translaminar Mode I Compression, 0/45/90 Fracture, 70, 180, 270 F/Wet (20X)	2-208
2-169	SEM Photographs of Translaminar Mode I Compression, 0/45/90 Fracture, 70, 180, 270 F/Wet (400X)	2-209
2-170	Optical and SEM Photographs of Translaminar Mode I Compression Fracture in Impact Damaged Gr/Ep - 32 Ply Quasi-Isotropic	2-210
2-171	Optical and SEM Photographs of Translaminar Mode I Compression Fracture in Gr/Ep - 32 Ply Quasi-Isotropic, Water Immersed Before Test	2-212
2-172	Optical and SEM Photographs of Translaminar Mode I Compression Fracture in Overcured Gr/Ep - 32 Ply Quasi-Isotropic	2-214
2-173	Optical and SEM Photographs of Translaminar Mode I Compression Fracture in High Resin Content Gr/Ep - 32 Ply Quasi-Isotropic	2-216
2-174	Side-Notched Rail Shear Type Test ..	2-218

LIST OF FIGURES (Continued)

Figure		Page
2-175	SEM Photographs of Translaminar Mode II Shear, 0/90 Fracture, 70 F/Dry	2-219
2-176	SEM Photographs of Translaminar Mode II Shear, 0/90 Fracture, -65, 180, 270 F/Dry (400X)	2-220
2-177	SEM Photographs of Translaminar Mode II Shear, 0/90 Fracture, -65, 180, 270 F/Dry (2000X)	2-221
2-178	SEM Photographs of Translaminar Mode II Shear, 0/90 Fracture, 70, 180, 270 F/Wet (400X)	2-222
2-179	SEM Photographs of Translaminar Mode II Shear, 0/90 Fracture, 70, 180, 270 F/Wet (2000X)	2-223
2-180	SEM Photographs of Translaminar Mode II Shear, 0/45/90 Fracture, 70 F/Dry ..	2-224
2-181	SEM Photographs of Translaminar Mode II Shear, 0/45/90 Fracture, -65, 180, 270 F/Dry (400X)	2-225
2-182	SEM Photographs of Translaminar Mode II Shear, 0/45/90 Fracture, -65, 180, 270 F/Dry (2000X)	2-226
2-183	SEM Photographs of Translaminar Mode II Shear, 0/45/90 Fracture, 70, 180, 270 F/Wet (400X)	2-227
2-184	SEM Photographs of Translaminar Mode II Shear, 0/45/90 Fracture, 70, 180, 270 F/Wet (2000X)	2-228
2-185	Laminate Flexure Type Test	2-229
2-186	SEM Photographs of Translaminar Flexure, 0/0 Fracture, 70 F/Dry	2-230
2-187	Double Cantilever Beam (DCB) for Mode I Fractures and Cracked-Lap Shear (CLS) for Mode II Fractures	2-231
2-188	Optical Photographs of Interlaminar Fatigue Mode I Tension, 0/0 Fracture, 70 F/Dry	2-232
2-189	Optical Photographs of Interlaminar Fatigue Mode I Tension, 0/0 Fracture, 70 F/Dry (400X and 1000X)	2-233
2-190	SEM Photographs of Interlaminar Fatigue Mode I Tension, 0/0 Fracture, 70 F/Dry (500X and 5000X)	2-234
2-191	Optical and SEM Photographs of Interlaminar Mode I DCB Spectrum Fatigue Fracture in AS4/3501-6 Gr/Ep - [0] _{24T}	2-235
2-192	SEM Photographs of Interlaminar Mode I DCB Spectrum Fatigue Fracture in AS4/3501-6 Gr/Ep - [+45/0/-45] _{4S}	2-237

LIST OF FIGURES (Continued)

Figure		Page
2-193	SEM Photographs of Interlaminar Mode I DCB Spectrum Fatigue Fracture in AS4/3501-6 Gr/Ep - [0/90] _{6S}	2-239
2-194	Optical Photograph of Interlaminar Fatigue Mode II Shear, 0/0 Fracture, 70 F/Dry	2-241
2-195	Optical Photographs of Interlaminar Fatigue Mode II Shear, 0/0 Fracture, 70 F/Dry (100X and 1000X)	2-242
2-196	SEM Photographs of Interlaminar Fatigue Mode II Shear, 0/0 Fracture, 70 F/Dry (5000X and 15000X)	2-243
2-197	SEM Photographs of Interlaminar Fatigue Mode II Shear, 0/0 Fracture, 70 F/Dry (1000X, 5000X and 15000X)	2-244
2-198	Macrophotographs of Interlaminar Mode I Tension, RT/Dry Creep, 0/90 Fracture	2-246
2-199	Optical Photomicrographs of Interlaminar Mode I Tension, RT/Dry Creep, 0/90 Fracture	2-247
2-200	SEM Fractographs of Interlaminar Mode I Tension, RT/Dry Creep, 0/90 Fracture	2-248
2-201	SEM Fractographs of Interlaminar Mode I Tension, RT/Dry, 0/90 Fracture (Area Shown in Figure 2-200a)	2-249
2-202	Macrophotographs of Interlaminar Mode I Tension, 270 F/Dry Creep, 0/90 Fracture	2-250
2-203	Optical Photomicrographs of Interlaminar Mode I Tension, 270 F/Dry Creep, 0/90 Fracture	2-251
2-204	SEM Fractographs of Interlaminar Mode I Tension, 270 F/Dry Creep, 0/90 Fracture	2-252
2-205	Photomicrographs of Interlaminar Mode II Shear, RT/Dry Creep, 0/90 Fracture	2-253
2-206	SEM Fractographs of Interlaminar Mode II Shear, RT/Dry Creep, 0/90 Fracture Showing Rough Surface (Area Shown in Figure 2-205b)	2-254
2-207	SEM Fractographs of Interlaminar Mode II Shear, RT/Dry Creep, 0/90 Fracture Showing Glassy Surface (Area Shown in Figure 2-205b)	2-255
2-208	Photomicrographs of Interlaminar Mode II Shear, 270 F/Dry Creep, 0/90 Fracture	2-256

LIST OF FIGURES (Continued)

Figure		Page
2-209	SEM Fractographs of Interlaminar Mode II Shear, 270 F/Dry Creep, 0/90 Fracture Showing Glassy Surface (Area Shown in Figure 2-208b)	2-257
2-210	SEM Fractographs of Interlaminar Mode II Shear, 270 F/Dry Creep, 0/90 Fracture Showing Rough Surface (Area Shown in Figure 2-208b)	2-258
2-211	Optical Photomicrographs of Interlaminar Mode I Tension, High Rate, Room Temperature Fracture Between the 0/90 Plies	2-260
2-212	SEM Fractographs of Interlaminar Mode I Tension, High Rate, Room Temperature Fracture (Region I of Figure 2-211)	2-261
2-213	SEM Fractographs of Interlaminar Mode I Tension, High Rate, Room Temperature Fracture (Region II of Figure 2-211)	2-262
2-214	Optical Photomicrographs of Interlaminar Mode II Shear, High Rate, Room Temperature Fracture Between the 0/90 Plies	2-263
2-215	SEM Fractographs of Interlaminar Mode II Shear, Room Temperature, High Rate Fracture (Region I of Figure 2-214)	2-264
2-216	SEM Fractographs of Interlaminar Mode II Shear, Room Temperature, High Rate Fracture (Region II of Figure 2-214)	2-265
2-217	Extent of Impact Damage Identified by Through Transmission Ultrasonic (TTU) Scan of Impact Specimen	2-267
2-218	Optical Photomicrographs of Interlaminar Fracture of Compression-After-Impact, RT/Dry, [0/+45/90/-45] ₄₅ Specimen	2-268
2-219	Cross-Sectional View of Compression-After-Impact, RT/Dry, [0/+45/90/-45] ₄₅ Specimen	2-269
2-220	SEM Photographs of Interlaminar/Translaminar Compression After Impact, 0/45/90 Fracture	2-270
2-221	SEM Photographs of Interlaminar Mode I Tension and Mode II Shear, 0/90 Fracture, Teflon Contamination, 70 F/Dry	2-272
2-222	SEM Photographs of Interlaminar Mode I Tension and Mode II Shear, 0/45 and 45/45 Fractures, Frekote Contamination, 70 F/Dry	2-273
2-223	SEM Photographs of Interlaminar Mode I Tension and Mode II Shear, 0/90 Fractures, With Voids, 70 F/Dry	2-275
3-1	Optical and SEM Photographs of Mode I DCB Interlaminar Tension Fracture in 49/3501-6 Kevlar/Ep - [0] _{24T} , Room Temperature Ambient	3-4

LIST OF FIGURES (Continued)

Figure		Page
3-2	Optical and SEM Photographs of Mode I DCB Interlaminar Tension Fracture in 49/3501-6 Kevlar/Ep - [+45/0/-45] ₄₈ , Room Temperature Ambient	3-5
3-3	Optical and SEM Photographs of Mode I DCB Interlaminar Tension Fracture in 49/3501-6 Kevlar/Ep - [0] _{24T} , Conditioned 180 F/Dry, 2 Weeks Before Test	3-6
3-4	Optical and SEM Photographs of Mode I DCB Interlaminar Tension Fracture in 49/3501-6 Kevlar/Ep - [+45/0/-45] ₄₈ , Water Immersed Before Test	3-7
3-5	Optical and SEM Photographs of Mode II ENF Interlaminar Shear Fracture in 49/3501-6 Kevlar/Ep - [0] _{24T} , Room Temperature Ambient	3-8
3-6	Optical and SEM Photographs of Mode II ENF Interlaminar Shear Fracture in 49/3501-6 Kevlar/Ep - [+45/0/-45] ₄₈ , Room Temperature Ambient	3-9
3-7	SEM Photographs of Mode II ENF Shear Crack-Growth Regions in 49/3501-6 Kevlar/Ep, Room Temperature Ambient	3-10
3-8	Optical and SEM Photographs of Mode II ENF Interlaminar Shear Fracture in 49/3501-6 Kevlar/Ep - [0] _{24T} , Conditioned 180 F Dry	3-11
3-9	Optical and SEM Photographs of Mode I and Mode II MMF Interlaminar Fracture in 49/3501-6 Kevlar/Ep - [0] _{24T} , Room Temperature Ambient	3-12
3-10	SEM Photographs of Mode I Translaminar Tension Fracture in 49/3501-6 Kevlar/Ep - [90/0] ₄₈ , Room Temperature Ambient	3-13
3-11	SEM Photographs of Mode I Translaminar Tension Fracture in 49/3501-6 Kevlar/Ep - [90/0] ₄₈ , Conditioned 180 F Dry	3-14
3-12	SEM Photographs of Mode I Translaminar Compression Fracture in 49/3501-6 Kevlar/Ep - [90/0] ₄₈ , Room Temperature Ambient	3-15
3-13	SEM Photographs of Mode I Translaminar Compression Fracture in 49/3501-6 Kevlar/Ep - 32 Ply/Quasi-Isotropic, Room Temperature Ambient	3-16
3-14	SEM Photographs of Mode I Translaminar Compression Fracture in 49/3501-6 Kevlar/Ep - [90/0] ₄₈ , Water Immersed Before Test	3-17
3-15	SEM Photographs of Mode I Translaminar Compression Fracture in 49/3501-6 Kevlar/Ep - 32 Ply/Quasi-Isotropic, Water Immersed Before Test	3-18
4-1	Optical Photomicrographs of Room Temperature/Dry, Interlaminar Mode I Tension, 0/90 Fracture in Boron/Epoxy	4-4
4-2	SEM Fractographs of Room Temperature/Dry, Interlaminar Mode I Tension, 0/90 Fracture in Boron/Epoxy	4-5

LIST OF FIGURES (Continued)

Figure		Page
4-3	Optical Photomicrographs of 270 F/Wet, Interlaminar Mode I Tension, 0/90 Fracture in Boron/Epoxy	4-6
4-4	SEM Fractographs of 270 F/Wet, Interlaminar Mode I Tension, 0/90 Fracture in Boron/Epoxy	4-7
4-5	SEM Fractographs of Room Temperature/Dry, Interlaminar Mode II Shear, 0/90 Fracture in Boron/Epoxy	4-8
4-6	Optical Photomicrographs of 270 F/Wet, Interlaminar Mode II Shear, 0/90 Fracture in Boron/Epoxy ..	4-9
4-7	SEM Fractographs of 270 F/Wet, Interlaminar Mode II Shear, 0/90 Fracture in Boron/Epoxy	4-10
4-8	SEM Fractographs of Room Temperature/Dry, Translaminar Tension, 0/90 Fracture in Boron/Epoxy	4-11
4-9	SEM Fractographs of Room Temperature/Dry, Translaminar Tension, 0/90 Fracture in Boron/Epoxy (0 Degree Tilt)	4-12
4-10	SEM Fractographs of 270 F/Wet, Translaminar Tension, 0/90 Fracture in Boron/Epoxy (45 and 0 Degree Tilts)	4-13
4-11	SEM Fractographs of Room Temperature/Dry, Translaminar Compression, 0/90 Fracture in Boron/Epoxy (40 Degree Tilt)	4-14
4-12	SEM Fractographs of Room Temperature/Dry, Translaminar Compression, 0/90 Fracture in Boron/Epoxy (0 Degree Tilt)	4-15
4-13	SEM Fractographs of 270 F/Wet, Translaminar Compression, 0/90 Fracture in Boron/Epoxy	4-16
4-14	SEM Fractographs of 270 F/Wet, Translaminar Compression, 0/90 Fracture in Boron/Epoxy (High Magnification).....	4-17
5-1	SEM Fractographs of Room Temperature/Dry, Interlaminar Mode I Tension, 0/90 Fracture in Fiberglass/Epoxy	5-3
5-2	SEM Fractographs of 200 F/Wet, Interlaminar Mode I Tension, 0/90 Fracture in Fiberglass/Epoxy	5-4
5-3	SEM Fractographs of Room Temperature/Dry, Interlaminar Mode II Shear, 0/90 Fracture in Fiberglass/Epoxy	5-5
5-4	SEM Fractographs of 200 F/Wet, Interlaminar Mode II Shear, 0/90 Fracture in Fiberglass/Epoxy	5-6

LIST OF FIGURES (Continued)

Figure		Page
	SEM Fractographs of 70 F/Dry, Translaminar Tension, 0/90 Fracture in Fiberglass/Epoxy	5-7
5-6	SEM Fractographs and Diagram of 70 F/Dry, Translaminar Compression, 0/90 Fracture in Fiberglass/Epoxy (0 Degree Tilt)	5-9
5-7	SEM Fractographs of 70 F/Dry, Translaminar Compression, 0/90 Fracture in Fiberglass/Epoxy (45 Degree Tilt)	5-10
5-8	SEM Fractographs of 200 F/Wet, Translaminar Compression, 0/90 Fracture in Fiberglass/Epoxy (45 Degree Tilt)	5-11
5-9	SEM Fractographs of 200 F/Wet, Translaminar Compression, 0/90 Fracture in Fiberglass/Epoxy (Higher Magnification)	5-12
6-1	Optical and SEM Photographs of Mode I DCB Interlaminar Tension Fracture in AS4/5250-3 Gr/BMI - [0] _{24T} , Room Temperature Ambient	6-3
6-2	Optical and SEM Photographs of Mode I DCB Interlaminar Tension Fracture in AS4/5250-3 Gr/BMI - [0] _{24T} , Water Immersed Before Test	6-5
6-3	Optical and SEM Photographs of Mode II ENF Interlaminar Shear Fracture in AS4/5250-3 Gr/BMI - [0] _{24T} , Room Temperature Ambient	6-6
6-4	Optical and SEM Photographs of Mode I and Mode II MMF Interlaminar Fracture in AS4/5250-3 Gr/BMI - [0] _{24T} , Room Temperature Ambient	6-7
6-5	SEM Photographs of Mode I Translaminar Tension Fracture in AS4/5250-3 Gr/BMI - [90/0] ₄₈ , Room Temperature Ambient	6-8
6-6	SEM Photographs of Mode I Translaminar Tension Fracture in AS4/5250-3 Gr/BMI - 32 Ply Quasi-Isotropic, Room Temperature Ambient	6-10
6-7	SEM Photographs of Mode I Translaminar Compression Fracture in AS4/5250-3 Gr/BMI - [90/0] ₄₈ , Room Temperature Ambient	6-12
7-1	Optical and SEM Photographs of Mode I DCB Interlaminar Tension Fracture in AS4/APC-2 Gr/PEEK - [0] _{24T} , Room Temperature Ambient	7-4
7-2	Optical and SEM Photographs of Mode I DCB Interlaminar Fracture in AS4/APC-2 Gr/PEEK - [+45/0/-45] ₄₈ , Mode I DCB, Room Temperature Ambient	7-6
7-3	SEM Fractographs of 270 F/Wet, Interlaminar Mode I Tension, 0/90 Fracture in AS4/APC-2	7-8
7-4	Optical and SEM Photographs of Mode I DCB Interlaminar Tension Fracture in AS4/APC-2 Gr/PEEK - [0] _{24T} , Conditioned 180 F/Dry	7-9

LIST OF FIGURES (Continued)

Figure		Page
7-5	Optical and SEM Photographs of Mode I DCB Interlaminar Tension Fracture in AS4/APC-2 Gr/PEEK - [+45/0/-45] _{gs} , Conditioned 180 F/Dry	7-10
7-6	Optical and SEM Photographs of Mode I DCB Interlaminar Tension Fracture in AS4/APC-2 Gr/PEEK - [90/0] _{gs} , Conditioned 180 F/Dry	7-11
7-7	Optical and SEM Photographs of Mode II ENF Interlaminar Shear Fracture in AS4/APC-2 Gr/PEEK - [0] _{24T} , Room Temperature Ambient	7-12
7-8	SEM Fractographs of 270 F/Wet, Interlaminar Mode II Shear, 0/90 Fracture in AS4/APC-2	7-15
7-9	Optical and SEM Photographs of Mode I and II MMF Fracture in AS4/APC-2 Gr/PEEK - [0] _{24T} , Room Temperature Ambient	7-16
7-10	Optical and SEM Photographs Mode I Translaminar Tension Fracture in AS4/APC-2 Gr/PEEK - [90/0] _{gs}	7-18
7-11	SEM Fractographs of 270/F Wet, Translaminar Tension, 0/90 Fracture in AS4/APC-2	7-19
7-12	Optical and SEM Photographs of Mode I Translaminar Compression Fracture in AS4/APC-2 Gr/PEEK - [90/0] _{gs} , Room Temperature Ambient	7-20
7-13.	SEM Fractographs of 270/F Wet, Translaminar Compression, 0/90 Fracture in AS4/APC-2	7-21
8-1	SEM Fractographs of Room Temperature, Mode I Interlaminar Tension Fracture in C3K 8-HS/PMR-15	8-4
8-2	SEM Fractographs of 500 F/Dry, Mode I Interlaminar Tension Fracture in C3K 8-HS/PMR-15	8-5
8-3	SEM Fractographs of Room Temperature, Mode II Interlaminar Shear Fracture in C3K 8-HS/PMR-15	8-6
8-4	SEM Fractographs of 500 F/Dry, Mode II Interlaminar Shear Fracture in C3K 8-HS/PMR-15	8-7
8-5	SEM Fractographs of Room Temperature/Dry, Translaminar Tension Fracture in C3K 8-HS/PMR-15	8-8
8-6	SEM Fractographs of 500 F/Dry, Translaminar Tension Fracture in C3K 8-HS/PMR-15	8-9
8-7	SEM Fractographs of Room Temperature/Dry, Translaminar Compression Fracture in C3K 8-HS/PMR-15	8-10

LIST OF FIGURES (Continued)

Figure		Page
8-8	SEM Fractographs of 500 F/Dry, Translaminar Compression Fracture in C3K 8-HS/PMR-15	8-11
9-1	Optical and SEM Photographs of Tension Failure in a AS4/3501-6 Gr/Ep Bolted Joint	9-3
9-2	Optical and SEM Photographs of Tension-Cleavage Failure in a AS4/3501-6 Gr/Ep Bolted Joint	9-5
9-3	Optical and SEM Photographs of Shear-Out Failure in a AS4/3501-6 Gr/Ep Bolted Joint	9-7
9-4	Optical and SEM Photographs of Bearing Failure in a AS4/3501-6 Gr/Ep Bolted Joint	9-9
9-5	Optical and SEM Photographs of Bolt Failure in a AS4/3501-6 Gr/Ep Bolted Joint	9-11
9-6	Optical and SEM Photographs of Bolt Failure in a AS4/3501-6 Gr/Ep Bolted Joint	9-13
10-1	Optical and SEM Photographs of Failure in Unidirectional AS4/3501-6 Gr/Ep Adherends Bonded With FM 300 Adhesive and Tested Under Interlaminar Mode I Tension	10-2
10-2	Optical and SEM Photographs of Failure in Unidirectional Gr/Ep Bonded to Quasi-Isotropic Gr/Ep With FM 300 Adhesive and Tested Under Mode I Tension	10-4
10-3	Optical and SEM Photographs of Failure in Unidirectional AS4/3501-6 Gr/Ep Adherends Bonded With FM 300 Adhesive and Tested Under Mode II Interlaminar Shear	10-5
10-4	Optical and SEM Photographs of Fracture in Unidirectional AS4/3501-6 Gr/Ep Adherends Bonded With FM 300 Adhesive, Having a Larger Lap/Strap Ratio, and Tested Under Mode II Interlaminar Shear	10-7
10-5	Optical and SEM Photographs of Fracture in Unidirectional Gr/Ep Bonded to Quasi-Isotropic Gr/Ep With FM 300 Adhesive and Tested Under Mode II Interlaminar Shear	10-9
10-6	Optical and SEM Photographs of Fracture in Unidirectional AS4/3501-6 Gr/Ep Adherends Bonded With FM 300 Adhesive and Tested Under Mode I Tension and Mode II Interlaminar Shear	10-11
10-7	Optical and SEM Photographs of Fracture in Unidirectional AS4/3501-6 Gr/Ep Adherends Bonded With FM 300 Adhesive, Larger Lap/Strap Ratio and Tested Under Mode I Tension and Mode II Interlaminar Shear	10-13

LIST OF FIGURES (Concluded)

Figure		Page
10-8	Optical and SEM Photographs of Fracture in Unidirectional Gr/Ep Bonded to Quasi-Isotropic Gr/Ep Using FM 300 Adhesive, Large Lap/Strap Ratio and Tested Under Mode I Tension and Mode II Interlaminar Shear	10-15
10-9	Optical and SEM Photographs of Failure in Unidirectional AS4/5250-3 Gr/BMI Bonded With EA 9673 Adhesive and Tested Under Interlaminar Mode I Tension	10-17
10-10	Optical and SEM Photographs of Failure in Unidirectional Gr/BMI Bonded to Quasi-Isotropic Gr/BMI With EA 9673 Adhesive and Tested Under Mode I Tension	10-19
10-11	Photographs of Fracture in Unidirectional AS4/5250-3 Gr/BMI Adhrends Bonded With EA 9673 Adhesive, and Tested Under Mode I Tension and Mode II Interlaminar Shear	10-21
10-12	Optical and SEM Photographs of Fracture in Unidirectional Gr/BMI Bonded to Quasi-Isotropic Gr/BMI Using EA 9673 Adhesive, Large Lap/Strap Ratio, Tested Under Mode I Tension and Mode II Interlaminar Shear	10-22

LIST OF TABLES

Table		Page
2-1	Test Matrix for Mode I DCB Specimens	2-4
2-2	Test Matrix for ENF Specimens	2-65
2-3	Test Matrix for Modes I and II MMF Specimens	2-120
2-4	Test Matrix for In-Plane Shear Specimens	2-145
2-5	Test Matrix for Translaminar Tension Specimens	2-155
2-6	Test Matrix for Translaminar Compression Specimens	2-189
2-7	Test Matrix for Translaminar Shear Specimens.....	2-218
3-1	Kevlar 49/3501-6 Epoxy Interlaminar Fracture Test Matrix	3-2
3-2	Kevlar 49/3501-6 Epoxy Translaminar Fracture Test Matrix	3-3
6-1	AS4/5250-3 Gr/BMI Interlaminar Fracture Test Matrix	6-2
6-2	AS4/5250-3 Gr/BMI Translaminar Fracture Test Matrix	6-2
7-1	AS4/APC-2 Gr/PEEK Interlaminar Fracture Test Matrix	7-2
7-2	AS4/APC-2 Gr/PEEK Translaminar Fracture Test Matrix	7-3
9-1	Test Matrix for Mechanically Joined Composites	9-1
9-2	Specimen Width/Fastener Diameter (w/d) and Fastener-Edge-Distance/ Fastener Diameter (e/d) Ratios	9-2
10-1	Test Matrix for Adhesively Bonded Composite Fractography	10-1

SECTION 1

INTRODUCTION AND PURPOSE

Advanced composites are rapidly emerging as a primary material for use in near-term and next-generation aircraft as they provide greater structural efficiency at lower weight than equivalent metallic components. Based on trends to date, the next generation of military aircraft could contain as much as 65 percent of their structural weight in advanced composite materials.

As composite materials continue to be developed and incorporated into airframe structures, needs have arisen for solving problems associated with their use. Composite structures can and will prematurely fail due to gross manufacturing defects, design errors or severe in-service damage. Needs exist for a systematic compilation of failure analysis techniques, procedures, and supporting fractographic data, in handbook form that can be used by experienced laboratory personnel, working in consultation with field investigators, to diagnose the cause for premature component failure and to make recommendations for prevention similar failures.

The goal of this Composite Failure Analysis Handbook is to provide a guide for conducting post-failure analysis of fiber-reinforced composite structures. It forms a compilation of the procedures, techniques, and sample data required to conduct analyses of composite structures. Volume II of this report is the Technical Handbook and it has been divided into three parts.

Part 2 of the Handbook is an atlas of fractographs and presents the results of fractographic evaluations performed by Northrop and Boeing under Air Force Contracts F33615-84-C-5010, F33615-87-C-5212, and F33615-86-C-5071. The atlas is centered on the model system AS4/3501-6 graphite/epoxy (Gr/Ep), because this composite system has been most extensively used in the aerospace industry. The object was to make the AS4/3501-6 Gr/Ep fractographic database as complete as possible, and then to extend the database to include information on other key composite systems including Kevlar/epoxy, boron/epoxy, fiberglass/epoxy, graphite/bismaleimide, graphite/polyetheretherketone, and carbon/polyimide. Fracture characteristics on simple test coupons loaded under interlaminar (Mode I tension, Mode II shear, and mixed mode) and translaminar (tension, compression, shear, and flexure) test conditions are described and shown. Results for in-plane shear, creep, and fatigue tests are also included, as well as the effects of manufacturing, processing, and post-failure variable conditions. The test matrices and testing procedures utilized by Boeing to establish the original fractographic data base are described in AFWAL-TR-86-4137 and WRDC-TR-89-4055. The test matrices and testing procedures utilized by Northrop to expand the fractographic database started under the Air Force/Boeing programs are described in Section 3.4 of Volume I. Additional discussion on mechanical test methods is presented in Section 7 of Volume II, Part 1.

The Gr/Ep fractographic data have also been extended to include information on mechanically joined Gr/Ep adherends. Test coupons were designed, fabricated, and tested to simulate the six macroscopic failure modes associated with bolted joint failures. Adhesively bonded Gr/Ep and graphite/bismaleimide (Gr/BMI) coupons in which adhesive, cohesive, and mixed failure modes were developed, are presented. In each case macroscopic and microscopic fracture characteristics were documented using optical and scanning electron microscopy (SEM) techniques.

In each test case, fracture was produced such that the crack direction and fracture mode was controlled. Where possible, the direction of crack growth has been noted, to aid the investigator in evaluation of the fracture surfaces during crack mapping. To demonstrate differences between the details identified by the various fractography tools, both optical and SEM photomicrographs are presented for most fracture conditions. To further familiarize the reviewer with the typical fracture characteristics, the photomicrographs have been arranged in increasing order of magnification showing a wide variety of ply orientations and environmental conditions.

The Handbook has been designed to be a living document that can be updated readily. This Handbook summarizes the results of six years of fundamental work that has been sponsored by the United States Air Force (USAF) and the Federal Aviation Administration (FAA). In this edition of the Atlas of Fractographs, most of the fractographs generated under the Air Force/Northrop/Boeing programs have been included for reference by failure analysts. Further clarification and verification of the fractographic characteristics that result from the various failure modes in each composite material system will be gained as composite failures are analyzed and the associated fractographic results are compared with the atlas. In the future, this atlas may be condensed to show only the essential fractographic characteristics that have become accepted by the aerospace industry through successful analyses of failed composites. At this point in the development of composites fractography as a failure analysis technique, it is useful to show fracture surfaces of different composite systems generated under similar conditions to establish the similarities and differences between these systems. The following observations and correlations were evident through comparison and analysis of the fractographic data generated under the Air Force/Northrop/Boeing programs.

1. Applied load was the principal parameter that affected the fracture surface characteristics in the Gr/Ep model system, Gr/BMI, and Gr/polyetheretherketone (PEEK).
2. For the systems studied, material form and processing variables (filament winding versus tape) indirectly affected the fracture characteristics, in that these may have caused localized variations in applied load, thereby altering fractographic features.
3. In fiber-dominated fracture events such as translaminar tension or compression, the type of fiber played a role in resultant fracture surface characteristics. In pitch base carbon fibers, fracture features such as DAF radials or chop marks occurred. These served as indicators of failure mode (tension, compression), and crack growth direction (DAF radials in tension failures). In organic fibers such as Kevlar 49,

defibrillation of the fibers occurred, thereby resulting in loss of fracture feature information.

4. Work on Gr/BMI and Gr/PEEK indicated that the resin plays a strong role in controlling the resulting fracture surface characteristics. Fracture in AS4/5250-3 Gr/BMI could be mapped in a manner similar to baseline Gr/Ep. In Gr/PEEK, the fracture surface morphology included features not observed in baseline Gr/Ep or Gr/BMI.
5. Fractographic evaluation of bolted Gr/Ep joints indicated that varying failure modes occur in these specimen based on applied loads, specimen, and fastener geometries.
6. Evaluations of Gr/Ep and Gr/BMI bonded structures indicate that specimen geometry, lap/strap ratios, and test load play roles in controlling fracture surface characteristics. Failures under adhesive or mixed-mode conditions could be mapped through evaluation of fracture features on the fractured adherends.
7. In-plane shear failure in Gr/Ep was characterized by the occurrence of hackles on fractured resin, and tension fracture characteristics on fractured fiber ends. Processing variables did not significantly alter fracture surface characteristics for Gr/Ep tested under in-plane shear.
8. In-plane shear in Gr/Ep could be distinguished from out-of-plane shear failure in Gr/Ep through examination of fractured fiber ends. Out-of-plane shear resulted in compressive features on fiber ends, whereas in-plane shear resulted in tension fracture characteristics on fractured fiber ends.
9. Environmental variables such as moisture, temperature, or humidity did not significantly affect the fracture surface characteristics in thermoplastic or thermoset composites. The only exception was in elevated temperature failures for situations where pyrolysis of the resin occurred (such as conditioning or testing above T_g). This led to loss of fracture information from the resin, thereby precluding unequivocal determination of crack-growth directions.
10. Processing variations such as fiber/prepreg variations, or post-consolidation treatments such as holes or impact, affected fracture surface characteristics only if they changed the local applied load state.

Parts 1 and 3 (the Procedures and Techniques and the Case Histories, respectively) of the Technical Handbook are discussed in the Summary of this report. Further information has been presented in the Introduction and Purpose section of each of these parts.

Section 1.1 has been taken from the Compendium of Post-Failure Analysis Techniques for Composite Materials (AFWAL TR-86-4137) developed by Boeing under Contract F33615-84-C-5010 and presented here to assist users of this Atlas of Fractographs in the development of the analytical methods and interpretive skills required to perform fractographic analyses of composites. Section 1.2 describes the organization of the atlas. A glossary of terms is available to users of this atlas in Section 11 of Volume II, Part 1.

1.1 FRACTOGRAPHIC APPLICATIONS, EXAMPLES AND INTERPRETIVE METHODS

Some of the most extensive investigations in a failure analysis involve the examination of the fracture surface of failed components. These surfaces may provide the only true physical record of the events and conditions involved in the failure process. Through detailed macroscopic and microscopic analyses, fractography can be used to attempt reconstruction of the failure sequence. Using the tools and methods outlined in Section 8 of Volume II, Part 1 of this report, primary emphasis is placed on interpreting the fractographic information obtained to answer the following questions:

1. Where did a crack start, that is, where is a crack origin?
2. What caused the crack to initiate at the origin?
3. By what modes did the crack propagate?
4. In what directions did the crack propagate?
5. What fracture types are present?
6. What loads or environmental conditions were operative at failure?
7. What was the sequence of failure in a case of multiple cracks or multiple component fracture?

The development of the analytical methods and interpretive skills required to answer these questions for composite material structures has only recently been initiated. In general, fractographic studies on other materials (metals and unreinforced polymers) have made significant strides toward (1) understanding the microscopic mechanisms of cracking and (2) identifying the causes of component failure. Of these two areas, the latter is perhaps the most important. Through fractographic examinations, the origin location and the direction of crack growth and load conditions involved in premature component fractures can generally be identified. In many cases, the definition of defects, damage conditions or anomalous fracture modes by such studies may be sufficient to identify the cause of fracture. In those cases where such causes are not apparent, understanding the sequence of events leading to fracture on a microscopic scale is often crucial to accurately direct other analytical techniques such as stress analysis or materials characterization.

The information presented in this section is intended to provide the investigator with a basic fundamental understanding of how laminated composite structures fracture. Primary emphasis is placed on analyses of carbon fiber reinforced and epoxy resin matrix systems, which have been proven to provide the aerospace industry with a material which exhibits high specific strength and modulus combined with excellent environmental durability. More specifically, the vast majority of the examples are from laminates constructed from prepreg tape. Fabric or three-dimensional product forms appear to fail under basically the same mechanisms, although slightly more complex in nature. Covered in this section are discussions on the following:

1. Fracture type and classification.
 - Translaminar

- Interlaminar
 - Intralaminar
2. Interlaminar and intralaminar fractures.
 - Tension versus shear fracture features
 - Mixed mode fractures
 - Relationships between features and crack growth directions
 - Cross-plying interfacial effects
 - Environment and fatigue effects
 3. Translaminar fractures.
 - Tension
 - Compression
 - Flexure
 - Environmental effects

1.1.1 Fracture Types

Because of their laminated anisotropic construction, fractures in composites can occur in a number of complex ways. The types and modes of failure which can be encountered depend upon both the direction of applied load and the orientation of fibers (plies) making up the composite material. As indicated in Figures 1-1 and 1-2, variations in either of these can produce strikingly different fracture appearances on a macroscopic scale. This range of diversity precludes the ability to assign well defined macroscopic fracture types for most applications. The definition of fracture types on a microscopic scale, however, provides a relatively useful means of classifying failure modes and fracture types in much the same way as with metals.

Fractures in continuous fiber reinforced composites can be divided into three basic fracture types; interlaminar, intralaminar, and translaminar. Each of these failure types are schematically illustrated in Figure 1-3. As with the intergranular and transgranular terminology commonly used with metals, each of these classifications describes the plane of fracture with respect to the microstructural constituents of the material. Translaminar fractures are those oriented transverse to the laminated plane in which conditions of fiber fracture are generated. Interlaminar fractures, on the other hand, describe failures oriented between plies whereas intralaminar fractures are those located internally within a ply. Translaminar fractures involve significant fiber fracture, while interlaminar or intralaminar fractures occur in the laminate plane, principally fracturing matrix resin and therefore breaking few or no fibers.

Commonly, a failed component will exhibit all three types of fracture. In this case, it is important to differentiate between the types so as to more easily prepare the analytical approach (per the fractography failure analysis logic network or FALN) and to define the analytical tools to

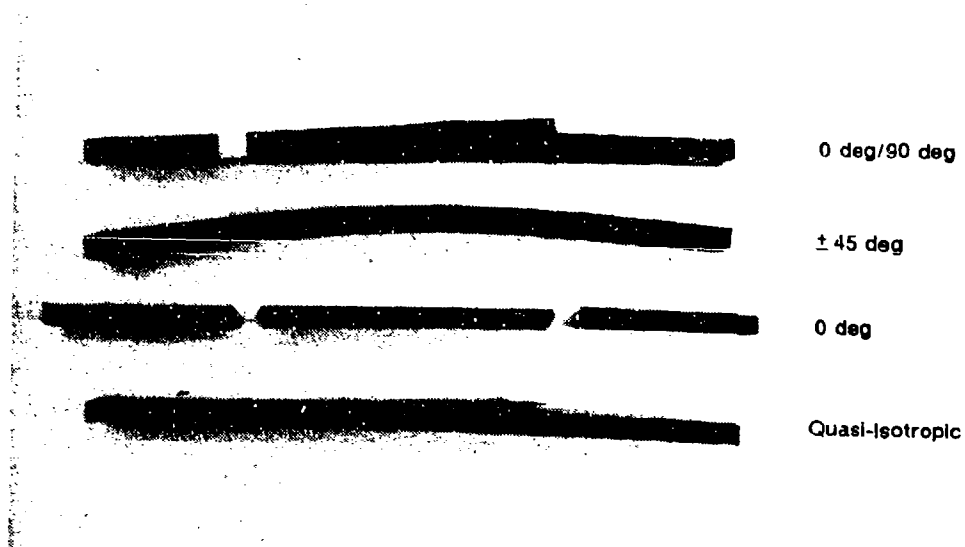
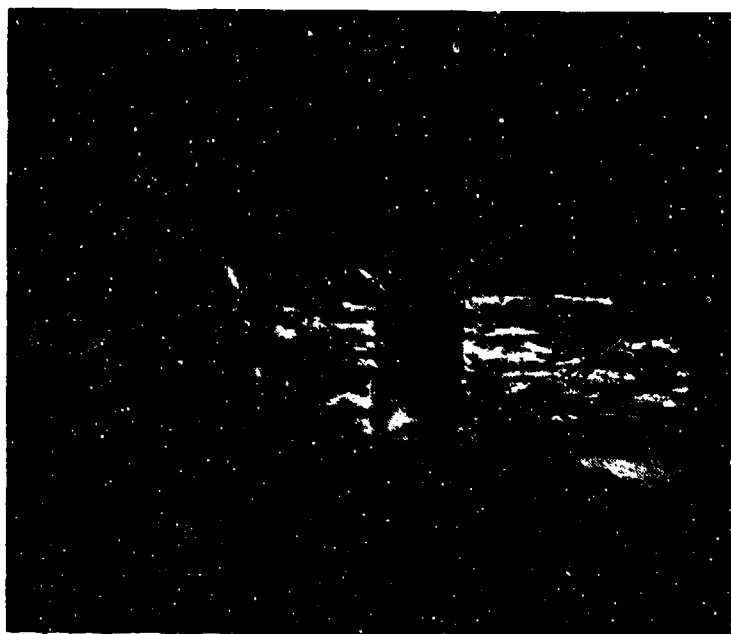


Figure 1-1. Laminate Flexure Specimens

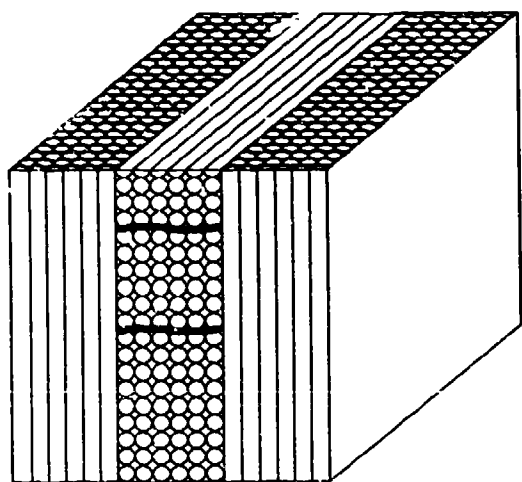


Tensile

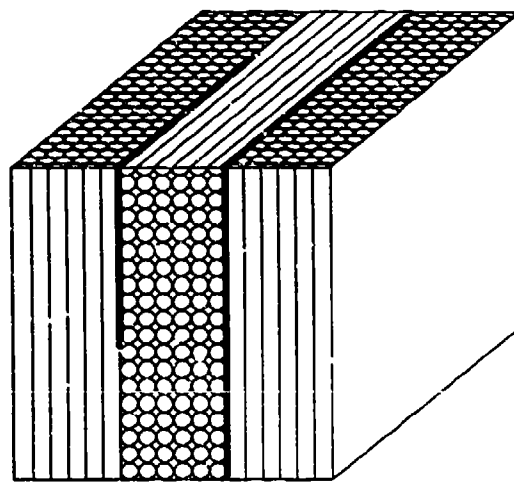


Compression

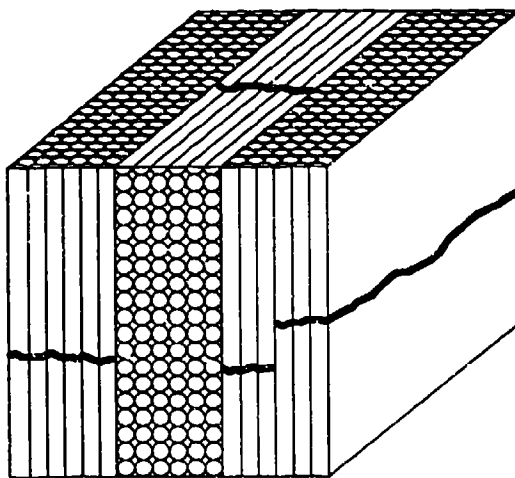
Figure 1-2. Tensile and Compression Translaminar Fractures



(a) Intralaminar Fracture



(b) Interlaminar Fracture



(c) Translaminar Fracture

Figure 1-3. The Basic Fracture Modes

be used. For instance, the optical microscope is the most accurate and quickest method of analyzing interlaminar or intralaminar fractures, in which the fracture of the matrix resin dominates. Conversely, the optical microscope cannot be used to investigate the translaminar, fiber-fracture dominated surfaces due to the rough topography. For such fractures in which a large depth of focus is required in conjunction with high magnification capabilities, the scanning electron microscope is invaluable. Although this is rather a simple analogy, it illustrates the need to define and understand the various fracture types so that planning of detailed analysis such as crack mapping can be developed early in the investigation process.

1.1.2 Fracture Modes, Features, and Growth Directions

Failures in composites can be described in terms of the failure mechanism exhibited on translaminar, interlaminar, and intralaminar fracture types. The first evaluation method available to define and differentiate between these fracture types is visual macroscopic. The ability to define fracture types at the macroscopic level can often be the most valuable capability for many investigators, particularly for those performing field investigations. When examining a failed composite structure, the investigator must assess the nature and direction of the applied load, identify the significance and time of fracture, and select portions of the structure for laboratory analyses. Visual examination alone can often provide sufficient information to answer these questions. However, this extremely valuable capability is very much in its infancy compared to the metals field. Figure 1-4 presents a brief overview of the relationships that various investigators have observed between fracture mode/load conditions and macroscopic fracture surface features. Figure 1-5 illustrates how a consistent pattern of crack branching of the skin surface was found to indicate the direction of macroscopic crack growth, and aided in identifying the initiation site in a very large structure which experienced compression buckling.

Although macroscopic methods are currently fairly limited, an extensive capability has been developed to evaluate the microscopic fracture features in the laboratory as related to each failure mechanism. The failure mechanism reflects the load under which microscopic separation occurs, either tension, shear, compression or fatigue. The following discussion presents each of the primary types of failure, with the interpretation of the fractographic features that identify the load type and localized crack propagation direction.

1.1.2.1 Interlaminar and Intralaminar

The extremely low in-plane fracture resistance ($G_{Ic} = 0.25 \text{ KJ/sq.m}$ versus translaminar G_{Ic} values of 100 KJ/sq.m) makes interlaminar and intralaminar fracture (commonly known as delaminations) a particularly significant mode of failure for nearly all composite fractures. When considered on a microscale, interlaminar and intralaminar fractures can be described similarly. In both cases fracture occurs on a plane parallel to that of the fiber reinforcement. In a manner similar to that described for metals, fracture of either type can occur under Mode I tension, Mode II in-plane shear, Mode III anti-plane shear. These three load states are illustrated in Figure 1-6. On a microscopic scale, nearly all delaminations separate in a combination of the first two types, with a predominance of either one or the other. All modes are recognized as

MODE	ENVIR. CONDITION	MACROSCOPIC FRACTURE FEATURES
Interlaminar Tension Dominated	Low Temperature/Dry	<ul style="list-style-type: none"> • Smooth, glassy fracture surface • Major portion of fracture between plies
	Hot or Hot/Wet	<ul style="list-style-type: none"> • Smooth but with loose fibers strewn on surface • A majority of the fracture within plies • May be permanent deformation of laminate
Interlaminar Shear Dominated	Low Temperature/Dry	<ul style="list-style-type: none"> • Surface flat, but with "milky" appearance when held at angle to light • Major portion of fracture between plies
	Hot or Hot/Wet	<ul style="list-style-type: none"> • Also exhibits "milky" appearance • Tends to fracture within a ply • Loose fibers on surface
Translaminar Tension	_____	<ul style="list-style-type: none"> • Rough, jagged fracture surface with individual fibers protruding from surface
Translaminar Compression	_____	<ul style="list-style-type: none"> • Extreme surface damage. Large regions of fibers fractured on same plane • Very few, if any, fibers protruding from surface
Translaminar Flexure	_____	<ul style="list-style-type: none"> • Two fairly distinct regions, one exhibiting translaminar tension and the other translaminar compression, the regions being separated by a neutral axis line

Figure 1-4. Visual Macroscopic Fracture Surface Features

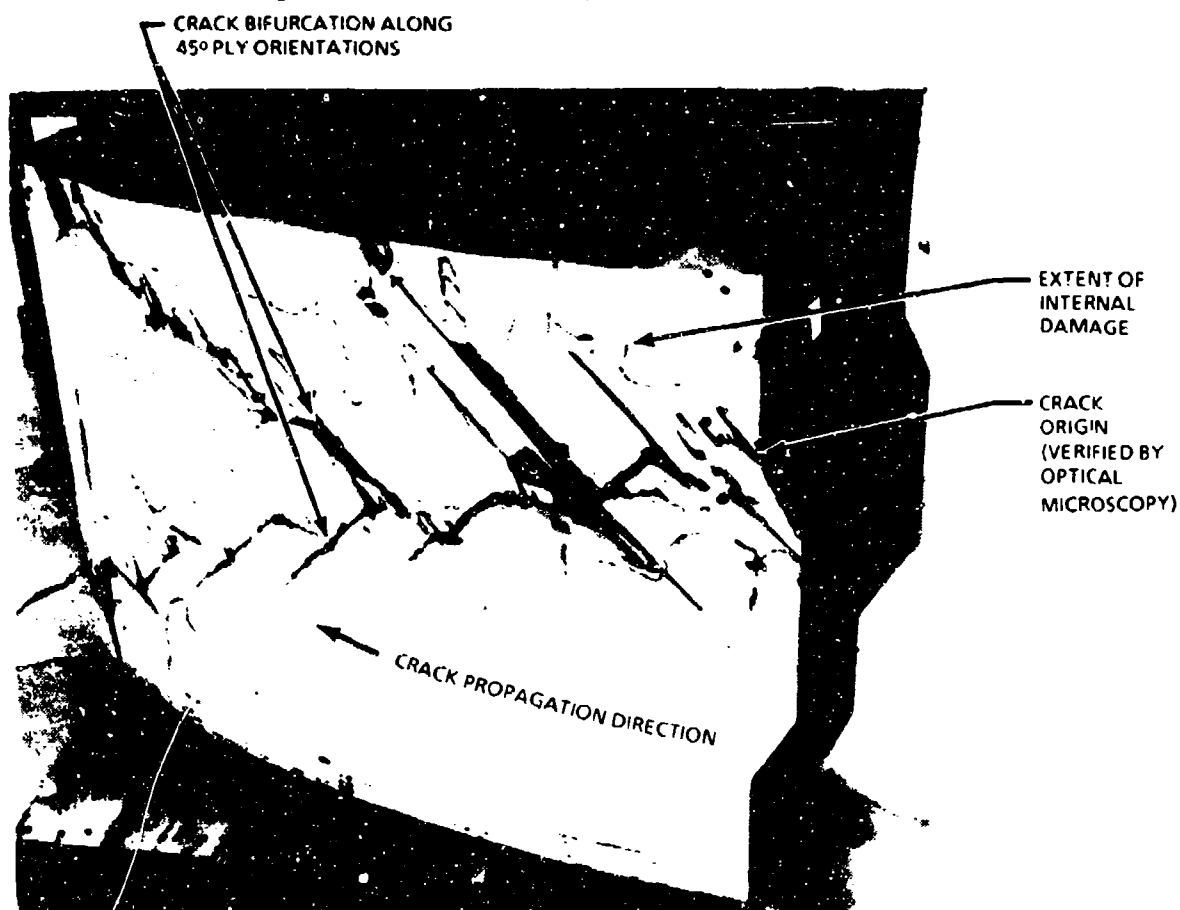
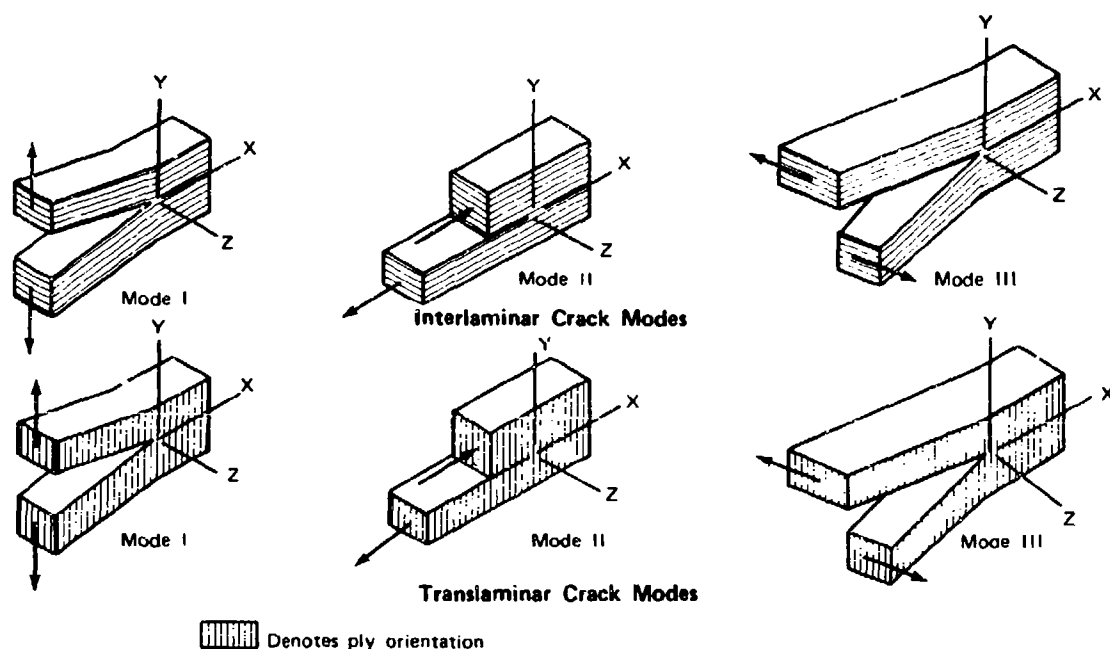


Figure 1-5. V-22 Osprey Wing Box Failure



- Mode I** Opening or tensile mode, where the crack surfaces move directly apart.
- Mode II** Sliding or in-plane shear mode, where the crack surfaces slide over one another in a direction perpendicular to the leading edge of the crack.
- Mode III** Tearing or antiplane shear mode, where the crack surfaces move relative to one another and parallel to the leading edge of the crack.

Figure 1-6. Basic Modes of Loading Involving Different Crack Types and Surface Displacements (Interlaminar and Translaminar)

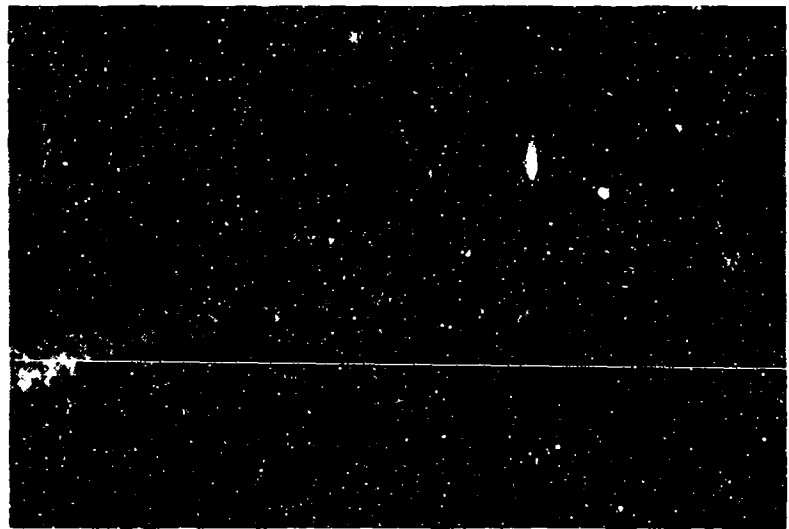
potentially critical in compression buckling, joint failures, and defect initiated failures such as impact. Each of these failure modes are still being actively investigated so as to further understand the actual microstructural separation mechanisms and the generated morphological features, as related to the macroscopic loading conditions. As a result, conditions such as Mode III anti-plane shear have not been thoroughly studied and will not be presented in this document. However, for Mode I tension and Mode II in-plane shear, enough data exists to accurately model their mechanisms of separation and describe their fracture characteristics.

Since interlaminar and intralaminar failures occur in the same plane as their fiber reinforcement, their fracture mechanism and appearance tend to be dominated by matrix fracture and fiber-to-matrix separation. In general, separation of the fiber from the matrix occurs at the interface for either Mode I tension or Mode II shear loading conditions. As a result, very little cohesive resin fracture occurs along the fiber, which often serves as a source of crack initiation. Fracture of the matrix resin between fibers exhibits pronounced cohesive fracture characteristics under both Mode I tension and Mode II shear loading.

For the majority of thermosetting matrices currently in use, cohesive matrix failure occurs in a brittle manner. Cohesive resin fracture characteristically exhibits relatively flat fracture planes with very little evidence of permanent material deformation. This is similar to brittle failure in metals (Figure 1-7), unreinforced polymers (Figure 1-8), and ceramics such as glass. The microscopic plane of such brittle failures is nearly always oriented normal to the direction of locally resolved tension. With reference to Figure 1-6, separation under either Mode I tension or Mode II shear occurs by the identical microscopic mechanism (that is, brittle tension). The only difference between these two modes is the orientation of principal tensile stress under which microscopic separation occurs.

Mode I Tension Delaminations. In the case of Mode I tension (which is the weakest fracture type with a G_{Ic} toughness at one-third of Mode II shear G_{IIc}), the maximum principal tensile stress lies perpendicular to the plane of failure. As a result, brittle cleavage of the matrix material occurs and fiber fracture rarely happens. These fractures are flat and are very shiny and smooth in appearance at macroscopic visual levels of magnification (Figure 1-9). Although not often identified, arced bands can be found that are similar to beach markings found in metals and unreinforced polymer fractures. Such markings, presented in Figure 1-10 from a controlled crack growth test coupon, are indicative of the crack-front geometry and are formed in response to pronounced changes in crack velocity. Numerous investigators have demonstrated that in neat polymeric materials, low crack velocities resulted in mirror-smooth fracture surfaces, and high crack velocities result in roughened, less reflective fracture topographies. This feature can be used to define the macroscopic direction of crack growth with the direction of growth moving from the concave to the convex side of the markings.

Microscopic examinations (optical and SEM) reveal distinctly flat areas of cohesive resin fracture between the areas of fiber-matrix separation. The extent to which either of these two features occurs depends upon both the volume fraction of fibers and the proximity of the fracture plane to these fibers (that is, intralaminar or interlaminar). In general, cohesive resin fractures dominate the overall surface topography. Such areas typically exhibit pronounced river markings



Crack growth direction

1.0X

Figure 1-7. Fracture Surface of 4340 M Steel Illustrating Cleavage Fracture Features Indicative of Crack Growth Direction

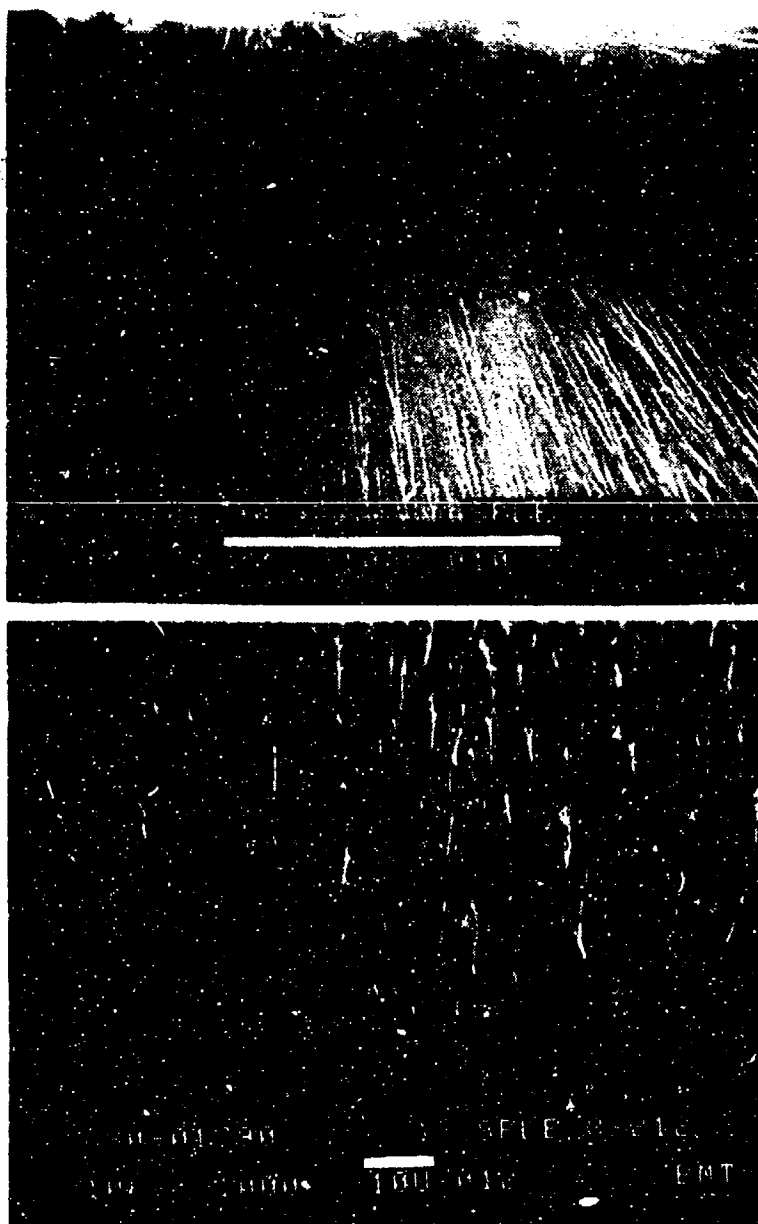


Figure 1-8. Fracture of Unreinforced Neat Epoxy Resin

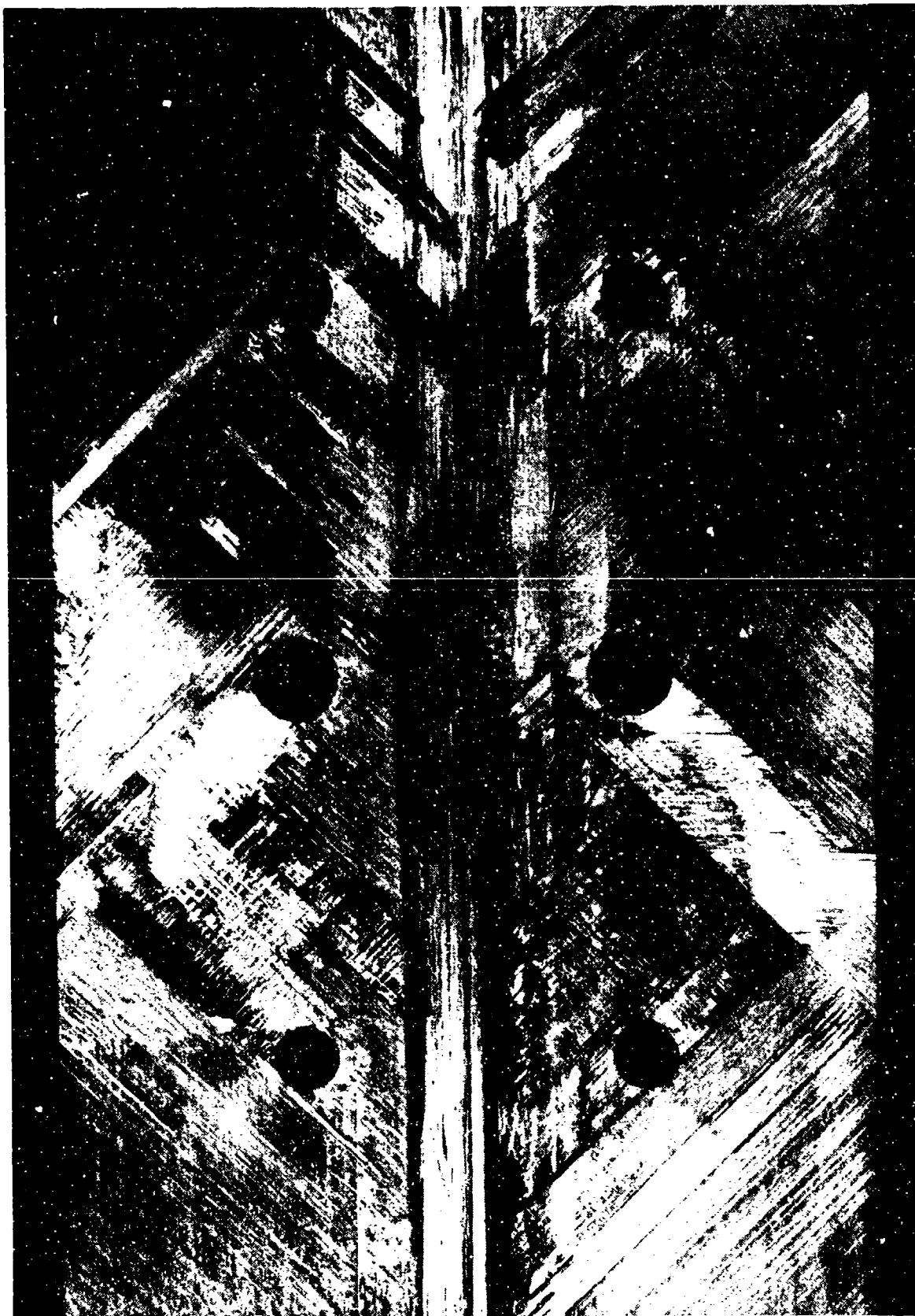
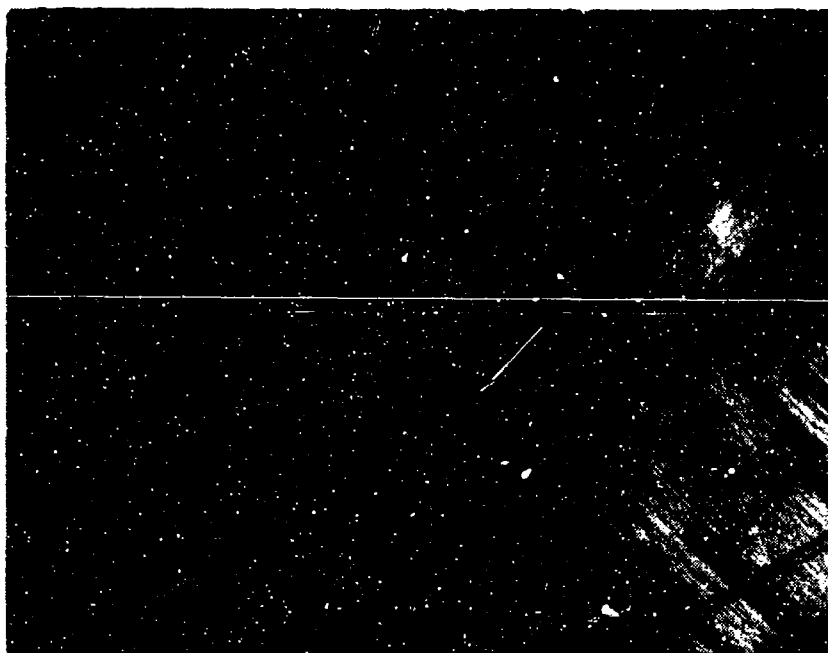


Figure 1-9. Mode I Tension Fracture



1X

Figure 1-10. Beach Marks Found in a Delamination Surface Indicative of Crack Front Shape and Crack Growth Direction During Fracture

and resin microflow as discussed below. The combination of these features appears unique to Mode I tension and provides a means of identifying the relative percentage of Mode I tension at fracture and the localized direction of crack propagation.

High magnification optical photomicrographs of interlaminar tension fractures which delaminated in the direction of fiber orientation are illustrated in Figure 1-11. The surface exhibits a reflective appearance with flat areas of resin fracture between the regions of fiber/matrix separation. Inspection reveals branching lines (river marks) in these flat resin fracture areas, along with an extremely fine texture of feathering (resin microflow); the direction of river mark coalescence corresponds with the direction of overall crack growth. These photomicrographs are taken from a region between plies that was rich in resin, primarily for illustrative purposes. Therefore more resin fracture and fewer fibers are evident than usually found. It should be noted that areas with different ratios of fiber reinforcement do not significantly effect the overall fracture features, although it can make optical inspections more difficult to resolve small resin fields between fibers.

The river markings, presented in Figure 1-12, are analogous to the cleavage fracture features commonly recognized in brittle materials such as metals, ceramics, and polymers. It has been determined through extensive studies that such features result from progressive joining of adjacent microscopic fracture planes during crack growth. More specifically, each line segment represents a local step formed when the thin ligament separating two adjacent planes is fractured during crack growth. The amount of strain energy involved in fracture is considered to be proportional to the areas of fracture surface created and the amount of plastic deformation at the crack tip. As a result, a large number of locally displaced fracture planes that initiate at the fiber/matrix interface represent a higher energy condition than a single continuous fracture surface. Since crack propagation tends to occur along the path requiring the least energy, there is a tendency for the planes to coalesce together. Thus the multitude of microplanes that initiate at the fiber/matrix interface link up as the crack propagates, resulting in a coalescence of the steps to form a branched pattern, or river marks.

Close inspection of the resin microplanes reveals a distinctly textured morphology referred to as resin microflow. Microflow is discernable at high magnifications and usually requires tilting of the specimen in the electron microscope (Figures 1-13 and 1-14) for this subtle feature to become visible. In many ways, the textured appearance is identical to the cleavage feathers characteristic of metallic fractures as shown in Figure 1-7. These feathery patterns exhibit a distinctive chevron type appearance, with the pointed end of the chevron oriented toward the origin of propagation. This chevron pattern results from the inherent tendency of a propagating crack to take the shortest path to a free surface. On a microscopic scale, these chevrons tend to rotate from the direction of overall crack growth toward adjacent free surfaces such as microplanes, transverse cracks, or fiber/matrix interfaces. However, by examining the direction and orientation of the microflow patterns in the center of each microplane, the localized direction of crack propagation can be determined.

Mode I tension fractures produced at angles relative to the direction of fiber reinforcement typically exhibit both the river markings and resin microflow as noted above. However,

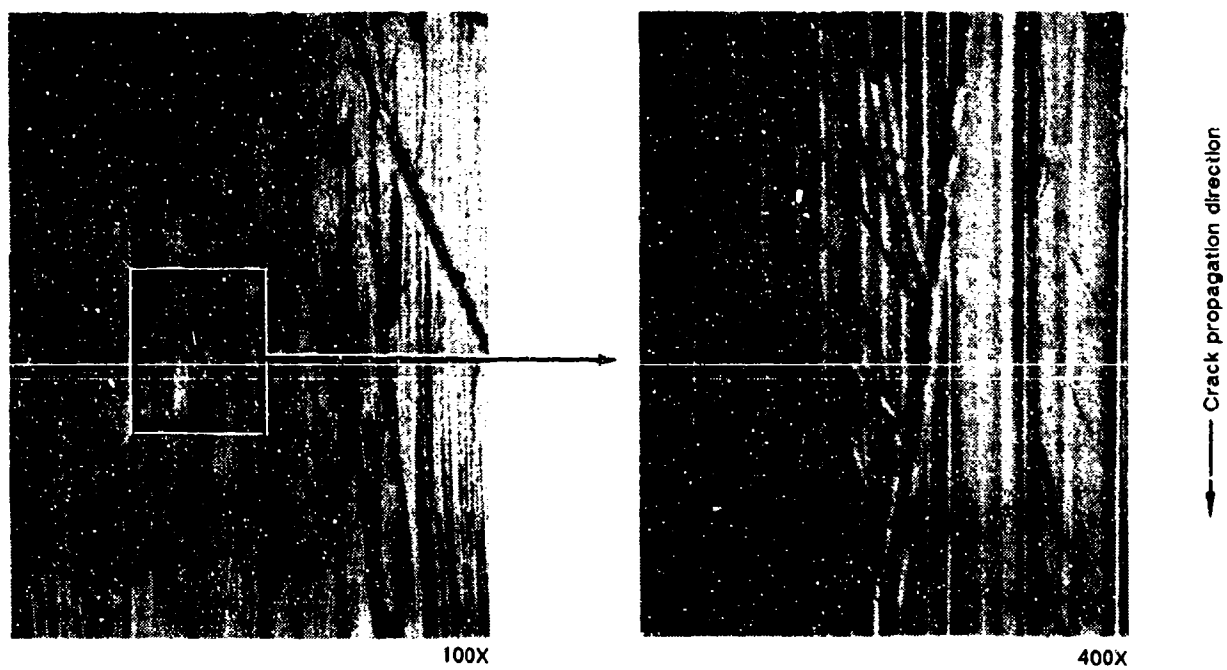


Figure 1-11. Optical Photomicrographs of Intended Fracture Plane Between 0/0 Degree Plies, DCB 21°C (70°F) Specimen



←
Mechanically induced crack direction

Legend:

- M Matrix fracture
- F Fiber matrix separation
- R River markings



Figure 1-12. SEM Fractographs of Mode I Deamination Between 0/0 Degree Plies

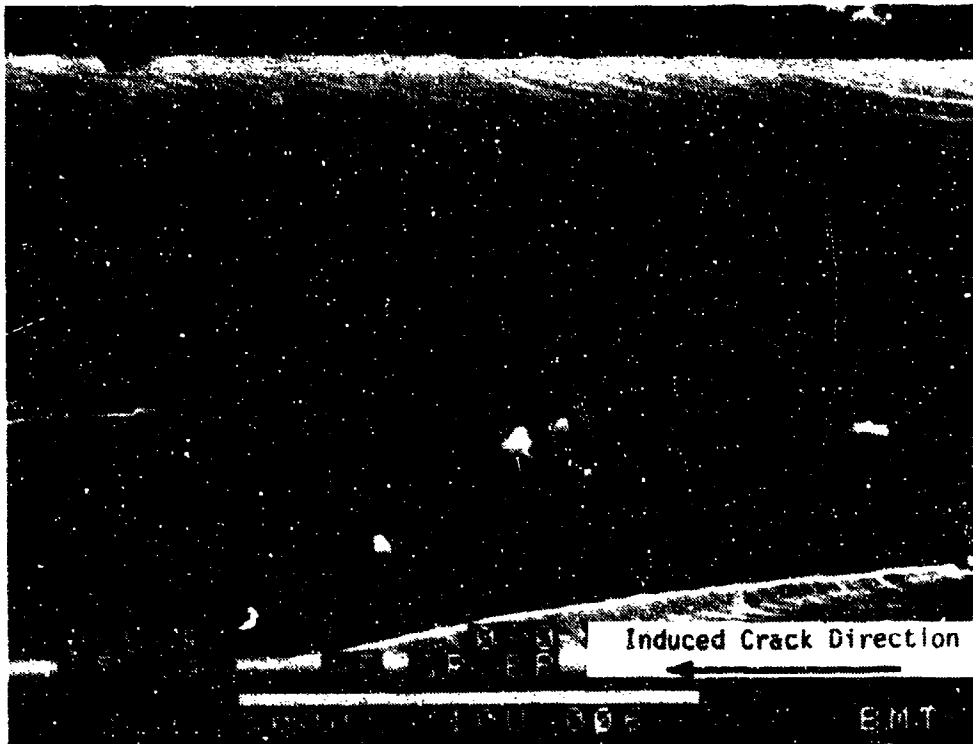


Figure 1-13. Photomicrograph Illustrating Adhesive Fracture Areas of Textured Microflow



300X

Figure 1-14. TEM Image of Resin Microplane With River Marks and Resin Microflow

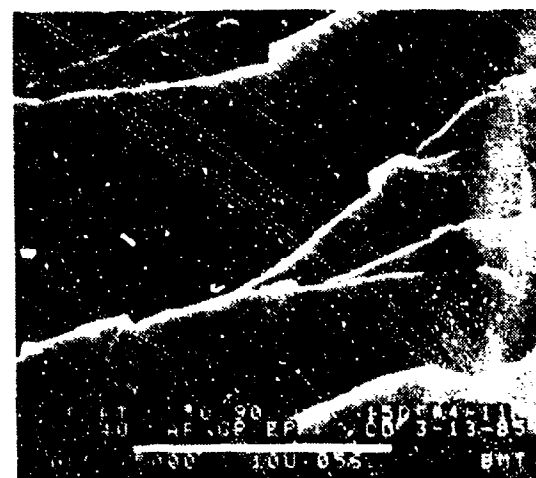
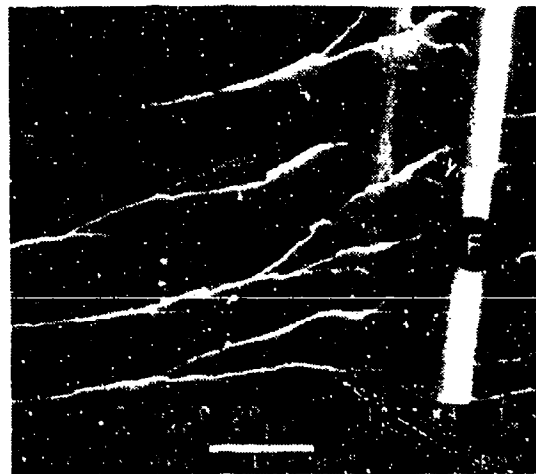
significant variations in the fracture topography can occur at the microscopic scale, depending upon the number of fibers exposed by the fracture and their orientation relative to the direction of microscopic crack growth (Figures 1-15 and 1-16). Cracking often occurs in the resin rich region between plies, particularly between plies of large angular differences (that is, 0° and 90°). Fractures which occur at the interface between plies exhibit relatively large areas of flat-resin fracture with distinct river marks in a fairly consistent microscopic direction. Alternatively, fractures which occur within a ply exhibit variable and often seemingly inconsistent localized microscopic directions of fracture. River marks and microflow are oriented in a wide variety of directions across the fracture surface. Variations in the direction of microscopic crack propagation can often be averaged together to obtain a more accurate estimate of the overall direction of crack propagation (Figure 1-17).

Variations in the direction of microscopic crack growth depend upon several factors. The two most notable factors that must be considered are the formation of localized zones due to fiber intrusion and the magnitude of stress concentration involved in fracture. In the first case, fiber/matrix areas tend to divide the crack tip into numerous microscopic zones, at which the crack must initiate a new crack front at the other side of the fiber to continue growth in this zone. In general, these zones will exhibit differing growth rates and slightly displaced planes of fracture. Consequently, the resultant crack front formed by these regions can be highly irregular, with narrow crack extensions in front of the main crack tip. This crack front profile can produce significant local variations in the crack directions as the extensions grow laterally to meet each other.

The second major condition that can lead to crack direction variations takes place when failure occurs without the formation of any appreciable stress concentration. This is similar to the condition generated with flatwise tension test coupons, in which failure tends to occur at a wide variety of locations within the laminate plane. As with ductile tensile separation rupture in metals, failure occurs when these multiple fracture planes intersect. Such fractures are characterized by the formation of an extensive number of fracture planes throughout the laminate with extreme variations in the direction of crack propagation such that no overall direction of crack propagation exists.

Mode II Shear Delaminations. Failures by interlaminar shear can occur by macroscopic loading sources such as tension, compression, or flexure. The duty of the matrix resin is to transfer the axial loads in each fiber to the adjacent similarly oriented fibers and to adjacent plies that are not oriented in the direction of primary loading. As a result, shear fractures tend to occur within, or adjacent to, plies that are oriented in the direction of maximum loading.

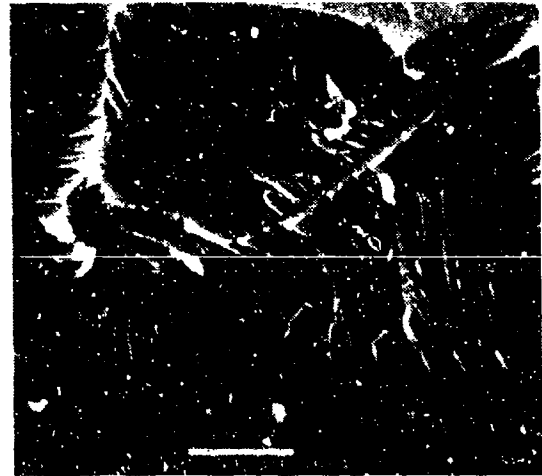
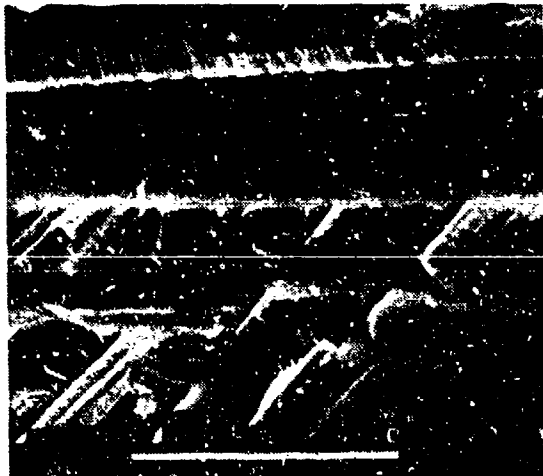
Failures produced under conditions of Mode II shear, while also occurring by brittle tensile separation, exhibit a distinctly different appearance than Mode I tensile failures. Macroscopic examinations reveal a dull and often "milky" appearance when held at oblique angles to a light source, due to opaque light scattering by the rough resin fracture features. Microscopic investigations show a much rougher topography than pure Mode I tension. Optical microscopy reveals a series of translucent, vertical, and parallel resin platelets found in the narrow resin fracture zones between the fibers. As shown in Figure 1-18, the platelets are aligned normal to the



Legend:

- M** Matrix fracture
- F** Fiber matrix separation
- R** River markings
- T** Textured microflow

1-22



Mechanically induced crack direction

Legend:

- M Matrix fracture
- F Fiber matrix separation
- R River markings
- T Textured microflow

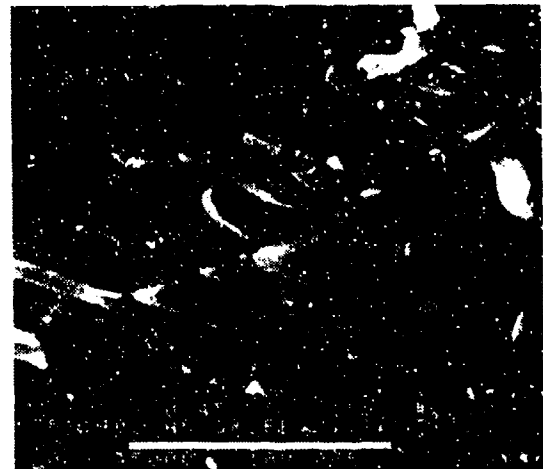
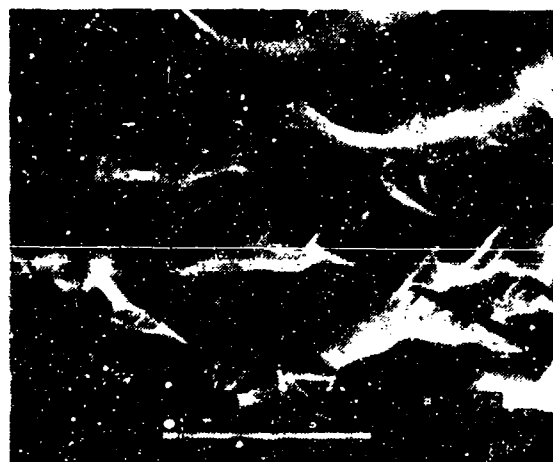
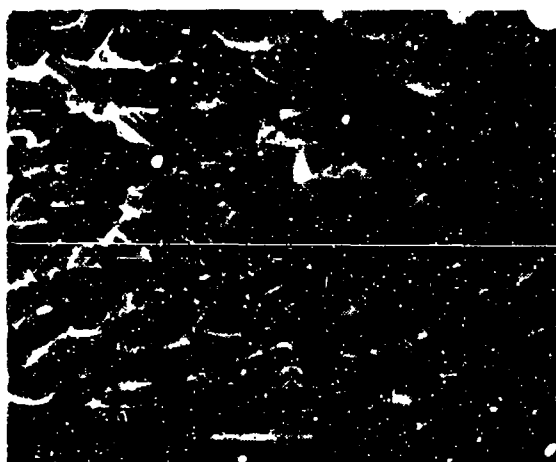


Figure 1-16. SEM Photomicrographs of Mode I Delamination Between 0/+45 Degree Plies



Mechanically induced crack direction

Legend:

- M Matrix fracture
- F Fiber matrix separation
- R River markings
- T Textured microflow



Figure 1-17. SEM Fractographs of Mode I Delamination Between +45/+45 Degree Plies

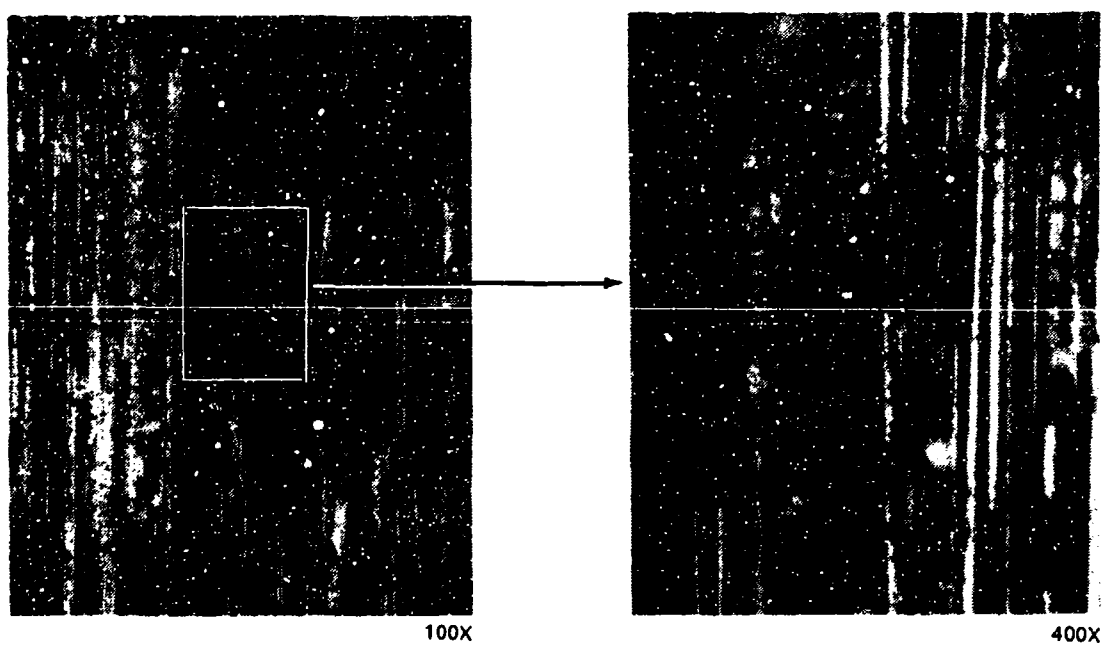


Figure 1-18. Optical Photomicrographs of Intended Fracture Plane Between 0/0 Degree Plies, ENF 21°C (70°F) Specimen

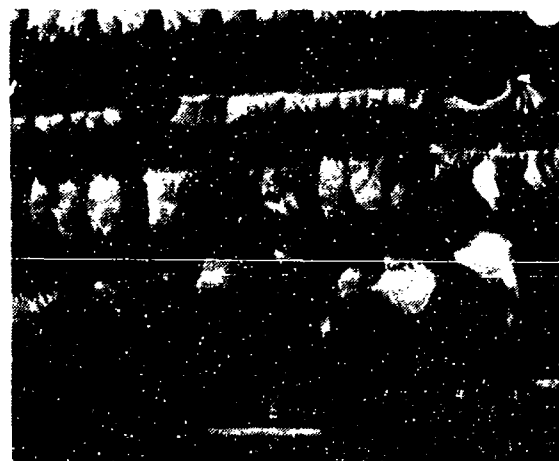
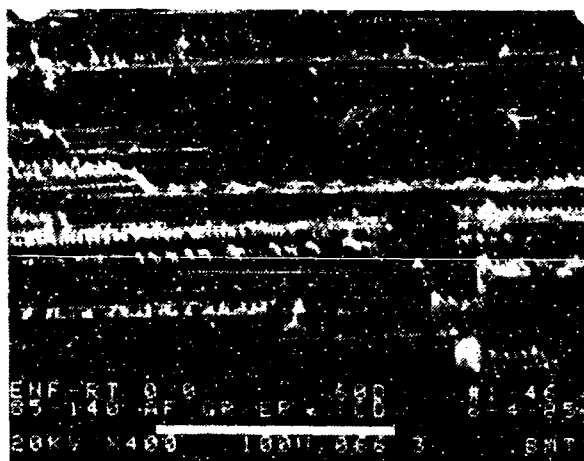
direction of crack propagation. The large flat matrix regions which exhibit river mark branching typical of Mode I delaminations are not present. These distinct differences permit the use of optical analyses to rapidly differentiate between Mode I and Mode II delaminations when either load condition dominates during fracture.

Under detailed SEM examination (Figure 1-19), the rows of curved vertical platelets are found in the cohesive resin fracture regions between fibers. As described by Mohr's circle, during in-plane shear loading the principle tensile stresses are oriented at forty-five degrees to the plane of applied shear, as shown in Figure 1-20. Since matrix fracture occurs in a microscopic plane normal to resolved tensile stress, a series of distinct inclined microcracks (Figure 1-21) are formed ahead of the main crack front. Increased strain or loading causes these small parallel microcracks to grow and coalesce, resulting in the formation of a series of upright curved platelets. Based upon these observations, the directions of applied shear (clockwise or counterclockwise moment) can be determined by examining the direction of platelet tilt. Concave areas are found on the mating fracture surfaces, opposite the these platelets (Figure 1-22). High magnification inspection of the platelets and the concave regions reveals small river marks and microflow, also indicative of resolved tensile separation. Several terms have been used to describe each of these features including lacerations or hackles for the upright platelets and scallops for the concave areas. For this document, the more common use of hackles to describe platelets and scallops to describe depressed concave areas is used.

Separation of hackles can result in two possible relationships (mechanisms A and B) between hackle tilt and the direction of crack propagation, depending on which fracture surface retains the hackle (Figure 1-23). In mechanism A, separation occurs such that the hackles are retained on the side in which the direction of crack propagation coincides with the direction of the local shear component. This condition produces hackles tilted in the direction of crack propagation, and normal to the direction of resolved tension (45 degrees). Conversely, in mechanism B, separation occurs such that hackles are retained on the side in which the direction of crack propagation opposes the direction of the local shear component. In this condition, the tilt of hackles oppose the direction of crack propagation.

Comparisons of the hackle tilt, scallop features, and the mating fracture surfaces by a variety of researchers indicated that the direction of crack growth cannot be established with the same confidence possible for Mode I delaminations. Mode II and mixed mode delaminations generally occur by a combination of the two possible mechanisms such that hackles are found on each mating fracture surface, preventing a definitive conclusion of the crack growth direction. However, the direction of hackle orientation can be used to estimate the direction parallel to which crack growth occurred.

The orientation of fiber reinforcement at, or adjacent to, the delamination plane can have a significant effect on the morphology of both hackles and scallops that must be considered when determining the direction of crack propagation. Surface fibers oriented parallel to the direction of crack growth tend to form orthogonal shaped hackles and scallops (Figure 1-24), whereas fibers intersecting the fracture surface at an angle to the direction of growth tend to form roughly triangular asymmetric hackles and scallops (Figure 1-25). In the first case, a distinct branched



←
Mechanically induced crack direction

Legend:

- F Fiber-matrix separation
- H Hackles
- R River markings
- T Textured microflow

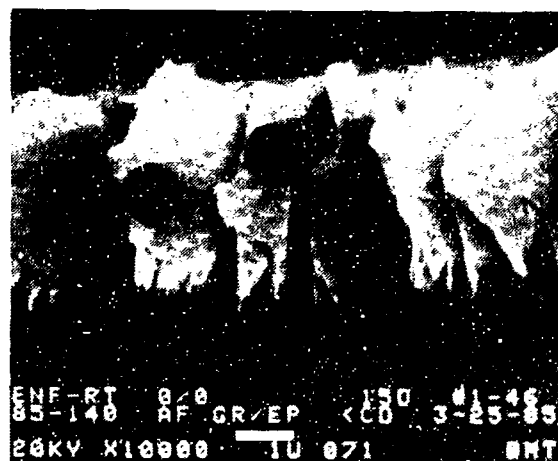


Figure 1-19. SEM Photomicrographs of Mode II Delamination Between 0/0 Degree Plies

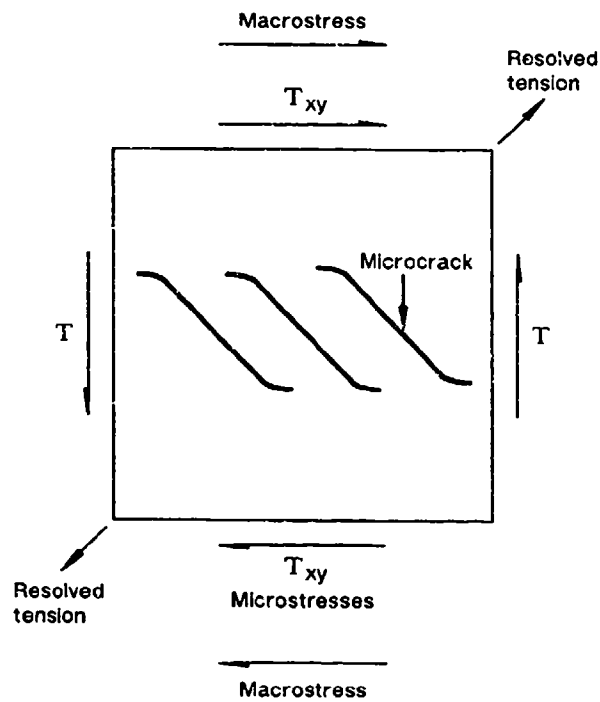
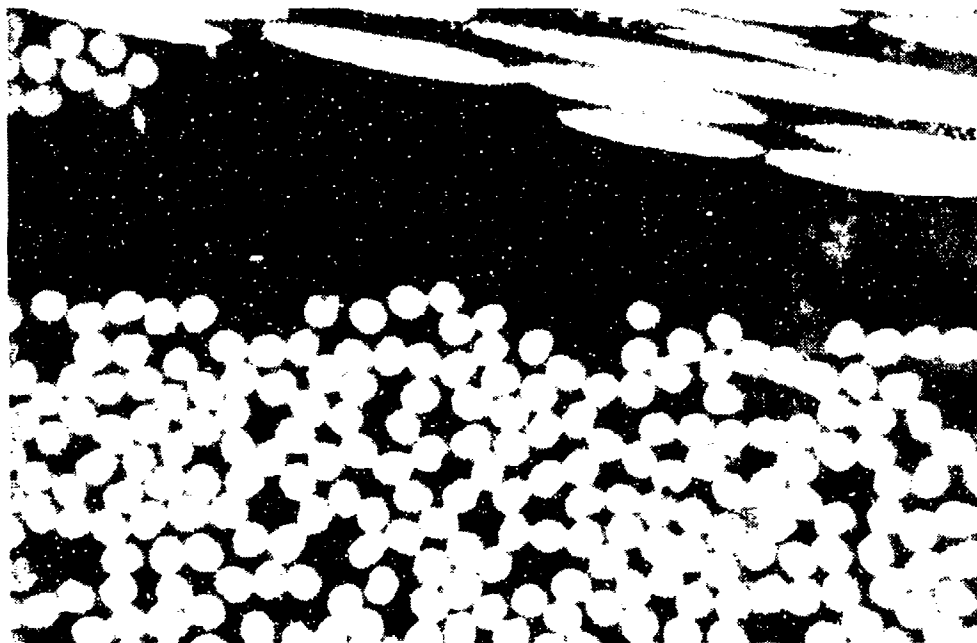


Figure 1-20. Free Body Diagram of Resolved Tensile Stresses and Inclined Microcracks



775X

(Copyright © ASTM reprinted with permission.)

Figure 1-21. Microstructure of Cracks Found in Short Beam Shear Specimen Tested at 132°C (270 °F)

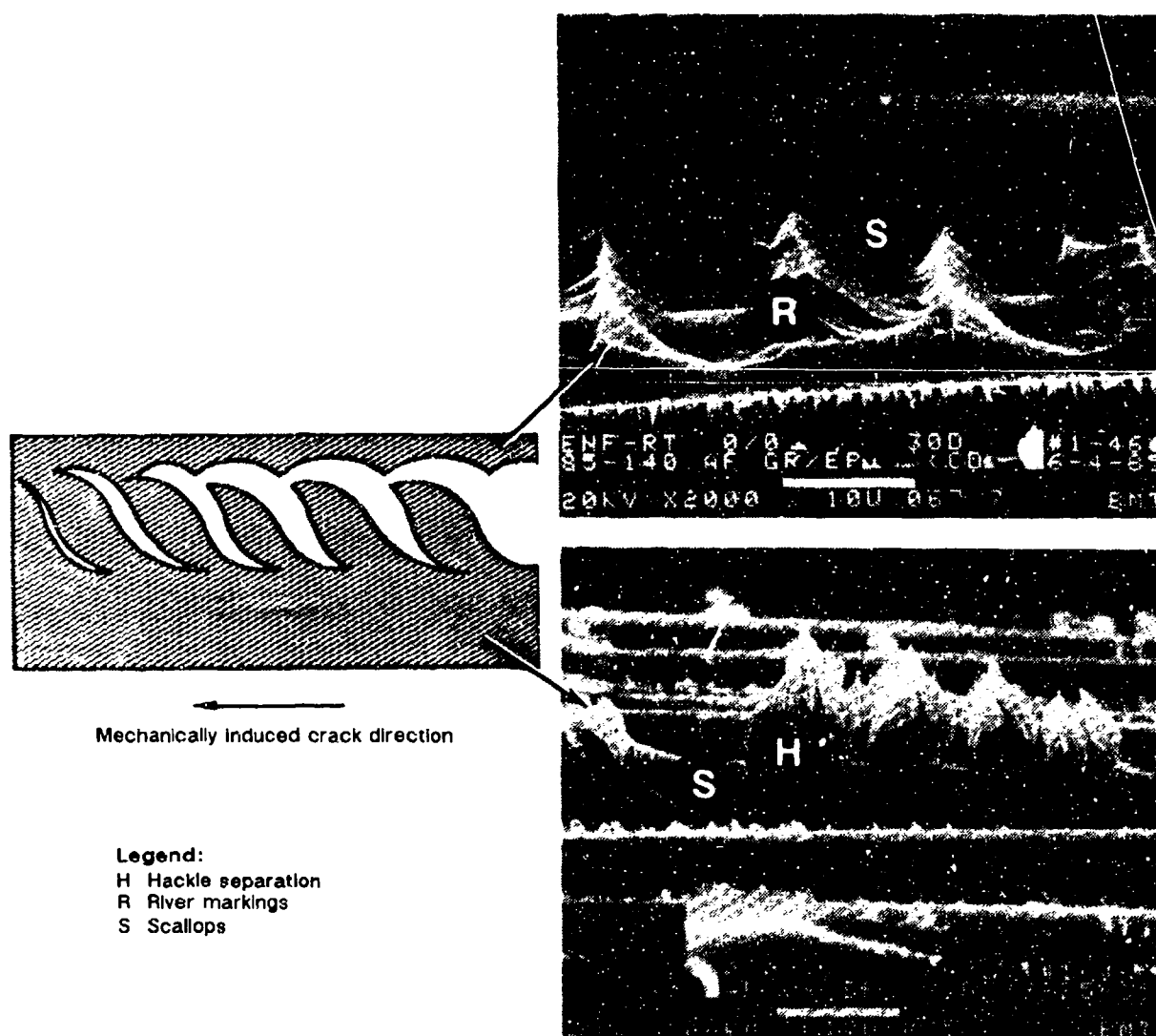
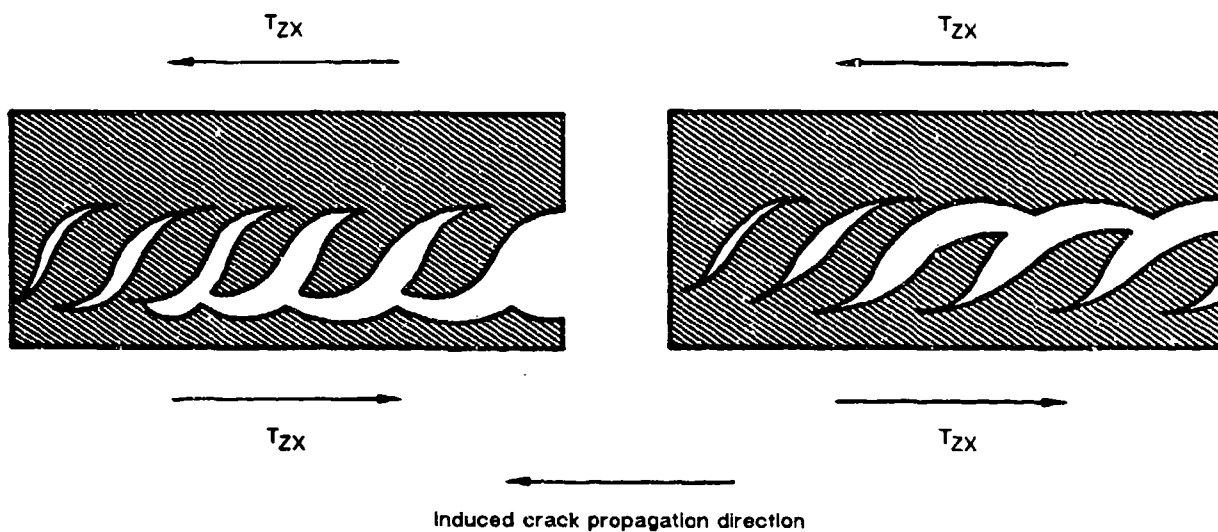


Figure 1-22. Scalloped Resin Fracture Areas and Their Development



Mechanism A
Hackle formation coincident with
the direction of crack propagation

Mechanism B
Formation of hackles opposite
to the direction of crack propagation

Figure 1-23. Possible Hackle Separation Mechanisms



Figure 1-24. Orthogonally Shaped Symmetrical Hackles

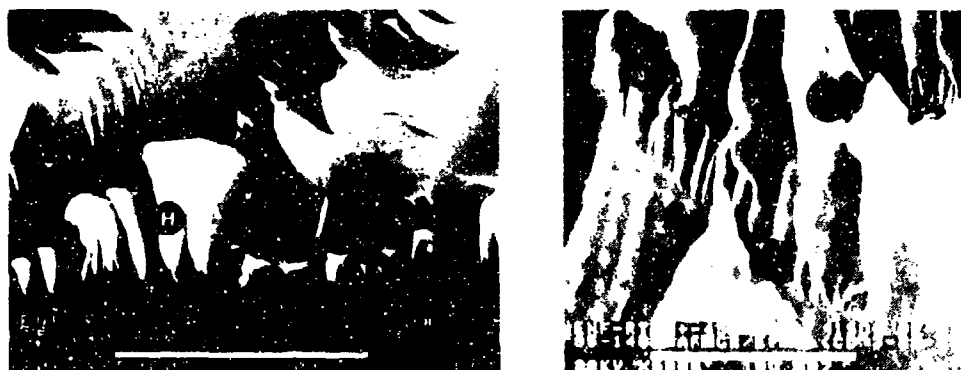


Figure 1-25. Triangular Asymmetric Hackles, With River Marks and Fiber-Matrix Separation

morphology generally exists on both sides of the hackles and scallops where they intersect adjoining areas of fiber/matrix separation. Since this symmetry and the orthogonal shape of these features correspond to propagation parallel to the direction of exposed fibers, these features provide a relatively rapid and easy means of identifying the direction parallel to which crack growth occurred. In the second case, when the asymmetric features are identified, the tilt of the triangular hackles is predominantly parallel to the direction of crack propagation.

Mixed Mode Delaminations. Interlaminar mixed mode delaminations commonly fail in a mixed mode loading condition, in which neither pure tension nor shear are operative. Failures due to complex loading such as flexure and compression buckling tend to exhibit delamination fracture morphologies that appear somewhat different to those found for the pure loading conditions presented in the above paragraphs. Since resin fracture separation occurs by resolved tensile forces in both pure shear and tension, so does fracture due to a mixed load state. The extent to which each of the predominant features exist (flat regions with river marks or vertical hackles) depends upon the ratio of Mode I to Mode II macroscopic stress. Therefore, delaminations with a predominance of Mode I tension mainly exhibit river marks and flat fracture topographies, with a tendency toward a slight tilt in each of the resin fracture microplanes, indicative of the slight rotation of the resolved tensile component (Figure 1-26). For these types of fractures, river marks and resin microflow are still useful for defining the localized crack growth direction and for use in crack mapping. As the percentage of Mode II increases, the tilt of these resin microplanes also increases relative to the rotation of the resolved tensile component. At percentages of Mode II above approximately 30%, these platelets take on an appearance of hackles, where there is pronounced separation between each hackle, and scallops present on the mating surface. Figure 1-27 presents the fracture morphology at approximately 43% Mode II shear and 57% Mode I tension. This fracture surface was generated with a Mixed Mode Flexural (MMF) specimen. Note the formation of the hackles, although they are not as vertical or upright as those found for pure shear fracture specimens. As indicated in the above paragraph on pure shear, hackles can be used to define the direction parallel to crack propagation. Precisely what percentage of Mode II or which fractographic features can be used to define crack growth directions have not been determined. Further studies on controlled crack growth specimens across the spectrum of mixed mode must be performed to gain a firm understanding of the validity of determining crack growth directions in a mixed mode loading state.

1.1.2.2 Translaminar

A significant portion of composite post-failure analyses involve translaminar fractures, usually in combination with delaminations located on either side of the through-thickness fracture. Due to the laminated nature of composites, combined with the excellent tensile strength of the fiber reinforcements, translaminar compression fractures tend to occur more often than translaminar tension fractures. Tension fractures exhibit a lesser amount of delamination and tend to be relatively less damaging to the fracture surfaces and surrounding structure. Compression dominated fractures commonly fail as a result of localized buckling instability with

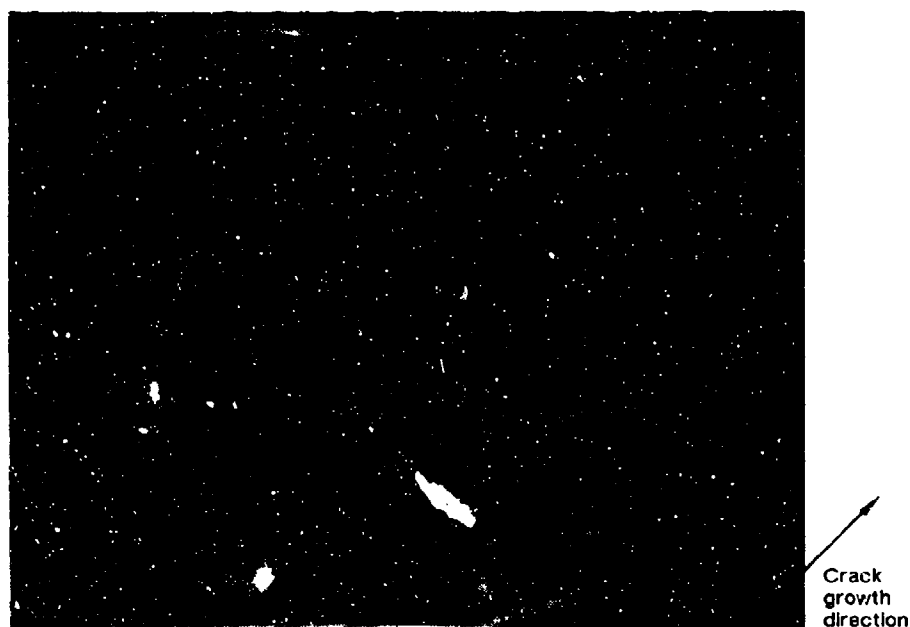


Figure 1-26. Interlaminar Mixed Mode (Tension and Shear) Fracture Morphology



Figure 1-27. Interlaminar Mixed Mode Flexural (MMF, Tension and Shear) Specimen Fracture Morphology

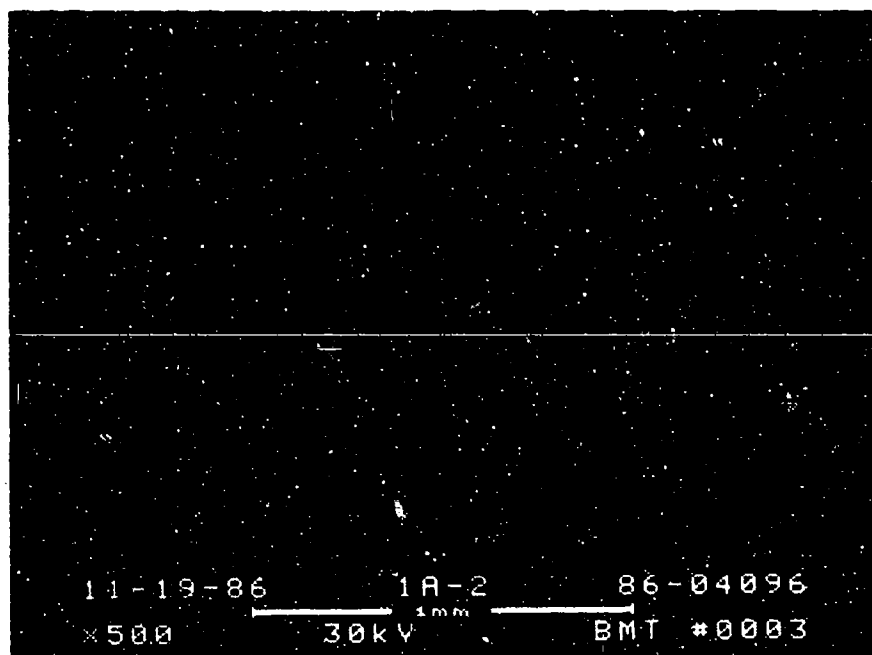
extensive delaminations and post-failure damage to the fracture surfaces. Often the compression fracture surfaces are pushed into each other, wedging open the delaminations even further.

Fractographic analyses of translaminar fractures are generally complicated since the dominating feature is broken fibers. This generally requires the use of the SEM microscope, which is tedious and time consuming for the accurate determination of the fracture modes and crack growth directions. The optical microscope does not have the depth of focus to evaluate these extremely rough surfaces. Crack mapping can be performed by first creating a photographic montage of the fracture region at low magnifications, followed by drawing arrows delineating crack growth directions on the montage during higher magnification inspections of the fiber ends.

The following paragraphs provide insight into the use of the SEM in identifying the salient features and relating them to determination of the failure sequence. Where applicable, macroscopic methods are presented which can be used to select smaller localized areas for investigations by the SEM.

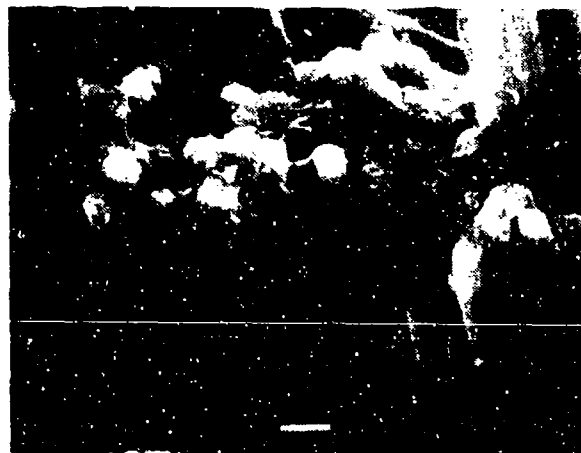
Translaminar Tension Fractures. Macroscopically, translaminar tension fractures exhibit an extremely rough topography, with large amounts of fibers protruding out of the major fracture plane, as presented in Figure 1-28. The general appearance depends largely upon the strength of the fiber matrix bond. Comparatively, strongly bonded laminates tend to be more planar and the fibers tend to fail in groups or bundles, while the lower bond strength materials are more complex and fibrous. Macroscopic inspection of plies that are oriented parallel to the principal tensile direction often exhibit radial lines, or ridges, that radiate from an origin source and can be used to more rapidly determine the overall direction of crack propagation (Figure 1-28). Macroscopic inspections of fracture surfaces of plies that are oriented at an angle to the loading direction and have failed by a combination of interlaminar and translaminar shear are extremely complicated and do not usually reveal any gross overall feature that can be used to determine fracture direction. This should be kept in mind when examining translaminar fractures of laminates that have multiple ply orientations.

Fiber end fracture, fiber pullout, and matrix fracture are the characteristic fractographic features of translaminar tension failures. Usually, little or no delamination is evident at the fracture surface, although secondary shear cracks running parallel to the fiber axis can often be found intersecting the main fracture surface. Brittle tensile failure of individual fibers is the primary operative failure mechanism, with shear fracture of the surrounding matrix considered as secondary. As stated, fibers fracture in groups (bundles) in high strength laminates, where the fibers in each bundle have a relatively flat, common fracture plane (Figure 1-29). Figure 1-30 presents the typical radial morphology found on the broken fiber ends. This radial pattern is analogous to the chevron features of tension fractures in metals with bar or rod forms. The faint lines radiate from the point of fiber fracture initiation and thus indicate the direction of crack propagation for each individual fiber. Consistent with brittle failures, the fiber origins are primarily located at flaws or notches in the rough surfaces, although some initiate at internal flaws such as voids.



500X

*Figure 1-28. Macroscopic View of a Translaminar Tension Fracture
From a Unidirectional Laminate*



Note: Fracture is primarily fiber dominated with some adjacent matrix fracture.

Figure 1-29. Translaminar Fracture Morphology

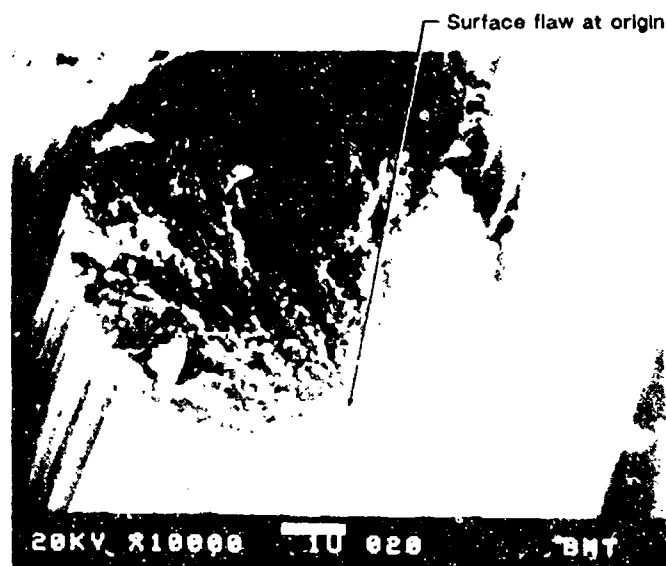


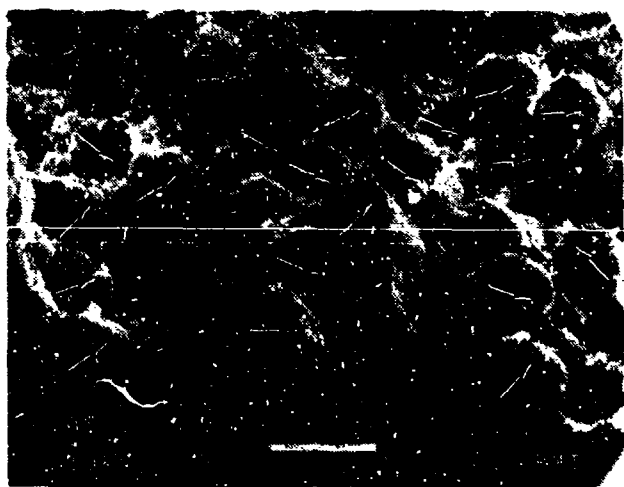
Figure 1-30. Typical Tensile Fiber Fracture Characteristics

Tension failure does not usually progress by a well defined crack front. Due to flaw sensitivity, the fracture process involves a series of zones in which all the fiber breaks within each zone originate at a single fiber. Thus, the crack front actually consists of numerous isolated fracture zones (at different planes) that coalesce and propagate in the overall growth direction. This phenomena produces the distinct fracture zones commonly referred to as fiber bundles. Fiber ends tend to fracture in a variety of directions, although they are often noticeably biased in a single overall direction. Through extensive SEM mapping of the fiber ends (Figure 1-31) the macroscopic growth direction can be determined. Extreme caution must be exercised in the evaluation of isolated fibers that protrude from the main surface. To increase accuracy, many areas of crack growth should be evaluated during the crack mapping process; particularly bundles which fracture on a plane relatively close to the overall fracture plane.

Translaminar Compression Fractures. Macroscopically, fractures produced under uniaxial compression exhibit gross buckling, extensive delamination, and over-running of the delamination planes (Figure 1-32). An end-on view of the broken fiber ends reveals a distinct, flat fracture surface with extensive post fracture damage. This condition of flat fracture is particularly evident for plies that are oriented parallel to the axial compression loading, as shown in Figure 1-33. Often, obliteration of the fracture surface details occurs due to relative post-failure motion between the fractured surfaces in contact (Figure 1-34). The surface is much flatter than the translaminar tension fractures and is virtually devoid of pulled-out fibers. Fiber buckling, fiber-end fracture, resin shear fracture, and post-fracture damage are the primary characteristic fractographic features of translaminar compression fractures.

Compression microbuckling is the primary operative failure mechanism for laminates which do not have extensive lateral through-thickness stability. This mechanism involves localized microscopic buckling of the individual fibers at a point in which a maximum lateral instability exists. Under compressive microbuckling, kinking of the fiber causes at least two fracture locations (Figure 1-35), with each fracture separated by 5 to 10 fiber diameters. Short sections of fibers with this length can often be seen on the fracture surface. Figure 1-36 illustrates the typical flexural fracture morphology found on the fiber ends. The portion of the fiber end which exhibits a radial morphology is due to tensile separation, while the smooth, or ratcheted topography represents the compressive portion of fiber fracture. The distinct line separating these portions on the fiber end is the neutral axis line. For each individual fiber, the direction of flexure and failure occurs normal to the neutral axis line. For a given fiber, the compression and tension portions are reversed when comparing the two breaks. Therefore, a singular crack direction cannot be determined, although the individual fiber fracture propagates perpendicularly to the neutral axes lines.

The neutral axis lines are commonly found parallel to one another in a given region, indicating that microbuckling occurs on a local scale in a concerted manner and in a unified direction, as presented in Figure 1-37. Preliminary controlled crack growth studies have shown that the neutral axis lines are often biased at an angle parallel to the direction of induced crack propagation. This indicates that flexural fiber collapse, and thus crack propagation on a



→
OVERALL CRACK
PROPAGATION
DIRECTION

250X.

Figure 1-31. SEM Photomicrograph Showing Direction of Crack Propagation

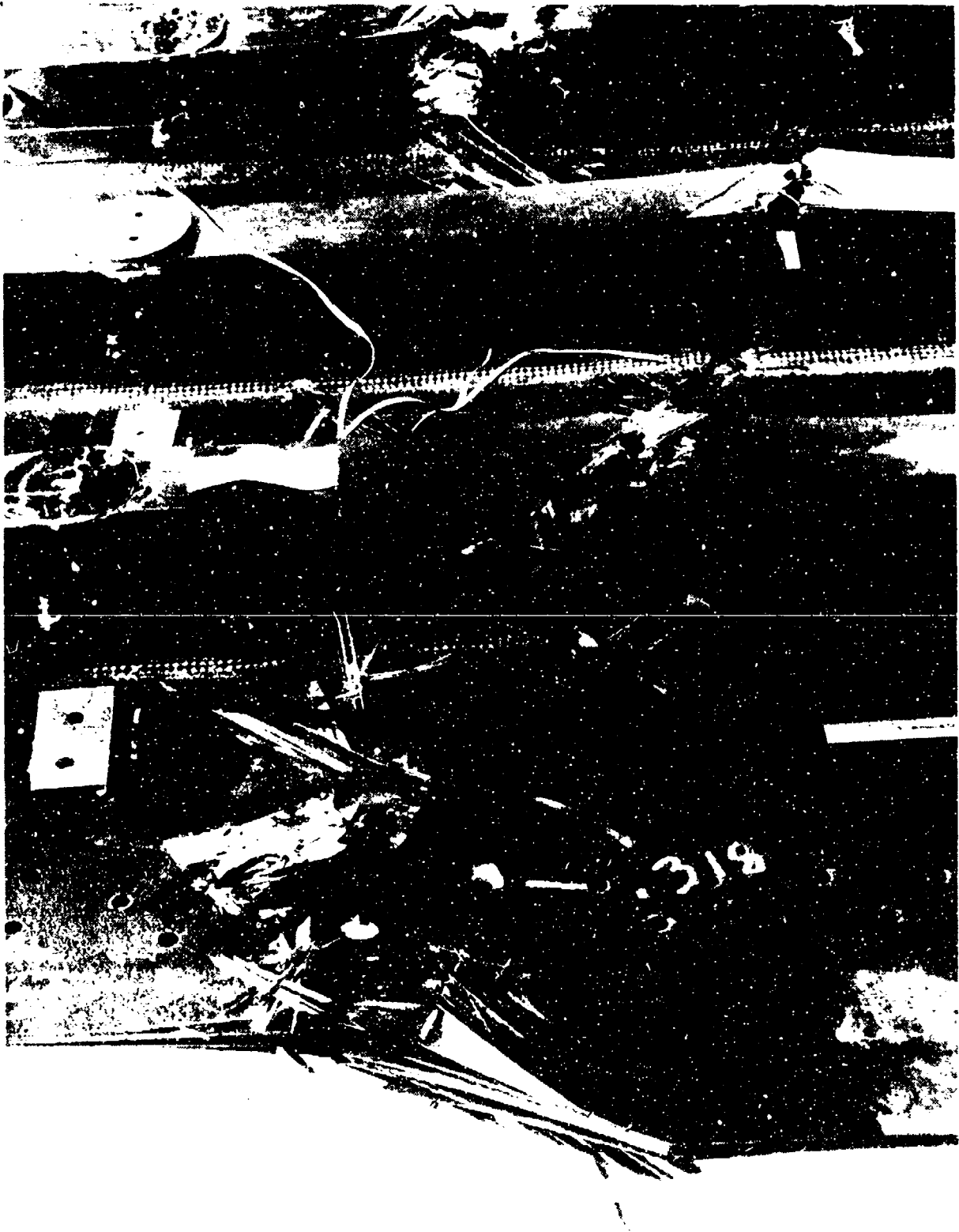


Figure 1-32. Compression Buckling Failure Damage of Stringer Stiffened Laminate



Figure 1-33. End-View of Translaminar Compression Fracture

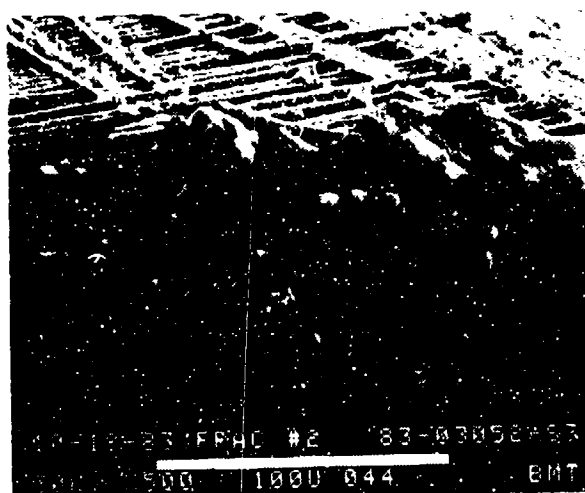
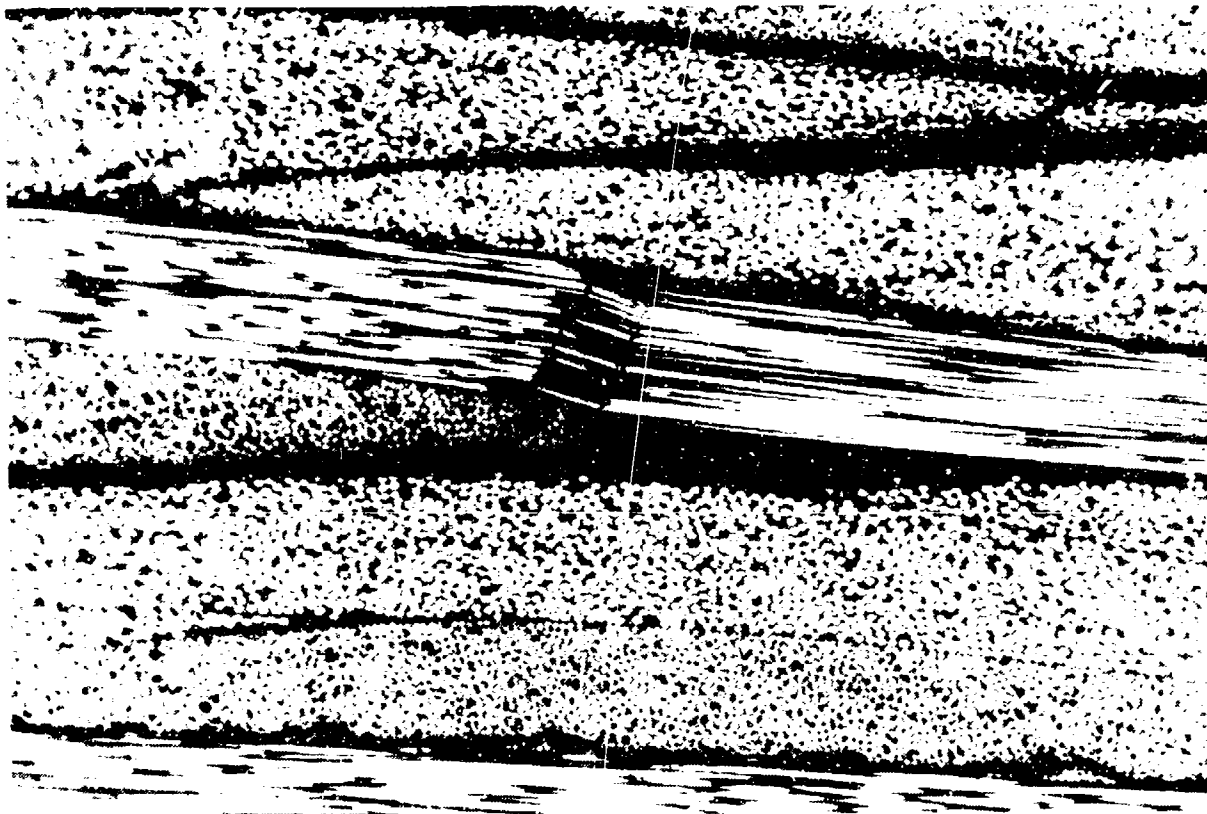


Figure 1-34. SEM Micrograph of Compression-Generated Fracture Surface Showing Severe Fracture Surface Damage



400X

Figure 1-35. Cross Section of Compressively Loaded Laminate With Microbuckling or Kinking of the Fiber Bundles Oriented Parallel to the Axial Compressive Load



Figure 1-36. Typical Flexural Fracture Morphology Found on the Fiber Ends From a Compression Failure

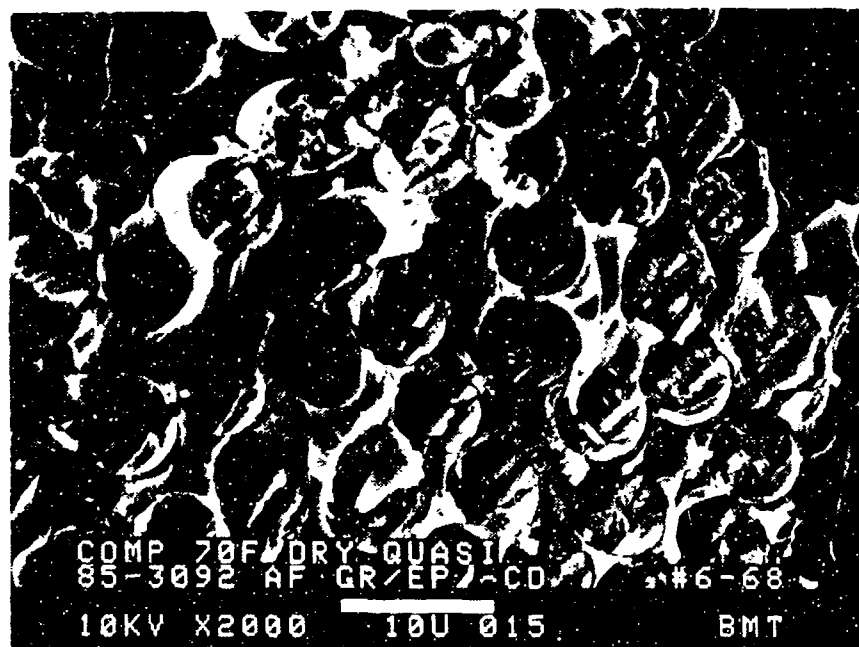


Figure 1-37. Fiber End Fracture Morphology From Compression Buckling Failure

microscopic scale, often occurs transverse to the gross overall crack direction; therefore, neutral axis lines cannot be used to determine the direction of crack propagation.

Laminates which have superior constraint in the through-thickness direction or excellent fiber/matrix interfacial strength are not as subject to localized delaminations or microbuckling of the plies. In this case, the fibers fracture on a microscale due to shear, with individual fiber ends exhibiting a slant type fracture, as shown in Figure 1-38.

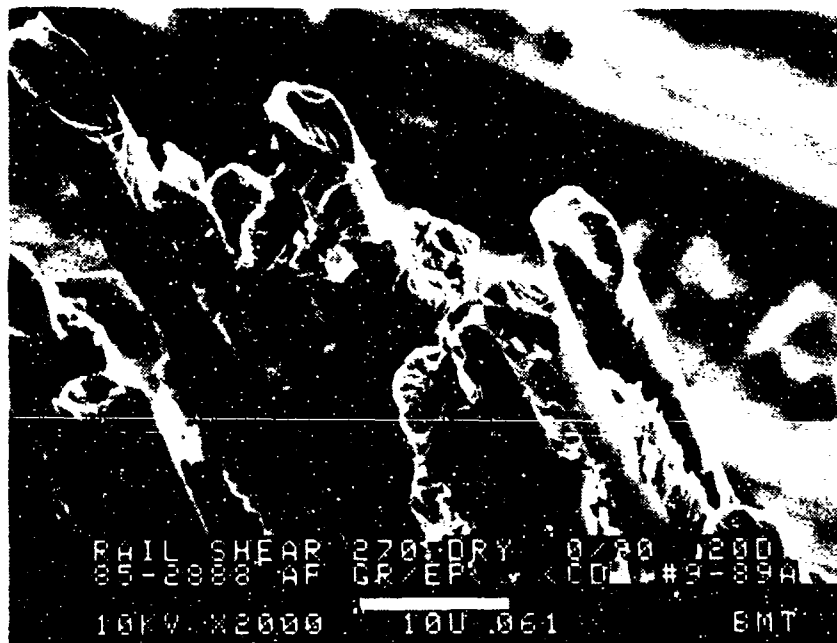
1.1.3 Interlaminar Fracture Mapping

Crack mapping has profound significance upon the success of determining the origin locations and sequence of failure. Using microscopic techniques presented in the following paragraphs, the localized direction of crack propagation can be determined. The recommended technique of crack mapping uses the lowest magnification capable of performing the job. This recommendation is made because one of the fundamental problems in detailed microscopy of large fractures is that there is an extremely limited perspective on how the area being examined relates to the part as a whole. The situation is similar to the old adage, "one can't see the forest for the trees." With a limited perspective, it is often possible to improperly characterize the direction, mode, or load state at fracture. By emphasizing the use of lower magnifications for early investigations, the FALN imposes a sense of perspective on the value of later, high magnification inspections.

The use of optical microscopy for crack mapping interlaminar fracture surfaces has been proven to provide the most information in a given time frame and therefore the most accurate and unbiased determination of the directions of crack propagation. Optical microscopy allows direct observation of relatively large specimens in a short period, eliminating the need for specimen preparation or specimen selection required for SEM analyses. SEM analysis is basically slow and cumbersome due to the need to constantly refocus during perusal of the fracture surface. As a result, the number of crack growth determinations per unit time is significantly reduced relative to optical microscopy, therefore greatly reducing the overall accuracy of the crack mapping process, particularly for ill-defined crack growth regions. Through direct scanning of the delamination surfaces with the optical microscope, features such as river marks and hackle formation can be resolved. These features, as described above, can be used to determine the localized crack propagation direction and allow the investigator to work back to the origin region. A few of the basic methods of optical crack mapping are discussed in the following paragraphs, however the photomicrographs presented were taken with the SEM, primarily due to its ability to document fracture features at higher magnifications better than the optical microscope.

The basic steps to crack mapping an interlaminar fracture surface area:

1. Sectioning open the fracture surfaces to minimize artifacts.
2. Reducing specimen size to fit on the optical microscope stage.
3. Producing a full size copy of the fracture surface.
4. Cleaning the fracture surfaces if necessary.



270°F, dry

←
Crack direction

Figure 1-38. Slant or Shear-Type Fracture From Compression-Induced Translaminar Failure

5. Performing crack growth determinations with the optical microscope.
6. Determining overall crack growth directions by averaging microscopic data.

Cutting open the delamination surfaces usually involves severing the laminate at the crack tip of the delamination as revealed by ultrasonic inspection. Successive cuts should be made until the laminate separates into two pieces. If localized fiber bridging occurs, they can be severed by cutting with a scissors. Effort should be made to prevent any delamination growth which often cannot be differentiated from cracking caused during the fracture event. Further cutting is often required to downsize the specimen to fit on the optical microscope stage (usually about 10 cm by 10 cm for an upright bench microscope).

For a worksheet by which to document the crack growth directions, a full size replica of the fracture surface can be made with a copy machine set in the lightest reproduction mode. This provides a worksheet which is superior to hand-drawn sketches (inaccurate) or photographs (expensive and time consuming).

A quick optical examination of the fracture surface can provide information regarding whether to clean the fracture surface prior to detailed crack mapping. Cleaning should not be performed if evidence of contamination is found.

Performance of the actual crack mapping process involves the interpretation of the identifiable microscopic fracture surface features as related to localized crack growth directions. Most optical microscope crack mapping requires magnifications in the range of 200X to 800X. This magnification is required to resolve the fine river marks and hackle features between the closely spaced fibers. Resin rich fracture areas such as those found between plies (or between tows for woven laminates) can be fairly easily mapped toward the lower end of this magnification range due to the larger features present. Caution should be taken when mapping these isolated resin rich regions, with direct substantiation by examination of the surrounding regions which have more fiber reinforcements. Since the fracture process actually involves a continual repetition of crack initiation at the fiber/matrix interface and subsequent crack growth in the matrix toward the next fiber, the fracture features can often be overwhelming and confusing. On a microscopic scale, the fracture details such as river marks and resin microflow are often found oriented in a variety of directions, even for delaminations with well defined crack fronts and macroscopic growth directions (Figure 1-39). As a result, accuracy during crack mapping is maximized by determining as many localized crack growth directions in a given area as economically feasible. This often requires mapping as many as 10 to 20 locations per square inch. This can be done by scanning the surface by stage translation and focussing at the same time. Once an "average" direction of the microscopic features has been obtained using the methods of determination of crack propagation described above, an arrow denoting this direction should be placed on the photocopy. For tension dominated growth regions, single-headed arrows and for shear dominated growth regions, double-headed arrows should be drawn on the map. By creating these maps for the entire fracture surface, the overall average microscopic crack growth directions, and possibly the origin location, can be determined.

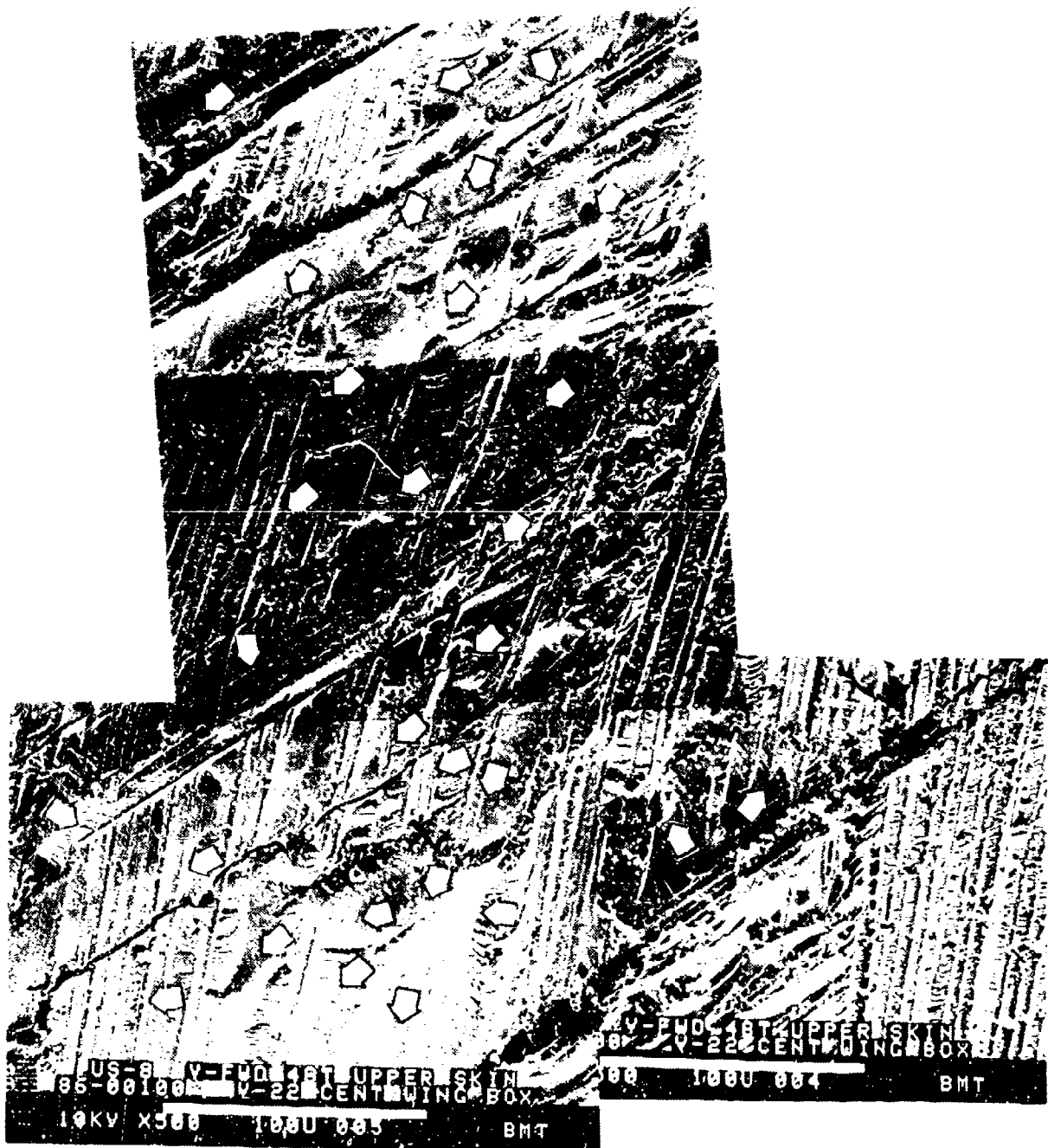


Figure 1-39. SEM Photographic Montage Showing Crack Propagation Direction Mapping

1.1.4 Crack Origin Analysis

When a crack origin has been determined, the primary emphasis is placed upon identifying the cause of crack initiation. Due to the complex nature of the fiber reinforced laminate, crack origins are often much less defined than found in metal fractures. While most metal fractures can be related to a very specific site of initiation, composites tend to exhibit origins that encompass a fairly large region. Sometimes this region can be as large as several inches in diameter, dependent upon the size of the part, the relative strain at failure, and other contributory conditions such as contamination and local part geometry. As a basic rule of thumb, fractures that have a large, relatively ill-defined origin with significant post-failure damage at the origin are exemplary of failures that occurred at a load close to the maximum strains for the entire part. This usually indicates a more desirable condition than failures exhibiting a relatively small origin which is easily defined on a microscopic scale. These origin types are often a result of localized defect conditions such that the strength at failure is low or the strains are locally magnified such as at a notch.

Analysis of the origin region should concentrate on determining if anomalous conditions existed which may have either caused or contributed to the failure event. A wide variety of defect conditions or design details should be considered when performing the analysis of the origin. Figure 1-40 presents a checklist of the possible defect conditions which can be considered. Information obtained regarding any of these defect conditions or fracture details such as local geometry, ply interfaces which delaminated, load conditions in the region (tension, shear, compression, etc) should all be evaluated for criticality. Often stress analysis is required to accurately assess the overall criticality of the specific information obtained in the origin region. Special care should be taken to not "brush off" seemingly small anomalous conditions since synergistic or accumulative situations can occur which may be immediately obvious to the investigator.

1.1.5 Environmental Effects

Conditions of environmental extremes have been shown to significantly reduce the overall strength of composites. Therefore, the investigator should be aware of the typical fracture features that can be identified when failure occurs under conditions of temperature and absorbed moisture. Environmental extremes at fracture tend to exhibit a more dramatic difference in the fracture features for translaminal fractures than delaminations, particularly on a macroscopic scale. Although small differences in environmental conditions cannot be readily identified in carbon/epoxy systems, large differences can be readily identified. Studies of fractures produced over a wide range of environmental conditions revealed that the general fractographic features that are used to identify the mode of fracture (tension, shear, etc) and identify the direction of crack propagation are not significantly affected.

1.1.5.1 Translaminal Fractures

Typical translaminal fractures generated at room temperature exhibit combined features of good fiber-matrix adhesion, limited fiber pullout, and a tendency of the fibers to fail in bundles.

DAMAGE DEFECT CHECKLIST
<ul style="list-style-type: none"> • FASTENER HOLE DAMAGE • BACK SURFACE DELAMINATION • NOTCHED BORE • EXCESSIVE COUNTERSINK • MANUFACTURING DEFECTS <ul style="list-style-type: none"> • SAW CUT • FOREIGN OBJECT INCLUSION • CONTAMINATION • VOIDS • PART DIMENSION AND TOLERANCE • MATERIAL STRUCTURE DISCONTINUITY <ul style="list-style-type: none"> — PLY DROPOFF — LAP/GAP — PLY ORIENTATION/STACKING SEQUENCE • INSERVICE/MAINTENANCE DAMAGE <ul style="list-style-type: none"> • IMPACT • ENVIRONMENTAL EFFECTS <ul style="list-style-type: none"> — CHEMICAL ATTACK — TEMPERATURE EXTREMES • REPAIR DAMAGE • OTHER

Figure 1-40. Damage Defect Checklist

However, translaminar fractures generated under hot/wet environmental conditions approaching the glass transition temperature exhibit greater levels of fiber pullout, combined with significantly less resin adhering to the fiber surface. Additionally, similar fractures generated under dry conditions at -65°F reveal very limited amounts of fiber pullout, with extensive amounts of residual resin on the fiber surface. In general, these observations are in agreement with published literature and illustrate the significant reduction in matrix shear strength or fiber-to-matrix interfacial strength that tends to occur under elevated-temperature and high absorbed moisture conditions. Figure 1-41 illustrates the tendency toward increased fiber/matrix separation and individual fiber pullout in wet specimens experiencing an increase in temperature.

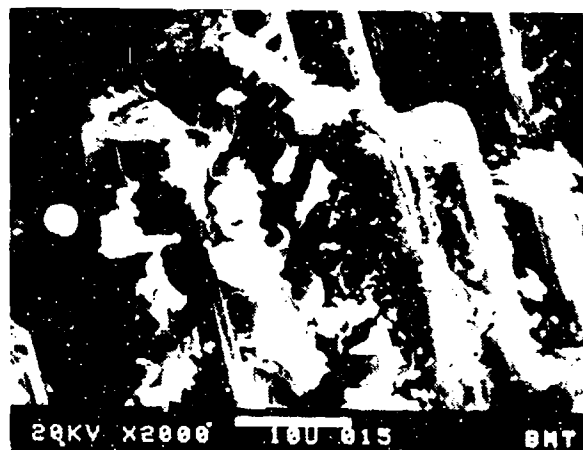
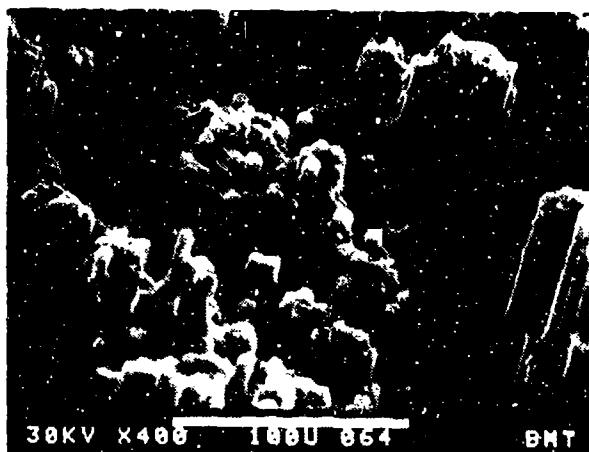
1.1.5.2 Delamination Fractures

For delamination fractures, similar tendencies are evident for conditions of increasing amounts of absorbed moisture and temperature. Fractures in 177°C (350°F) cure epoxy systems which occur at temperatures below approximately 90°C (194°F) are very similar in appearance to the room temperature fractures. However, above this temperature range, increased fiber/matrix separation is evident and the fracture plane tends to occur within, or adjacent to, densely packed fiber regions within the lamina, resulting in a fiber-dominated fracture appearance, with small, localized regions of resin fracture (Figures 1-42 and 1-43).

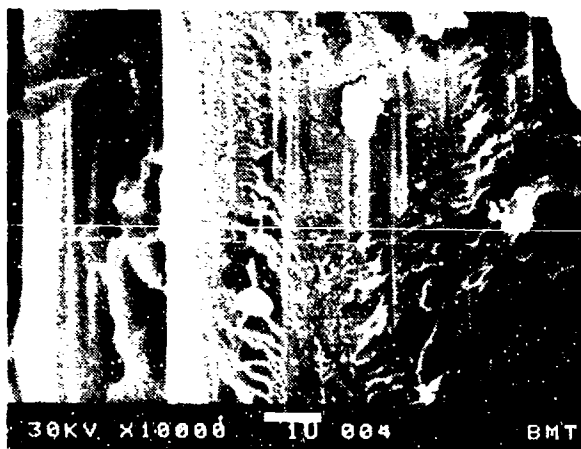
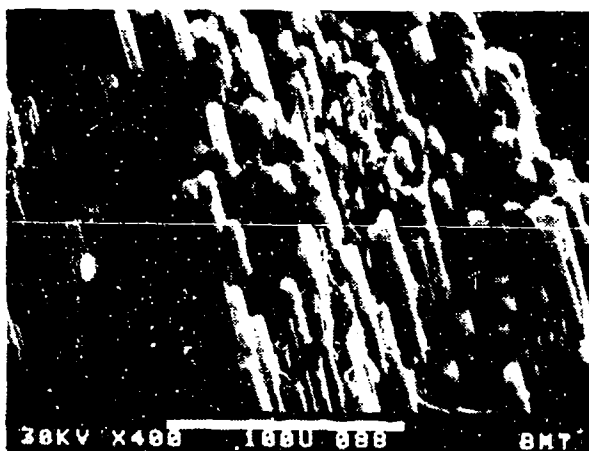
1.1.6 Summary of Composite Materials Fractography

The information presented in the following paragraphs provides the reader with a short summary of the current understanding of fractography of composite materials. The items included are:

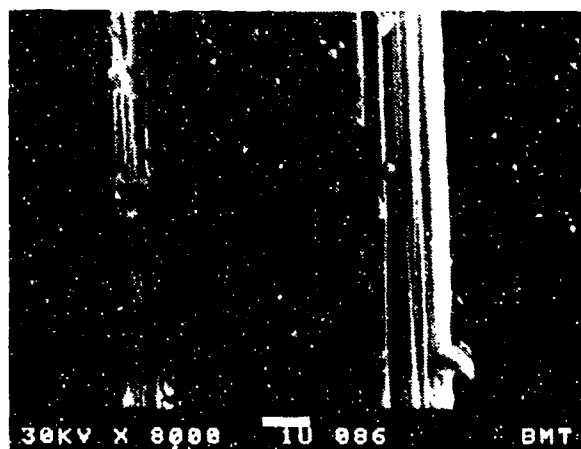
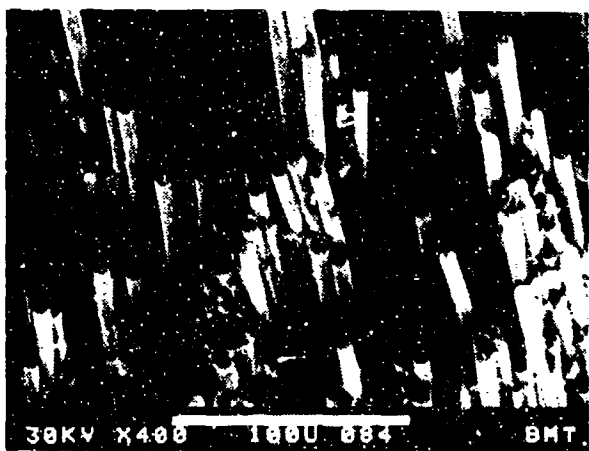
1. Crack propagation in brittle resin based composites.
2. Crack propagation in ductile resin based composites.
3. Determination of fracture modes (tension, shear, compression).
4. Variables affecting fracture appearance.
 - Mixed modes
 - Temperature and absorbed moisture
 - Processing defects
 - Chemical release agents
 - Voids/porosity
 - Material forms
 - Post-failure environment
 - Water immersion after fracture
 - Fatigue loading



-65° test condition



70° test condition

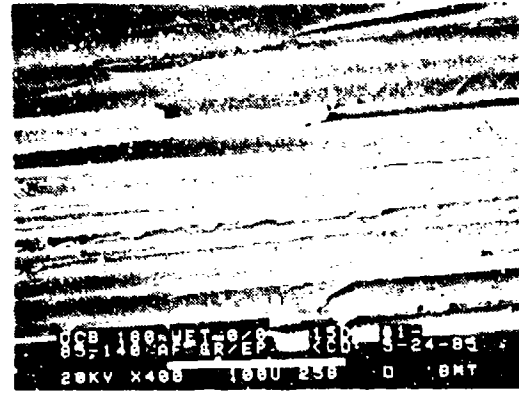


270° F wet condition

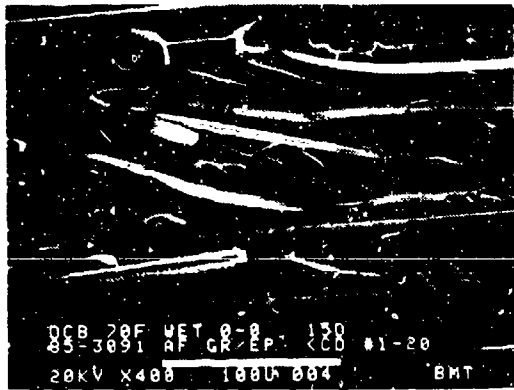
Figure 1-41. SEM Micrographs of Translaminar Fracture Conditions at Different Temperatures



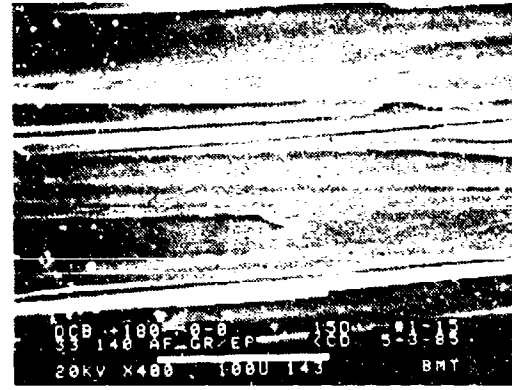
-54°C (-65°F) Dry



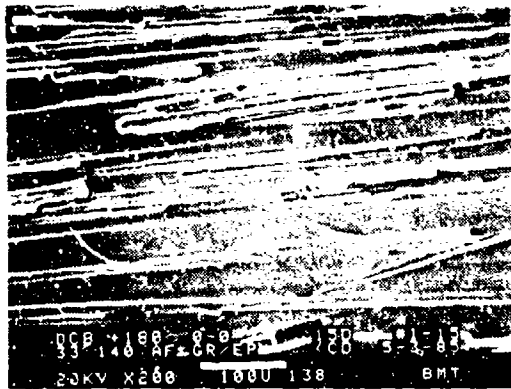
82°C (180°F) Wet



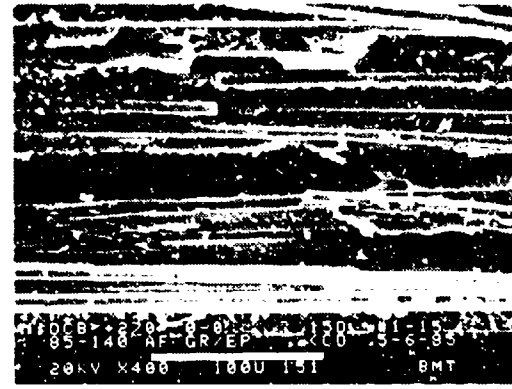
21°C (70°F) Wet



132°C (270°F) Dry



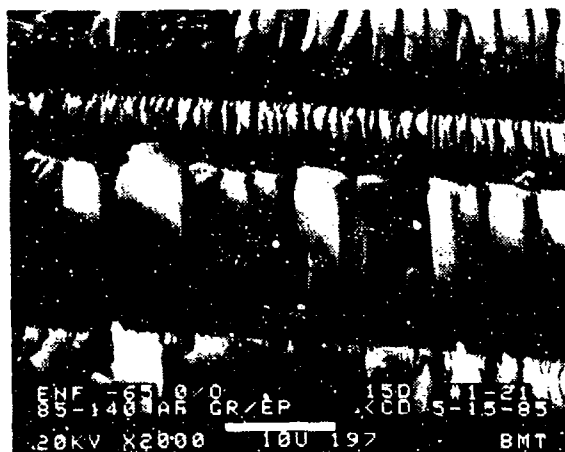
82°C (180°F) Dry



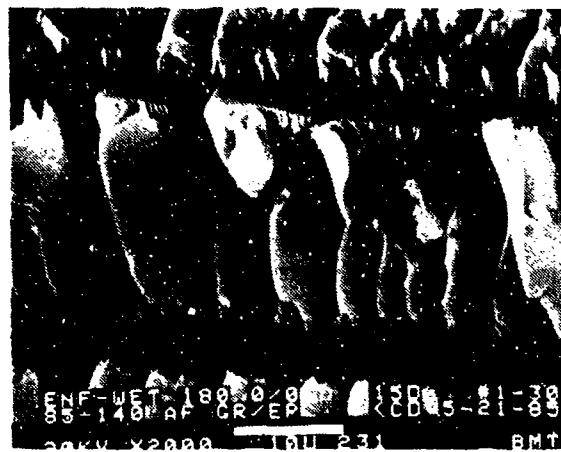
132°C (270°F) Wet

←
Mechanically Induced crack direction

Figure 1-42. Low Magnification Series of Characteristic 0/0 Degree Interface Mode I Fractures at Each Environmental Condition



-54°C (-65°F) Dry



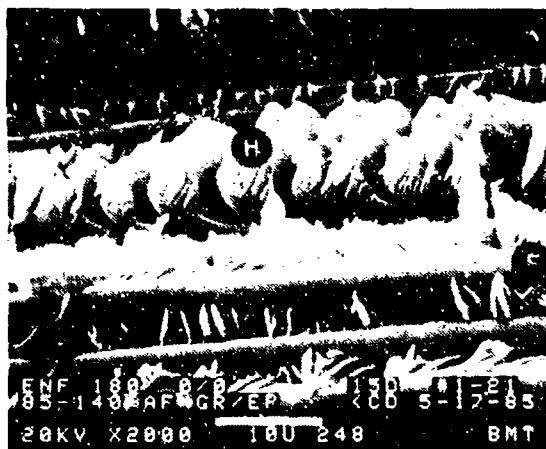
82°C (180°F) Wet



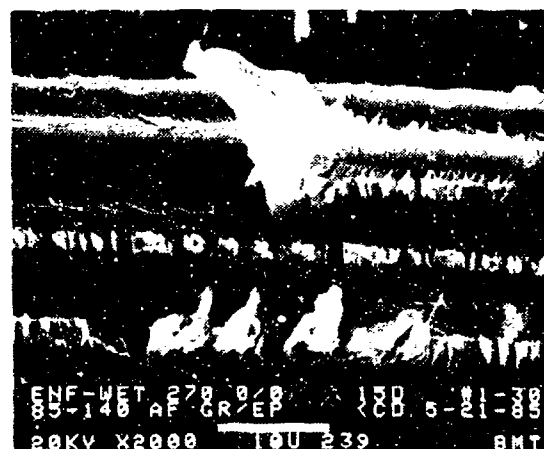
21°C (70°F) Wet



132°C (270°F) Dry



82°C (180°F) Dry



132°C (270°F) Wet

← Mechanically Induced crack direction

Figure 1-43. High Magnification Series of 0/0 Degree Interface Mode II (Shear) Fractures Showing Features of Fiber-Matrix Separation

With an exception of the paragraph on crack growth of ductile resin based materials, the discussion is focused on the carbon fiber/epoxy resin system which currently is extensively used in the aerospace industry.

1.1.6.1 Brittle Resin Composite Crack Growth

The term "brittle" in regard to fractography denotes a material that fractures with very little plastic deformation during crack growth and thus absorbs a small amount of energy during failure. Obviously this is simply a relative term which can be used to compare two or more materials in terms of fracture toughness. Crosslinked thermosets and some thermoplastics (which fracture well below their T_g) are included in this category. Microstructurally, brittle resins fracture due to locally resolved tensile stresses, resulting in a cleavage type fracture appearance with river marks and resin microflow. Mode I tension resin fracture regions appear flat, normal to the applied load. The Mode II shear resin fracture regions exhibit the telltale 45 degree tilted resin platelets, or hackles. In these conditions of pure in-plane shear, the fracture occurs by resolved tension resulting in hackles and scallops with river marks and resin microflow present. Cracking is continually reinitiating and propagating from the fiber-matrix interface. Crack growth occurs in the direction of river mark coalescence (Mode I tension), and for Mode II shear delaminations, growth is parallel to the direction of hackle tilt. Crack mapping utilizes these features to identify macroscopic loading conditions, overall crack growth directions and origin locations.

1.1.6.2 Ductile Resin Composite Crack Growth

As with the term of "brittle", "ductile" is a relative term denoting material systems which exhibit high fracture toughness and ductility, or plastic deformation, at the crack tip. These materials are the thermoplastic resin based systems. Microstructurally, ductile resins fracture by shear banding, shear banding, and void coalescence. During cracking, the long chain molecules are aligned in the locally resolved tension direction and microvoids form in this region. These microvoids account for the visible stress-whitening commonly observed in many fractured or highly stressed plastics. During crack growth, extensive local deformation occurs, somewhat similar to that seen in ductile aluminum alloys during static tension fracture, in which no cleavage features are generated. To date, no conclusive methods or telltale fracture features have been identified which could be used to determine the crack growth directions. However, some resins do exhibit tilted platelets (similar to hackles) under Mode II shear conditions, such that the investigator can differentiate between Mode I tension and Mode II shear fractures.

1.1.6.3 Fracture Mode Determination (Tension, Shear and Compression)

For interlaminar fractures, the mode can be determined as follows:

1. Mode I tension dominated fractures exhibit flat resin fracture between each fiber, with river marks and resin microflow as the dominant features.

2. Mode II shear dominated fractures exhibit rough resin fracture between each fiber, with hackles and scallops as the dominant features.
3. Tension dominated fractures exhibit a rough morphology, with fibers protruding at various heights from the surface. Close inspection of the individual fiber ends reveals radial lines indicative of tensile failure.
4. Compression dominated fractures exhibit a smooth morphology, with most of the fibers broken at a common plane. Extensive damage is common due to rubbing between the mating fracture surfaces. Close inspection of the individual fiber ends reveals a neutral axis line with tensile radials on one side of the line and compression fracture on the other side.

1.1.6.4 Mixed Mode Loading Effects

Currently, the understanding is rather incomplete in regard to how the appearance of the interlaminar fracture surface is affected when fracture occurs under loading conditions between pure Mode I tension and pure Mode II shear (mixed mode). The accepted theory is that since cracking occurs on a microscale due to locally resolved tensile stresses, as the laminate stresses move from Mode I to Mode II the resolved principal tensile stresses rotate. As a result, the flat resin fracture regions between fibers become progressively more tilted until they reach a 45 degree angle (hackles). Until a firm understanding of how this relates to the ability to determine crack growth directions, it is advisable to concentrate analyses in delamination regions which exhibit a dominance of either tension or shear loading at fracture.

1.1.6.5 Temperature and Absorbed Moisture Effects

For the brittle thermoset materials systems, the effects of temperature and moisture content do not significantly alter the overall fracture mechanisms or features. As a result, examination of the characteristic fracture features remains a viable means of determining the mode and direction of crack growth. Slight differences in features are usually apparent only when temperatures exceed one half of the T_g , and temperature appears to have more of a pronounced effect than absorbed moisture. These differences are usually not great enough to verify conditions at fracture unless great care is taken to compare features with controlled fracture specimens for the identical material system. The general theory is that increased temperature and absorbed moisture contents decrease the strength of the fiber-matrix interface and increase the ductility of the resin. As a result, the interlaminar fractures tend to occur at locations with higher fiber volume fractions, as opposed to the resin rich region between plies. For the translaminar tension fractures, elevated temperatures and absorbed moisture contents result in increased fiber pullout and lower amounts of resin seen adhering to the sides of the fibers.

1.1.6.6 Processing Defects Effects

Some of the processing defects which can have a direct effect on the fracture appearance include porosity, chemical and particulate contamination, fiber waviness, and resin rich/starved

regions. These defects result in reduced strength of the laminate and often contribute to crack initiation and growth. Voids appear smooth, lack fracture features, and their perimeter is distinct and rounded. Usually the voids do not act as crack initiation sites, but rather reduce the overall delamination strength by simply a reduction in resin volume. Chemical release agents present a situation where a bondline does not cohesively bond, resulting in a smooth and featureless adhesive separation. These areas differ in appearance to voids since they affect a much larger area and are not bounded by a distinct perimeter.

1.1.6.7 Material Forms Effects

Generally, fractures in laminates produced from tape, fabric, or filament winding raw material forms all exhibit the basic resin and fiber fracture features that have been presented in this document. The methods used to determine the crack growth directions and the mode of fracture are identical for all forms.

For interlaminar fractures, crack mapping is easiest and often more reliable in the local regions which exhibit the highest resin volume fraction, that is between cross-ply of tape and at the intersection points of the fabric tows. This is particularly true for Mode I tension cracks where river marks are larger and more easily identified. With this in mind, it is understandable that filament winding is more difficult to analyze since very few, if any, of these resin rich regions exist.

For translaminar fractures, the filament wind and tape forms appear identical for both tension and compression features. Translaminar fabric forms exhibit each individual tow on a microscopic scale; however, at high magnifications the features present on the fiber ends are similar to the other two forms. Often less fraying and splitting of the laminate occurs with fabric since it is held together by cross-weaving each tow.

1.1.6.8 Post-Failure Environment Effects

Several sources of damage to the fracture surfaces exist following a component failure. These sources can be categorized as either chemical or mechanical.

The chemically induced damage sources include solvents, acids, alkaline, and complex compounds such as hydraulic fluid or flame retardant. The general result is usually a softening or loss of fine fracture surface details such as river marks, resin microflow, hackles, and scallops. Often a by-product or residue is present which can be determined by chemical analysis methods.

Mechanical damage sources include fatigue or sonic rubbing between the mating fracture surfaces during service or involves damage by poor handling practices. In nearly all cases the fracture surfaces are mechanically abraded and exhibit fine parallel lines on the fracture surfaces due to rubbing.

1.1.6.9 Fatigue Effects

The specific mechanisms for fatigue of brittle composite materials is not fully understood at this time. The major unanswered question is whether cracking occurs due to plastic deformation of the crack tip (such as seen in aluminum) or due to a simple crack arrest/crack initiation (similar to beach marks seen visually). Laboratory induced interlaminar fractures of small coupons have been produced which exhibit finely spaced lines similar to striations in metals. In Mode I tension the "striations" appear in the resin fracture regions, whereas the Mode II shear fractures reveal these sets of parallel lines at the fiber-matrix interface. Larger structures which have been cyclically loaded to failure exhibit only very isolated and faint striations. These regions of fatigue are often extremely difficult to locate; since so far we have not visually or macroscopically identified any differences between the slow growth and rapid fracture regions. Further studies are a must in this area since future, higher toughness materials will be pushed into higher service loads and strains which will be more susceptible to fatigue fracture.

1.2 ORGANIZATION OF THE ATLAS OF FRACTOGRAPHS

The fractographs shown in the following sections are grouped primarily by the composite material system that is represented. Sections 2 through 8 are arranged by material system in the following order: graphite/epoxy, Kevlar/epoxy, boron/epoxy, fiberglass/epoxy, graphite/bismaleimide, graphite/thermoplastic and carbon/polyimide. Bolted and adhesively bonded composites are characterized in Sections 9 and 10, respectively.

The extensive fractography of the graphite/epoxy system in Section 2 has been subdivided primarily by the mechanically induced failure mode. Subsections 2.1 through 2.12 are arranged by failure mode in the following order: interlaminar tension, interlaminar shear, interlaminar mixed mode flexural, in-plane shear, translaminar tension, translaminar compression, translaminar shear, translaminar flexure, fatigue, creep, high rate, and compression-after-impact. Defects are shown in subsection 2.13. In those subsections where a large number of laminate lay-ups and test conditions are characterized, a test matrix has been presented, and the fractographs have been arranged in the same order that the variables are listed in the test matrix. In the small subsections, the fractography has been arranged in the order that it is discussed at the beginning of the subsection. Similar test matrices and/or discussions are presented in Sections 3 through 10 indicating the arrangement of the fractography in those sections.

Inconsistencies exist in the format of the figures, tables and text of this Atlas of Fractographs because it represents a compilation of three reports. The integration of the relevant parts of these reports into this single atlas with the organization described in the previous paragraphs emphasizes function rather than form.

SECTION 2
GRAPHITE/EPOXY
AS4/3501-6

2.1 INTERLAMINAR TENSION (MODE I DCB)

The primary features observed in fracture surfaces generated by interlaminar Mode I tension double cantilever beam testing (Figure 2-1) are as follows:

1. Macroscopically and microscopically flat fracture surface
2. Flat resin fracture between fibers, exhibiting river marks and very fine resin microflow
3. Smooth appearance of the resin at the fiber-matrix separation.

Crack growth direction (CD) can be determined by examining the matrix between fibers. River mark coalescence and the radiating nature of the resin microflow are two fracture surface features which can be used to identify the direction of crack growth (Figures 2-2 and 2-3). Care must be taken to examine many locations on the fracture surface for accuracy and reliability of crack growth direction determination, since various conditions can cause localized crack growth in a direction other than the overall macroscopic crack growth direction.

Where the overall cracking progresses in a direction parallel to the fibers, river marks are concentrated adjacent to the fibers where cracking tends to continually reiterate on a microscale. In other cases, where overall cracking progresses in a direction other than parallel to the fibers, these river marks are concentrated on the side of the fiber away from the origin of the failure. In all cases, Mode I tension interlaminar fracture is characterized by river patterns on the fracture surfaces that are oriented at an angle or parallel to the direction of macroscopic fracture.

Processing variations (overcure or undercure), material form (filament winding, fabric or tape), or post fracture environmental conditions (rain, fuels, fluids), do not significantly alter the fracture characteristics. Absorbed moisture or elevated temperature present during fracture do not alter the ability to determine crack growth and fracture mode. Cracking does, however, tend to occur within the plies (intralaminar) at elevated temperature, as opposed to between the plies (interlaminar) at room temperature. This is likely due to either the decreased strength of the fiber-matrix interface or the increased ductility of the resin. Fractures created at 270°F often exhibit large amounts of loose fibers on the fracture surface.

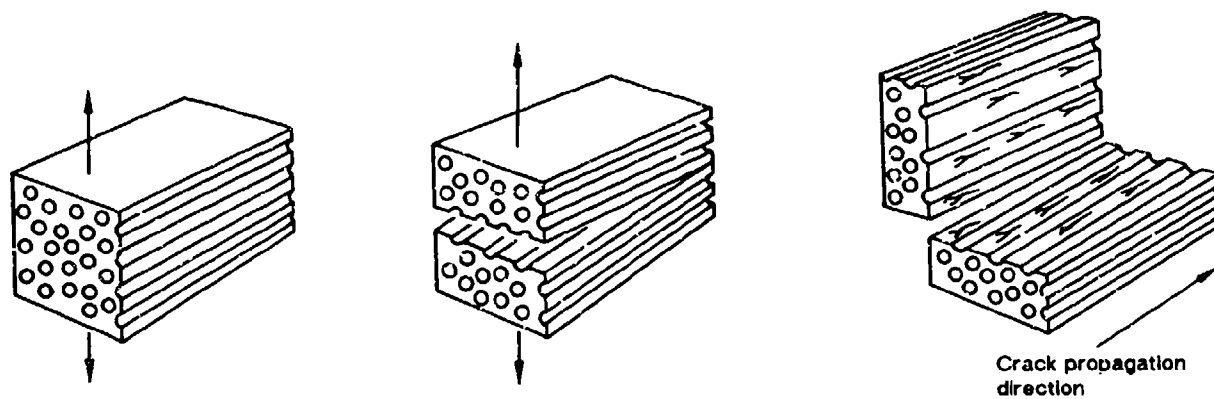


Figure 2-1. Double-Cantilever Beam Test Type

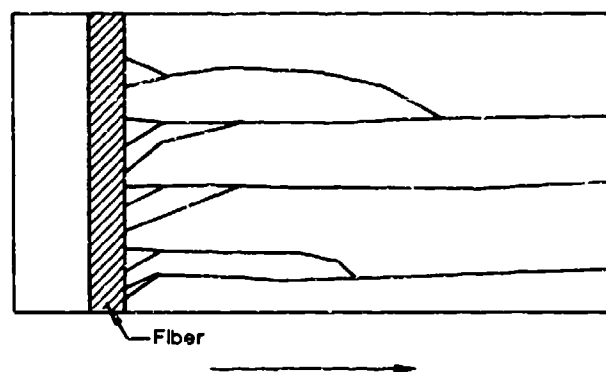


Figure 2-2. Overall Crack-Growth Direction by River Markings

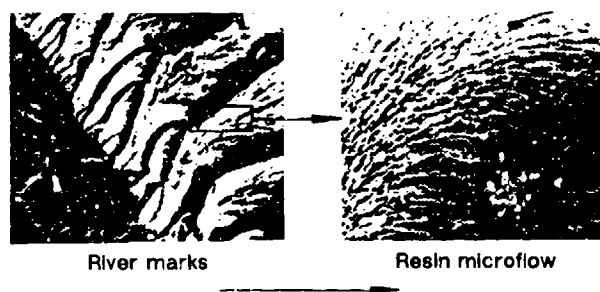


Figure 2-3. Overall Crack-Growth Direction by Resin Microflow

Fracture surfaces exposed to 2000°F flame for five minutes exhibited resin-starved carbon fibers on the outermost ply. Due to the minimal resin content, there were no signs of river marks or resin microflow to indicate crack propagation direction.

Table 2-1 shows the test matrix for the double cantilever beam (DCB) test type. Results of the testing listed in Table 2-1 are depicted in Figures 2-4 through 2-57. These figures are arranged in the same order that the corresponding tests are listed in Table 2-1.

Table 2-1. Test Matrix for Mode I DCB Specimens

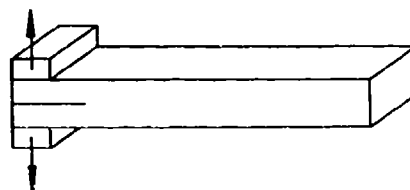
PLY/ORIENTATION	VARIABLE CONDITIONS	CONTRIBUTOR
24/0 24/± 45 24/0, ± 45 24/0, 90 24/90	RT/Dry (Baseline), -65°F/Dry, 270°F/Dry, RT/Wet, 180°F/Wet (Conditions During Tests)	Boeing
24/± 45 24/0, ± 45 24/0, 90	Filament Wound	Northrop
24/0, 90	Fabric	Boeing
24/± 45 24/0, ± 45 24/0, 90	3-D Weave	Northrop
24/0 24/0, ± 45	Impact Damaged Before Test	Northrop
24/0	Water Immersion Before Test	Northrop
24/0, 90	Water Immersion or Humidity Exposure (100% RH), 4 weeks at 160°F, After Test	Boeing
24/0 24/0, ± 45 24/0, 90	Undercured	Northrop

Table 2-1. Test Matrix for Mode I DCB Specimens (Continued)

PLY/ORIENTATION	VARIABLE CONDITIONS	CONTRIBUTOR
24/0 24/0, ± 45	Overcured	Northrop
24/0, 90	Low Resin	Boeing
24/0	High Resin	Northrop
24/0 24/ ± 45 24/0, ± 45	High Resin + Conditioned 180°F/Dry After Test	Northrop
24/0 24/0, ± 45	Overcured + Conditioned 180°F/Wet After Test	Northrop
24/0, 90	2000°F/Dry (5 Minutes) After Test	Boeing

Optical photomicrographs

Fracture type	Interlaminar mode I tension
Ply layup	[0] 24
Test type	DCB
• Test conditions	21°C dry
• Fracture between	0/0 plies
Material	Hercules 3501-6/177°C cure AS4 fibers



100X

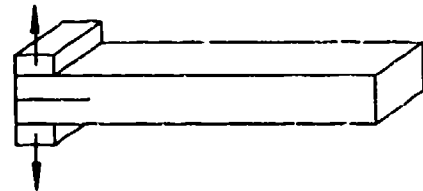


400X

Figure 2-4. Photographs of Interlaminar Mode I Tension, 0/0 Fracture, 70 F/Dry

SEM photomicrographs

Fracture type	Interlaminar mode I tension
Ply layup	[0]24
Test type	DCB
• Test conditions	21°C dry
• Fracture between	0/0 plies
Material	Hercules 3501-6/177°C cure AS4 fibers



Mechanically induced
crack direction

Legend:

- F Fiber matrix separation
- M Matrix fracture
- R River markings

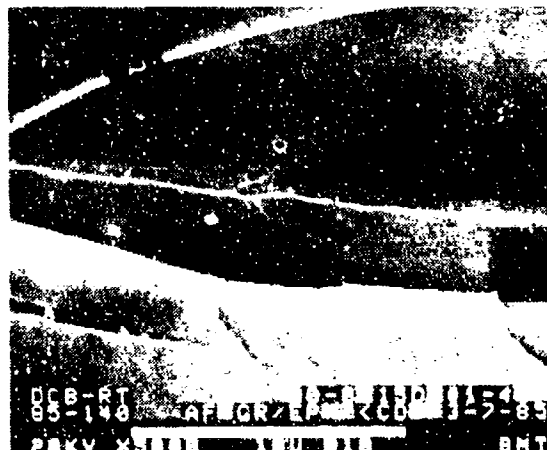
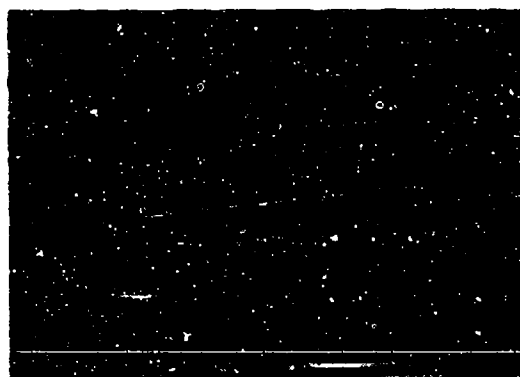
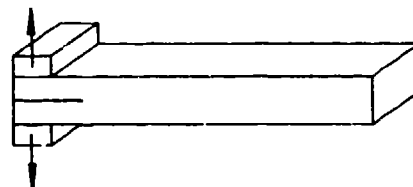


Figure 2-5. SEM Photographs of Interlaminar Mode I Tension Fracture, 0/0, 70 F/Dry

Optical photomicrographs

Fracture type	Interlaminar mode I tension
Ply layup	[0]24
Test type	DCB
• Test conditions	Dry
• Fracture between	0/0 plies
Material	Hercules 3501-6/177°C cure AS4 fibers



-65°F, dry

400X



70°F, dry

400X

→
Mechanically induced
crack direction



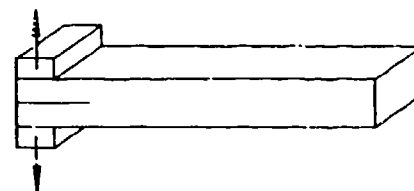
270°F, dry

400X

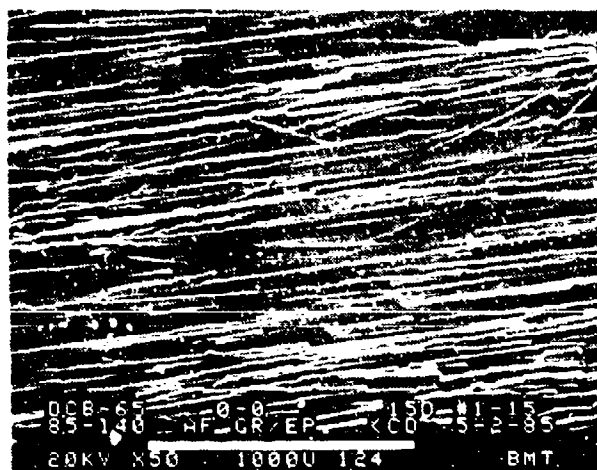
Figure 2-6. Photographs of Interlaminar Mode I Tension, 0/0 Fracture, -65, 70, and 270 F/Dry

SEM photomicrographs

Fracture type	Interlaminar mode I tension
Ply layup	[0] 24
Test type	DCB
• Test conditions	Dry
• Fracture between	0/0 plies
Material	Hercules 3501-6/177°C cure AS4 fibers



Mechanically Induced crack direction



-55°F, dry



70°F, dry

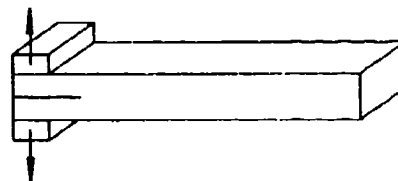


270°F, dry

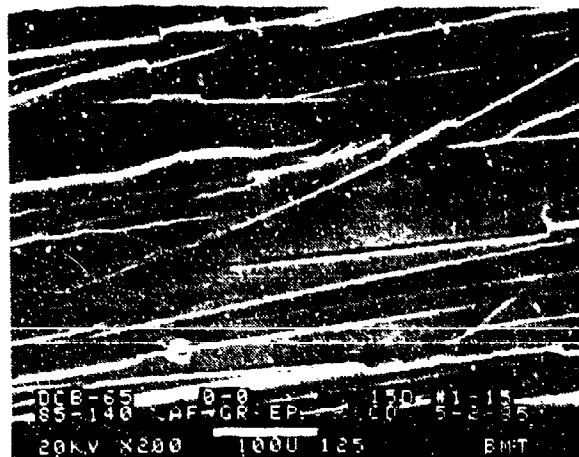
Figure 2-7. SEM Photographs of Interlaminar Mode I Tension, 0/0 Fracture, -65, 70 and 270 F/Dry (50X)

SEM photomicrographs

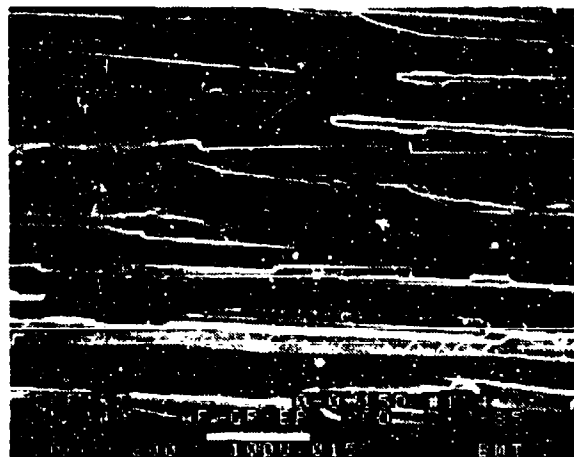
Fracture type	Interlaminar mode I tension
Ply layup	[0] 24
Test type	DCB
• Test conditions	Dry
• Fracture between	0/0 plies
Material	Hercules 3501-6/177° C cure AS4 fibers



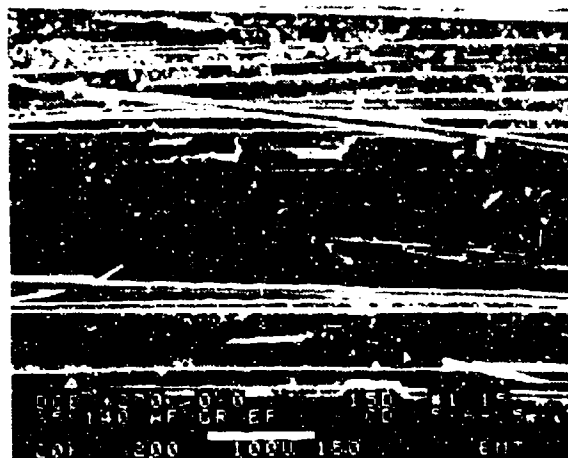
←
Mechanically induced crack direction



-65°F, dry



70°F, dry

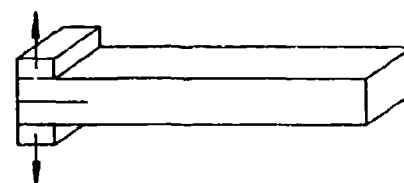


270°F, dry

Figure 2.8. SEM Photographs of Interlaminar Mode I Tension, 0/0 Fracture, -65, 70, and 270 F/Dry (200X)

SEM photomicrographs

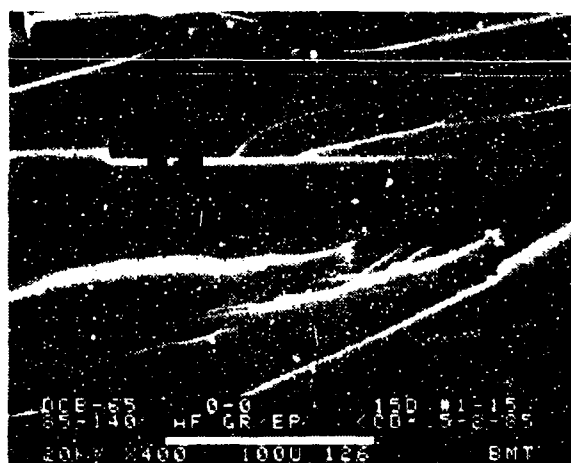
Fracture type	Interlaminar mode I tension
Ply layup	[0] 24
Test type	DCB
• Test conditions	Dry
• Fracture between	0/0 plies
Material	Hercules 3501-6/177°C cure AS4 fibers



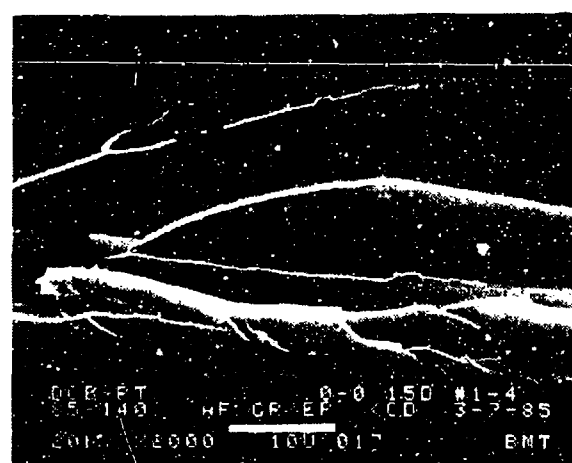
Legend:

F Fiber matrix separation
R River markings
M Matrix fracture

← Mechanically induced crack direction



-65°F, dry

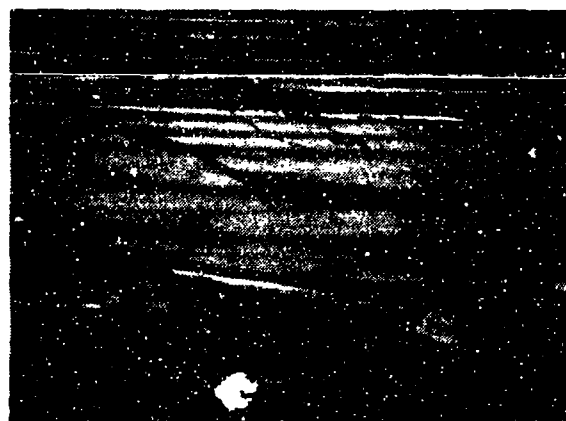
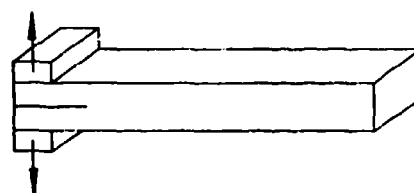


70°F, dry

Figure 2-9. SEM Photographs of Interlaminar Mode I Tension, 0/0 Fracture, -65 and 70 F/Dry

Optical photomicrographs

Fracture type	Interlaminar mode I tension
Ply layup	[0]24
Test type	DCB
• Test conditions	70°F wet
• Fracture between	0/0 plies
Material	Hercules 3501-6/177° C cure AS4 fibers



70°F wet

400X



180°F wet

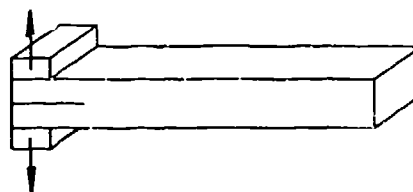
400X

← Mechanically induced crack direction

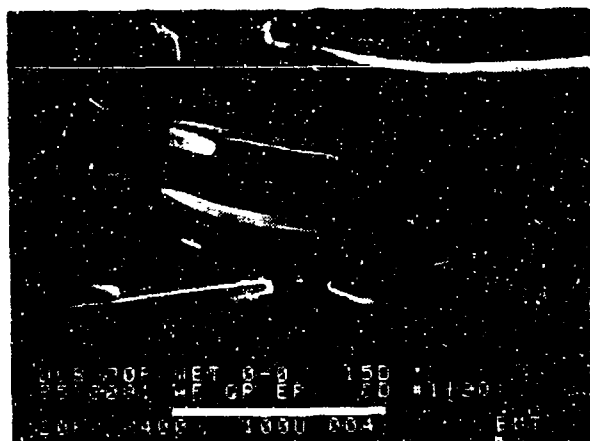
Figure 2-10. Photographs of Interlaminar Mode I Tension, 0/0 Fracture, 70 and 180 F/Wet

SEM photomicrographs

Fracture type	Interlaminar mode I tension
Ply layup	[0] 24
Test type	DCB
• Test conditions	Wet
• Fracture between	0/0 plies
Material	Hercules 3501-6/177°C cure AS4 fibers



←
Mechanically Induced crack direction



70°F, wet

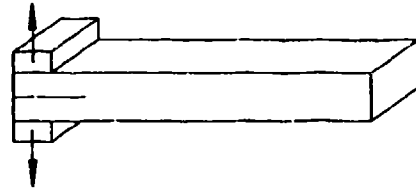


180°F, wet

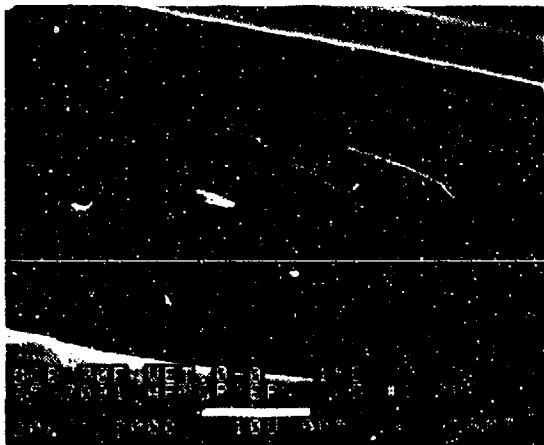
Figure 2-11. SEM Photographs of Interlaminar Mode I Tension, 0/0 Fracture, 70 and 180 F/Wet

SEM photomicrographs

Fracture type	Interlaminar mode I tension
Ply layup	[0] 24
Test type	DCB
• Test conditions	Dry/wet
• Fracture between	0/0 plies
Material	Hercules 3501-6/177°C cure AS4 fibers

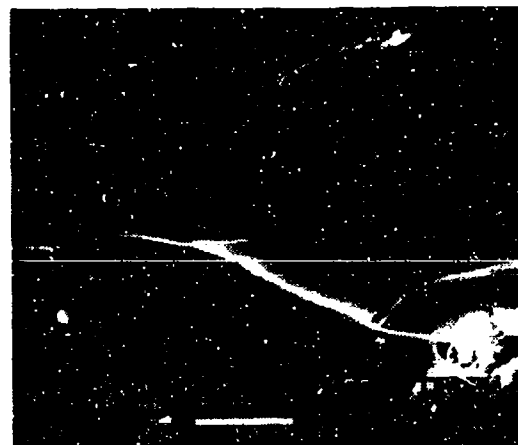


←
Mechanically Induced crack direction



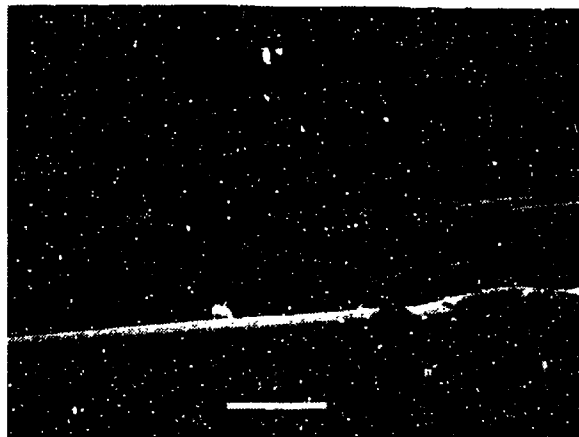
70°F, wet

2000X



180°F, dry

2000X



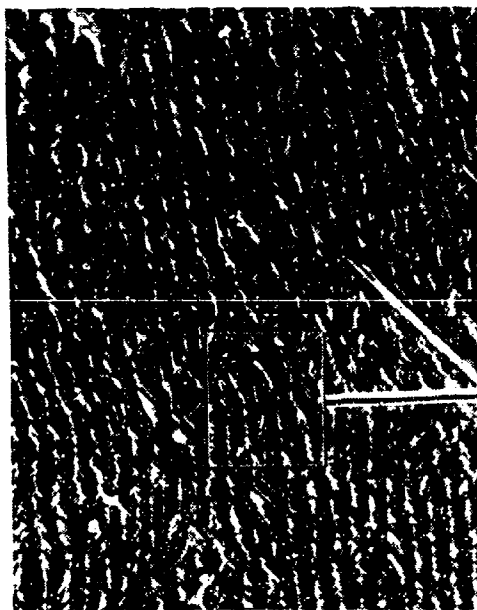
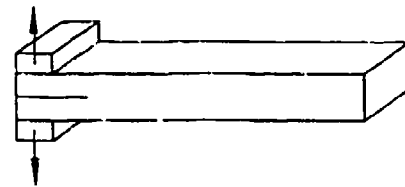
180°F, wet

2000X

Figure 2-12. SEM Photographs of Interlaminar Mode I Tension, 0/0 Fracture, 70 F/Wet, 180 F/Dry, and 180 F/Wet

Optical photomicrographs

Fracture type	Interlaminar mode I tension
Ply layup	[+45, -45] 12S
Test type	DCB
• Test conditions	21°C dry
• Fracture between	+45/-45 plies
Material	Hercules 3501-6/177°C cure AS4 fibers



100X



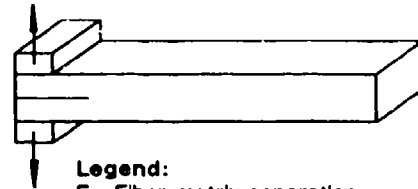
400X

← Mechanically Induced crack direction

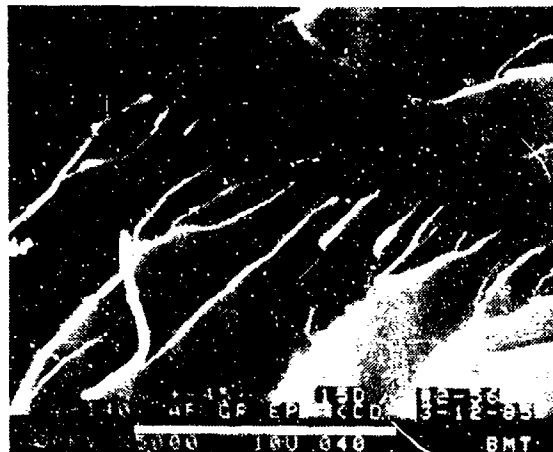
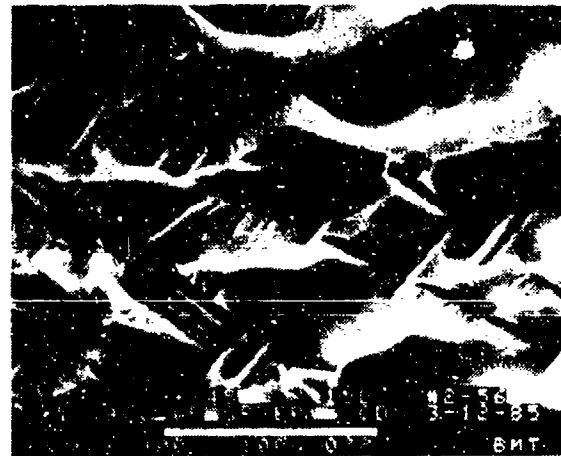
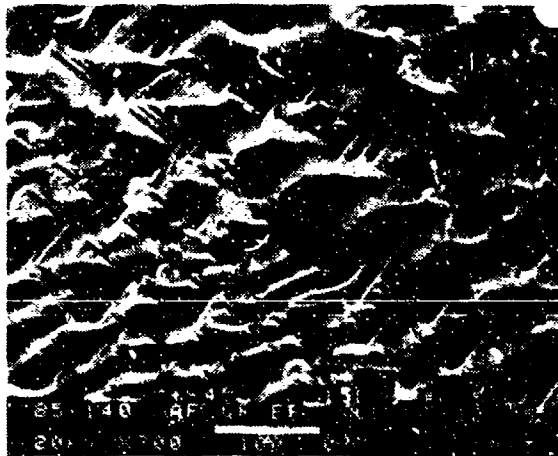
Figure 2-13. Photographs of Interlaminar Mode I Tension, +45/-45 Fracture, 70 F/Dry

SEM photomicrographs

Fracture type	Interlaminar mode I tension
Ply layup	[+45, -45] 12S
Test type	DCB
• Test conditions	21°C dry
• Fracture between	+45/-45 plies
Material	Hercules 3501-6/177°C cure AS4 fibers



Legend:
 F Fiber matrix separation
 M Matrix fracture
 R River markings
 T Textured microflow

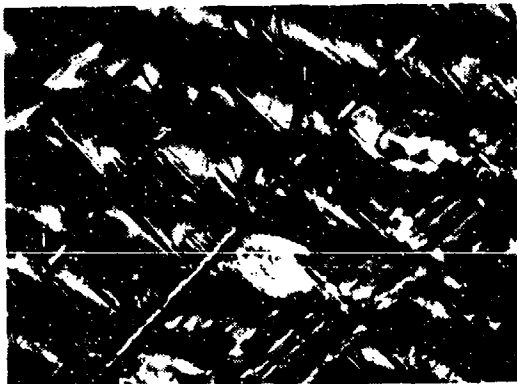
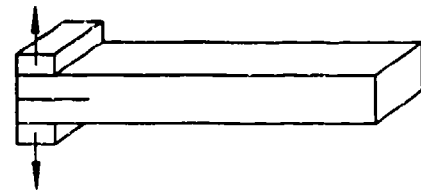


←
 Mechanically induced crack direction

Figure 2-14. SEM Photographs of Interlaminar Mode I Tension, +45/-45 Fracture, 70 F/Dry

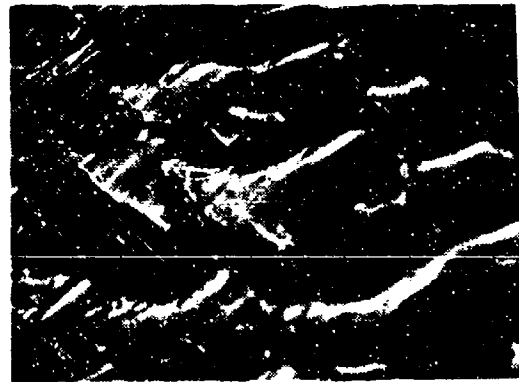
Optical photomicrographs

Fracture type	Interlaminar mode I tension
Ply layup	[+45, -45] _{12S}
Test type	DCB
• Test conditions	Dry
• Fracture between	+45/-45 plies
Material	Hercules 3501-6/177°C cure AS4 fibers



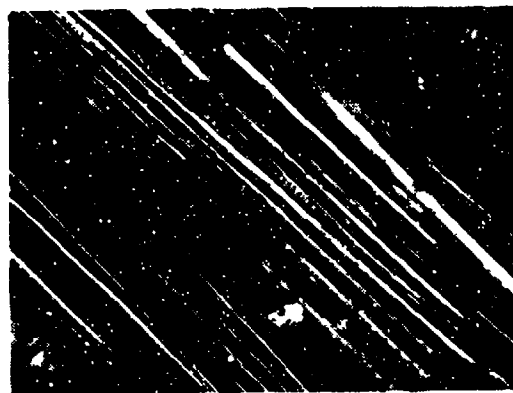
-65°F, dry

400X



70°F, dry

400X



270°F, dry

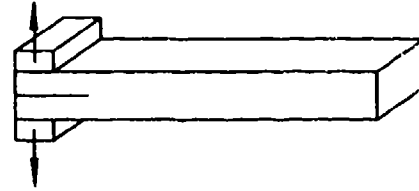
400X

→
Mechanically Induced crack direction

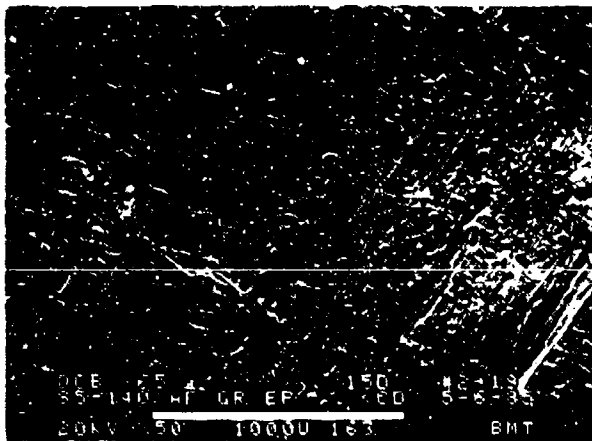
Figure 2-15. Photographs of Interlaminar Mode I Tension, +45/-45 Fracture, -65, 70, and 270 F/Dry

SEM photomicrographs

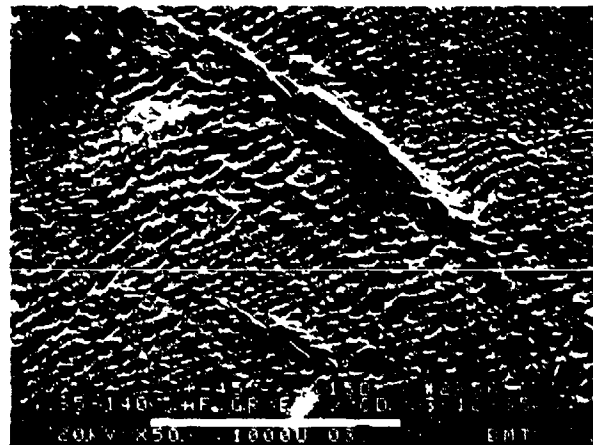
Fracture type	Interlaminar mode I tension
Ply layup	[+45,-45] 12S
Test type	DCB
• Test conditions	Dry
• Fracture between	+45/-45 plies
Material	Hercules 3501-6/177°C cure AS4 fibers



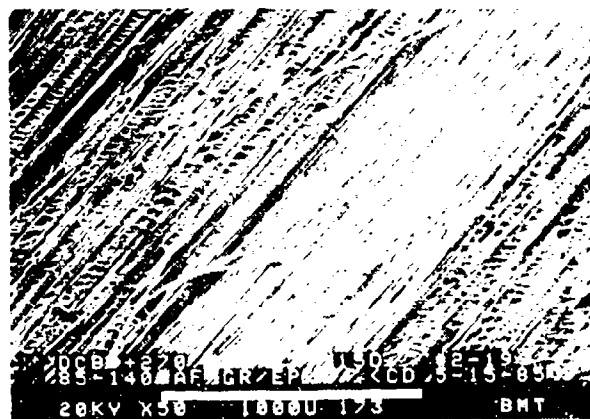
Mechanically induced crack direction



-65°F, Dry



70°F, Dry

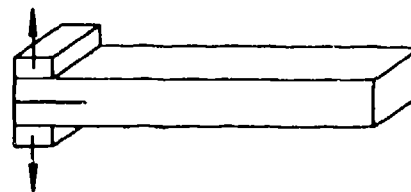


270°F, Dry

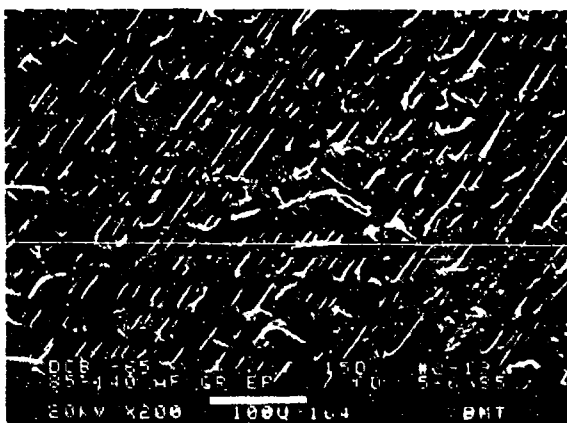
Figure 2-16. SEM Photographs of Interlaminar Mode I Tension, +45/-45 Fracture, -65, 70, and 270 F/Dry (50X)

SEM photomicrographs

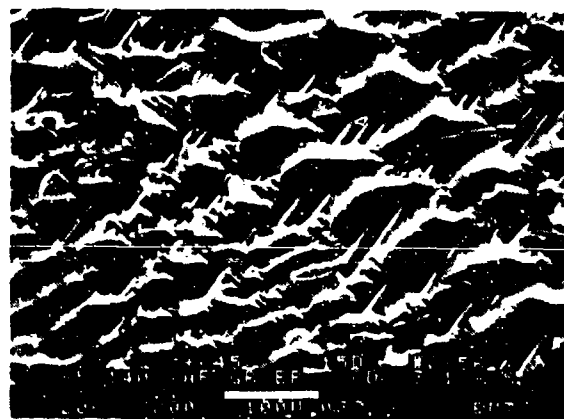
Fracture type	Interlaminar mode I tension
Ply layup	[+45,-45] 12S
Test type	DCB
• Test conditions	Dry
• Fracture between	+45/-45 plies
Material	Hercules 3501-6/177°C cure AS4 fibers



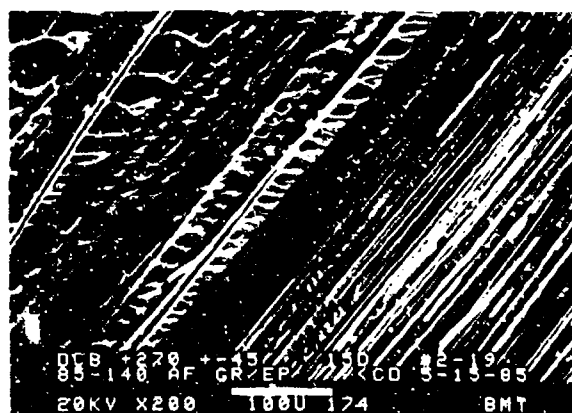
Mechanically Induced crack direction



-65°F, Dry



70°F, Dry

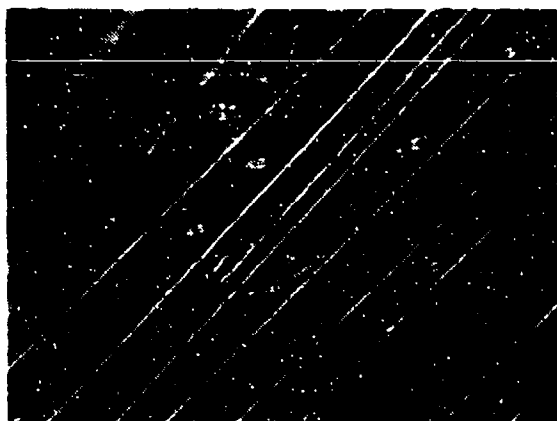
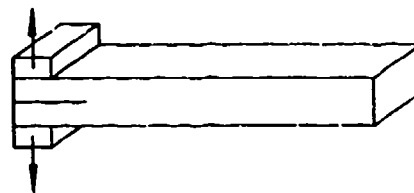


270°F, Dry

Figure 2-17. SEM Photographs of Interlaminar Mode I Tension, +45/-45 Fracture, -65, 70, and 270 F/Dry (200X)

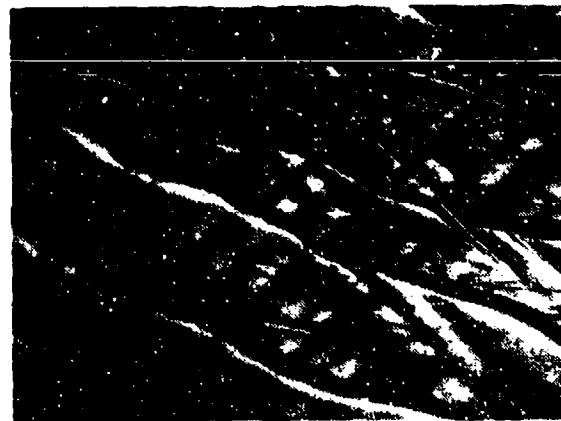
Optical photomicrographs

Fracture type	Interlaminar mode I tension
Ply layup	[+45, -45] _{12S}
Test type	DCB
• Test conditions	Wet
• Fracture between	+45/-45 plies
Material	Hercules 3501-6/177°C cure AS4 fibers



70°F, wet

400X



180°F, wet

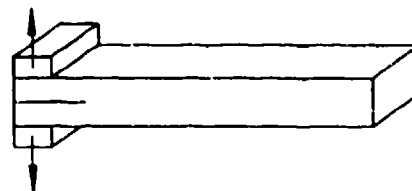
400X

←
Mechanically induced crack direction

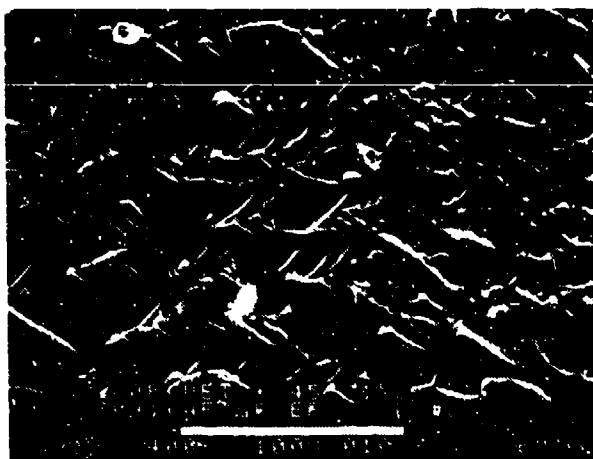
Figure 2-18. Photographs of Interlaminar Mode I Tension, +45/-45 Fracture, 70 and 180 F/Wet

SEM photomicrographs

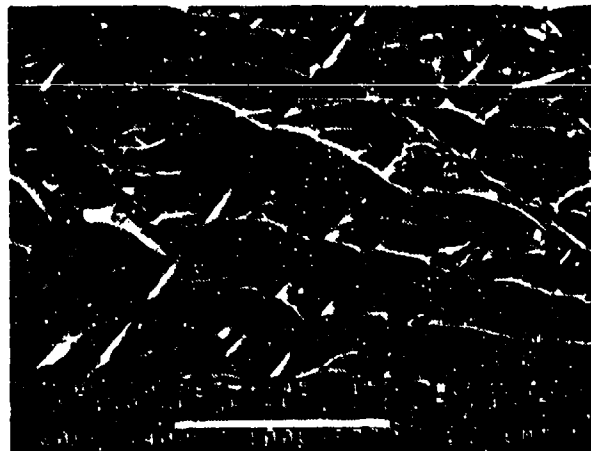
Fracture type	Interlaminar mode I tension
Ply layup	[+45,-45] 12S
Test type	DCB
• Test conditions	Wet
• Fracture between	+45/-45 plies
Material	Hercules 3501-6/177°C cure AS4 fibers



Mechanically induced crack direction



70°F, Wet

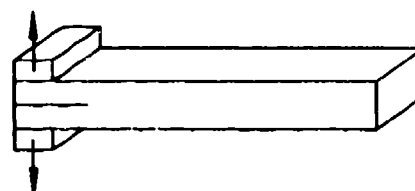


180°F, Wet

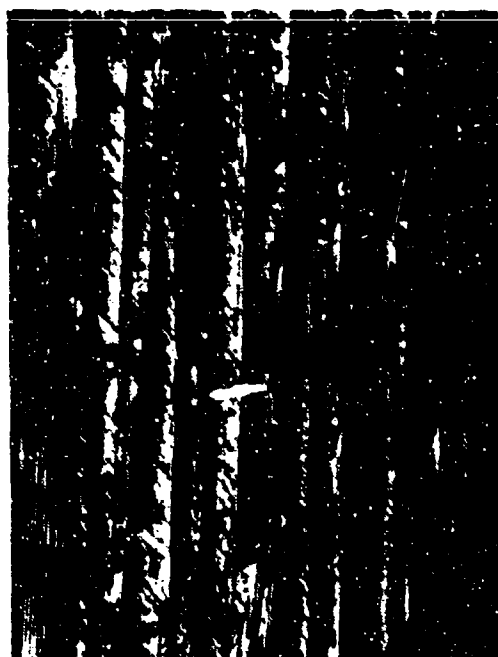
Figure 2-19. SEM Photographs of Interlaminar Mode I Tension, +45/-45 Fracture, 70 and 180 F/Wet

Optical photomicrographs

Fracture type	Interlaminar mode I tension
Ply layup	[0.45] ₁₂ S
Test type	DCB
• Test conditions	2 °C dry
• Fracture between	0/45 plies
Material	Hercules 3501-6/177 °C cure AS4 fibers



Mechanically
induced crack
direction



100X

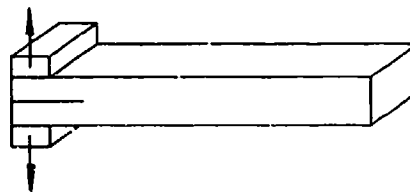


400X

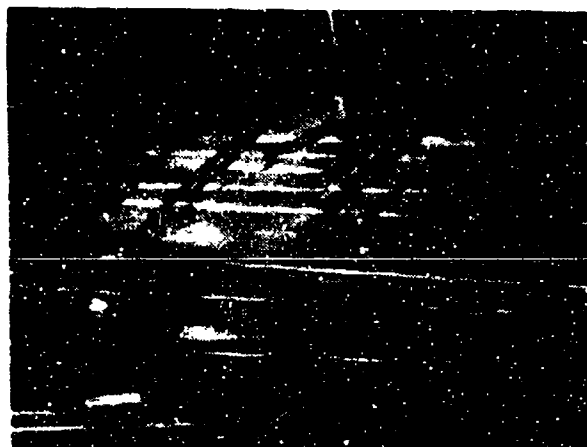
Figure 2-20. Photographs of Interlaminar Mode I Tension, 0/45 Fracture, 70 F/Dry

Optical photomicrographs

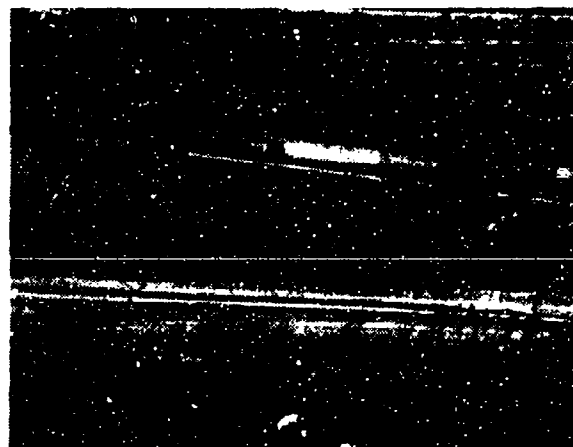
Fracture type	Interlaminar mode I tension
Ply layup	[0, 45] ₁₂ S
Test type	DCB
• Test conditions	Dry
• Fracture between	0/45 plies
Material	Hercules 3501-6/177°C cure AS4 fibers



Mechanically induced crack direction →



-65°F, dry



70°F, dry

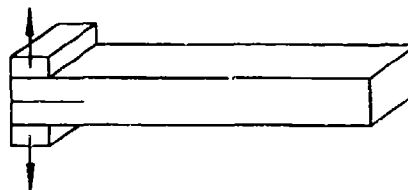


270°F, dry

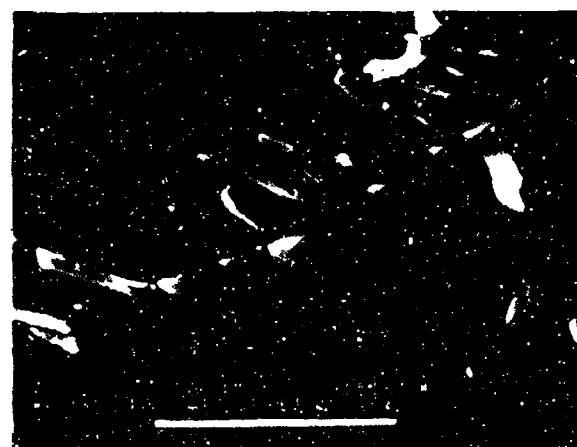
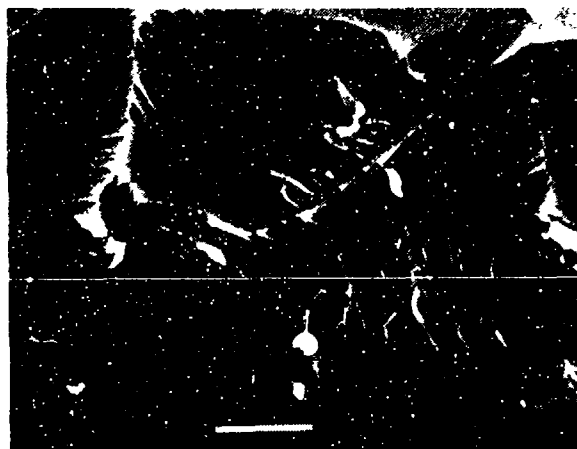
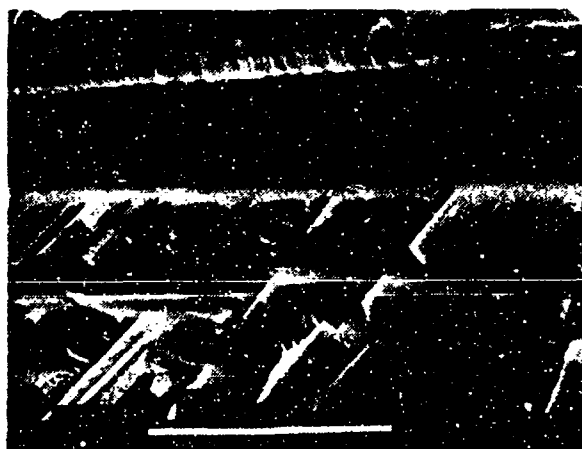
Figure 2-21. Photographs of Interlaminar Mode I Tension, 0/45 Fracture, -65, 70 and 270 F/Dry (400X)

SEM photomicrographs

Fracture type	Interlaminar mode I tension
Ply layup	[0.45] _{12S}
Test type	DCB
• Test conditions	Wet
• Fracture between	0/45 plies
Material	Hercules 3501-6/177°C cure AS4 fibers



←
Mechanically Induced crack direction



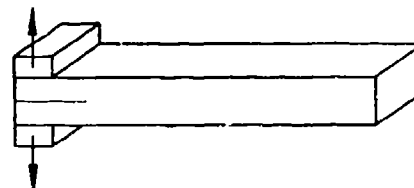
Legend:

- F Fiber matrix separation
- M Matrix fracture
- R River markings
- T Textured microflow

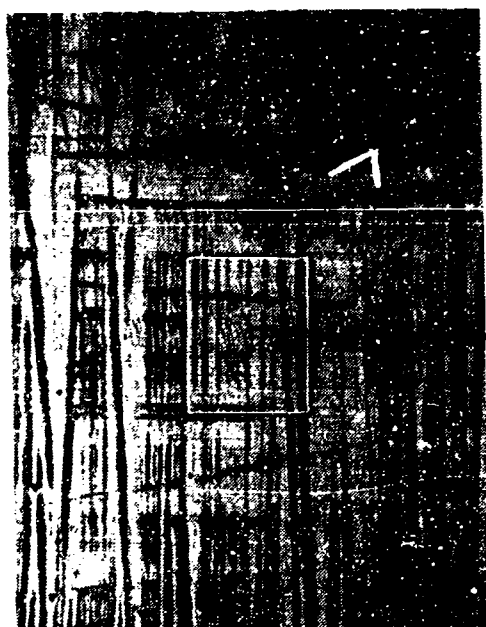
Figure 2-22. SEM Photographs of Interlaminar Mode I Tension, 0/45 Fracture, 70 F/Wet

Optical photomicrographs

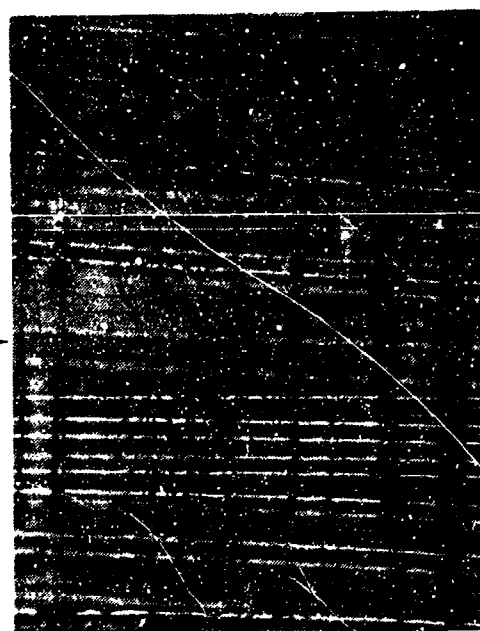
Fracture type	Interlaminar mode I tension
Ply layup	[0, 90] ₂ S
Test type	DCB
• Test conditions	21°C, dry
• Fracture between	0/90 plies
Material	Hercules 3501-6/177°C cure AS4 fibers



Mechanically induced crack direction



100X

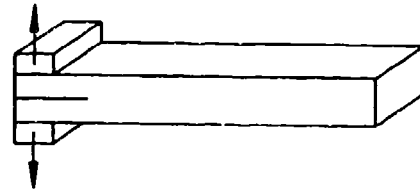


400X

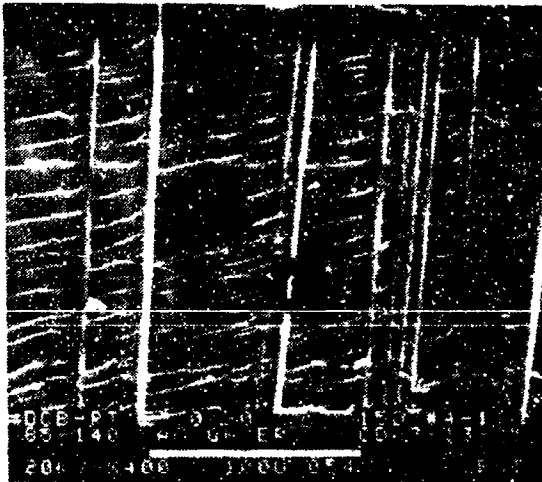
Figure 2-23. Photographs of Interlaminar Mode I Tension, 0/90 Fracture, 70 F/Dry

SEM photomicrographs

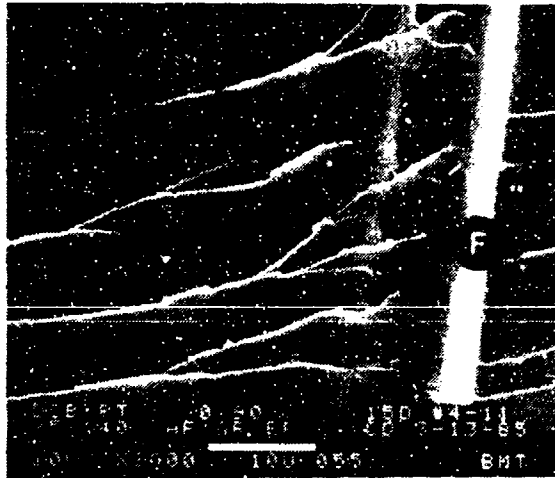
Fracture type	Interlaminar mode I tension
Ply layup	[0, 90] _{12S}
Test type	DCB
• Test conditions	21°C, dry
• Fiber end fracture	
Material	Hercules 3501-6/177°C cure AS4 fibers



← Mechanically Induced crack direction



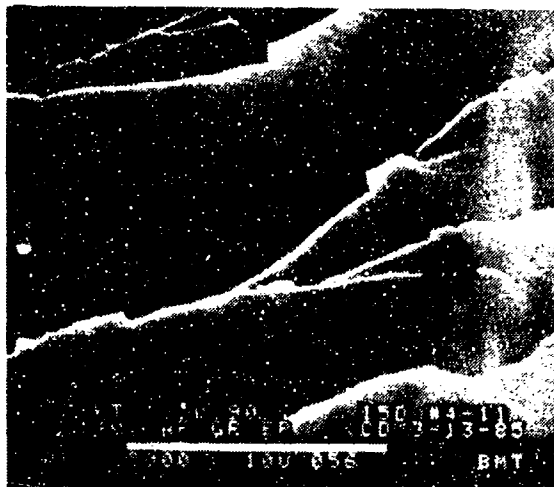
400X



2000X

Legend:

- F Fiber matrix separation
- M Matrix fracture
- R River markings
- T Textured microflow

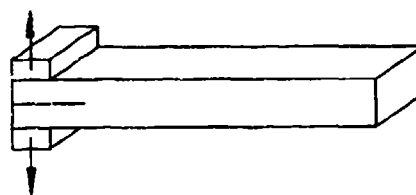


5000X

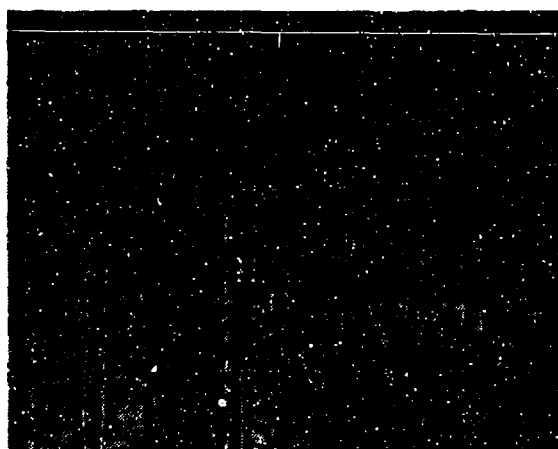
Figure 2-24. SEM Photographs of Interlaminar Mode I Tension, 0/90 Fracture, 70 F/Dry

Optical photomicrographs

Fracture type	Interlaminar mode I tension
Ply layup	[0, 90] ₁₂ S
Test type	DCB
• Test conditions	Dry
• Fracture between	0/90 plies
Material	Hercules 3501-6/177°C cure AS4 fibers

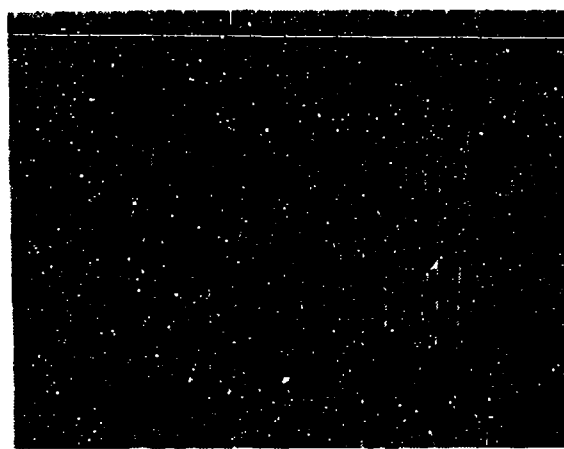


Mechanically induced crack direction →



-65°F, dry

400X



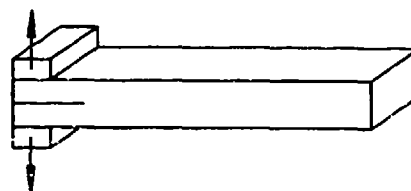
70°F, dry

400X

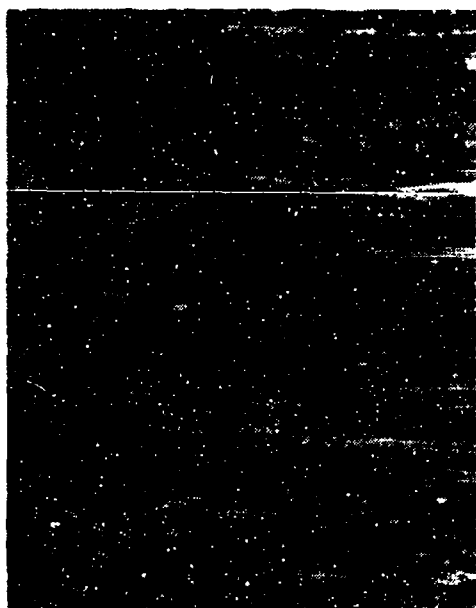
Figure 2-25. Photographs of Interlaminar Mode I Tension, 0/90 Fracture, -65 and 70 F/Dry

Optical photomicrographs

Fracture type	Interlaminar mode I tension
Ply layup	[90]24
Test type	DCB
• Test conditions	21°C, dry
• Fracture between	90/90 plies
Material	Hercules 3501-6/177°C cure AS4 fibers



↓ Mechanically induced crack direction



100X

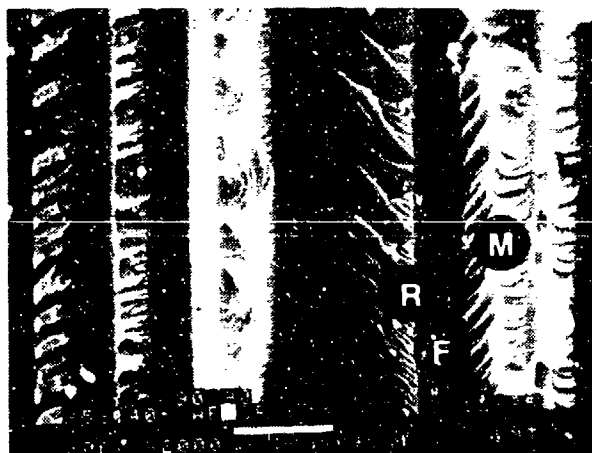
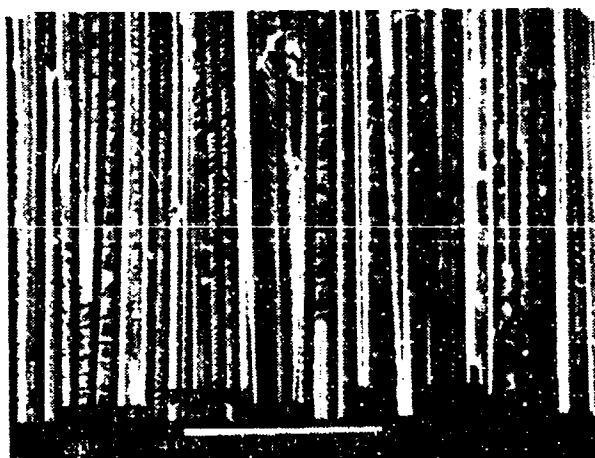
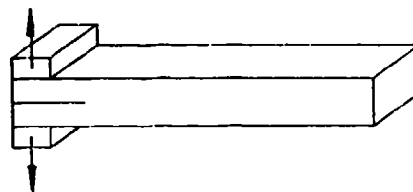


400X

Figure 2-26. Photographs of Interlaminar Mode I Tension, 90/90 Fracture, 70 F/Dry

SEM photomicrographs

Fracture type	Interlaminar mode I tension
Ply layup	[90]24
Test type	DCB
• Test conditions	21°C, dry
• Fracture between	0/90 plies
Material	Hercules 3501-6/177°C cure AS4 fibers



Mechanically induced crack direction

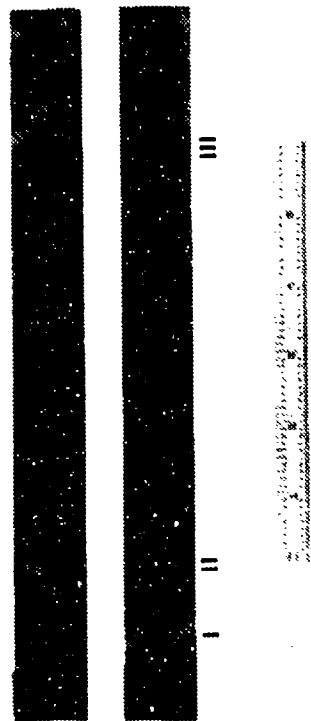


Legend:

- F Fiber matrix separation
- M Matrix fracture
- R River markings



Figure 2-27. SEM Photographs of Interlaminar Mode I Tension, 90/90 Fracture, 70 F/Dry



(a)

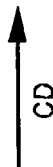
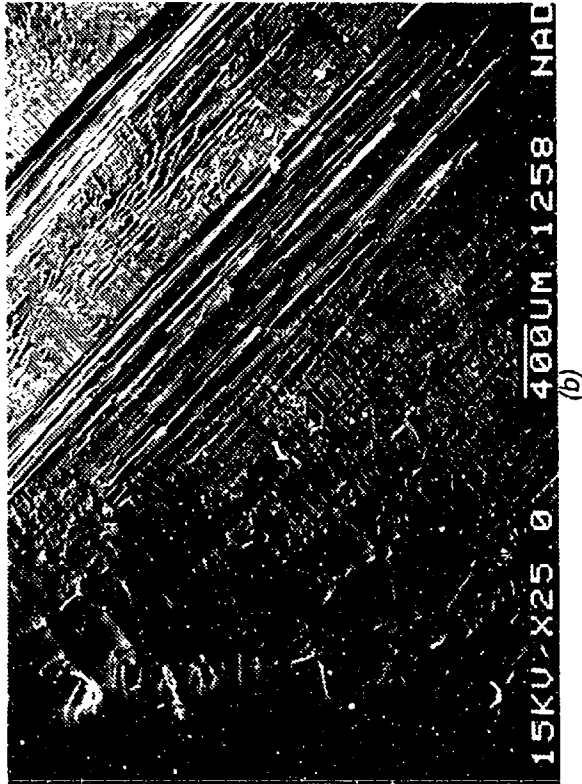
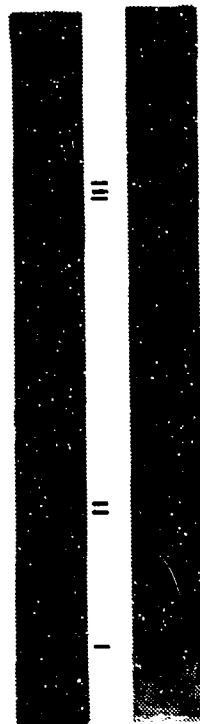


Figure 2-28. Optical and SEM Photographs of Mode I DCB Interlaminar Fracture in Filament Wound Gr/Ep - [+45/-45] _{ss}, Room Temperature Ambient
 (a) Macro photograph
 (b) Initiation in Precrack
 (c) River Patterns in Mode I Area

CD = Crack propagation direction
 R = River patterns





Optical photograph of the filament wound Grl/Ep laminate showing the three regions I, II, and III.

(a)

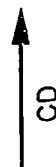
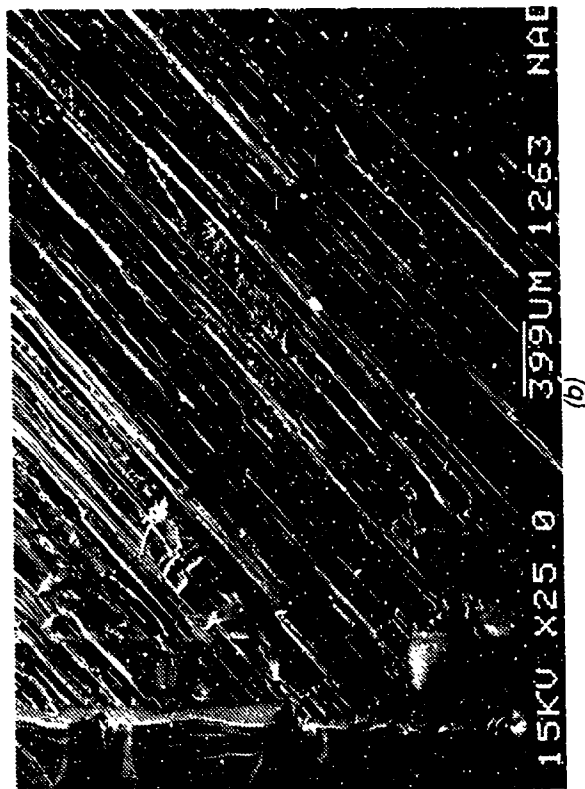
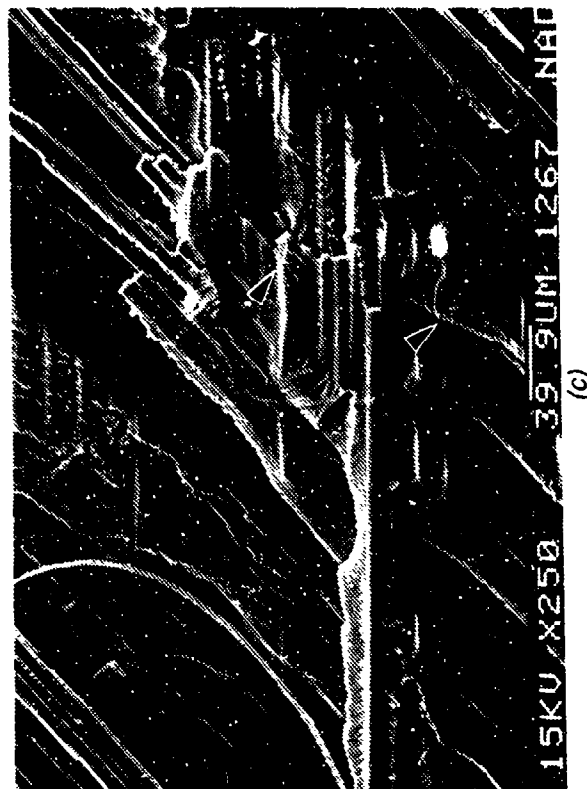


Figure 2-29. Optical and SEM Photographs of Mode I DCB Interlaminar Fracture in Filament Wound Grl/Ep - [+45/0/-45]_{4s}, Room Temperature Ambient
 (a) Macro photograph
 (b) Initiation in Precrack Region
 (c) River Patterns in Mode I Tension Fracture

CD = Crack propagation direction
 R = River patterns



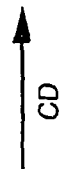
(b)



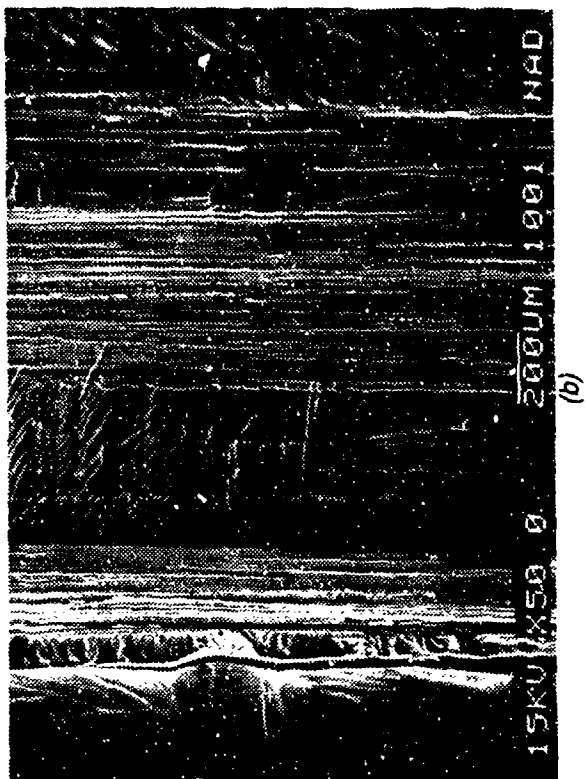
(c)



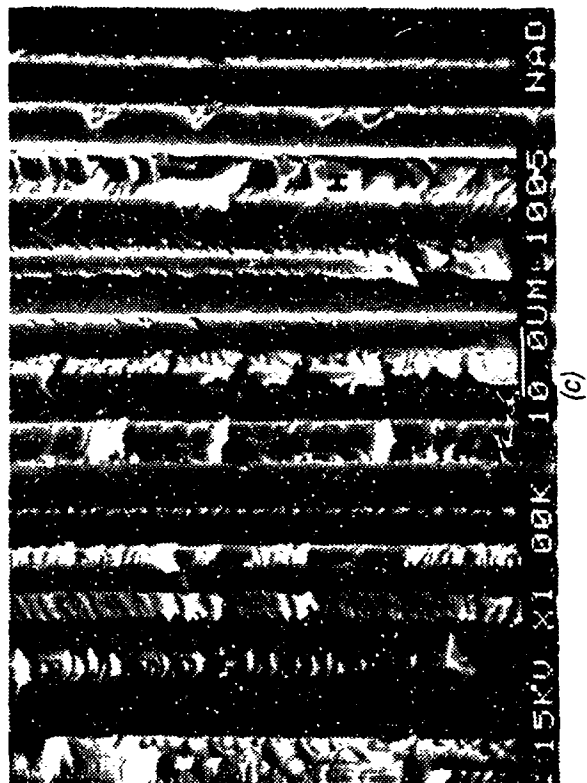
(a)



CD



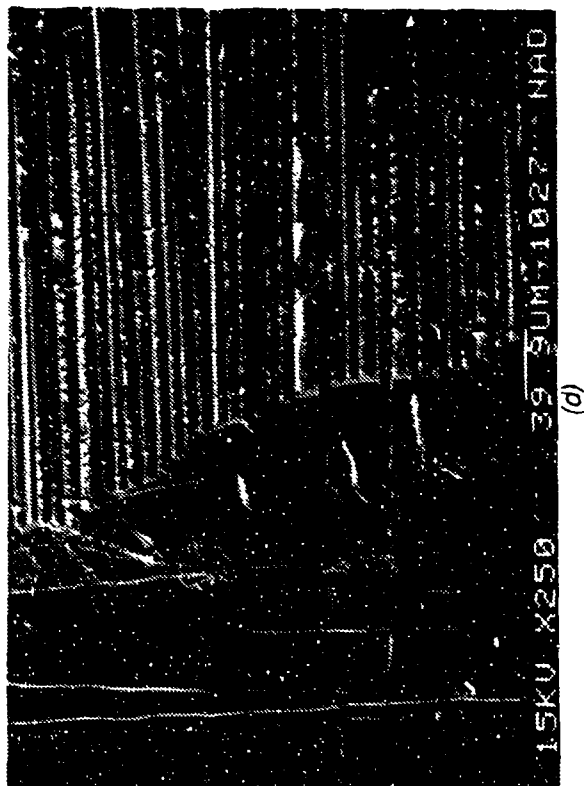
(b)



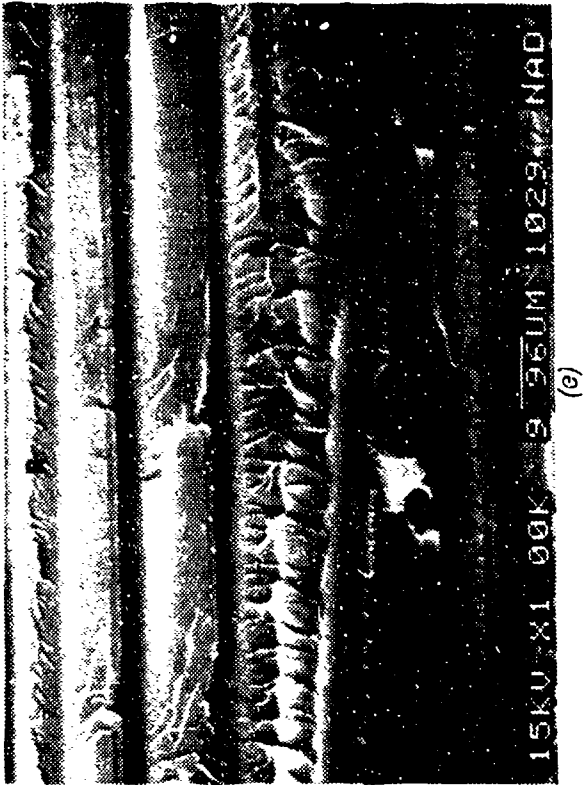
(c)

Figure 2-30. Optical and SEM Photographs of Mode I DCB Interlaminar Fracture in Filament Wound Gr/Ep - [0/90] 6S, Room Temperature Ambient
(a) Macro photograph
(b) Initiation in Precrack Region
(c) Local Hackles in 90 Degree Ply

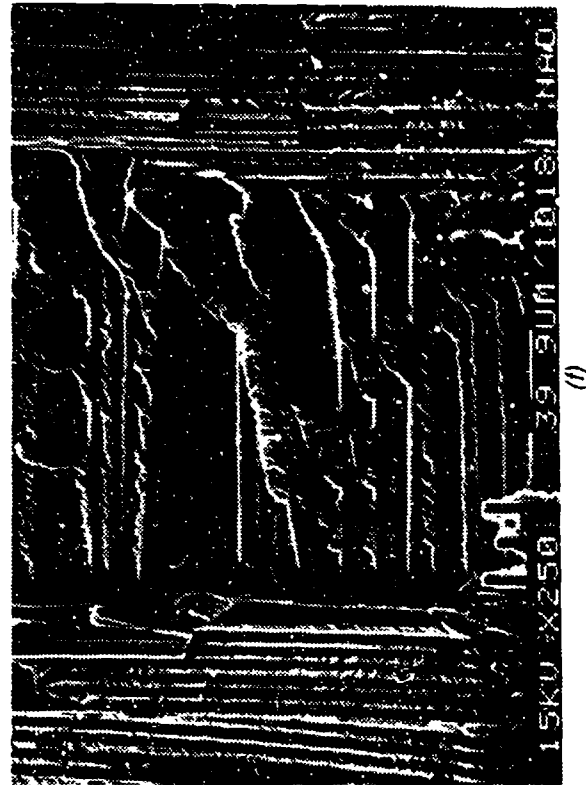
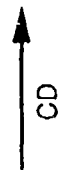
CD = Crack-propagation direction
H = Hackles



(d)



(e)



(f)

Figure 2-30. (Continued)
 (d) Precrack/Crack-Growth Interface
 (e) River Patterns in Epoxy
 (f) River Patterns in Epoxy Away From Interface
 CD = Crack-propagation direction
 R = River patterns

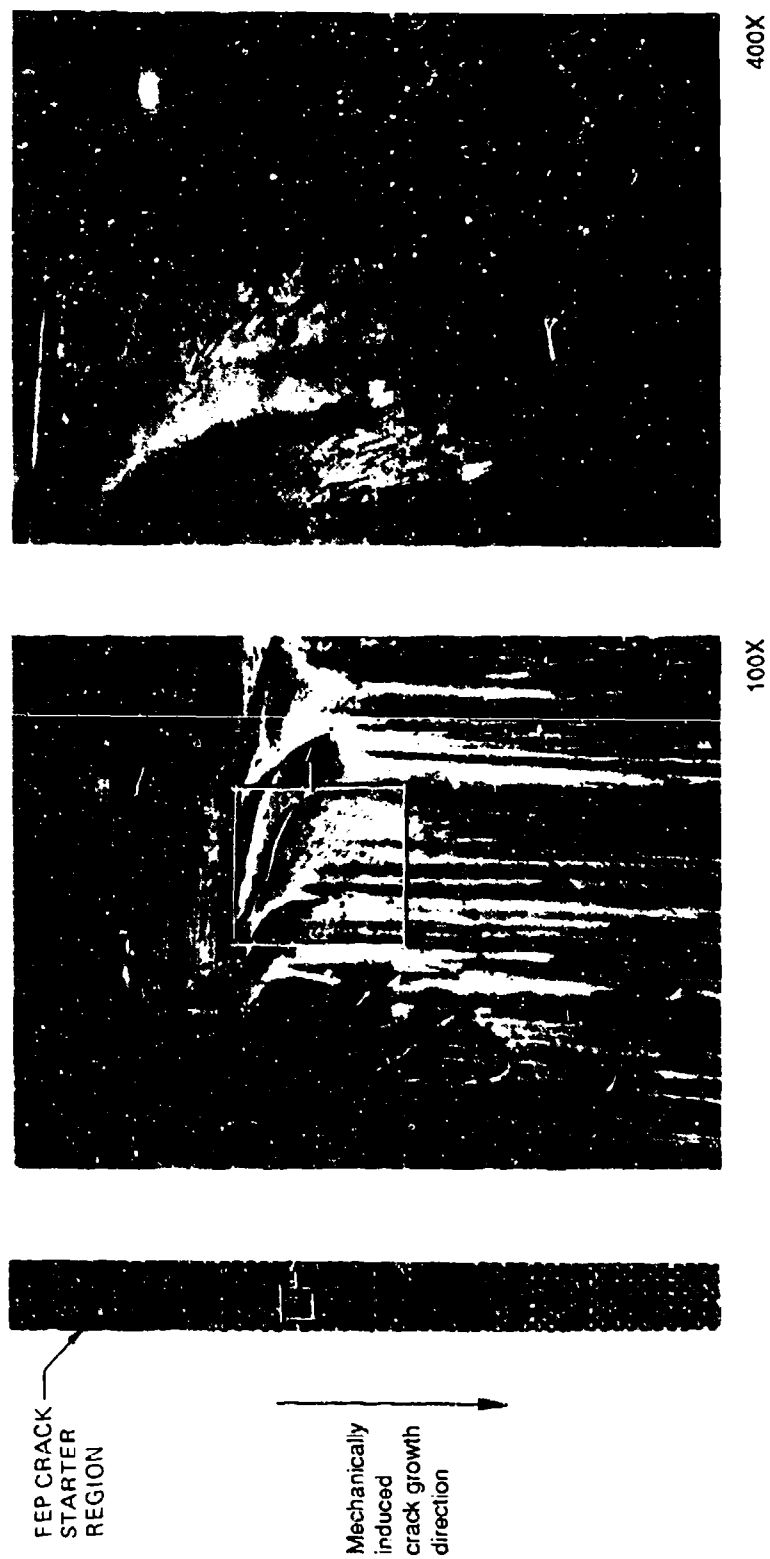
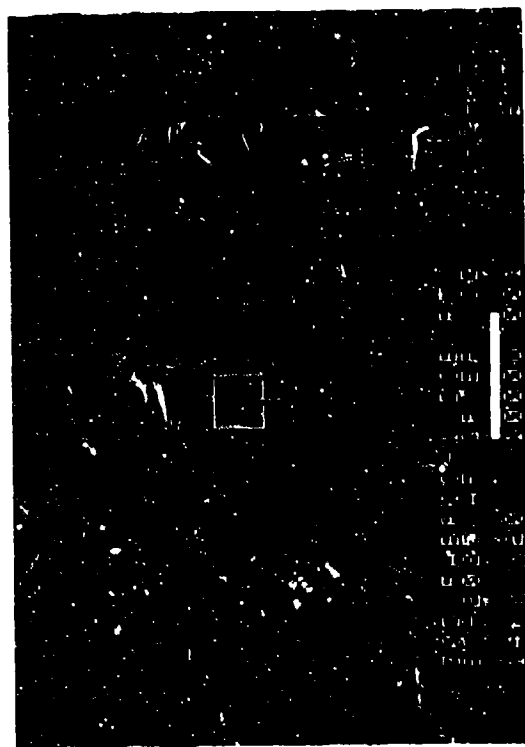
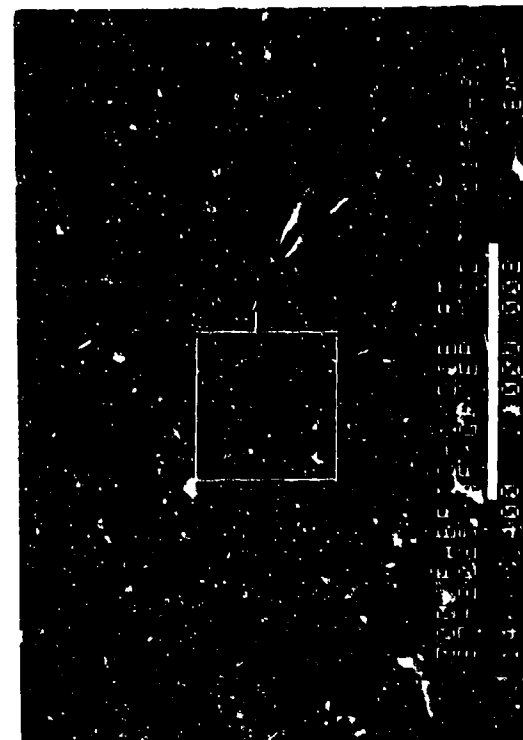


Figure 2-31. Optical Photomicrographs of Interlaminar Mode I Tension, Room Temperature, Fabric Fracture, $[0/90]_{6s}$



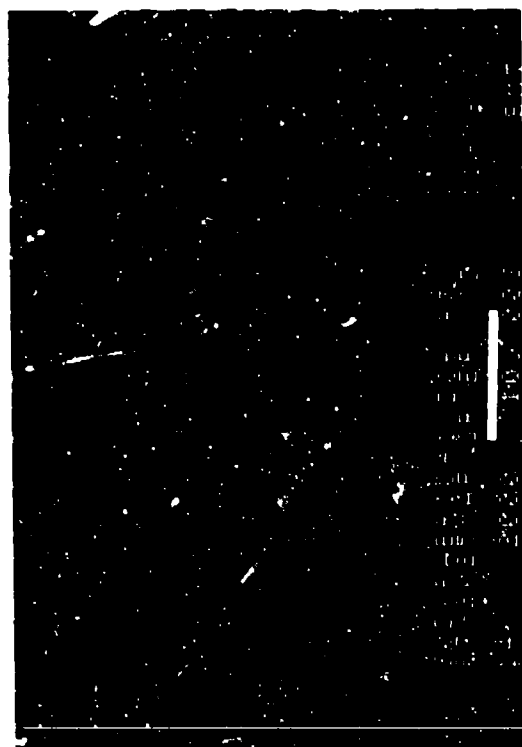
20X

30 degree tilt



400X

30 degree tilt



2,000X

30 degree tilt

Legend:

R rivermarks

Mechanically induced
crack direction



Figure 2-32. SEM Fractographs of Interlaminar Mode I Tension, Room Temperature, Fabric Fracture, [0/90]₆₅

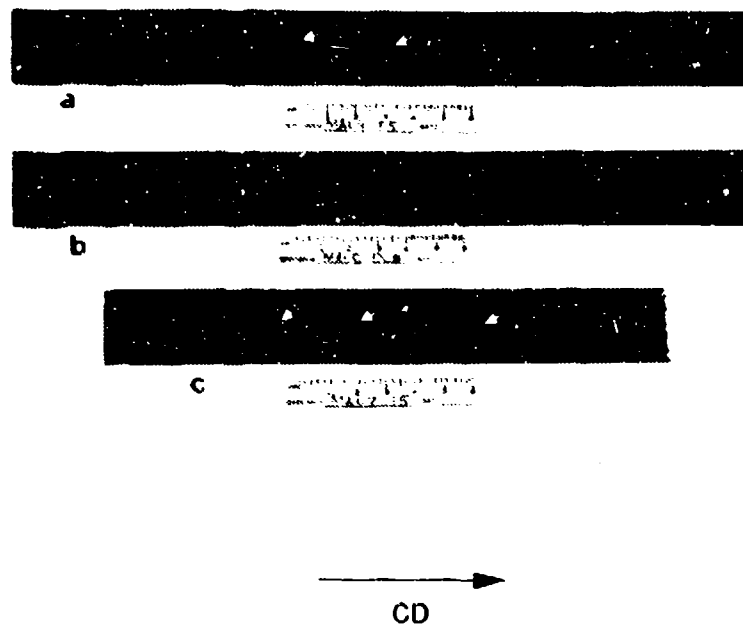
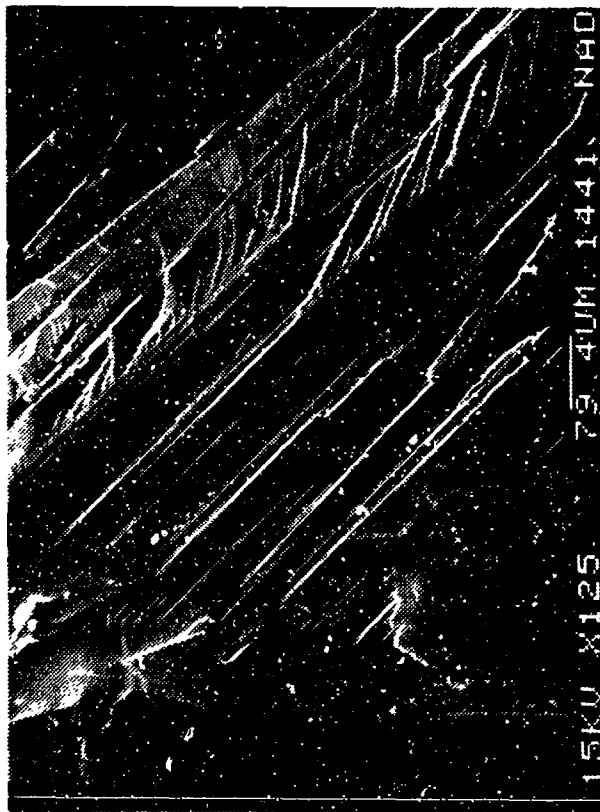


Figure 2-33. Macrophotograph of 3-D Weave Mode I DCB Gr/Ep Coupons
 (a) $[+45/-45]_{6S}$
 (b) $[+45/0/-45]_{4S}$
 (c) $[90/0]_{6S}$

Note: Arrows indicate coarse bands (nbs).
 CD = Crack-propagation direction



(a)



(b)

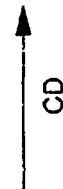


Figure 2-34. SEM Photographs of Mode I DCB Interlaminar Fracture in 3-D Weave Gr/Ep - [+45/-45]_{6s}

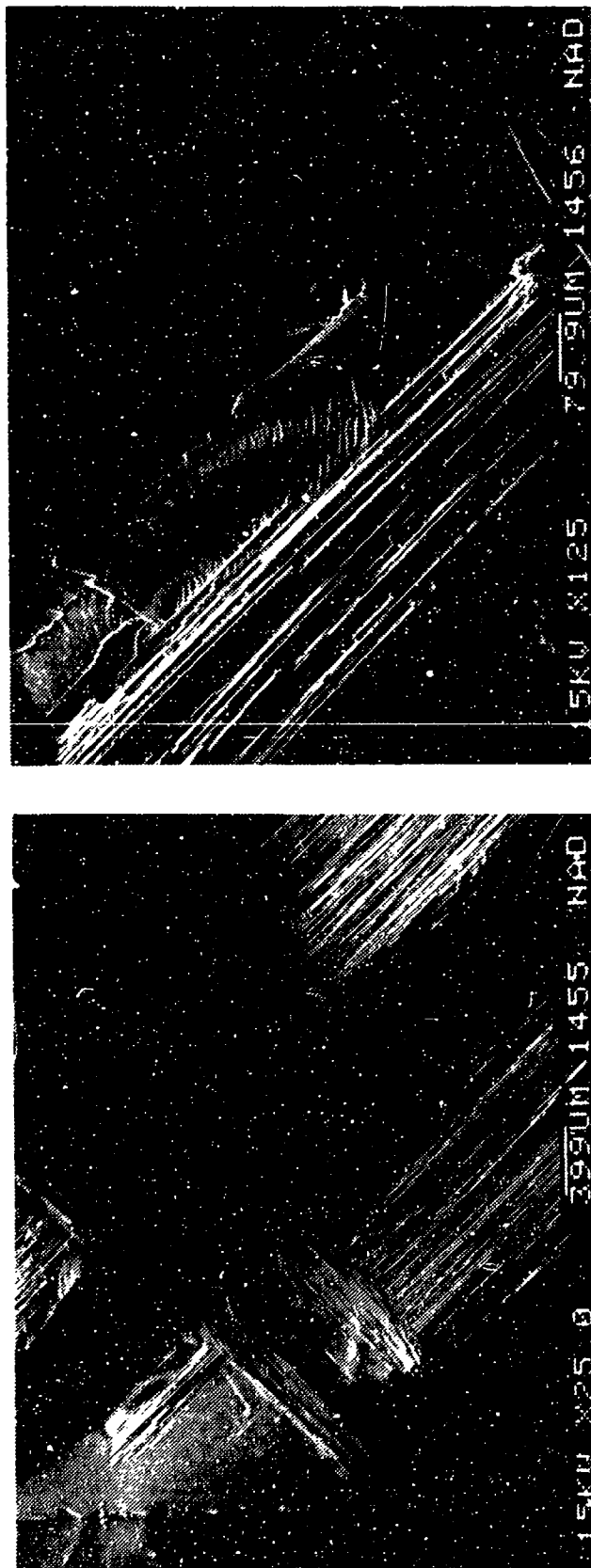
(a) Initiation in Precrack Region of Coupon

(b) River Patterns in Precrack Region

CD = Crack-propagation direction

F = Frayed carbon fibers used in weave

R = River patterns



(a)

(b)

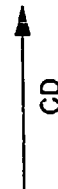


Figure 2-35. SEM Photographs of Mode I DCB Interlaminar Fracture in 3-D Weave Gr/Ep - [+45/0/-45]_{4s}
 (a) Initiation in Precrack Region of Coupon
 (b) River Patterns in Precrack Region

CD = Crack propagation direction
 R = River patterns

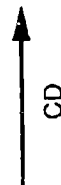
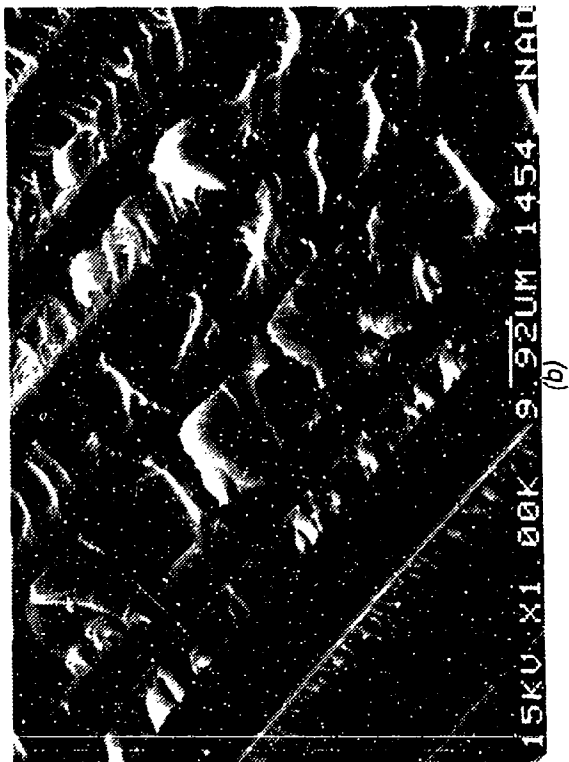
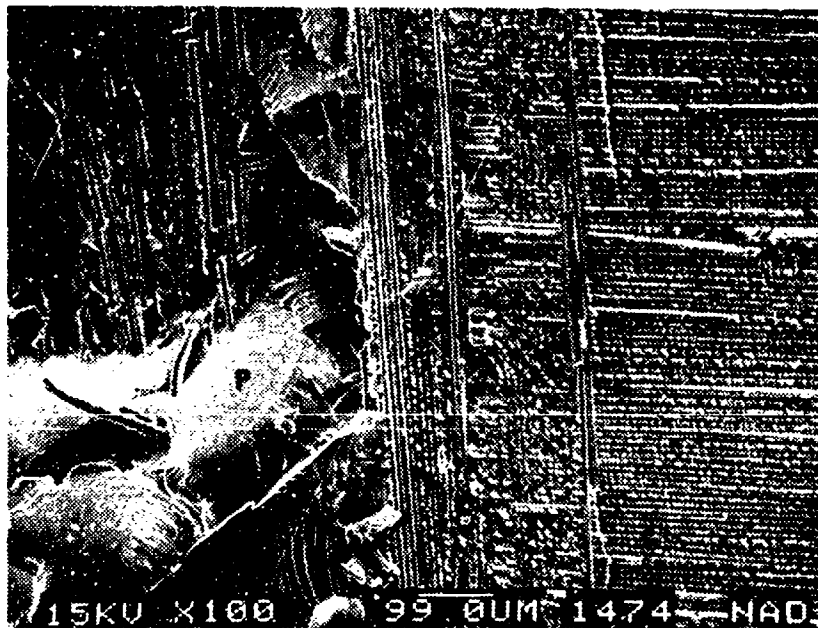
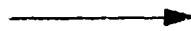


Figure 2-36. SEM Photographs of Mode I DCB Interlaminar Fracture in 3-D Weave Grl/Ep
 (a) Crack-Growth Region in $[+45/-45]_{ss}$
 (b) Higher Magnification of (a) Showing Hackles
 (c) Fractured Resin Pocket and Hackles in Crack-Growth Region of $[+45/0/-45]_{4s}$

CD = Crack-propagation direction
 F = Frayed carbon fibers
 H = Hackles
 P = Resin pocket
 R = River patterns




 CD

**Figure 2-37. SEM Photographs of Mode I DCB Fracture in 3-D Weave
 Gr/Ep - $[0/90]_{6S}$ in Crack-Growth Region**
 CD = Crack-propagation direction
 P = Resin pocket adjacent to carbon fiber used in weave



(a)

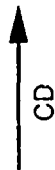
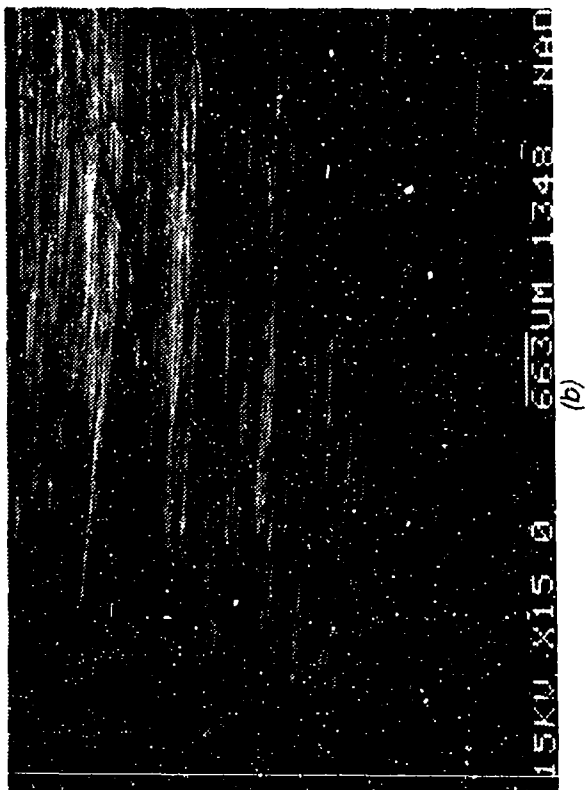
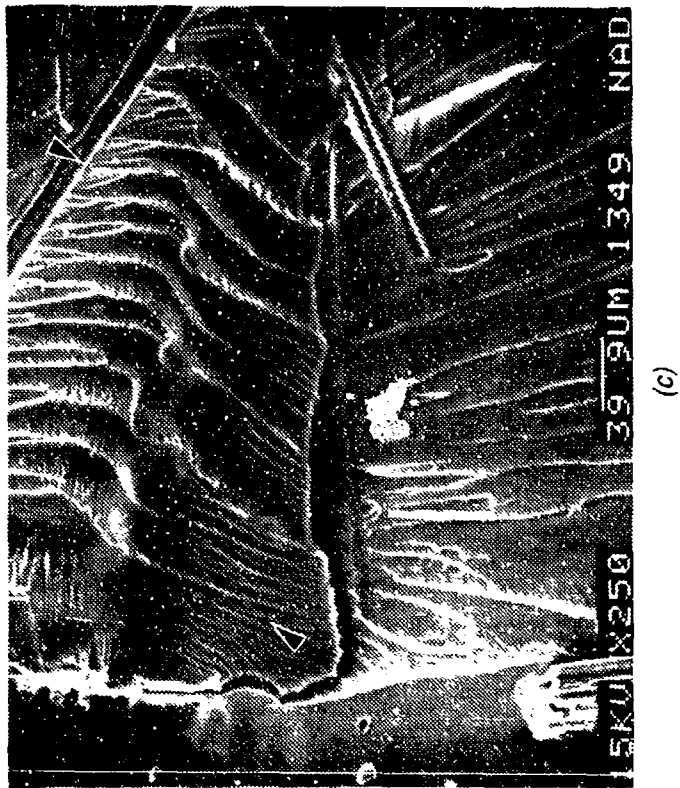


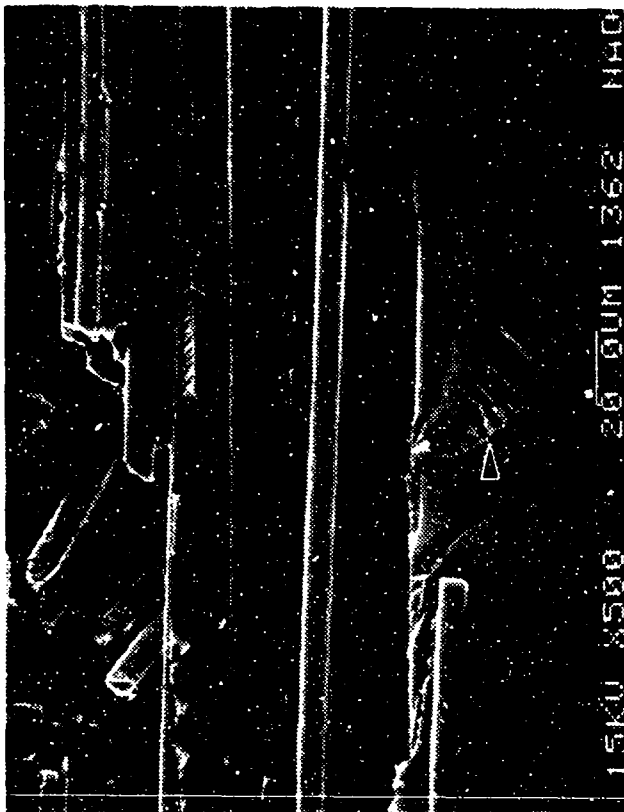
Figure 2-38. Optical and SEM Photographs of Mode I DCB Interlaminar Fracture in $\text{Gr/Ep} - [0]_{24T}$, Impact Damaged Before Test
 (a) Macrophotograph
 (b) Initiation in Precrack
 (c) River Patterns (R) in Mode I Region
 CD = Crack-propagation direction



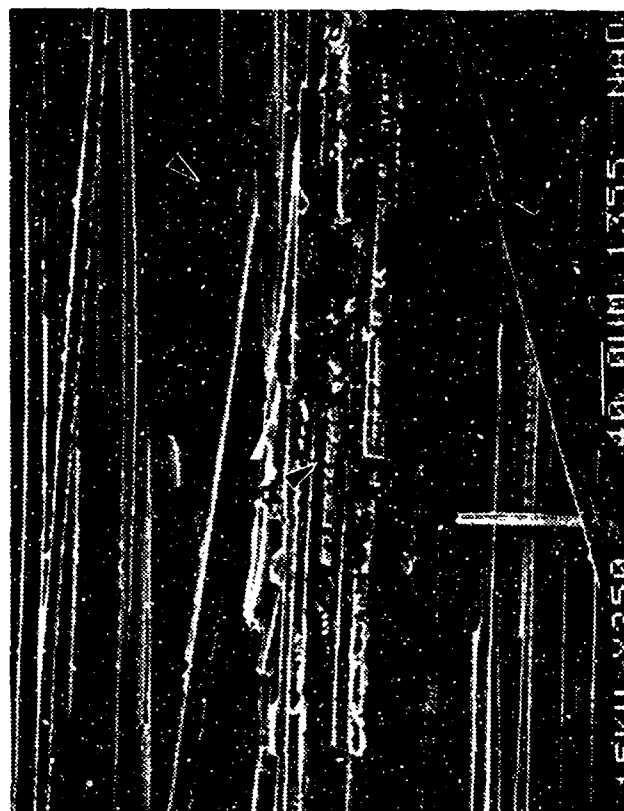
(b)



(c)



(d)



(e)

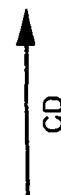
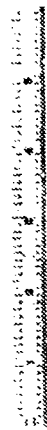


Figure 2-38. (Continued)
 (d) Impact Center
 (e) Broken Fibers in Impact Area
 Note river patterns in resin
 CD = Crack-propagation direction
 H = Hackles (cusps)
 R = River patterns



(a)

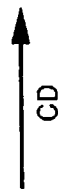
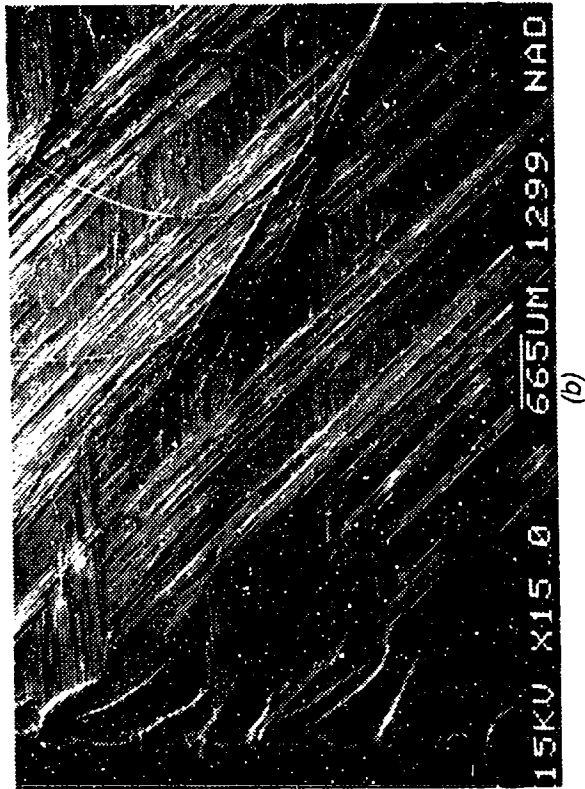


Figure 2-39. Optical and SEM Photographs of Mode I DCB Interlaminar Fracture in Gr/Ep - [+45/0/-45]_{4s}. Impact Damaged Before Test
 (a) Macro photograph
 (b) Initiation in Precrack Region
 (c) River Patterns (R) in Region I

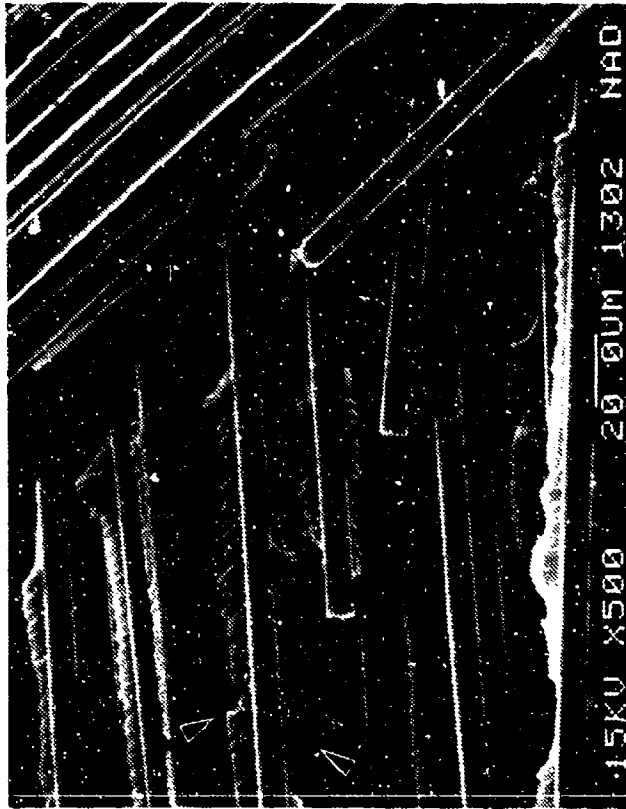
CD = Crack-propagation direction



(b)



(c)



(e)



(d)

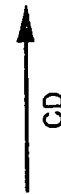
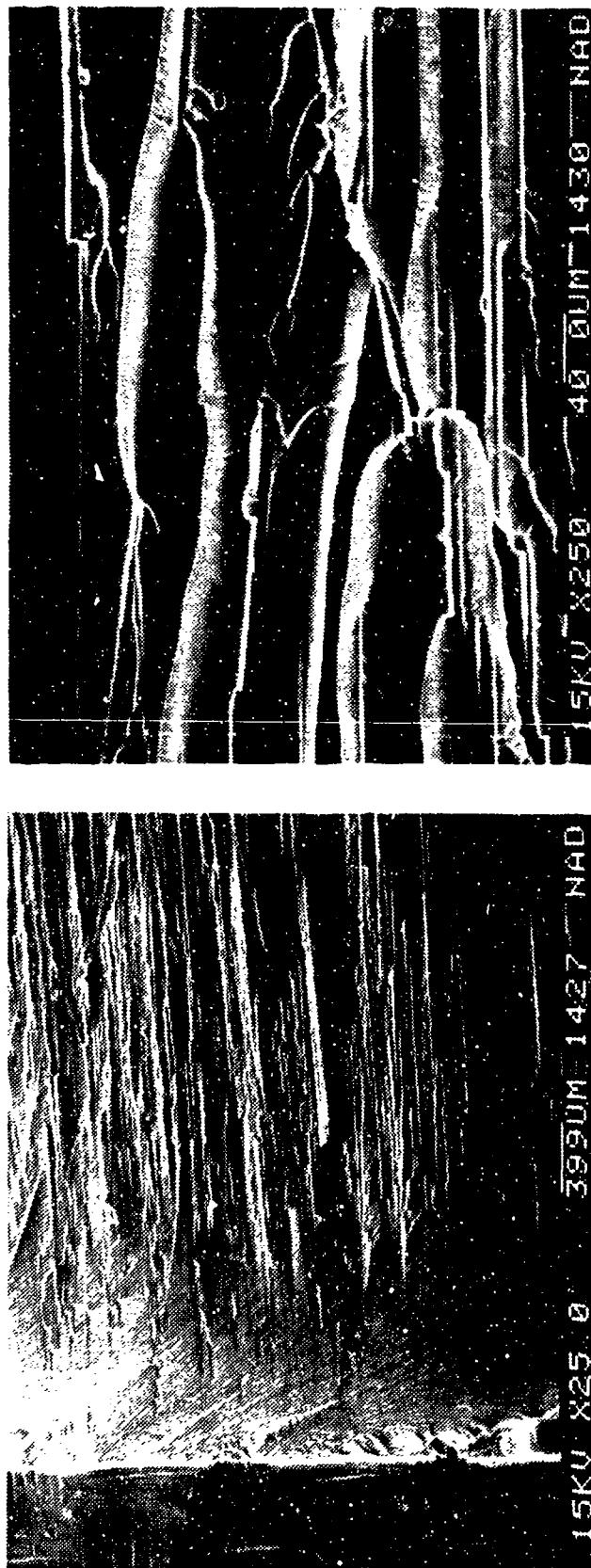


Figure 2-39. (Continued)
 (d) Impact Center
 (e) Interlaminar Fracture Away From Impact

CD = Crack propagation direction
 H = Hackles (cusps)
 R = River patterns



(a)

(b)

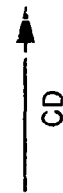


Figure 2-40. SEM Photographs of Mode I DCB Interlaminar Fracture in Gr/Ep - [0]_{24T}, Water Immersed Before Test

(a) Initiation in Precrack Region

(b) River Patterns in Crack-Growth Region

CD = Crack-propagation direction

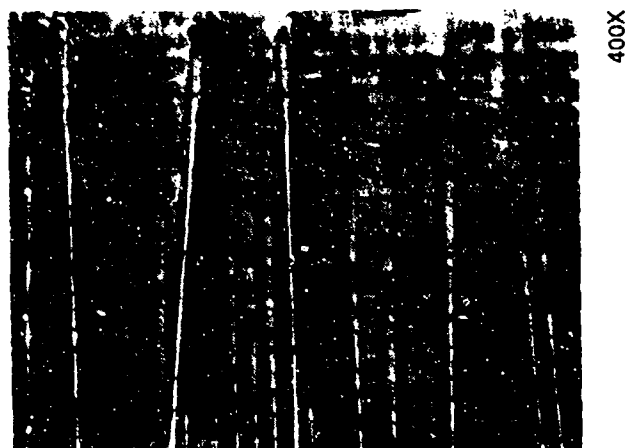
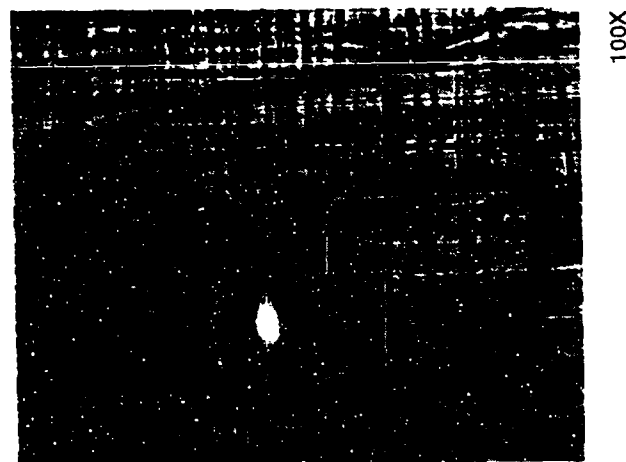
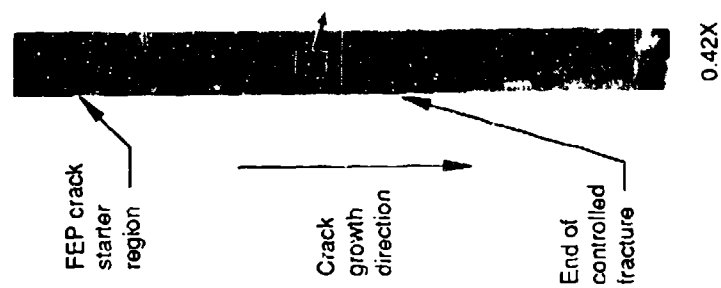
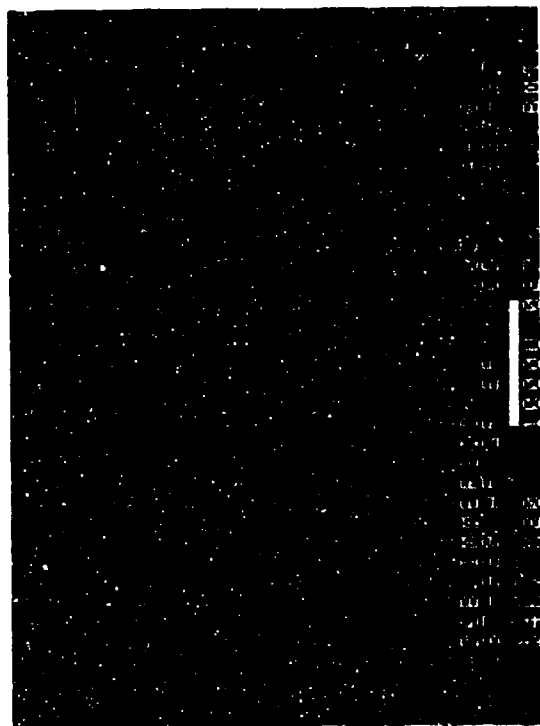


Figure 2-41. Optical Photomicrographs of Interlaminar Mode I Tension, 0/90 Fracture, Water Immersed (160 F) After Test



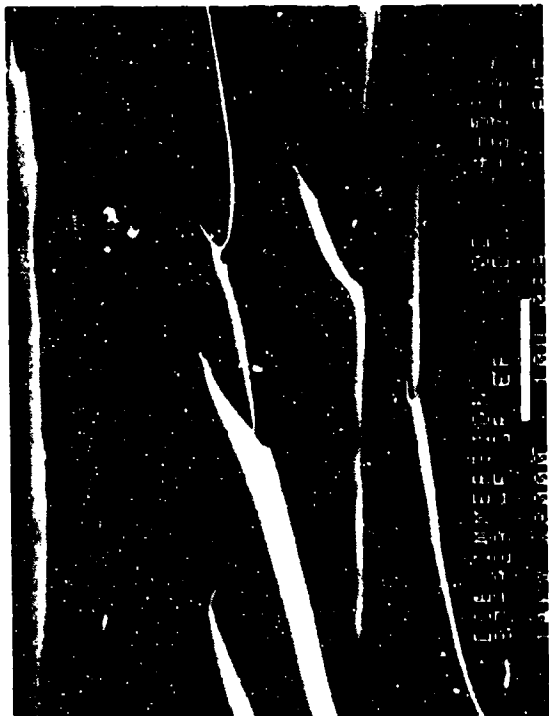
0 degree tilt

20X



0 degree tilt

400X



0 degree tilt

2,000X

Legend:

- M matrix fracture
- F fiber matrix separation
- R rivermarks

Mechanically induced
crack direction



Figure 2-42. SEM Fractographs of Interlaminar Mode I Tension, 0/90 Fracture, Water Immersed (160 F) After Test

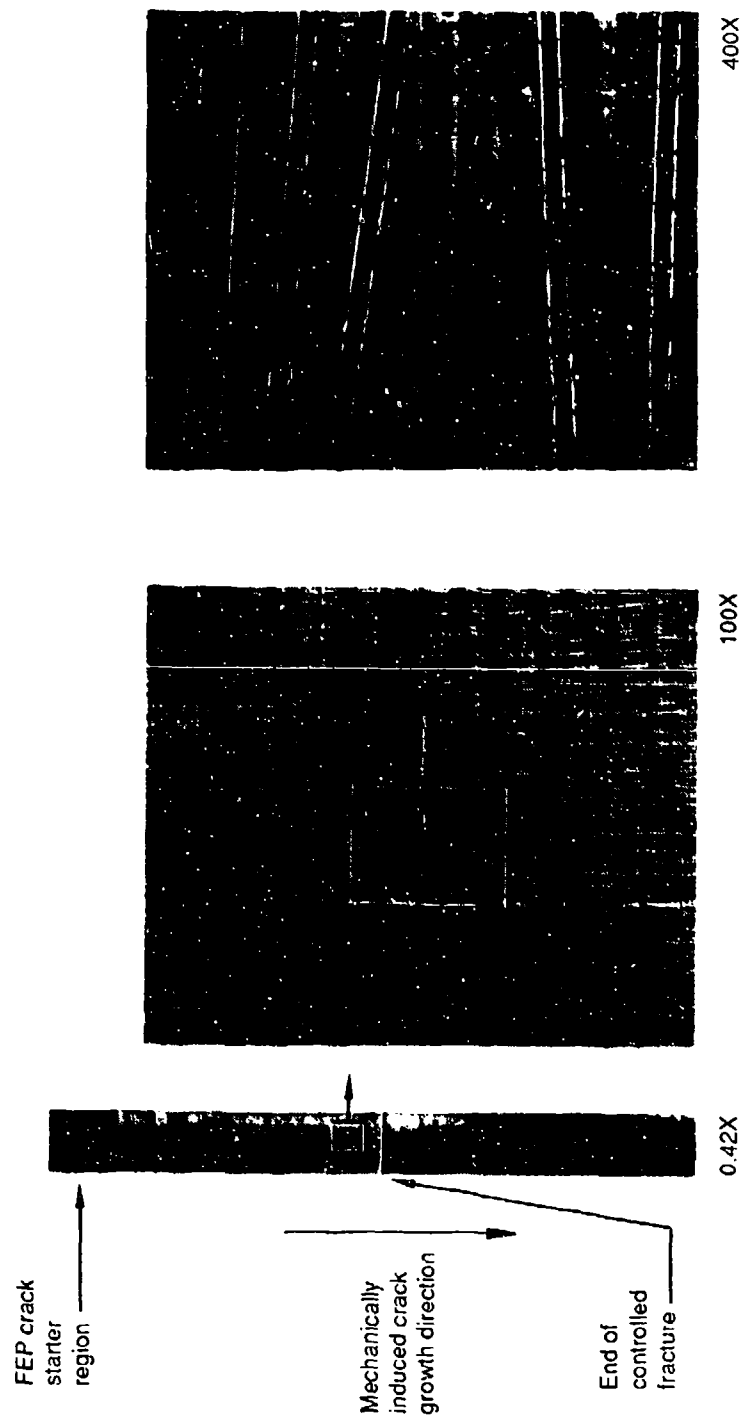
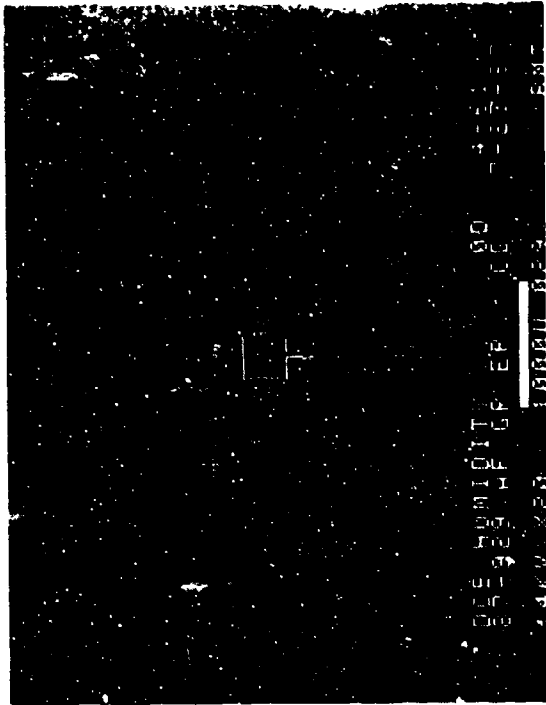
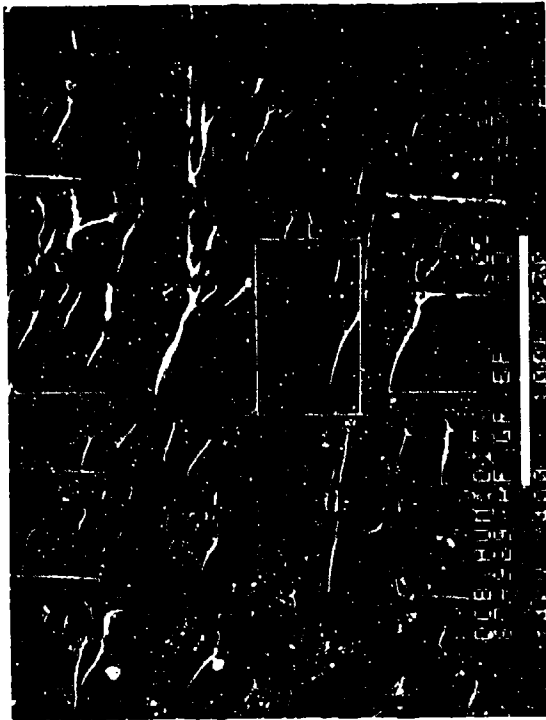


Figure 2-43. Optical Photomicrographs of Interlaminar Mode I Tension, 0/90 Fracture, Exposure to Humidity (160 F) After Test



0 degree tilt 20X

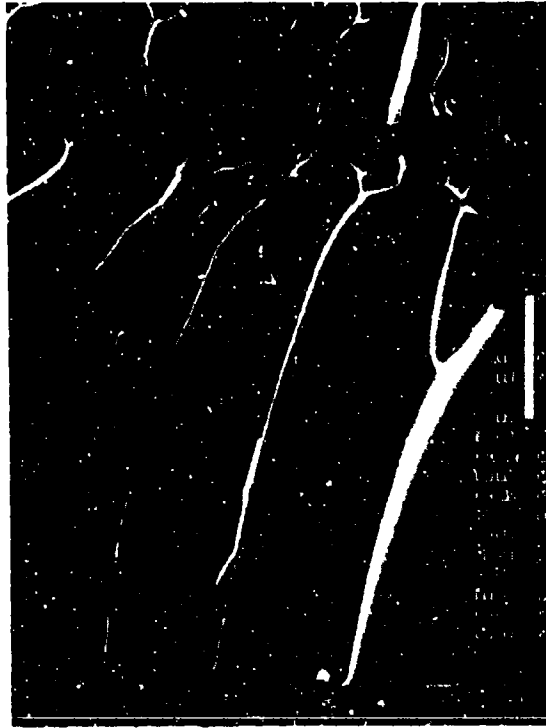


0 degree tilt 400X

Legend:

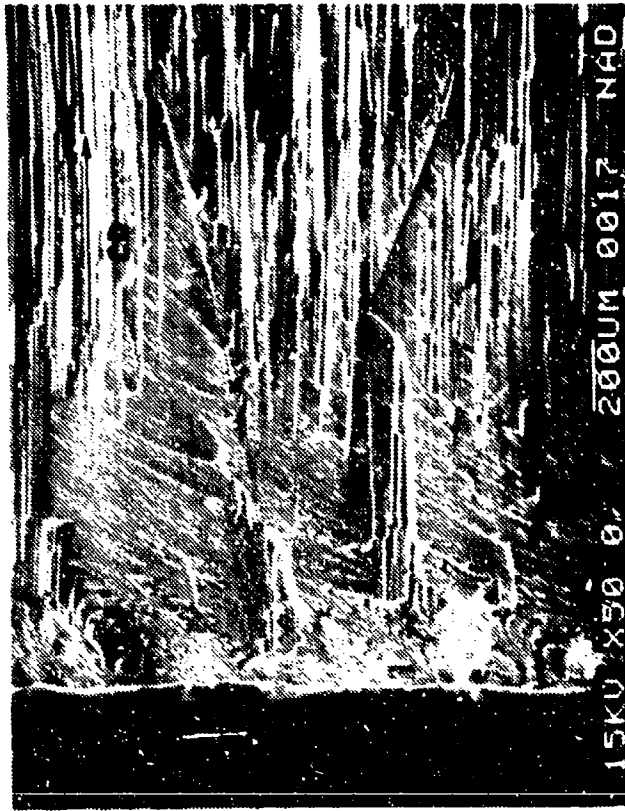
- M matrix fracture
- F fiber matrix separation
- R rivermarks

Mechanically induced
crack direction

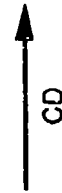


0 degree tilt 2,000X

Figure 2-44. SEM Fractographs of Interlaminar Mode I Tension, 0/90 Fracture, Exposure to Humidity (160 F) After Test



(b)



(a)

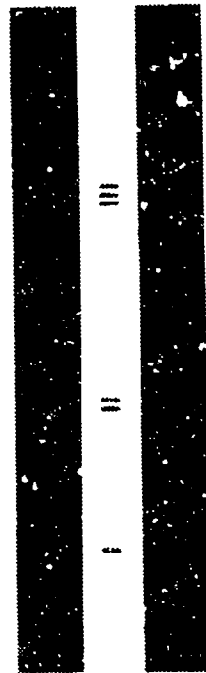
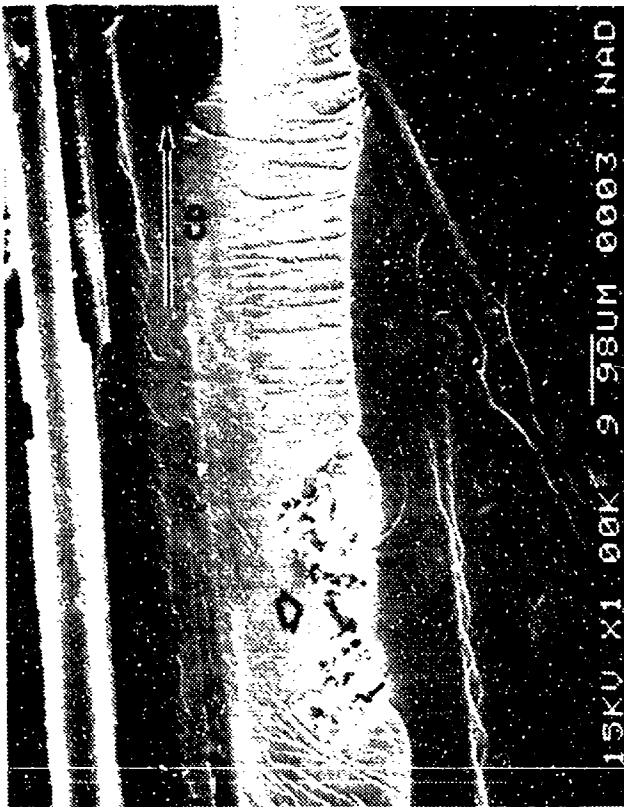
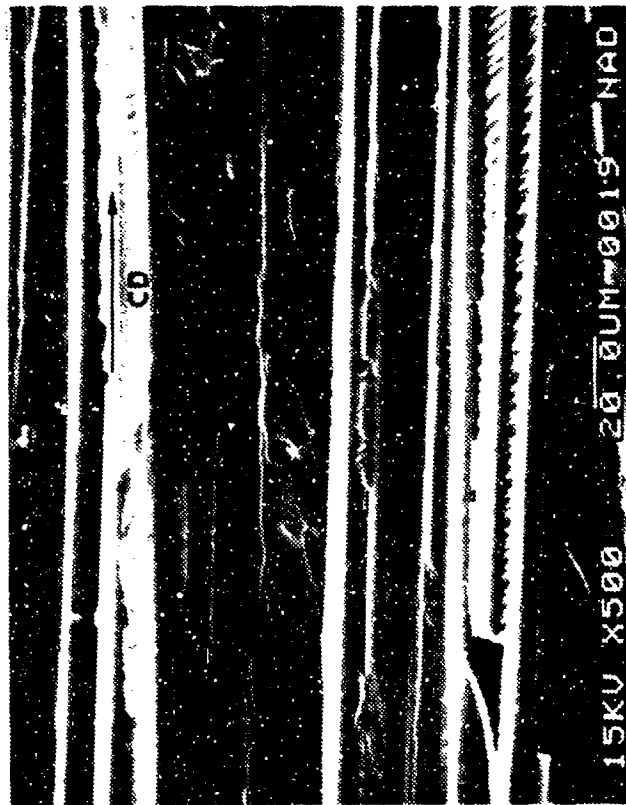


Figure 2-45. Optical and SEM Photographs of Mode I DCB Interlaminar Fracture in Undercured Gr/Ep - [0]_{24T}
 (a) Macro photograph showing Regions I, II, and III
 (b) Initiation in Region I Adjacent to Armalor (A)

CD = Crack-propagation direction



(c)



(d)

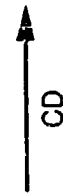


Figure 2-45. (Continued)
 (c) River Patterns Indicating Crack-Propagation Direction
 (d) Porosity (Arrows)

CD = Crack-propagation direction

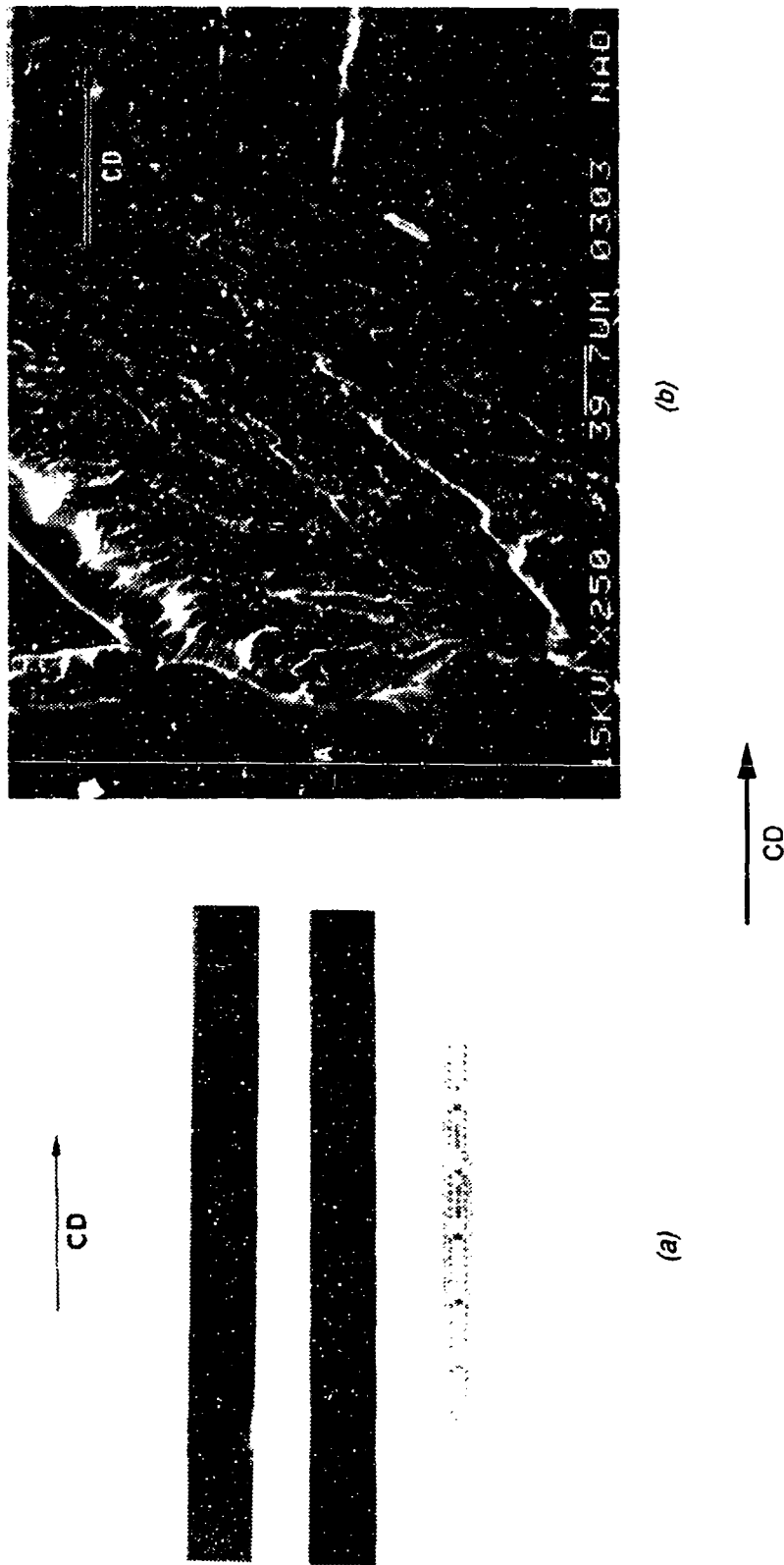


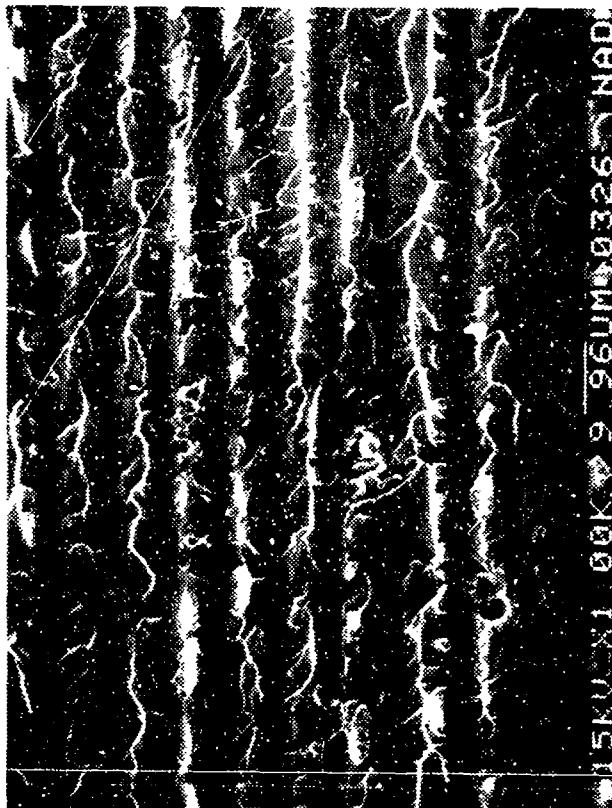
Figure 2-46. Optical and SEM Photographs of Mode I DCB Interlaminar Fracture in Undercured Gr/Ep - [+45/0/-45]_{4s}
 (a) Macro photograph Showing Radial Bands
 (b) Local Fracture Initiating in Region I

A = Armaton Insert

CD = Crack-propagation direction



(c)



(d)

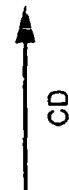


Figure 2-46. (Continued)
 (c) River Patterns in Fractured Epoxy
 (d) Local Porosity in Specimen

CD = Crack-propagation direction



(a)

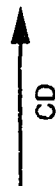
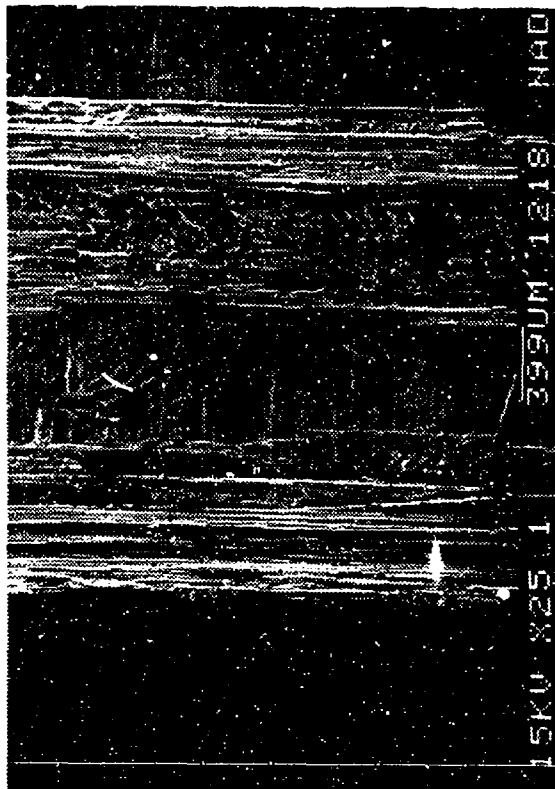
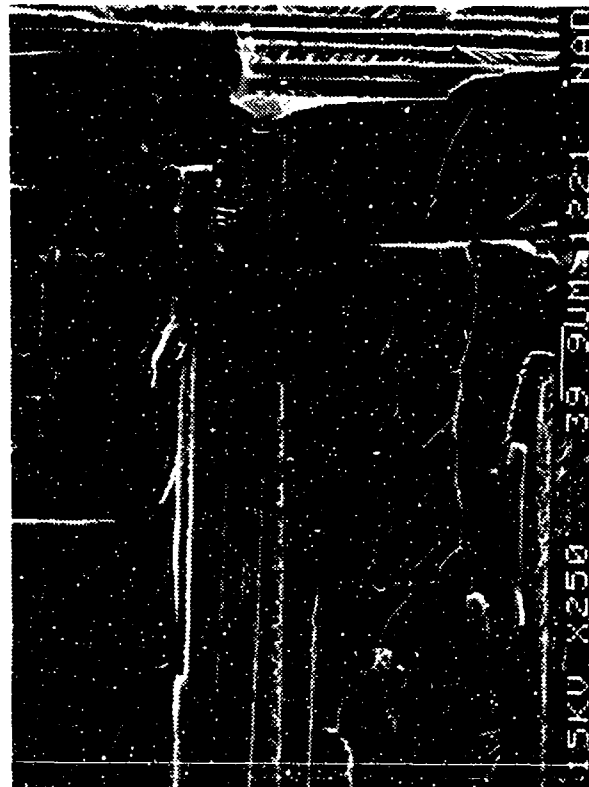


Figure 2-47. Optical and SEM Photographs of Mode I DCB Interlaminar Fracture in Undecured Gr/Ep - [0/90]_{as}
 (a) Macro photograph
 (b) Initiation in Precrack Region
 (c) River Patterns (R) in Region II

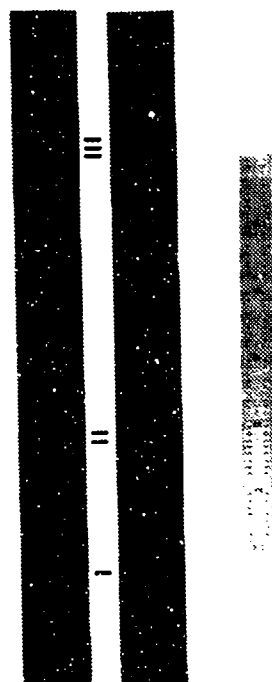
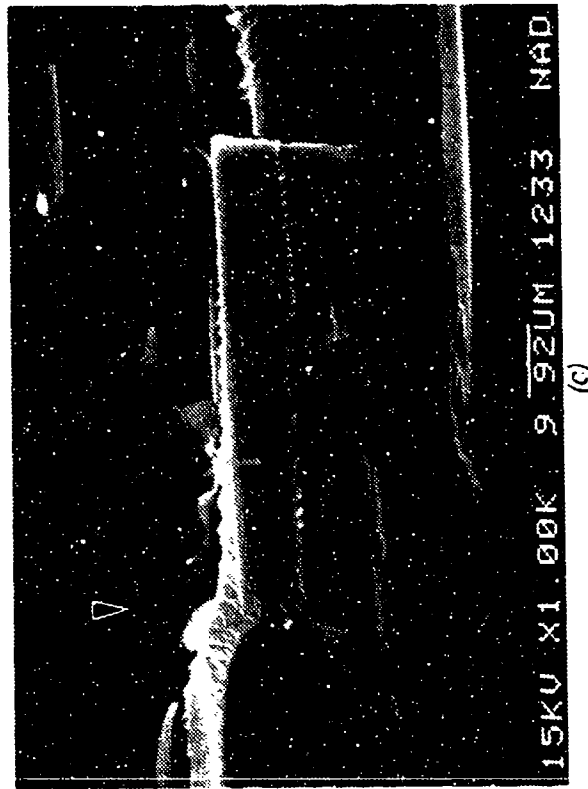
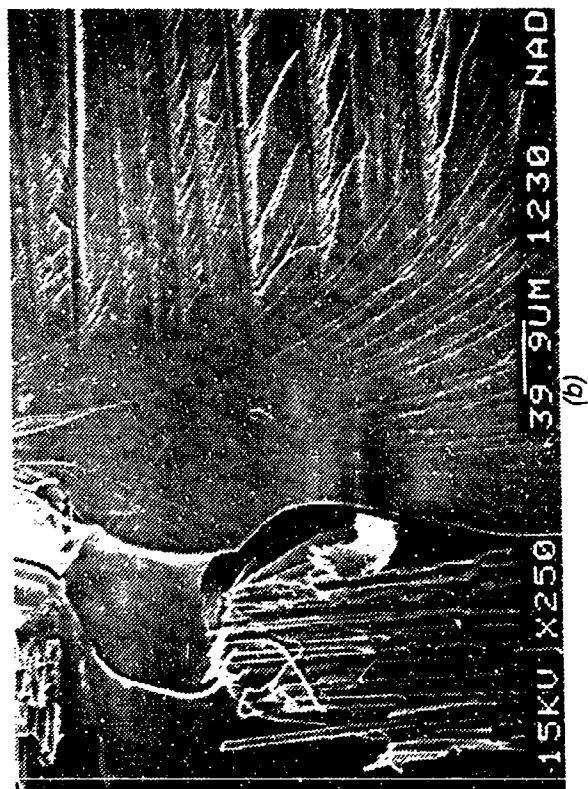
CD = Crack-propagation direction



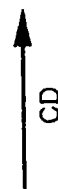
(b)



(c)



(a)



CD

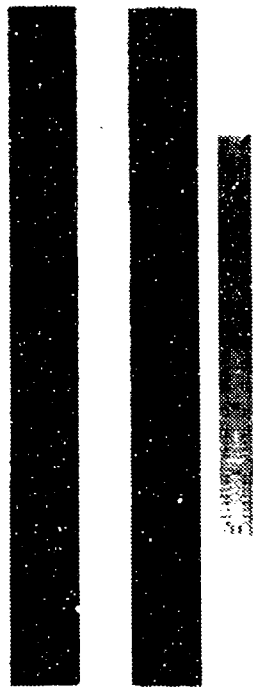
Figure 2-48. Optical and SEM Photographs of Mode I DCB Interlaminar Fracture in Overcured Gr/Ep - [0]_{24T}

(a) Macrophotograph

(b) Initiation in Precrack Region

(c) River Patterns (R) in Region II

CD = Crack-propagation direction



(a)

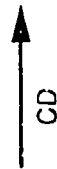


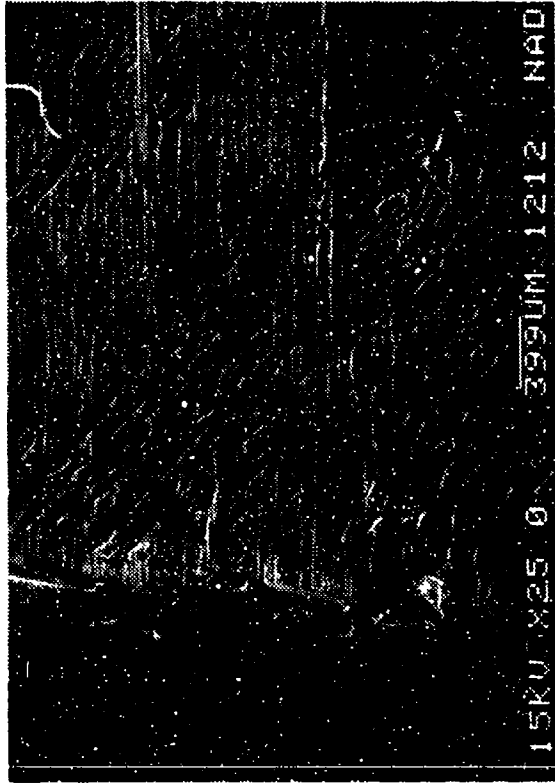
Figure 2-49. Optical and SEM Photographs of Mode I DCB Interlaminar Fracture in Overcured Gr/Ep - [+45/0/-45] _{4s}

(a) Macrophotograph

(b) Initiation in Precrack Region

(c) River Patterns (R) in Mode I Region

CD = Crack-propagation direction



(b)



(c)

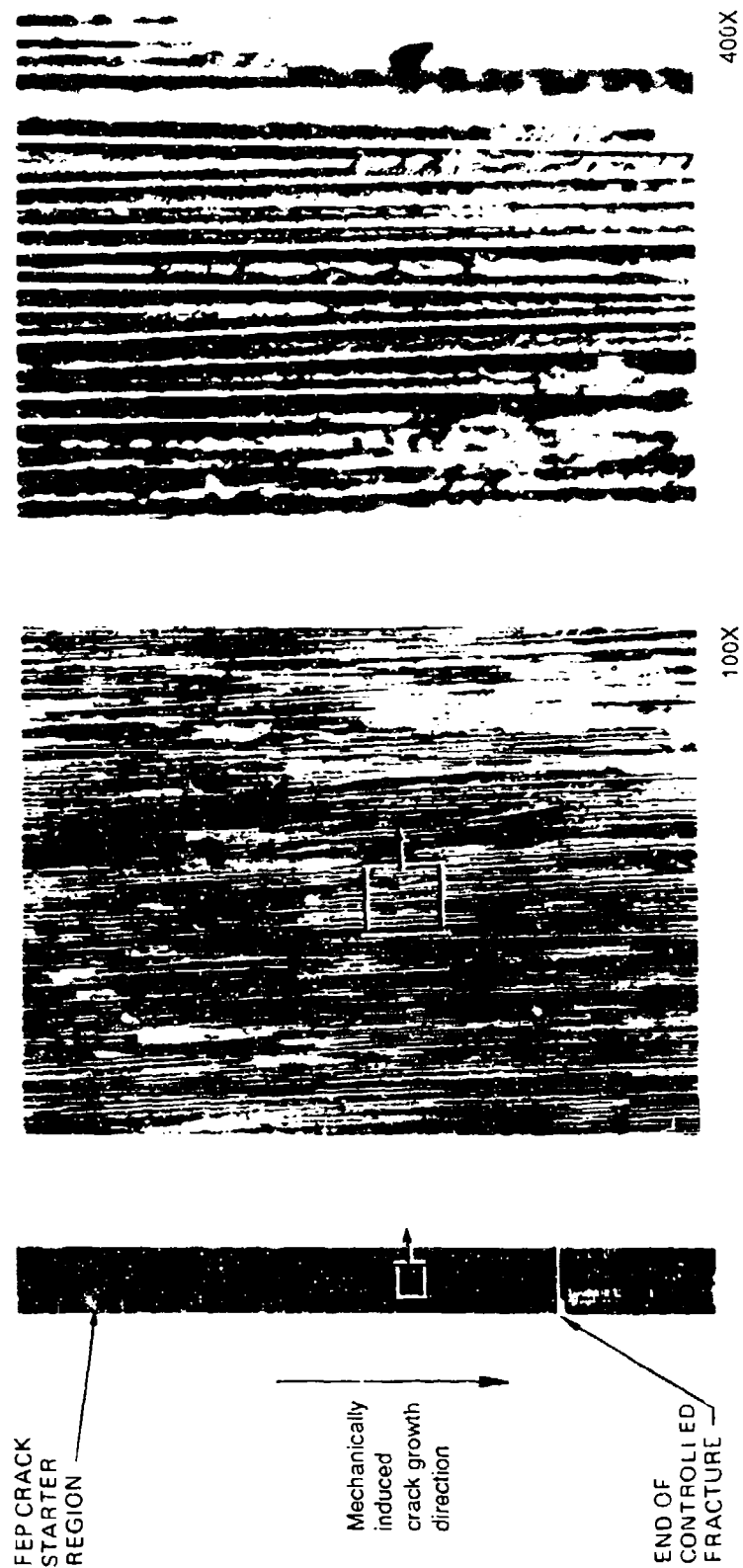
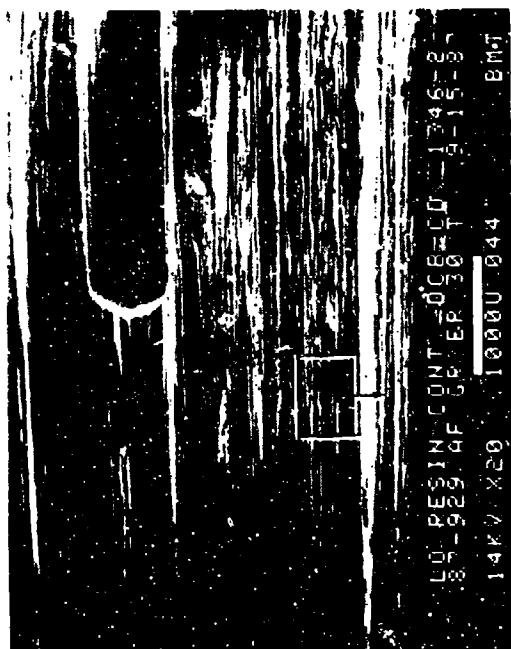
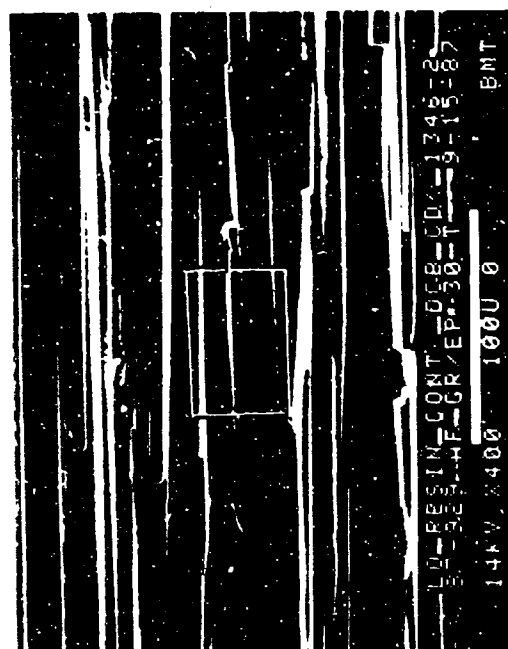


Figure 2-50. Optical Photomicrographs of Interlaminar Mode I Tension, 0/90 Fracture of Low Resin Content Specimen



30 degree tilt

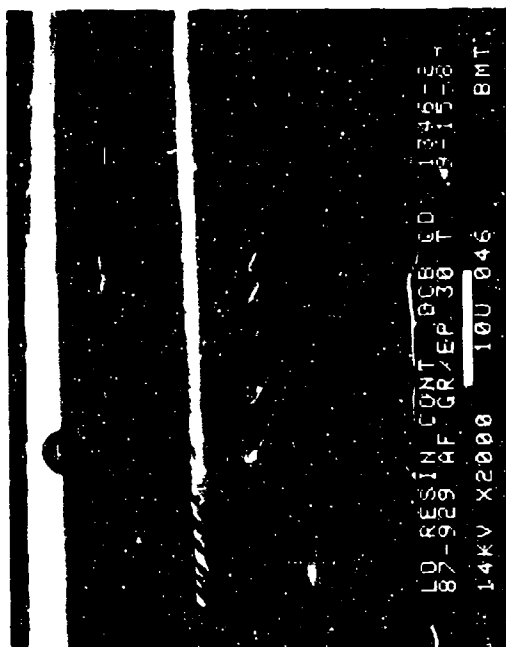


30 degree tilt

Legend:

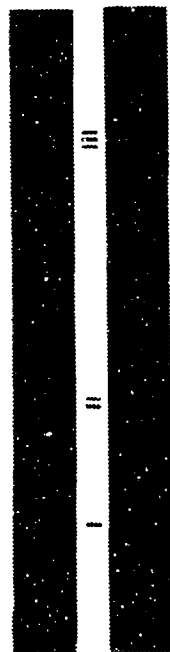
- M matrix fracture
- F fiber/matrix separation
- R rivermarks

Mechanically induced crack direction

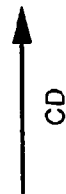


30 degree tilt

Figure 2-51. SEM Fractographs of Interlaminar Mode I Tension, 0/90 Fracture of Low Resin Content Specimen



(a)



CD

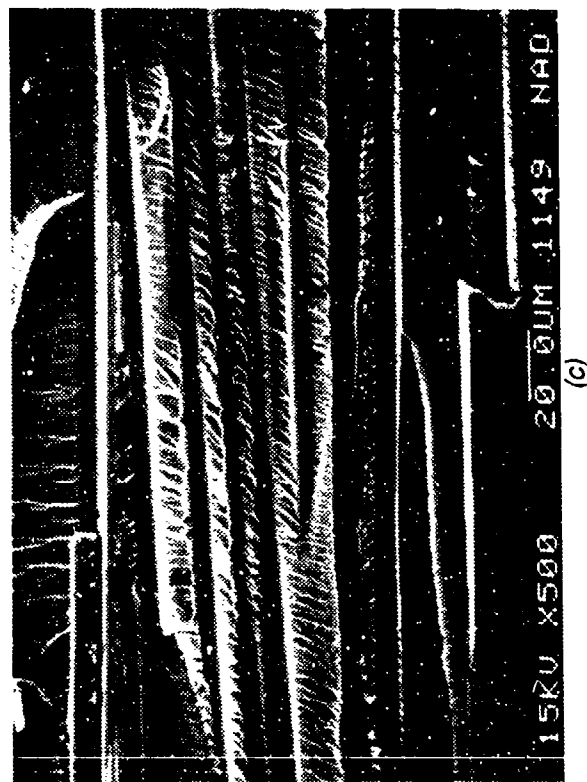
Figure 2-52. Optical and SEM Photographs of Mode I DCB Interlaminar Fracture in High Resin Content Gr/Ep - [0] ^{24T}

- (a) Macro photograph
- (b) Low Magnification SEM Photograph of Precrack Region
- (c) River Patterns in Mode I Region

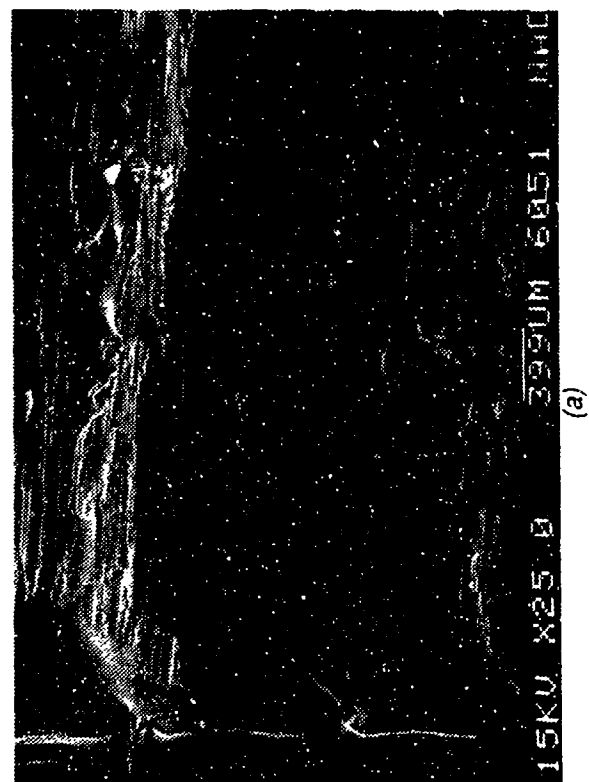
CD = Crack propagation direction



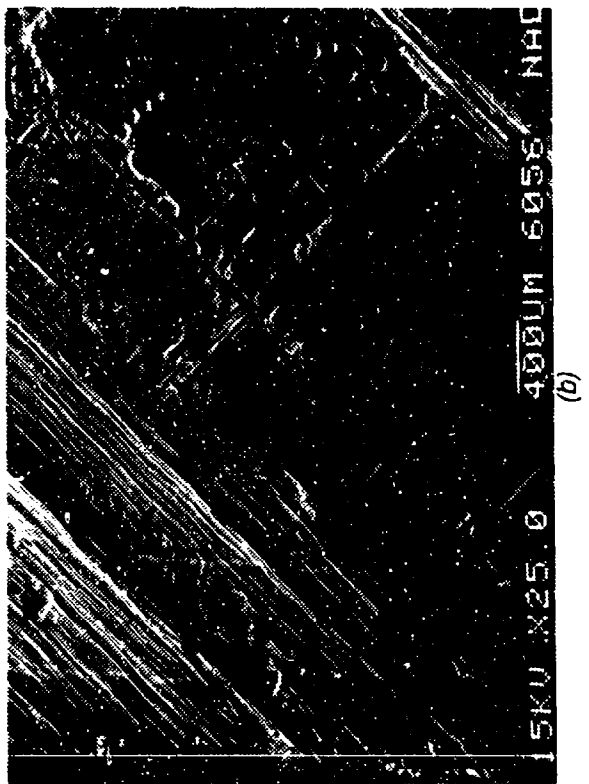
(b)



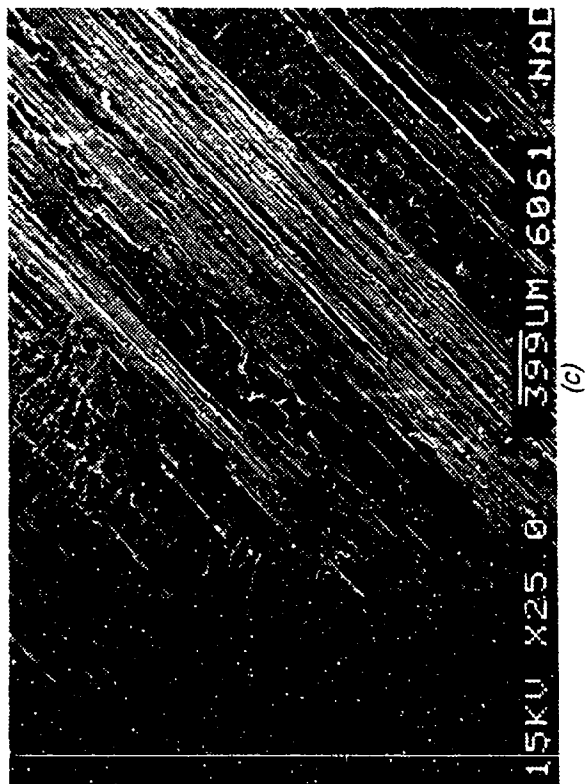
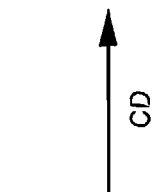
(c)



(a)



(b)



(c)

Figure 2-53. SEM Photographs of Mode I DCB Interlaminar Fracture in High Resin Content Gr/Ep, Conditioned 180 F Dry (a), (b), and (c) Initiation in Precrack Regions of [0]_{24T}, [+45/-45]_{4S}, and [+45/0/-45]_{6S} Coupons, Respectively

CD = Crack-propagation direction



(a)



(b)



Figure 2-54. SEM Photographs of Mode I DCB Interlaminar Fracture Details in High Resin Content Gr/Ep, Conditioned 180 F Dry After Test

(a) $[0]_{24T}$

(b) $[+45/0/-45]_{4S}$

CD = Crack-propagation direction
R = River patterns

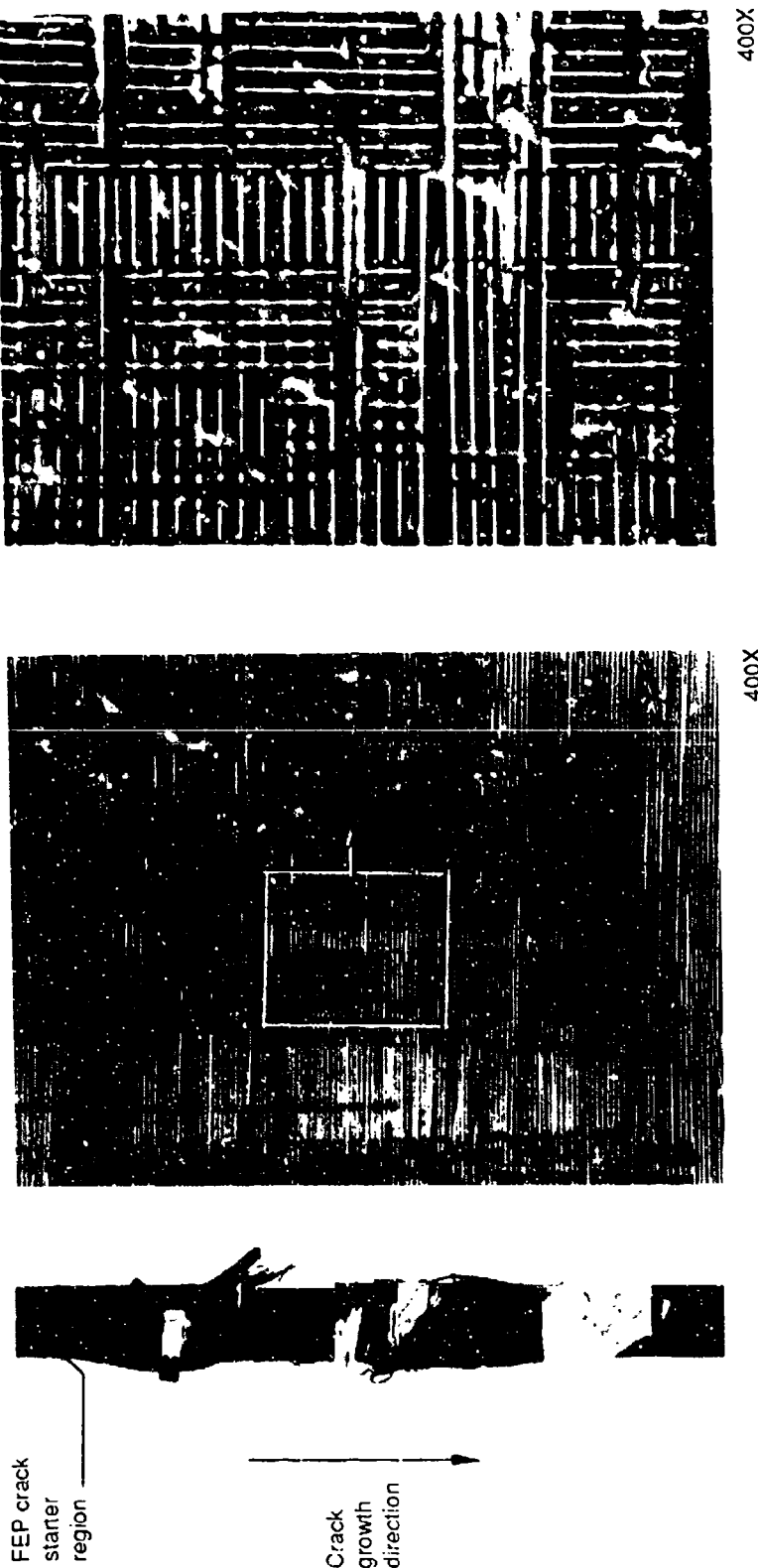


Figure 2-56. Optical Photomicrographs of Interlaminar Mode I Tension, 0/90 Fracture, 2000 F Exposure for 5 Minutes After Test



45 degree tilt

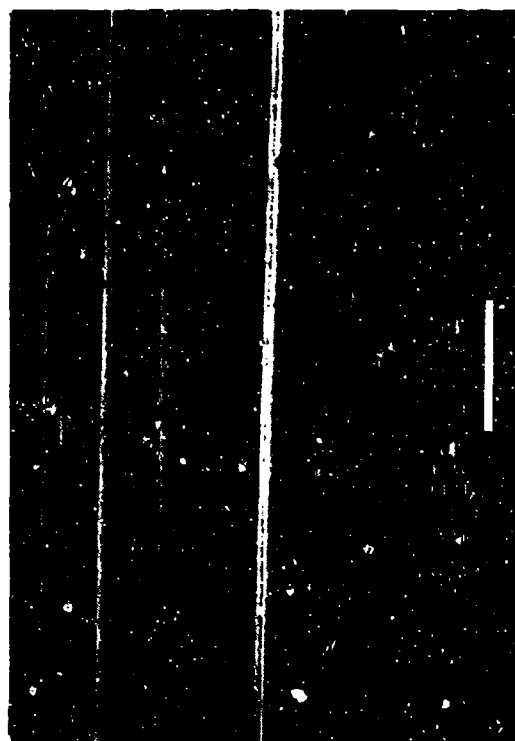
20X

Mechanically induced
crack direction



45 degree tilt

400X



45 degree tilt

2,000X

Figure 2-57. SEM Fractographs of Interlaminar Mode I Tension, 0/90 Fracture, 2000 F Exposure for 5 Minutes After Test

2.2 INTERLAMINAR SHEAR (MODE II ENF)

The primary features observed in fracture surfaces generated under predominantly Mode II shear are as follows:

1. Macroscopically flat surface
2. Microscopically rough resin fracture between fibers, exhibiting hackles and scallops
3. Smooth appearance at fiber-matrix separation
4. Secondary cracking (transverse to fracture plane).

The characteristic fracture features consist of hackles and scallops that are of different fracture initiation site(s), and therefore, cannot be used to determine initiation site(s) or crack-propagation direction(s) in Mode II shear interlaminar fracture failures. Processing variations (overcure or undercure), material form (filament winding versus tape), or post-processing variables (impact-damage) do not significantly alter the fracture characteristics. Exposure to 2000°F flame for 5 minutes after the test resulted in resin starved carbon fibers on the outermost ply. Due to the minimal resin content, there were no resin fracture surface characteristics to indicate crack propagation direction.

Table 2-2 shows the test matrix for the end-notched flexural (ENF) test type. Figure 2-58 shows the ENF test geometry. The fractographs from the interlaminar shear testing are shown in Figures 2-59 through 2-99. These figures are arranged in the same order that the corresponding tests are listed in Table 2-2.

Table 2-2. Test Matrix for ENF Specimens

PLY/ORIENTATION	VARIABLE CONDITIONS	CONTRIBUTOR
24/0 24/± 45 24/0, ± 45 24/0, 90 24/50	Conditions During Tests- RT Dry (Baseline), -65°F Dry, 270°F Dry, RT/Wet, 180°F/Wet	Boeing
24/0 24/0, ± 45	Filament Wound	Northrop
24/0, 90	Fabric	Boeing

Table 2-2. Test Matrix for ENF Specimens (Continued)

PLY/ORIENTATION	VARIABLE CONDITIONS	CONTRIBUTOR
24/0, ± 45	3-D Weave	Northrop
24/0, 90	Impact Damaged Before Test	Northrop
24/0 24/0, 90	Water Immersion Before Test	Northrop
24/0, 90	Water Immersion, 4 weeks at 160°F, After Test	Boeing
24/0, 90	Humidity Exposure 100% RH, 4 weeks at 160°F, After Test	Boeing
24/0 24/0, ± 45	Undercured	Northrop
24/0 24/0, ± 45	Overcured	Northrop
24/0, 90	Low Resin	Boeing
24/0 24/0, 90	High Resin + Conditioned 180°F Dry, After Test	Northrop
24/0 24/0, ± 45	Overcured + Conditioned 180°F/Wet, After Test	Northrop
24/0, 90	2000°F/Dry (5 Minutes) After Test	Boeing

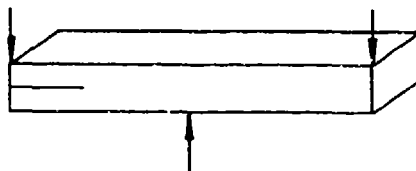


Figure 2-58. End-Notched Flexural Test Type

Optical photomicrographs

Fracture type	Interlaminar mode II shear
Ply layup	[0] 24
Test type	ENF
• Test conditions	21°C, dry
• Fracture between	0/0 plies
Material	Hercules 3501-6/177°C cure AS4 fibers

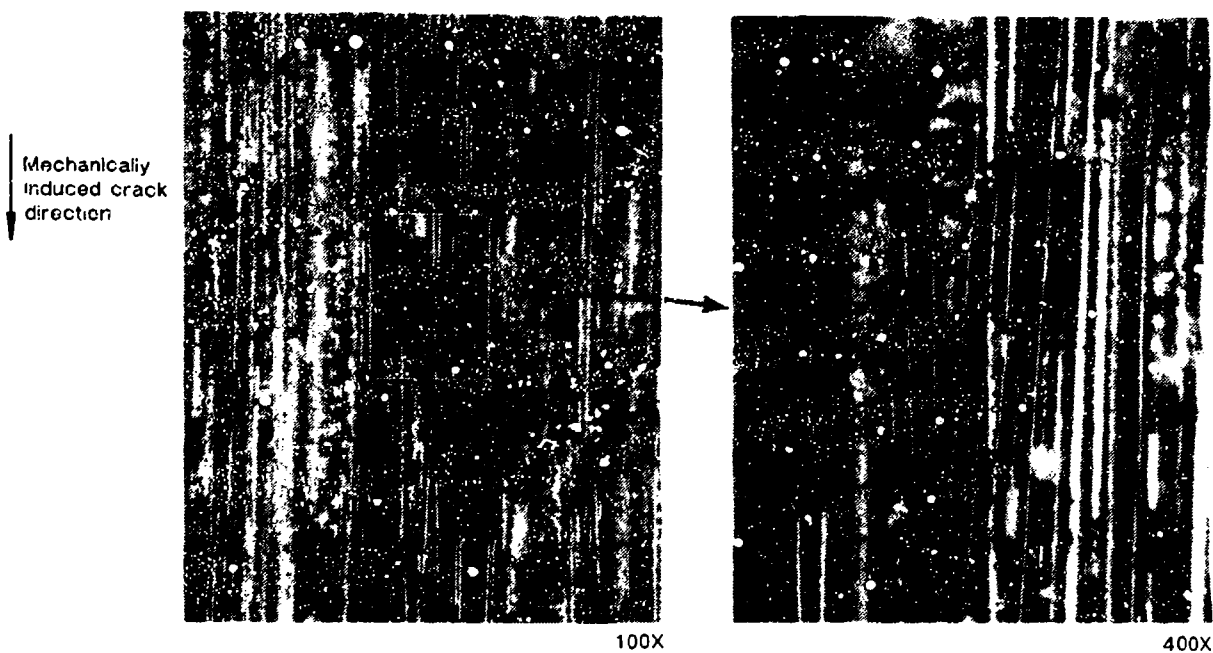
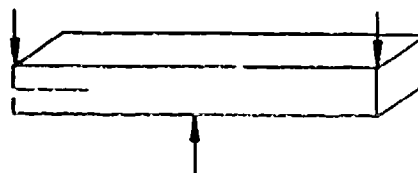
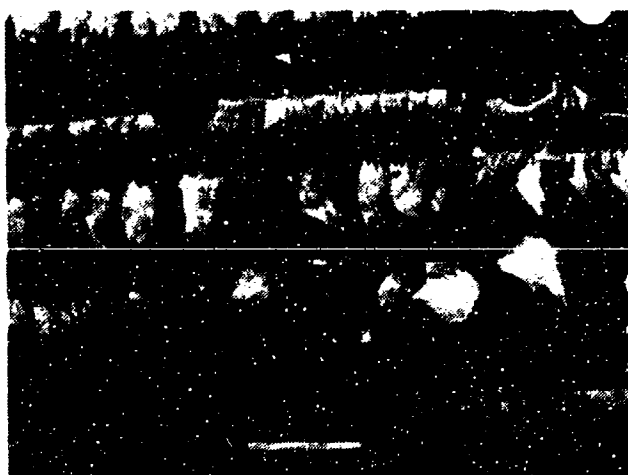
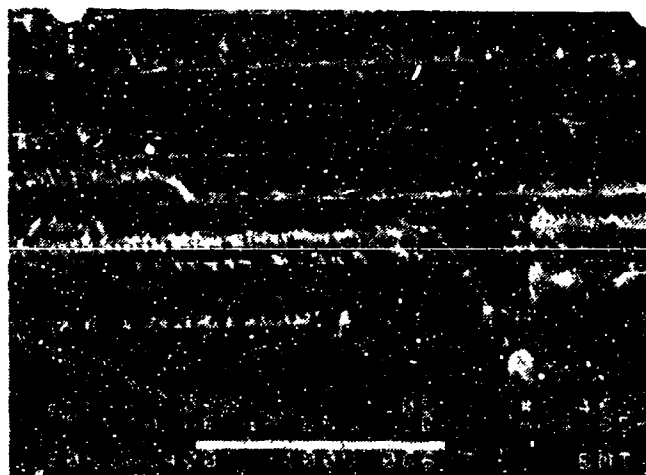
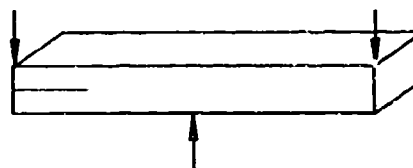


Figure 2-59. Photographs of Interlaminar Mode II Shear, 0/0 Fracture, 21°C/Dry

SEM photomicrographs

Fracture type	Interlaminar mode II shear
Ply layup	[0] 24
Test type	ENF
• Test conditions	21°C, dry
• Fracture between	0/0 plies
Material	Hercules 3501-6/177° C cure AS4 fibers



Mechanically induced crack direction

Legend:

- F Fiber matrix separation
- H Hackles
- R River markings
- T Textured microflow



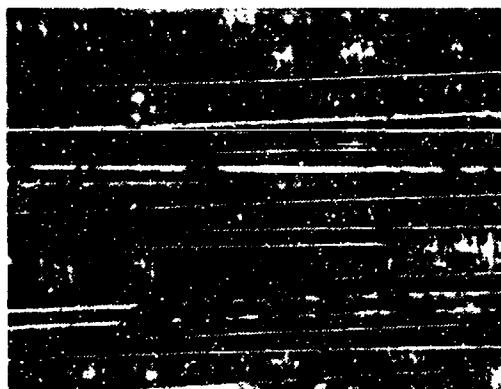
Figure 2-60. SEM Photographs of Interlaminar Mode II Shear, 0/0 Fracture, 70 F/Dry

Optical photomicrographs

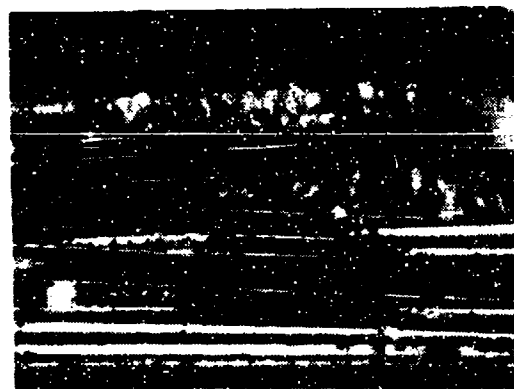
Fracture type	Interlaminar mode II shear
Ply layup	[0] 24
Test type	ENF
• Test conditions	Dry
• Fracture between	0/0 plies
Material	Hercules 3501-6/177° C cure AS4 fibers



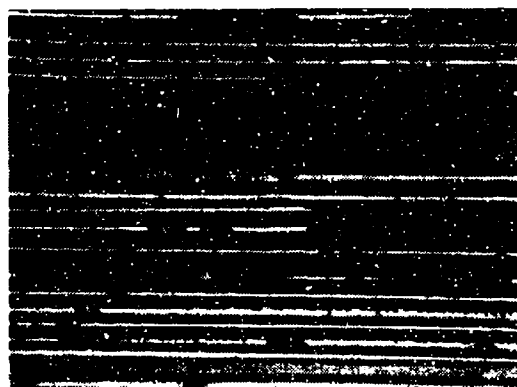
Mechanically induced crack direction



-65°F, dry



70°F, dry



270°F, dry

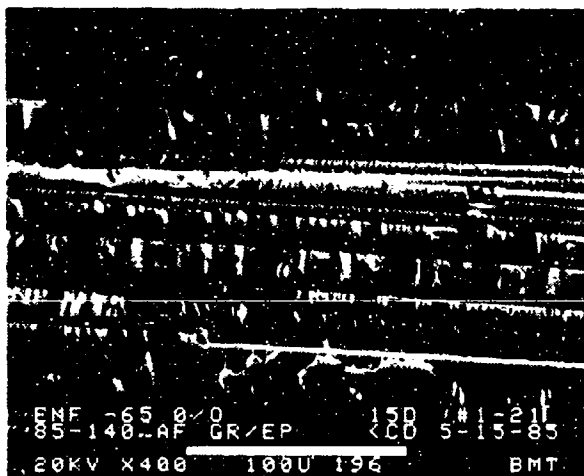
Figure 2-61. Photographs of Interlaminar Mode II Shear, 0/0 Fracture, -65, 70, and 270 F/Dry (400X)

SEM photomicrographs

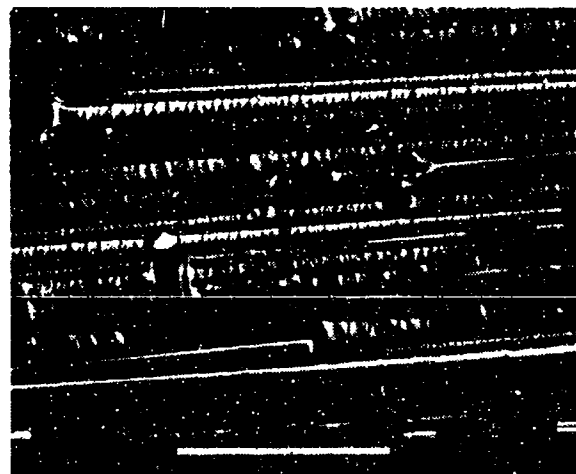
Fracture type	Interlaminar mode II shear
Ply layup	[0] 24
Test type	ENF
• Test conditions	Dry
• Fracture between	0/0 plies
Material	Hercules 3501-6/177° C cure AS4 fibers



Mechanically induced crack direction



-65°F, dry



70°F, dry

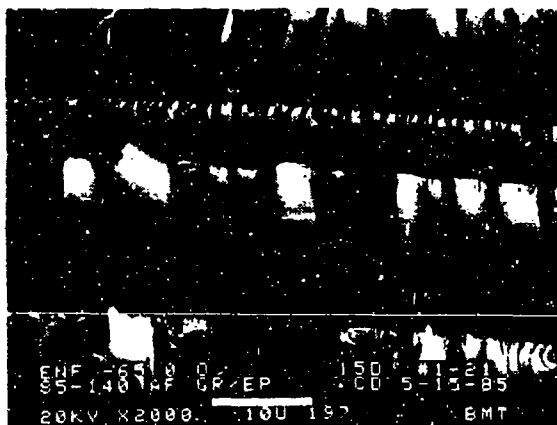


270°F, dry

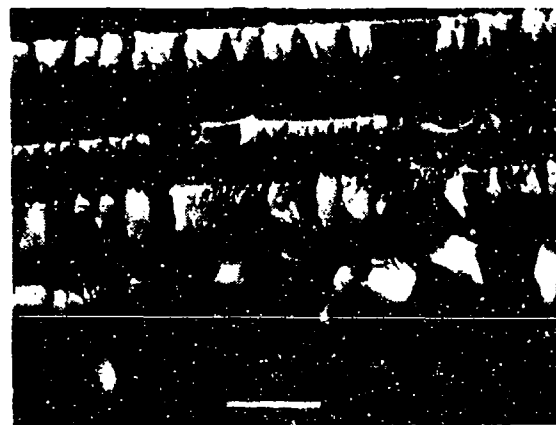
Figure 2-62. SEM Photographs of Interlaminar Mode II Shear, 0/0 Fracture, -65, 70, and 270 F/Dry (400X)

SEM photomicrographs

Fracture type	Interlaminar mode II shear
Ply layup	[0] 24
Test type	ENF
• Test conditions	Dry
• Fracture between	0/0 plies
Material	Hercules 3501-6/177°C cure AS4 fibers

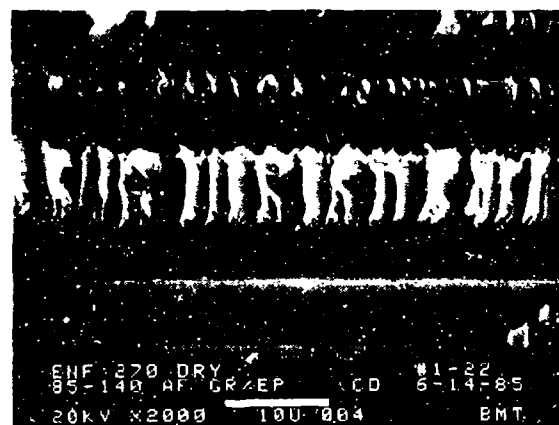


-65°F, dry



70°F, dry

Mechanically Induced crack direction



270°F, dry

Legend:

- F Fiber matrix separation
- H Hackles

Figure 2-63. SEM Photographs of Interlaminar Mode II Shear, 0/0 Fracture, -65, 70, and 270 F/Dry (2000X)

Optical photomicrographs

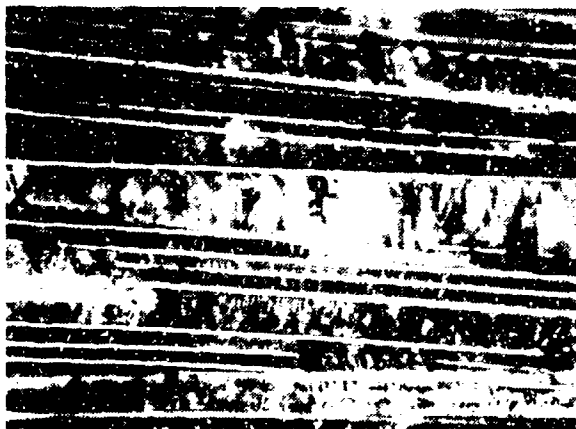
Fracture type	Interlaminar mode II shear
Ply layup	[0, 0] 12S
Test type	ENF
• Test conditions	Dry/wet
• Fracture between	0/0 plies
Material	Hercules 3501-6/177°C cure AS4 fibers



Mechanically induced crack direction



70°F, wet



180°F, dry

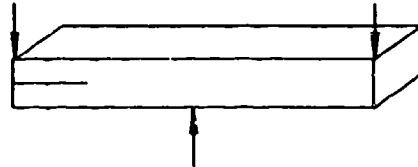


180°F, wet

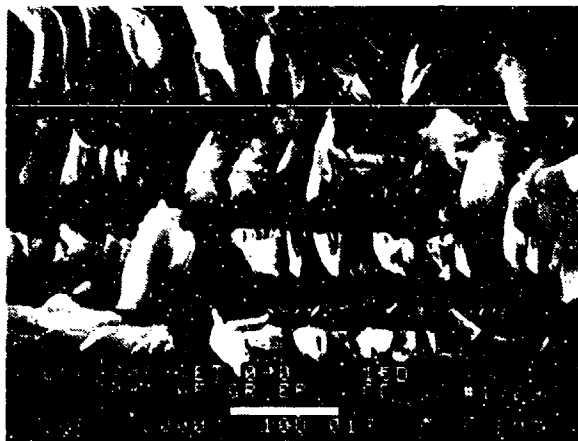
Figure 2-64. Photographs of Interlaminar Mode II Shear, 0/0 Fracture, 70 F/Wet, 180 F/Dry, and 180 F/Wet (400X)

SEM photomicrographs

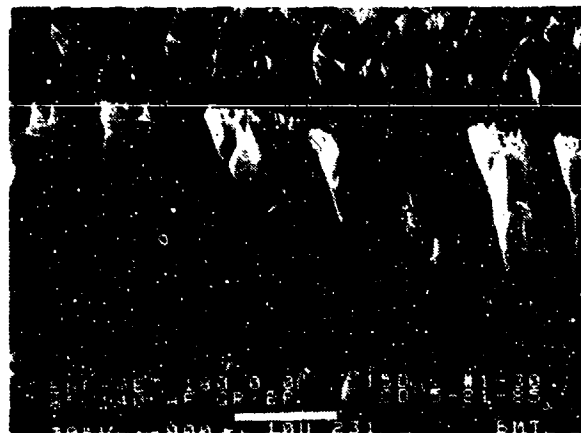
Fracture type	Interlaminar mode II shear
Ply layup	[0] 24
Test type	ENF
• Test conditions	Wet
• Fracture between	0/0 plies
Material	Hercules 3501-6/177° C cure AS4 fibers



Mechanically induced crack direction



70°F, wet



180°F, wet

Legend:

F Fiber matrix separation
H Hackles

Figure 2-65. SEM Photographs of Interlaminar Mode II Shear, 0/0 Fracture, 70 and 180 F/Wet

Optical photomicrographs

Fracture type	Interlaminar mode II shear
Ply layup	[+45/-45] 12S
Test type	ENF
• Test conditions	21°C, dry
• Fracture between	+45/-45 plies
Material	Hercules 3501-6/177°C cure AS4 fibers

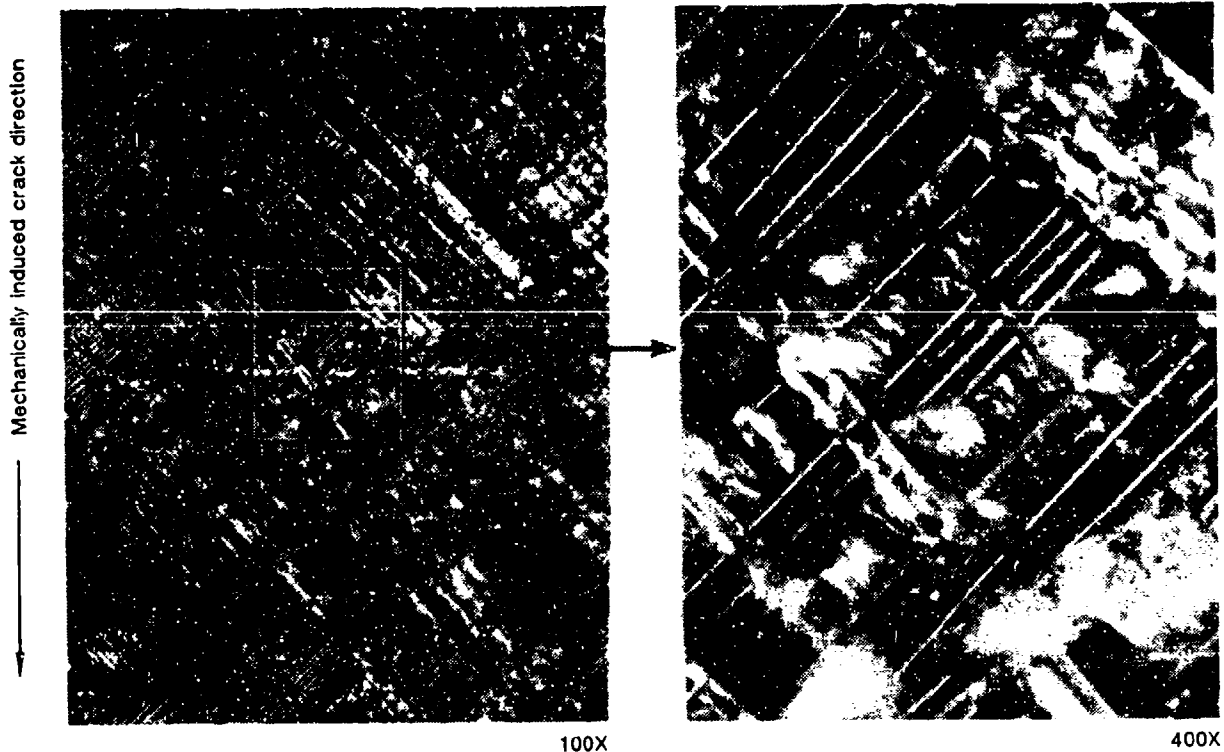
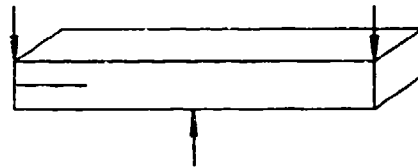


Figure 2-66. Photographs of Interlaminar Mode II Shear, +45/-45 Fracture, 70 F/Dry

SEM photomicrographs

Fracture type	Interlaminar mode II shear
Ply layup	[+45/-45] 12S
Test type	ENF
• Test conditions	21°C, dry
• Fracture between	+45/-45 plies
Material	Hercules 3501-6/177°C cure AS4 fibers



Mechanically induced crack direction



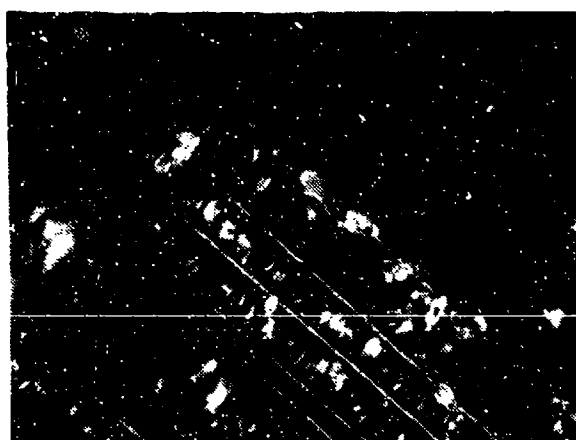
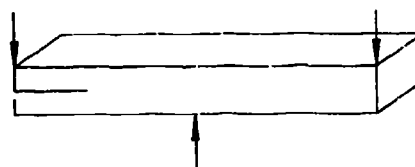
Legend:

- F Fiber matrix separation
- H Hackles
- R River markings

Figure 2-67. SEM Photographs of Interlaminar Mode II Shear, +45/-45 Fracture, 70 F/Dry

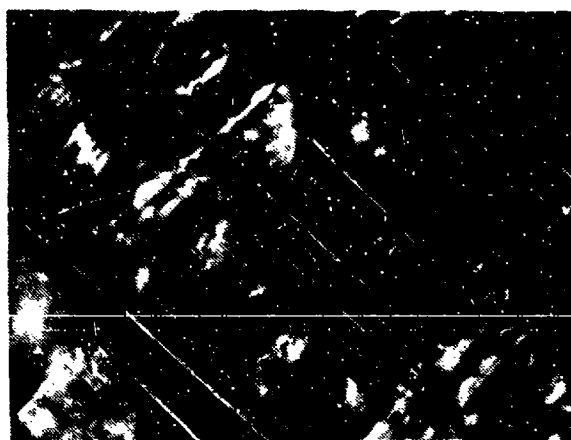
Optical photomicrographs

Fracture type	Interlaminar mode II shear
Ply layup	[+45/-45] 12S
Test type	ENF
• Test conditions	Dry
• Fracture between	+45/-45 plies
Material	Hercules 3501-6/177°C cure AS4 fibers



-65°F, dry

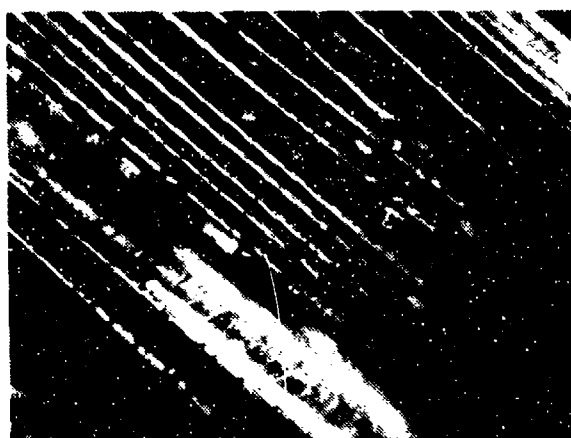
400X



70°F, dry

400X

Mechanically induced crack direction →



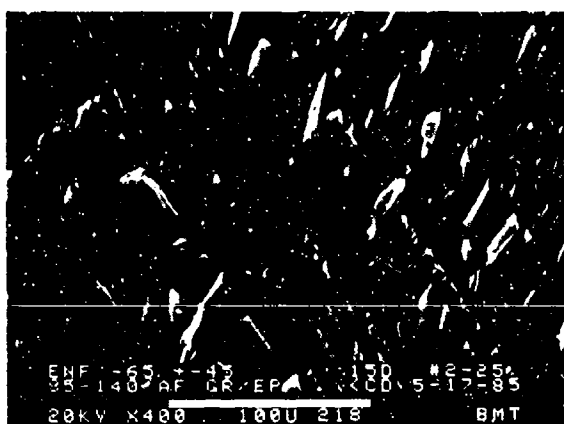
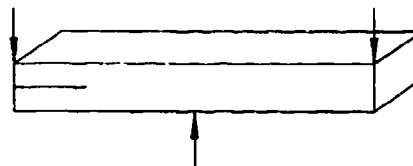
270°F, dry

400X

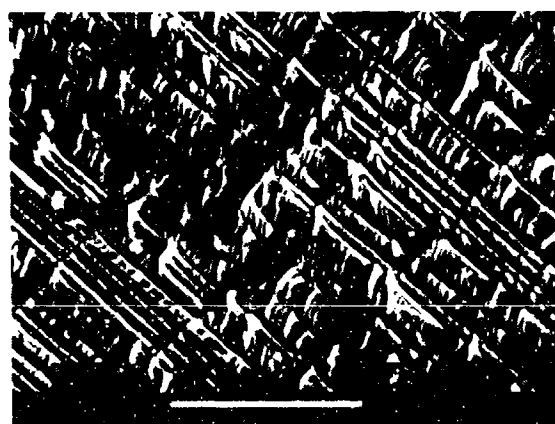
Figure 2-68. Photographs of Interlaminar Mode II Shear, +45/-45 Fracture, -65, 70 and 270 F/Dry

SEM photomicrographs

Fracture type	Interlaminar mode II shear
Ply layup	[+45, -45] ₁₂ S
Test type	ENF
• Test conditions	Dry
• Fracture between	+45/-45 plies
Material	Hercules 3501-6/177°C cure AS4 fibers

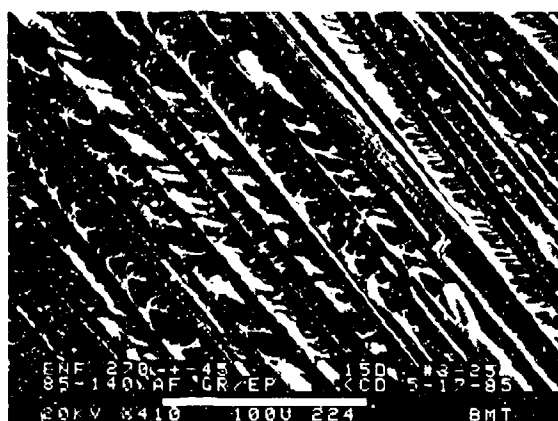


-65°F, dry



70°F, dry

←
Mechanically Induced crack direction

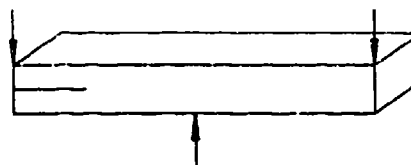


270°F, dry

Figure 2-69. SEM Photographs of Interlaminar Mode II Shear, +45/-45 Fracture, -65, 70 and 270 F/Dry (400X)

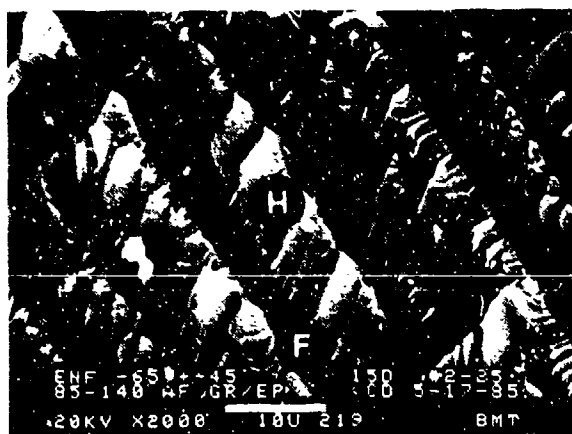
SEM photomicrographs

Fracture type	Interlaminar mode II shear
Ply layup	[+45/-45] 12S
Test type	ENF
• Test conditions	Dry
• Fracture between	+45/-45 plies
Material	Hercules 3501-6/177°C cure AS4 fibers

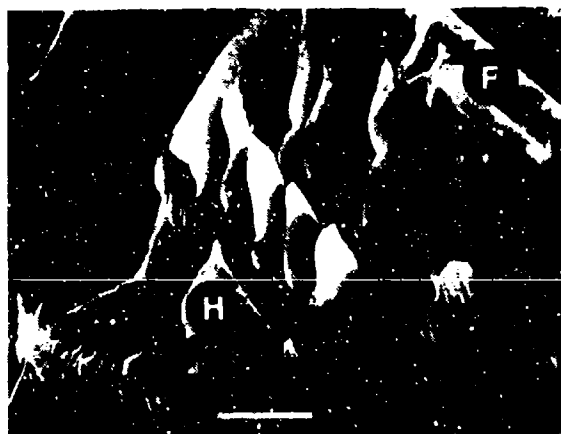


Legend:

F Fiber matrix separation
H Hackles



-65°F, dry



70°F, dry

← Mechanically Induced crack direction



270°F, dry

Figure 2-70. SEM Photographs of Interlaminar Mode II Shear, +45/-45 Fracture, -65, 70 and 270 F/Dry (2000X)

Optical photomicrographs

Fracture type	Interlaminar mode II shear
Ply layup	[0, 45] _{12S}
Test type	ENF
• Test conditions	21°C, dry
• Fracture between	0/45 plies
Material	Hercules 3501-6/177°C cure AS4 fibers

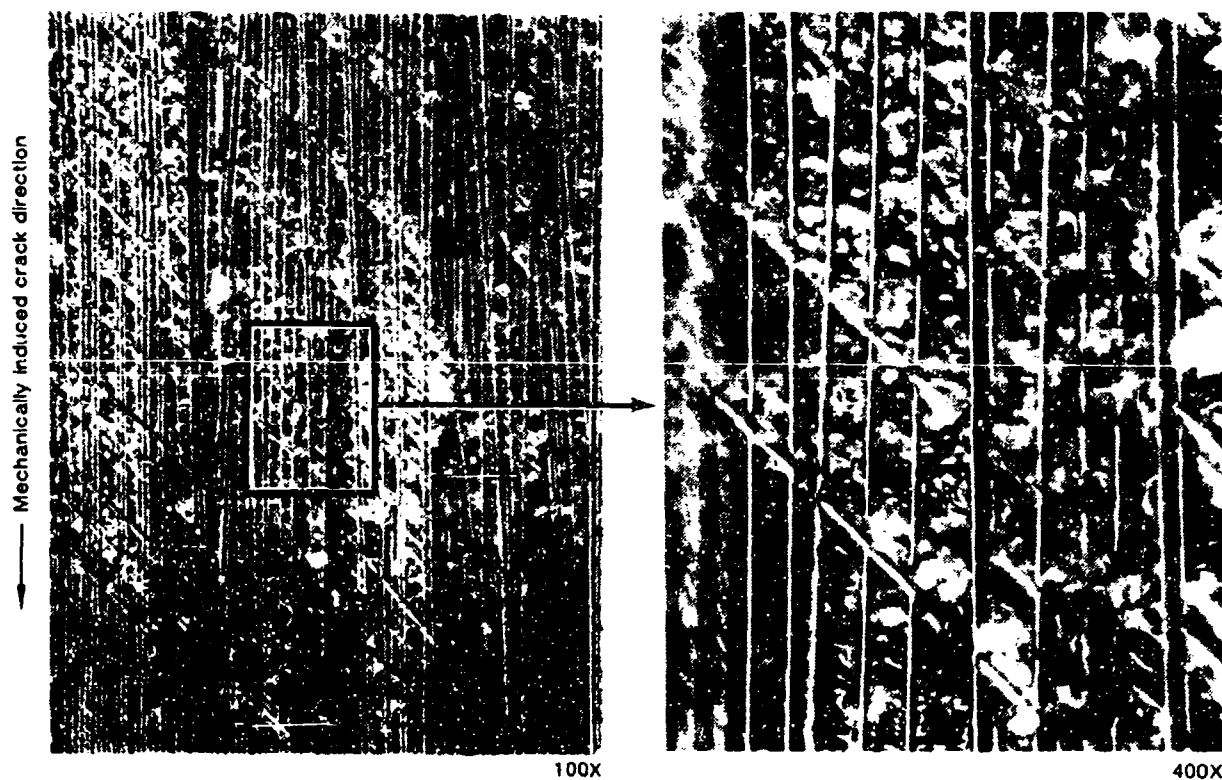
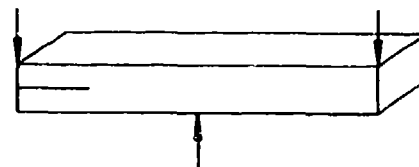
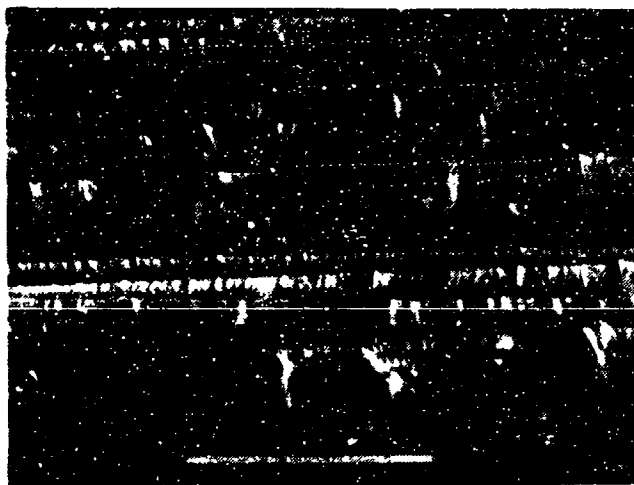
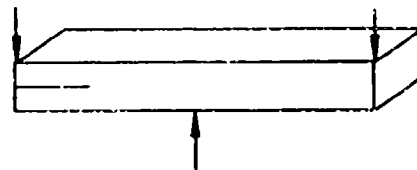


Figure 2-71. Photographs of Interlaminar Mode II Shear, 0/45 Fracture, 70 F/Dry

SEM photomicrographs

Fracture type	Interlaminar mode II shear
Ply layup	[0, 45] _{12S}
Test type	ENF
• Test conditions	RT
• Fracture between	0/45 plies
Material	Hercules 3501-6/177°C cure AS4 fibers



Mechanically induced crack direction



Legend:

- F Fiber matrix separation
- H Hackles
- R River markings
- T Textured microflow



Figure 2-72. SEM Photographs of Interlaminar Mode II Shear, 0/45 Fracture, 70 F/Dry

Optical photomicrographs

Fracture type	Interlaminar mode II shear
Ply layup	[0, 90] ₁₂ S
Test type	ENF
• Test conditions	21°C, dry
• Fracture between	0/90 plies
Material	Hercules 3501-6/177°C cure AS4 fibers

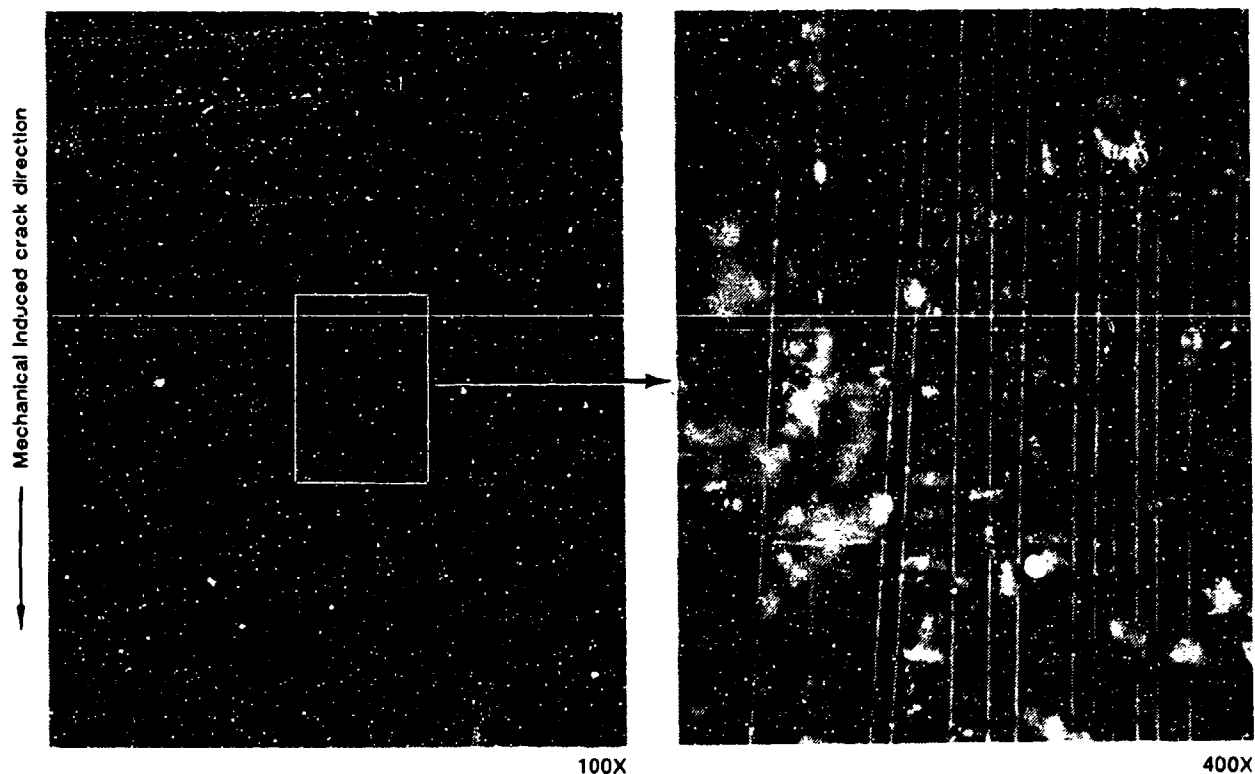
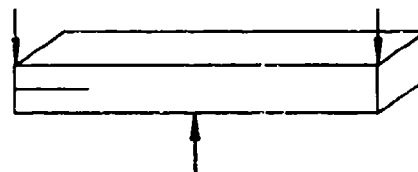


Figure 2-73. Photographs of Interlaminar Mode II Shear, 0/90 Fracture, 70 F/Dry

Optical photomicrographs

Fracture type	Interlaminar mode II shear
Ply layup	[90] 24
Test type	ENF
• Test conditions	21°C, dry
• Fracture between	90/90 plies
Material	Hercules 3501-6/177°C cure AS4 fibers

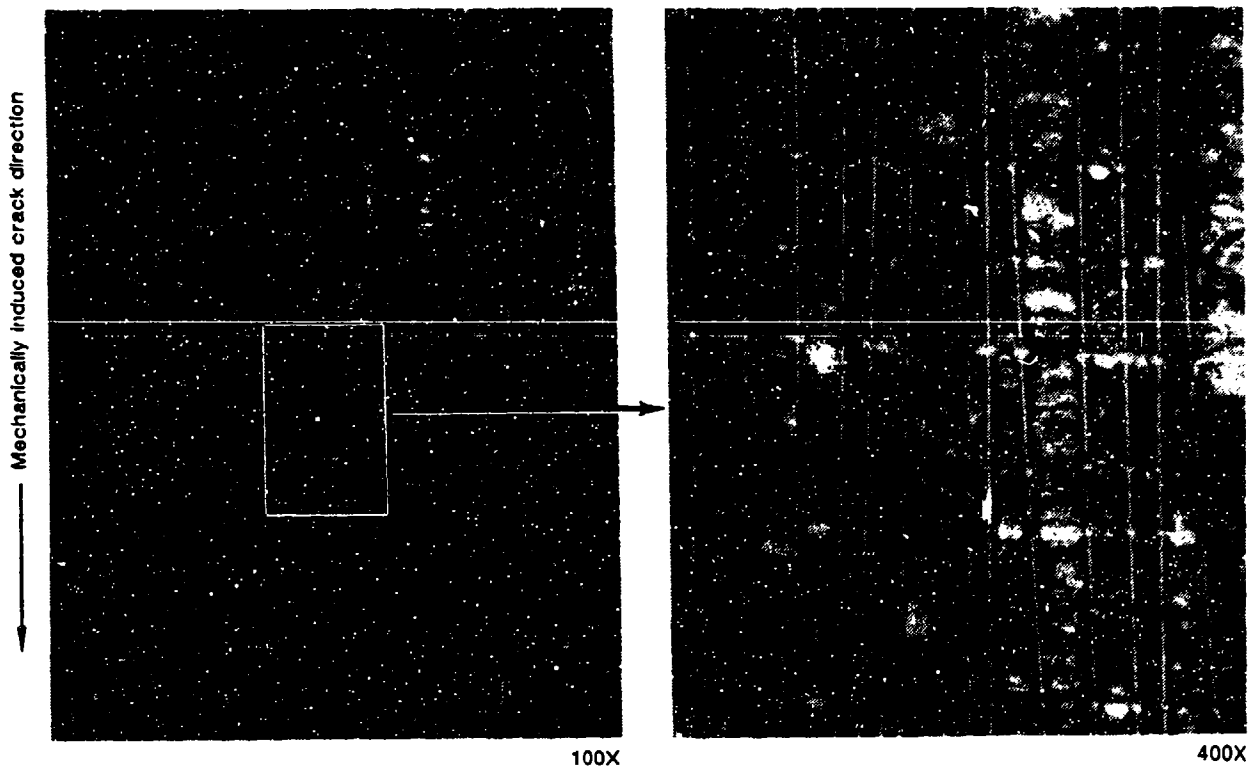
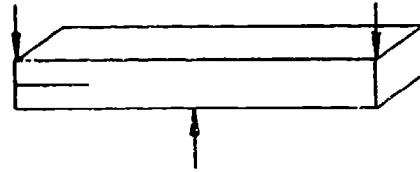
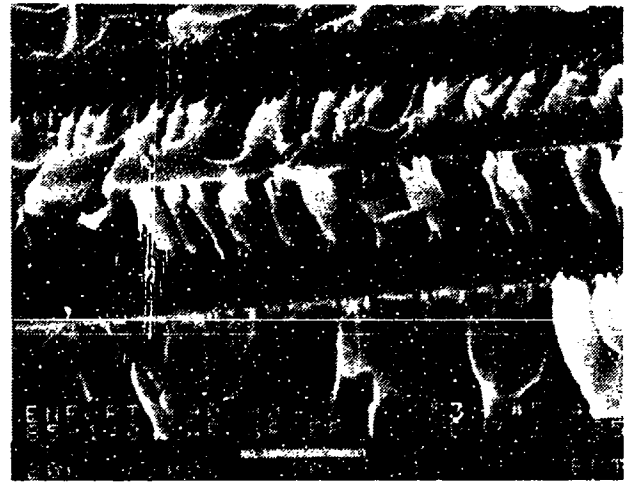
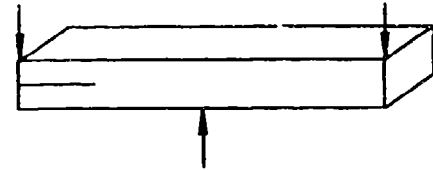


Figure 2-74. Photographs of Interlaminar Mode II Shear, 90/90 Fracture, 70 F/Dry

SEM photomicrographs

Fracture type	Interlaminar mode II shear
Ply layup	[90] 24
Test type	ENF
• Test conditions	21°C, dry
• Fracture between	90/90 plies
Material	Hercules 3501-6/177°C cure AS4 fibers



Mechanically Induced crack direction



Legend:

- F Fiber matrix separation
- H Hackles
- R River markings



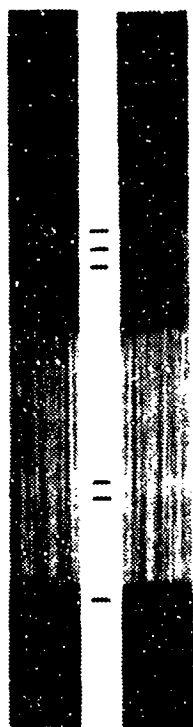
Figure 2-75. SEM Photographs of Interlaminar Mode II Shear, 90/90 Fracture, 70 F/Dry



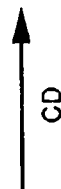
(a)



(b)



(c)



CD

Figure 2-76. Optical and SEM Photographs of Mode II ENF Interlaminar Shear Fracture in Filament Wound Gr/Ep - [0] _{24T}, Room Temperature Ambient
(a) Macro photograph
(b) Low Magnification SEM Photograph of Initiation
(c) River Patterns at Larger Crack Lengths

CD = Crack-propagation direction
R = River patterns

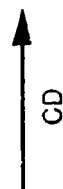
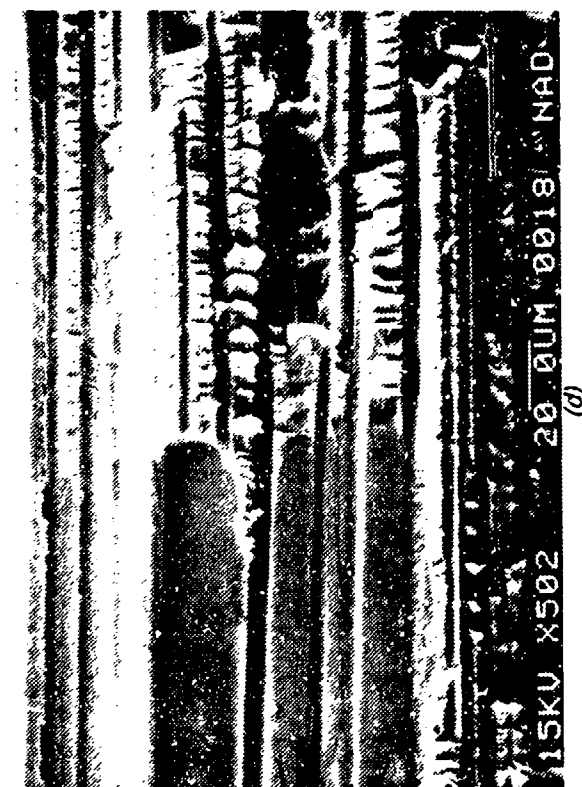
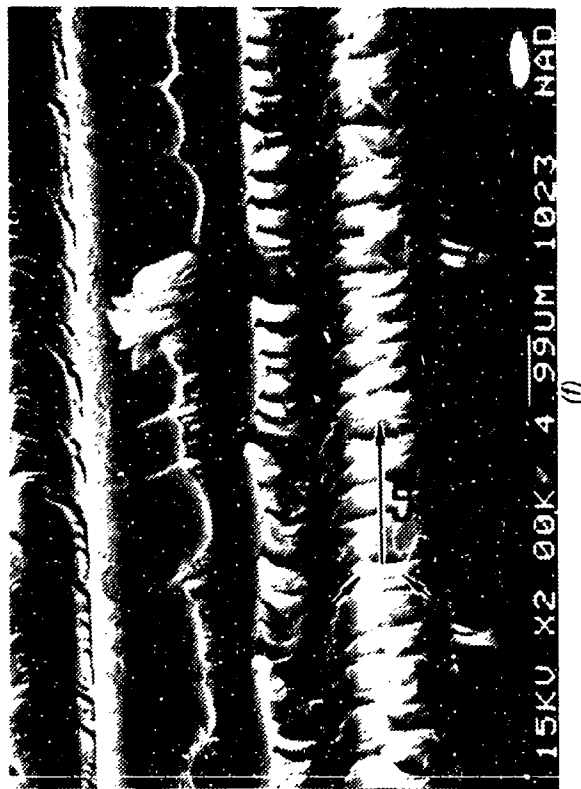
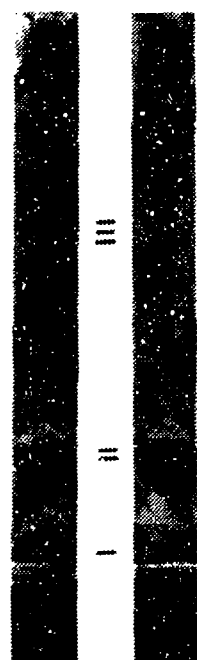


Figure 2-76. (Continued)
 (d) Region I/Region II Boundary
 (e) Hackles (H) and Scallops (S) in Region II
 (f) River Patterns (R) at Roots of Hackles

CD = Crack-propagation direction



(a)

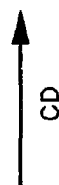


Figure 2-77. Optical and SEM Photographs of Mode II ENF Interlaminar Shear Fracture in Filament Wound Gr/Ep - [J45/0/-45]_{4s}, Room Temperature Ambient

(a) Macro photograph of Fracture

I = Precrack, II = Crack-growth region, III = Laboratory overload

(b) Fracture Initiation in Region I

(c) River Patterns (Arrows) in Region I

CD = Crack-propagation direction

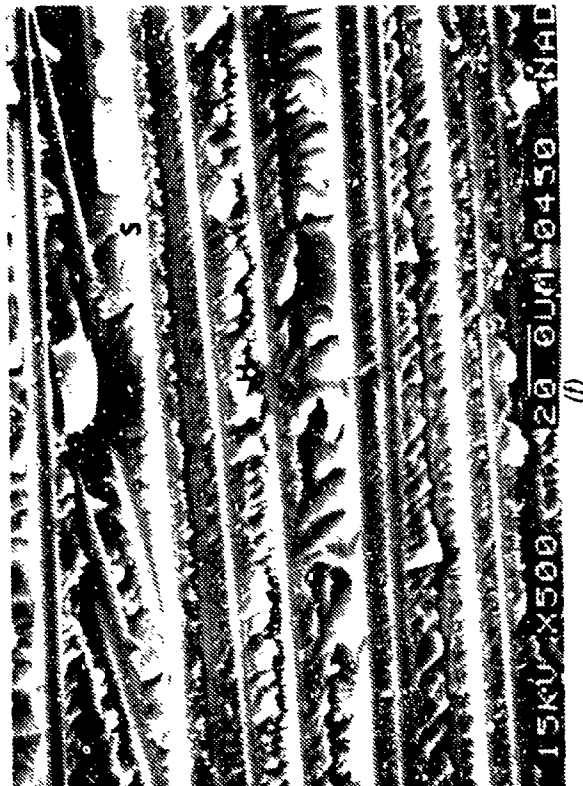
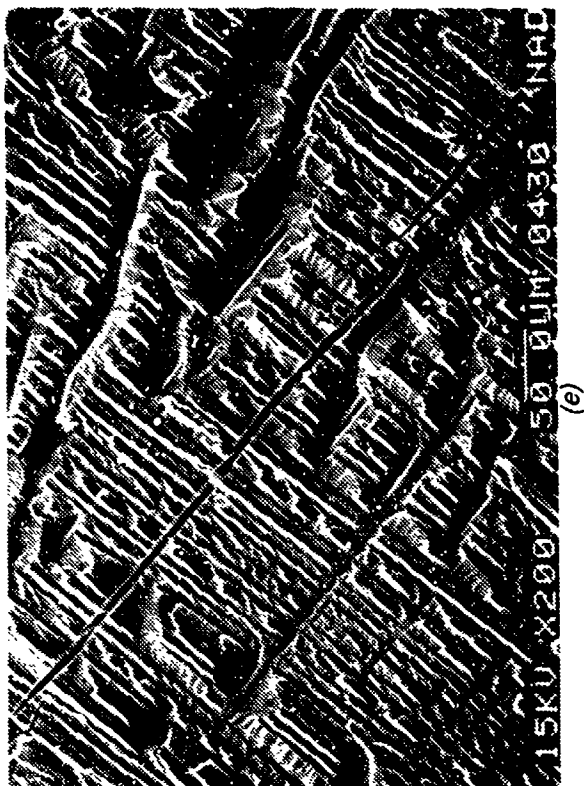
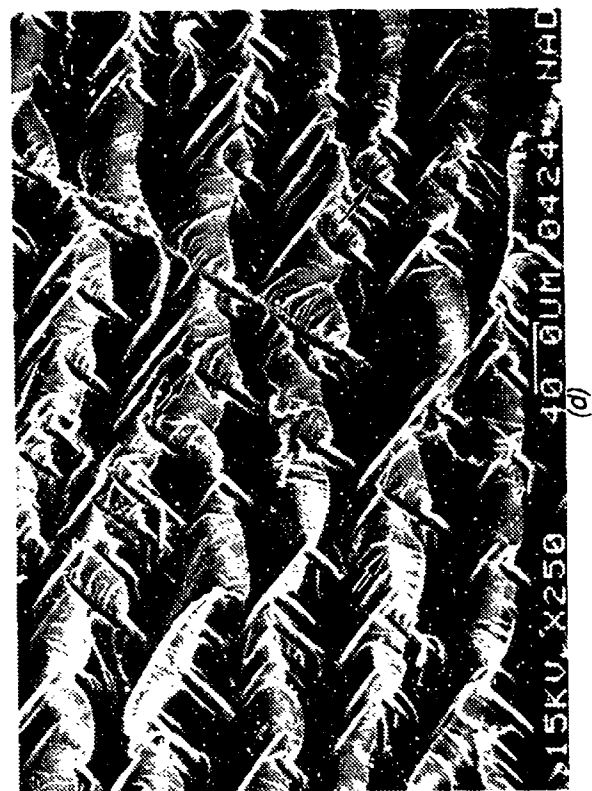


Figure 2-77. (Continued)
 (d) River Patterns (Arrows) in Resin Between 0 and 45 Degree Plies
 (e) Cracks in Ply
 (f) Hackles (H) and Scallops (S) in Mode II Shear Region

CD = Crack propagation direction

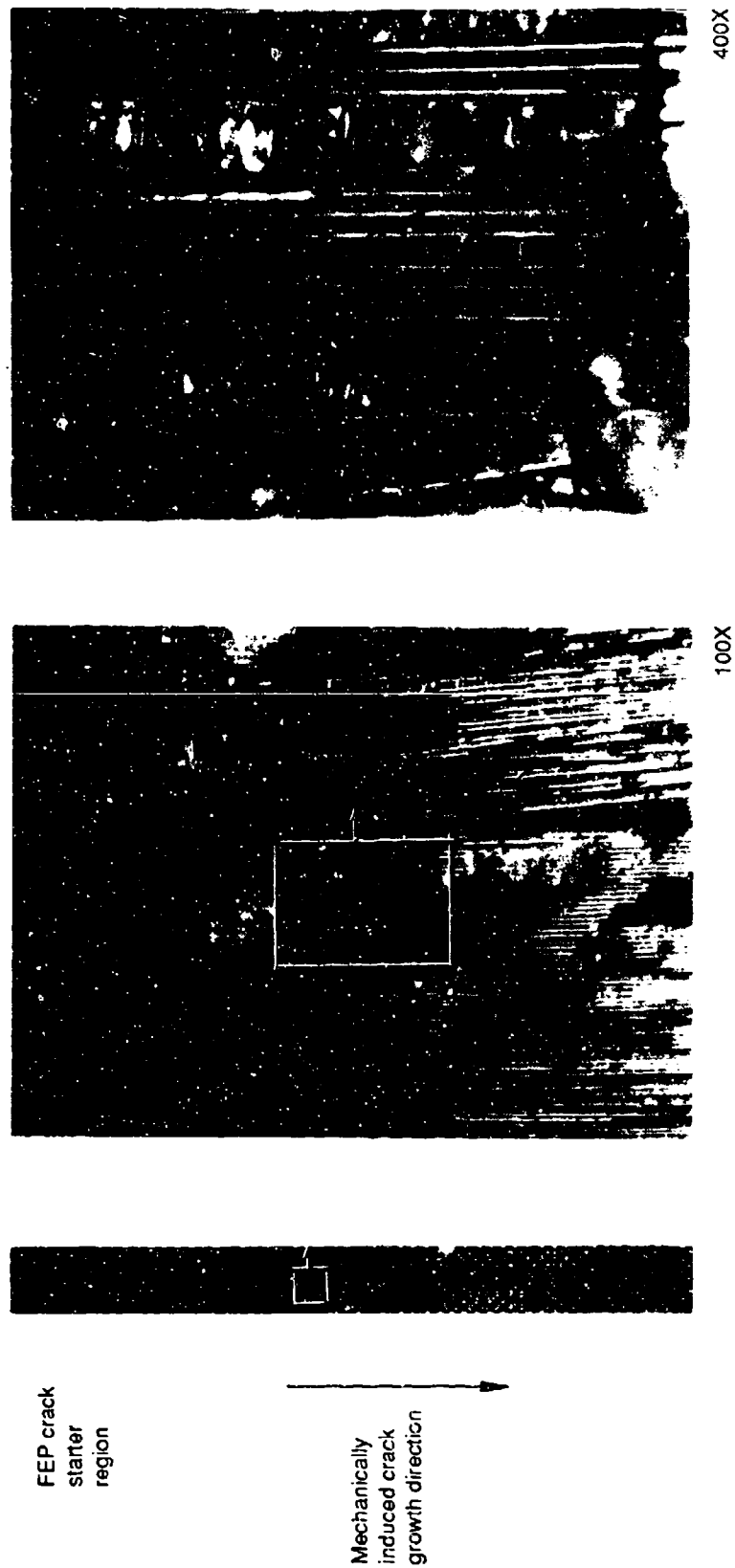


Figure 2-78. Optical Photomicrographs of Interlaminar Mode II Shear, Room Temperature, 0/90 Fabric Fracture



30 degree tilt

20X

Legend:

Hackles

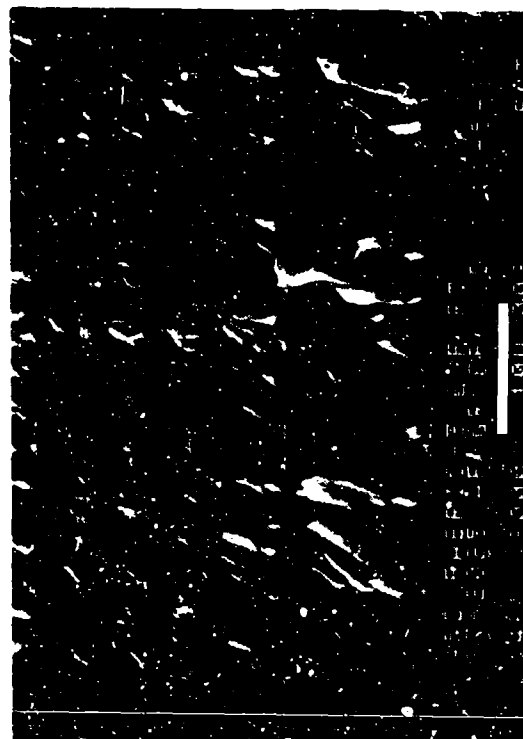
S scallops

Mechanically induced crack direction



30 degree tilt

40CX.



45 degree tilt

2,000X

Figure 2-79. SEM Fractographs of Interlaminar Mode II Shear, Room Temperature, 0/90 Fabric Fracture

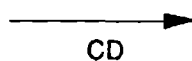
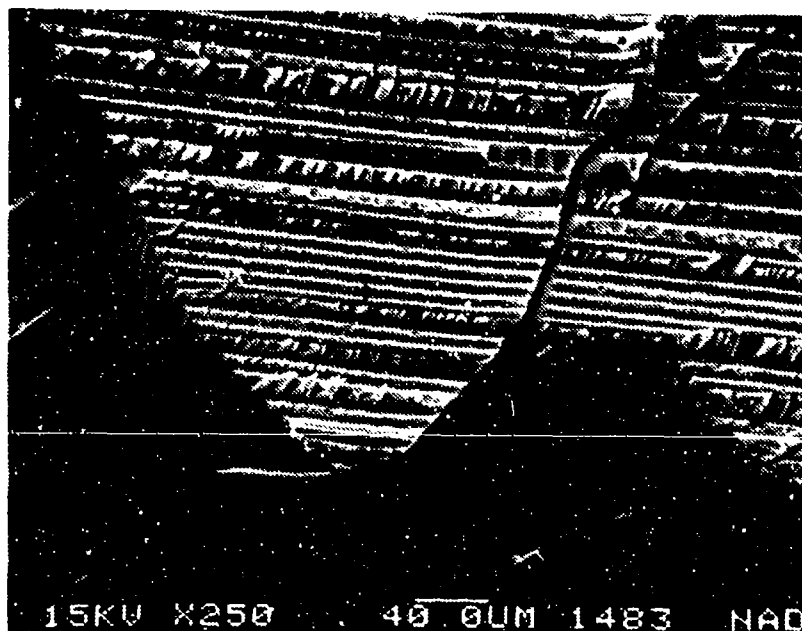
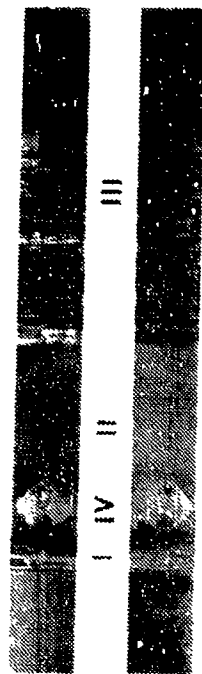


Figure 2-80. SEM Photograph of Mode II ENF Interlaminar Shear Fracture in 3-D Weave Gr/Ep - [+45/0/-45]_{4S} in Crack-Growth Region

Note: Arrows indicate mixed-mode interlaminar fracture features.

CD = Crack-propagation direction

P = Resin pocket adjacent to weave



100X 1000 0373 NAD

(a)

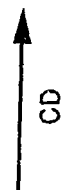
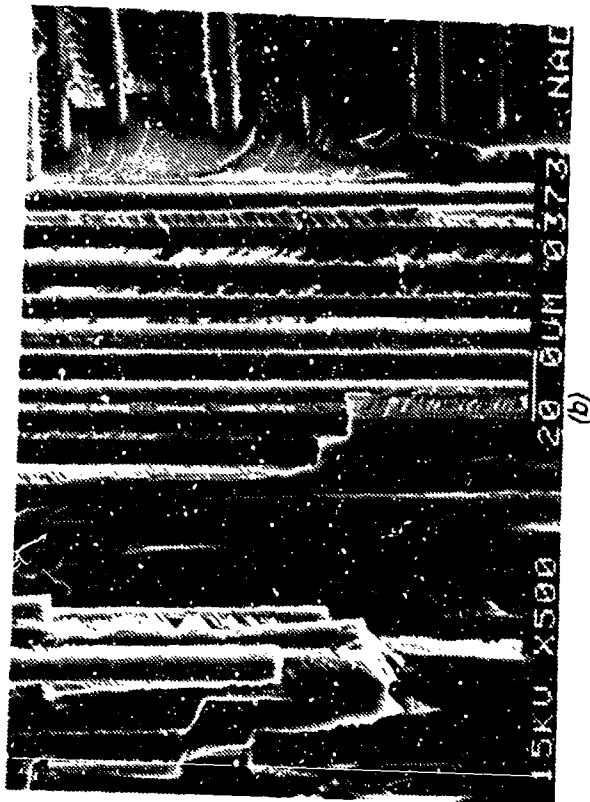
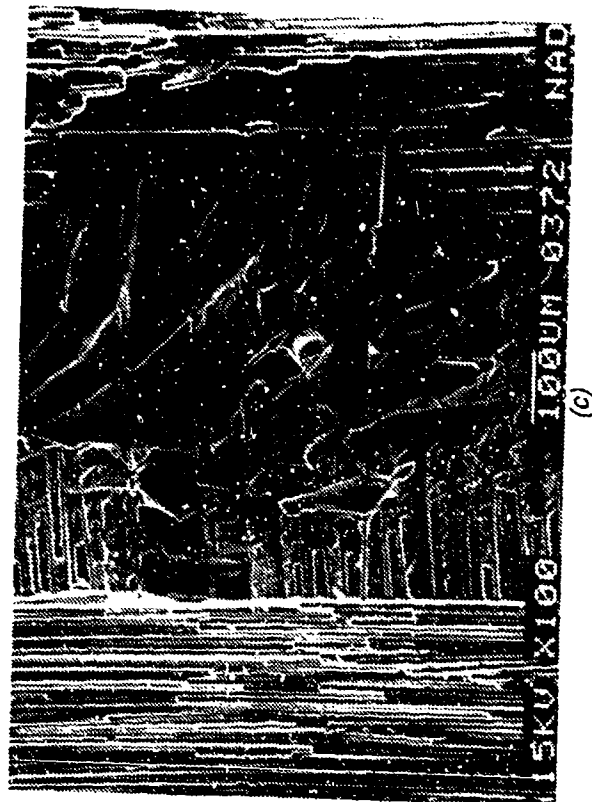


Figure 2-81. Optical and SEM Photographs of Mode II ENF Interlaminar Shear Fracture in Gr/Ep - [0/90]ss, Impact Damaged Before Test
 (a) Macrograph of Fracture
 (b) Local Fracture in 90 Degree Ply in Region I (Arrow)
 (c) River Patterns in 0 Degree Ply in Region I (Arrow)

CD = Crack propagation direction



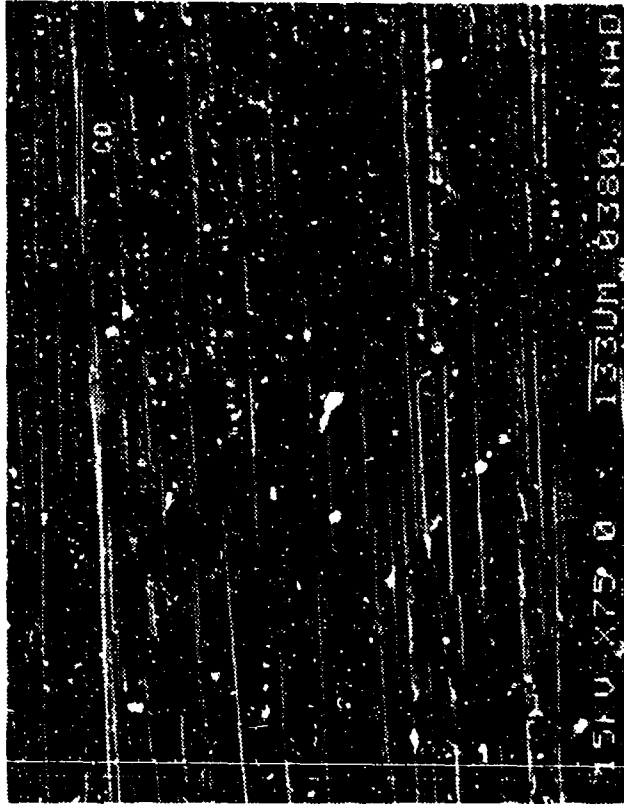
(b)



(c)



(d)



(e)



Figure 2-81. (Continued)
 (d) Interface Between Mode I (T), Mode II (S), and Impact (I) Fracture Areas
 (e) Mode I/Mode II Interface Regions
 CD = Crack propagation direction

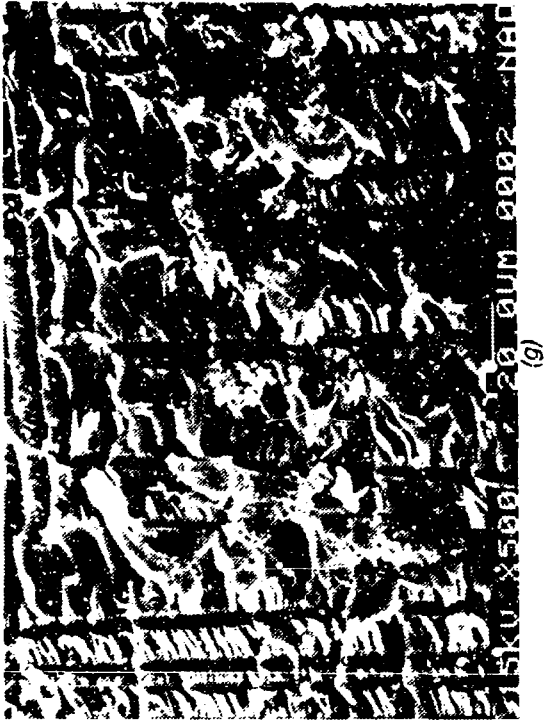
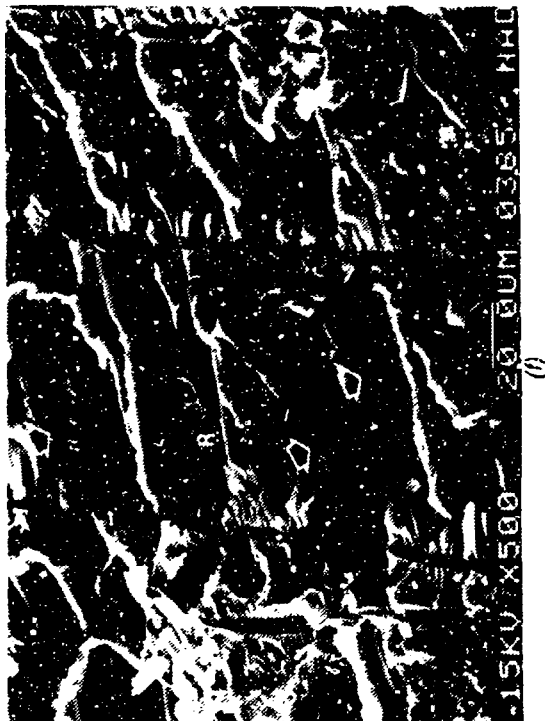


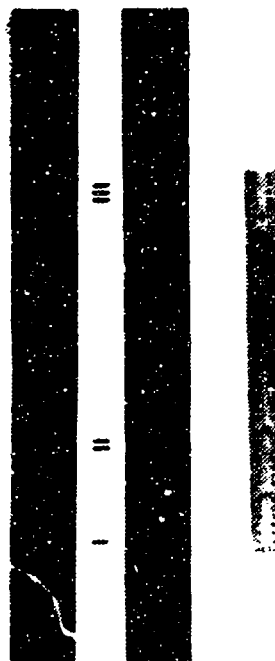
Figure 2-81. (Continued)
 (i) Smooth Resin Surface With River Patterns (R) and
 Crushed Resin (C) in Impacted Region
 (g) Hackles (H) and Delamination Fracture in Impact
 Area
 (h) Details of Delamination Fracture Shown in (g)
 Note river patterns oriented along CD
 CD = Crack propagation direction



(b)



(c)



(a)

Figure 2-82. Optical and SEM Photographs of Mode II ENF Interlaminar Shear Fracture in Gr/Ep - [0] _{24T} Water Immersed Before Test

- (a) Macro photograph
- (b) Initiation in Precrack Region
- (c) Details of Initiation

CD = Crack propagation direction



(d)



(e)

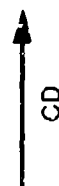


Figure 2-82. (Continued)
 (d) River Patterns in Region I
 (e) Region I/II Interface
 (f) Hackles in Region II

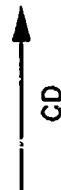
CD = Crack propagation direction



(f)



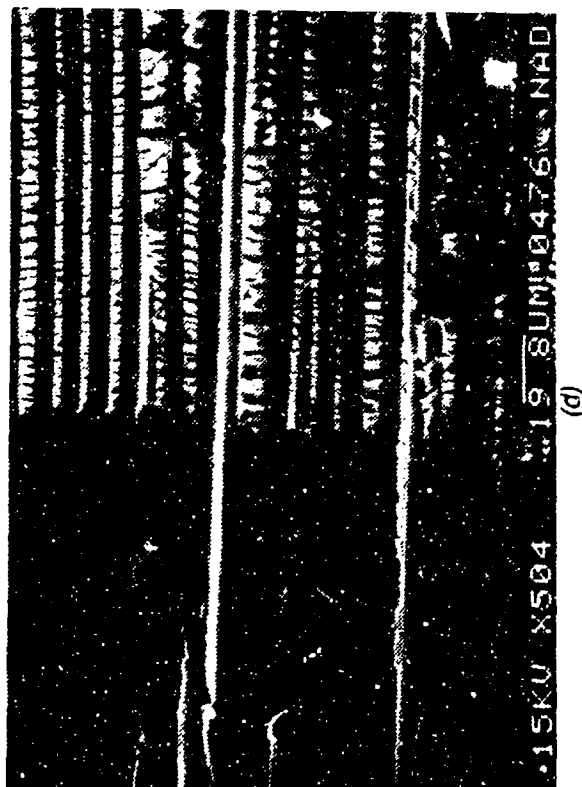
(a)



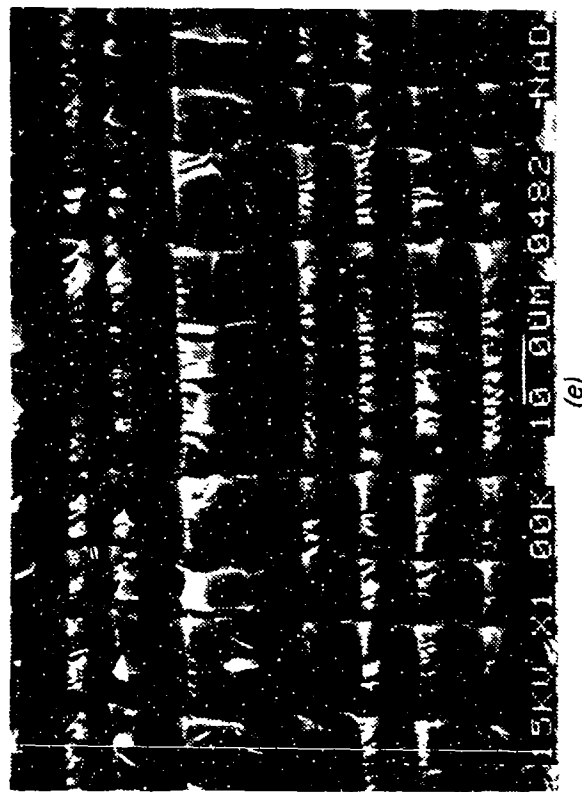
(c)

Figure 2-83. Optical and SEM Photographs of Mode II ENF Interlaminar Shear Fracture in Gr/Ep - [0°/90] es. Water immersed Before Test
(a) Macro photograph Showing Regions I, II, and III (Precrack, Mode II Shear, and Laboratory Overload)
(b) Initiation Occurring at Resin-Rich Areas Adjacent to Armalon (A) Insert
(c) River Patterns (Arrows) in Mode I Fracture

CD = Crack propagation direction



(d)



(e)

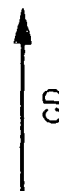
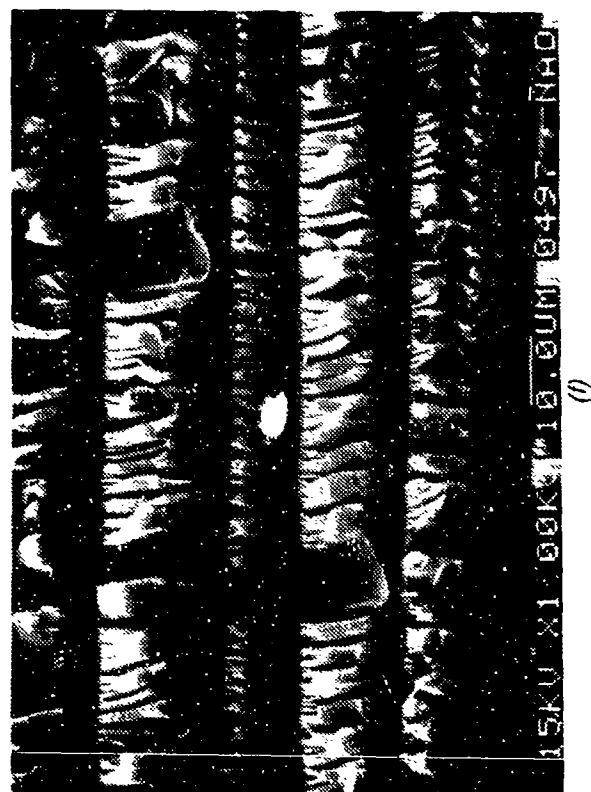


Figure 2-83. (Continued)
 (d) Mode I/Mode II Interface
 (e) Cracks Found in Mode II Fracture Region
 (f) Mode II Hackles (H) and Scallops (S)

CD = Crack propagation direction



(f)

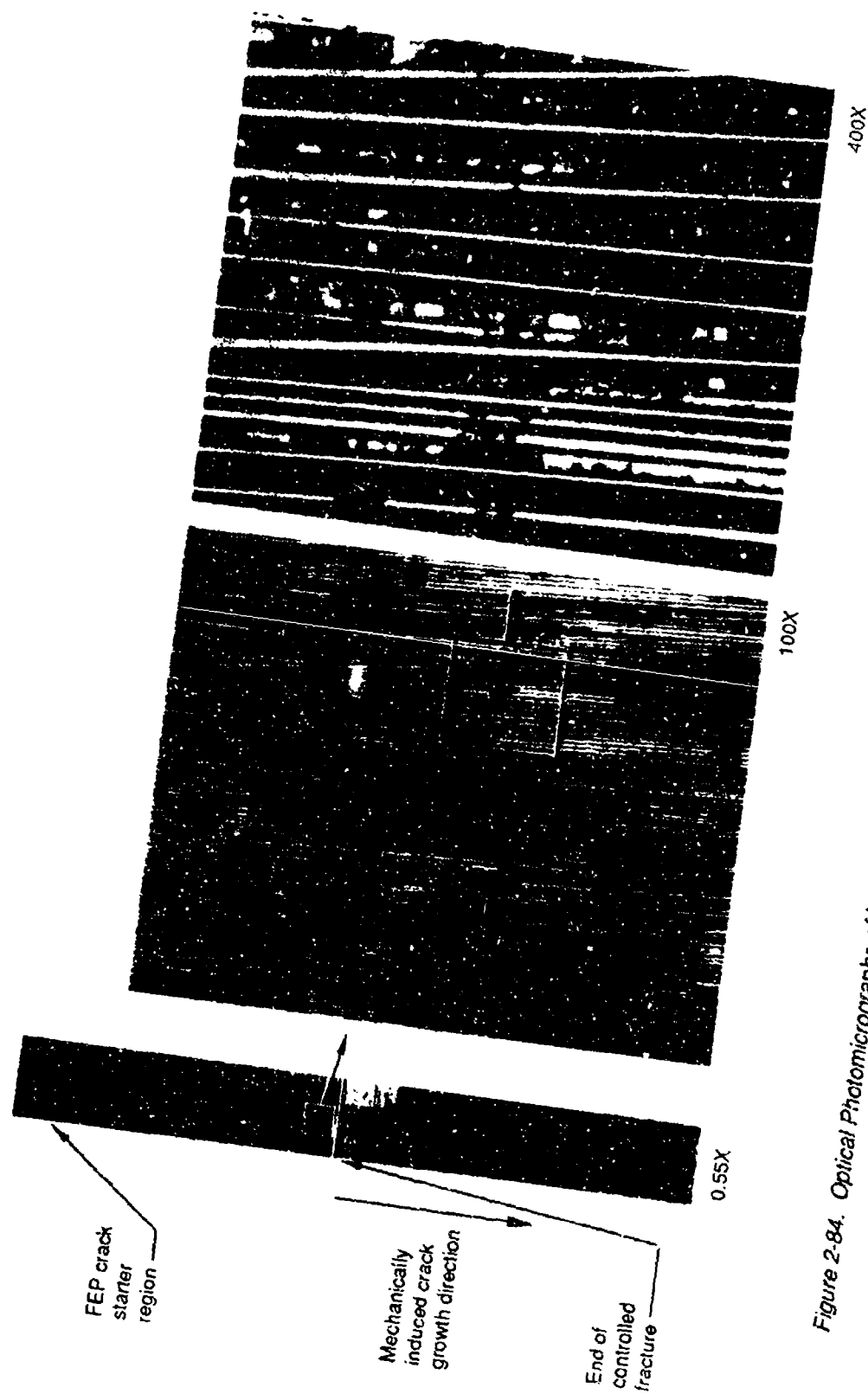
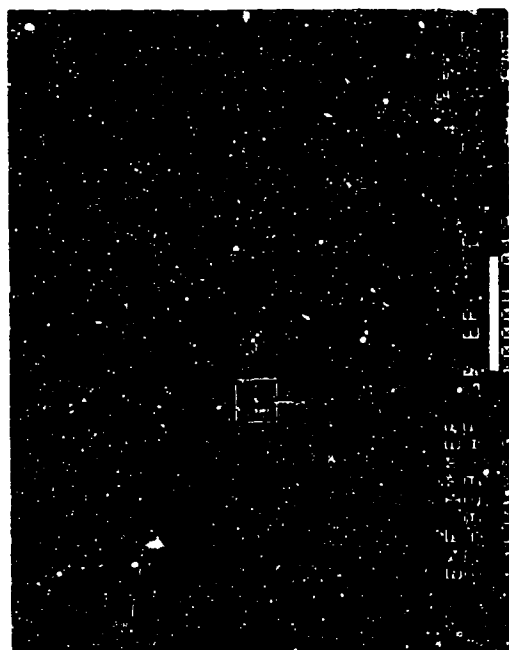
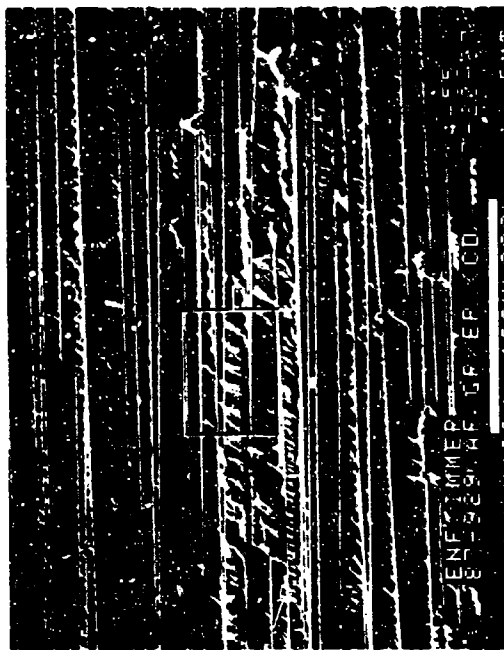


Figure 2-84. Optical Photomicrographs of Interlaminar Mode II Shear, 0/90 Fracture, Water Immersion (160 F) After Test



20X

60 degree tilt



400X

60 degree tilt

Legend:

- F fiber matrix separation
- H hackles
- R rivermarks

Mechanically induced
crack direction



2,000X

60 degree tilt

Figure 2-85. SEM Fractographs of Interlaminar Mode II Shear, 0/90 Fracture, Water Immersion (160 F) After Test

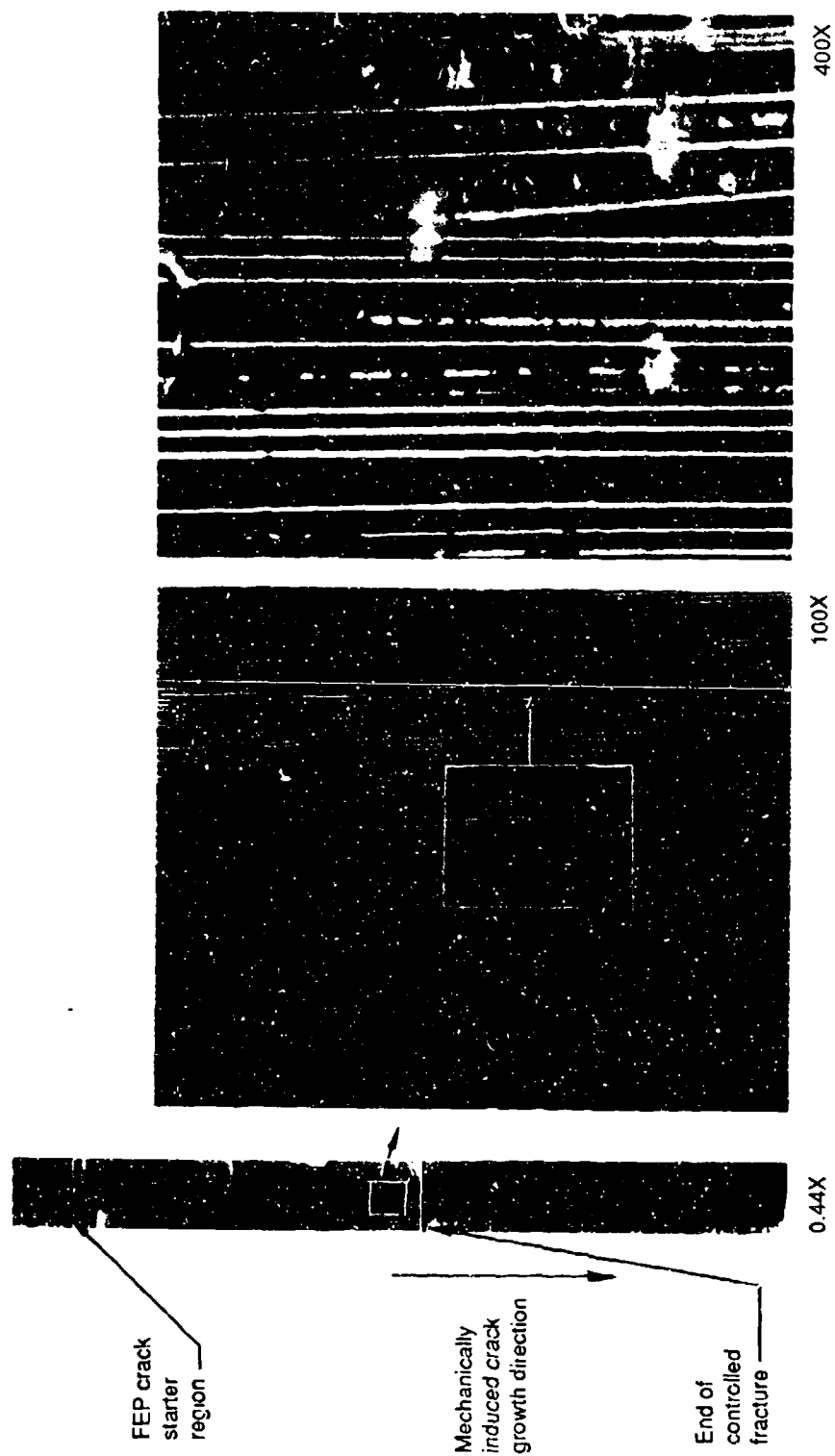
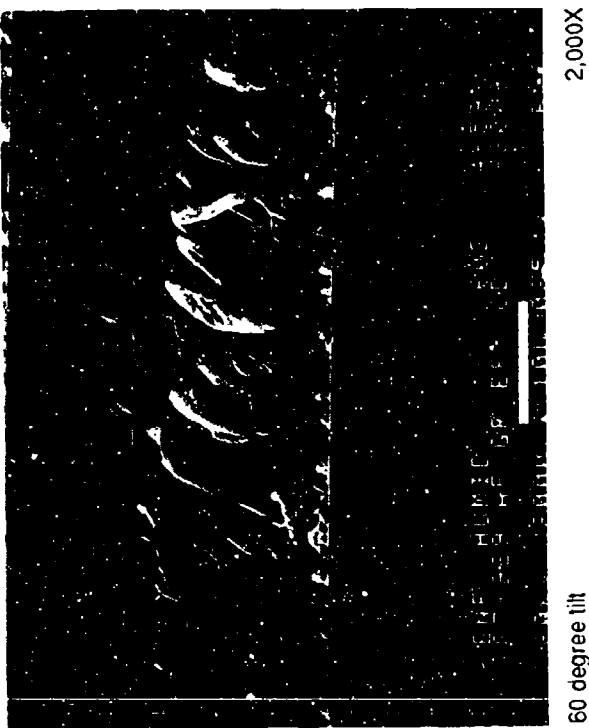
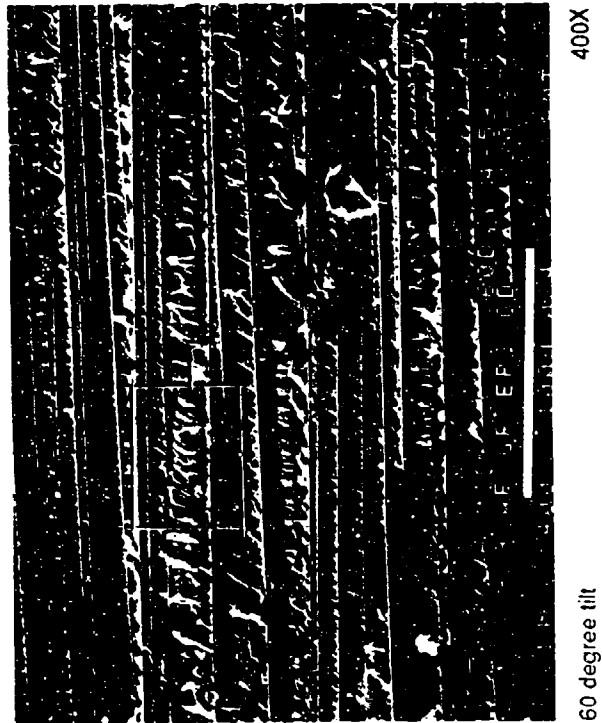
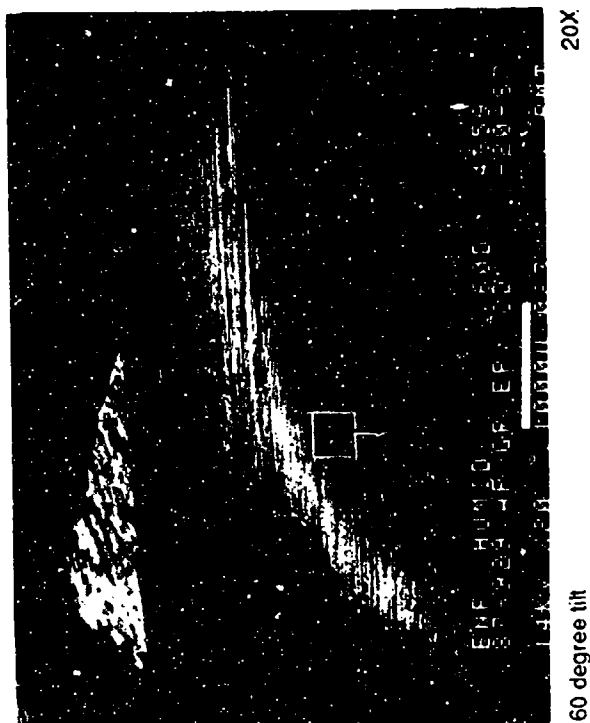


Figure 2-86. Optical Photomicrographs of Interlaminar Mode II Shear, 0/90 Fracture, Exposure to Humidity (160 F) After Test



Legend:

F fiber matrix separation

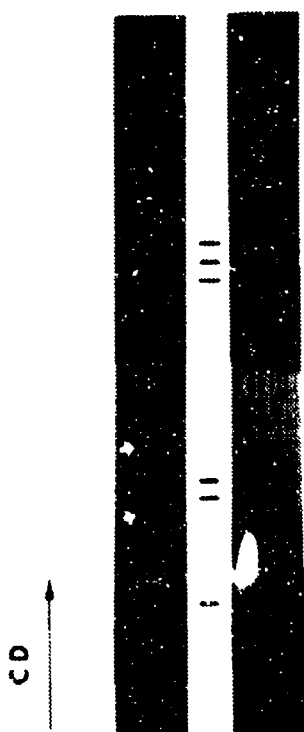
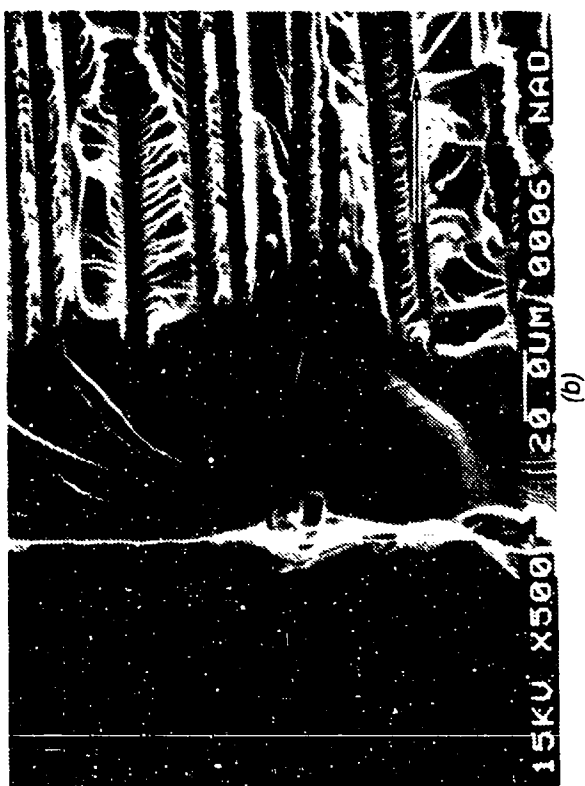
H hackles

R rivermarks

Mechanically induced crack direction



Figure 2-87. SEM Fractographs of Interlaminar Mode II Shear, 0/90 Fracture, Exposure to Humidity (160 F) After Test

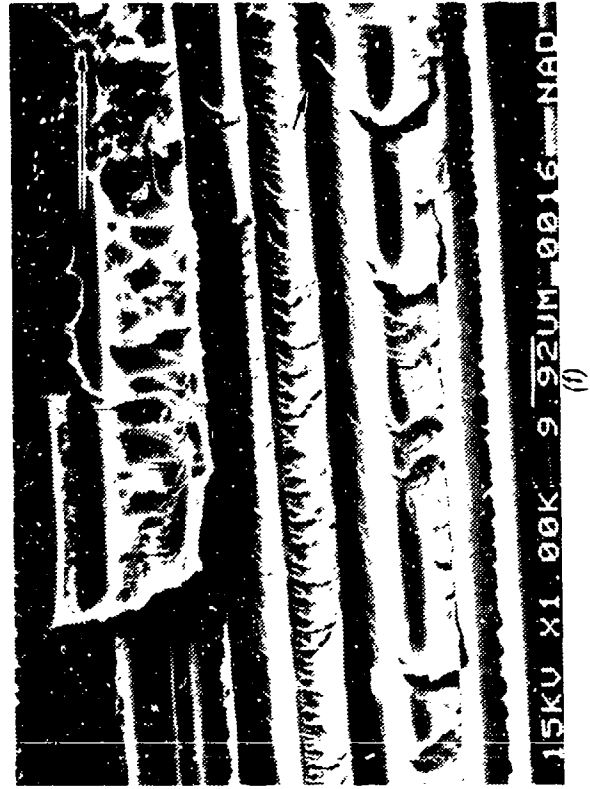


(a)

CD
↑

Figure 2-88. Optical and SEM Photographs of Mode II ENF Shear Interlaminar Fracture in Undercured Gr/Ep - [0]_{24T}
 (a) Macrophotograph of Fracture
 (b) Initiation Site in Region I
 (c) River Patterns (R) in Region I

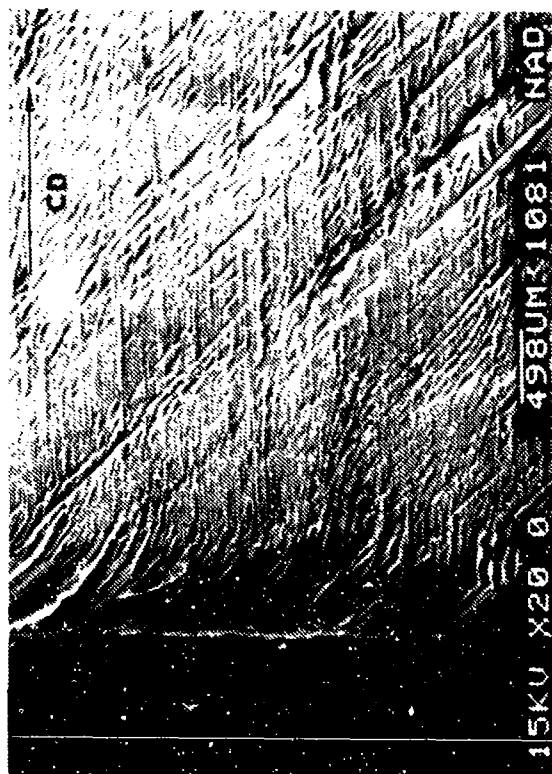
CD = Crack-propagation direction



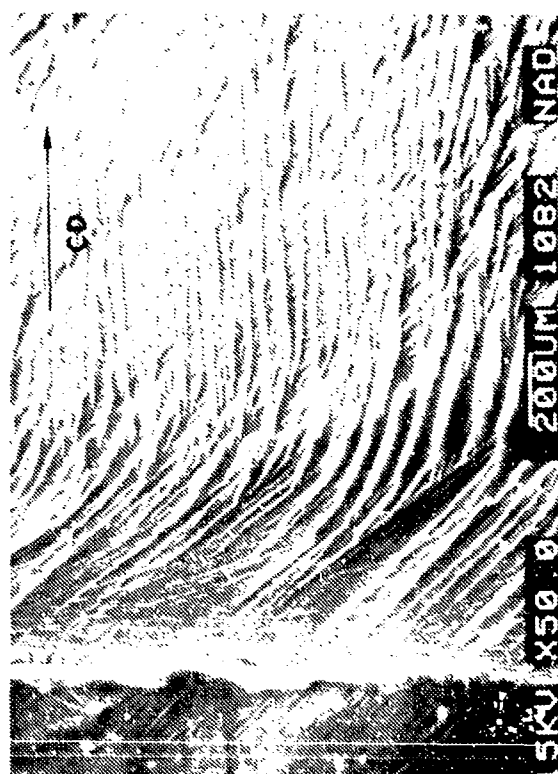
CD
↑

Figure 2-88. (Continued)
 (d) Region I/II Interface
 (e) Hackles (H) and Scallops (S) in Region II
 (f) V-Shaped Tears (Arrow) in Region II

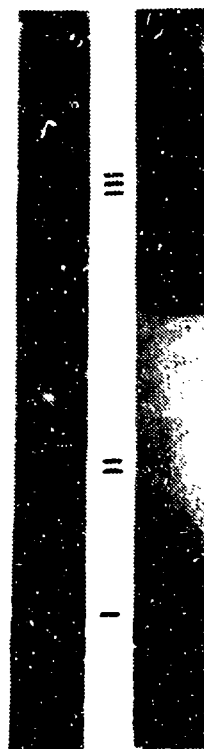
CD = Crack propagation direction



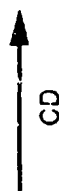
(a)



(b)



(c)



CD

Figure 2-89. Optical and SEM Photographs of Mode II ENF Shear Interlaminar Fracture in Undecured Gr/Ep - [+45/0/-45]_s
 (a) Macrophotograph Showing Regions I, II, and III
 (b) Local Initiation sites in Region I
 (c) River Patterns in Region I

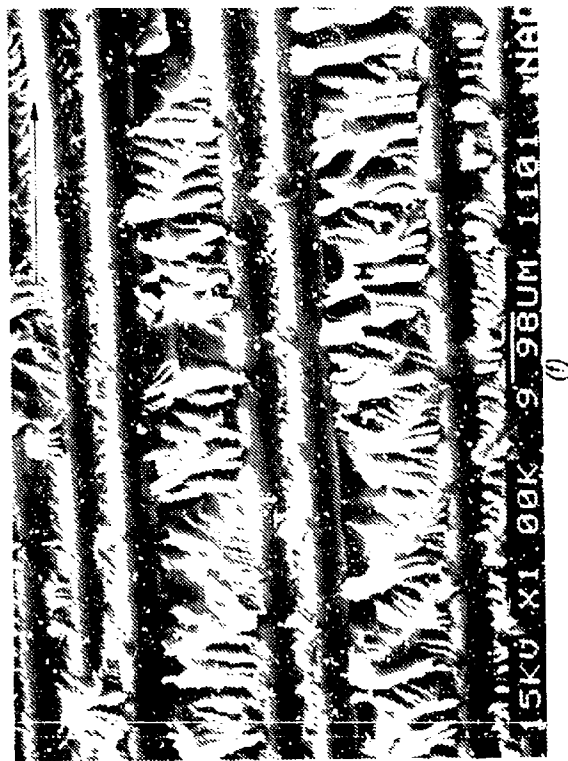
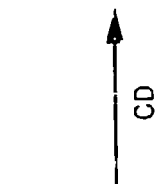
CD = Crack-propagation direction



(d)

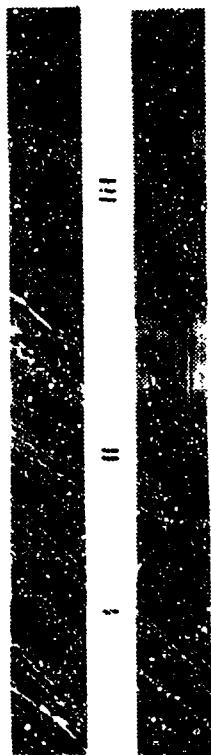


(e)



(f)

Figure 2-89. (Continued)
 (d) River Patterns in Resin Between 0 and 45 Degree Piles
 (e) Mode I/Mode II Interface
 (f) Hackles (H) in Region II
 CD = Crack propagation direction



(a)

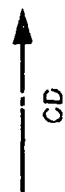
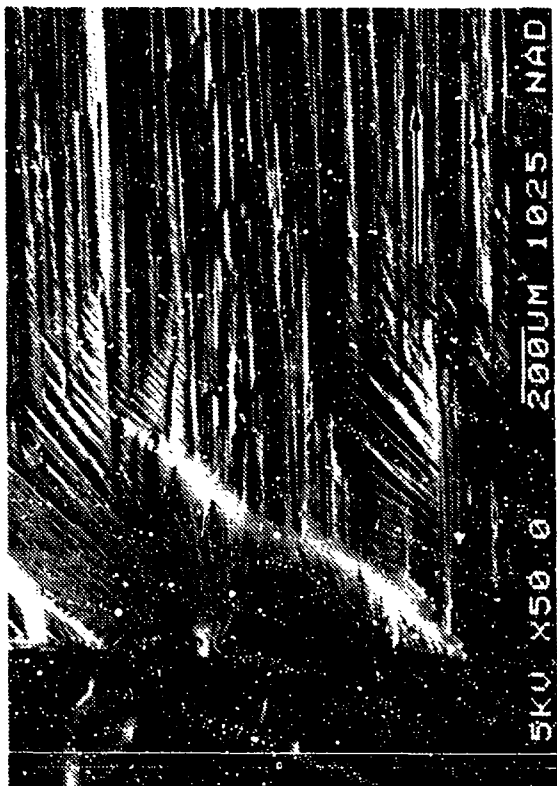
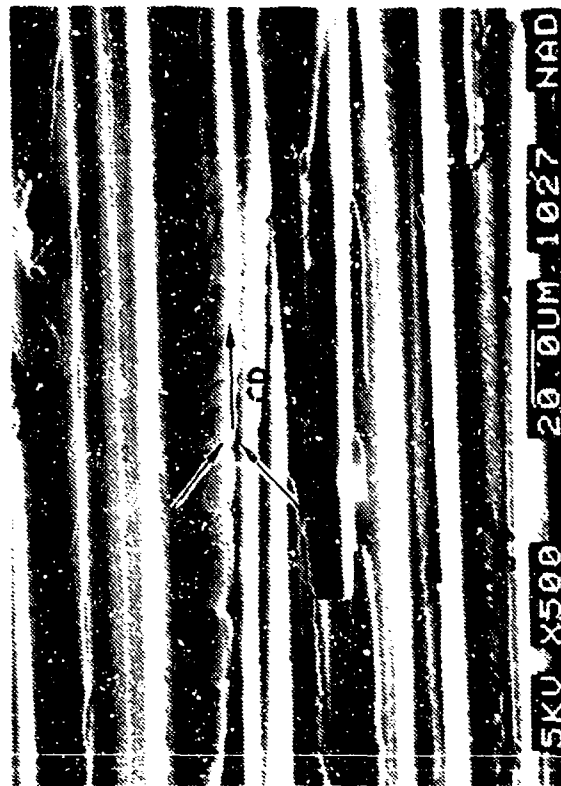


Figure 2-90. Optical and SEM Photographs of Mode II ENF Shear Interlaminar Fracture in Overcured Gr/Ep - [0]_{24T}
 (a) Macro photograph of Fracture
 (b) Initiation Site in Region I
 (c) Mapping of CD With River Patterns (Arrows)

CD - Crack propagation direction



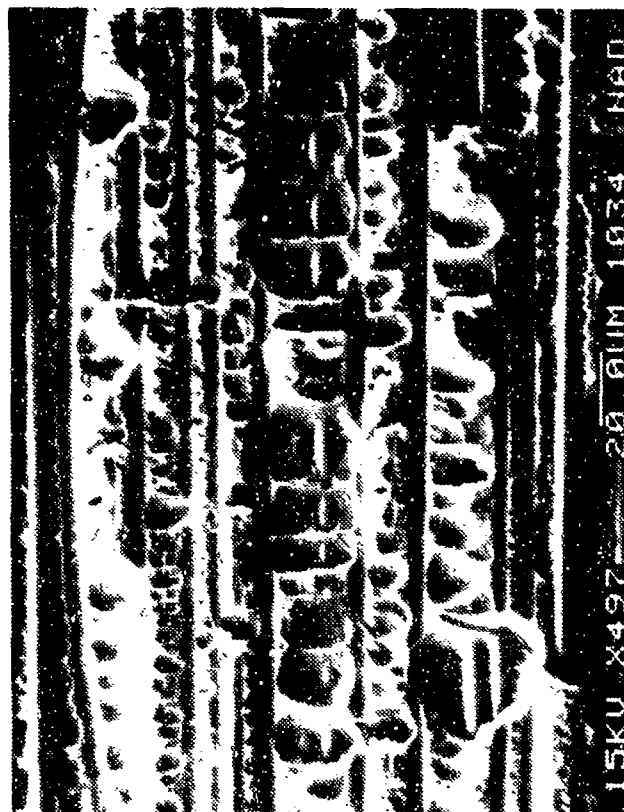
(b)



(c)



(d)



(e)

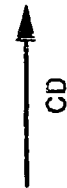


Figure 2-90. (Continued)
 (d) Hackles (H) and Scallops (S) in Region II
 (e) Microflow Lines in Scallops in Region II

CD = Crack propagation direction

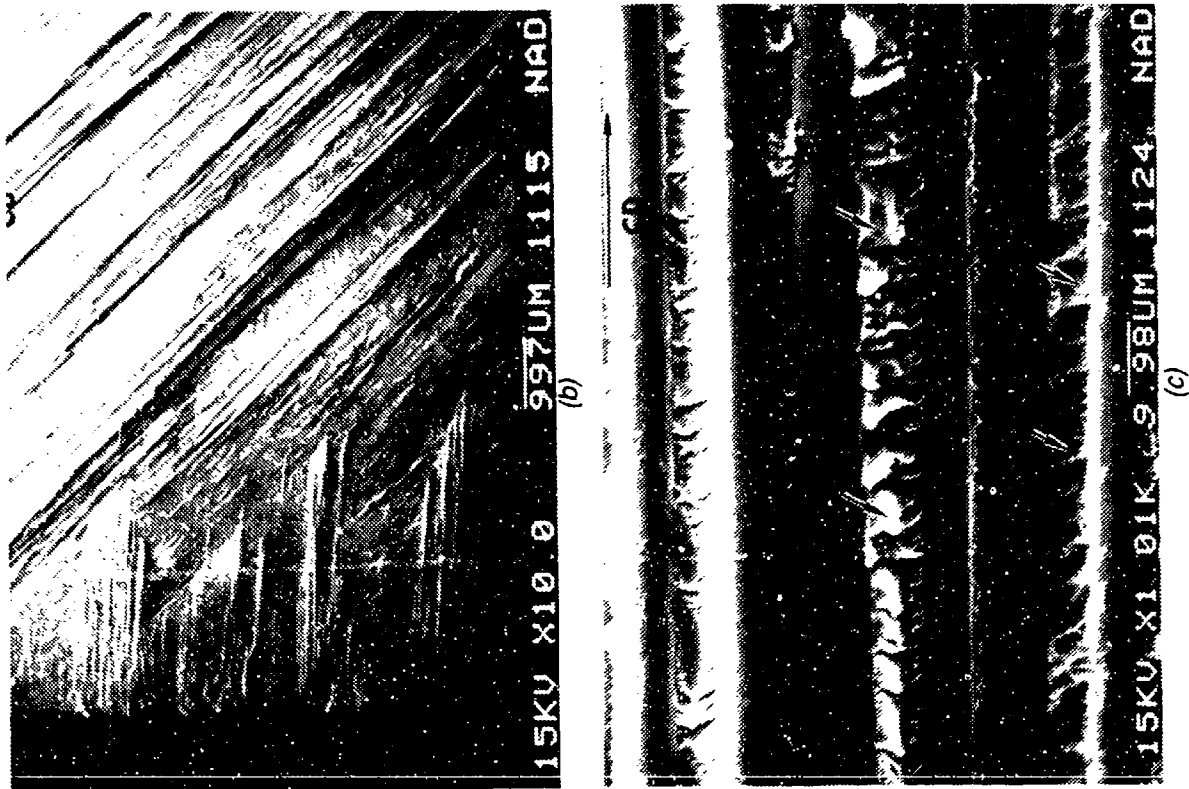


Figure 2-91. Optical and SEM Photographs of Mode II ENF Shear Interlaminar Fracture in Overcured Gr/Ep - [+45/0/-45]_s
 (a) Macro photograph Showing Regions I, II, and III (Precrack, Crack-Growth, Laboratory Overload)
 (b) Initiation in Resin Between 0 and 45 Degree Plies (c) Hackles (H) and Scallop (S) in Region II
 CD = Crack-propagation direction

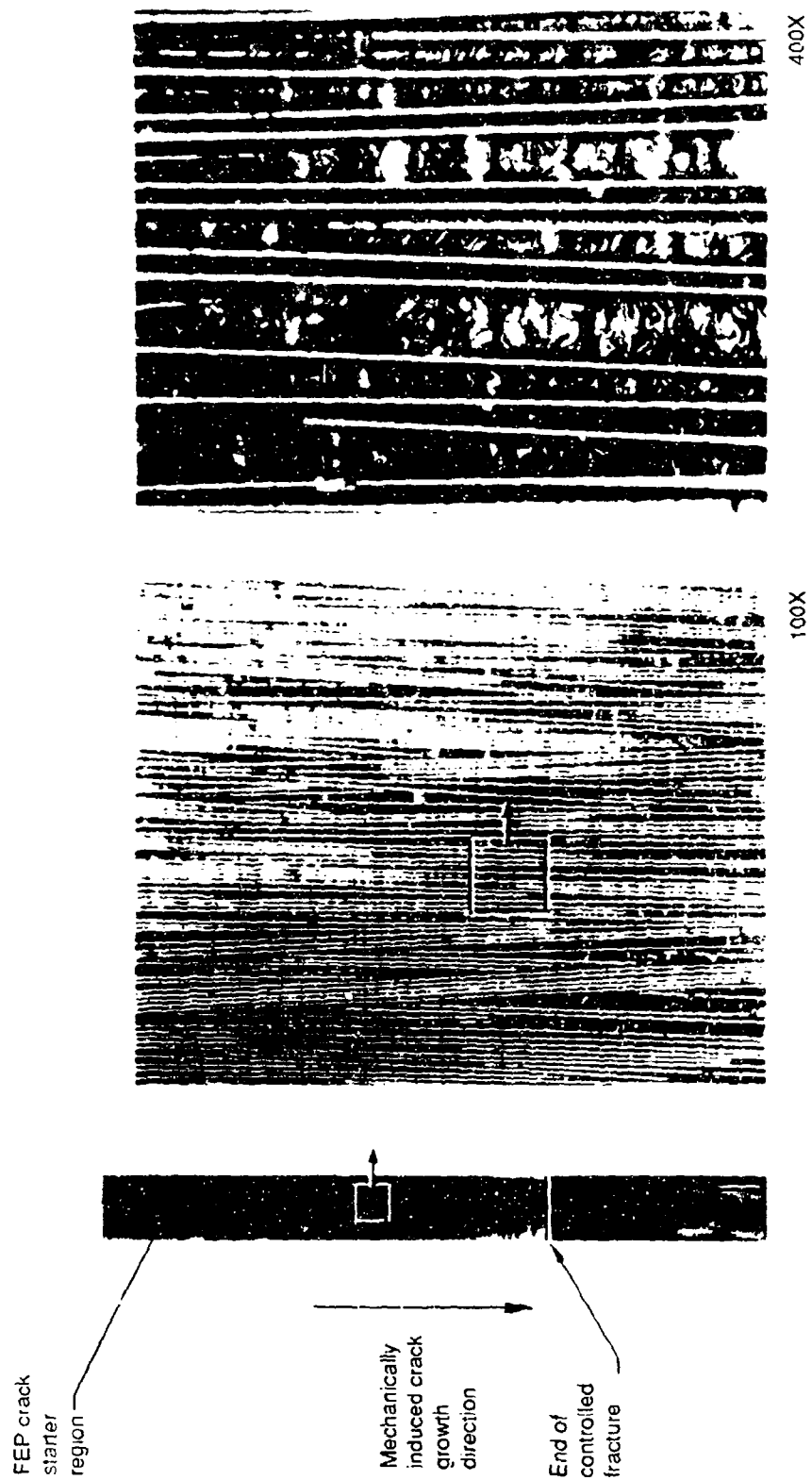
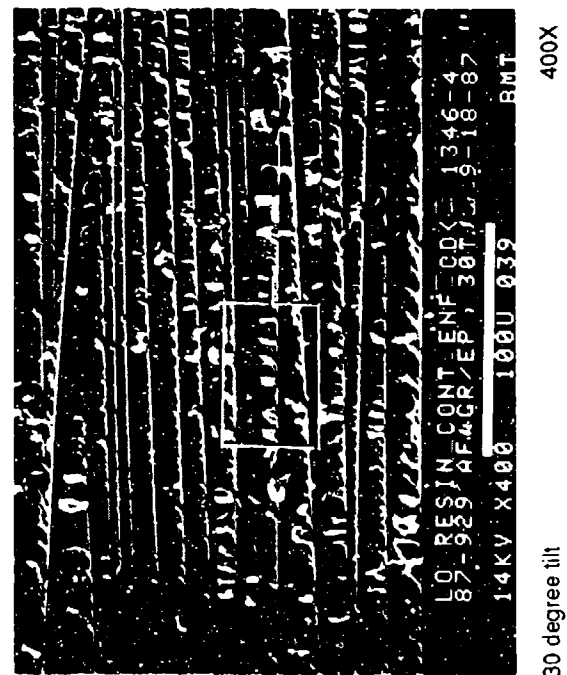
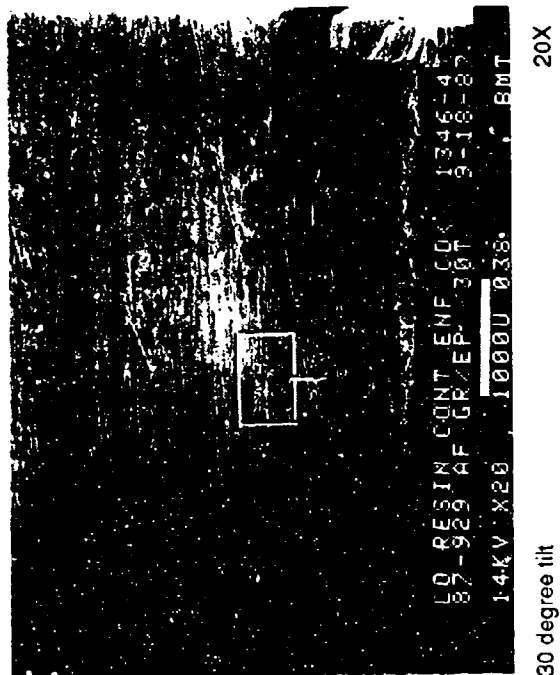


Figure 2-92. Optical Photomicrographs of Interlaminar Mode II Shear, 0/90 Fracture of Low Resin Content Specimen



Legend:
 F fiber/matrix separation
 H hackles
 R rivermarks
 Mechanically induced crack direction
 →

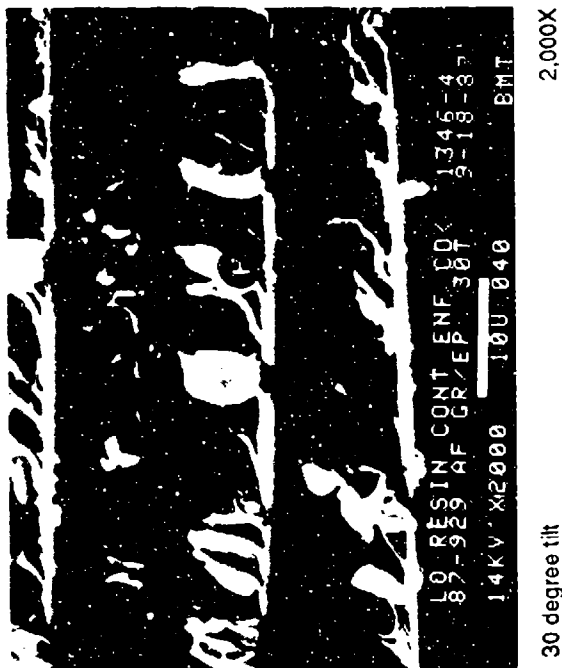
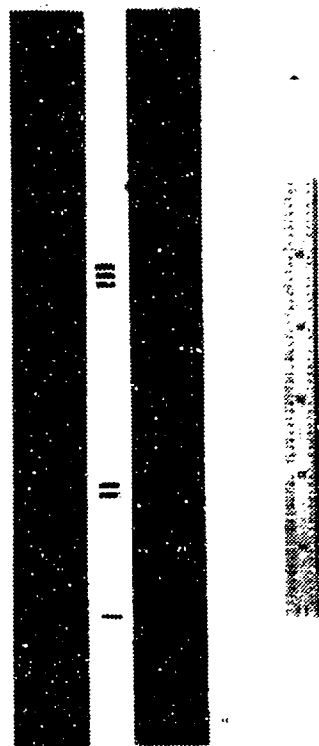
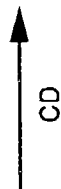


Figure 2-93. SEM Fractographs of Interlaminar Mode II Shear, 0/90 Fracture of Low Resin Content Specimen



(a)



CD



(b)



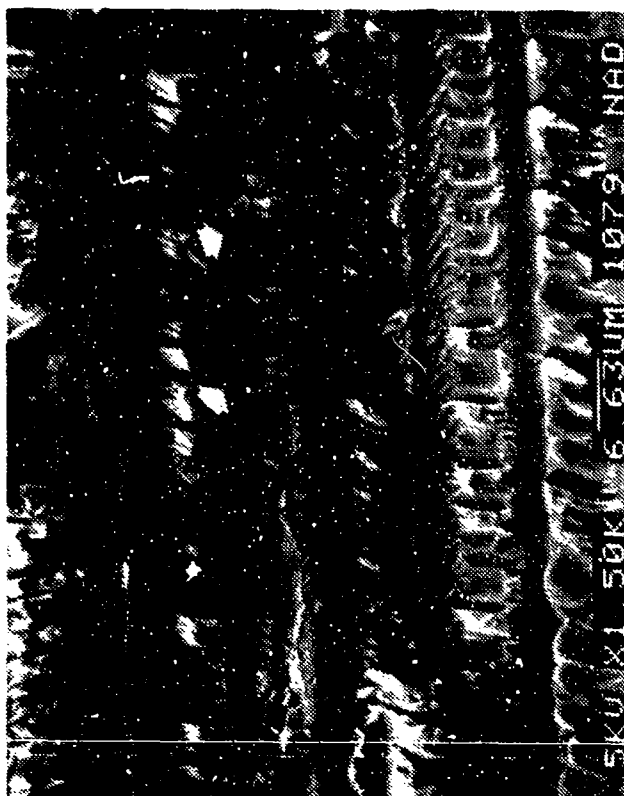
(c)

Figure 2-94. Optical and SEM Photographs of Mode II ENF Shear Interlaminar Fracture in High Resin Content Gr/Ep - [0]_{24T}
 (a) Macro photograph Showing Region I, II, and III
 (b) Local Initiation in Region I
 (c) River Patterns Indicate CD

CD = Crack propagation direction



(d)



(e)

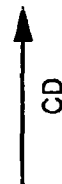
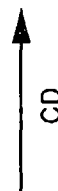


Figure 2-94. (Continued)
 (d), (e) Mode II Shear Fracture in Region II
 Note hackles (H), scallops (S), resin micro-flow
 (Arrows) and S-shaped cracks

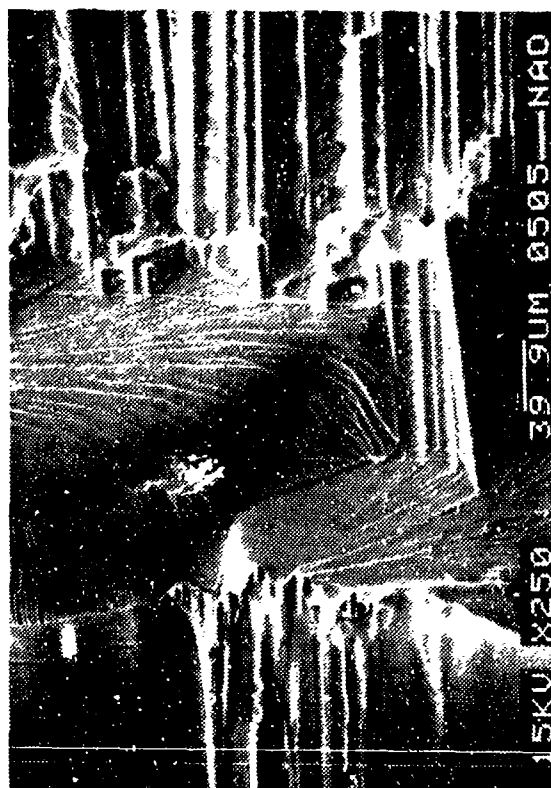
CD = Crack-propagation direction



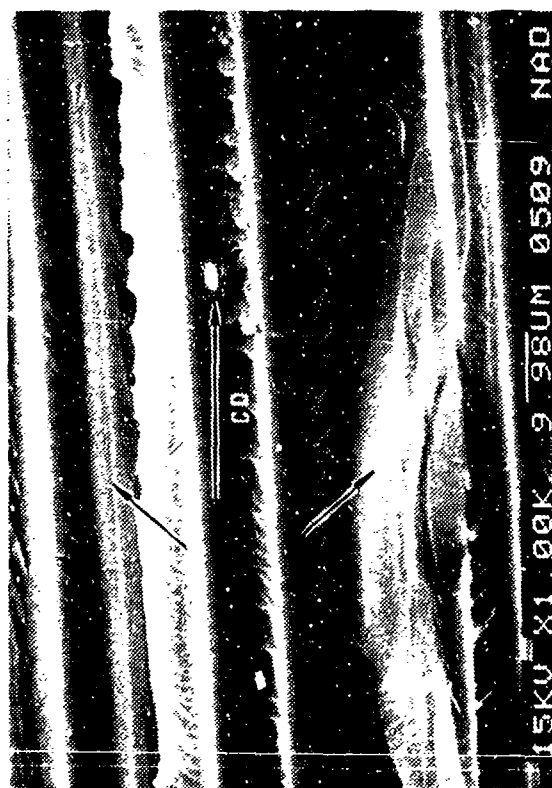
(a)



CD



(b)



(c)

Figure 2-95. Optical and SEM Photographs of Mode II ENF Interlaminar Shear Fracture in High Resin Content Gr/Ep - [0/90]_{6s}
 (a) Macrograph Showing Regions I, II, and III (Precrack, Mode II Shear, Laboratory Overlay)
 (b) Initiation Occurring in Mode I Resin-Rich Areas
 (c) River Patterns (Arrows) in Mode I Tension Fracture Area That Can Be Used to Map CD

CD = Crack propagation direction



(d)



(e)

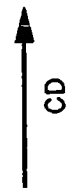


Figure 2-95. (Continued)
 (d) Mode I/Mode II Interface
 (e) Hackles (H) and Scallops (S) in Mode II Fracture
 CD = Crack-propagation direction

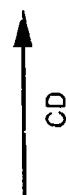
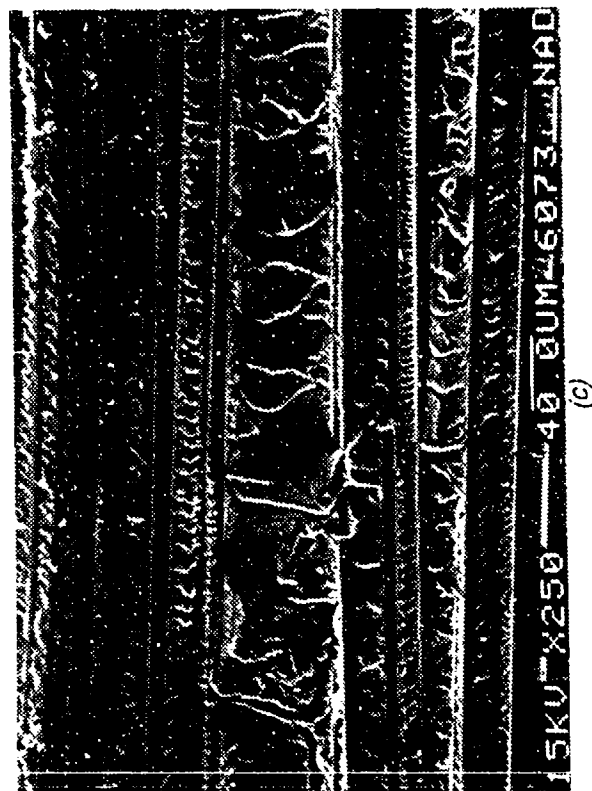
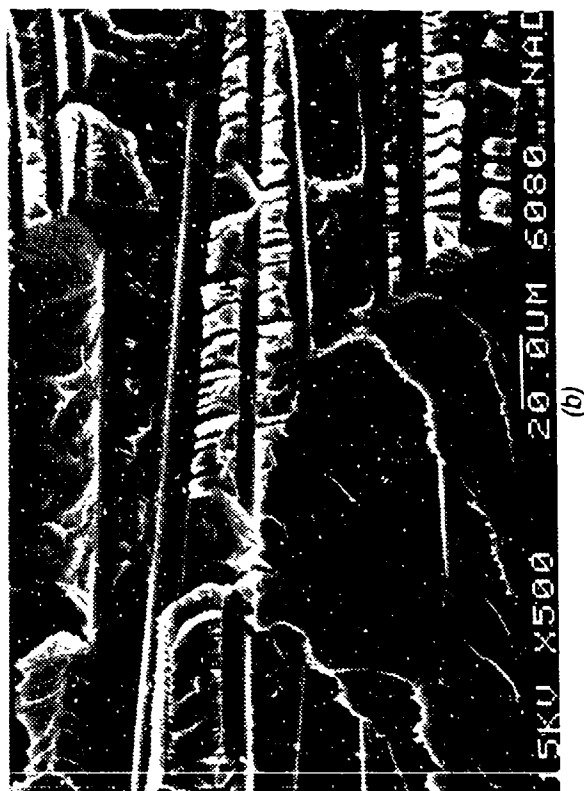
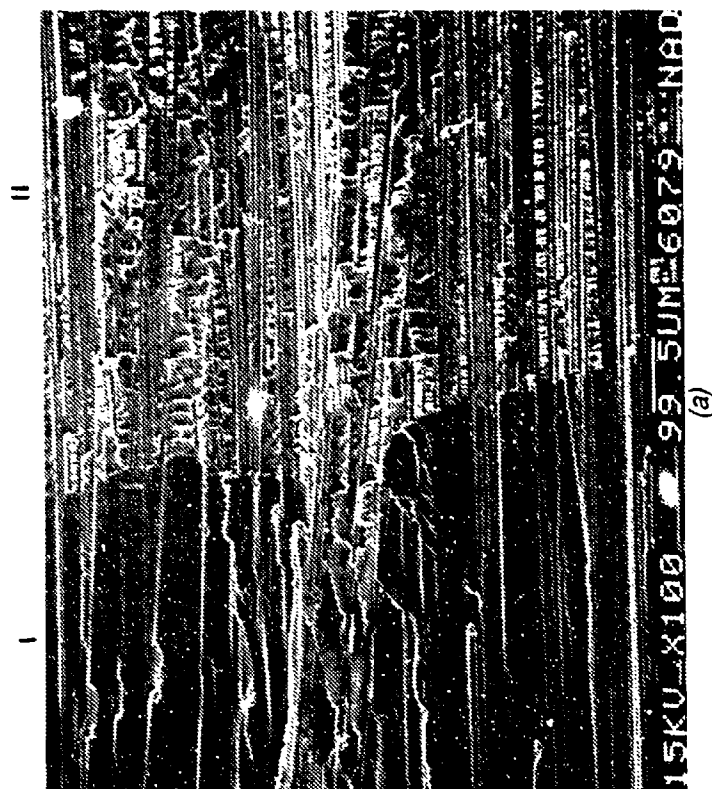


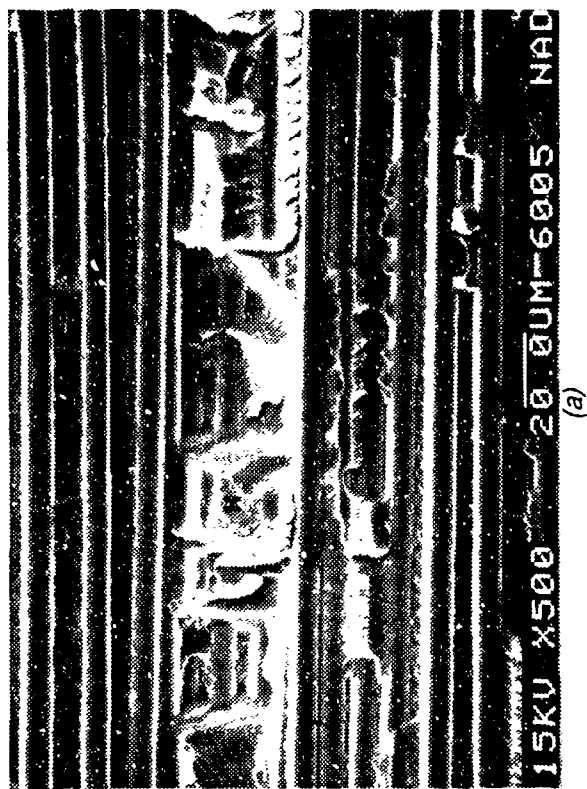
Figure 2-96. SEM Photographs of Mode II ENF Interlaminar Shear Fracture in High Resin Content Gr/Ep, Conditioned 180 F/Dry After Test

(a) Precrack to Crack-Growth Transition Region in [0] 24T Coupon
 I = Precrack, II = Crack-growth

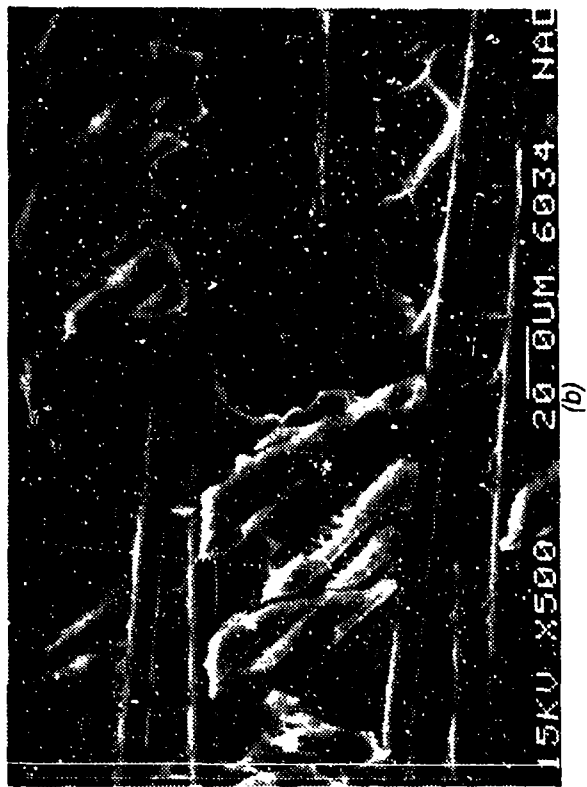
(b) Details of Fracture in (a)
 R = River patterns, H = Hackles, S = Scallops

(c) Hackles (H) in Crack-Growth Region of [0/90]_{es} Coupon

CD = Crack-propagation direction



(a)



(b)



(c)

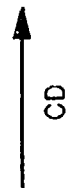


Figure 2-97. SEM Photographs of Mode II ENF Interlaminar Shear Fracture in Overcured Gr/Ep, Conditioned 180 F/Wet After Test

(a), (b) Crack-Growth Regions in $[0]_{24T}$ and $[\pm 45/0/\pm 45]_{4S}$ Coupons, Respectively
Note bare fibers and hackles (H)

(c) Detail of Area Shown in (b)
Note random river patterns on hackles

CD = Crack-propagation direction

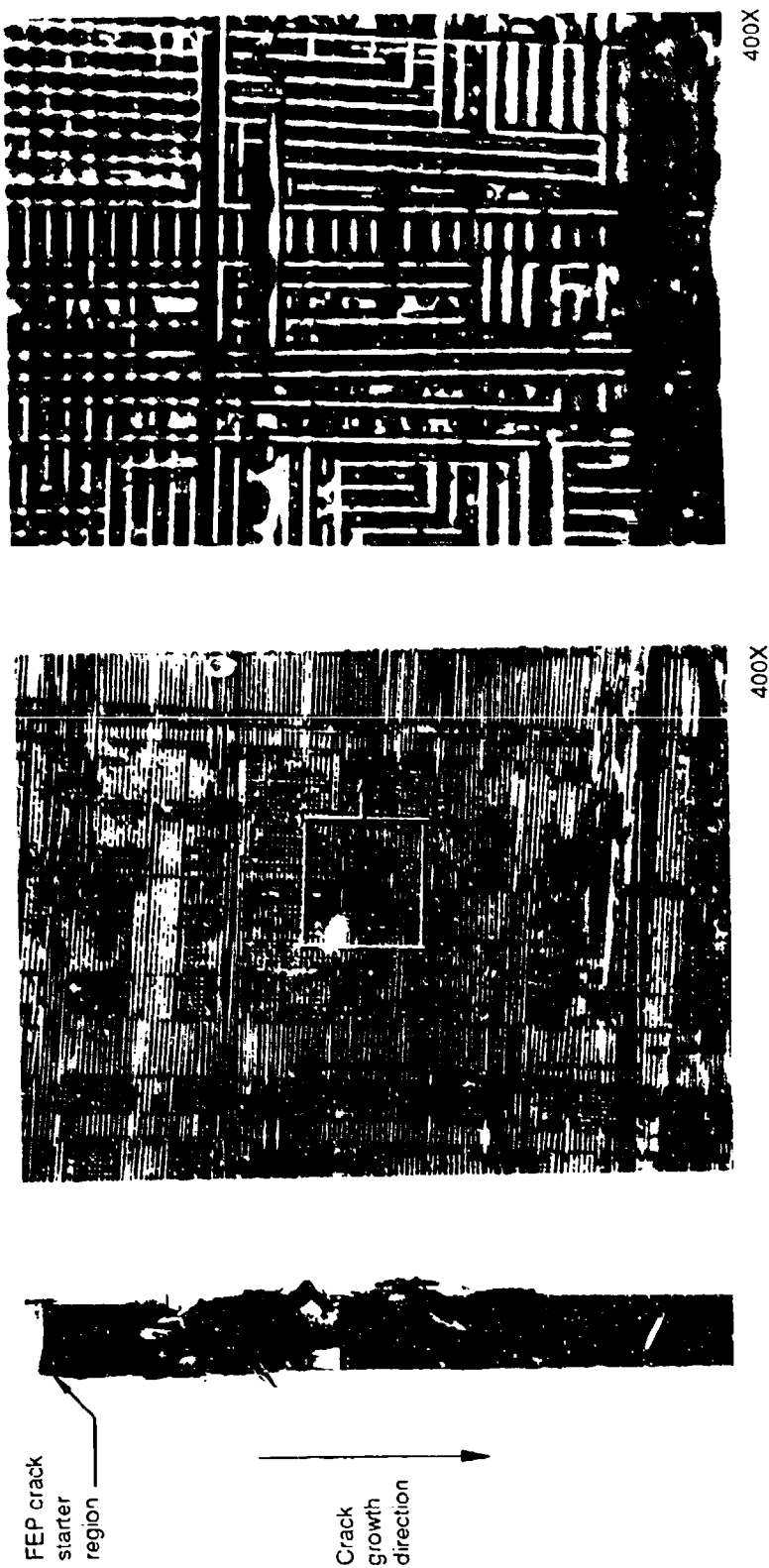
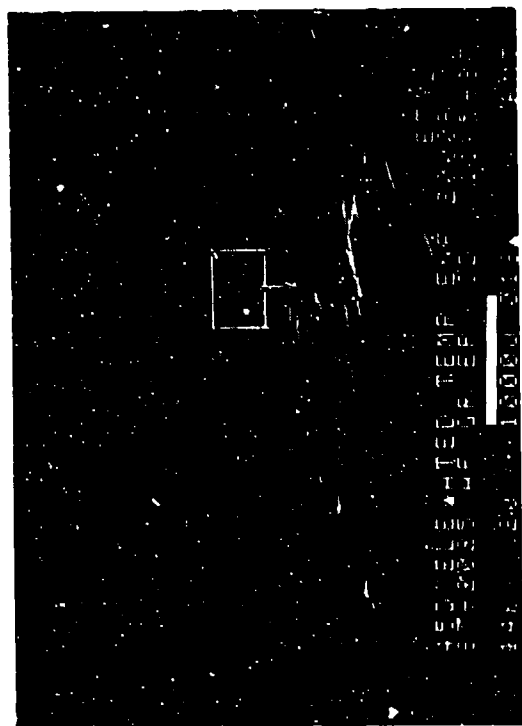


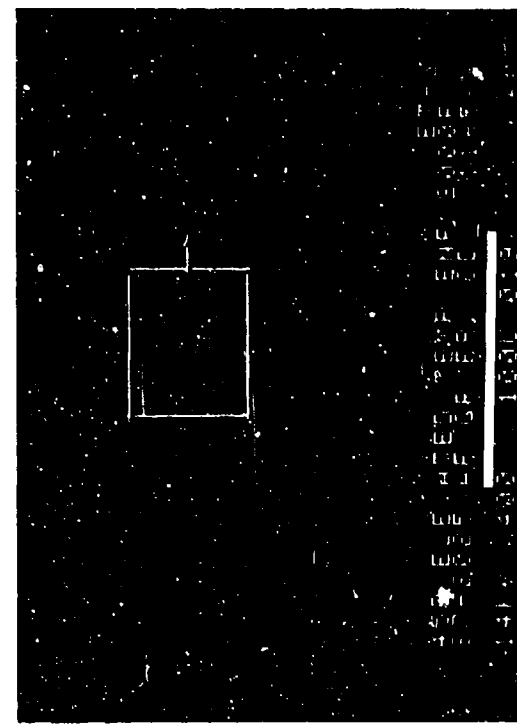
Figure 2-98. Optical Photomicrographs of Interlaminar Mode II Shear, 0.90 Fracture, 2000 F Exposure for 5 Minutes After Test



20X

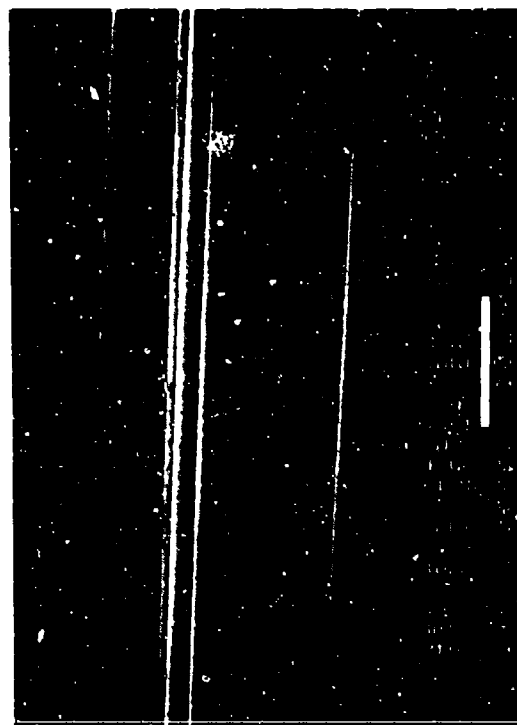
45 degree tilt

Mechanically induced
crack direction



400X

45 degree tilt



2,000X

45 degree tilt

Figure 2-99. SEM Fractographs of Interlaminar Mode II Shear, 0/90 Fracture, 2000 F Exposure for 5 Minutes After Test

2.3 INTERLAMINAR MIXED MODE FLEXURAL

The mixed mode flexural (MMF) test geometry, shown in Figure 2-100, produces 57 percent Mode I tension and 43 percent Mode II shear at the crack tip. The macroscopic fracture surface characteristics are as follows:

1. Macroscopically flat surface
2. Microscopically rough resin fracture with a predominance of hackles and scallops
3. Small localized regions of flat resin fracture exhibiting only river marks and resin microflow.

SEM examination of mixed-mode interlaminar failures indicates that these are characterized by mixtures of hackles or scallops and river patterns that are generally interspersed between the hackles. The river patterns can be used to map local fracture origins and direction as for pure Mode I tension. Processing variations (overcure or undercure), material form (filament winding versus tape), or post-processing variables (impact-damage) do not significantly alter the fracture characteristics.

The test matrix for MMF testing is provided in Table 2-3 and the related fractographs are shown in Figures 2-101 through 2-117. These figures are arranged in the same order that the corresponding tests are listed in Table 2-3.

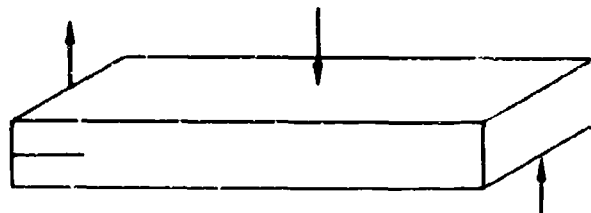


Figure 2-100. Mixed Mode Flexural Test Type

Table 2-3. Test Matrix for Modes I and II MMF Specimens

PLY/ORIENTATION	VARIABLE CONDITIONS	CONTRIBUTOR
24/0 24/± 45 24/0, ± 45 24/0, 90	RT/Dry (Baseline), During Test	Boeing
24/0 24/0, ± 45	Filament Wound	Northrop
24/0, ± 45	3-D Weave	Northrop
24/0 24/0, ± 45	Impact Damaged Before Test	Northrop
24/0	Water Immersion Before Test	Northrop
24/0 24/0, ± 45	Undercured	Northrop
24/0 24/0, ± 45	Overcured	Northrop
24/0	High Resin	Northrop
24/0	High Resin + Conditioned 180°F/Dry, After Test	Northrop
24/0, ± 45	Overcured + Conditioned 180°F/Wet, After Test	Northrop

Fracture type	Interlaminar mixed mode (I and II)
Ply layup	[0] ₂₄
Test type	Mixed mode flexure (MMF)
• Test conditions	21°C, dry
• Fracture between	0/0 plies
Material	Hercules 3501-6/177°C cure AS4 fibers

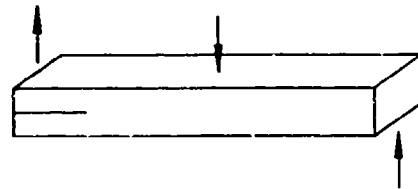
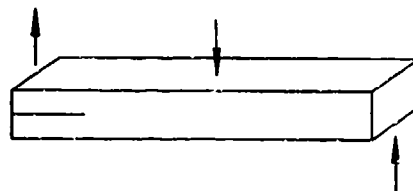


Figure 2-101. SEM Photograph of Interlaminar Mode I and Mode II, 0/0 Fracture, 70 F/Dry

Optical photomicrographs

Fracture type	Interlaminar mixed mode (I and II)
Ply layup	[+45, -45] 12S
Test type	Mixed-mode flexure (MMF)
• Test conditions	21°C, dry
• Fracture between	+45/-45 plies
Material	Hercules 3501-6/177°C cure AS4 fibers



← Mechanically induced crack direction

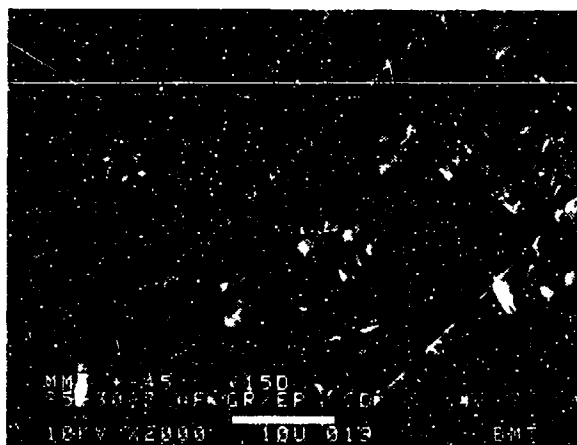
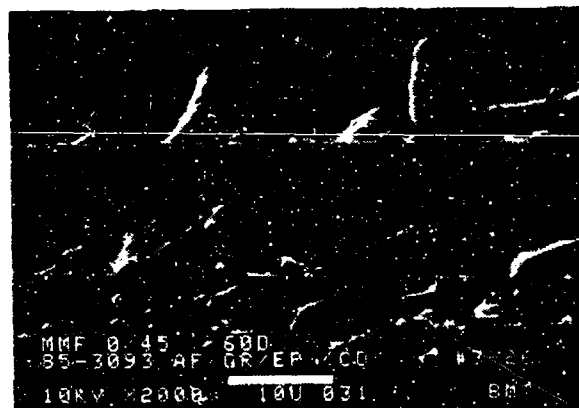
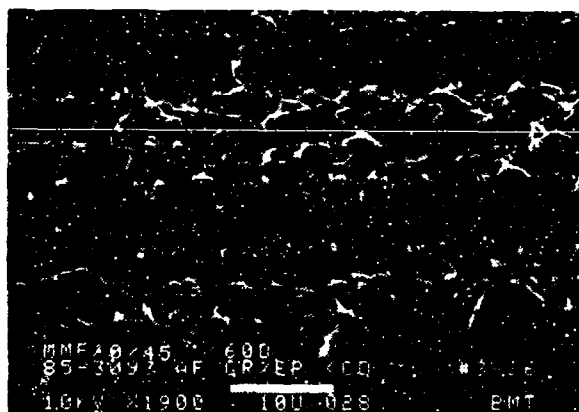
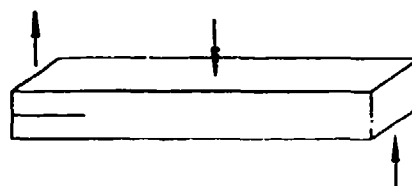


Figure 2-102. SEM Photographs of Interlaminar Mode I and Mode II, +45/-45 Fracture, 70 F/Dry

SEM photomicrographs

Fracture type	Interlaminar mixed mode (I and II)
Ply layup	[0, 45] _{12S}
Test type	Mixed-mode flexure (MMF)
• Test conditions	21°C, dry
• Fracture between	0/45 plies
Material	Hercules 3501-6/177°C cure AS4 fibers

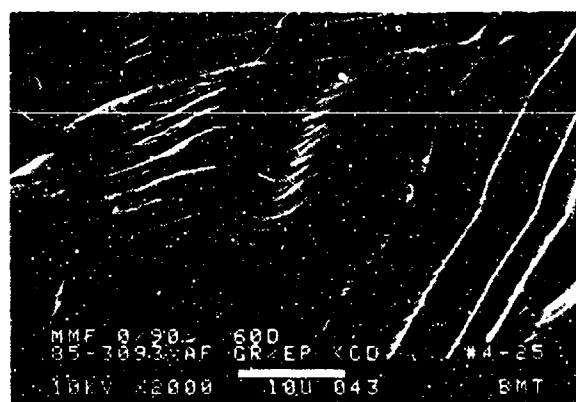
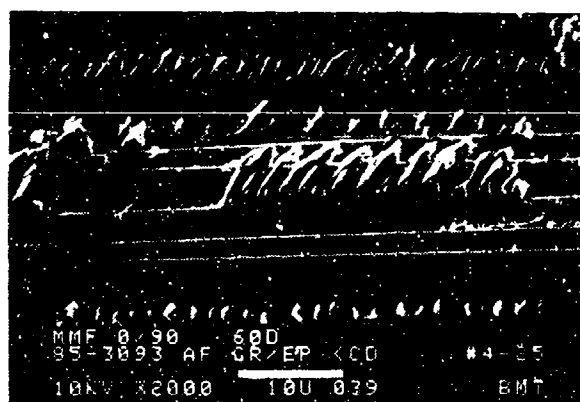
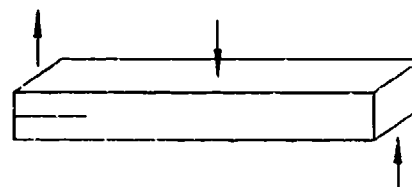


←
Mechanically induced crack direction

Figure 2-103. SEM Photographs of Interlaminar Mode I and Mode II, 0/45 Fracture, 70 F/Dry

SEM photomicrographs

Fracture type	Interlaminar mixed mode (I and II)
Ply layup	[0, 90] ₁₂ S
Test type	Mixed-mode flexure (MMF)
• Test conditions	21°C, dry
• Fracture between	0/90 plies
Material	Hercules 3501-6/177°C cure AS4 fibers



←
Mechanically Induced crack direction

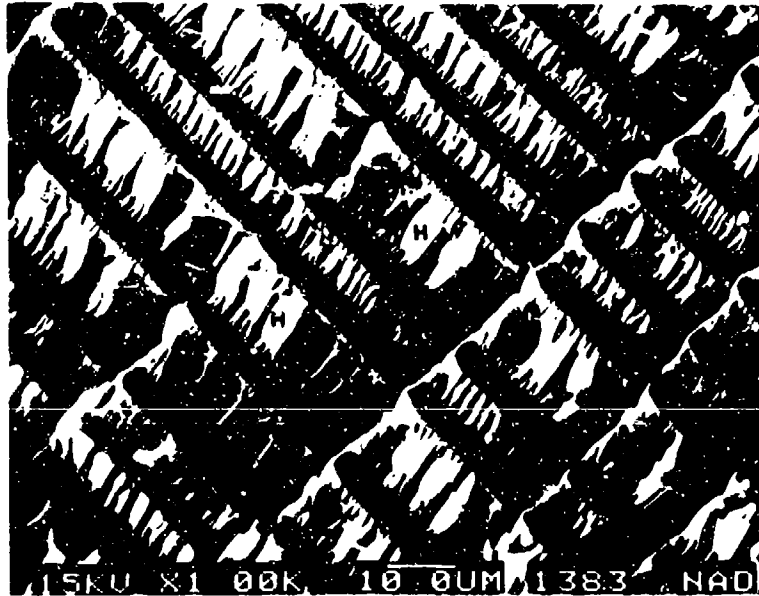
Figure 2-104. SEM Photographs of Interlaminar Mode I and Mode II, 0/90 Fracture, 70 F/Dry



CD
↑

Figure 2-105. SEM Photographs of Mode I and Mode II MMF Interlaminar Fracture in Filament Wound Gr/Ep - [0]_{24T}
 (a) River Patterns (R) at Initiation Site (Precrack Region)
 (b) Precrack to Crack-Growth Transition Region (Mode I Tension to Mixed Mode I Tension and Mode II Shear)
 (c) Hackles (H) and River Patterns (R) in Crack-Growth Region

CD = Crack-propagation direction





 CD

Figure 2-106. SEM Photograph of Mode I and Mode II MMF interlaminar Fracture in Crack-Growth Region of Filament Wound Gr/Ep - [+45/0/-45]_{4s}

CD = Crack-propagation direction
 H = Hackles
 R = River patterns

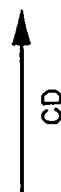
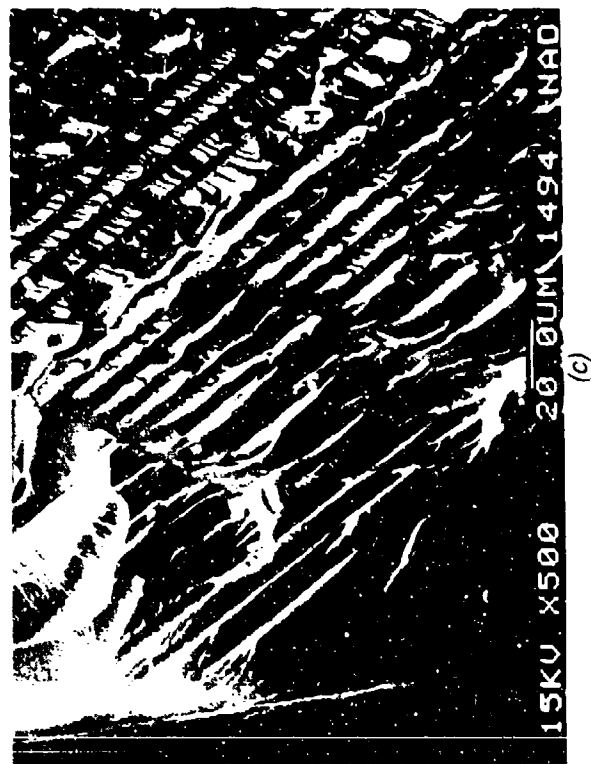
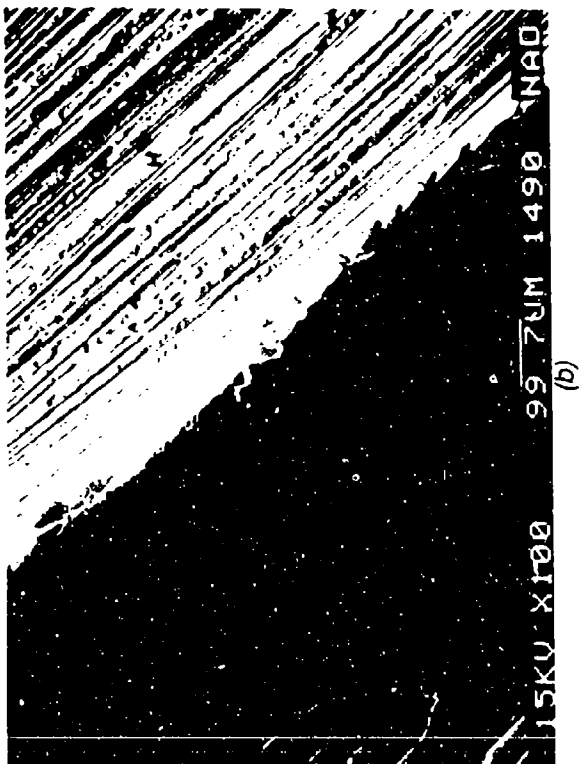


Figure 2-107. SEM Photographs of Mode I and Mode II MMF Interlaminar Fracture in 3-D Weave Gr/Ep - [+45/0/-45] ₄₅

(a) Initiation in Precrack Region of Coupon

(b) Hackles (H) and River Patterns (R) in Precrack Region

(c) Hackles (H) and River Patterns (R) in Crack-Growth Region

CD = Crack-propagation direction

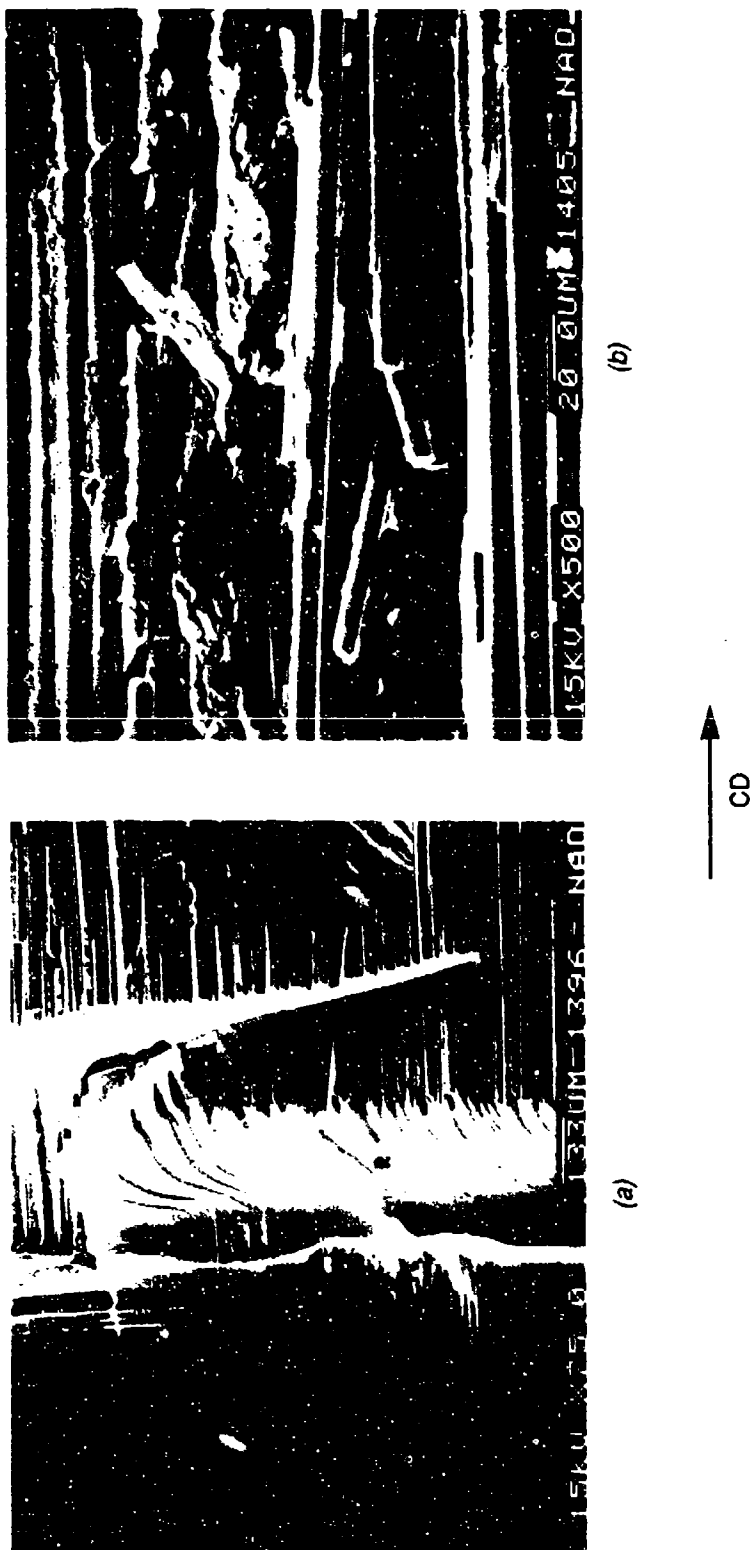


Figure 2-108. SEM Photographs of Mode I and Mode II MMF Interlaminar Fracture in Impact Damaged Gr/Ep - [0] _{24T}

(a) River Patterns in Precrack Initiation Region

(b) Impact Damage Area in Crack-Growth Region

Note broken fibers and crushed resin

CD = Crack-propagation direction



(a)

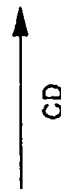
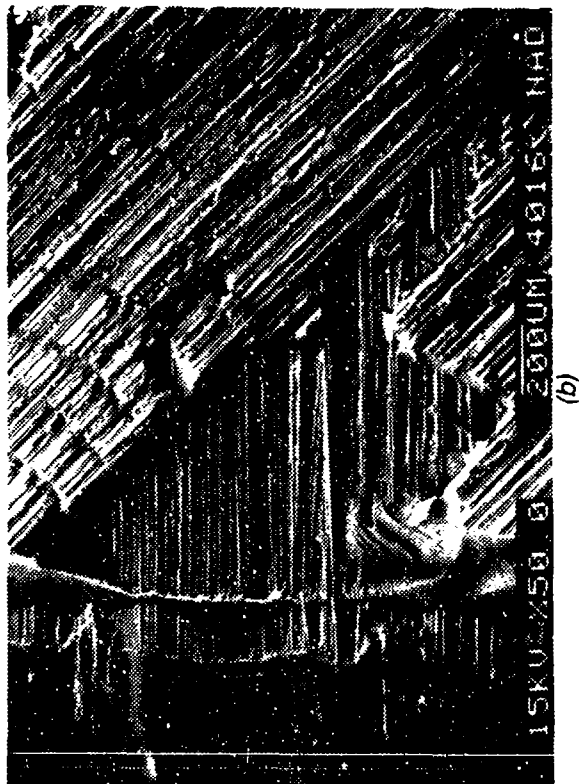
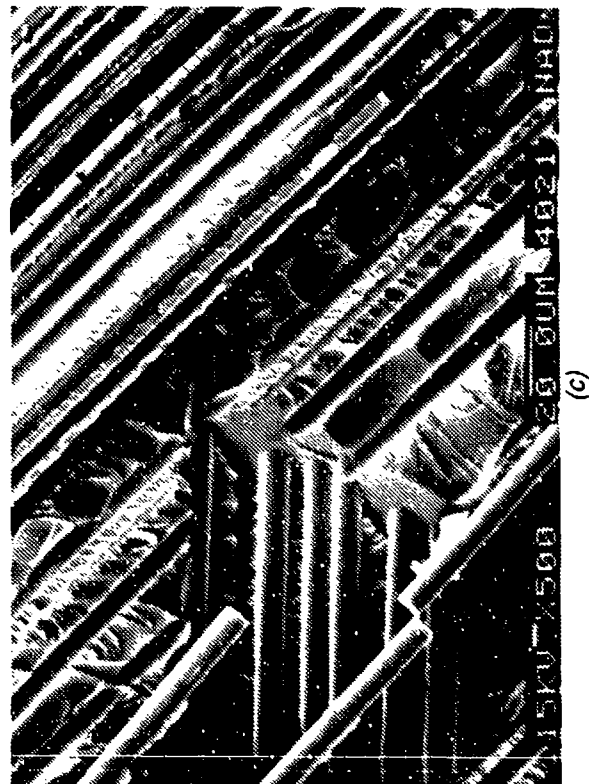


Figure 2-109. Optical and SEM Photographs of Mode I and Mode II MMF Impact Damaged Grl/Ep - [+45/0/-45]_{4S}
 (a) Macrophotograph Showing Regions I, II, III and IV (Precrack, Crack Growth Under Mode I Tension and Mode II Shear, Laboratory Overload, Impact Damage)
 (b) Initiation in Resin-Rich Areas
 (c) River Patterns in the Mode I Fracture Region

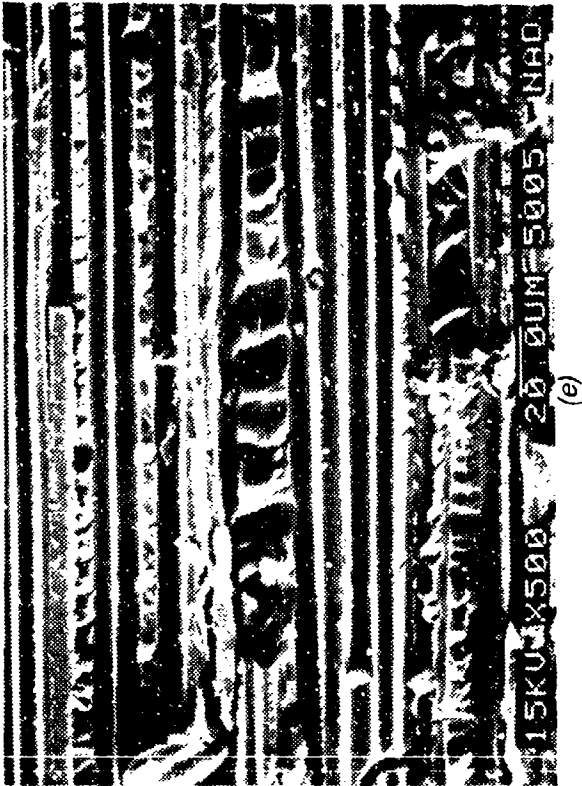
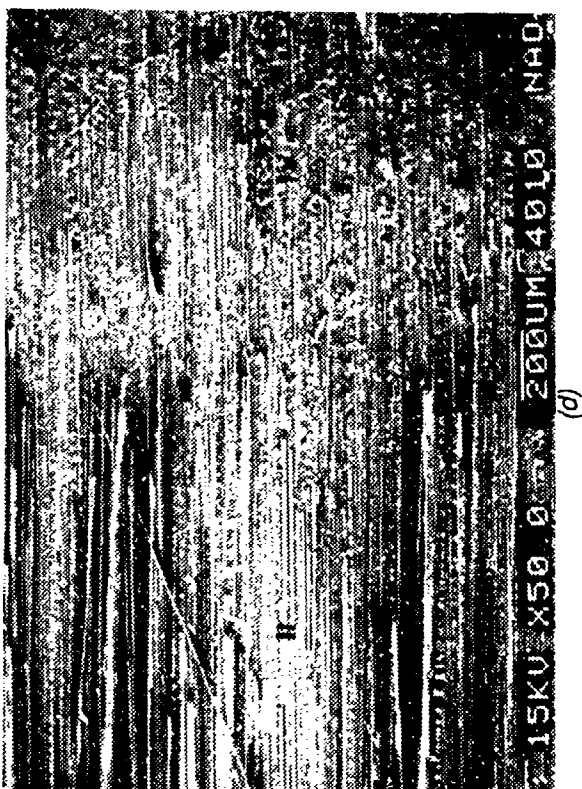
CD = Crack propagation direction



(b)



(c)




 CD



Figure 2-109. (Continued)
 (d) Interface Between the Mixed-Mode Region II and the Impact Region IV
 (e) Crushed Resin and Debris in the Impact Damaged Area
 (f) Mode I Tension and Mode II Shear Fracture Region
 Note the presence of river patterns (R), hackles (H), scallops (S) and localized cracks

CD = Crack-propagation direction

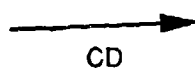
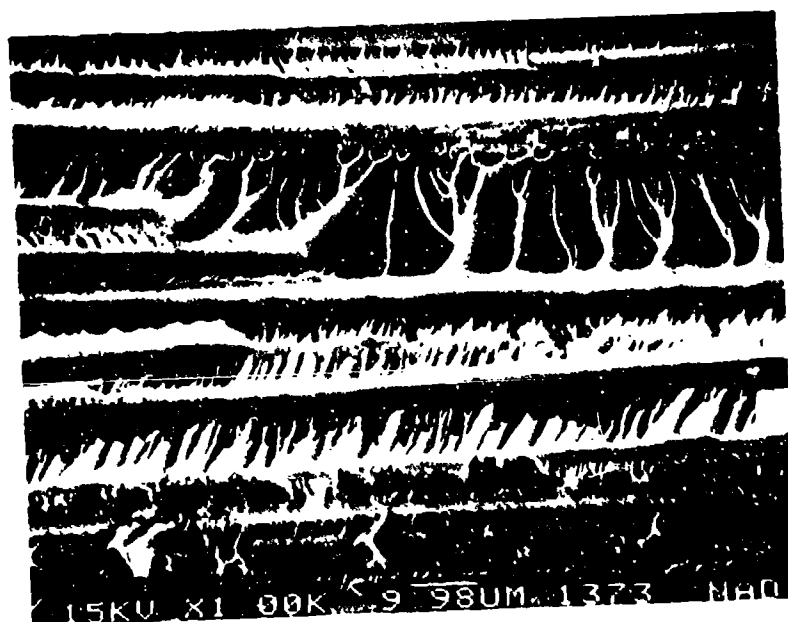
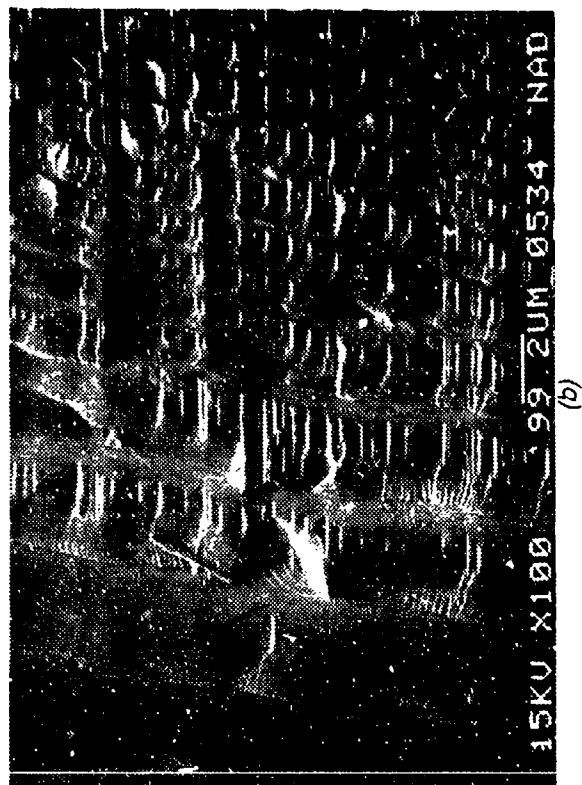
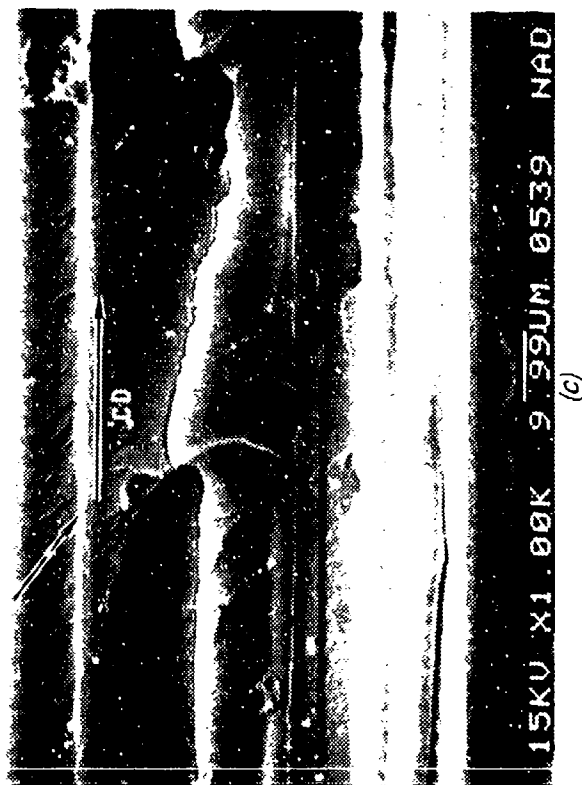


Figure 2-110. SEM Photograph of Mode I and Mode II MMF Interlaminar Fracture in Gr/Ep - [0] _{24T}, Water Immersion Before Test
 Note hackles and river patterns
 CD = Crack-propagation direction
 H = Hackles
 R = River patterns



(a)



(b)



(c)

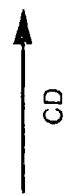
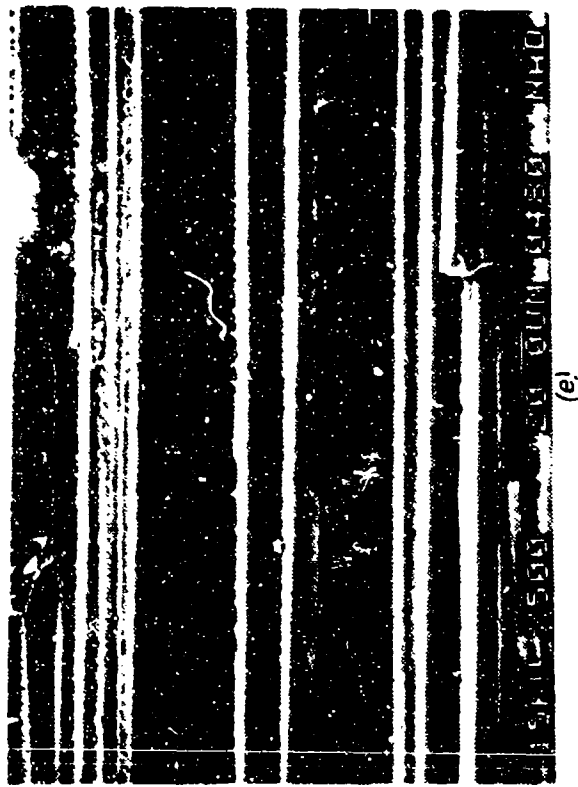


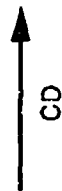
Figure 2-111. Optical and SEM Photographs of Mode I and Mode II MMF Interlaminar Fracture in Undercured Gr/Ep - [0]_{24T}
 (a) Macro photograph showing Regions I, II, and III (Pre-crack, Mode I and II Growth, and Laboratory Overload)
 (b) Mode I Tension Fracture Initiation in Resin-Rich Areas
 (c) River Patterns (Arrows) on Fractured Epoxy
 CD = Crack-propagation direction



(d)

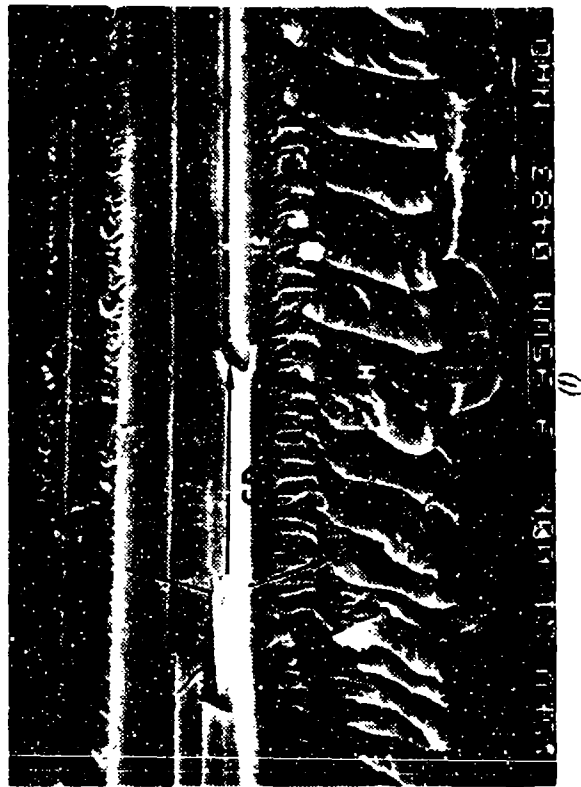


(e)

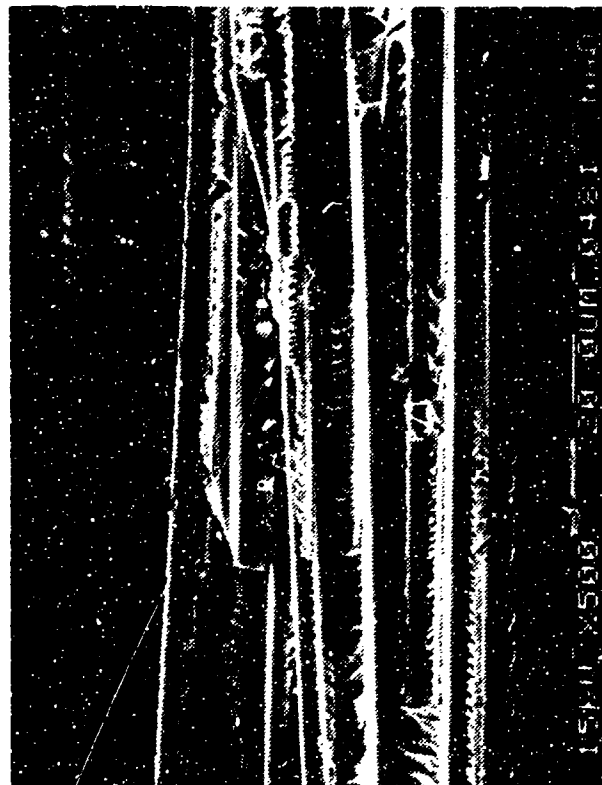


CD

Figure 2-111. (Continued)
 (d) Local Porosity (P) in Region I
 (e) Interface Between Mode I and Mixed-Mode Regions
 (f) River Patterns (Arrows) and Hackles (H) in the Mixed-Mode Region
 CD = Crack-propagation direction



(f)



(g)



(h)

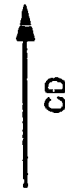


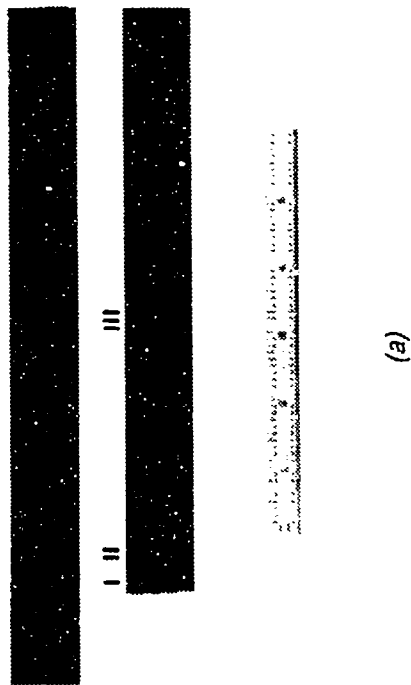
Figure 2-111. (Continued)

(g) Local Porosity (P) in Region II

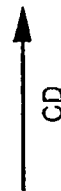
(h) River Patterns (Arrows) and Hackles (H) Present in the Mixed-Mode Regions

Note: The river patterns can be used to establish direction of fracture.

CD = Crack-propagation direction



(a)



CD



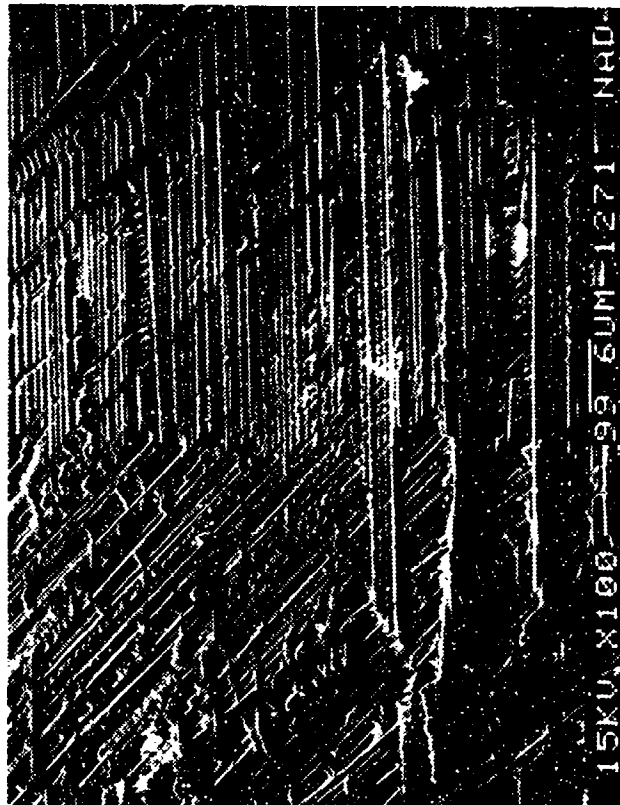
(b)



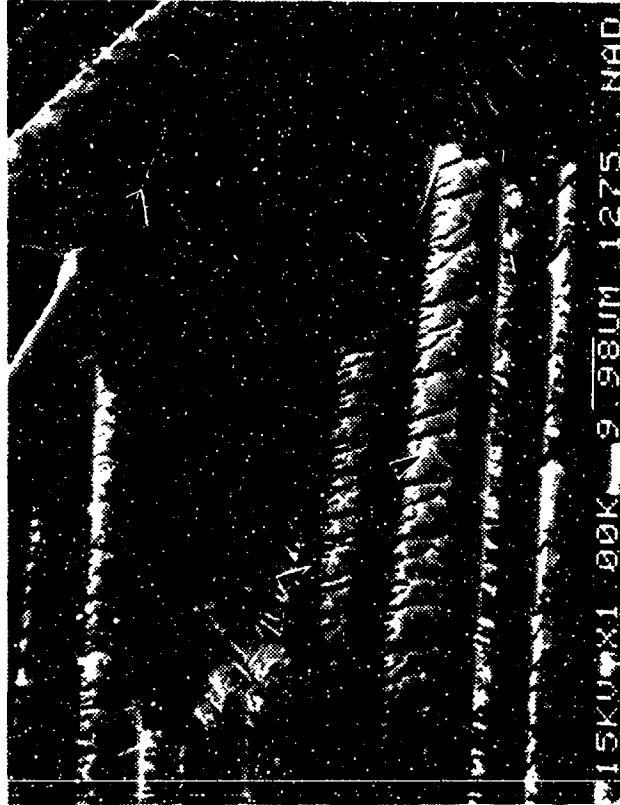
(c)

Figure 2-112. Optical and SEM Photographs of Mode I and Mode II
MMF Interlaminar Fracture in Undercured Gr/Ep -
[+45/0/-45] ₄₅
(a) Macro photograph
(b) Initiation in Precrack
(c) High Magnification Photograph of Precrack
Showing River Patterns (R)

CD = Crack propagation direction



(d)



(e)

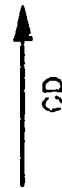
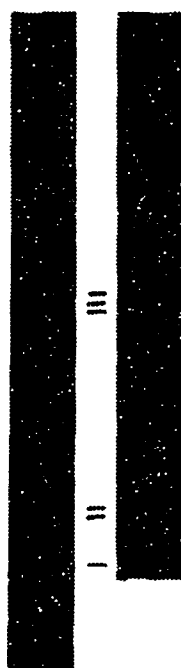
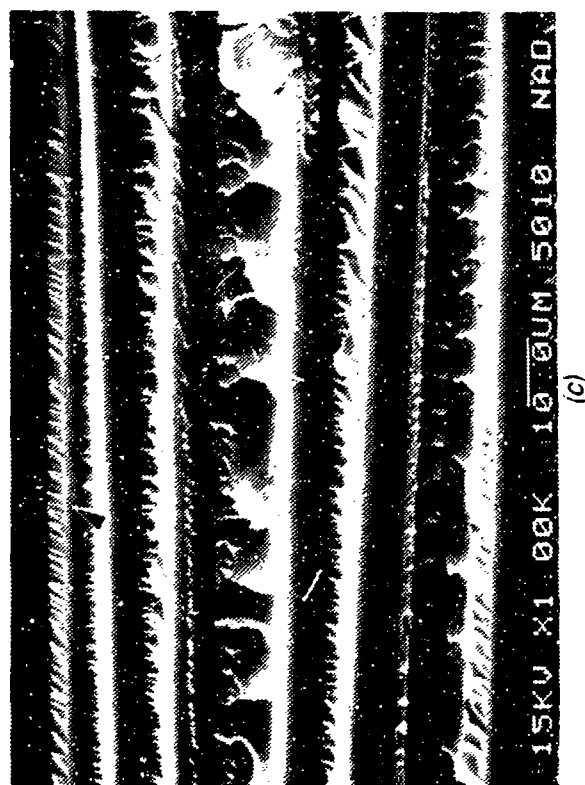
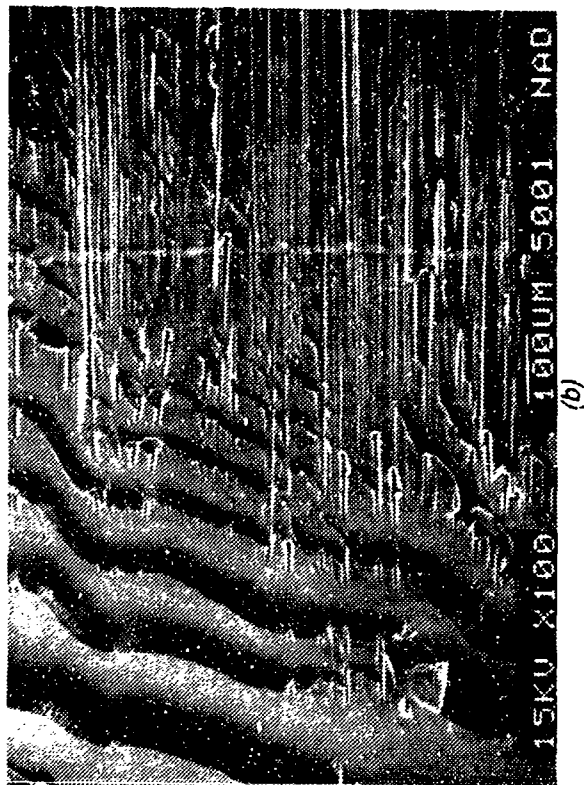


Figure 2-112. (Continued)
 (d) Mode I/Mixed-Mode Interface
 (e) Mixed-Mode Region
 Note local deviation of river patterns from CD

CD = Crack-propagation direction
 H = Hackles
 R = River patterns



(a)

CD
→

Figure 2-113. Optical and SEM Photographs of Mode I and Mode II MMF Interlaminar Fracture in Overcured Gr/Ep - [0]₂₄T
(a) Macrograph Showing Regions I, II, and III
(b) Pre-crack, Crack-Growth Under Mode I Tension and Mode II Shear, and Laboratory Overload
(c) Initiation in Resin-Rich Areas
(d) Mode I River Patterns (Arrows)

CD = Crack propagation direction

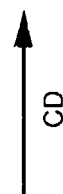
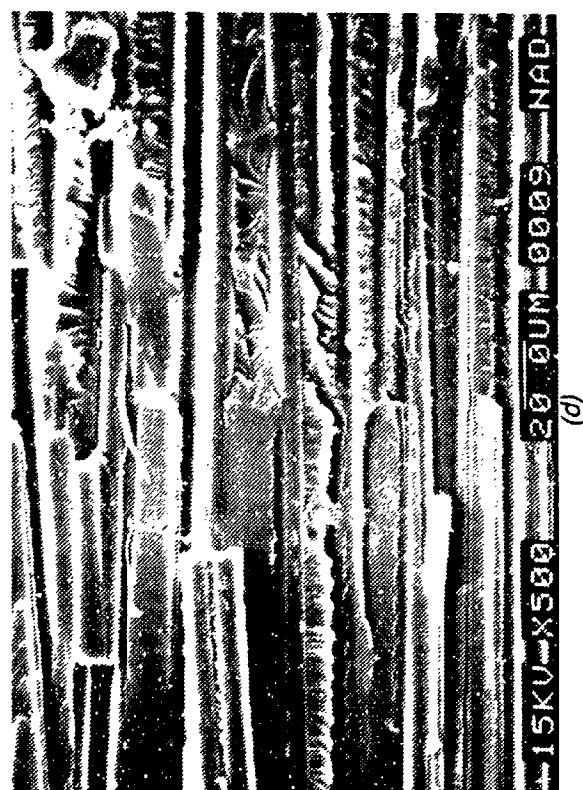
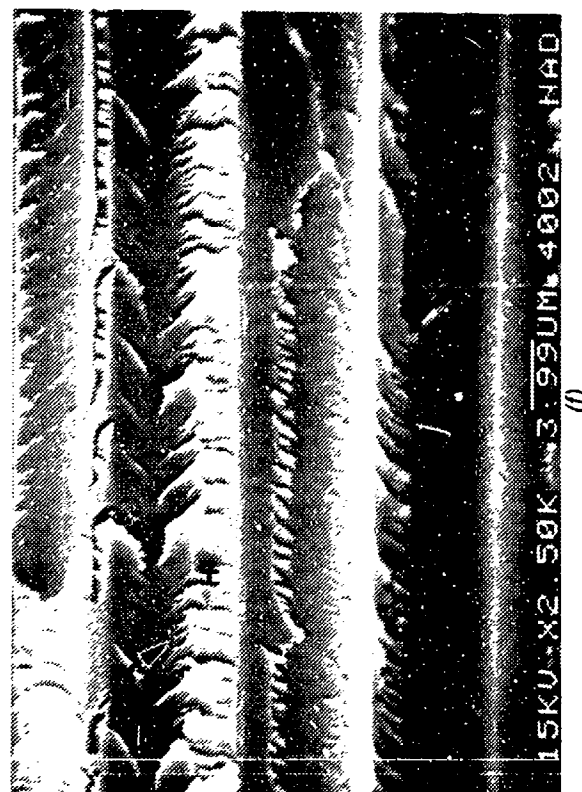
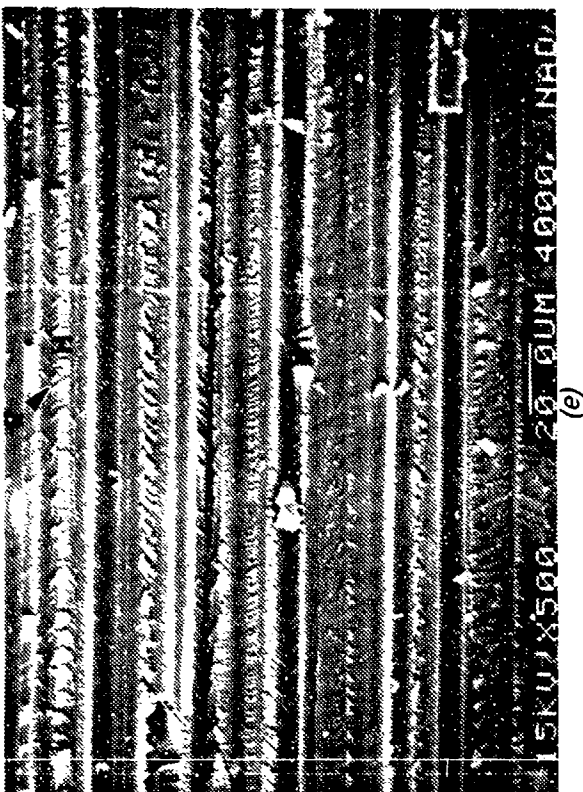
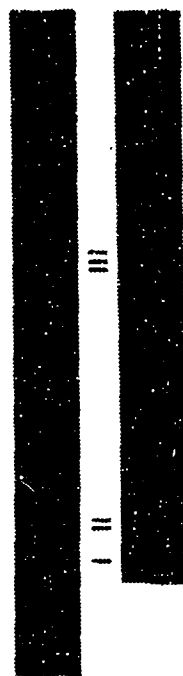


Figure 2-113. (Continued)
 (d) Interface Between Mode I and Mixed-Mode Regions
 (e), (f) River Patterns (R) and Hackles (H) in the Mixed-Mode Fracture Surface

CD = Crack-propagation direction



(a)

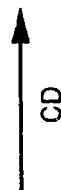


Figure 2-114. Optical and SEM Photographs of Mode I and Mode II
MMF Interlaminar Fracture in Overcured Gr/Ep -

[+45/0/-45]_{4S}

(a) Macrograph Showing Regions I, II, and III
(Precrack, Crack-Growth Under Mode I Tension
and Mode II Shear, Laboratory Overload)

(b) Initiation in Resin-Rich Areas

(c) Mode I River Patterns (Arrows)

CD = Crack-propagation direction



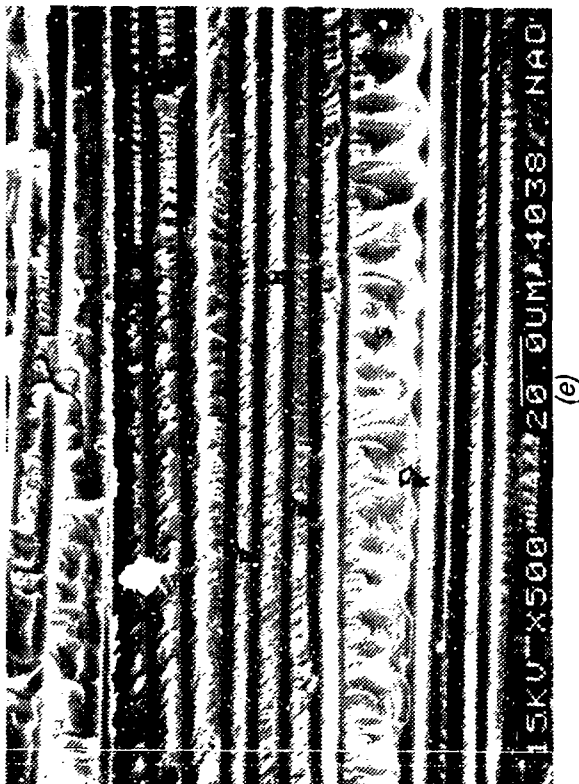
(b)



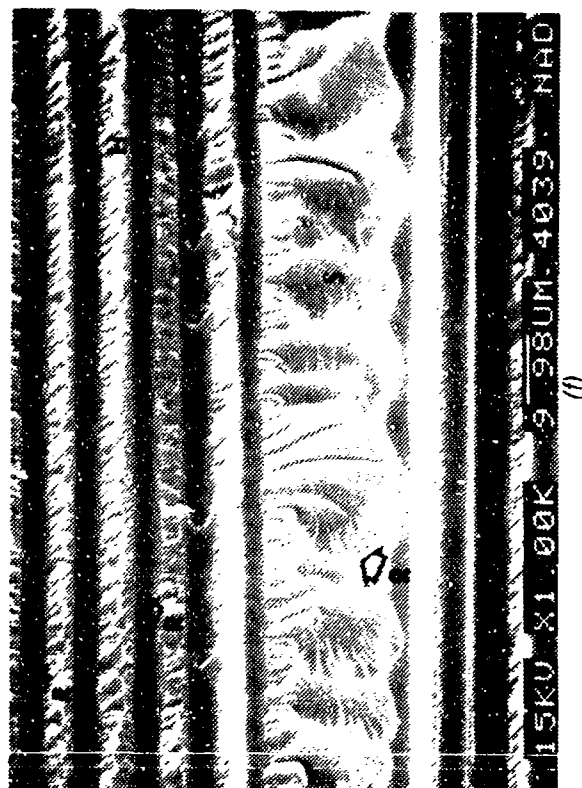
(c)



(d)



(e)



(f)

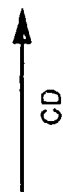


Figure 2-114. (Continued)
 (d) Interface Between Mode I and Mixed-Mode Regions
 (e), (f) River Patterns (R), Hackles (H), and Scallop (S) in the Mixed-Mode Fracture Surface
 CD = Crack-propagation direction

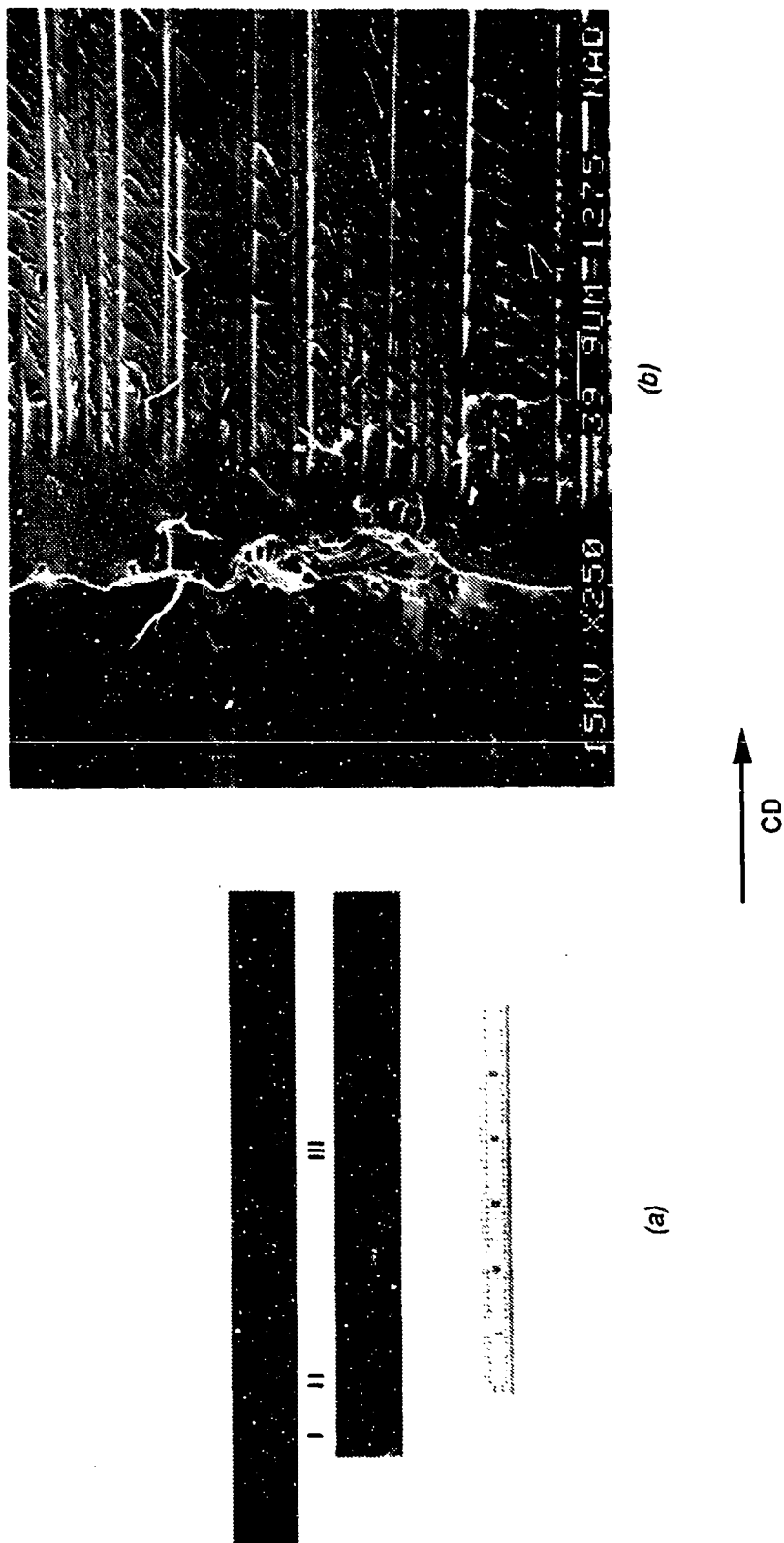


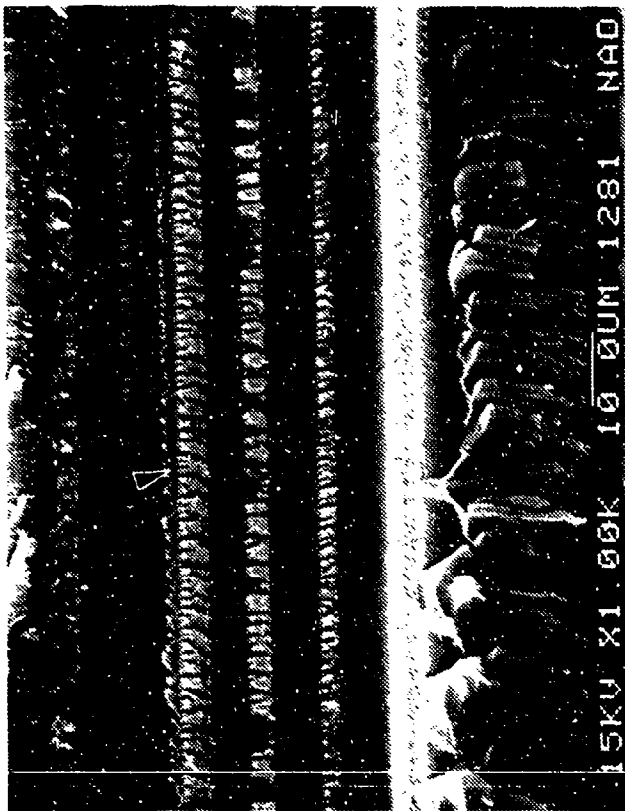
Figure 2-115. Optical and SEM Photographs of Mode I and Mode II MMF Interlaminar Fracture in High Resin Content Gr/Ep - $[0]_{24T}$

(a) Macro photograph

(b) Initiation in Precrack

CD = Crack-propagation direction

R = River patterns



(c)



(d)

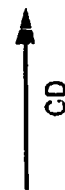
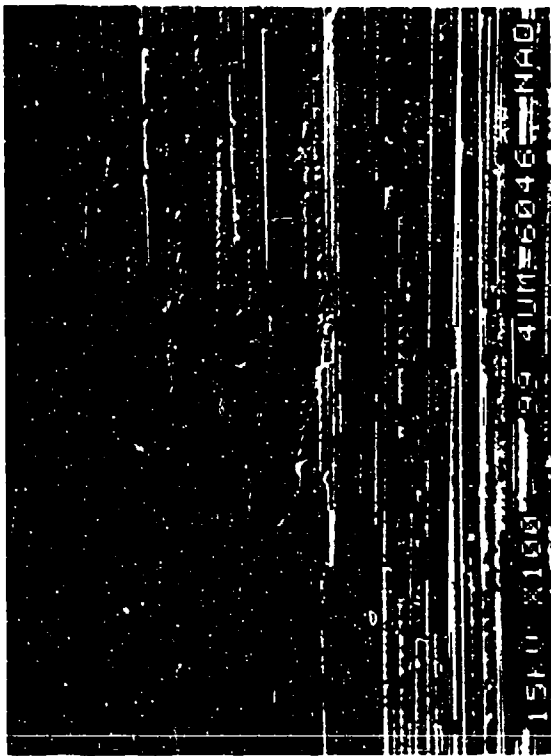


Figure 2-115. (Continued)
 (c) Mode I/Mixed-Mode Interface
 (d) Mixed-Mode Region

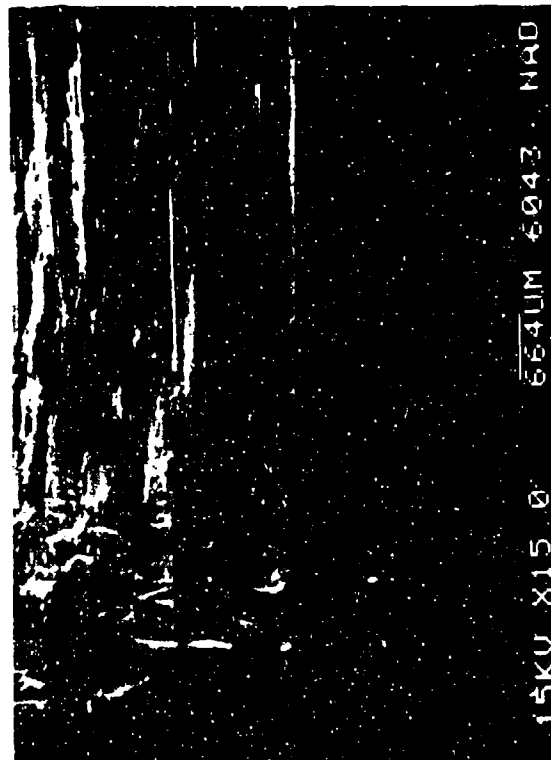
CD = Crack-propagation direction
 H = Hackles (Cusps)
 R = River patterns



(a)



(b)



(c)

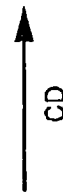


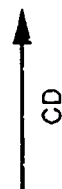
Figure 2-116. SEM Photographs of Mode I and Mode II MMF Interlaminar Fracture in High Resin Gr/Ep - $[0]_{24T}$ Conditioned 180 F Dry After Test
 (a) Initiation in Precrack Region
 (b) Mode I Tension to Mixed-Mode Tension and Shear Transition
 (c) Mixed-Mode Failure
 CD = Crack propagation direction
 H = Hackles
 R = River patterns



(a)



(b)



CD

Figure 2-117. SEM Photographs of Mode I and Mode II MMF Interlaminar Fracture in Overcured Gr/Ep - [+45/0/-45] _{4s}, Conditioned 180 F/Wet After Test
(a) Mode I Tension to Mixed-Mode Transition
(b) Detail in Transition Region
(c) Mixed-Mode Fracture

CD = Crack-propagation direction
H = Hackles
R = River patterns

2.4 IN-PLANE SHEAR

In-plane shear fracture regions can easily be distinguished because fracture regions have a relatively smoother topography than the transverse tensile fracture regions. On a macroscopic scale, in-plane shear failures are characterized as follows:

1. Localized "bowing" of fiber bundles
2. Secondary transverse tensile fractures of fiber bundles.

Microscopic examination indicates that plies oriented parallel to the applied shear loads exhibit hackles and compression debris. Plies oriented normal to the applied shear loads exhibit transverse tensile fracture characteristics, with individual fibers exhibiting DAF radials oriented toward the direction of macroscopic fracture.

Overcure or undercure does not significantly alter fracture characteristics. Water immersion before or after testing has no effect on the fracture features.

Table 2-4 shows the test matrix used for characterized in-plane shear failures in Gr/Ep. The test matrix includes baseline Gr/Ep, processing variations, and post-failure variables. The rail-shear test specimen is shown in Figure 2-118. The in-plane shear fractographs are provided in Figures 2-119 through 2-122. This contribution was made by Northrop.

Table 2-4. Test Matrix for In-Plane Shear Specimens

VARIABLE CONDITION	NUMBER CF PLIES/ORIENTATION	
	24/ ± 45	24/0, 90
BASILINE (DEFECT-FREE)	3	3
IMPACT DAMAGE	3	—
WATER IMMERSION BEFORE TEST	3	3
WATER IMMERSION AFTER TEST	3	3
UNDERCURE	3	--
OVERCURE	3	—

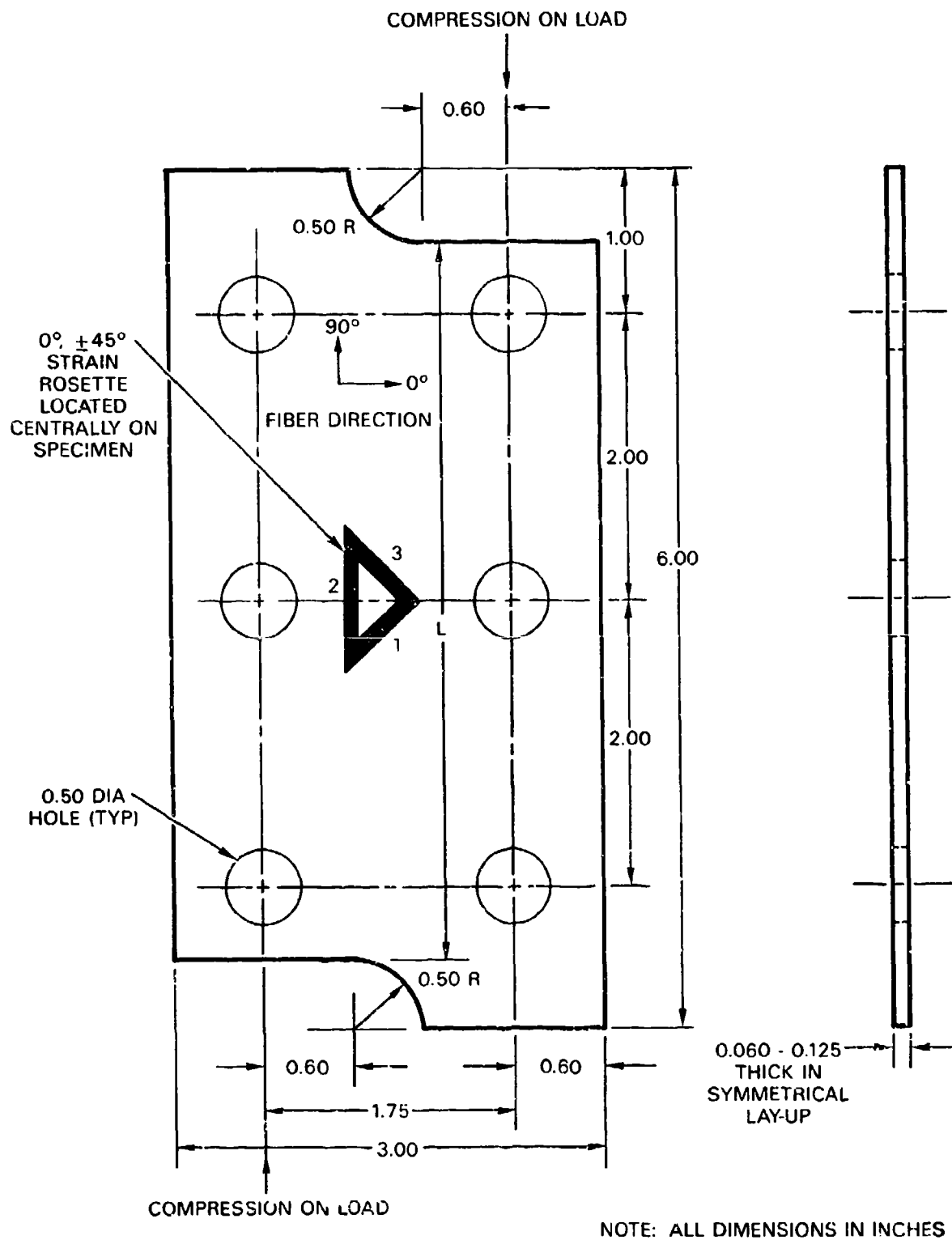
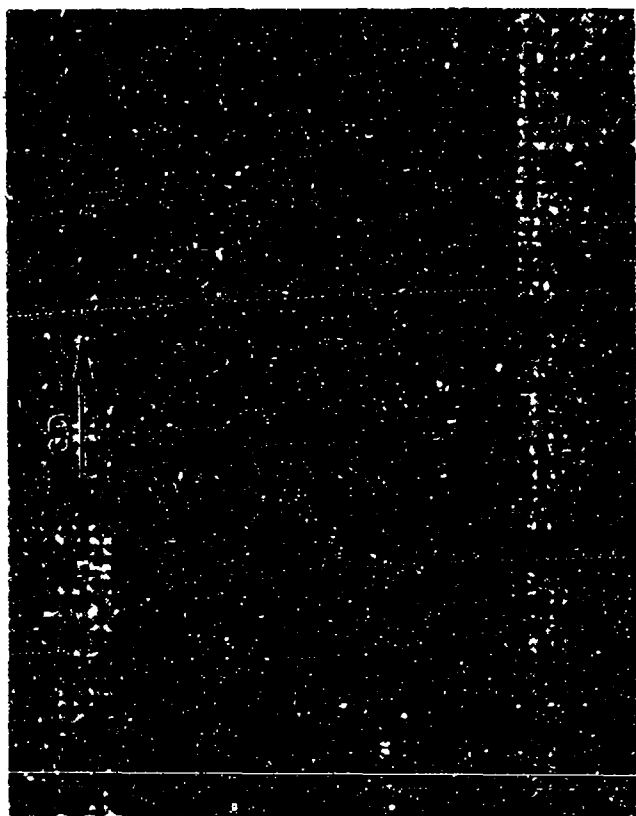
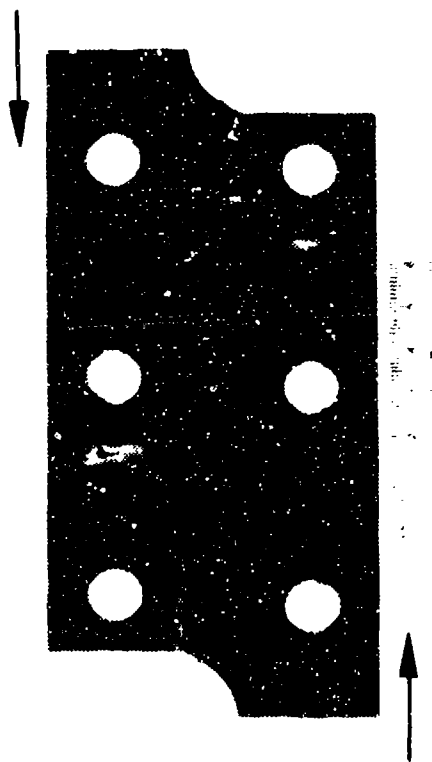


Figure 2-118. Rail-Shear Specimen



(b)



(a)

Figure 2-119. Optical and SEM Photographs of AS4/3501-6 Gr/Ep - [0/90]_{es} . In-Plane Shear-Tested (Baseline)

(a) Macro photograph of Rail-Shear Specimen

Note: Arrows indicate loading direction.

(b) Close-Up View of In-Plane Shear Region

CD = Crack-propagation direction

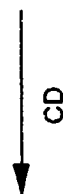
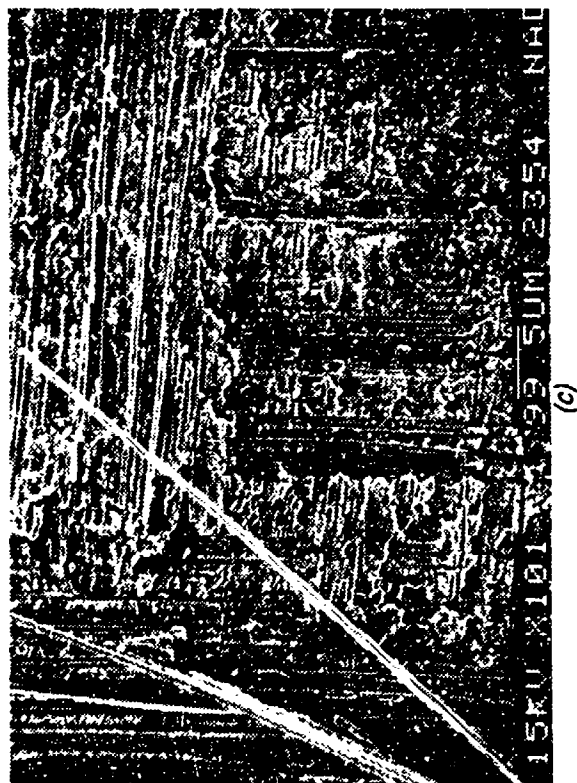


Figure 2-119. (Continued)
 (c) Delaminated Fracture Surface of Region
 Exposed by Sectioning Outer Plies
 (d), (e) Fracture in 90 and 0 Degree Plies

CD = Crack-propagation direction
 D = Compression debris
 H = Hackles

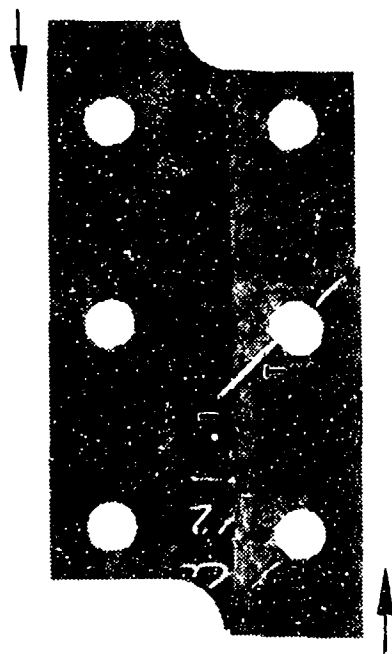


Figure 2-12c. Optical and SEM Photographs of AS4/3501-6 Gr/Ep - [+45/-45]_{6s}, In-Plane Shear Tested (Baseline)

(a) Macro photograph of Rail-Shear Specimen

Note: Arrows indicate loading directions.

(b) Close-up View of Fracture Viewed End-On

Note: Arrows indicate chevrons oriented toward bolt-hole.

B = Bolt-hole

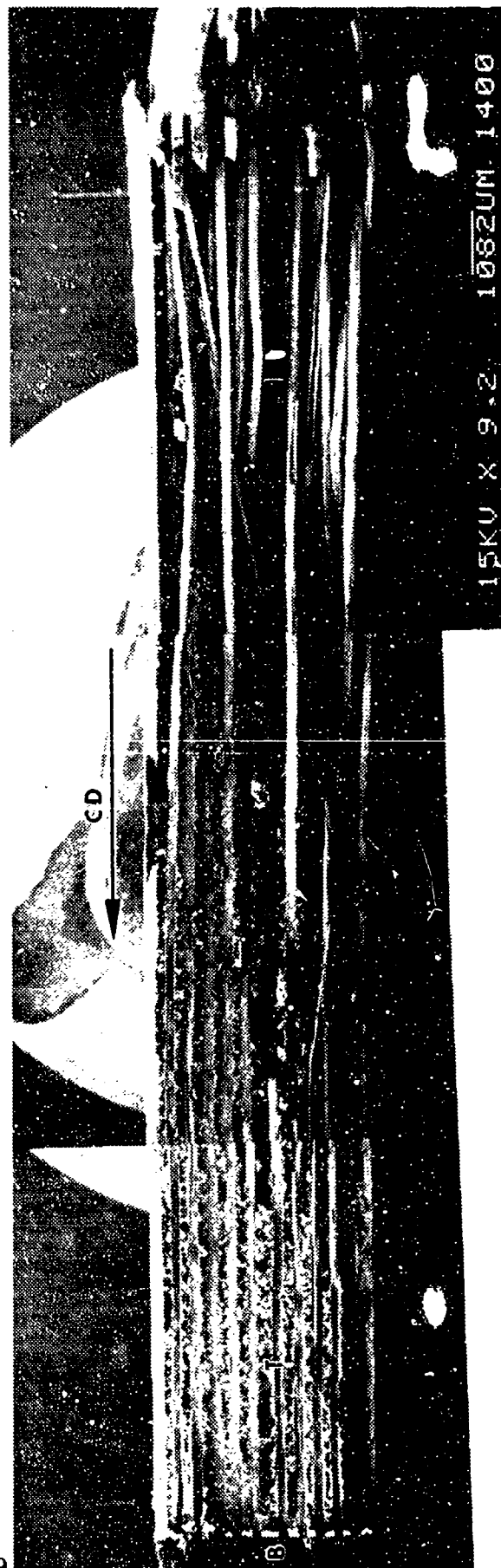
CD = Crack-propagation direction

I = In-plane shear region

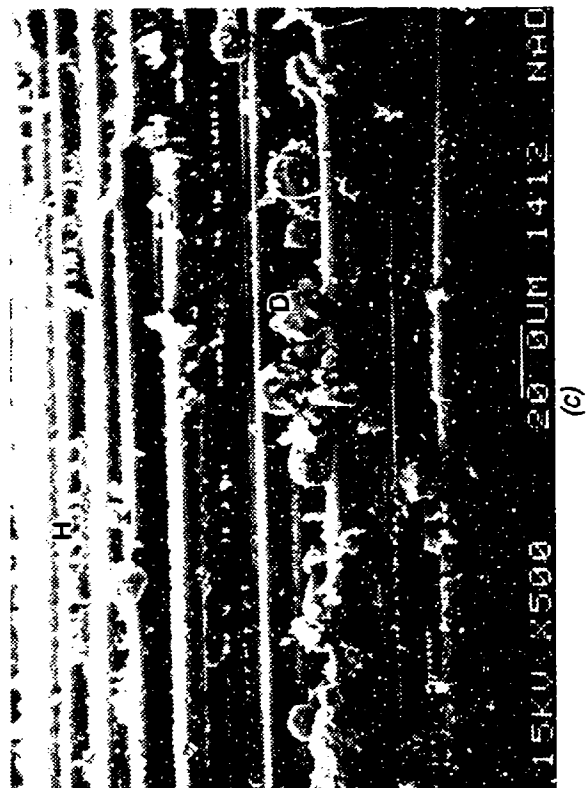
T = Secondary transverse tensile fracture

(a)

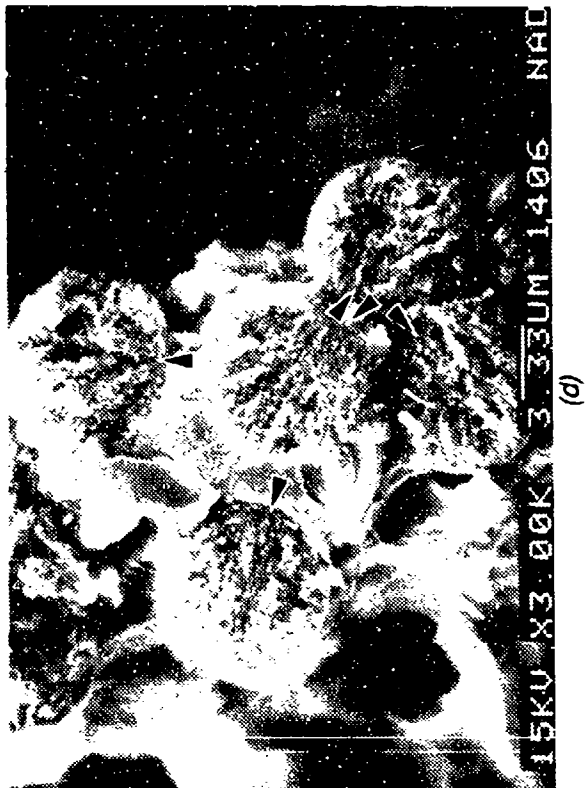
2-149



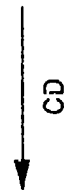
(b)



(c)



(d)



CD

Figure 2-120. (Continued)

(c) Fracture in +45 Degree Ply Showing Hackles (H) and Compression Debris (D)

(d) Fracture in -45 Degree Ply Showing Tensile Fiber Breaks

Note DAF radials (arrows)

(e) Transverse Tensile Fracture in Secondary Failure Region Showing Rivers (R) and Hackles (H)

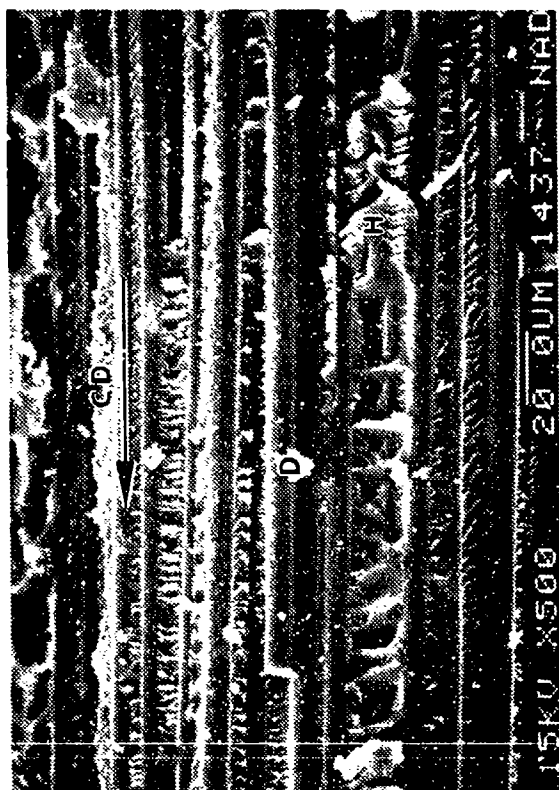
Note rivers oriented away from bolt hole

CD = Crack-propagation direction

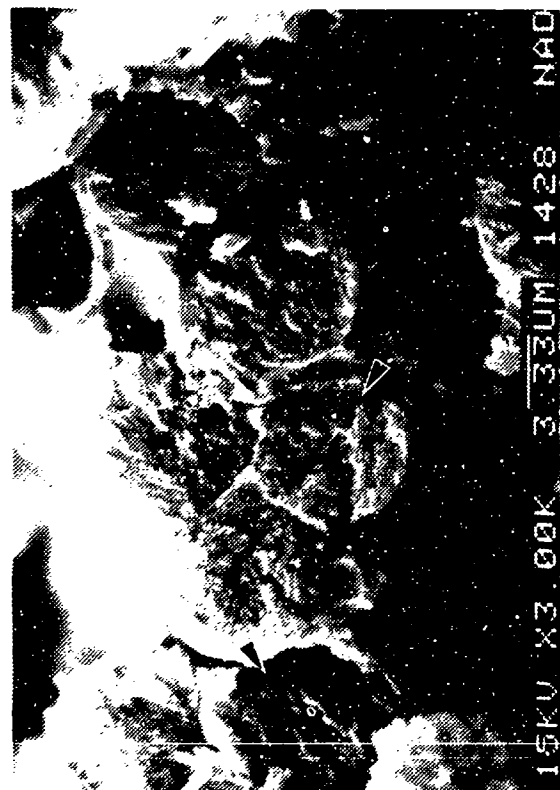
D = Compression debris

H = Hackles

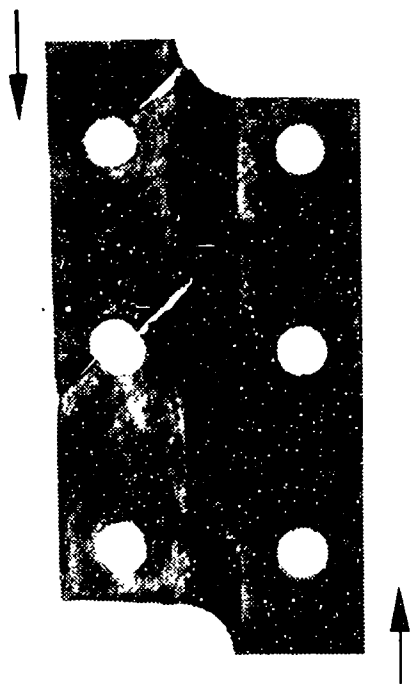
R = Rivers



(a)



(b)



(c)

Figure 2-121. Optical and SEM Photographs of AS4/3501-6 Undercured Gr/Ep - [+45/-45]_{6s} In-Plane Shear Tested

(a) Macrophotograph of Rail-Shear Specimen

Note arrows indicating loading directions

(b) Fracture in +45 Degree Ply Showing Hackles (H) and Compression Debris (D)

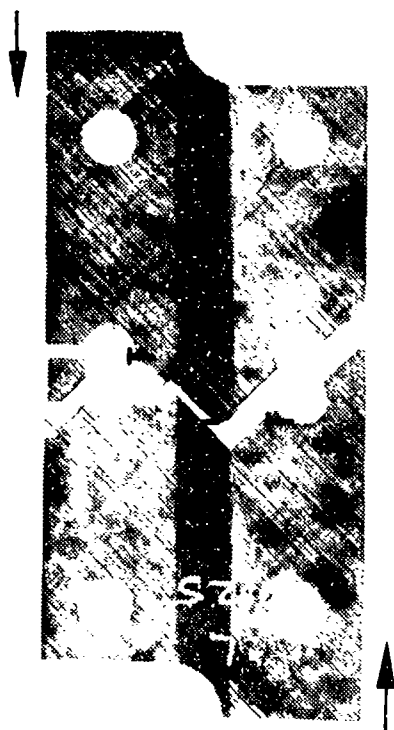
(c) Fracture in -45 Degree Ply Showing Tensile Fiber Breaks

Note DAF radials (arrows)

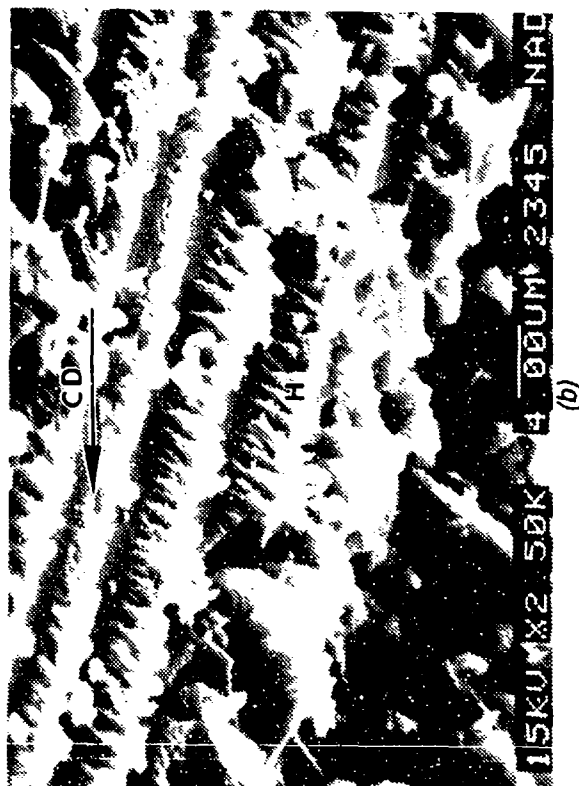
CD = Crack-propagation direction

I = In-plane shear region

T = Secondary transverse tensile fracture



(a)



(b)



(c)

Figure 2-122. Optical and SEM Photographs of AS4/3501-6 Overcured Gr/Ep - [+45/-45]_{6s}, In-Plane Shear Tested
(a) Macrograph of Rail-Shear Specimen
(b) Fracture in +45 Degree Ply Showing Hackles (H)
(c) Transverse Tensile Fracture in Secondary Failure Region

CD = Crack-propagation direction
I = In-plane shear region
T = Secondary transverse tensile fracture

2.5 TRANSLAMINAR TENSION

The primary features observed in translaminar fracture surfaces generated by Mode I tension are as follows:

1. Macroscopically rough fracture surface
2. Fibers protruding from the surface (fiber pullout) at a wide variety of heights
3. Radial feature on each fiber end
4. Fractured resin on sides of fibers, ranging from shear dominated hackle morphology to a very smooth nearly adhesive fracture.

During the fracture process an individual fiber will break, possibly leading to fracture of adjacent fibers. Fiber fracture continues at various planes throughout the laminate, resulting in a rough surface of broken fibers and/or bundles. Close inspection of the fiber ends (using SEM) reveals a radiating pattern indicative of the fracture direction for each individual fiber. Inspection of the fiber ends at several locations along the fracture surface is required to determine the overall crack growth direction. For laminates with a wide variety of ply orientations, the fibers which are oriented 90 degrees to the fracture plane should be examined to obtain the best results. When plies with fibers oriented parallel to the fracture plane are present, inspection of the intralaminar river marks may also be used to determine crack growth direction.

Exposure to 2000°F flame for 5 minutes after the test resulted in a fracture surface with rows of bare fibers. Most of the resin was burned off near the fracture surface. Radial patterns typically seen on fiber ends after translaminar tension fracture were present before but not after the flame exposure. Instead, the fibers showed extensive cracking on their end surfaces.

Figure 2-123 depicts the translaminar tension test configuration, and Figure 2-124 shows typical orientations of fibers and radial patterns of adjacent fibers at both low and high magnifications. Table 2-5 is the test matrix for the translaminar tension test specimens. Translaminar tension fractographs are shown in Figures 2-125 through 2-147. These figures are arranged in the same order that the corresponding tests are listed in Table 2-5.

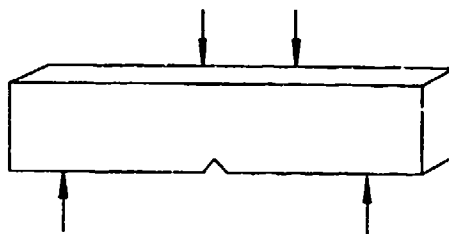


Figure 2-123. Four-Point Bend Tension Test Specimen

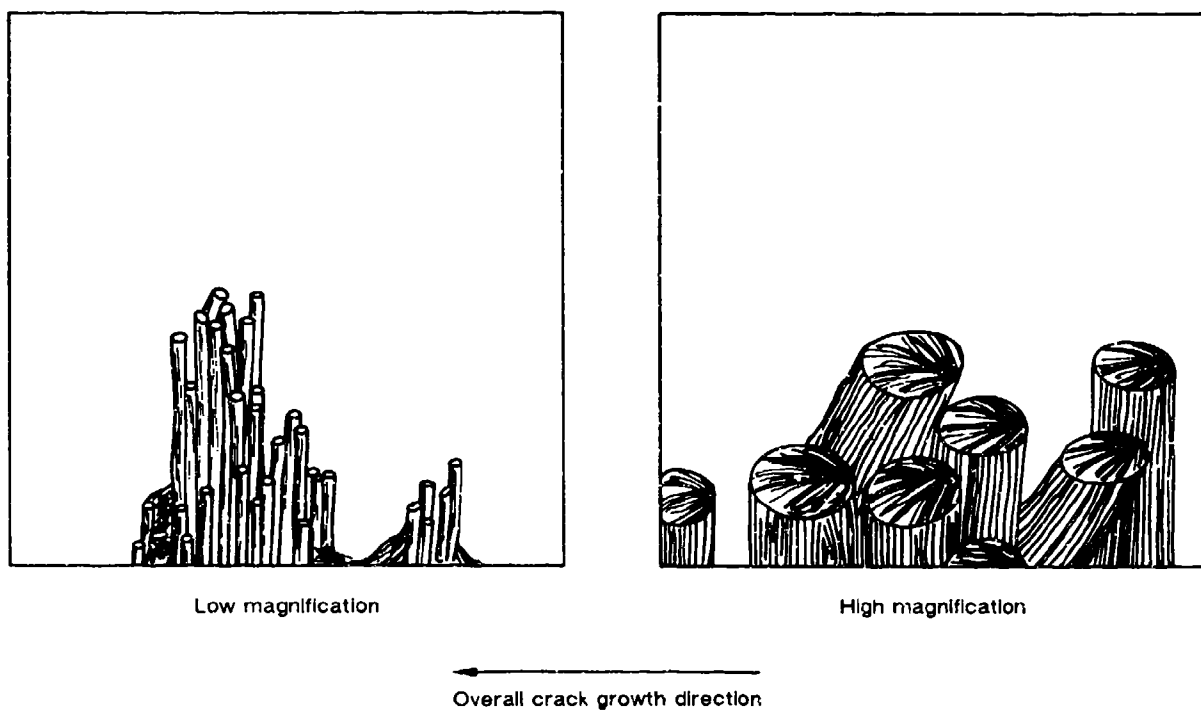


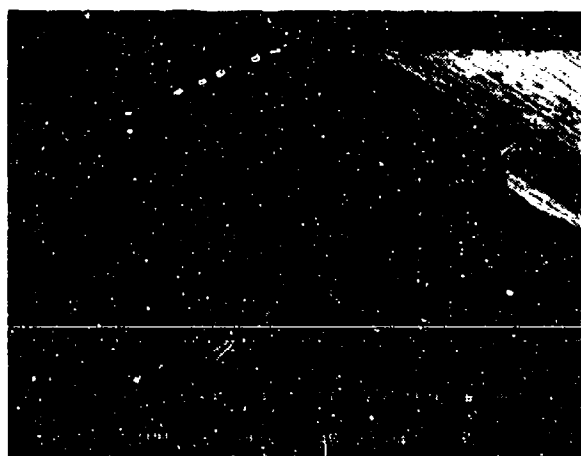
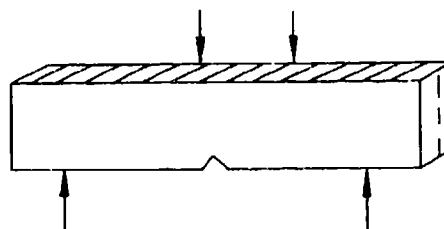
Figure 2-124. Fracture of Adjacent Fibers

Table 2-5. Test Matrix for Translaminar Tension Specimens

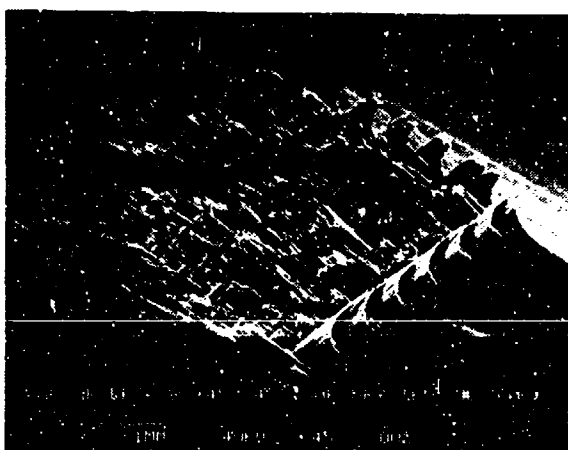
PLY/ORIENTATION	VARIABLE CONDITIONS	CONTRIBUTOR
32/± 45 32/0,90 32/Quasi	Conditions During Tests- RT/Dry (Baseline), -65°F/Dry, 180°F/Dry, 270°F/Dry, RT/Wet, 180°F/Wet, 270°F/Wet	Northrop
32/Quasi	Filament Wound	Northrop
32/0, 90	Fabric	Boeing
32/Quasi	Impact Damaged Before Test	Northrop
32/Quasi	Water Immersed Before Test	Northrop
32/0, 90	Water Immersed After Test	Boeing
32/0, 90	Humidity Exposure	Boeing
32/Quasi	Undercured	Northrop
32/0, 90	Low Resin	Boeing
32/Quasi	High Resin	Northrop
32/0, 90	2000°F/Dry (5 Minutes) After Test	Boeing

SEM photomicrographs

Fracture type	Translaminar mode I tension
Ply layup	[+45, -45] 16S
Test type	Four-point bend
• Test conditions	Dry
• Fiber end fracture	
Material	Hercules 3501-6/177°C cure AS4 fibers

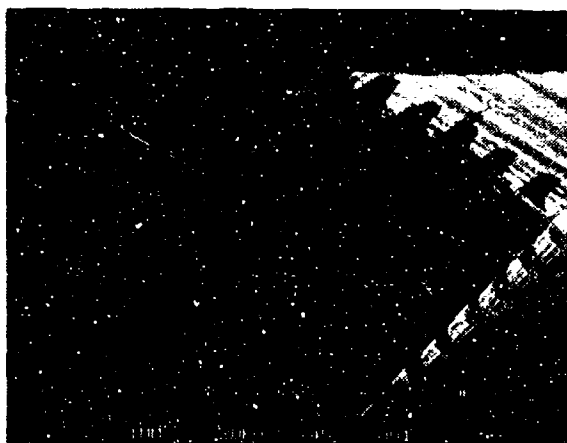


-65°F, dry



180°F, dry

Mechanically induced crack direction

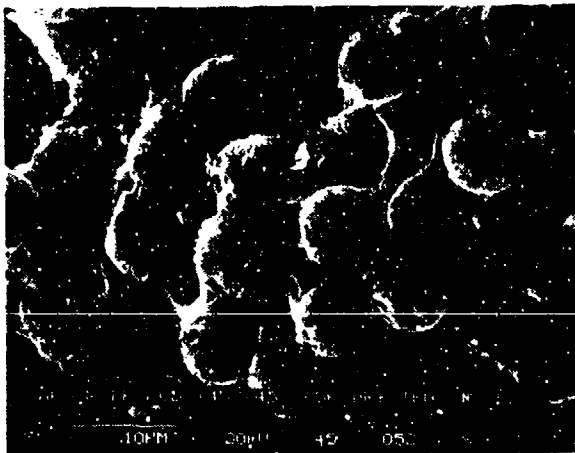
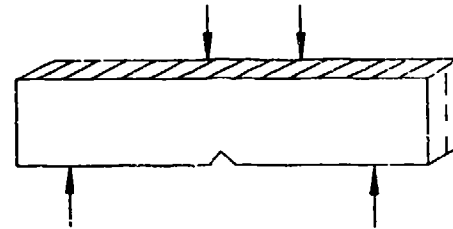


270°F, dry

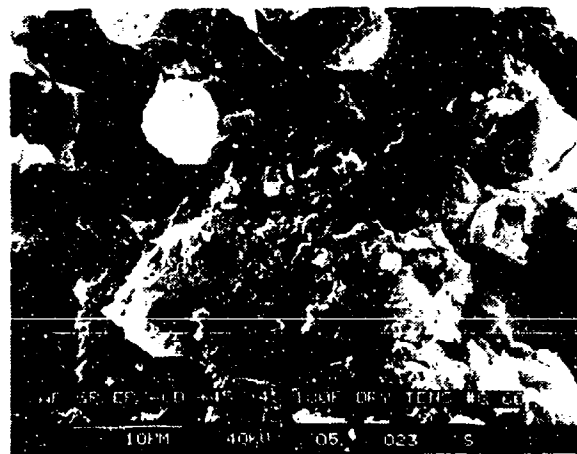
Figure 2-125. SEM Photographs of Translaminar Mode I Tension, +45/-45 Fracture, -65, 180, and 270 F/Dry (Fiber Pullout)

SEM photomicrographs

Fracture type	Translaminar mode I tension
Ply layup	[+45, -45] ₁₆ S
Test type	Four-point bend
• Test conditions	Dry
• Fiber end fracture	
Material	Hercules 3501-6/177°C cure AS4 fibers

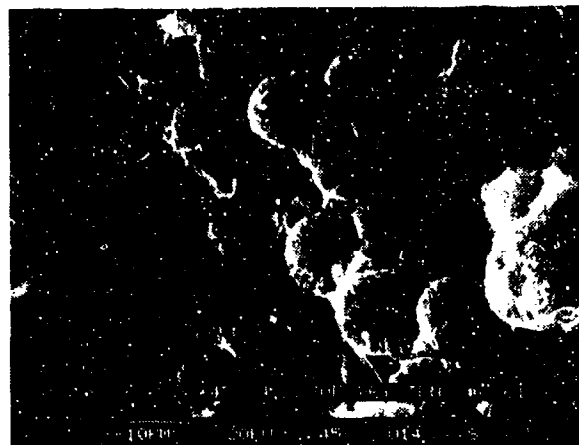


-65°F, dry



180°F, dry

Mechanically Induced crack direction

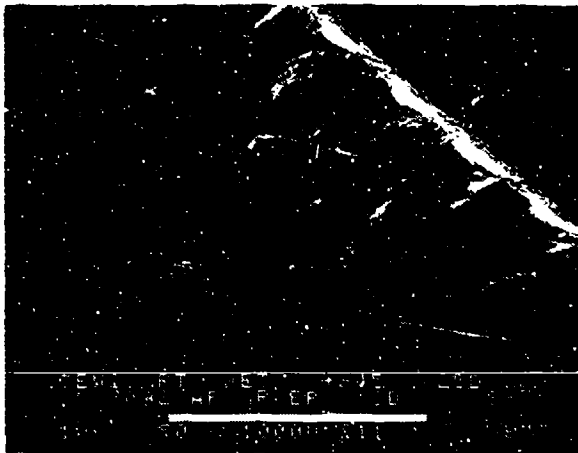
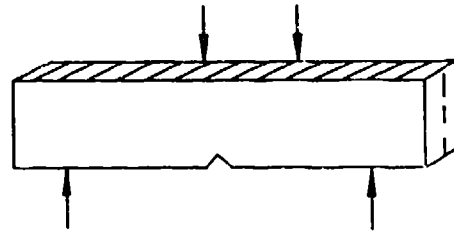


270°F, dry

Figure 2-126. SEM Photographs of Translaminar Mode I Tension, +45/-45 Fracture, -65, 180, and 270 F/Dry (Fiber Breakage)

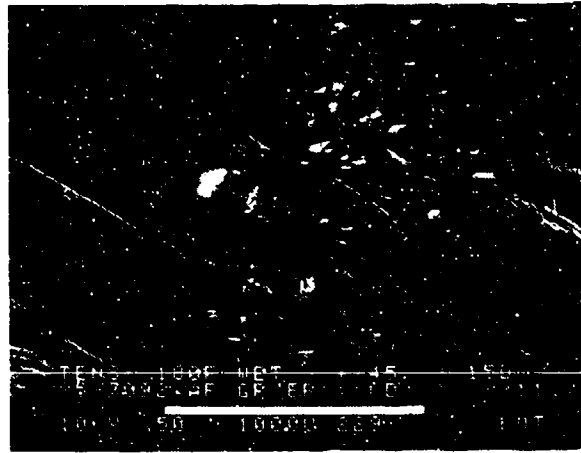
SEM photomicrographs

Fracture type	Translaminar mode I tension
Ply layup	[+45, -45] 16S
Test type	Four-point bend
• Test conditions	Wet
• Fiber end fracture	
Material	Hercules 3501-6/177°C cure AS4 fibers



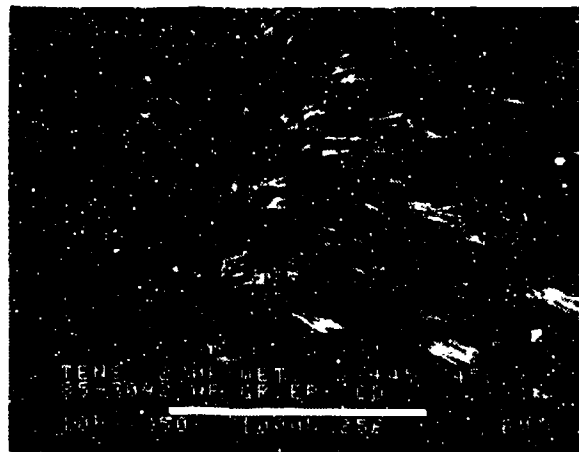
70°F, wet

Mechanically Induced crack direction



180°F, wet

Mechanically Induced crack direction



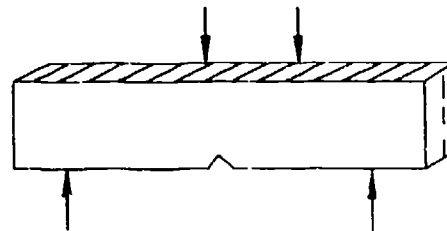
270°F, wet

Mechanically Induced crack direction

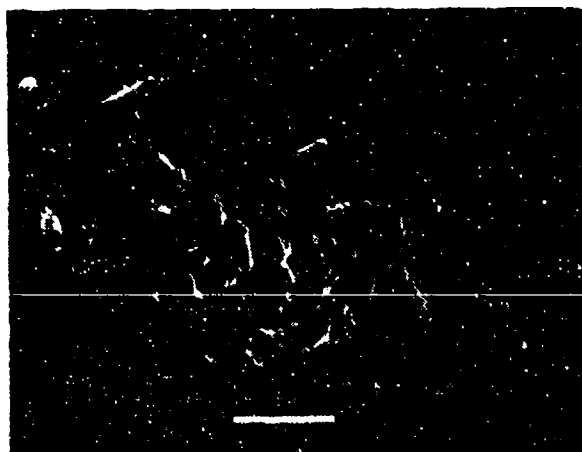
Figure 2-127. SEM Photographs of Translaminar Mode I Tension, +45/-45 Fracture, 70, 180, and 270 F/Wet (50X)

SEM photomicrographs

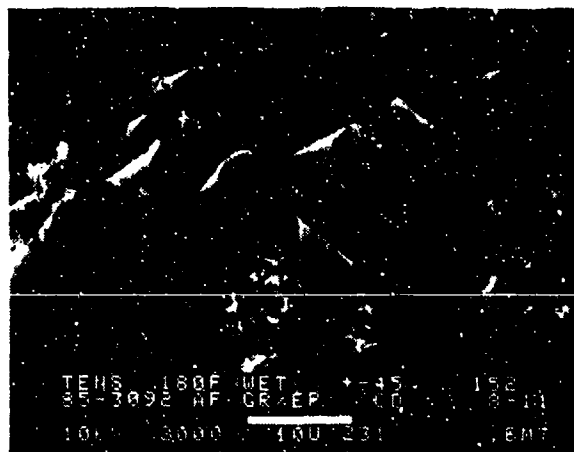
Fracture type	Translaminar mode I tension
Ply layup	[+45, -45] _{16S}
Test type	Four-point bend
• Test conditions	Wet
• Fiber end fracture	
Material	Hercules 3501-6/177°C cure AS4 fibers



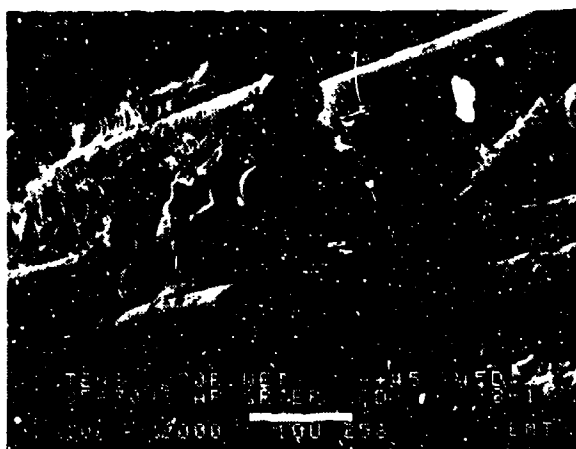
Mechanically induced crack direction



70°F, wet



180°F, wet



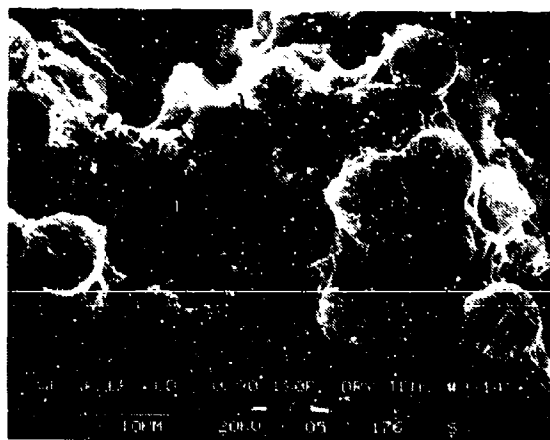
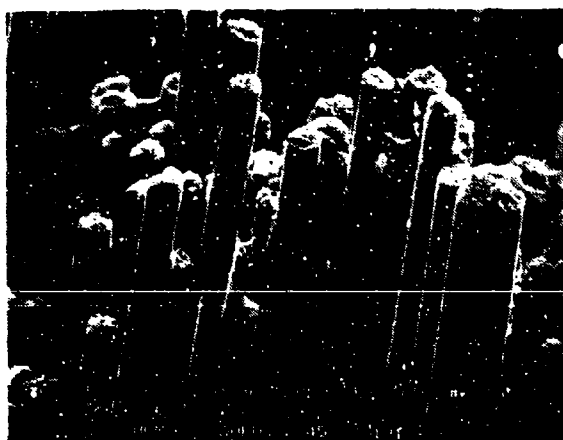
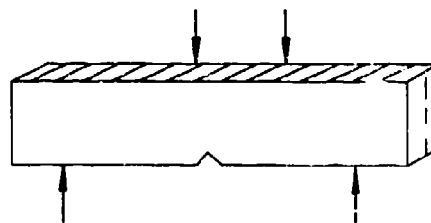
270°F, wet

Mechanically induced crack direction

Figure 2-128. SEM Photographs of Translaminar Mode I Tension, +45/-45 Fracture, 70, 180, and 270 F/Wet (2000X)

SEM photomicrographs

Fracture type	Translaminar mode I tension
Ply layup	[0, 90] ₁₆
Test type	Four-poin. bend
• Test conditions	82°C, dry
• Fiber end fracture	
Material	Hercules 3501-6/177°C cure AS4 fibers



←
Mechanically Induced crack direction

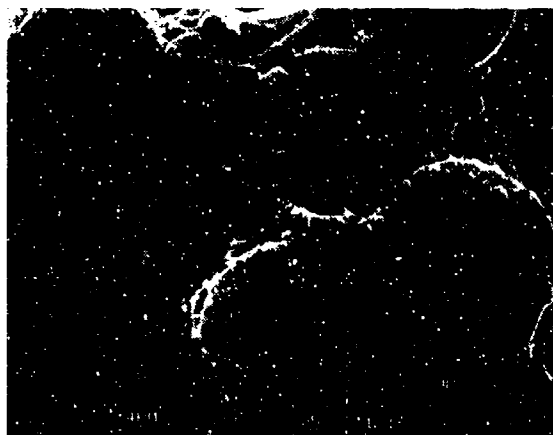
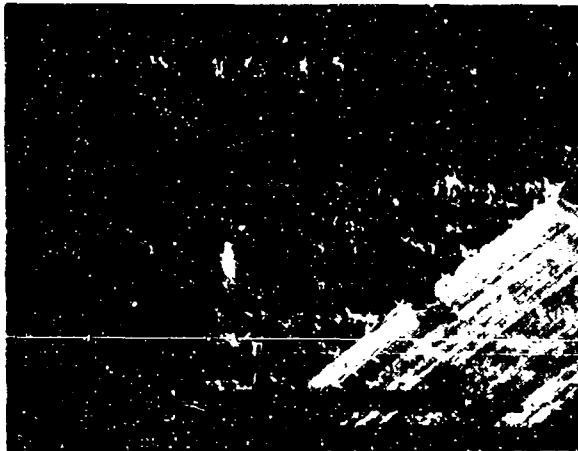
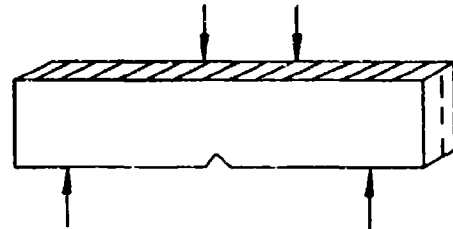


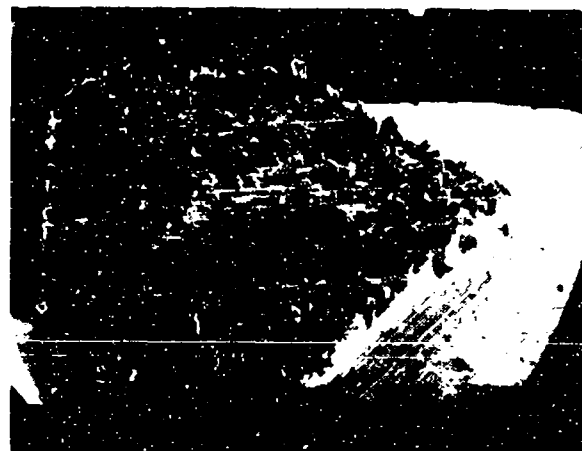
Figure 2-129. SEM Photographs of Translaminar Mode I Tension, 0/90 Fracture, 180 F/Dry (Various Magnifications)

SEM photomicrographs

Fracture type	Translaminar mode I tension
Ply layup	[0, 90] 16S
Test type	Four-point bend
• Test conditions	Dry
• Fiber end fracture	
Material	Hercules 3501-6/177°C cure AS4 fibers

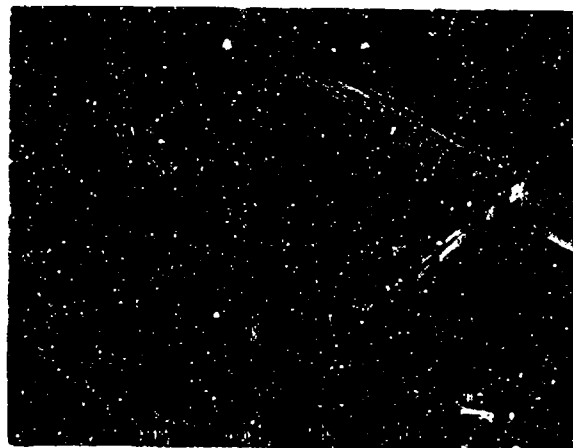


-65°F, dry



160°F, dry

Mechanically induced crack direction

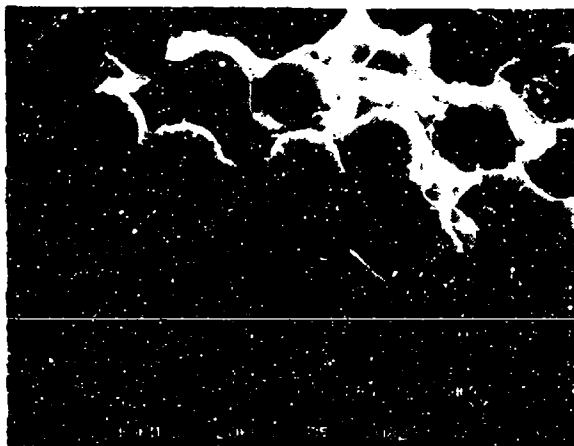
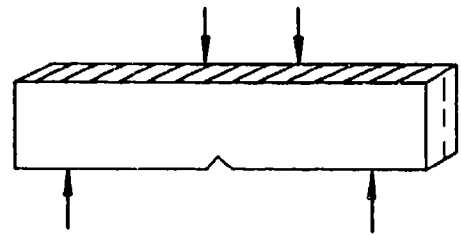


270°F, dry

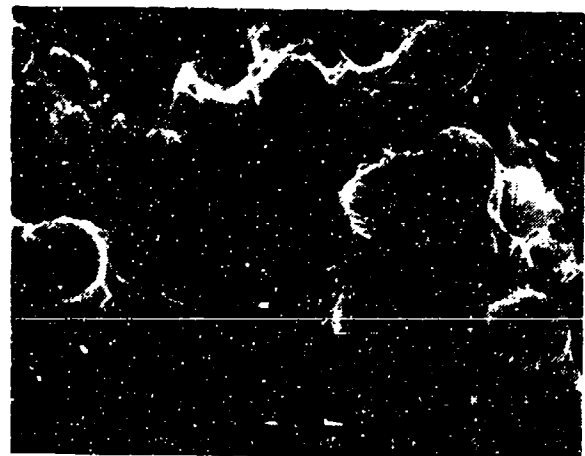
Figure 2-130. SEM Photographs of Translaminar Mode I Tension, 0/90 Fracture, -65, 180, and 270 F/Dry (Low Magnification)

SEM photomicrographs

Fracture type	Translaminar mode I tension
Ply layup	[0, 90]16S
Test type	Four-point bend
• Test conditions	Dry
• Fiber and fracture	
Material	Hercules 3501-6/177°C cure AS4 fibers

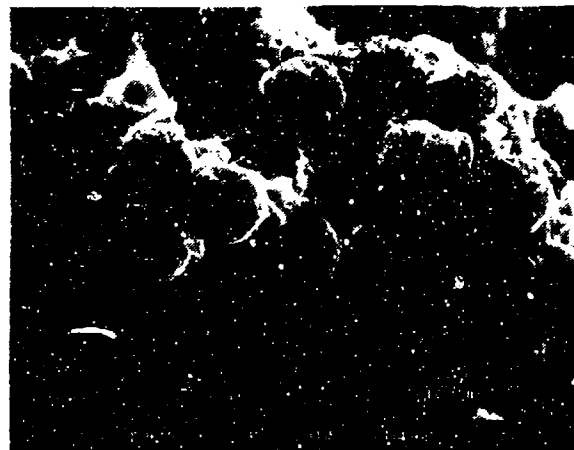


-65°F, dry



180°F, dry

Mechanically induced crack direction

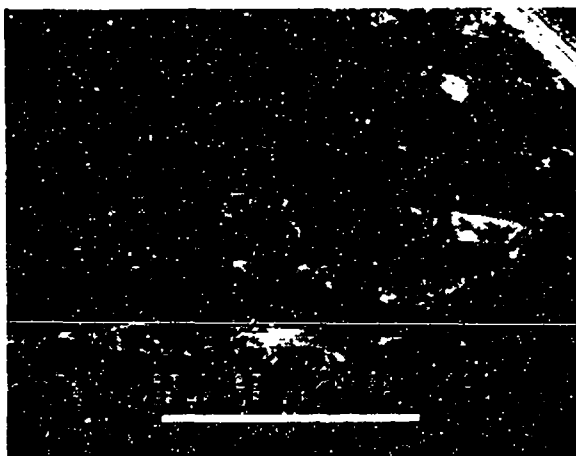
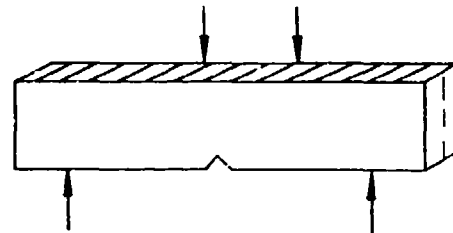


270°F, dry

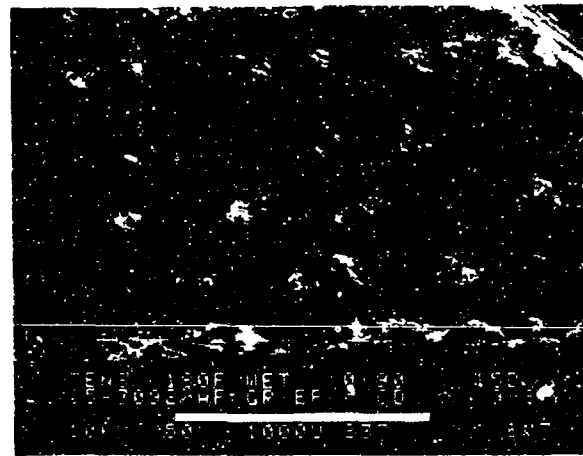
Figure 2-131. SEM Photographs of Translaminar Mode I Tension, 0/90 Fracture, -65, 180, 270 F/Dry (High Magnification)

SEM photomicrographs

Fracture type	Translaminar mode I tension
Ply layup	[0, 90] _{16S}
Test type	Four-point bend
• Test conditions	Wet
• Fiber end fracture	
Material	Hercules 3501-6/177°C cure AS4 fibers

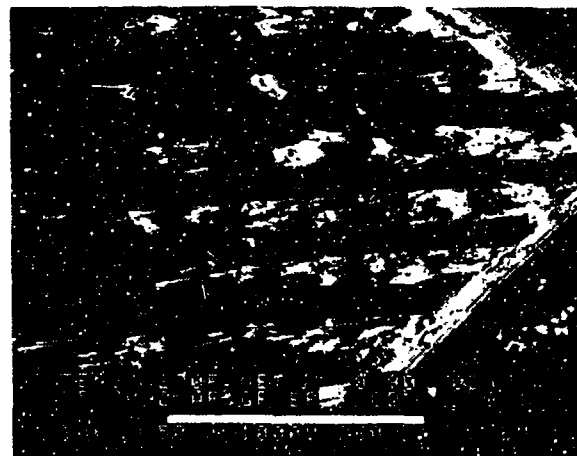


70°F, wet



180°F, wet

Mechanically induced crack direction

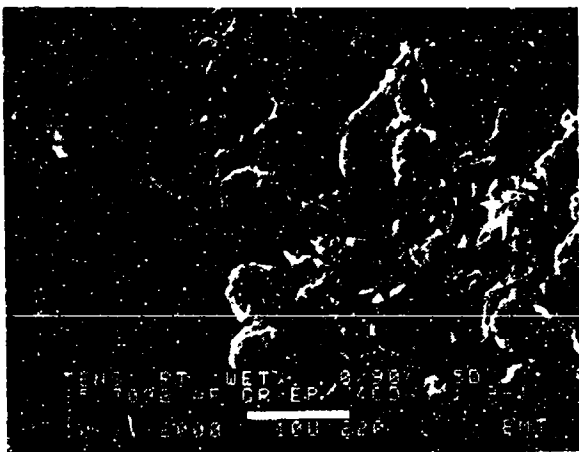
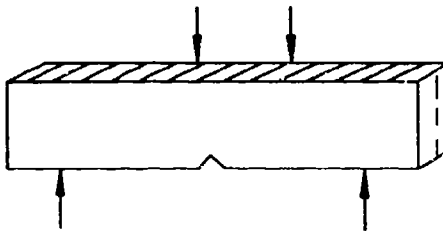


270°F, wet

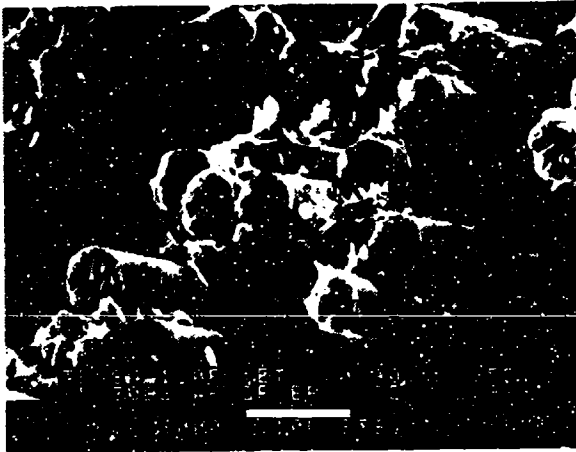
Figure 2-132. SEM Photographs of Translaminar Mode I Tension, 0/90 Fracture, 70, 180, 270 F/Wet (50X)

SEM photomicrographs

Fracture type	Translaminar mode I tension
Ply layup	[0, 90] ₁₆ S
Test type • Test conditions • Fiber end fracture	Four-point bend Wet
Material	Hercules 3501-6/177°C cure AS4 fibers

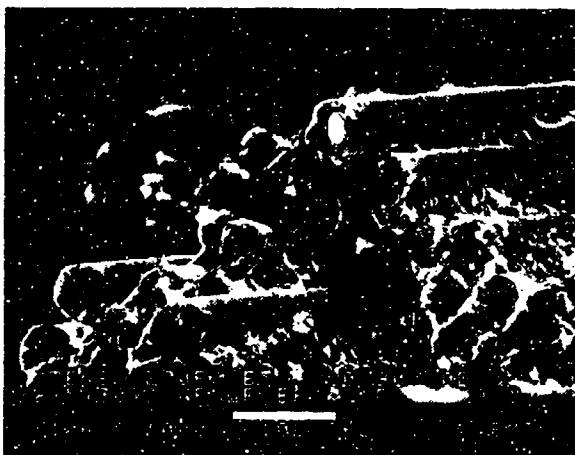


70°F, wet



180°F, wet

Mechanically induced crack direction

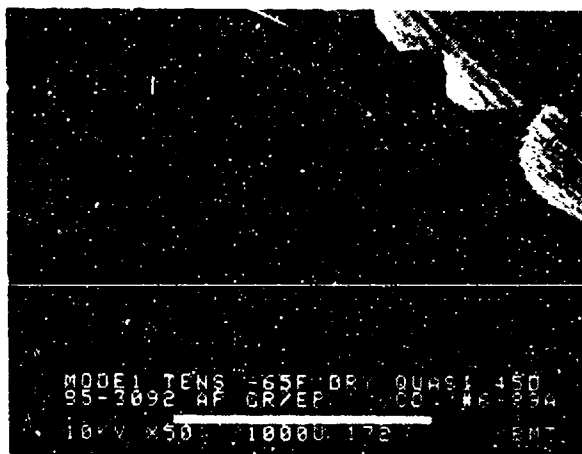
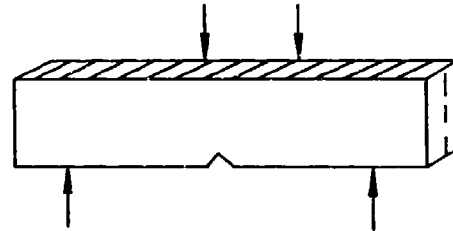


270°F, wet

Figure 2-133. SEM Photographs of Translaminar Mode I Tension, 0/90 Fracture, 70, 180, 270 F/Wet (2000X)

SEM photomicrographs

Fracture type	Translaminar mode I tension
Ply layup	[0, 45, 90] _{16S}
Test type	Four-point bend
• Test conditions	Dry
• Fiber end fracture	
Material	Hercules 3501-6/177°C cure AS4 fibers



-65°F, dry



180°F, dry

Mechanically induced crack direction

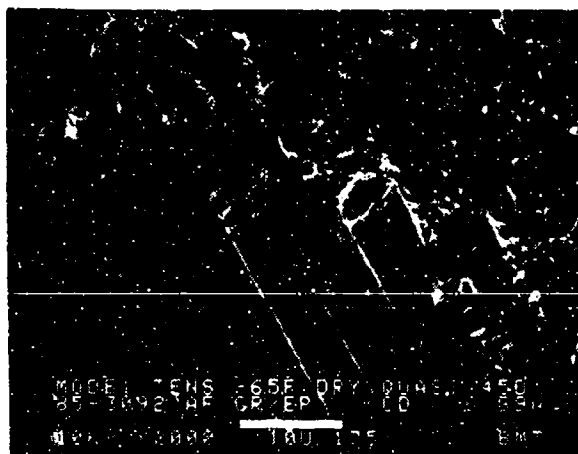
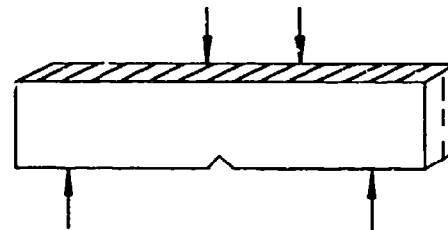


270°F, dry

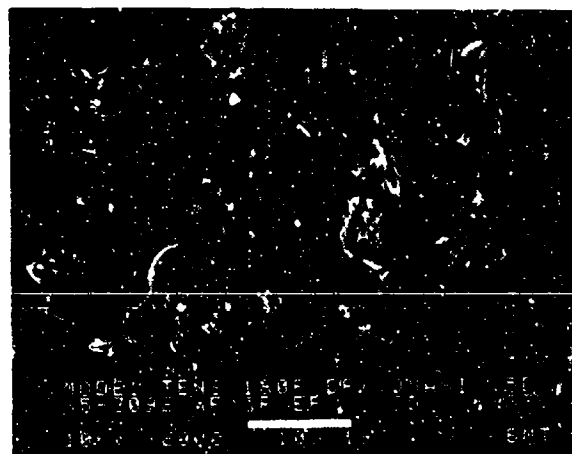
Figure 2-134. SEM Photographs of Translaminar Mode I Tension, 0/45/90 Fracture, -65, 180, 270 F/Dry (50X)

SEM photomicrographs

Fracture type	Translaminar mode I tension
Ply layup	[0, 45, 90] ₁₆ S
Test type	Four-point bend
• Test conditions	Dry
• Fiber end fracture	
Material	Hercules 3501-6/177°C cure AS4 fibers

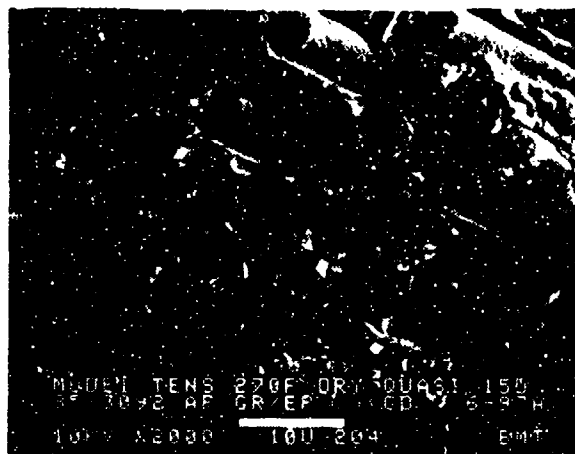


-65°F, dry



180°F, dry

Mechanically Induced crack direction

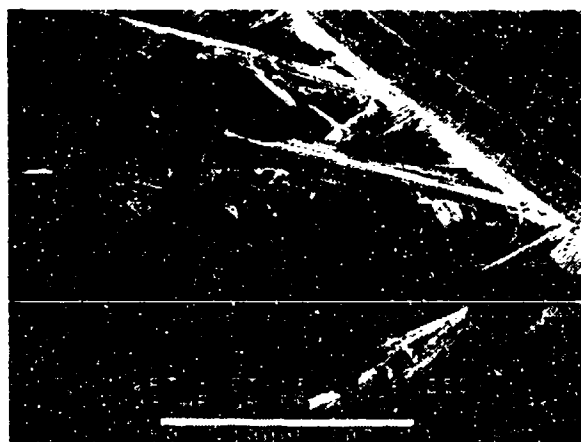
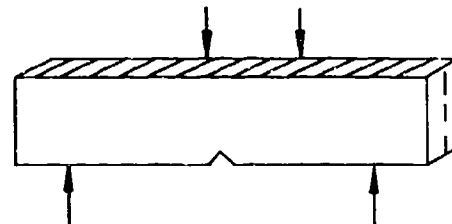


270°F, dry

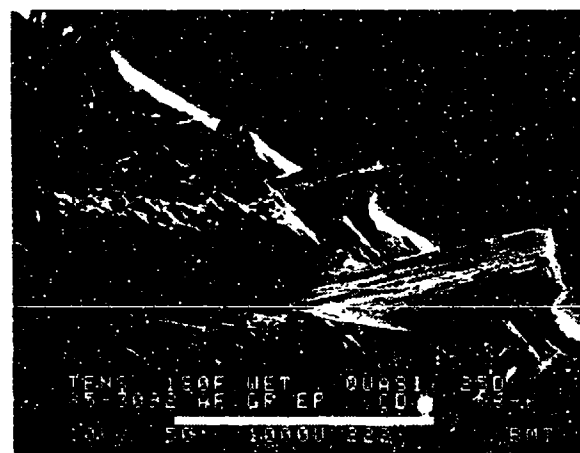
Figure 2-135. SEM Photographs of Translaminar Mode I Tension, 0/45/90 Fracture, -65, 180, 270 F/Dry (2000X)

SEM photomicrographs

Fracture type	Translaminar mode I tension
Ply layup	[0, 45, 90] _{16S}
Test type	Four-point bend
• Test conditions	Wet
• Fiber end fracture	
Material	Hercules 3501-6/177°C cure AS4 fibers



70°F. wet



180°F. wet

Mechanically Induced crack direction



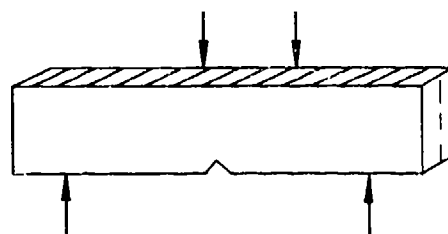
270°F. wet

Mechanically Induced crack direction

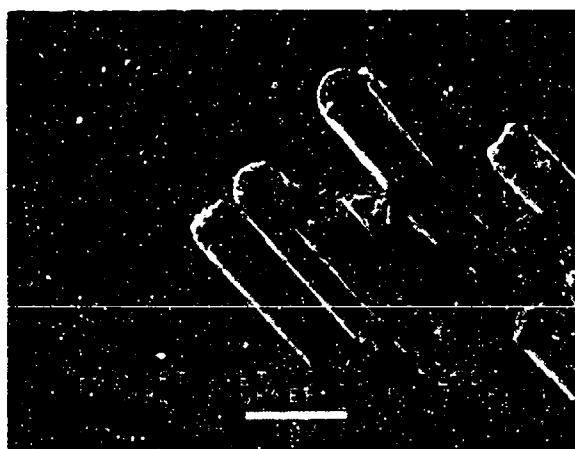
Figure 2-136. SEM Photographs of Translaminar Mode I Tension, 0/45/90 Fracture, 70, 180, 270 F/Wet (50X)

SEM photomicrographs

Fracture type	Translaminar mode I tension
Fiber layup	[0, 45, 90] _{16S}
Test type	Four-point bend
• Test conditions	Wet
• Fiber end fracture	
Material	Hercules 3501-6/177°C cure AS4 fibers



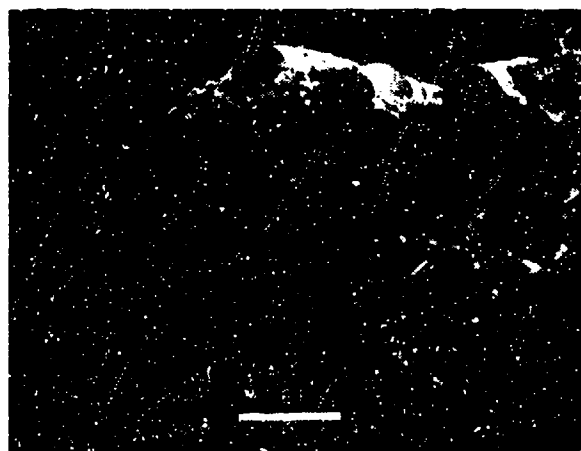
← Mechanically induced crack direction



70°F, wet



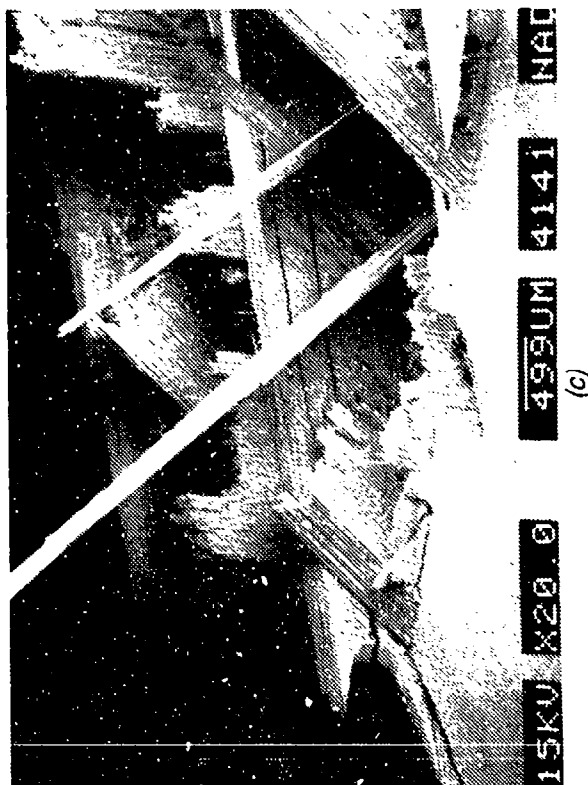
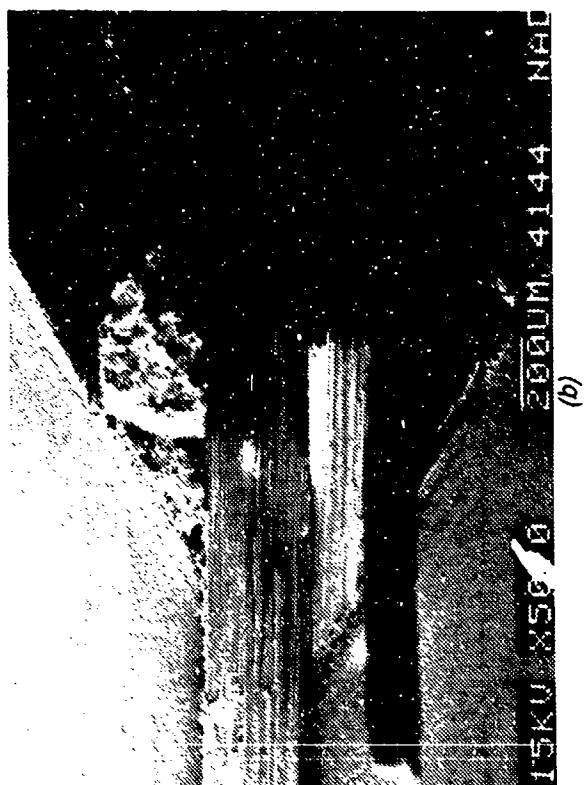
180°F, wet



270°F, wet

→ Mechanically induced crack direction

Figure 2-137. SEM Photographs of Translaminar Mode I Tension, 0/45/90 Fracture, 70, 180, 270 F/Wet (2000X)

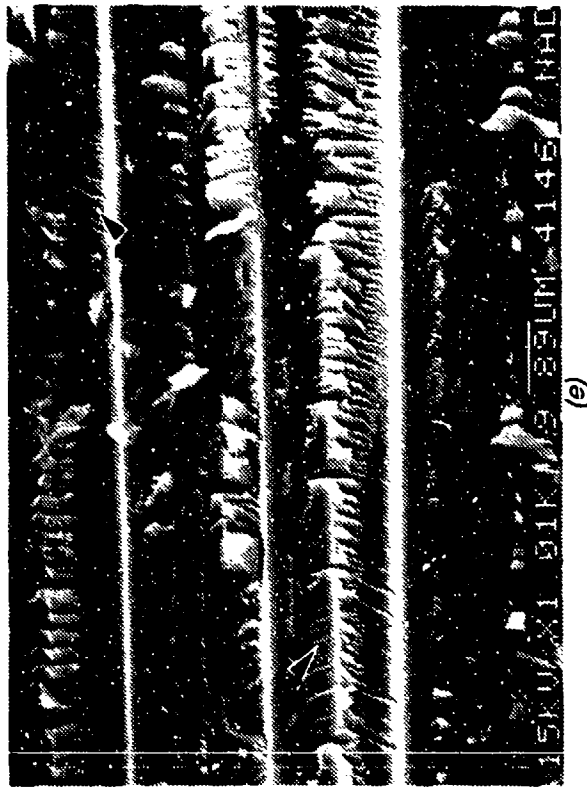
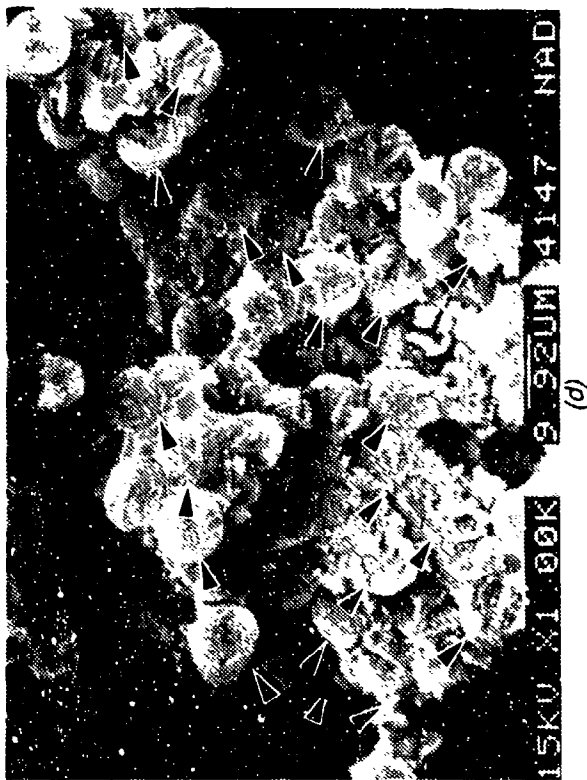


(a)



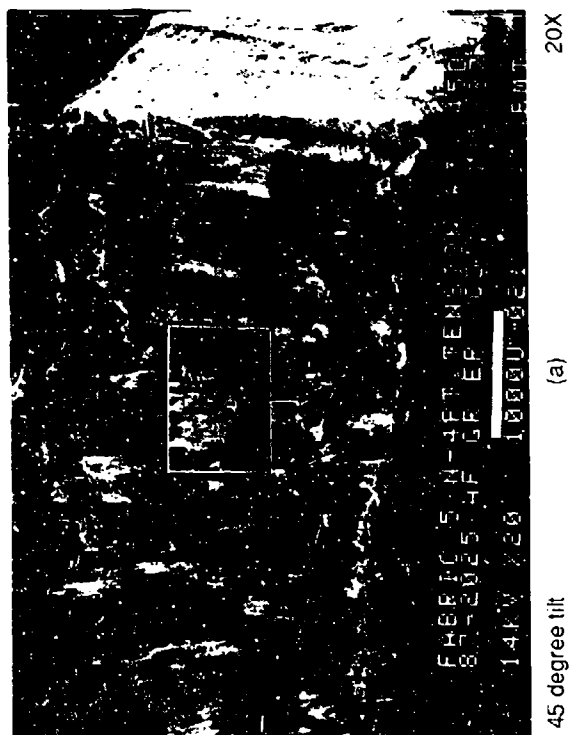
Figure 2-138. Optical and SEM Photographs of Translaminar Tension Fracture in Filament Wound Gr/Ep - 32 Ply/Quasi-Isotropic
(a) Macro photograph of Fractured Fragments
(b), (c) Normal and Oblique Views of Fracture Near the Apex

CD = Crack-propagation direction



CD
↑

Figure 2-138. (Continued)
 (d) Arrows Point to DAF Radial Lines on Fractured
 Fiber-Ends and Indicate Local Fracture Path
 (e), (f) Fracture Features Present in Ply Orientation
 Parallel to Fracture
 Note hackles (H) and river patterns (R)
 CD = Crack-propagation direction



Mechanically induced
crack direction

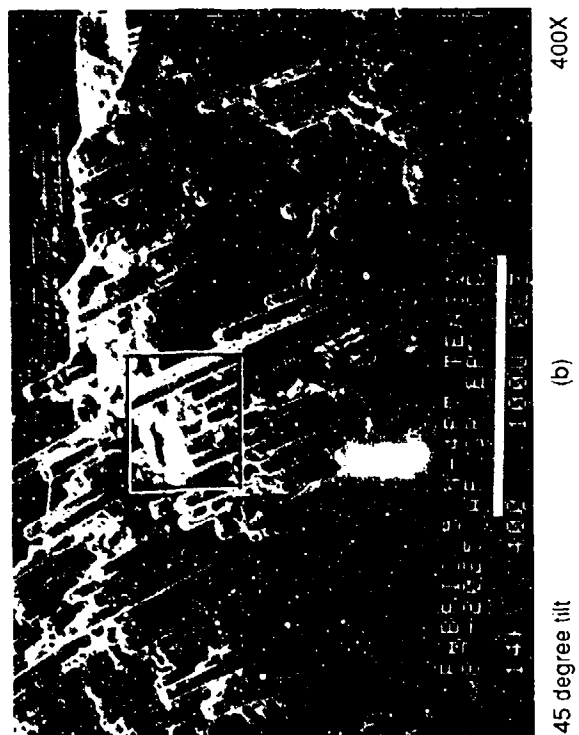
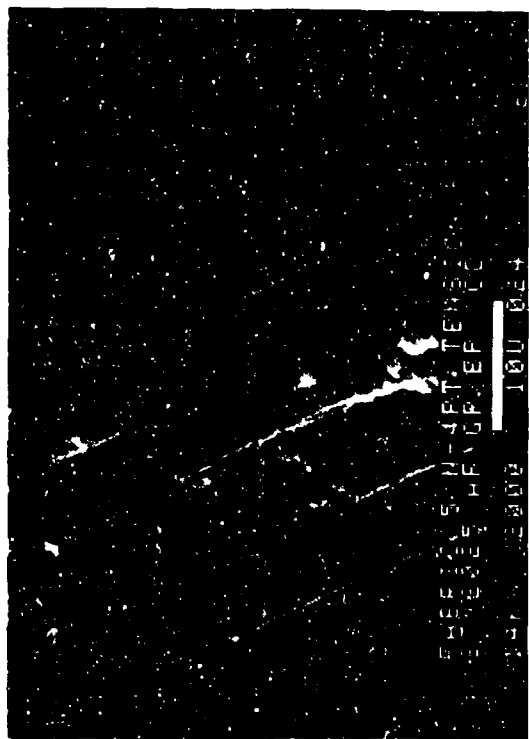
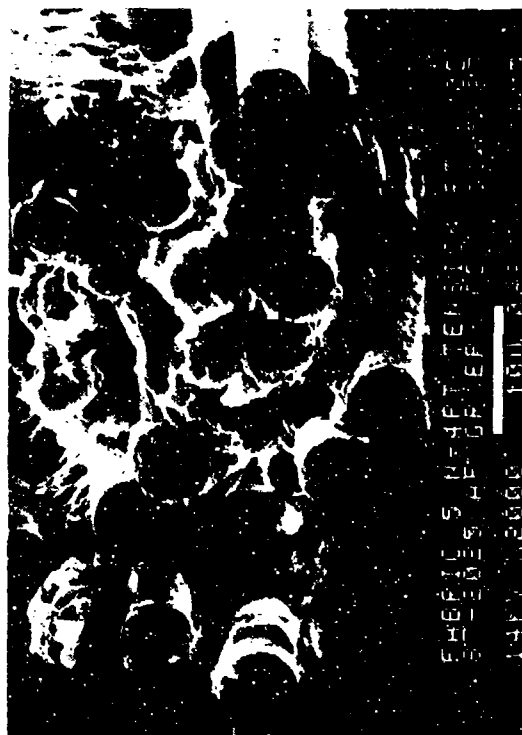


Figure 2-139. SEM Fractographs of Translaminar Tension, Room Temperature, 0/90 Fabric Fracture



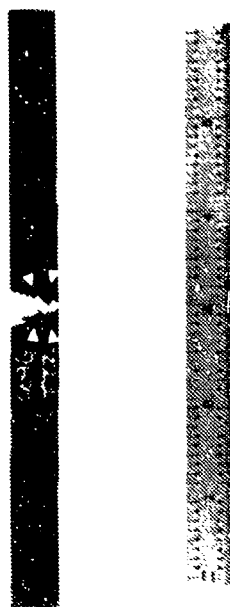
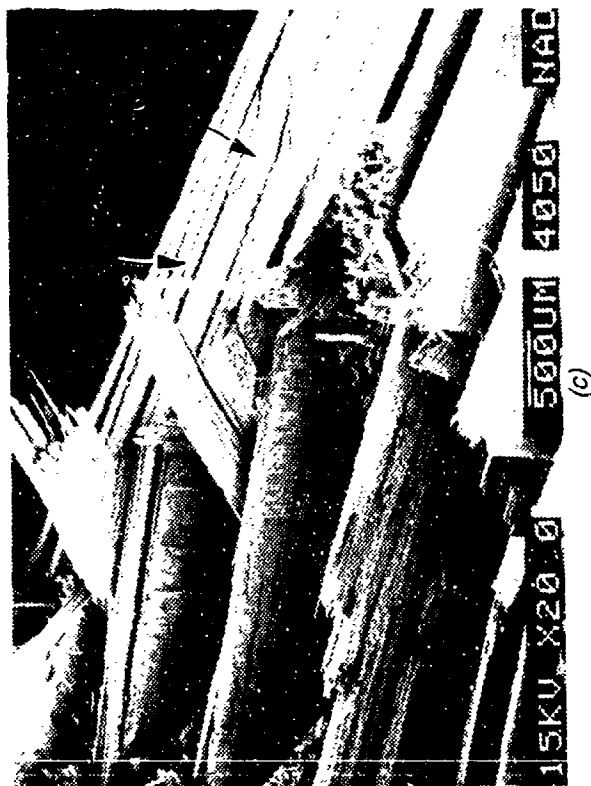
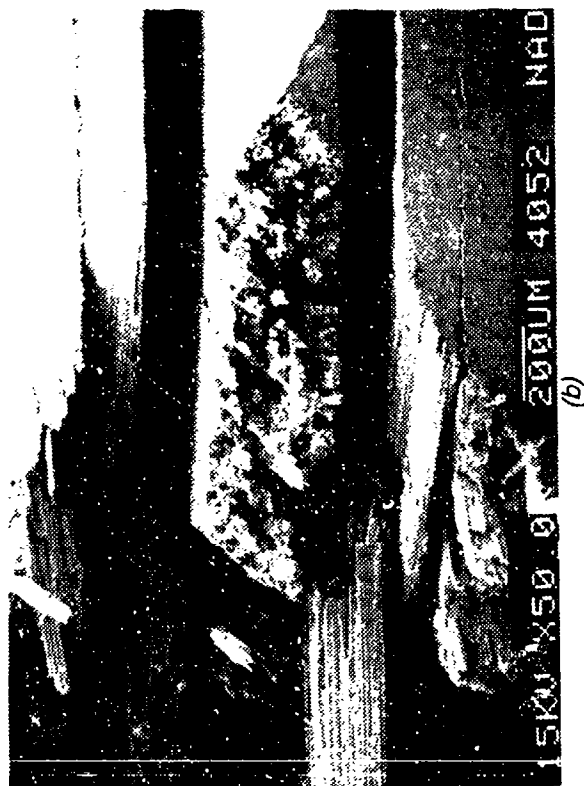
45 degree tilt (c) Typical fracture along the fibers 2,000X

Mechanically induced
crack direction



0 degree tilt (d) Illustration of crack mapping using the radial patterns on the fiber ends 2,000X

Figure 2-139. (Continued)



(a)



CD

Figure 2-140. Optical and SEM Photographs of Translaminar Tension Fracture in Impact Damaged Gr/Ep -32 Ply/Quasi-Isotropic

(a) Macro photograph of Fractured Fragments

Arrows indicate damage zone

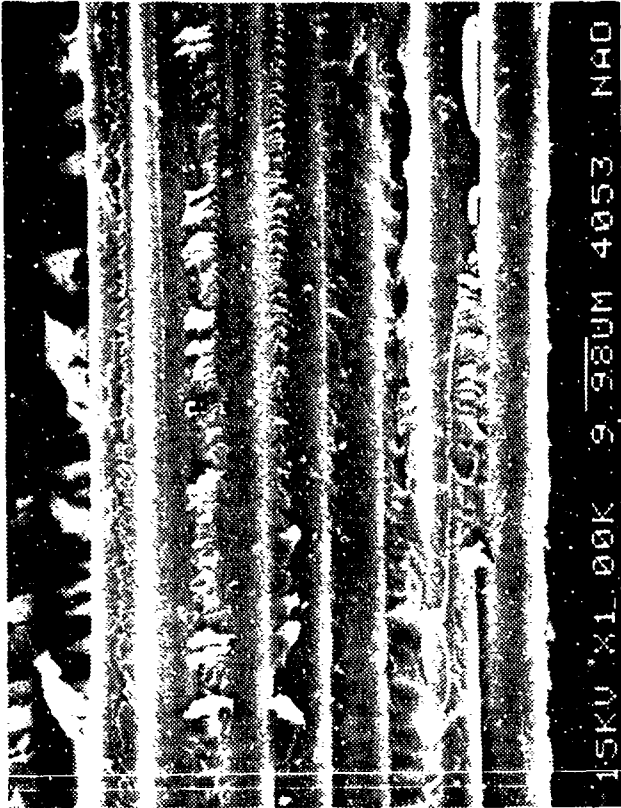
(b), (c) Normal and Oblique Views of Fracture Near the Apex

1 = Impact point

CD = Crack-propagation direction



(d)



(e)

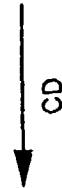
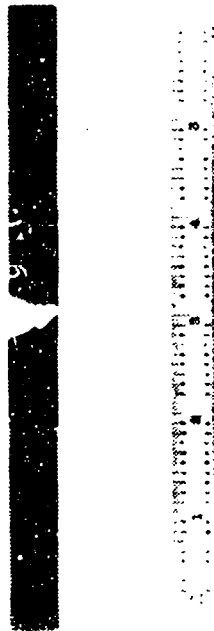


Figure 2-140. (Continued)
 (d) Arrows Point to DAF Radial Lines on Fractured Fiber-Ends and
 Indicate Local Fracture Path
 (e) Fracture Features Present in Ply Oriented Parallel to Fracture
 H = Hackles
 R = River patterns
 CD = Crack propagation direction



(a)

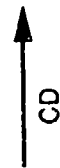


Figure 2-141. Optical and SEM Photographs of Translaminar Tension Fracture in Gr/Ep-32 Ply/Quasi-Isotropic, Water Immersed Before Test
(a) Macrofracture of Fractured Fragments
(b), (c) Normal and Oblique Views of Fracture Near the Apex

CD = Crack propagation direction



(b)



(c)



(d)



(e)

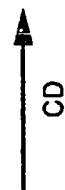
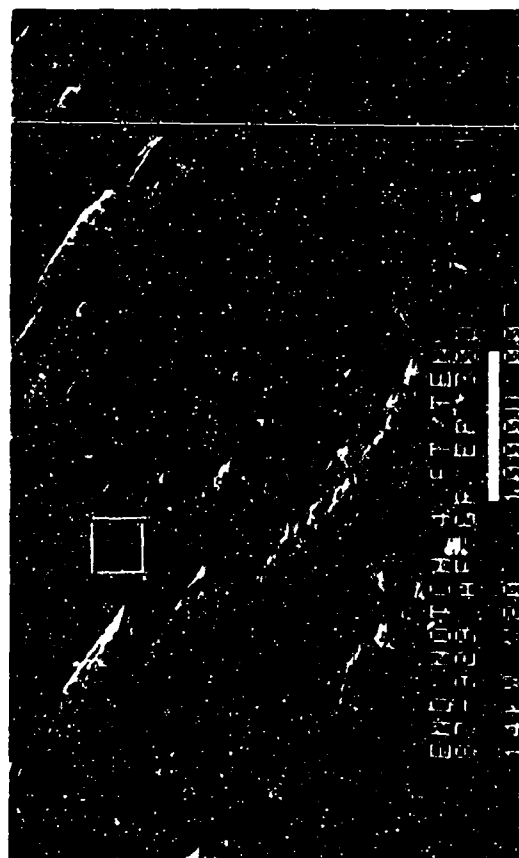


Figure 2-141. (Continued)
 (d) Arrows Point to DAF Radial Lines on Fractured Fiber-Ends and Indicate Fracture Path
 (e) Fracture Features Present in Ply Oriented Parallel to Fracture
 H = Hackles
 R = River patterns
 CD = Crack-propagation direction



30 degree tilt

(a)

20X



30 degree tilt

(b)

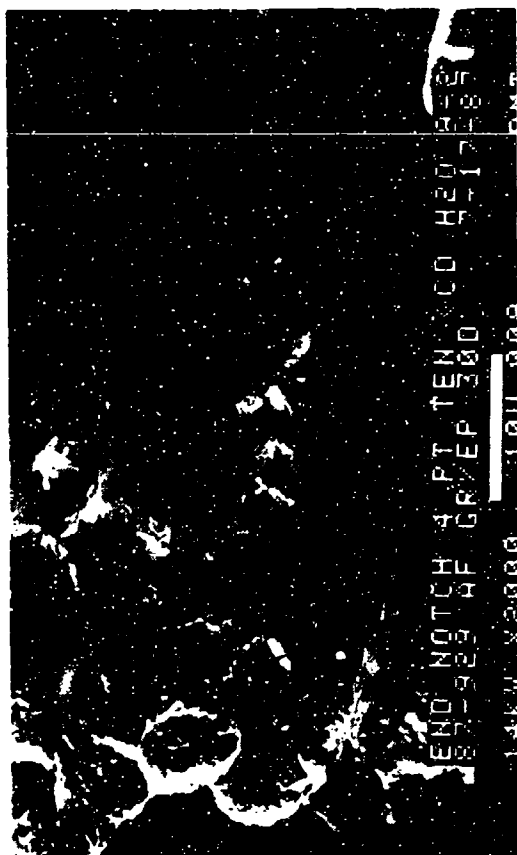
400X

Note:
Location a is magnified in (c)
Location b is magnified in (d)

Mechanically induced
crack direction



Figure 2-142. SEM Fractographs of Translaminar Tension, 0/90 Fracture, Water Immersion (160 F) After Test



30 degree tilt (c) Typical fracture along the fibers 2,000X

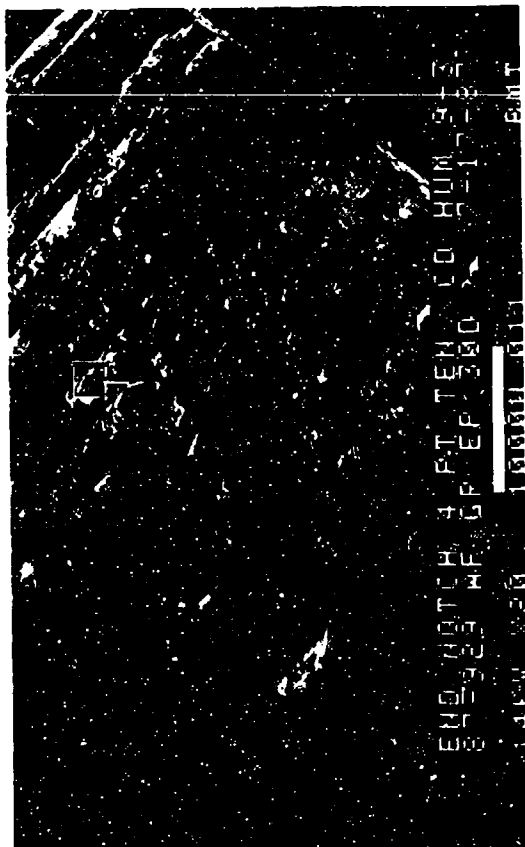


30 degree tilt (d) Illustration of crack mapping using the radial patterns on the fiber ends 2,000X

Mechanically induced
crack direction



Figure 2-142. (Continued)



20X

(a)

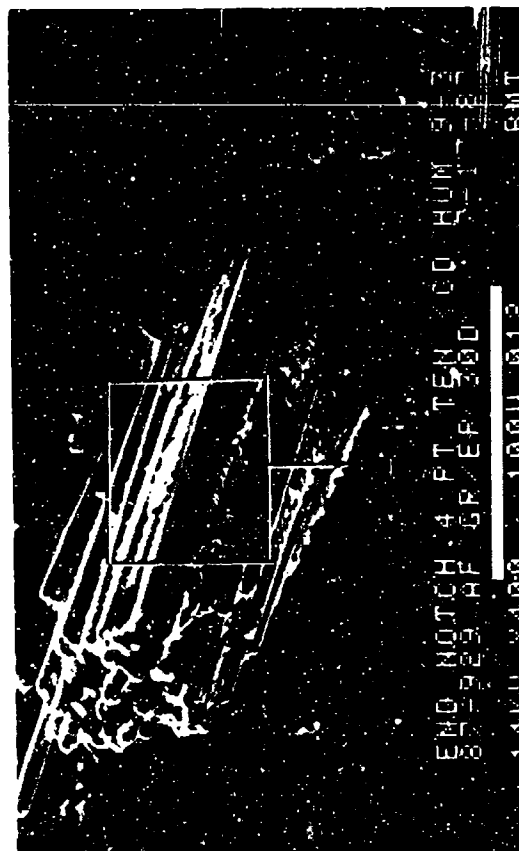
30 degree tilt

Illustration of crack mapping using
the radial patterns on the fiber ends

Mechanically induced
crack direction



2-179

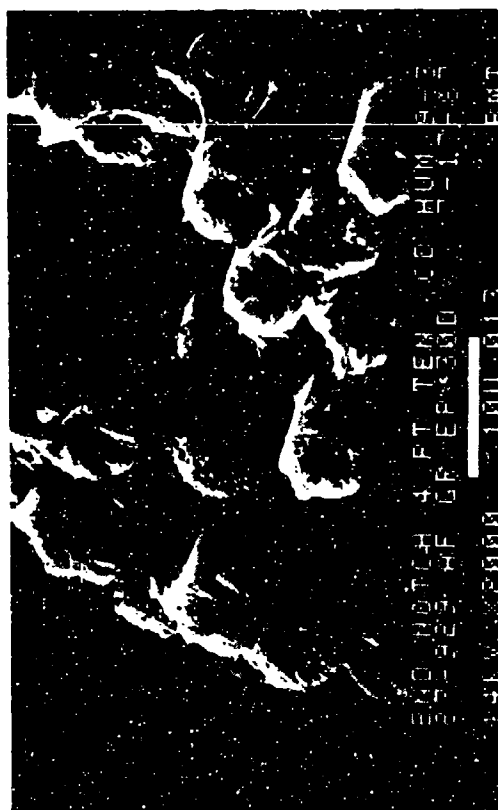


400X

(b)

30 degree tilt

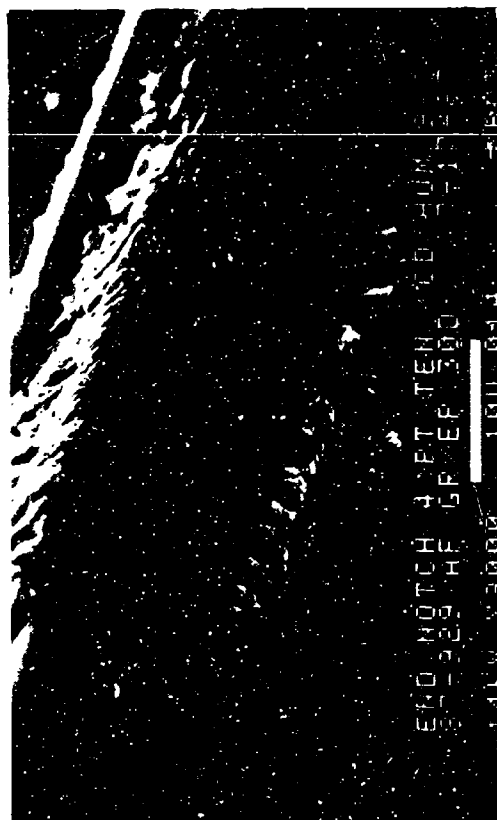
Figure 2-143. SEM Fractographs of Translaminar Tension, 0/90 Fracture, 100% Relative Humidity (160 F) Exposure After Test



30 degree tilt

(c)

2,000X



30 degree tilt

(d)

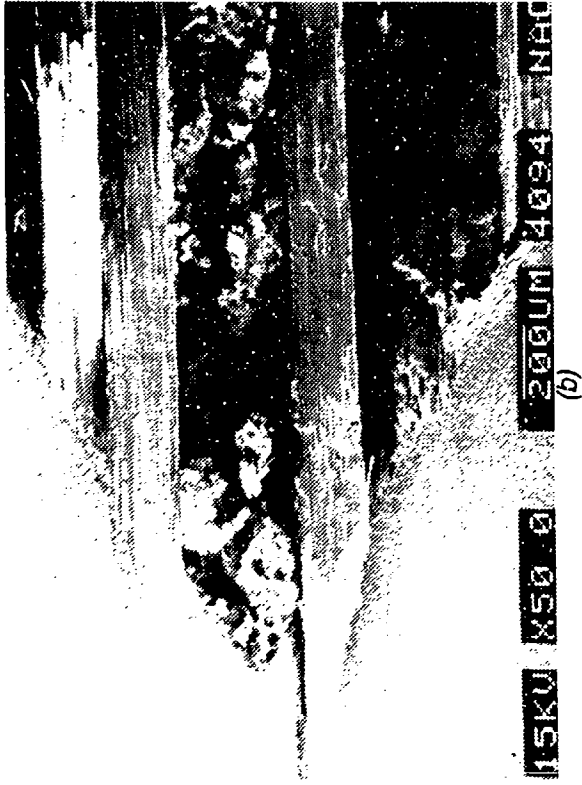
2,000X

Illustration of crack mapping using
the radial patterns on the fiber ends

Mechanically induced
crack direction



Figure 2-143. (Continued)



Optical photograph of fractured fragments. The image shows a dark, rectangular specimen with a bright, irregular fracture line.

(a)

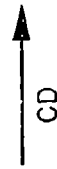
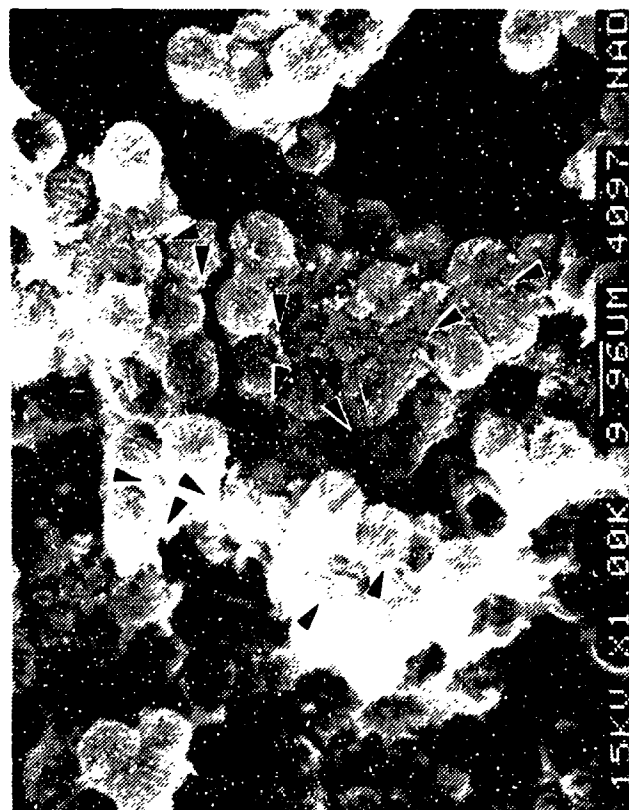


Figure 2-144. Optical and SEM Photographs of Translaminar Tension Fracture in Undercured Gr/Ep -32 Ply/Quasi-Isotropic
(a) Macro photograph of fractured fragments
(b), (c) Normal and Oblique Views of Fracture Near the Apex

CD = Crack propagation direction



(d)



(e)

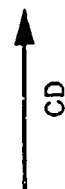


Figure 2-144. (Continued)
 (d) Arrows Point to DAF Radial Lines on Fractured Fiber-Ends and Indicate Fracture Path
 (e) Fracture Features Present in Ply Oriented Parallel to Fracture

H = Hackles
 R = River patterns
 S = Scallops

CD = Crack-propagation direction

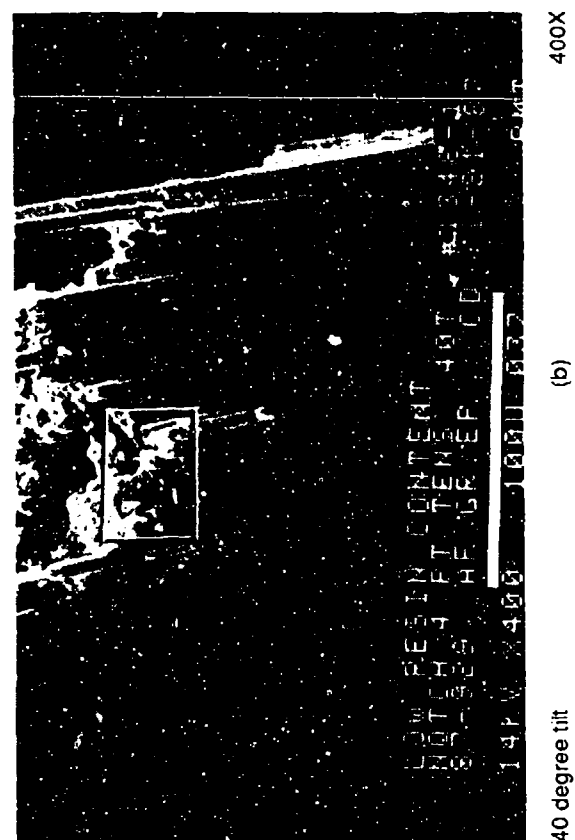
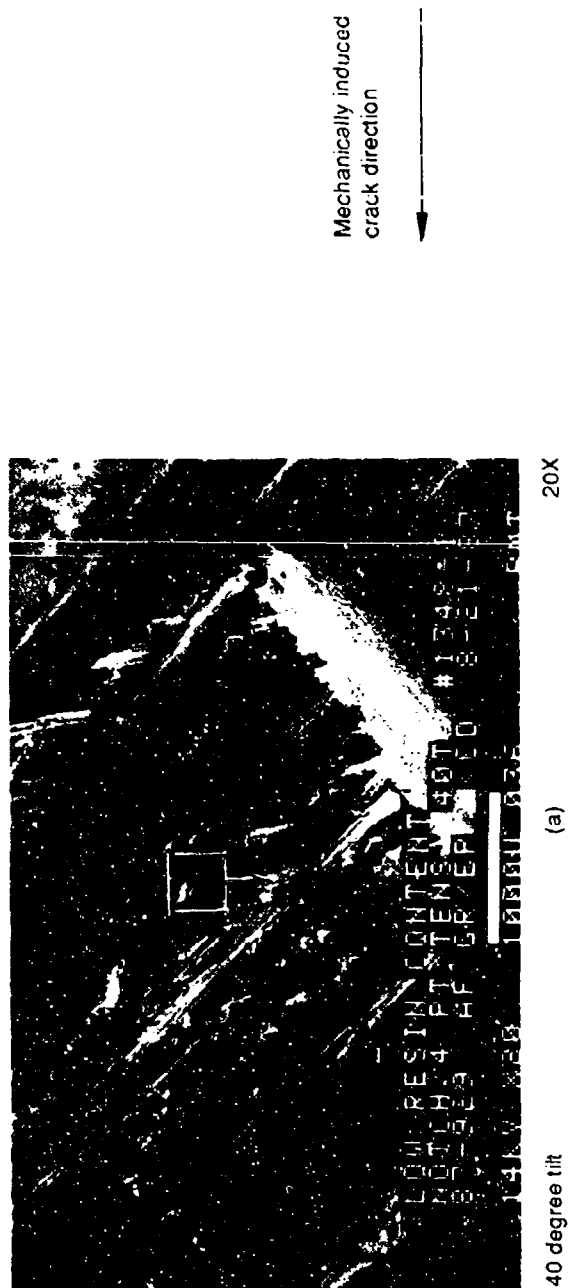
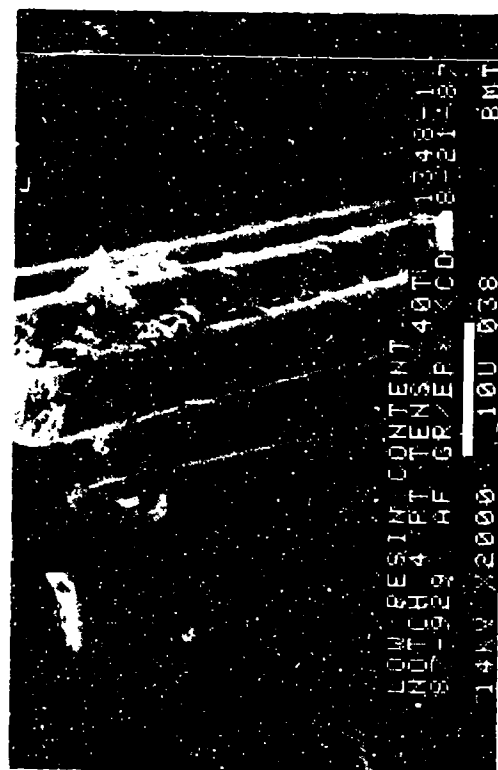
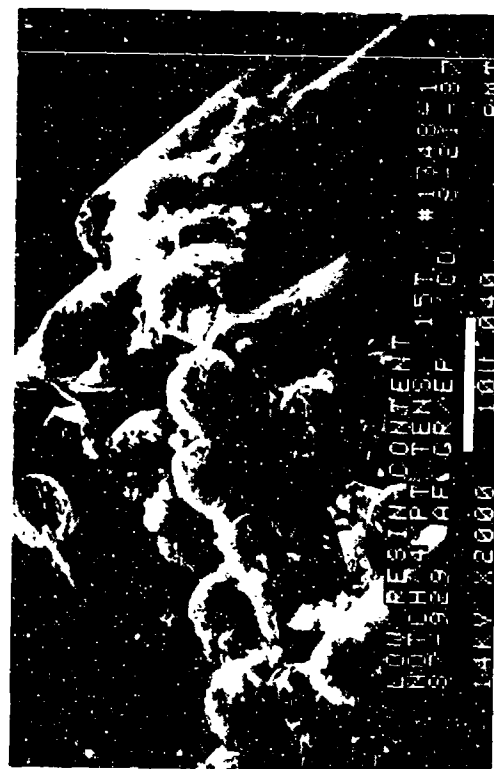


Figure 2-145. SEM Fractographs of Translaminar Tension, 0/90 Fracture, Low Resin Content



40 degree tilt (c) Typical fracture along the fibers 2,000X

Mechanically induced
crack direction



15 degree tilt (d) Illustration of crack mapping using the radial patterns on the fiber ends 2,000X

Figure 2-145. (Continued)

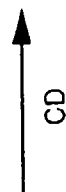
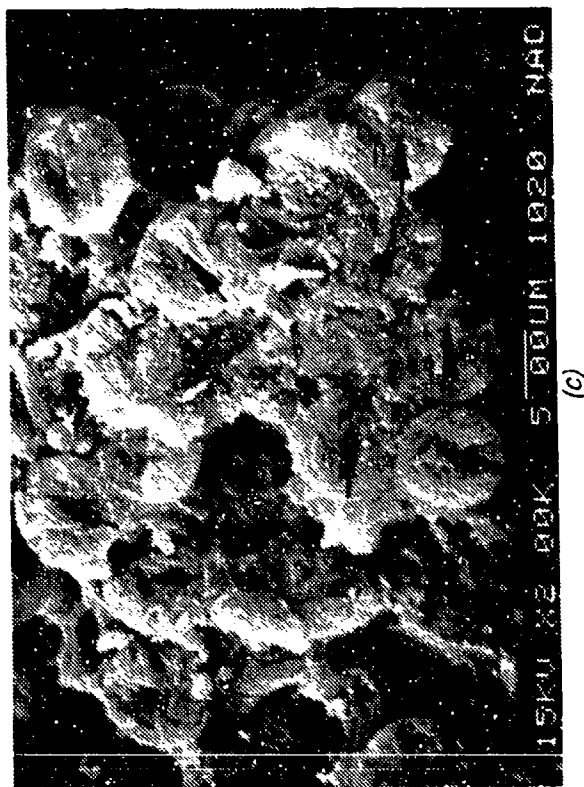
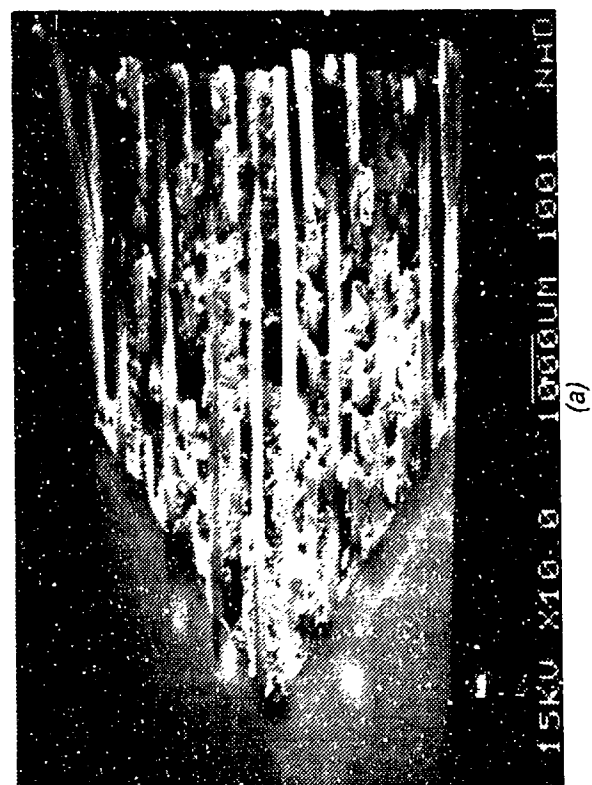
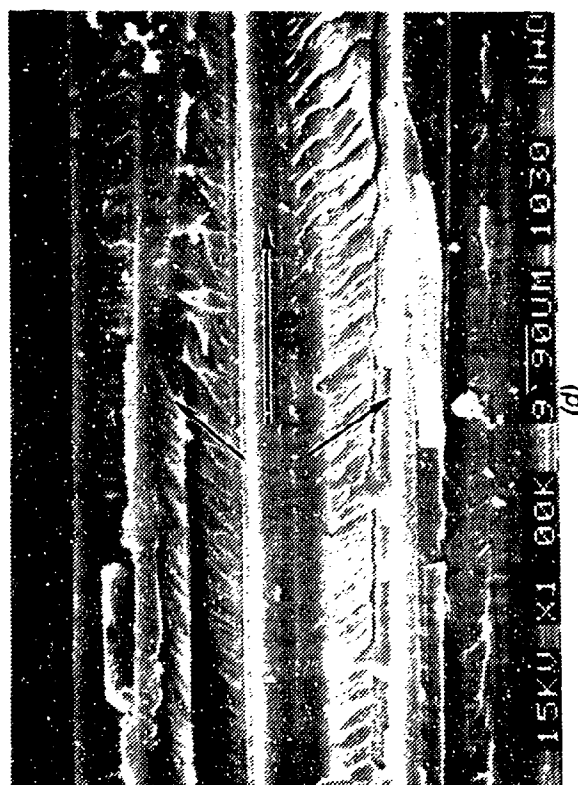
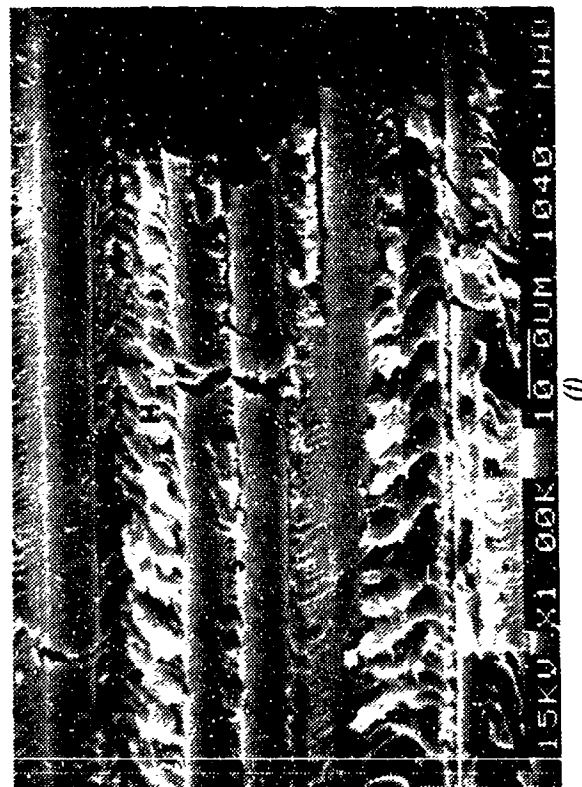


Figure 2-146. SEM Photographs of Translamellar Tension Fracture in High Resin Content Gr/Ep - 32 Ply Quasi-Isotropic (a), (b) River Patterns (Arrows) in Fractured Epoxy Region of a 90 Degree Ply (c) Hackles (H), Scallops (S), and Broken Fibers in a 45 Degree Ply

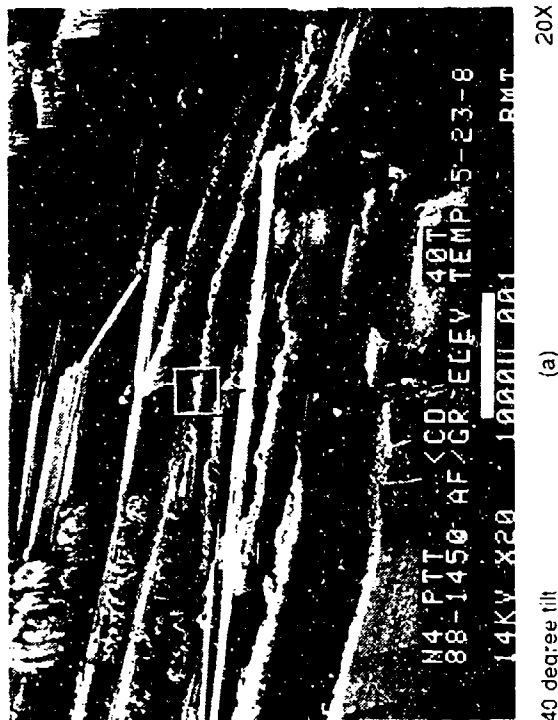
CD = Crack-propagation direction



↑
CD

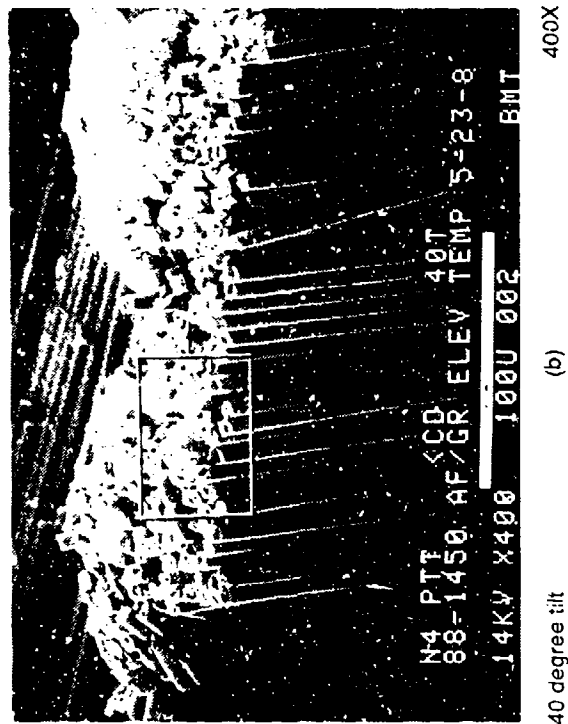
Figure 2-146. (Continued)
(d), (e) River Patterns (Arrows) Present in the
Fractured Epoxy Regions of a 90 Degree Ply
(f) Hackles (H), Scallops (S), and Broken Fibers in a
45 Degree Ply

CD = Crack-propagation direction

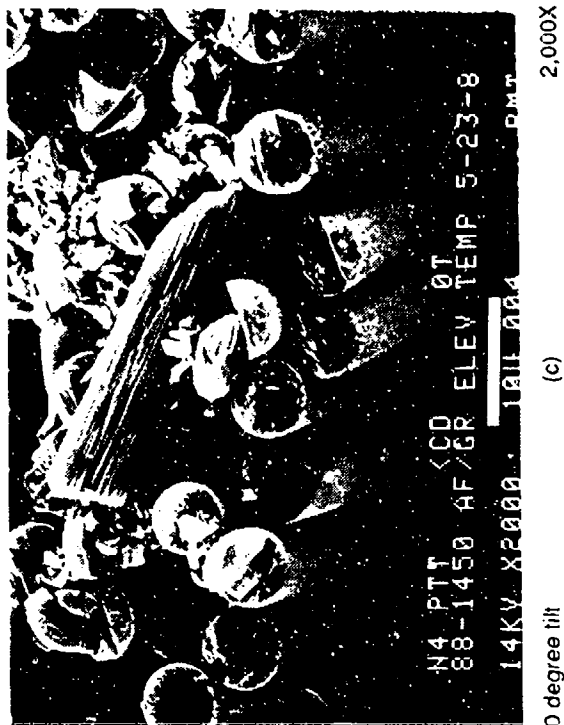


20X

Mechanically induced
crack direction



400X



2,000X

Figure 2-147. SEM Fractiographs of Translaminar Tension, 0/90 Fracture, 2000 F Exposure for 5 Minutes After Test

2.6 TRANSLAMINAR COMPRESSION

The primary features observed in translaminar fractures generated under Mode I compression are as follows:

1. Macroscopically, a relatively flat fracture surface, particularly on plies oriented parallel to axial compression load
2. Fiber kink bands (short fiber segments) protruding from the fracture surface
3. Fiber end flexural fracture features known as chop marks, exhibiting tension features on one side and compression features on the other side of a neutral axis line
4. Post-failure damage due to rubbing contact between mating fracture surfaces (This feature can often completely obscure the features normally found on individual fiber ends).

Figure 2-148 shows the translaminar compression test configuration. Translaminar compression fracture usually occurs by a combination of fiber microbuckling and delamination fractures. Chop marks on the fiber ends (Figure 2-149) indicate a flexural fiber fracture. Studies of the neutral axis lines of the chop marks have indicated that no direct correspondence to crack propagation is inferred.

Fractures produced at high temperatures in specimens with high absorbed moisture content exhibit a rougher macroscopic fracture surface, with longer fiber segments and more secondary intralaminar shear cracks on the microscopic scale.

The test matrix for this section is provided in Table 2-6. Figures 2-150 through 2-173 are the translaminar compression fractographs. The reader should note that the low-magnification SEM photomicrographs reveal both compression fracture (flat) and tension fracture (fibers protruding). This is because the flexural nature of the test specimen, where cracking is initiated at the notch in compression. The high magnification photographs are from the compression fracture region. The fractography figures are arranged in the same order that the corresponding tests are listed in Table 2-6.

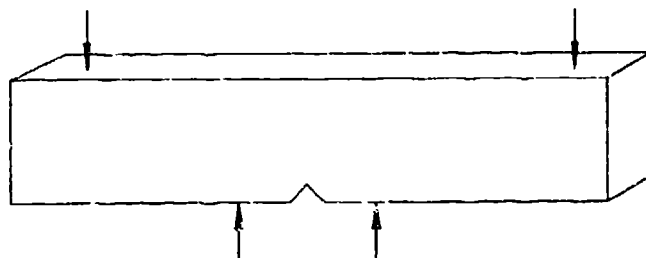


Figure 2-148. Four-Point Bend Test Type

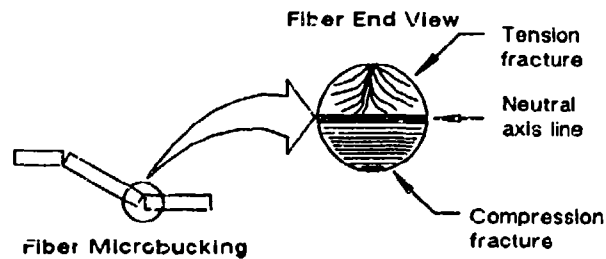


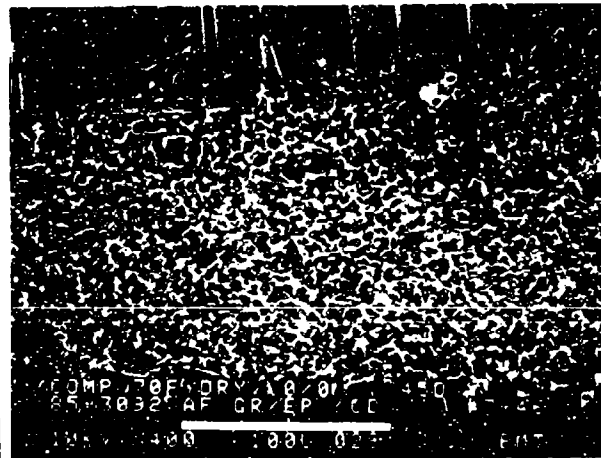
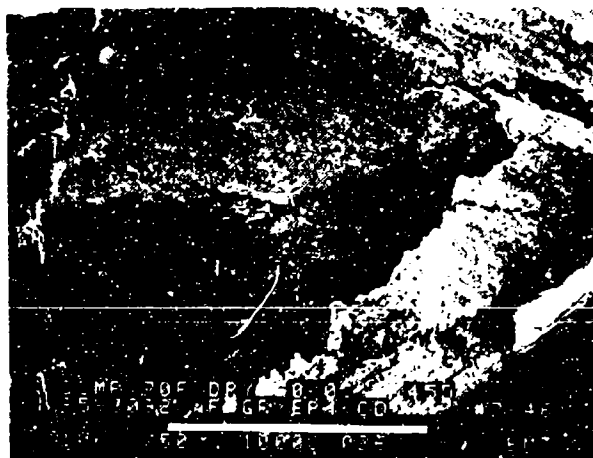
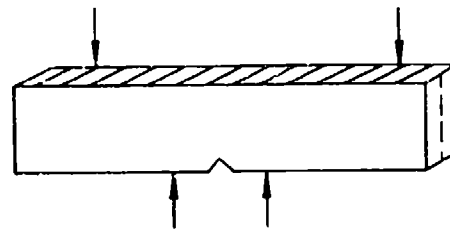
Figure 2-149. Translaminar Compression Fracture

Table 2-6. Test Matrix for Translaminar Compression Specimens

PLY/ORIENTATION	VARIABLE CONDITIONS	CONTRIBUTOR
32/0 32/+ 45 32/0,90 32/Quasi	RT/Dry (Baseline), -65°F/Dry, 180°F/Dry, 270°F/Dry, RT/Wet, 270°F/Wet	Boeing
32/Quasi	Impact Damage Before Test	Northrop
32/Quasi	Water Immersion Before Test	Northrop
32/Quasi	Overcured	Northrop
32/Quasi	High Resin	Northrop

SEM photomicrographs

Fracture type	Translaminar mode I compression
Ply layup	[0] 32
Test type	Four-point bend
• Test conditions	21°C, dry
• Fiber end fracture	
Material	Hercules 3501-6/177°C cure AS4 fibers



Mechanically induced crack direction

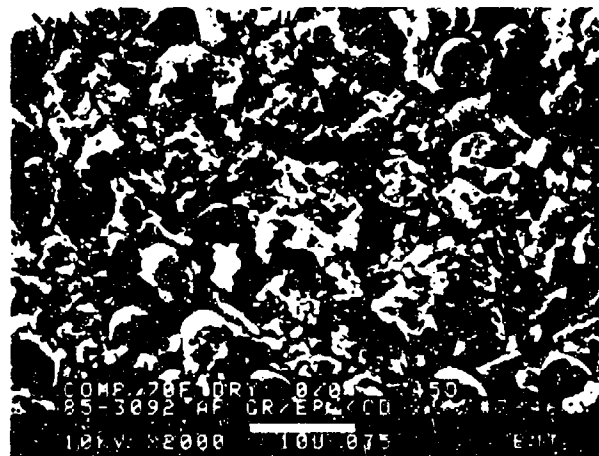
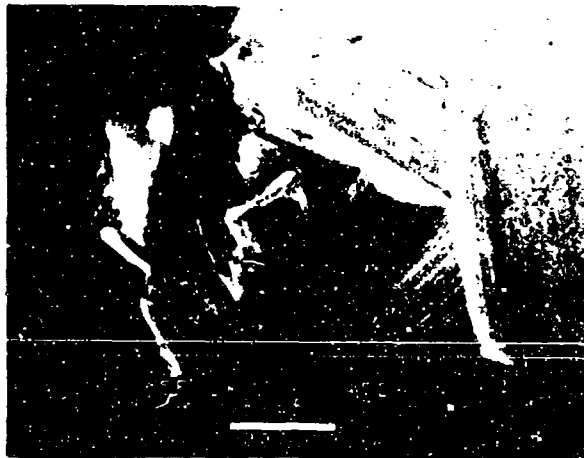
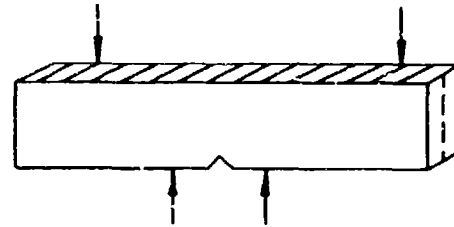


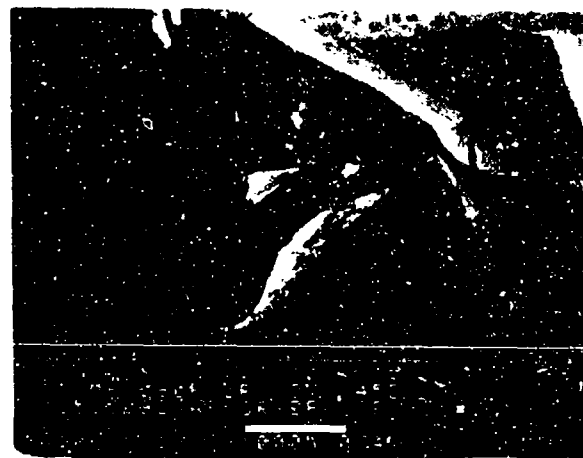
Figure 2-150. SEM Photographs of Translaminar Mode I Compression, 0/0 Fracture, 70 F/Dry

SEM photomicrographs

Fracture type	Translaminar mode I compression
Ply layup	[0] 32
Test type	Four-point bend
• Test conditions	Dry
• Fiber end fracture	
Material	Hercules 3501-6/177°C cure AS4 fibers

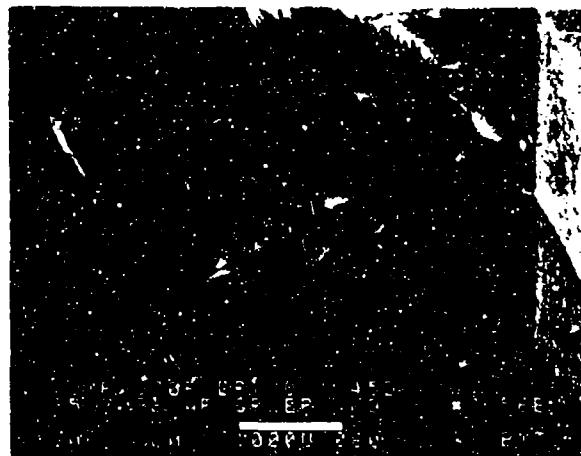


-65°F. dry



180°F. dry

————— Mechanically induced crack direction

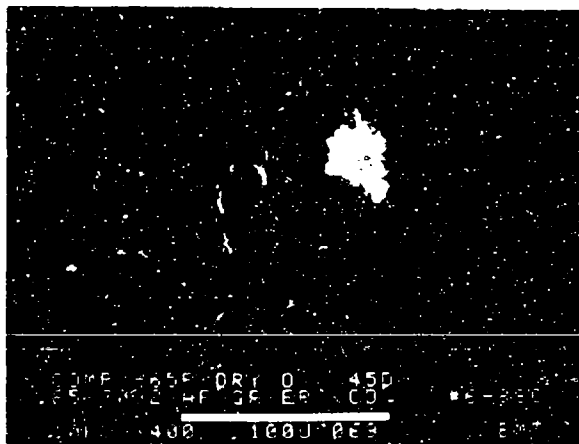
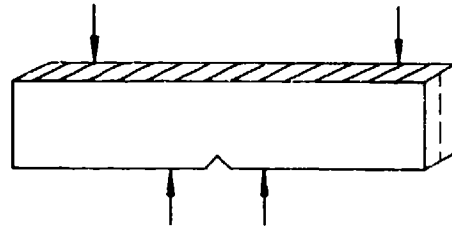


270°F. dry

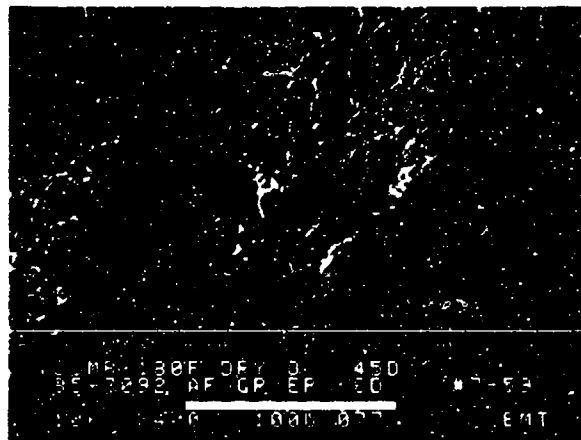
Figure 2-151. SEM Photographs of Translaminar Mode I Compression, 0/0 Fracture.
-65, 180, 270 F/Dry (20X)

SEM photomicrographs

Fracture type	Translaminar mode I compression
Ply layup	[0] 32
Test type	Four-point bend
• Test conditions	Dry
• Fiber end fracture	
Material	Hercules 3501-6/177°C cure AS4 fibers

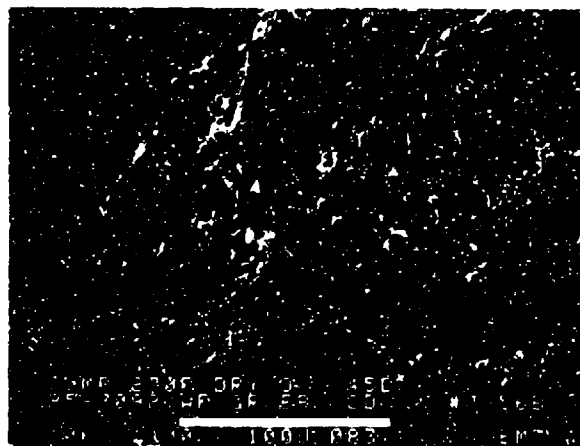


-65°F, dry



180°F, dry

← Mechanically induced crack direction

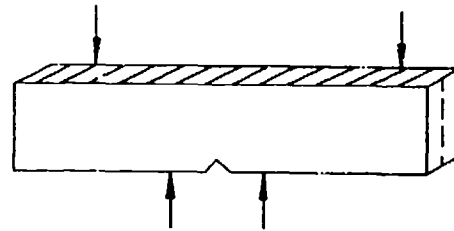


270°F, dry

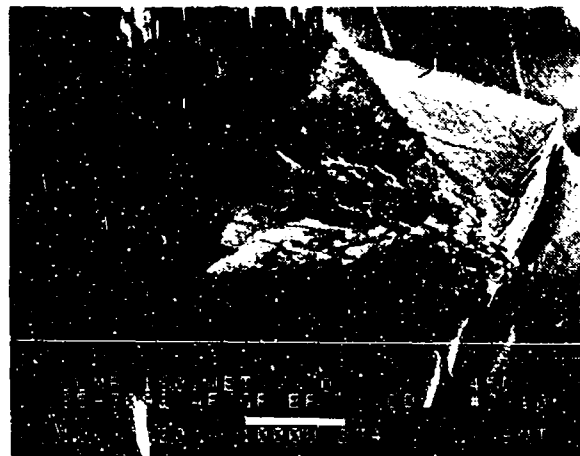
Figure 2-152. SEM Photographs of Translaminar Mode I Compression, 0/0 Fracture, -65, 180, 270 F/Dry (400X)

SEM photomicrographs

Fracture type	Translaminar mode I compression
Ply layup	[0] 32
Test type	Four-point bend
• Test conditions	Wet
• Fiber end fracture	
Material	Hercules 3501-6/177°C cure AS4 fibers

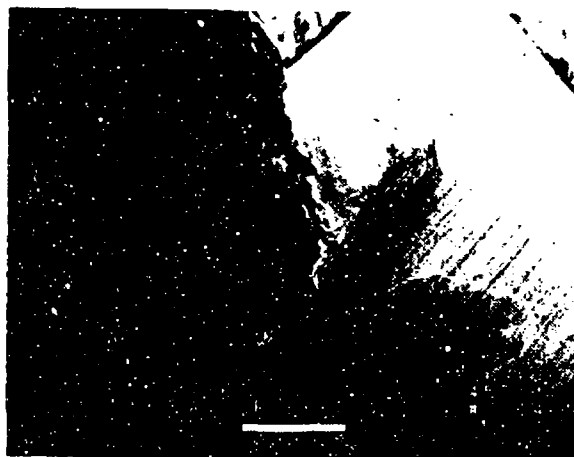


70°F, wet



180°F, wet

Mechanically induced crack direction

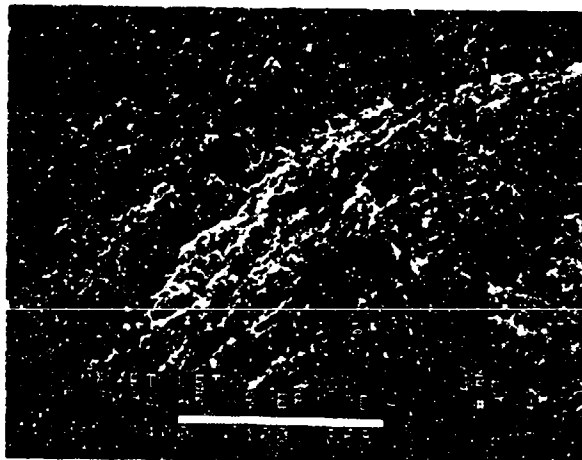
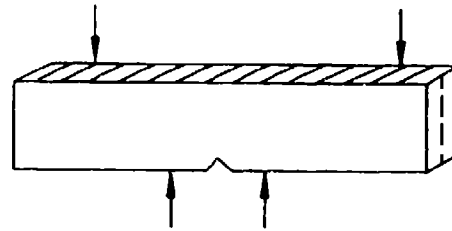


270°F, wet

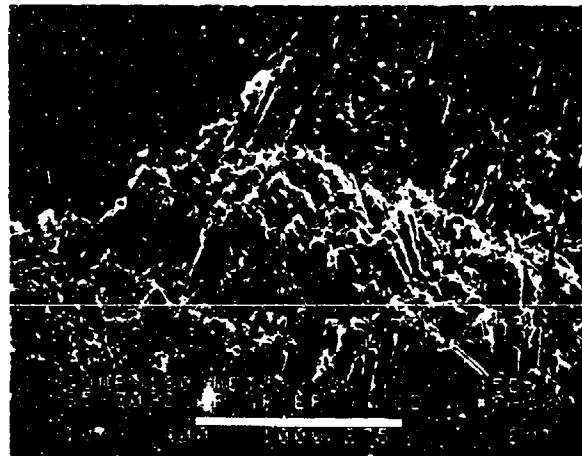
Figure 2-153. SEM Photographs of Translaminar Mode I Compression, 0/0 Fracture, 70, 180, 270 F/Wet (20X)

SEM photomicrographs

Fracture type	Translaminar mode I compression
Ply layup	[0] ₃₂
Test type	Four-point bend
• Test conditions	Dry
• Fiber end fracture	
Material	Hercules 3501-6/177°C cure AS4 fibers

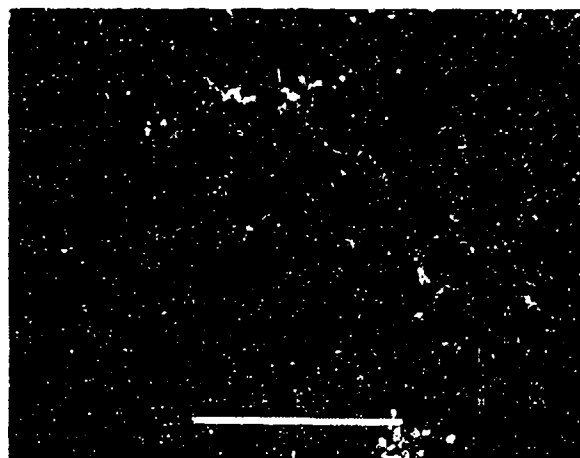


70°F, wet



180°F, wet

Mechanically induced crack direction

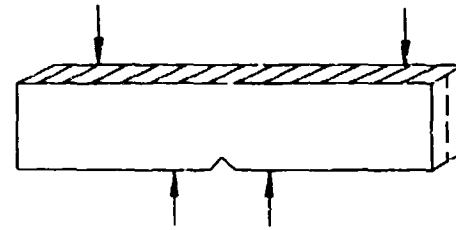


270°F, wet

Figure 2-154. SEM Photographs of Translaminar Mode I Compression, 0/0 Fracture, 70, 180, 270 F/Wet (400X)

SEM photomicrographs

Fracture type	Translaminar mode I compression
Ply layup	[+45, -45] 16S
Test type	Four-point bend
• Test conditions	21°C, dry
• Fiber end fracture	
Material	Hercules 3501-6/177°C cure AS4 fibers



Mechanically induced crack direction

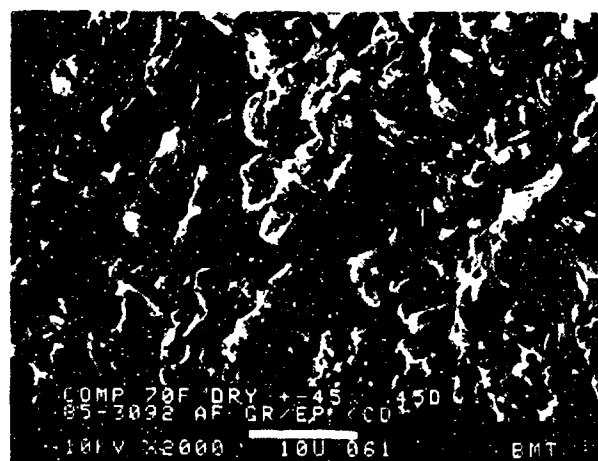
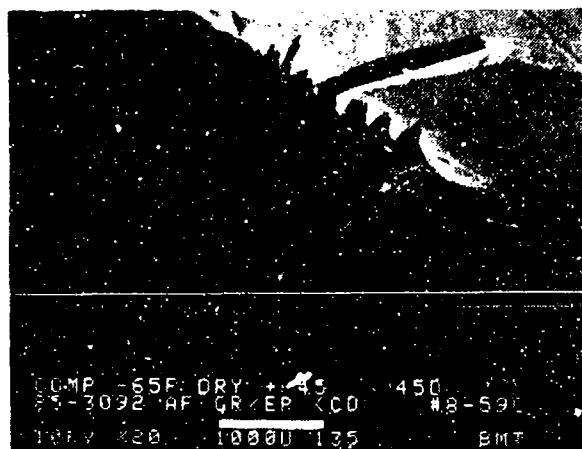
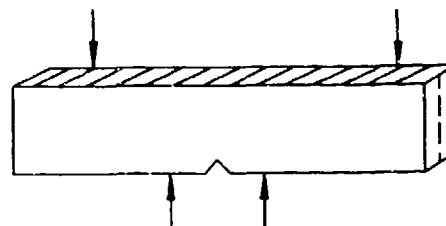


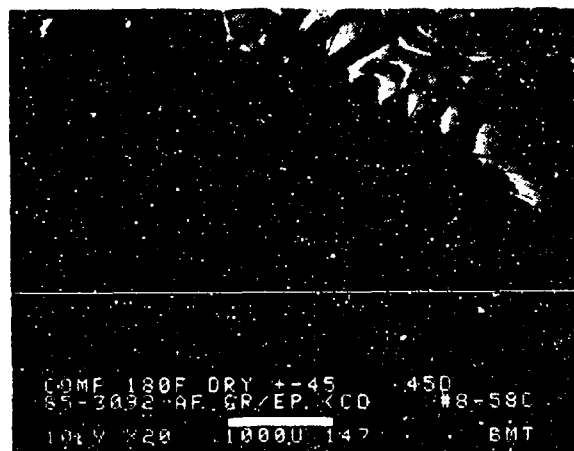
Figure 2-155. SEM Photographs of Translaminar Mode I Compression, +45/-45 Fracture, 70 F/Dry

SEM photomicrographs

Fracture type	Translaminar mode I compression
Ply layup	[+45, -45] 16S
Test type	Four-point bend
• Test conditions	Dry
• Fiber end fracture	
Material	Hercules 3501-6/177°C cure AS4 fibers

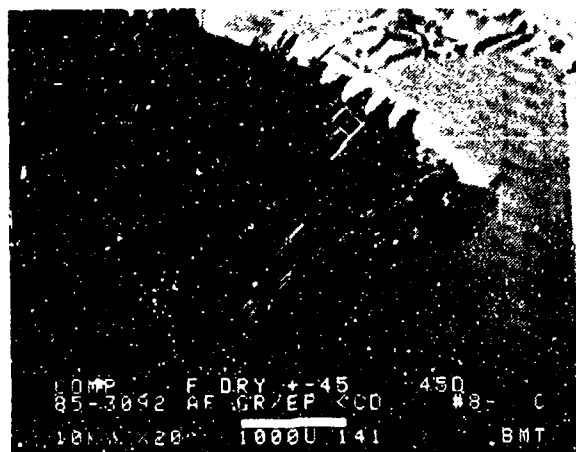


-65°F, dry



180°F, dry

Mechanically induced crack direction

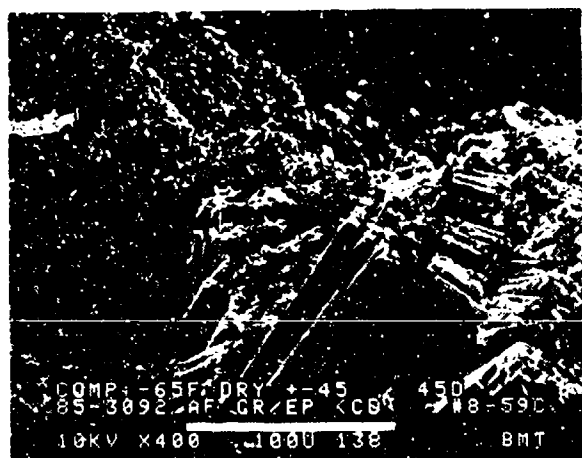
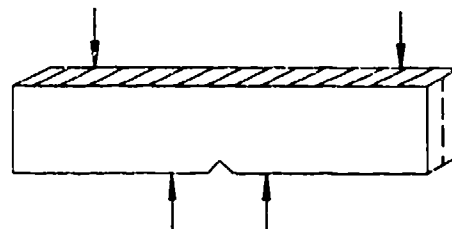


270°F, dry

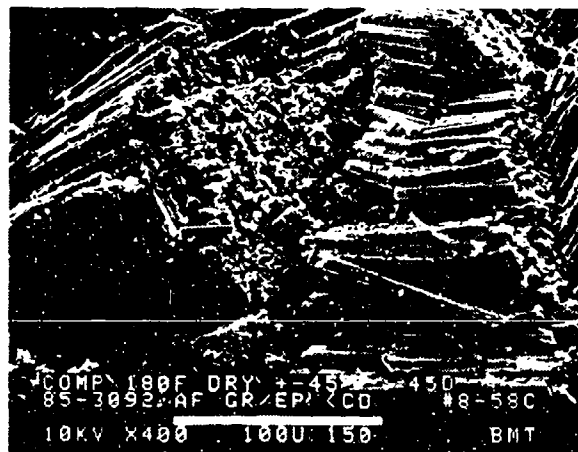
Figure 2-156. SEM Photographs of Translaminar Mode I Compression, +45/-45 Fracture, -65, 180, 270 F/Dry (20X)

SEM photomicrographs

Fracture type	Translaminar mode I compression
Ply layup	[+45, -45] 16S
Test type	Four-point bend
• Test conditions	Dry
• Fiber end fracture	
Material	Hercules 350i-6/177°C cure AS4 fibers

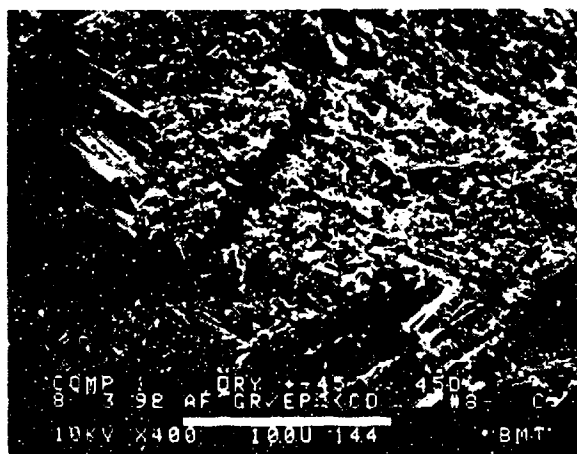


-65°F, dry



180°F, dry

————— Mechanically induced crack direction

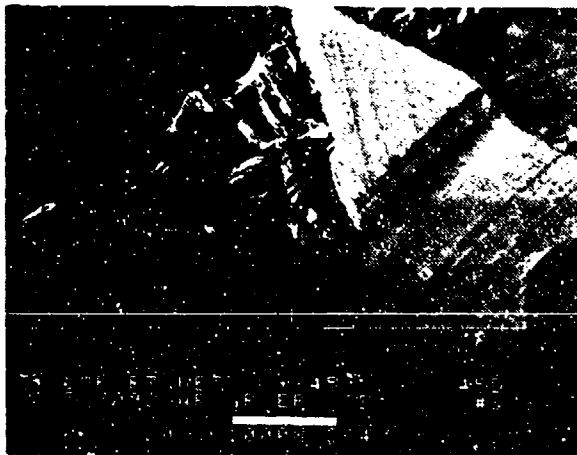
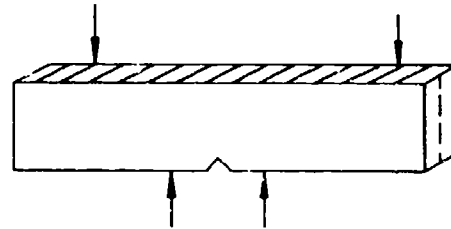


270°F, dry

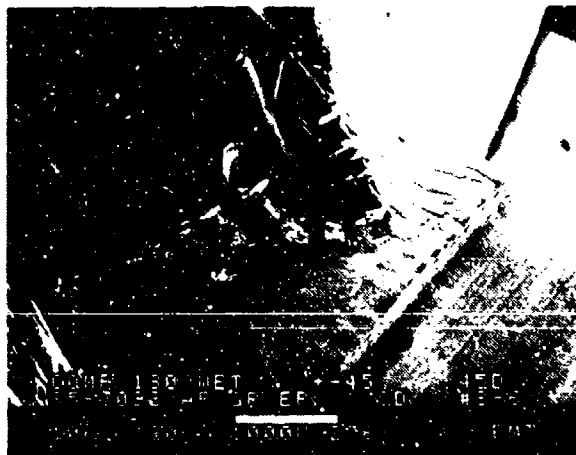
Figure 2-157. SEM Photographs of Translaminar Mode I Compression, +45/-45 Fracture, -65, 180, 270 F/Dry (400X)

SEM photomicrographs

Fracture type	Translaminar mode I compression
Ply layup	[+45, -45] 16S
Test type	Four-point bend
• Test conditions	Wet
• Fiber end fracture	
Material	Hercules 3501-6/177°C cure AS4 fibers

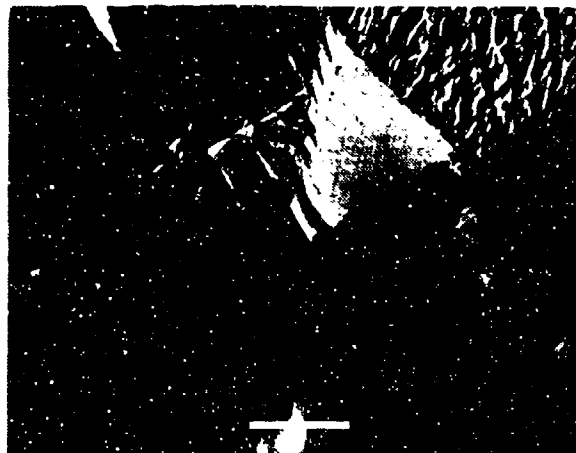


-65°F, wet



180°F, wet

Mechanically induced crack direction

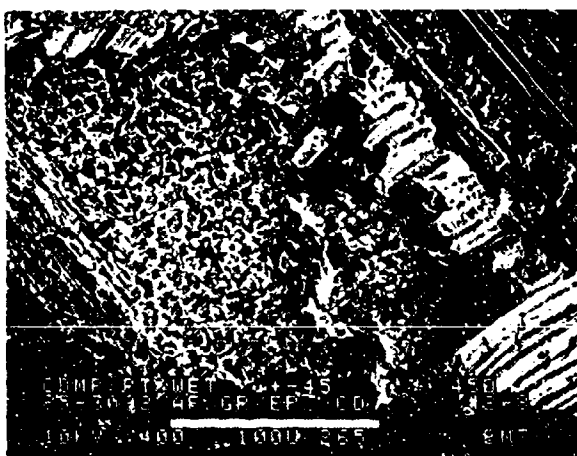
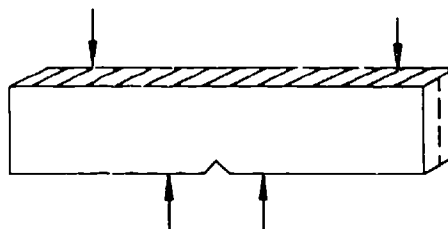


270°F, wet

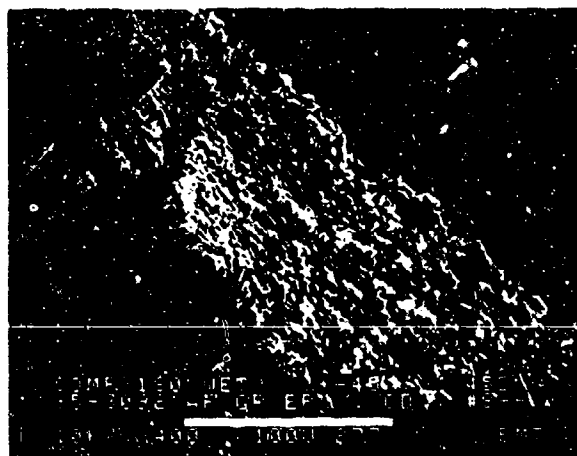
Figure 2-158. SEM Photographs of Translaminar Mode I Compression, +45/-45 Fracture, 70, 180, 270 F/Wet (20X)

SEM photomicrographs

Fracture type	Translaminar mode I compression
Ply layup	[+45, -45] 16S
Test type	Four-point bend
• Test conditions	Dry
• Fiber end fracture	
Material	Hercules 3501-6/177°C cure AS4 fibers

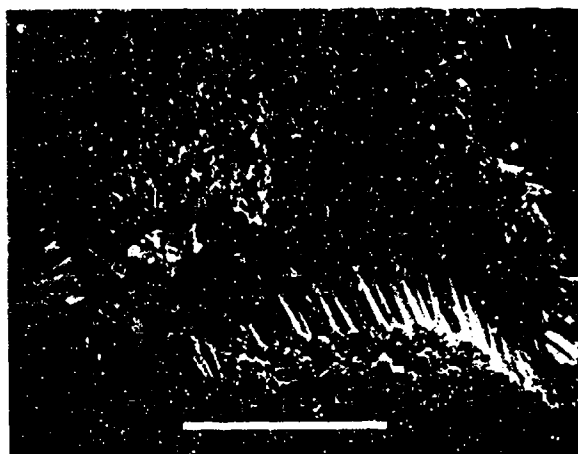


70°F, wet



180°F, wet

Mechanically induced crack direction

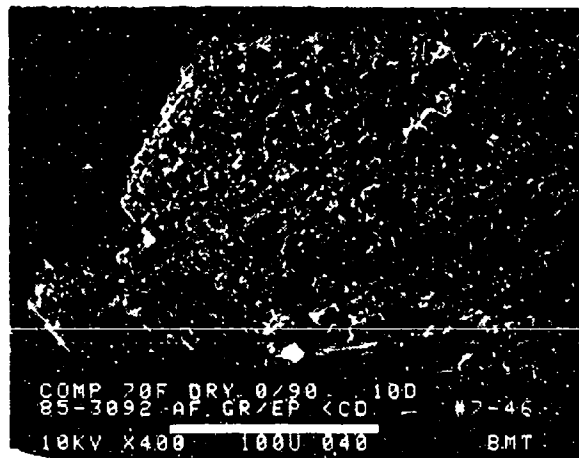
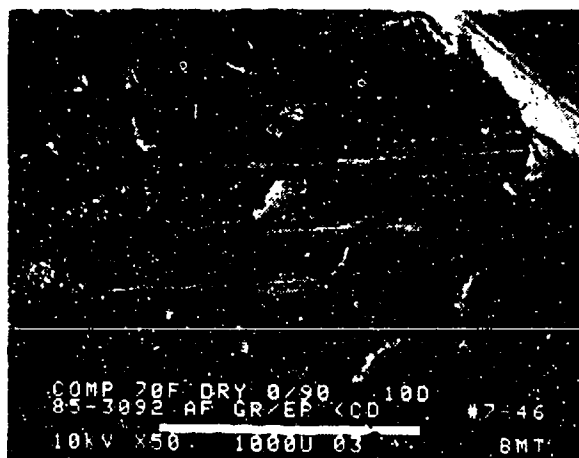
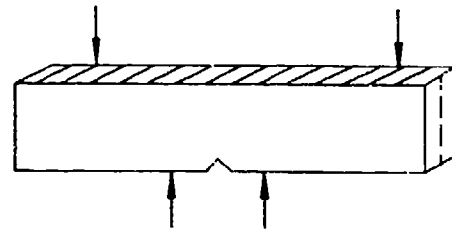


270°F, wet

Figure 2-159. SEM Photographs of Translaminar Mode I Compression, +45/-45 Fracture, 70, 180, 270 F/Wet (400X)

SEM photomicrographs

Fracture type	Translaminar mode I compression
Ply layup	[0, 90] 16S
Test type	Four-point bend
• Test conditions	21°C, dry
• Fiber end fracture	
Material	Hercules 3501-G/177°C cure AS4 fibers



← Mechanically induced crack direction

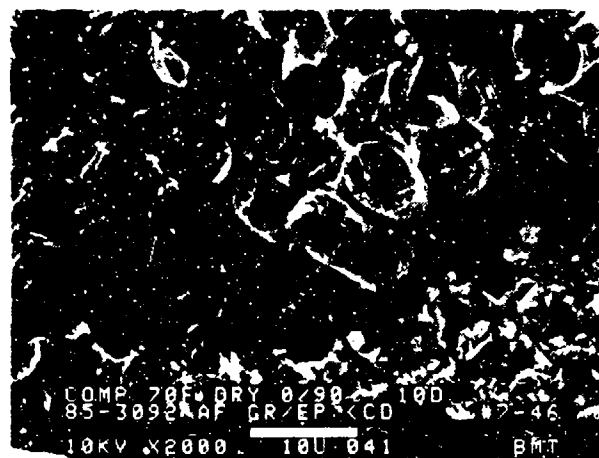
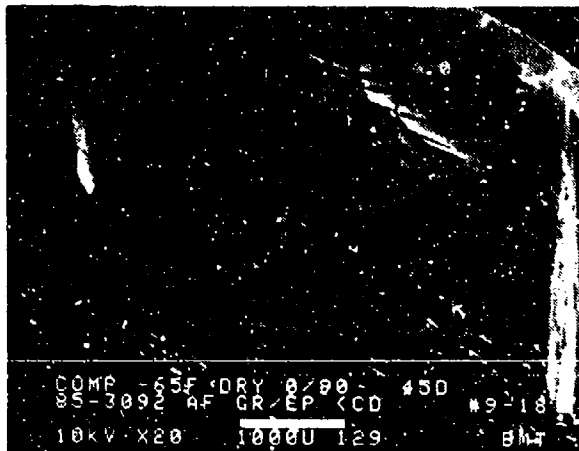
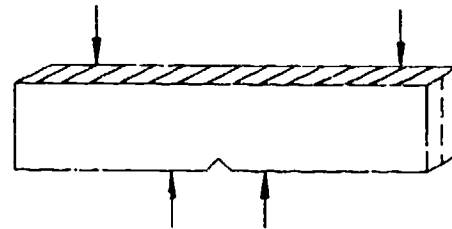


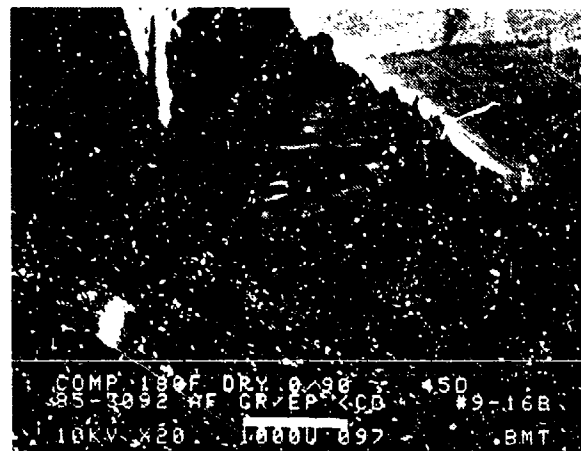
Figure 2-160. SEM Photographs of Translaminar Mode I Compression, 0/90 Fracture, 70 F/Dry

SEM photomicrographs

Fracture type	Translaminar mode I compression
Ply layup	[0, 90] _{16S}
Test type	Four-point bend
• Test conditions	Dry
• Fiber end fracture	
Material	Hercules 3501-6/177°C cure AS4 fibers

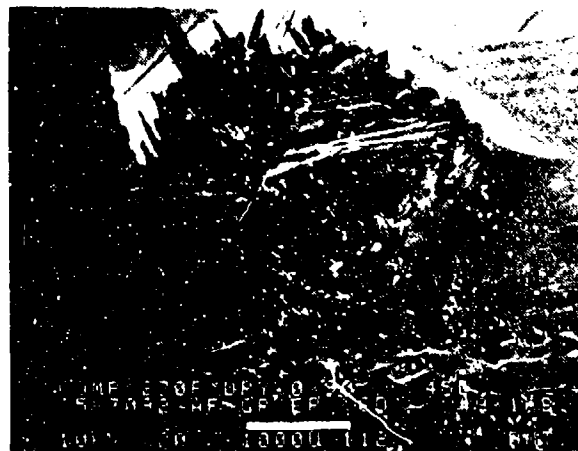


-65°F, dry



180°F, dry

Mechanically induced crack direction

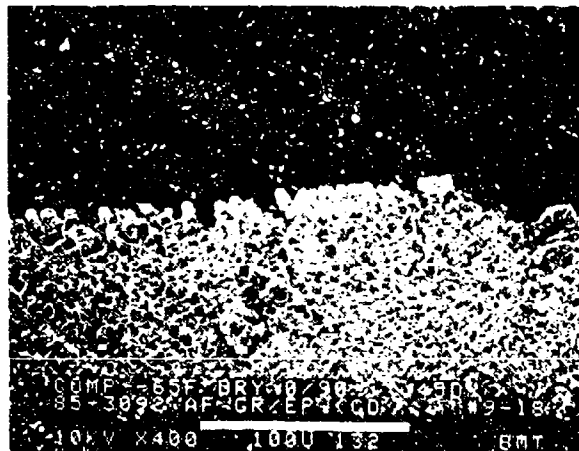
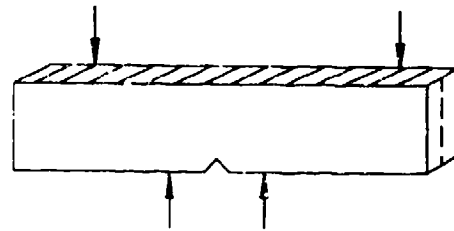


270°F, dry

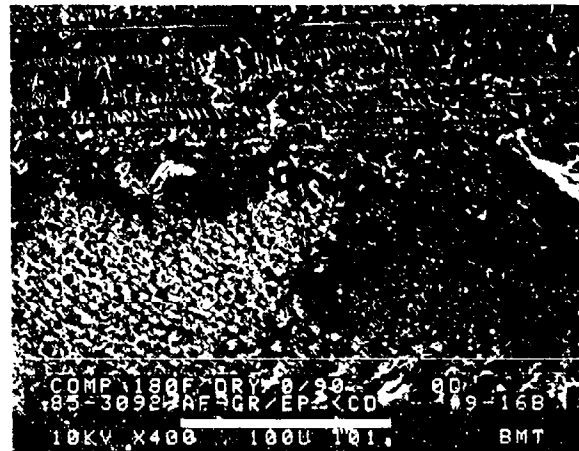
Figure 2-161. SEM Photographs of Translaminar Mode I Compression, 0/90 Fracture, -65, 180, 270 F/Dry (20X)

SEM photomicrographs

Fracture type	Translaminar mode I compression
Ply layup	[0, 90]16S
Test type	Four-point bend
• Test conditions	Dry
• Fiber end fracture	
Material	Hercules 3501-6/177°C cure AS4 fibers

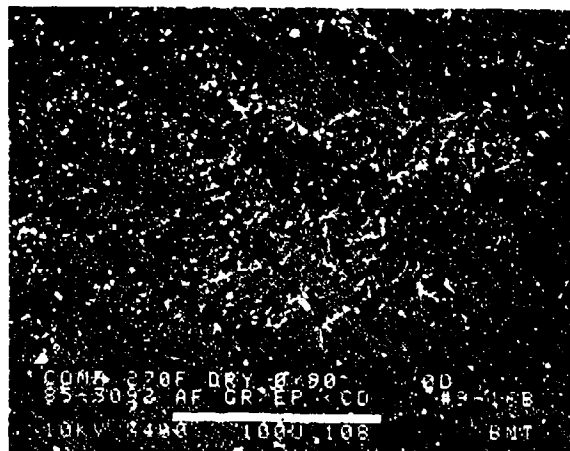


-65°F, dry



180°F, dry

Mechanically Induced crack direction

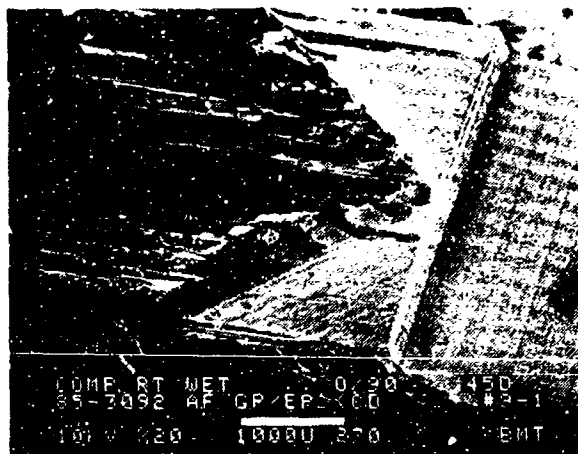
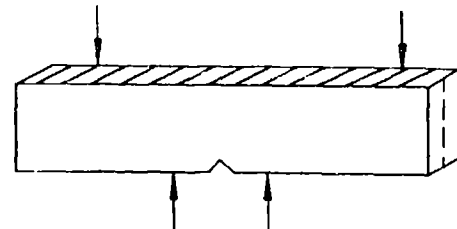


270°F, dry

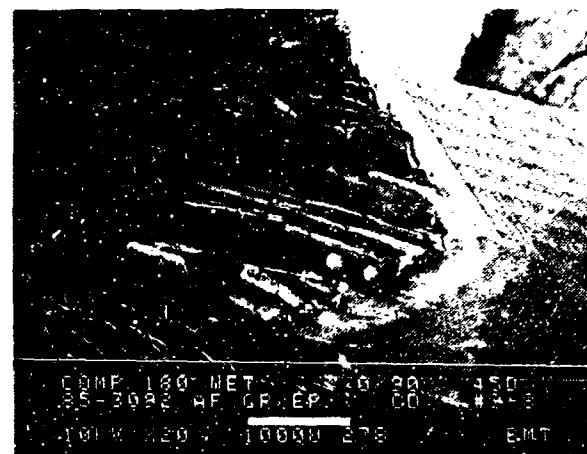
Figure 2-152. SEM Photographs of Translaminar Mode I Compression, 0/90 Fracture, -65, 180, 270 F/Dry (400X)

SEM photomicrographs

Fracture type	Translaminar mode I compression
Ply layup	{0, 90}16S
Test type	Four-point bend
• Test conditions	Wet
• Fiber end fracture	
Material	Hercules 3501-6/177°C cure AS4 fibers

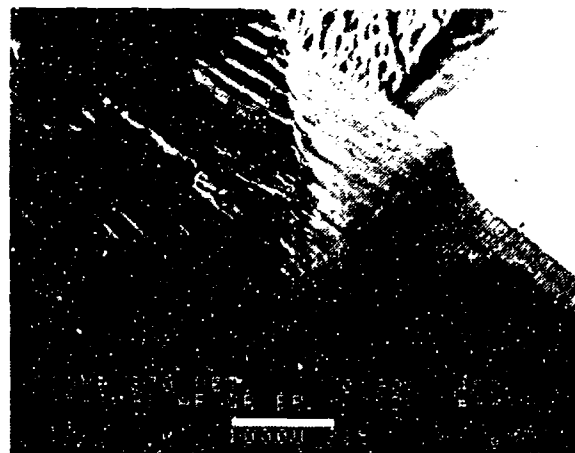


70°F, wet



180°F, wet

Mechanically induced crack direction

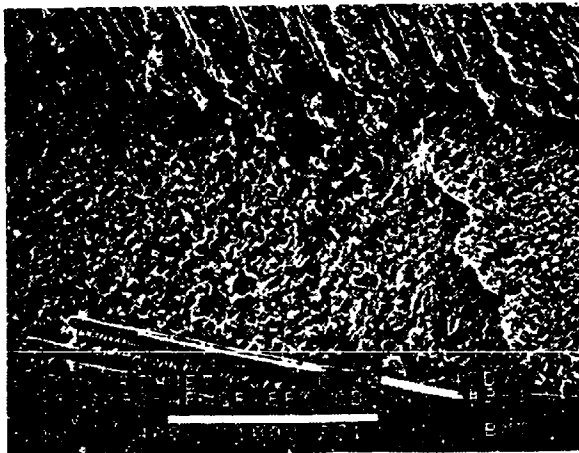
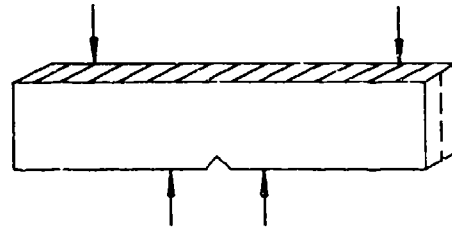


270°F, wet

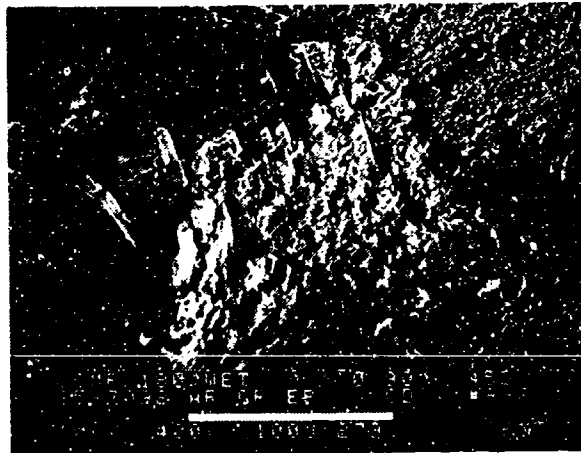
Figure 2-163. SEM Photographs of Translaminar Mode I Compression, 0/90 Fracture, 70, 180, 270 F/Wet (20X)

SEM photomicrographs

Fracture type	Translaminar mode I compression
Ply layup	[0, 90] _{16S}
Test type	Four-point bend
• Test conditions	Wet
• Fiber end fracture	
Material	Hercules 3501-6/177°C cure AS4 fibers

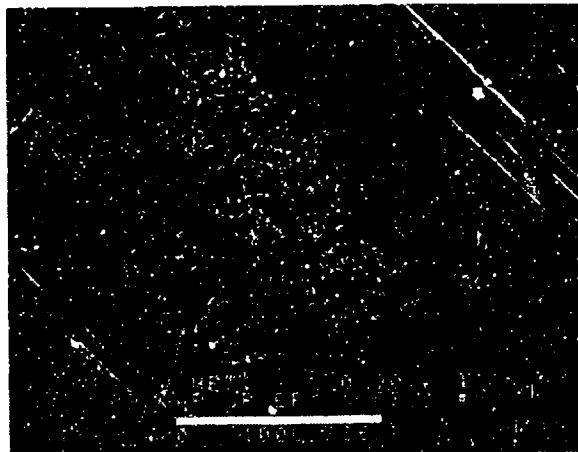


70°F, wet



180°F, wet

Mechanically induced crack direction

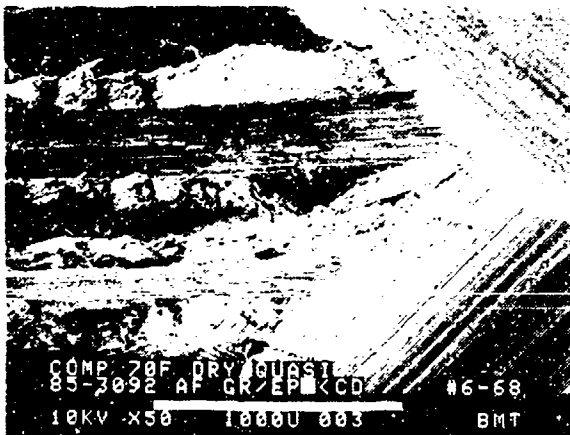
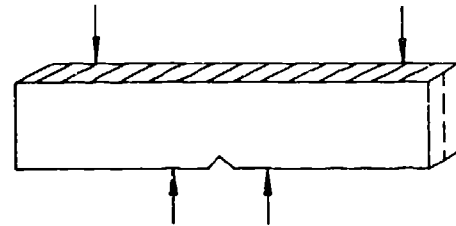


270°F, wet

Figure 2-164. SEM Photographs of Translaminar Mode I Compression, 0/90 Fracture, 70, 180, 270 F/Wet (400X)

SEM photomicrographs

Fracture type	Translaminar mode I compression
Ply layup	[0, 45, 90] 16S
Test type	Four-point bend
• Test conditions	21°C, dry
• Fiber end fracture	
Material	Hercules 3501-6/177°C cure AS4 fibers



Mechanically Induced crack direction

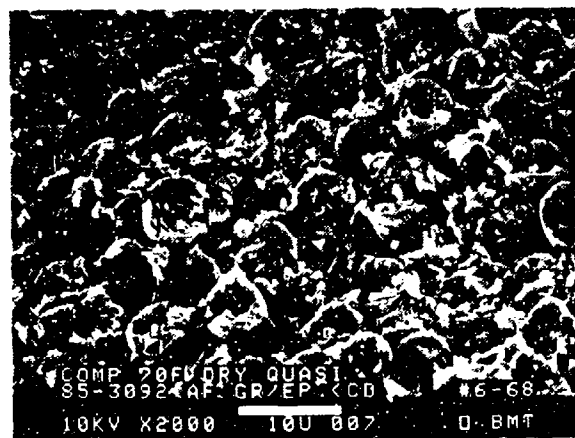
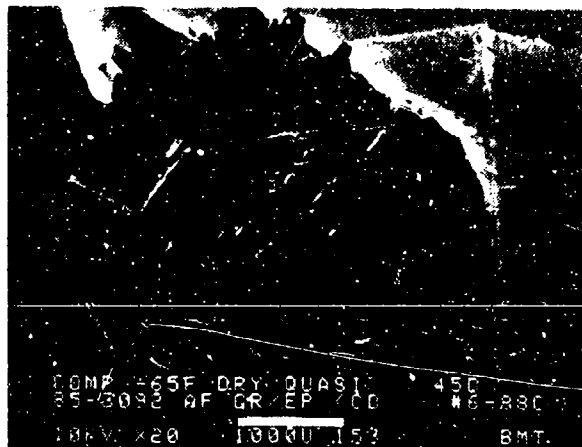
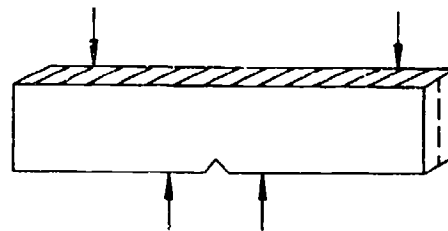


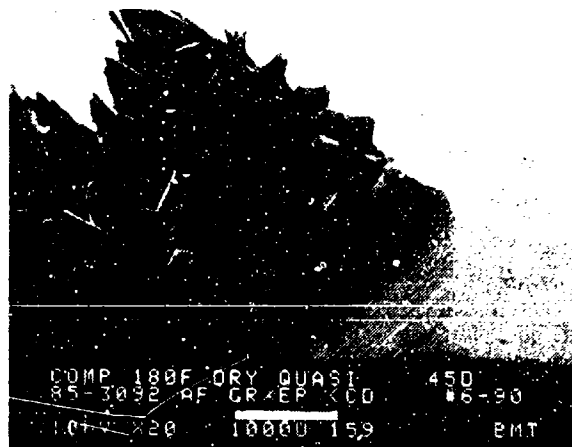
Figure 2-165. SEM Photographs of Translaminar Mode I Compression, 0/45/90 Fracture, 70 F/Dry

SEM photomicrographs

Fracture type	Translaminar mode I compression
Ply layup	[0, 45, 90] _{16S}
Test type	Four-point bend
• Test conditions	Dry
• Fiber end fracture	
Material	Hercules 3501-6/177°C cure AS4 fibers



-65°F, dry



180°F, dry

← Mechanically induced crack direction

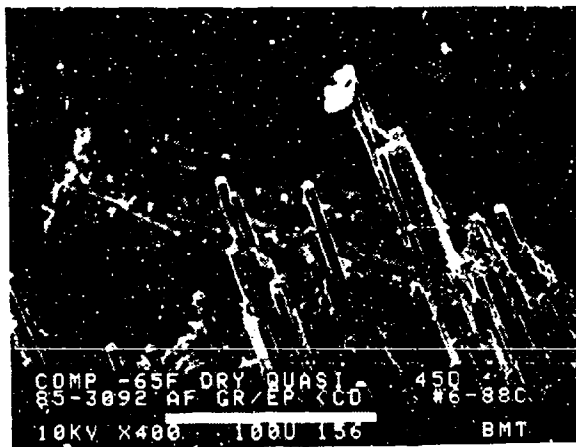
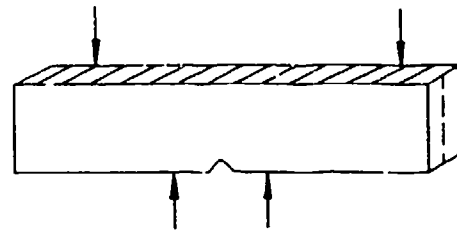


270°F, dry

Figure 2-166. SEM Photographs of Translaminar Mode I Compression, 0/45/90 Fracture, -65, 180, 270 F/Dry (20X)

SEM photomicrographs

Fracture type	Translaminar mode I compression
Ply layup	[0, 45, 90] _{16S}
Test type	Four-point bend
• Test conditions	Dry
• Fiber end fracture	
Material	Hercules 3501-6/177°C cure AS4 fibers



-65°F, dry



180°F, dry

Mechanically induced crack direction

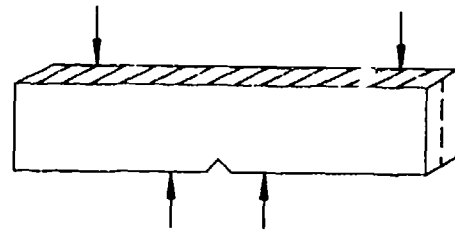


270°F, dry

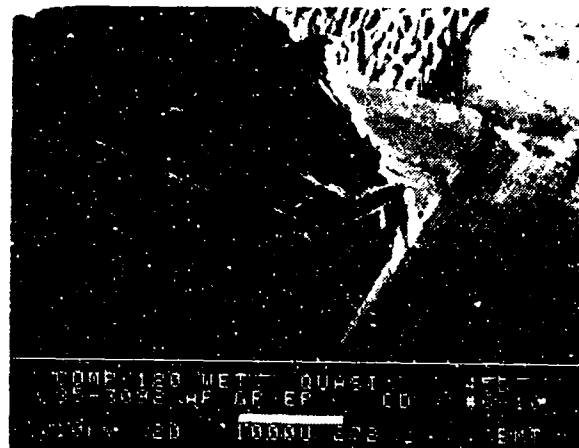
Figure 2-167. SEM Photographs of Translaminar Mode I Compression, 0/45/90 Fracture, -65, 180, 270 F/Dry (400X)

SEM photomicrographs

Fracture type	Translaminar mode I compression
Ply layup	[0, 45, 90] _{16S}
Test type	Four-point bend
• Test conditions	Wet
• Fiber end fracture	
Material	Hercules 3501-6/177°C cure AS4 fibers

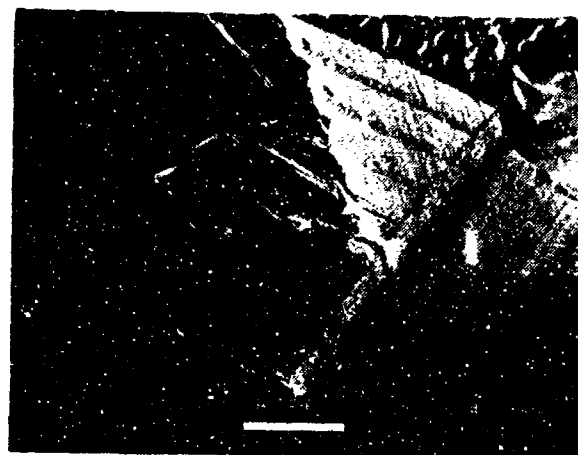


70°F, wet



180°F, wet

Mechanically Induced crack direction

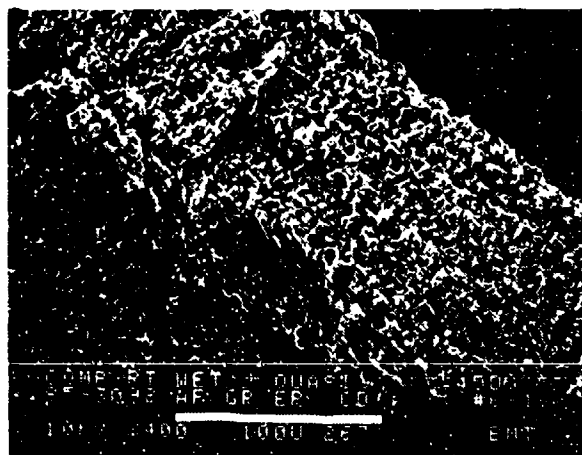
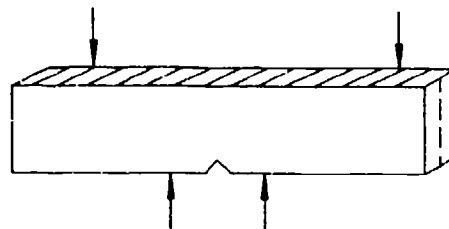


270°F, wet

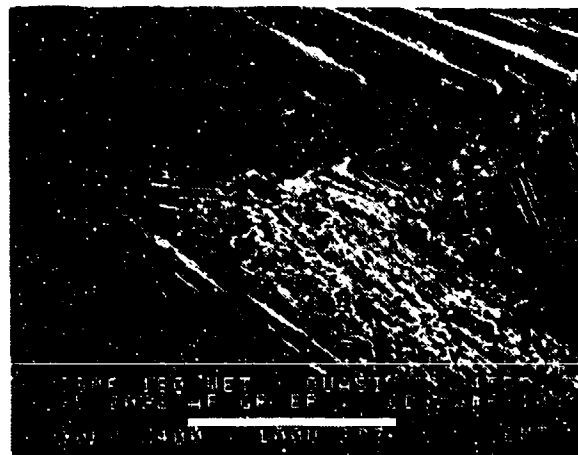
Figure 2-168. SEM Photographs of Translaminar Mode I Compression, 0/45/90 Fracture, 70, 180, 270 F/Wet (20X)

SEM photomicrographs

Fracture type	Translaminar mode I compression
Ply layup	[0, 45, 90] _{16S}
Test type	Four-point bend
• Test conditions	Wet
• Fiber end fracture	
Material	Hercules 3501-6/177°C cure AS4 fibers

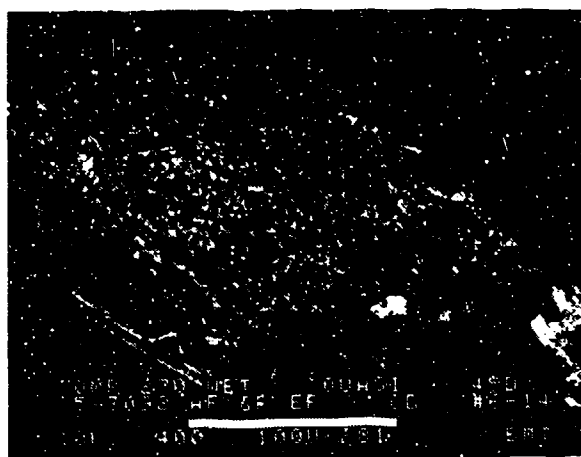


70°F, wet



180°F, wet

Mechanically induced crack direction



270°F, wet

Figure 2-169. SEM Photographs of Translaminar Mode I Compression, 0/45/90 Fracture, 70, 180, 270 F/Wet (400X)

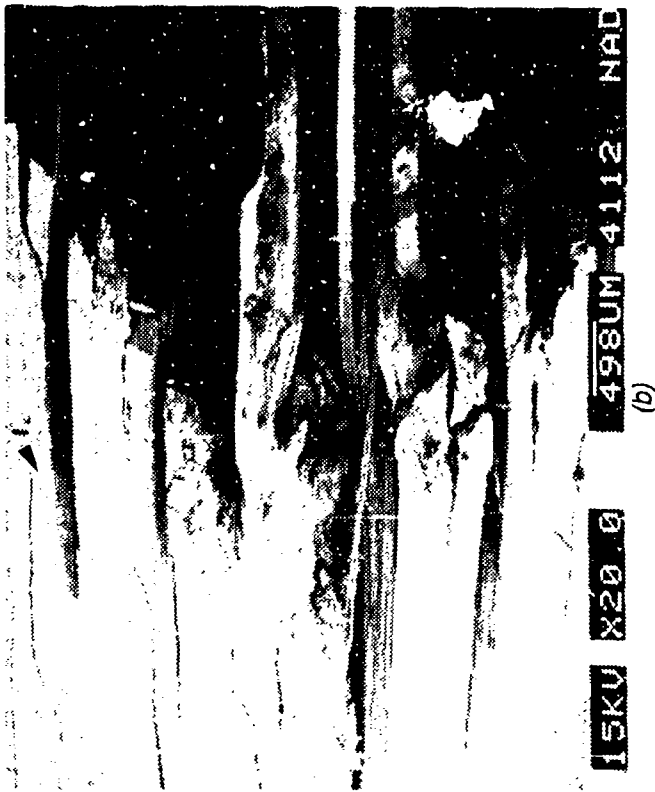


Figure 2-170. Optical and SEM Photographs of Translaminar Mode I Compression Fracture in Impact Damaged Gr/Ep - 32 Ply Quasi-Isotropic

(a) Macro photograph of Fractured Fragments

Note damage zone shown by arrows

(b), (c) Normal and Oblique Views of Fracture Near the Apex

1 = Impact damage

CD = Crack propagation direction



(d)



(e)

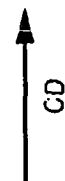


Figure 2-170. (Continued)
 (d) Microbuckling Features (Chop Marks) on Fractured Fiber Ends
 (e) Broken Fibers

CD = Crack-propagation direction



Figure 2-171. Optical and SEM Photographs of Translaminar Mode
I Compression Fracture in Gr/Ep - 32 Ply
Quasi-Isotropic, Water Immersed Before Test
(a) Macro photograph of Fractured Fragments
(b), (c) Normal and Oblique Views of Fracture Near
the Apex

CD = Crack-propagation direction



(d)



(e)

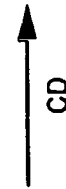
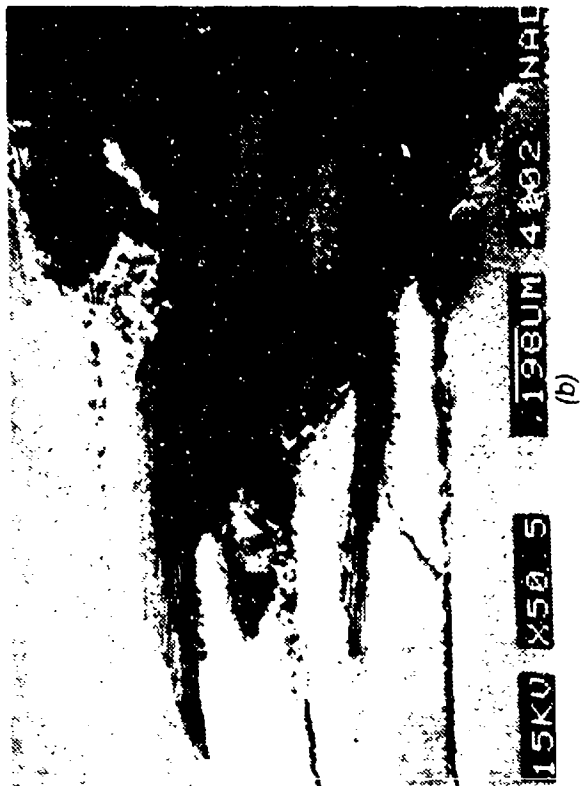


Figure 2-171. (Continued)
 (d) Microbuckling Features (Chop Marks) on Fractured Fiber Ends
 (e) Broken Fibers
 CD = Crack propagation direction



(a)

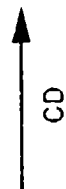


Figure 2-172. Optical and SEM Photographs of Translaminar Mode I Compression Fracture in Overcured Gr/Ep - 32 P/ly Quasi-Isotropic
(a) Macro photograph of fractured fragments
(b), (c) Normal and Oblique Views of Fracture Near the Apex

CD = Crack propagation direction



(e)



(d)

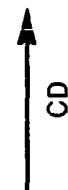
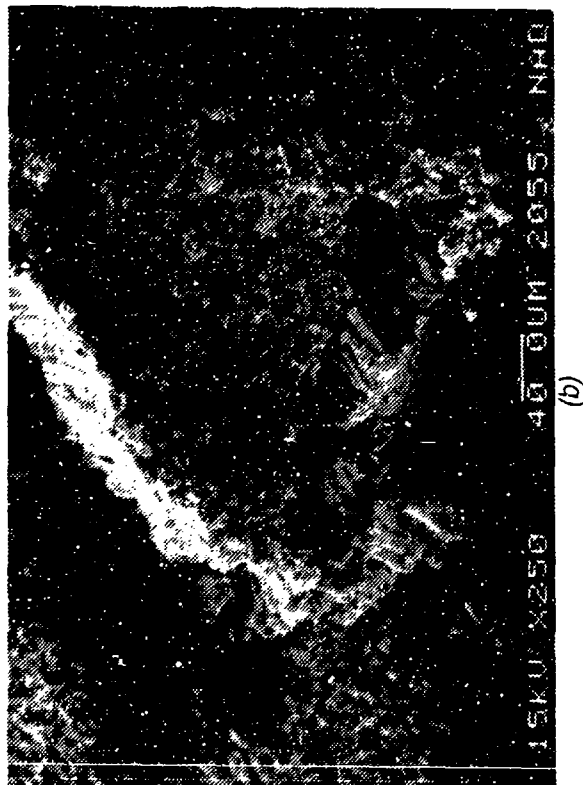


Figure 2-172. (Continued)
 (d) Microbuckling Features (Chop Marks) on Fractured Fiber Ends
 (e) Broken Fibers
 CD = Crack-propagation direction



(a)



(b)



(c)

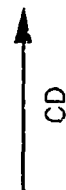


Figure 2-173. Optical and SEM Photographs of Translaminar Mode I Compression Fracture in High Resin Content Gr/Ep - 32 Ply Quasi-Isotropic

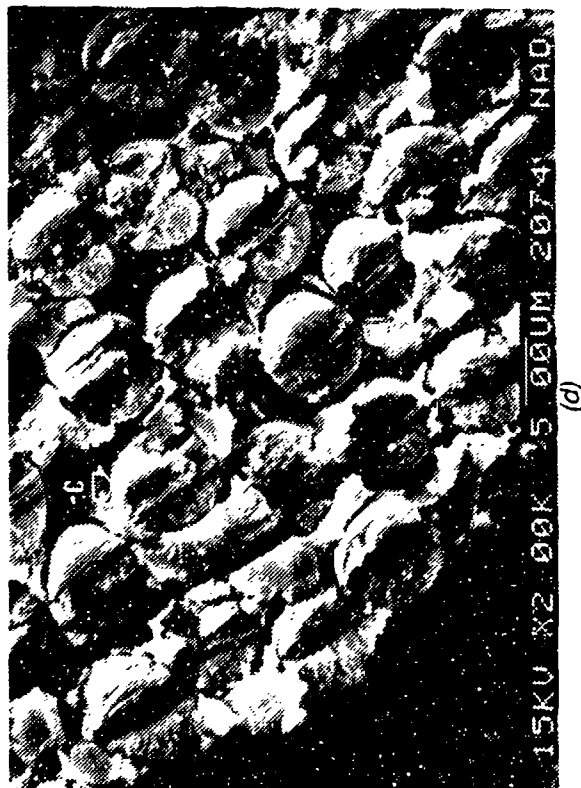
(a) Macro photograph of the Fracture and Apex

(b) Fracture Near the Apex

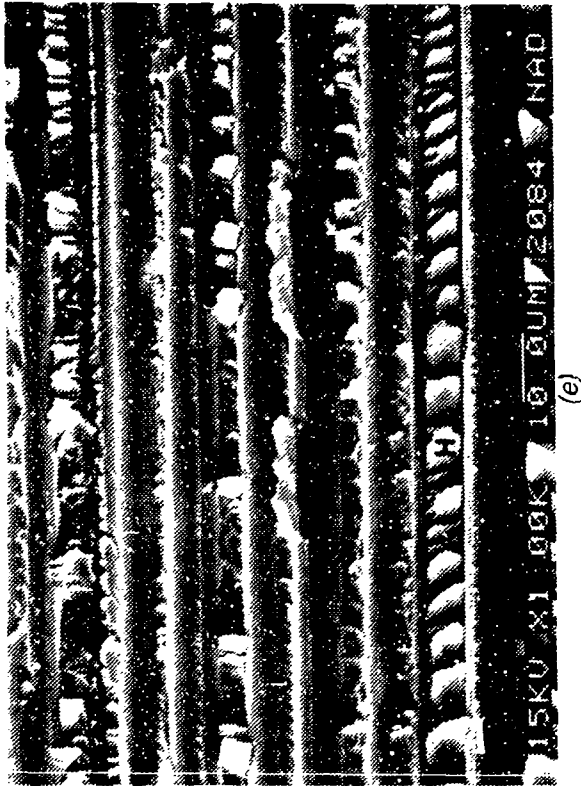
Note the flat fracture surface and the post fracture damage

(c) High Magnification of (b) Showing Crushed Fibers

CD = Crack propagation direction



(d)



(e)



(f)

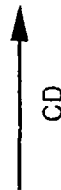


Figure 2-173. (Continued)
 (d) Flexural Fracture Features
 Note: Chop marks (C) on individual fiber ends are typical of flexural fractures in compression.
 (e) Hackles (H) and Scallops (S) in a 90 Degree Ply
 (f) Multiple Fiber Breaks Due to Microbuckling

CD = Crack propagation direction

2.7 TRANSLAMINAR SHEAR

The primary features observed in these specimens are very complex and generally a combination of features identified for the translaminar Mode I tension and compression fractures. The key features are as follows:

1. Fiber microbuckling and fiber slant fracture
2. Post-failure compression damage to fiber ends
3. Fiber pullout and extensive lateral displacement between the protruding fibers
4. Hackle features on the sides of the fibers.

As with compression dominated fractures, fractographic features by which the direction of fracture can be identified, do not exist. Figure 2-174 shows the side-notched rail shear test configuration and Table 2-7 provides the test matrix for the translaminar shear testing. Figures 2-175 through 2-184 are the corresponding fractographs.

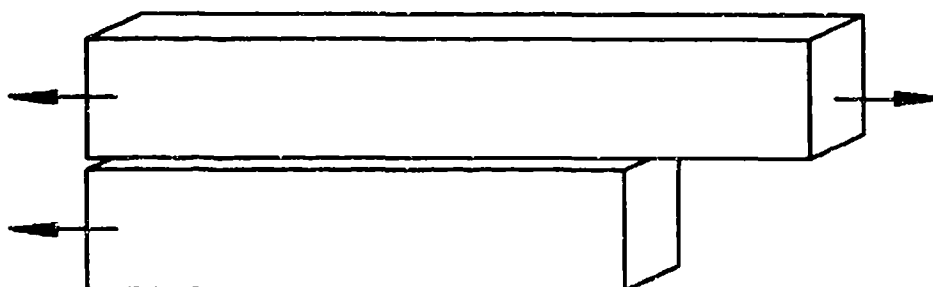


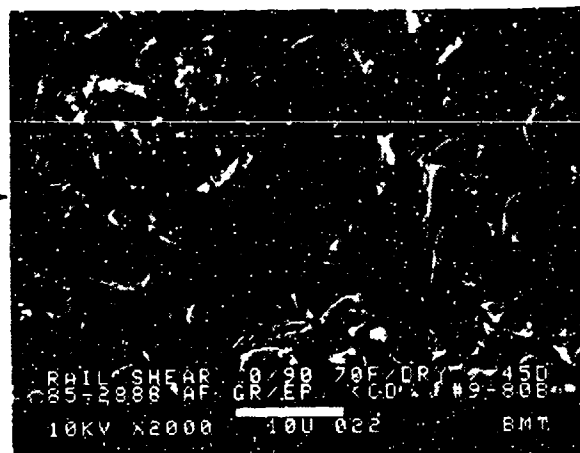
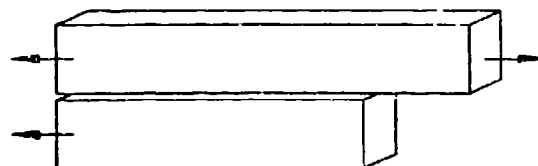
Figure 2-174. Side-Notched Rail Shear Type Test

Table 2-7. Test Matrix for Translaminar Shear Specimens

PLY/ORIENTATION	VARIABLE CONDITIONS	CONTRIBUTOR
32/0,90	RT/Dry (Baseline), -65°F/Dry, 180°F/Dry, 270°F/Dry, RT/Wet, 180°F/Wet, 270°F/Wet	Boeing
32/Quasi		

SEM photomicrographs

Fracture type	Translaminar mode II shear
Ply layup	[0, 90]16S
Test type	Side-notched rail shear
• Test conditions	21°C, dry
• Fiber end fracture	
Material	Hercules 3501-6/177°C cure AS4 fibers



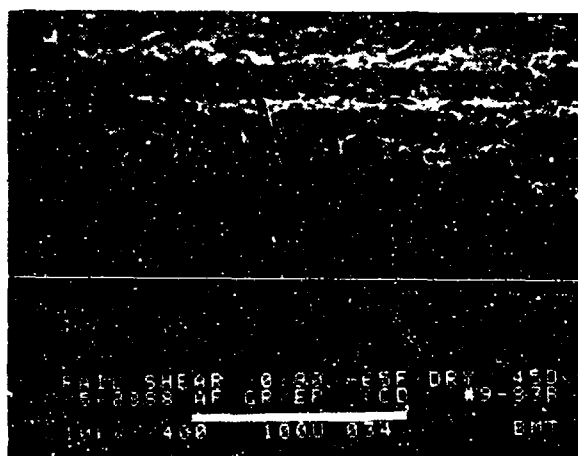
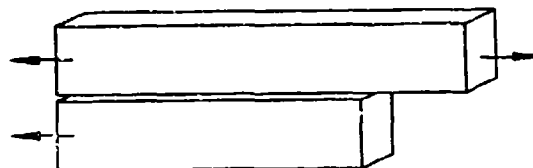
Mechanically induced crack direction



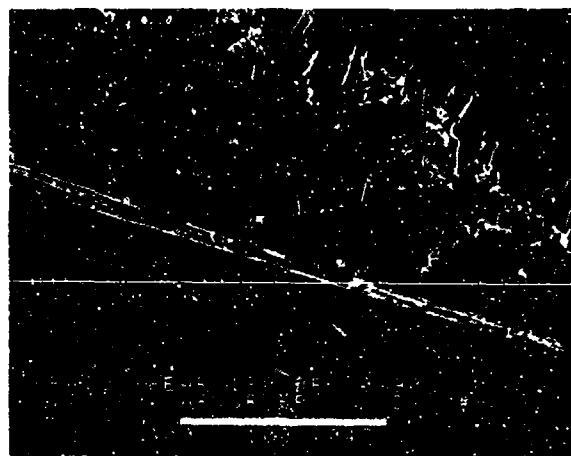
Figure 2-175. SEM Photographs of Translaminar Mode II Shear, 0/90 Fracture, 70 F/Dry

SEM photomicrographs

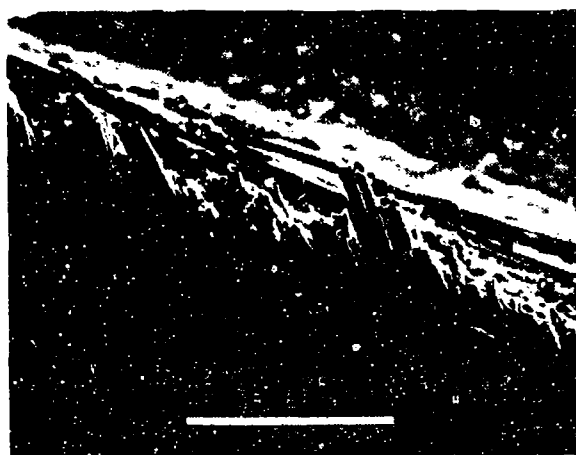
Fracture type	Translaminar mode II shear
Ply layup	[0, 90] _{16S}
Test type	Side-notched rail shear
• Test conditions	Dry
• Fiber end fracture	
Material	Hercules 3501-6/177°C cure AS4 fibers



-65°F, dry



180°F, dry

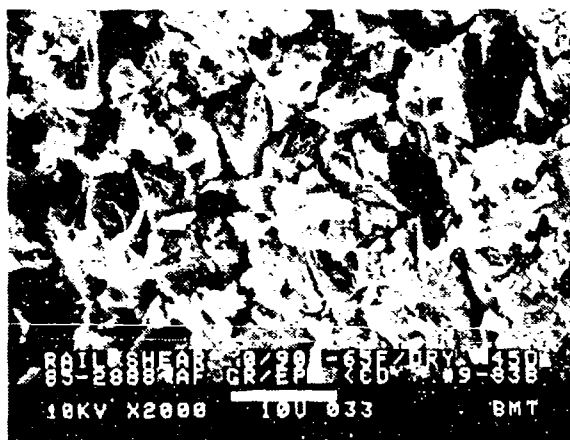
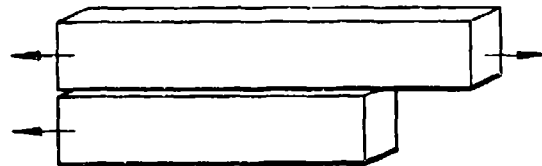


270°F, dry

Figure 2-176. SEM Photographs of Translaminar Mode II Shear, 0/90 Fracture, -65, 180, 270 F/Dry (400X)

SEM photomicrographs

Fracture type	Translaminar mode II shear
Ply layup	[0, 90] ₁₆ S
Test type	Side-notched rail shear
• Test conditions	Dry
• Fiber end fracture	
Material	Hercules 3501-6/177°C cure AS4 fibers



-65°F, dry



180°F, dry

Mechanically Induced crack direction

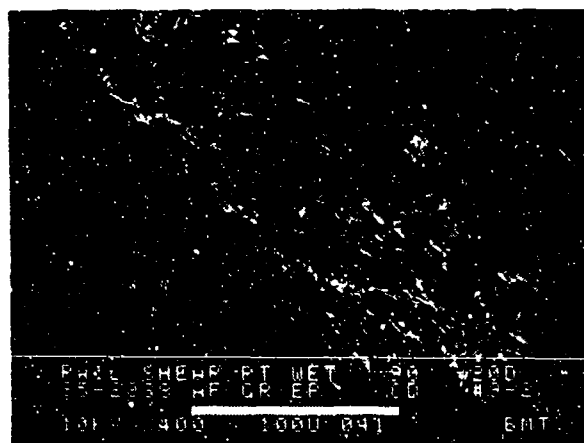
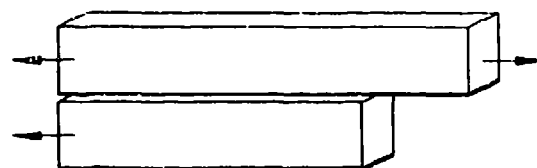


270°F, dry

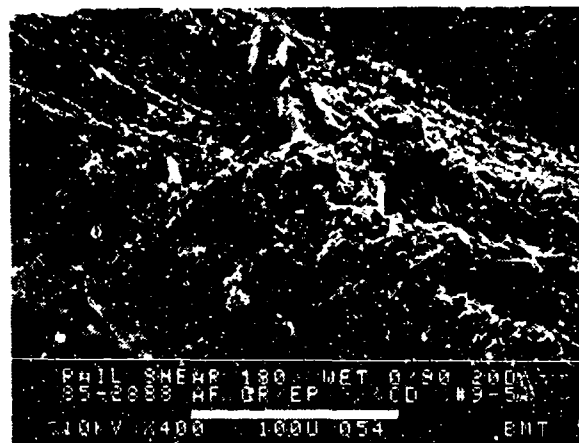
Figure 2-177. SEM Photographs of Translaminar Mode II Shear, 0/90 Fracture, -65, 180, 270 F/Dry (2000X)

SEM photomicrographs

Fracture type	Translaminar mode II shear
Ply layup	[0, 90] _{16S}
Test type	Side-notched rail shear
• Test conditions	Wet
• Fiber end fracture	
Material	Hercules 3501-6/177°C cure AS4 fibers

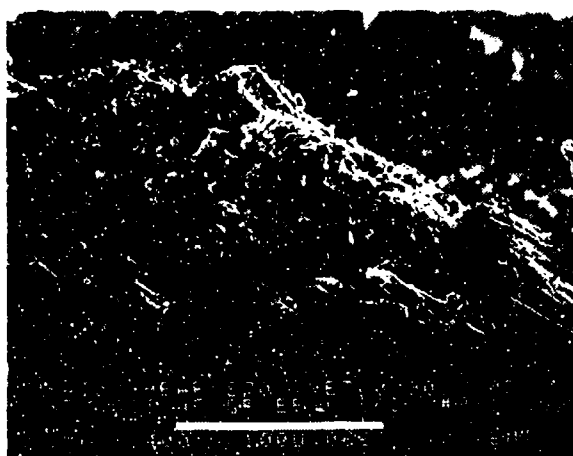


70°F, wet



180°F, wet

Mechanically induced crack direction

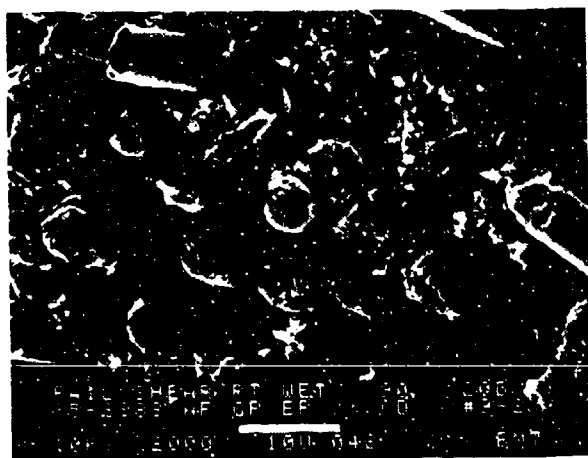
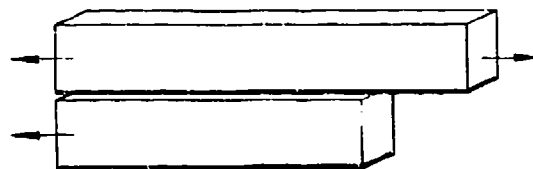


270°F, wet

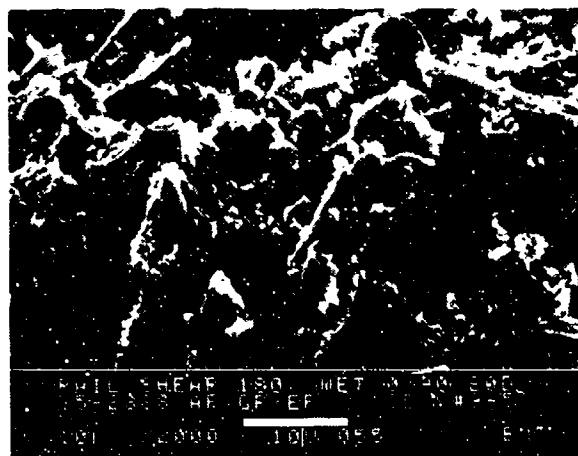
Figure 2-178. SEM Photographs of Translaminar Mode II Shear, 0/90 Fracture, 70, 180, 270 F/Wet (400X)

SEM photomicrographs

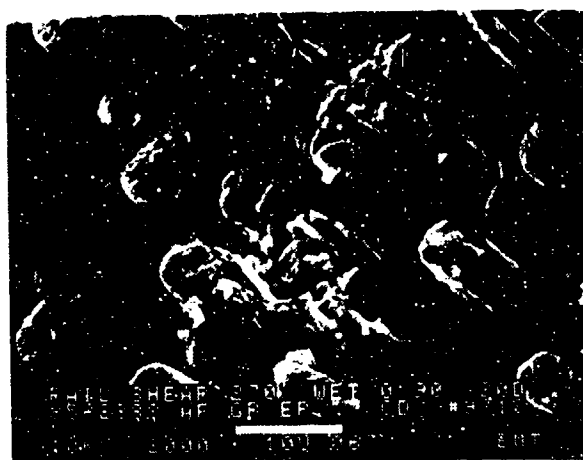
Fracture type	Translaminar mode II shear
Ply layup	[0, 90] _{16S}
Test type	Side-notched rail shear
• Test conditions	Wet
• Fiber end fracture	
Material	Hercules 3501-6/177°C cure AS4 fibers



70°F. wet



180°F. wet

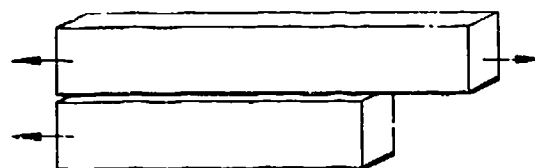


270°F. wet

Figure 2-179. SEM Photographs of Translaminar Mode II Shear, 0/90 Fracture, 70, 180, 270 F/Wet (2000X)

SEM photomicrographs

Fracture type	Translaminar mode II shear
Ply layup	[0, 45, 90] _{16S}
Test type	Side-notched rail shear
• Test conditions	21°C, dry
• Fiber end fracture	
Material	Hercules 3501-6/177°C cure AS4 fibers



Mechanically Induced crack direction



Mechanically Induced crack direction

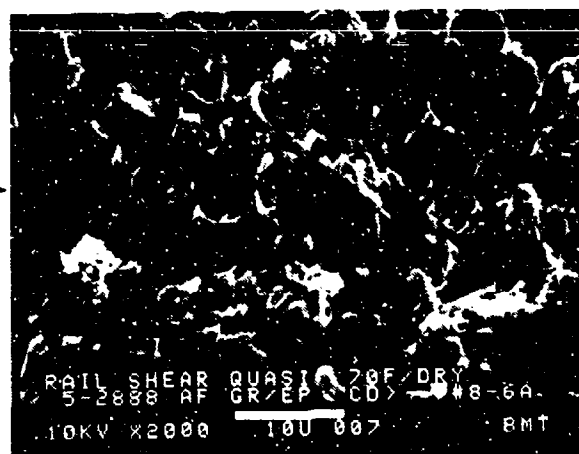
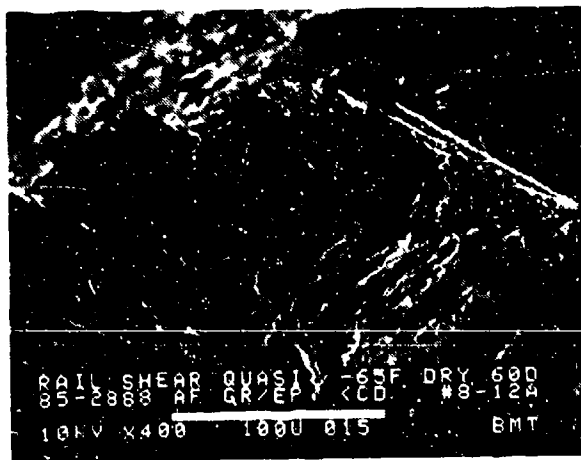
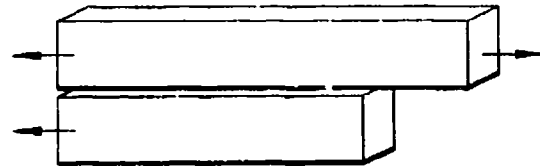


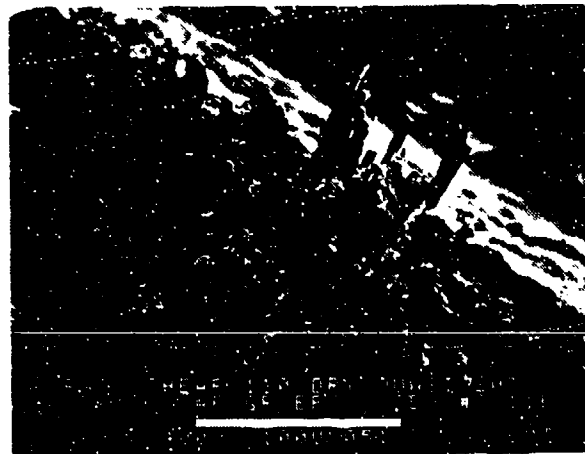
Figure 2-180. SEM Photographs of Translaminar Mode II Shear, 0/45/90 Fracture, 70 F/Dry

SEM photomicrographs

Fracture type	Translaminar mode II shear
Ply layup	[0,45, 90] _{16S}
Test type	Side-notched rail shear
• Test conditions	Dry
• Fiber end fracture	
Material	Hercules 3501-6/177°C cure AS4 fibers

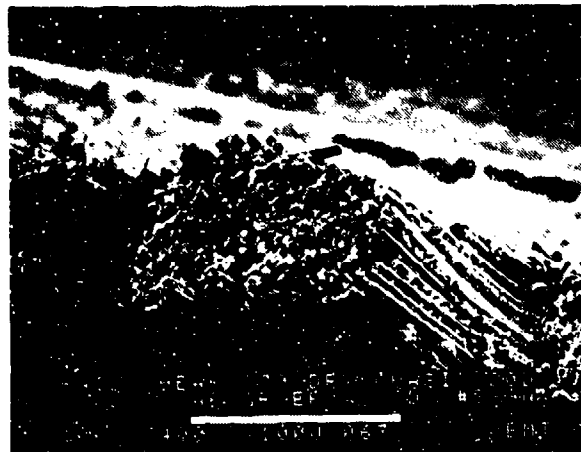


-65°F. dry



180°F. dry

Mechanically induced crack direction

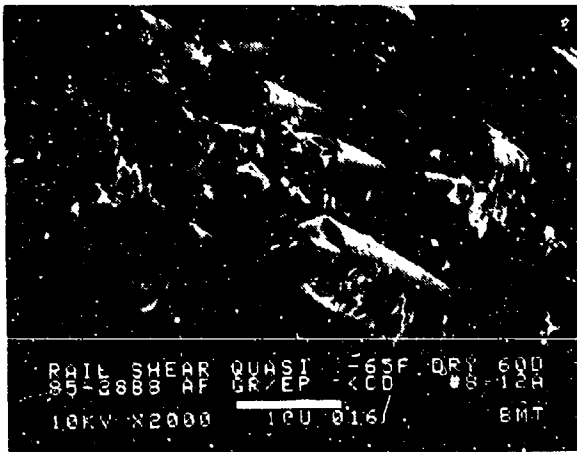
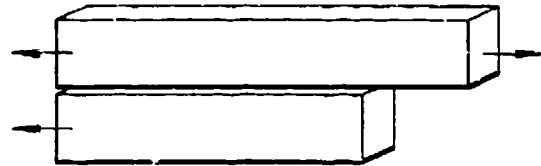


270°F. dry

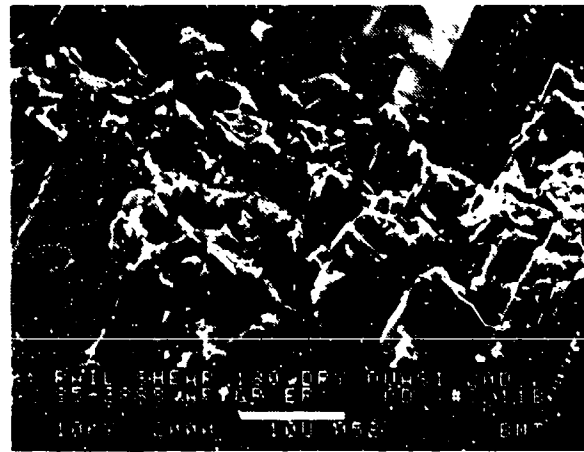
Figure 2-181. SEM Photographs of Translaminar Mode II Shear, 0/45/90 Fracture, -65, 180, 270 F/Dry (400X)

SEM photomicrographs

Fracture type	Translaminar mode II shear
Ply layup	[0, 45, 90] _{1,2,3} S
Test type	Side-notched rail shear
• Test conditions	Dry
• Fiber end fracture	
Material	Hercules 3501-6/177°C cure AS4 fibers

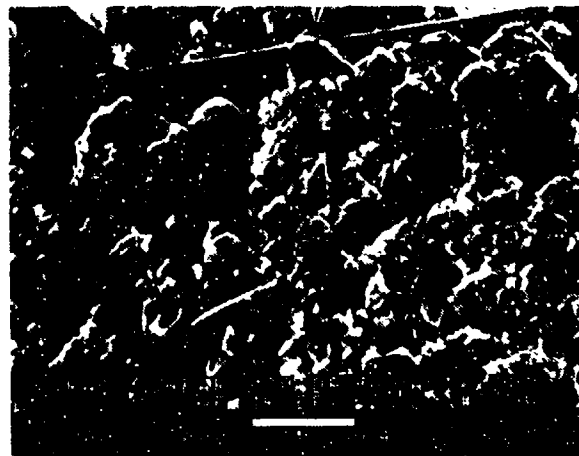


-65°F, dry



180°F, dry

Mechanically induced crack direction

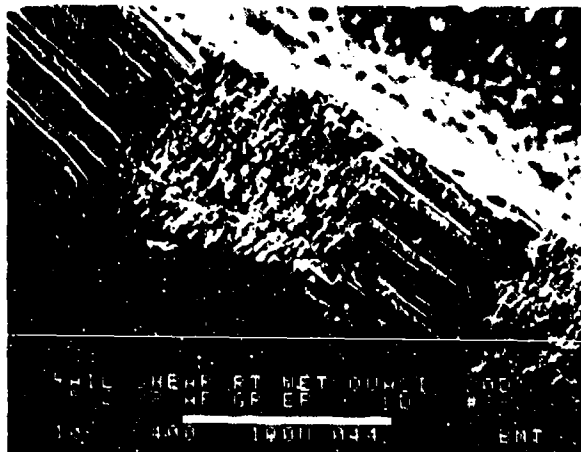
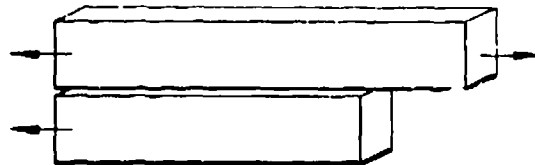


270°F, dry

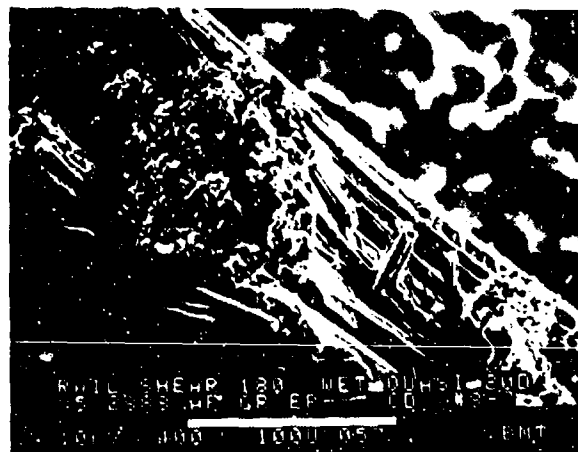
Figure 2-182. SEM Photographs of Translaminar Mode II Shear, 0/45/90 Fracture, -65, 180, 270 F/Dry (2000X)

SEM photomicrographs

Fracture type	Translaminar mode II shear
Ply layup	[0, 45, 90] 16S
Test type	Side-notched rail shear
• Test conditions	Wet
• Fiber end fracture	
Material	Hercules 3501-6/177°C cure AS4 fibers

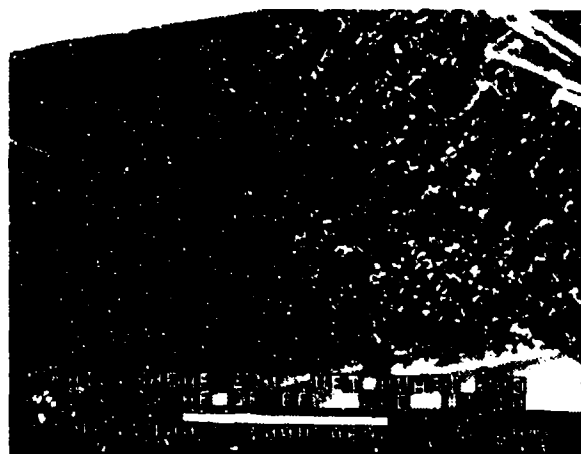


70°F, wet



180°F, wet

Mechanically induced crack direction

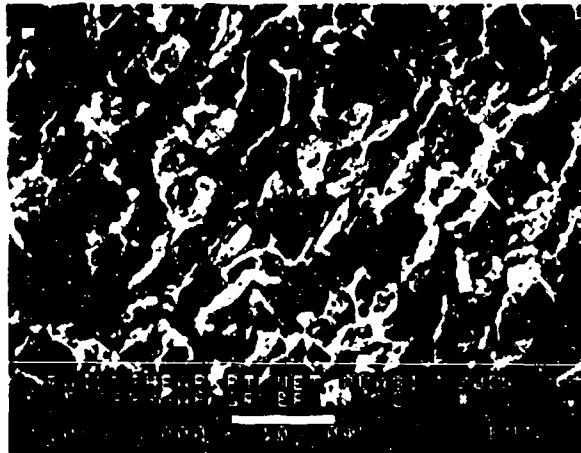
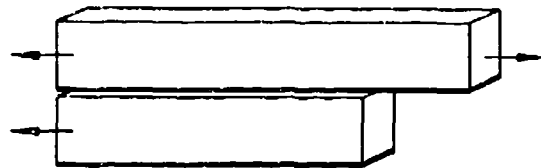


270°F, wet

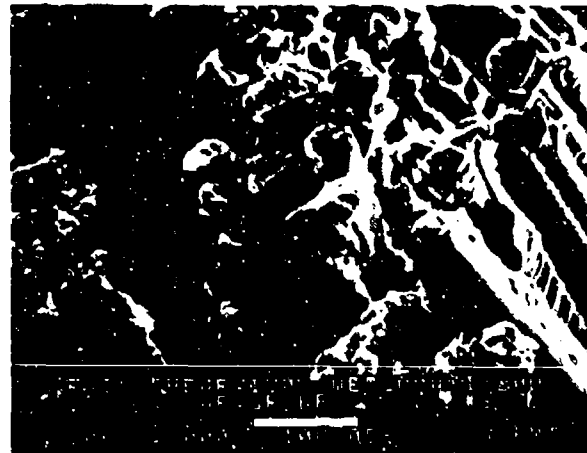
Figure 2-183. SEM Photographs of Translaminar Mode II Shear, 0/45/90 Fracture, 70, 180, 270 F/Wet (400X)

SEM photomicrographs

Fracture type	Translaminar mode II shear
Ply layup	[0, 45, 90] _{16S}
Test type	Side-notched rail shear
• Test conditions	Wet
• Fiber end fracture	
Material	Hercules 3501-6/177°C cure AS4 fibers

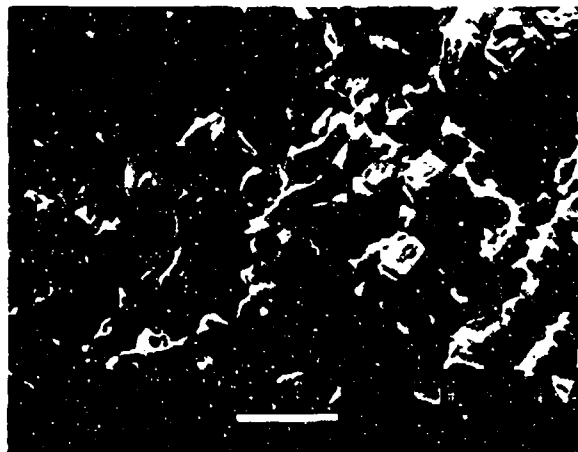


70°F, wet



180°F, wet

→ Mechanically induced crack direction



270°F, wet

Figure 2-184. SEM Photographs of Translaminar Mode II Shear, 0/45/90 Fracture, 70, 180, 270 F/Wet (2000X)

2.8 TRANSLAMINAR FLEXURE

The primary features observed in unnotched specimens which fail because of flexural loading are as follows:

1. Macroscopic identification of rough (tensile) and smooth (compressive) fracture regions
2. Distinct separation between tension and compression regions (as indicated by a neutral axis region)
3. Tensile fractures tend to initiate along the outer surface and progress toward the neutral line (as indicated by analysis of fiber end radials).

Figure 2-185 shows the laminate flexure test type and Figure 2-186 provides the corresponding fractographs. This contribution was made by Boeing.

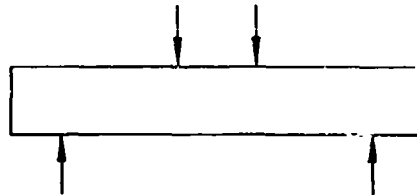
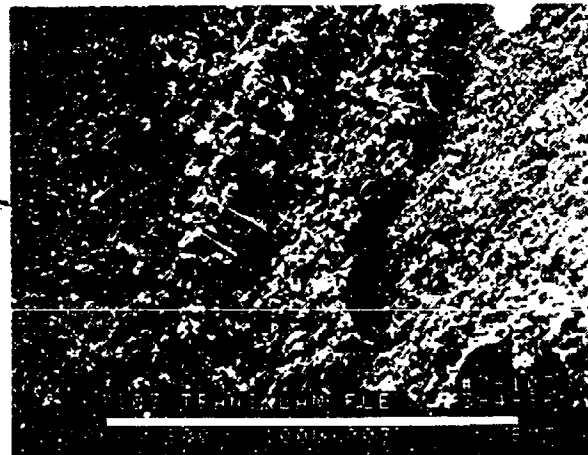


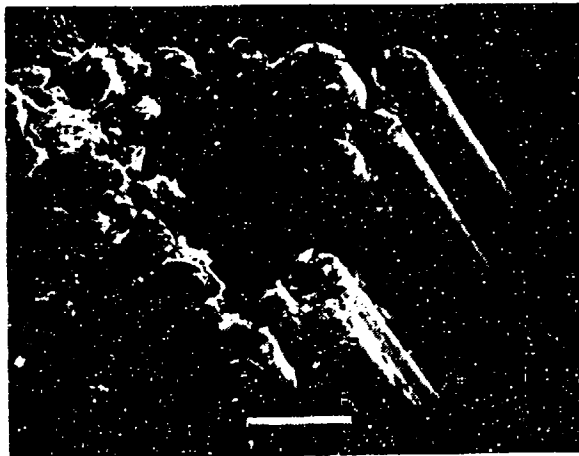
Figure 2-185. Laminate Flexure Type Test

SEM photomicrographs

Fracture type	Translaminar flexure
Ply layup	[0] ₃₂
Test type	Laminate flexure
• Test conditions	20°C, dry
• Fiber end fracture	
Material	Hercules 3501-6/177°C cure AS4 fibers



Compression Fracture Region



Tensile Fracture Region

Overall growth direction →

Mechanically induced crack direction



Figure 2-186. SEM Photographs of Translaminar Flexure, 0/0 Fracture, 70 F/Dry

2.9 FATIGUE

The primary features observed in DCB Mode I tension fatigue fractures are:

1. Striations
2. River marks and resin microflow features identical to static fractures.

DCB striations are parallel sets of curved lines located in the resin fracture regions between fibers and orientated toward the direction of crack-growth.

The primary features observed in CLS Mode II shear fatigue fractures are:

1. Striations
2. Hackle and scallop features identical to static fractures.

CLS striations are present mainly at the fiber-matrix separation region, with isolated locations exhibiting striations in the resin fracture planes. Currently, it is unclear whether these striations are being formed due to a plastic deformation mechanism at the crack tip (as seen in aluminum alloys) or whether these are simply crack arrest features. However, the striation spacing does not appear to increase as the test loads are increased. Spacing between striations often varies greatly along the length of a single fiber as well as between immediately adjacent fibers. This inconsistency prevents the investigator from accurately determining crack-growth rates or loads at fracture.

Figure 2-187 shows the test configuration of double cantilever beam (DCB) for Mode I fractures and cracked-lap shear (CLS) for Mode II fractures. Figures 188, 189 and 190 are Mode I DCB constant amplitude fatigue fractographs contributed by Boeing. Figures 191, 192 and 193 are Mode I DCB variable amplitude (Spectrum) fatigue fractographs contributed by Northrop. Figures 194 through 197 are Mode II CLS constant amplitude fatigue fractographs contributed by Boeing.

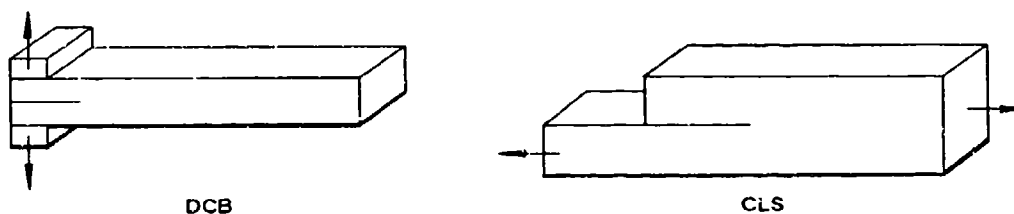
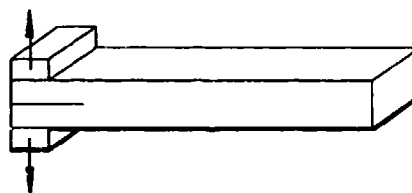


Figure 2-187. Double Cantilever Beam (DCB) for Mode I Fractures and Cracked-Lap Shear (CLS) for Mode II Fractures

Optical photomicrographs

Fracture type	Interlaminar fatigue mode I tension
Ply layup	[0] ₂₄
Test type	Fatigue DCB
• Test conditions	21°C, dry
• Fracture between	0/0 plies
Material	Hercules 3501-6/177°C cure AS4 fibers

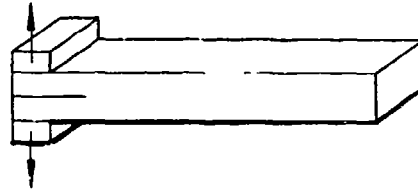


Mechanically Induced crack direction →

Figure 2-188. Optical Photographs of Interlaminar Fatigue Mode I Tension, 0/0 Fracture, 70 F/Dry

Optical photomicrographs

Fracture type	Interlaminar fatigue mode I tension
Ply layup	[0] ₂₄
Test type	Fatigue DCB
• Test conditions	21°C, dry
• Fracture between	0/0 plies
Material	Hercules 3501-6/177°C cure AS4 fibers



Mechanically induced crack direction



400X



1000X

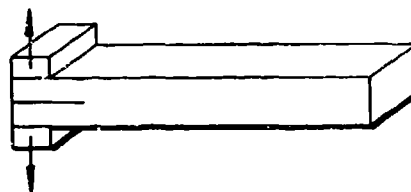
Static
growth

Cyclic
growth

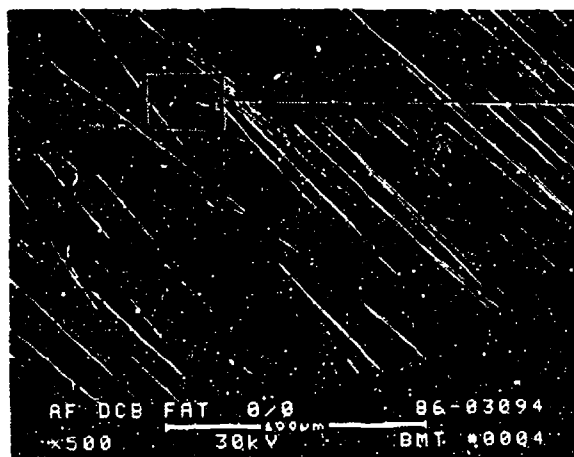
Figure 2-189. Optical Photographs of Interlaminar Fatigue Mode I Tension, 0/0 Fracture, 70 F/Ly (400X and 1000X)

SEM photomicrographs

Fracture type	Interlaminar fatigue mode I tension
Ply layup	[0]24
Test type	Fatigue DCB
• Test conditions	21°C, dry
• Fracture between	0/0 plies
Material	Hercules 3501-6/177°C cure AS4 fibers

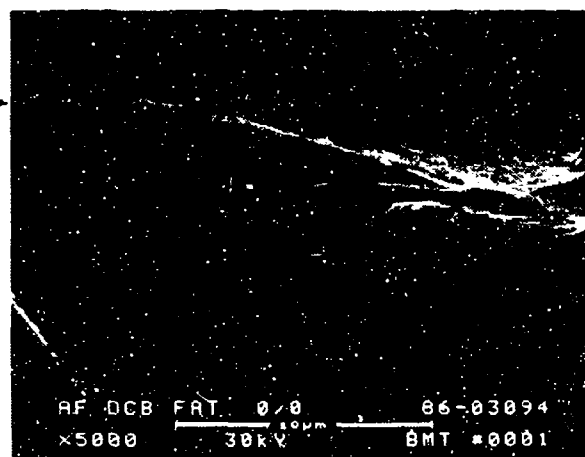


Mechanically Induced crack direction



75-deg tilt

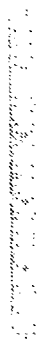
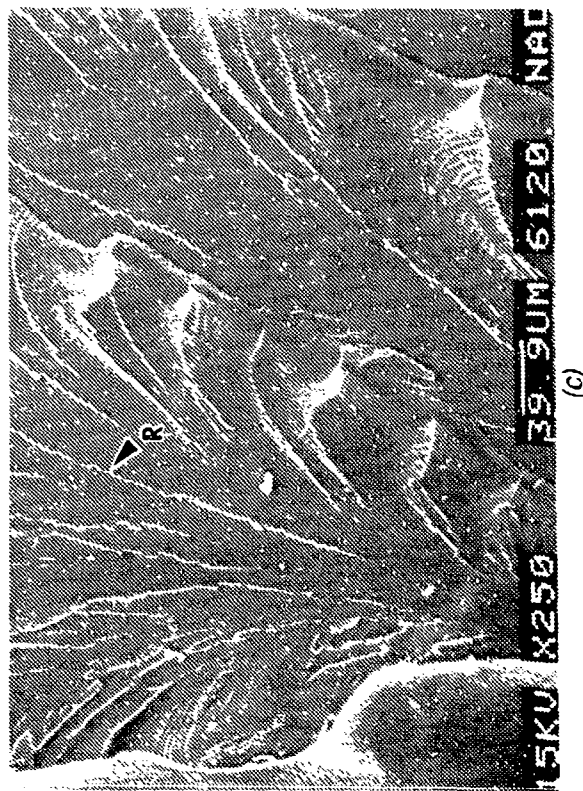
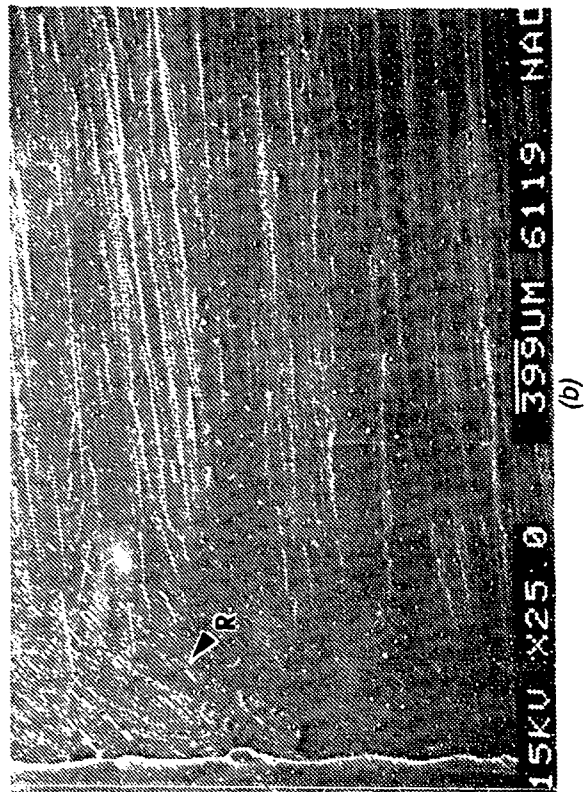
500X



75-deg tilt

5000X

Figure 2-190. SEM Photographs of Interlaminar Fatigue Mode I Tension, 0/0 Fracture, 70 F/Dry (500X and 5000X)



(a)

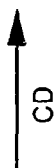


Figure 2-191. Optical and SEM Photographs of Interlaminar Mode I DCB Spectrum Fatigue Fracture in AS4/3501-6 Gr/Ep - [0]_{24T}
 (a) Macro photograph
 (b), (c) Initiation in Resin Rich Areas

CD = Crack-propagation direction
 R = River patterns



(d)

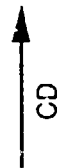
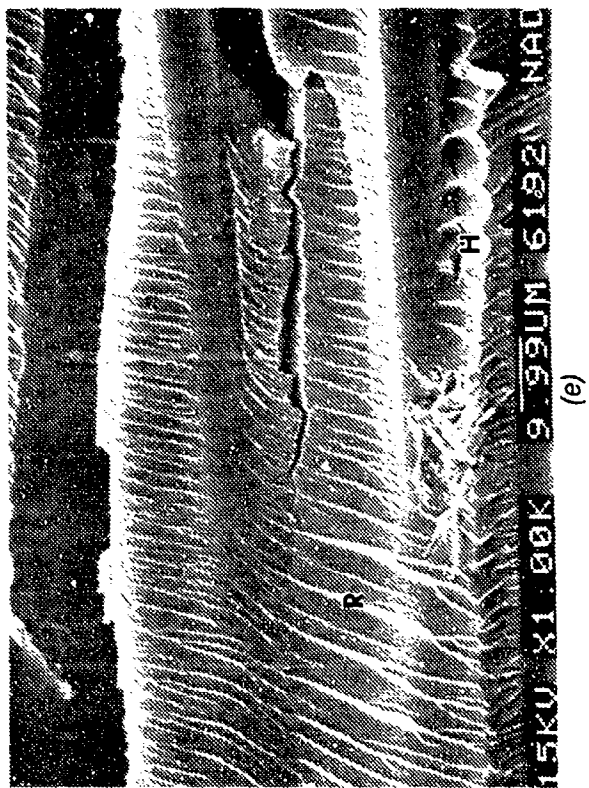
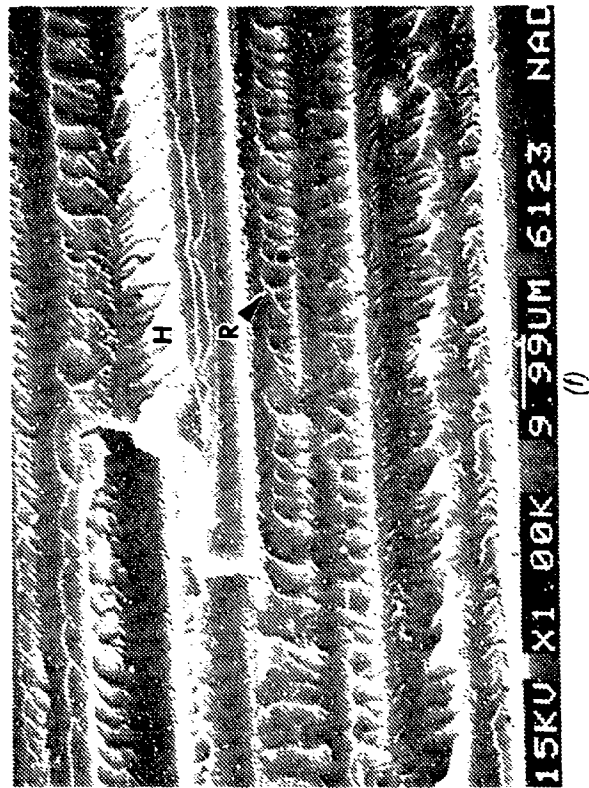


Figure 2-191. (Continued)
 (d) Low Magnification Photograph of Crack Growth
 Region
 Note regular arrangement of river patterns and occasional hackles
 (e), (f) Fracture Details

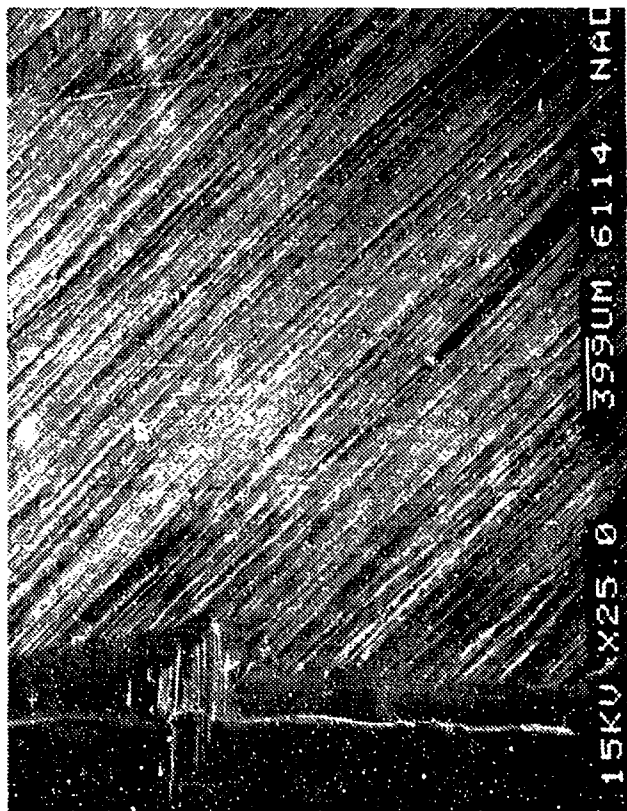
CD = Crack-propagation direction
 H = Hackles
 R = River patterns



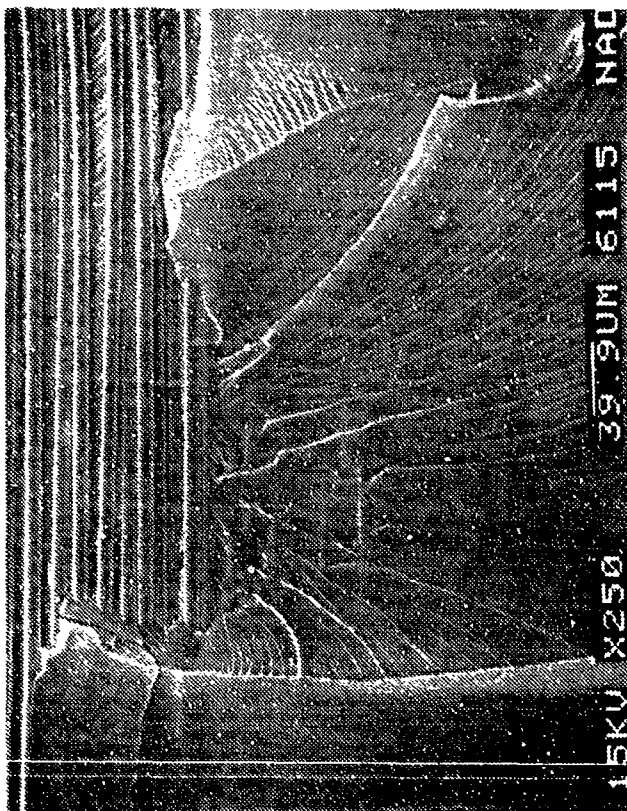
(e)



(f)



(a)



(b)

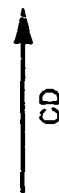


Figure 2-192. SEM Photographs of Interlaminar Mode I DCB Spectrum Fatigue Fracture in AS4/3501-6 Gr/Ep - [+45/0/-45]_{4s}
 (a) Macro photograph of Fracture
 (b) Initiation in Resin-Rich Area in Precrack Region

CD = Crack-propagation direction

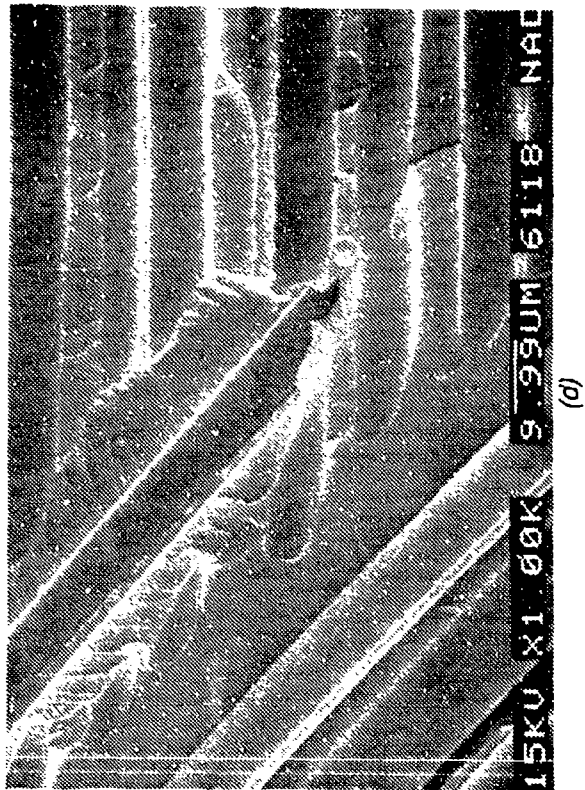
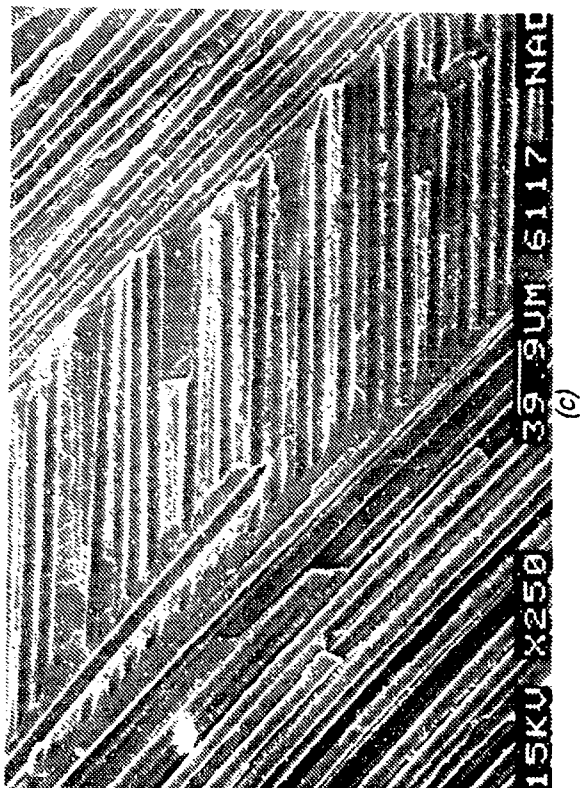
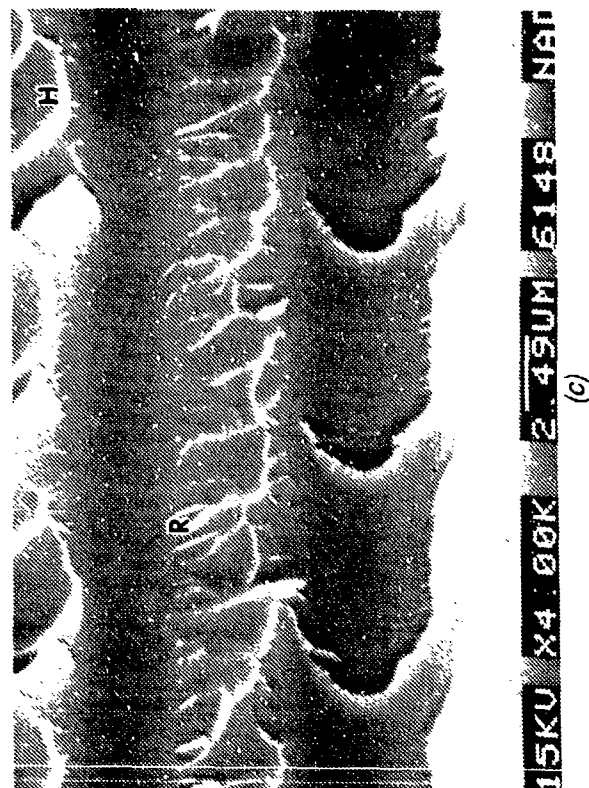
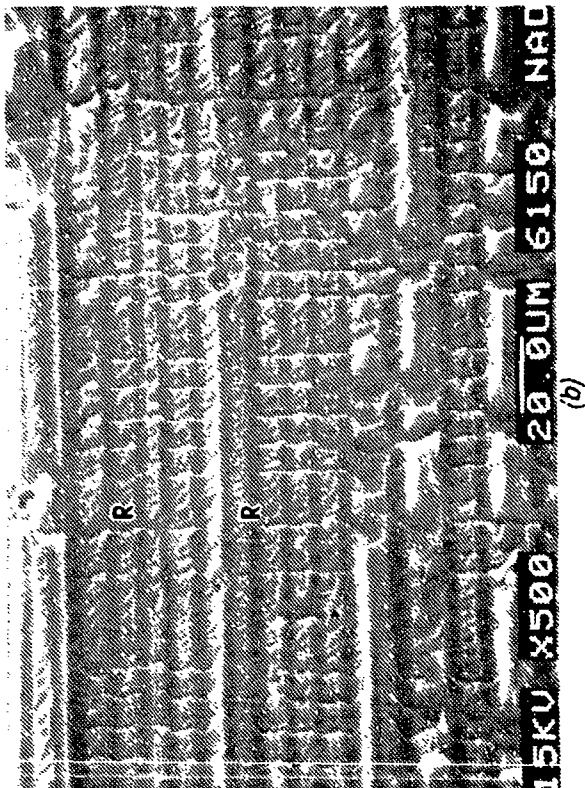
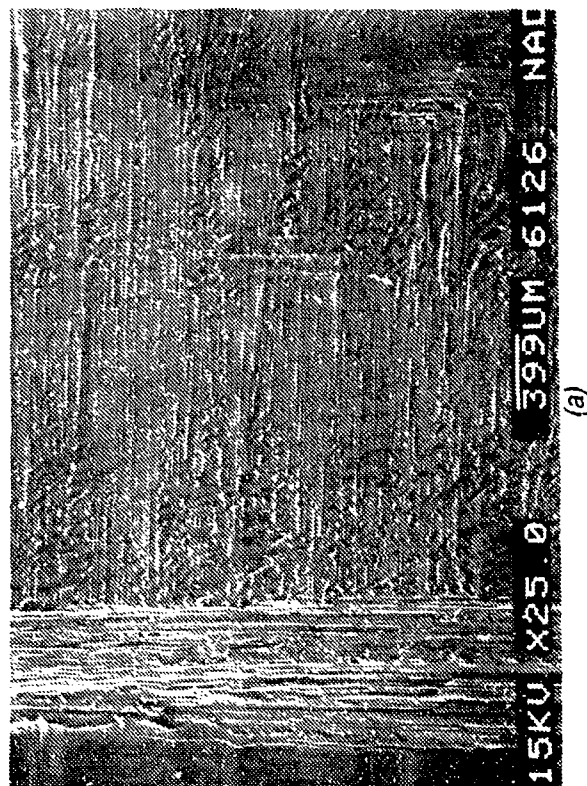


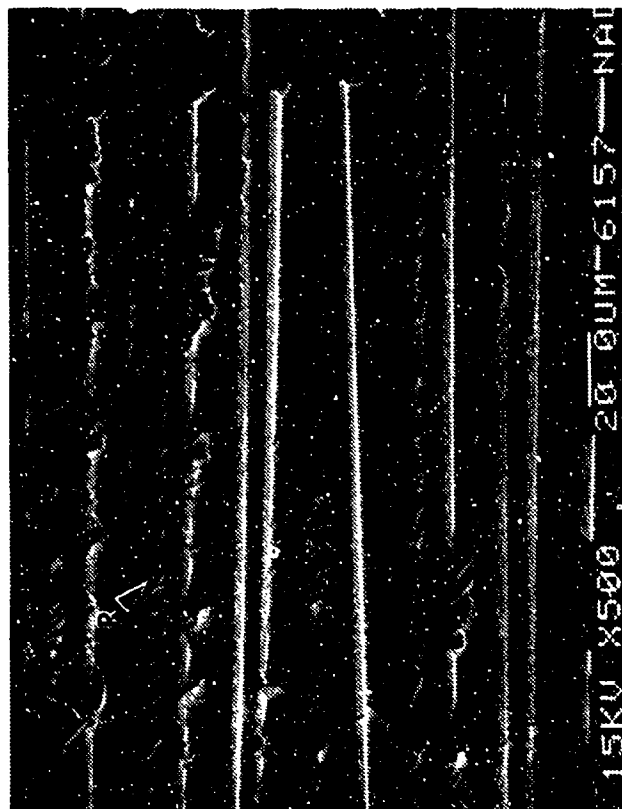
Figure 2-192. (Continued)
 (c), (d) Low and Intermediate Magnification
 Photographs Showing Fracture Traversing from
 45 Degree Ply to 0 Degree Ply and Back in
 Crack-Growth Region
 (e) High Magnification Photograph Showing Regular
 Array of Rivers (R) Oriented Toward CD
 CD = Crack-propagation direction



→
CD

Figure 2-193. SEM Photographs of Interlaminar Mode I DCB
Spectrum Fatigue Fracture in AS4/3501-6 Gr/Ep -
[0/90]_{6S}
(a) Macro photograph of Fracture
(b), (c) Fracture Details in Spectrum Fatigue Region
Close to 90 Degree Fibers

CD = Crack-propagation direction



(d)



(e)

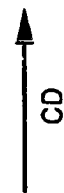
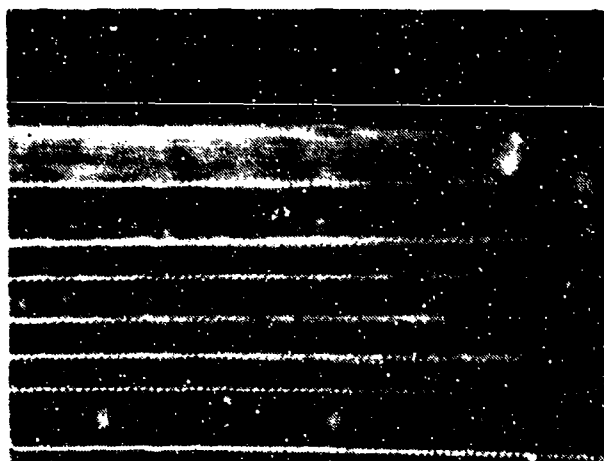
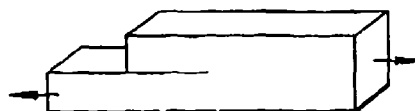


Figure 2-193. (Continued)
 (d), (e) Crack-Growth Region Close to 0 Degree Fibers
 CD = Crack propagation direction

Optical photomicrographs

Fracture type	Interlaminar fatigue mode II shear
Ply layup	[0] ₂₄
Test type	Fatigue CLS
• Test conditions	21°C, dry
• Fracture between	0/0 plies
Material	Hercules 3501-6/177°C cure AS4 fibers



Mechanically induced crack direction →

Figure 2-194. Optical Photograph of Interlaminar Fatigue Mode II Shear, 0/0 Fracture, 70 F/Dry

Optical photomicrographs

Fracture type	Interlaminar fatigue mode II shear
Ply layup	[0] 24
Test type	Fatigue C.I.S
• Test conditions	21°C, dry
• Fracture between	0/0 plies
Material	Hercules 3501-6/177°C cure AS4 fibers

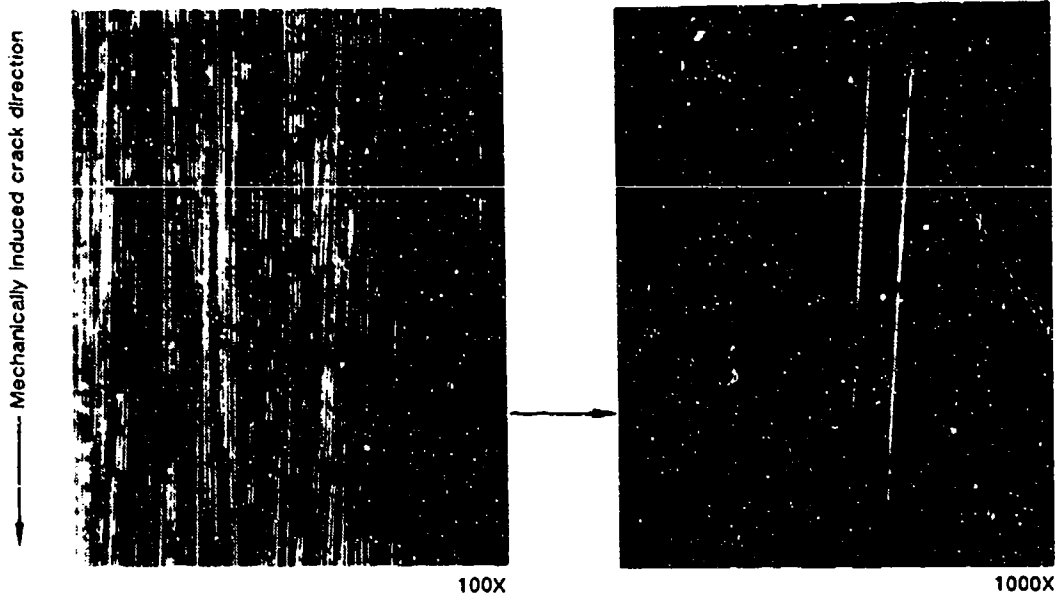
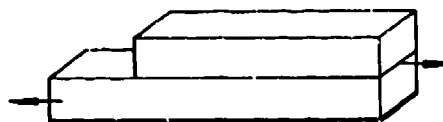
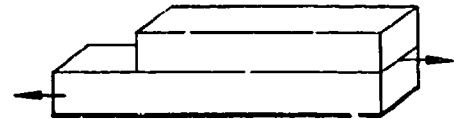


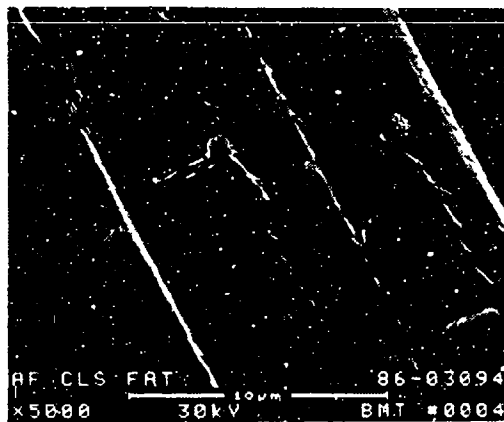
Figure 2-195. Optical Photographs of Interlaminar Fatigue Mode II Shear, 0/0 Fracture, 70 F/Dry (100X and 1000X)

SEM photomicrographs

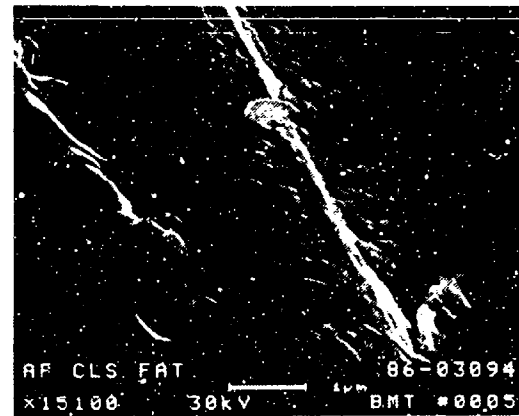
Fracture type	Interlaminar fatigue mode II shear
Ply layup	[0] 24
Test type	Fatigue CLS (80% to 20% G _{II} C)
• Test conditions	21°C, dry
• Fracture between	0/0 plies
Material	Hercules 3501-6/ 177°C cure AS4 fibers



Mechanically induced crack direction



5000X

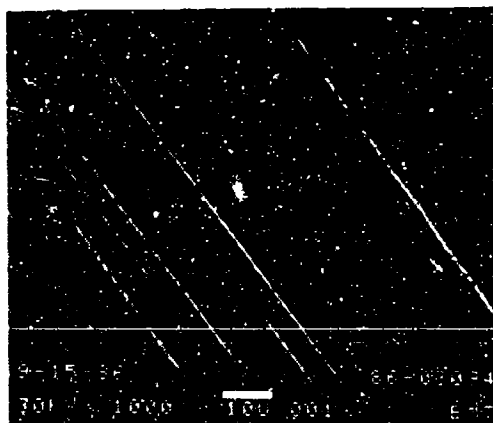


15000X

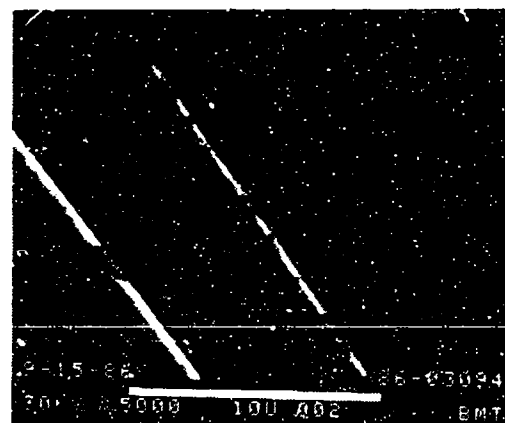
Figure 2-196. SEM Photographs of Interlaminar Fatigue Mode II Shear, 0/0 Fracture, 70 F/Dry (5000X and 15000X)

SEM photomicrographs

Fracture type	Interlaminar fatigue mode II shear
Ply layup	[0] 24
Test type	Fatigue CLS (80% to 40% GIIIC)
• Test conditions	21°C, dry
• Fracture between	0/0 plies
Material	Hercules 3501-6/177°C cure AS4 fibers

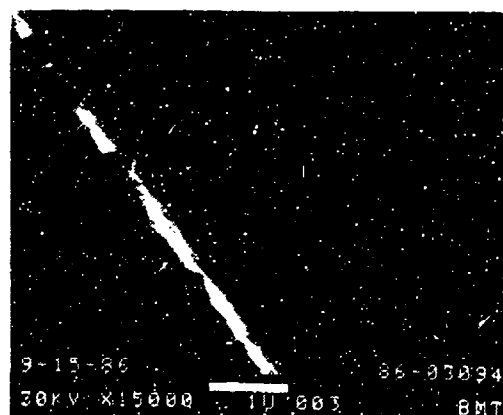


1000X



5000X

Mechanically induced crack direction



15000X

Figure 2-197. SEM Photographs of Interlaminar Fatigue Mode II Shear, 0/0 Fracture, 70 F/Dry (1000X, 5000X and 15000X)

2.10 CREEP

Room temperature (RT)/dry and elevated temperature (270°F)/dry creep specimens were tested by Boeing under interlaminar tension and shear. Tapered specimens of 0/90 laminates were tested in a Satec 25,000-lb capacity Universal test machine with the crosshead speed set at .001 in/min. Deflection was measured at the crosshead using a motion transducer.

2.10.1 Interlaminar Mode I Tension, RT/Dry

Visual observation revealed a smooth, glassy surface typical of an interlaminar Mode I tension fracture. There were visible crack arrest marks ("beach marks") running perpendicular to the mechanically induced crack direction (Figure 2-198). The spacing between these marks was quite consistent due to the constant loading rate throughout the creep test. Optical fractography focused on what appeared to be a striped fracture region. Due to the re-initiation of the crack, the location just after crack arrest appeared much rougher than the region just prior to it (Figure 2-199). The river marks were more readily observed in the region prior to the crack arrest.

SEM fractographs of the three regions of fracture were taken, including the location of the crack arrest (Figure 2-200). The fracture topography was smooth with distinct river marks just prior to the periodic crack arrest. After reinitiation of the crack, the fracture appeared uneven with very fine river marks (Figure 2-201).

2.10.2 Interlaminar Mode I Tension, 270°F/Dry

Visual observation revealed a smooth, glassy fracture surface similar to that of the RT specimen. Crack arrest marks were again observed (Figure 2-202). However, there were fragments of loose fibers on the fracture surface. These fibers may have separated from the resin matrix prematurely due to poor adhesion. The fracture topography at the region before and after the crack arrest was smooth (Figure 2-203), unlike that of the fracture created at RT. The SEM analysis confirmed the observations made during the optical analysis (Figure 2-204).

2.10.3 Interlaminar Mode II Shear, RT/Dry

Visually, the mating fracture surfaces looked somewhat different: one surface was smooth and glassy, while the other was rough and dull (Figure 2-205). Crack arrest marks were observed on the fracture surfaces at the ends of and at the center of the specimen. SEM fractographs revealed that the glassy surface consisted largely of scallops with some hackles (Figure 2-206), and the rough surface exhibited mainly hackles with some scallops (Figure 2-207).

2.10.4 Interlaminar Mode II Shear, 270°F/Dry

Visual examination revealed a fracture with a smooth and glassy surface on one of the mating sides and a rough and dull surface on the other side (Figure 2-208). This was similar to the

fracture surfaces created at room temperature. The glassy surface exhibited mostly scallops (with some hackles, Figure 2-209), and the rough surface consisted mostly of hackles (with some scallops, Figure 2-210). Optical and SEM analyses showed no significant features to distinguish the RT and 270°F creep specimens.

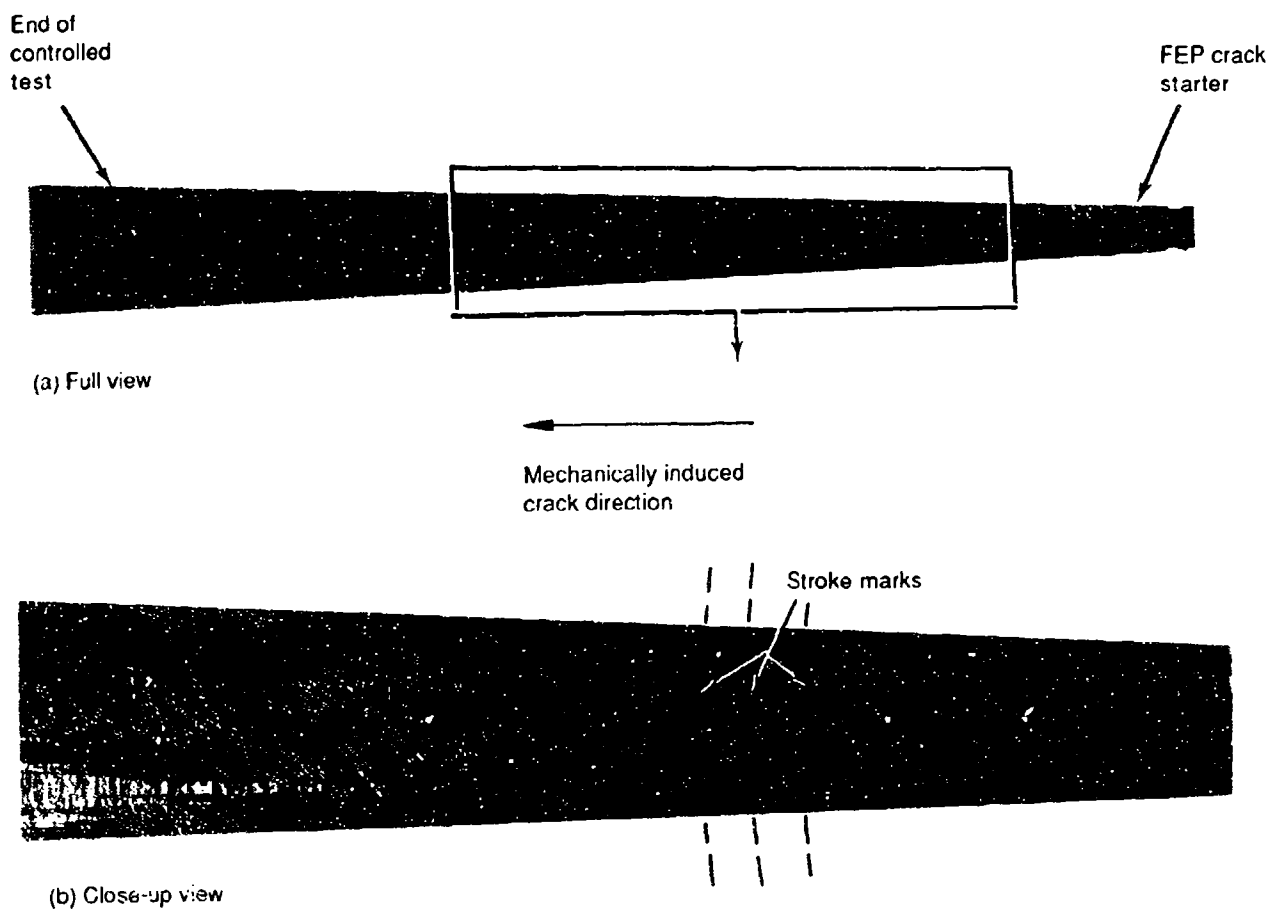


Figure 2-196. Macrophotographs of Interlaminar Mode I Tension, RT/Dry Creep, 0/90 Fracture

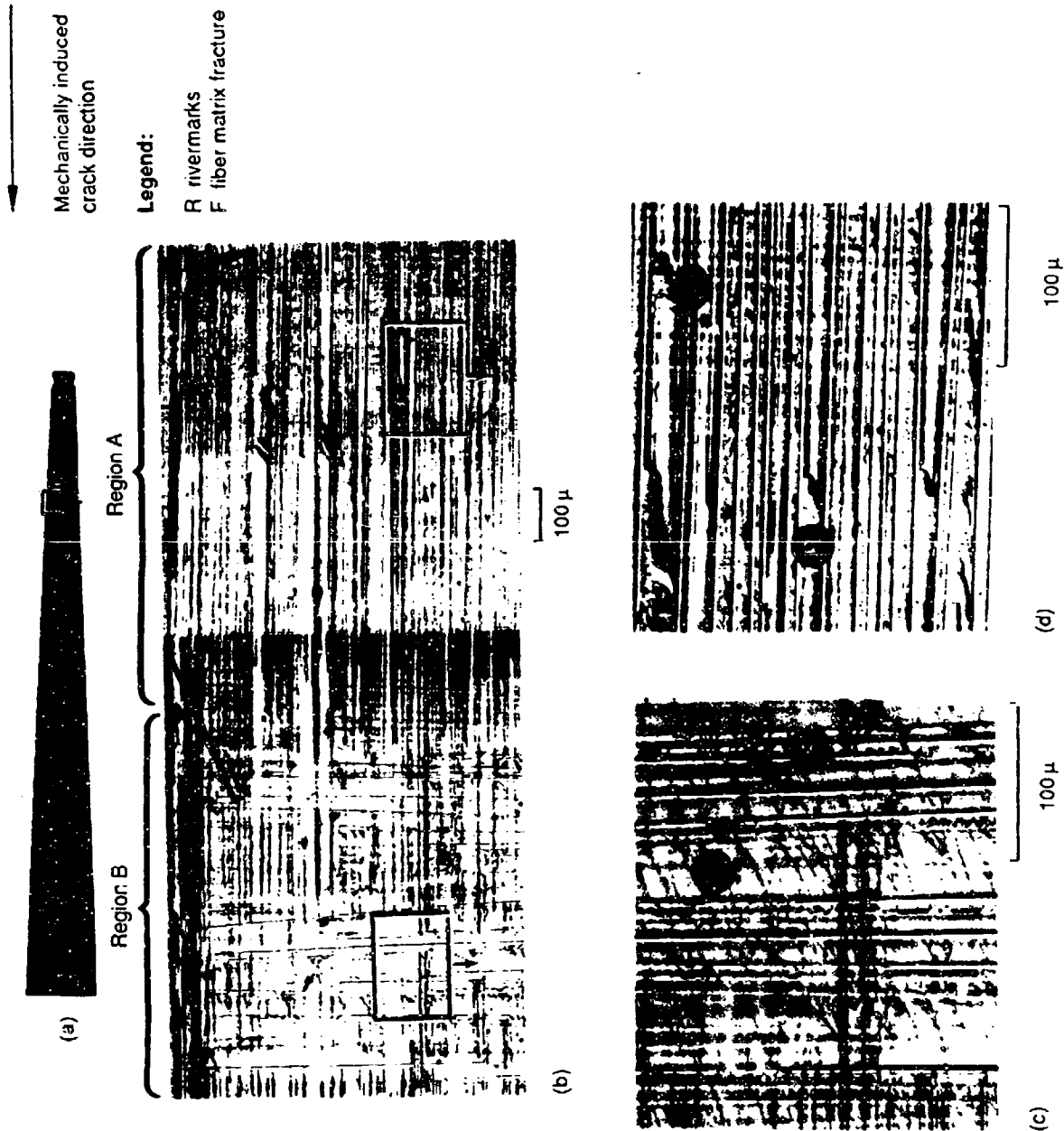


Figure 2-199. Optical Photomicrographs of Interlaminar Mode I Tension, RT/Dry Creep, 0/90 Fracture

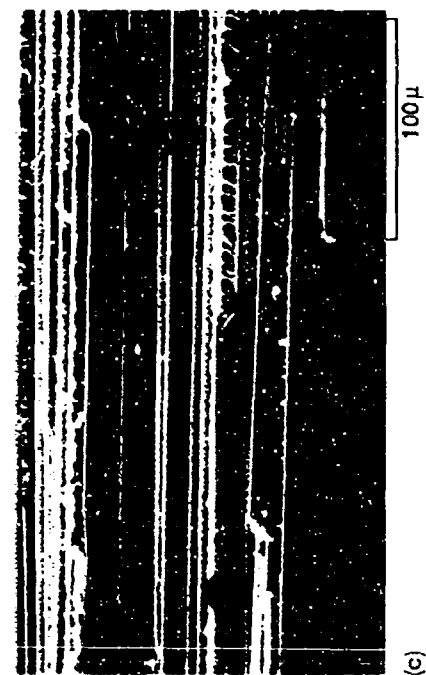
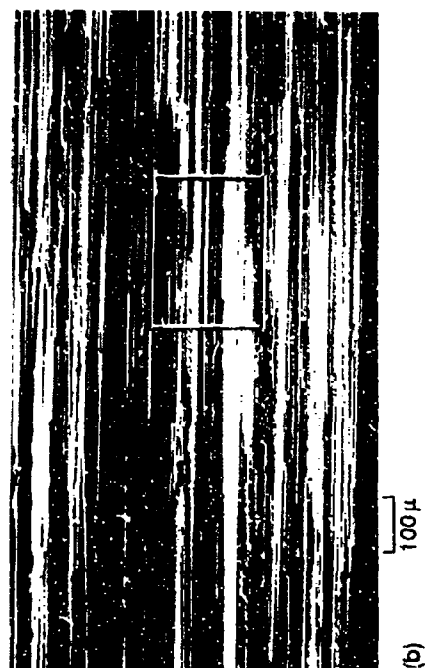
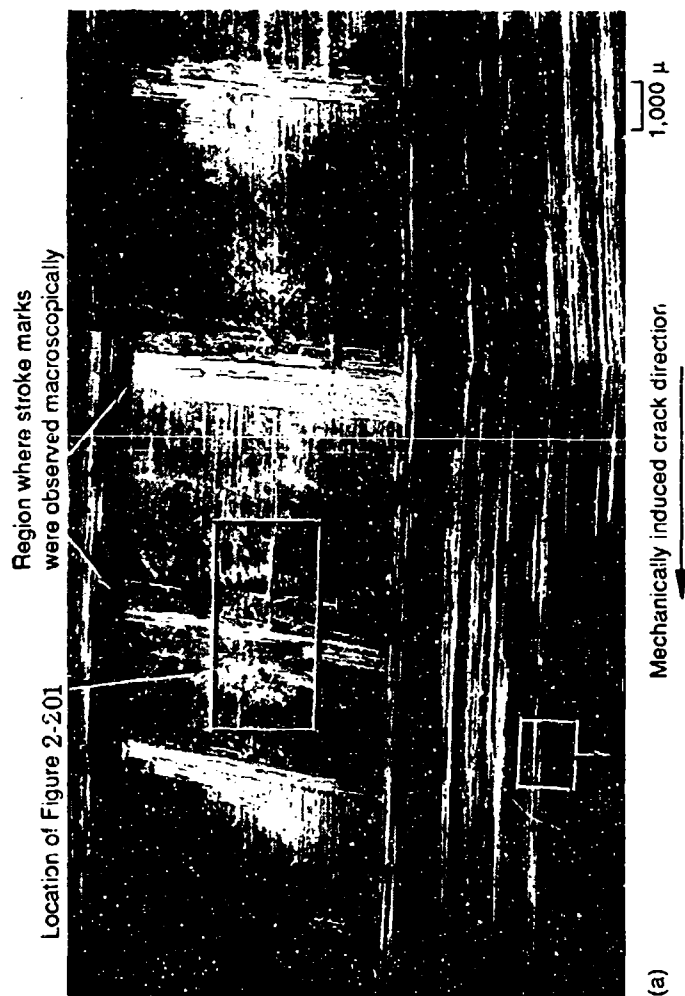


Figure 2-200. SEM Fractographs of Interlaminar Mode I Tension, RT/Dry Creep, 0.90 Fracture

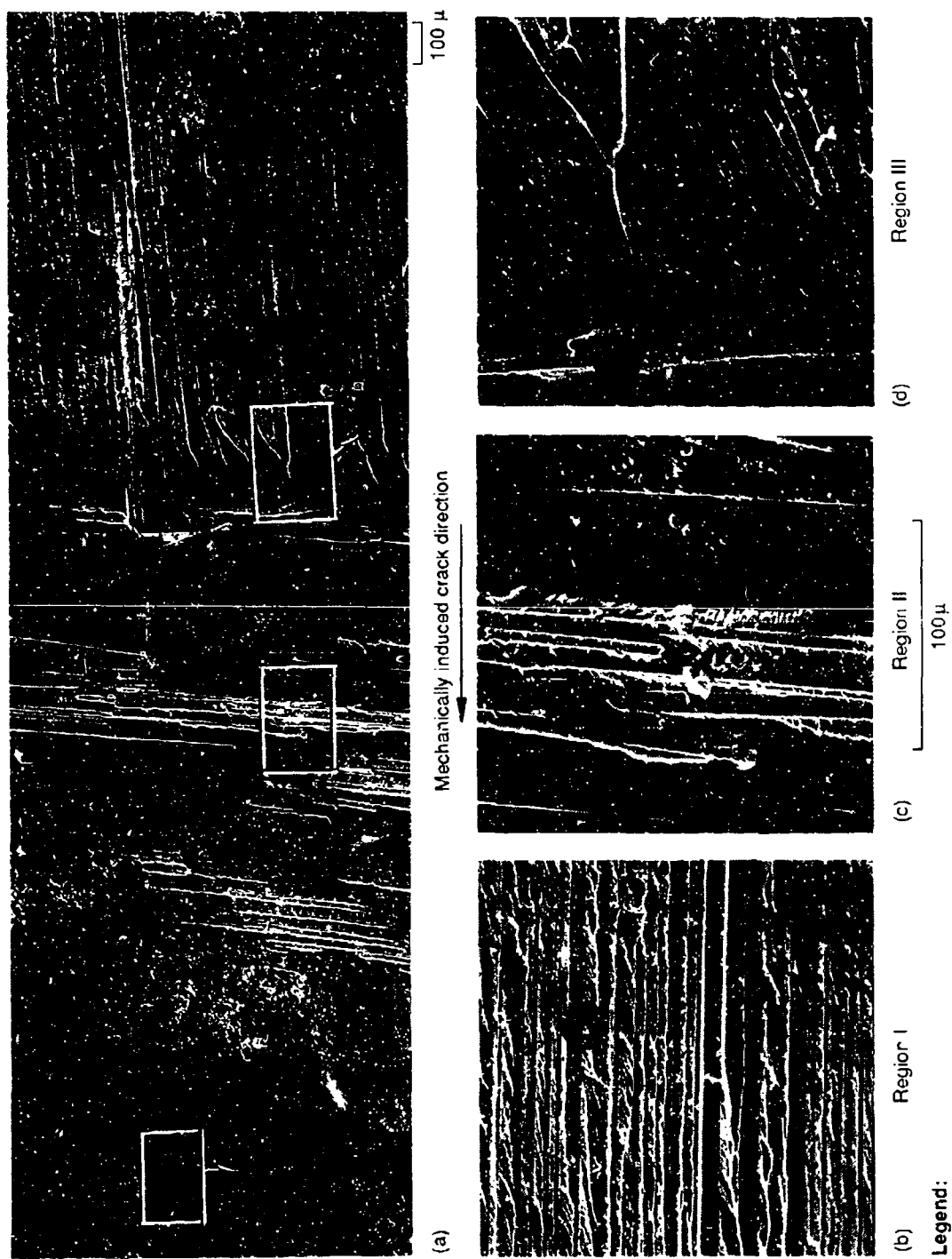


Figure 2-201. SEM Fractographs of Interlaminar Mode I Tension, RT/Dry, 0/90 Fracture (Area Shown in Figure 2-200a)

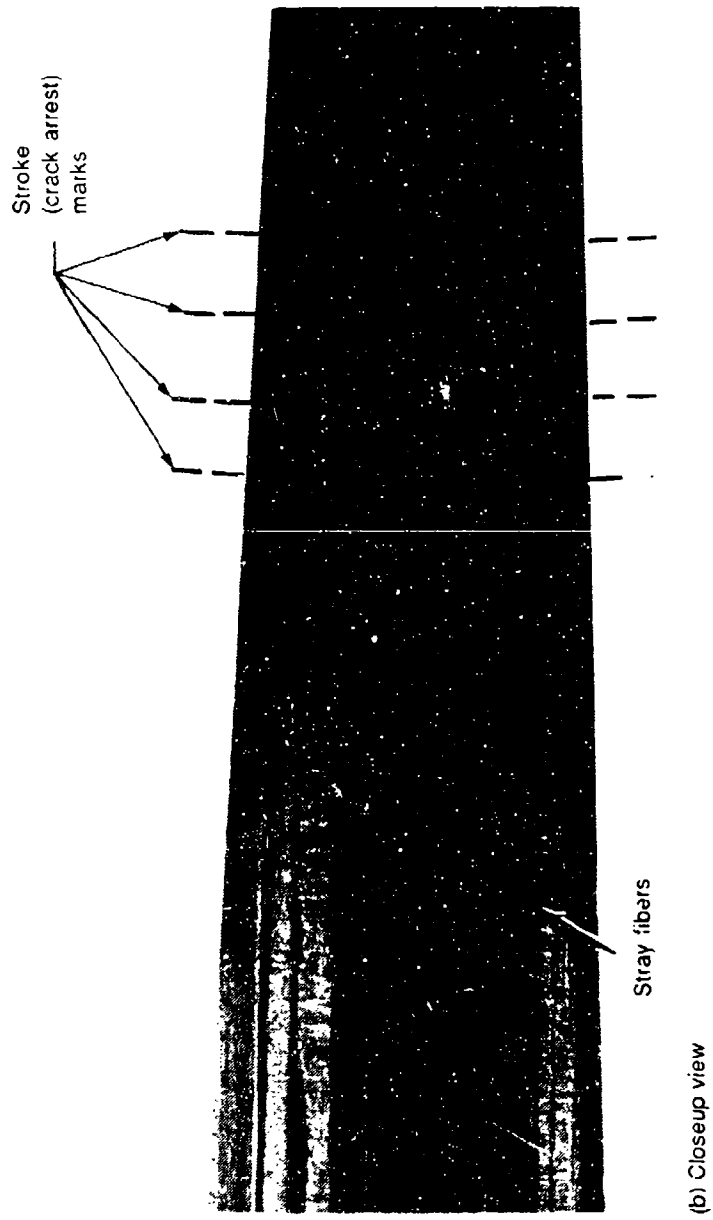
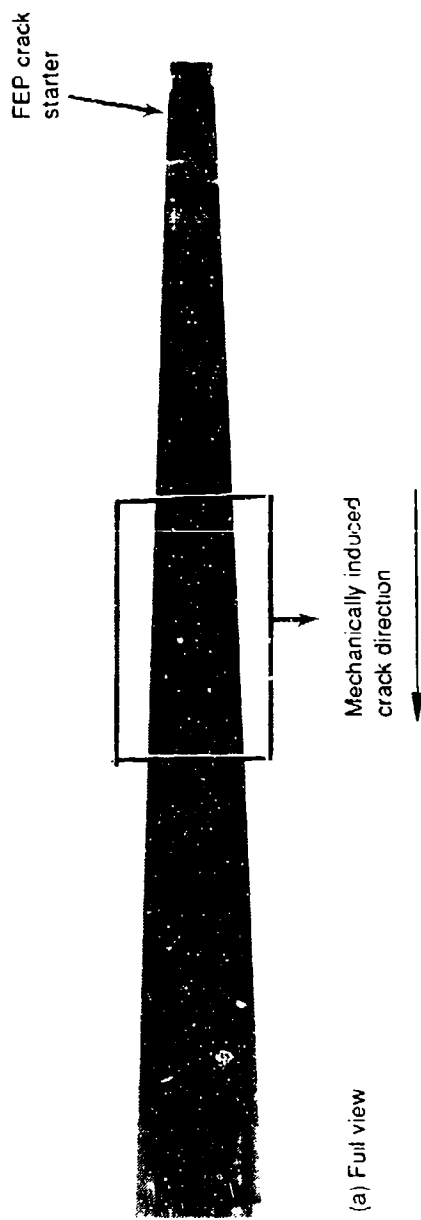


Figure 2-202. Macrophotographs of Interlaminar Mode I Tension, 270 F/Dry Creep, 0/90 Fracture

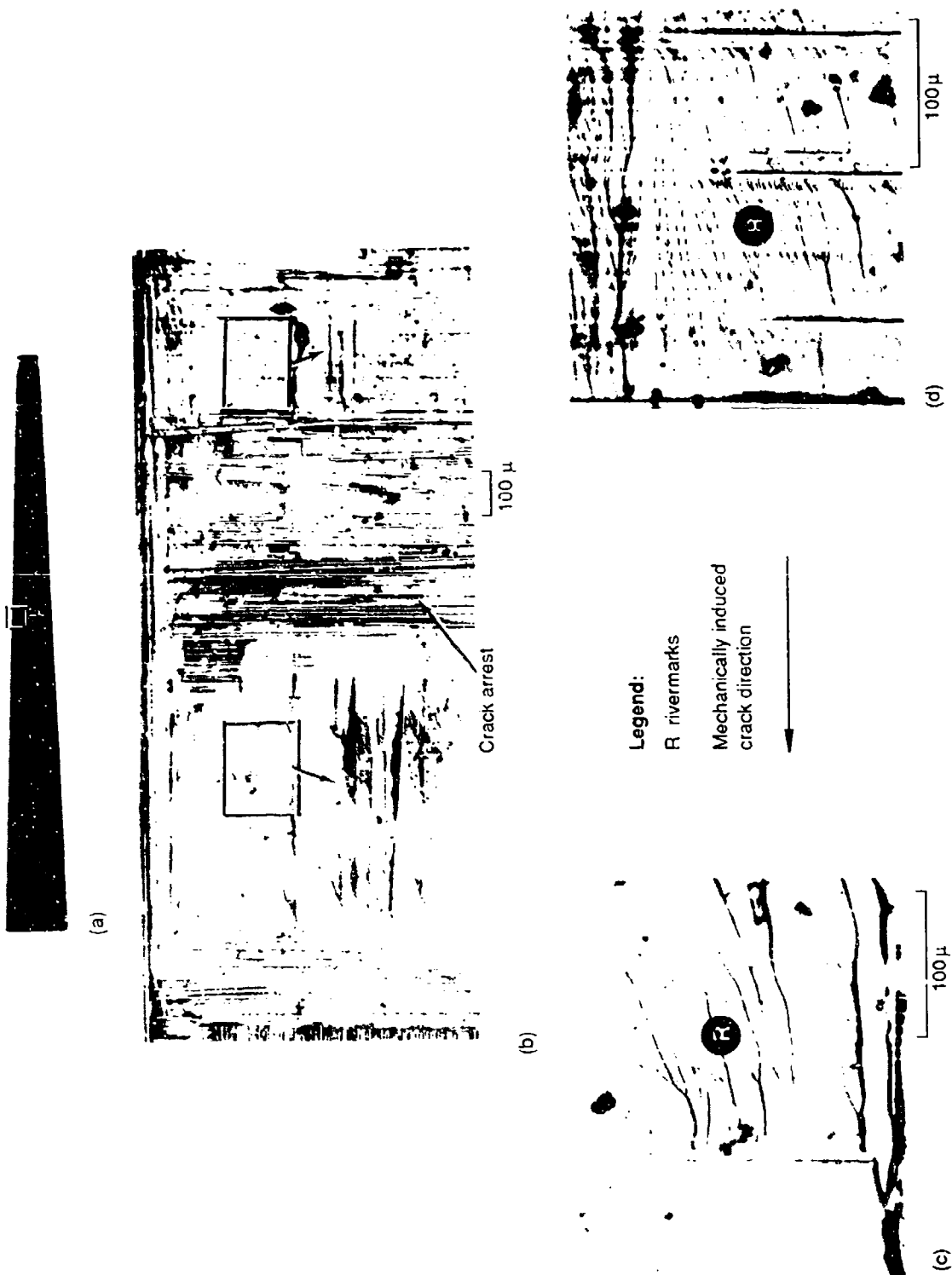
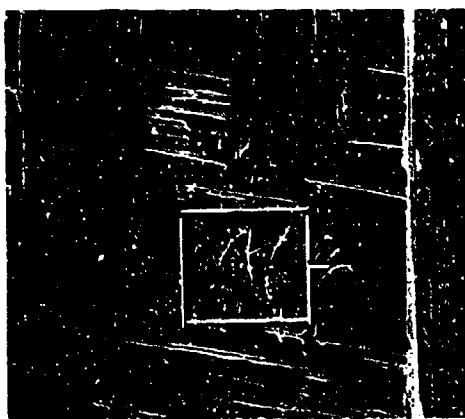
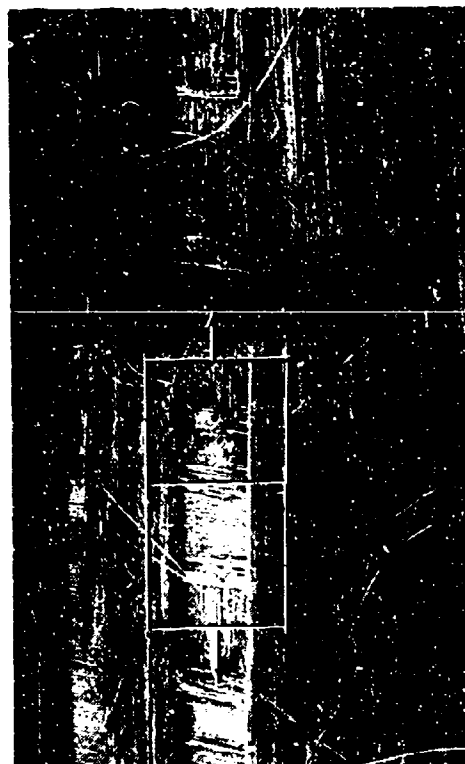


Figure 2-203. Optical Photomicrographs of Interlaminar Mode I Tension, 270 Fil/Dry Creep, 0/90 Fracture



(c)

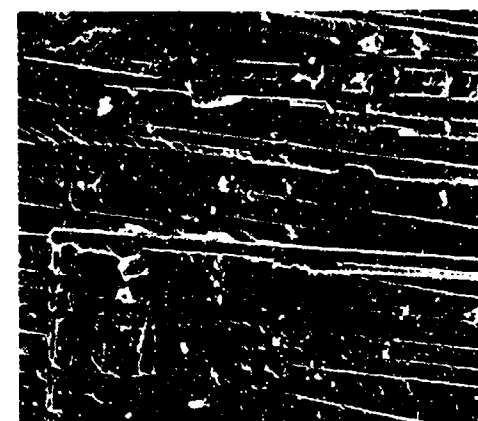


(b)

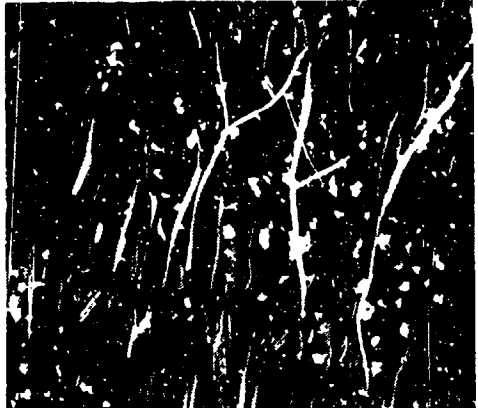


(a)

Legend:
 R rivermarks
 F fiber/matrix fracture
 Mechanically induced crack direction



(d)



(e)

Figure 2-204. SEM Fractographs of Interlaminar Mode I Tension, 270 F/Dry Creep, 0/90 Fracture

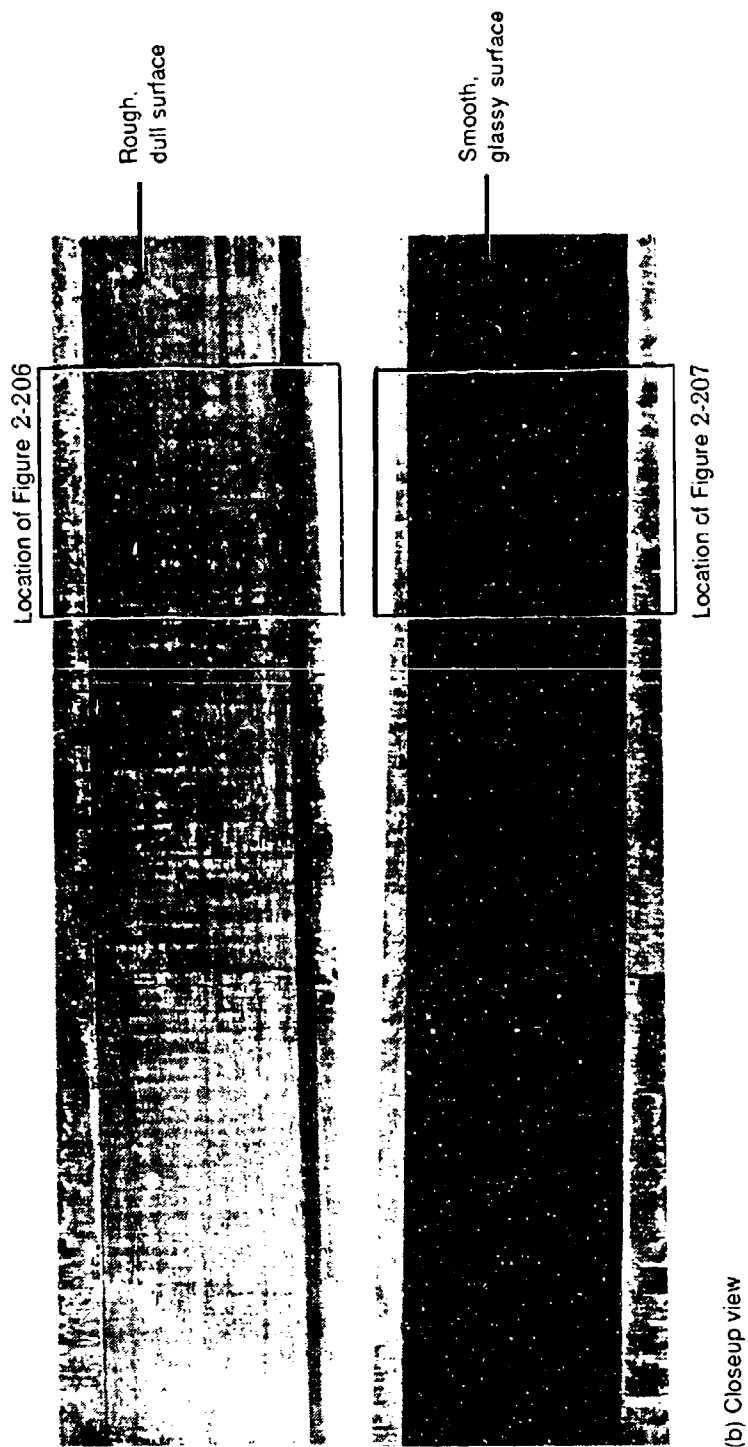
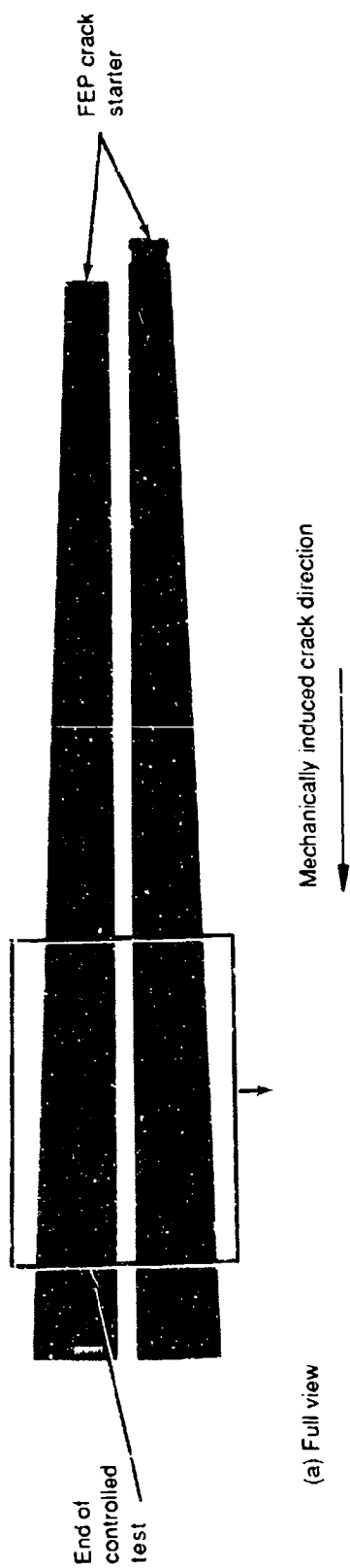


Figure 2-205. Photomicrographs of Interlaminar Mode II Shear, RT/Dry Creep, 0/90 Fracture

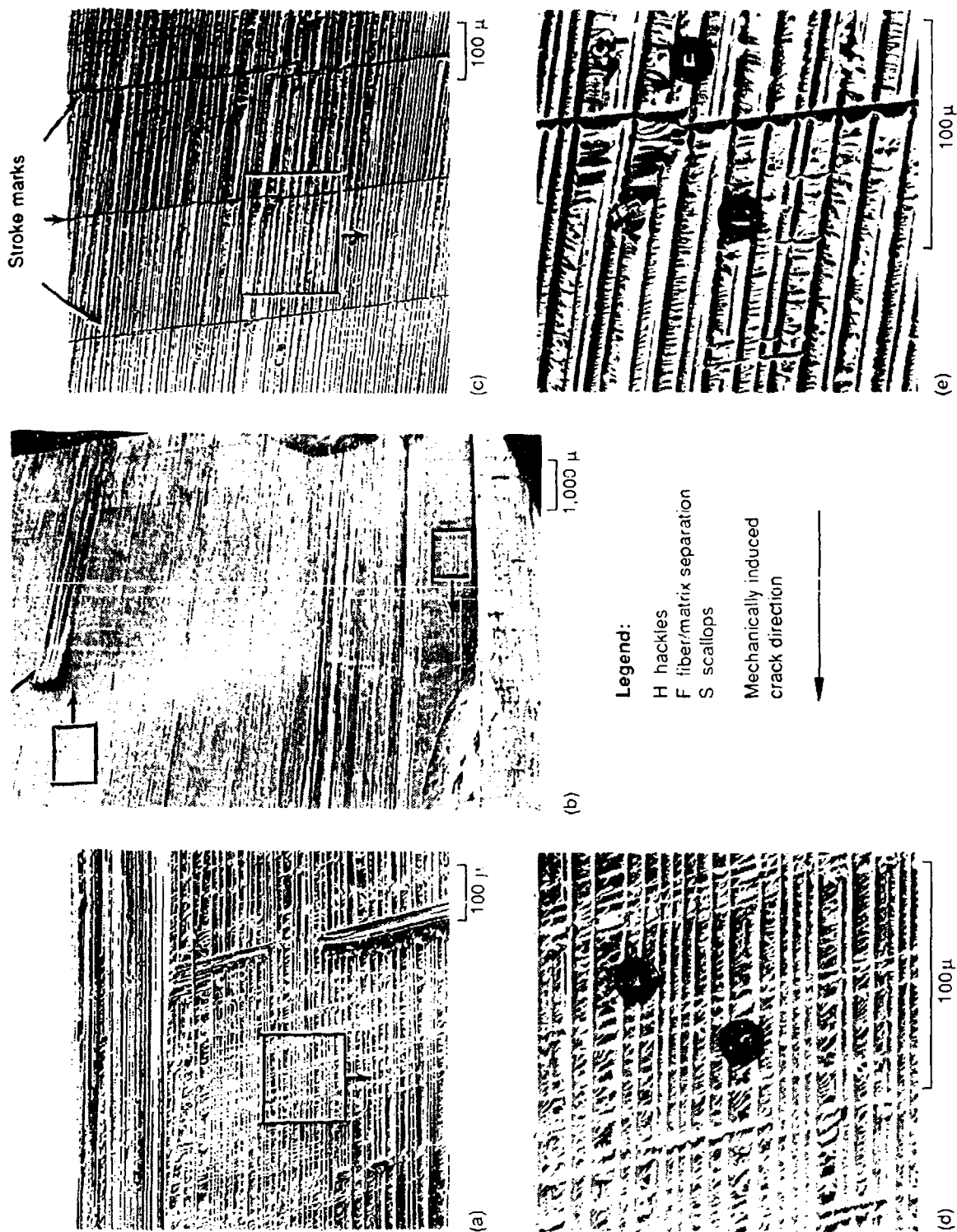
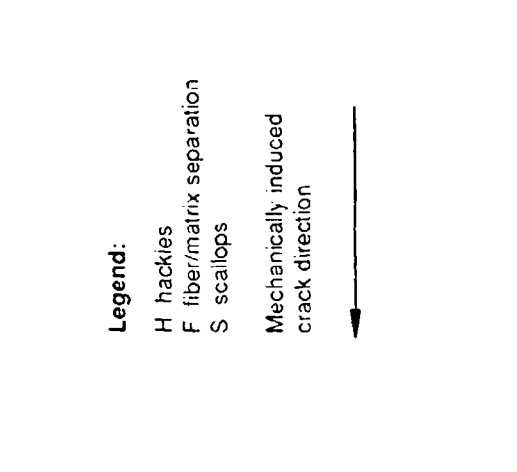
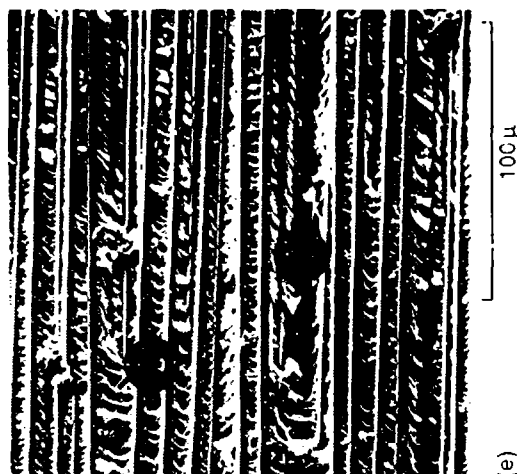
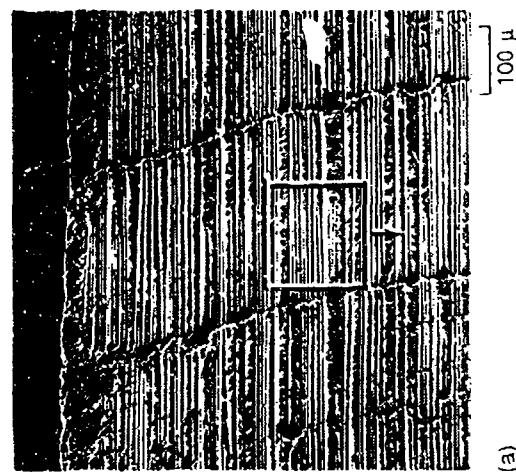
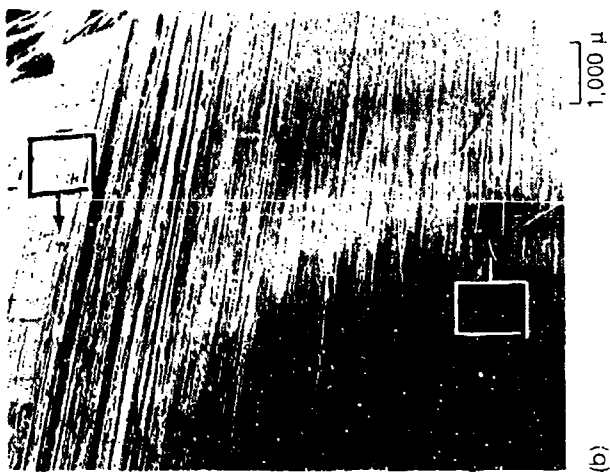
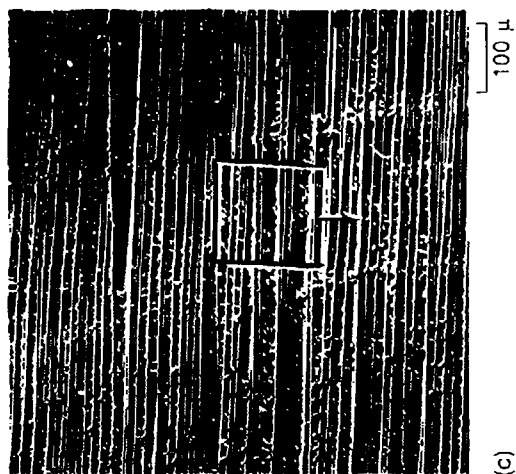


Figure 2-206. SEM Fractographs of Interlaminar Mode II Shear, RT/Dry Creep, 0/90 Fracture Showing Rough Surface
(Area Shown in Figure 2-205b)

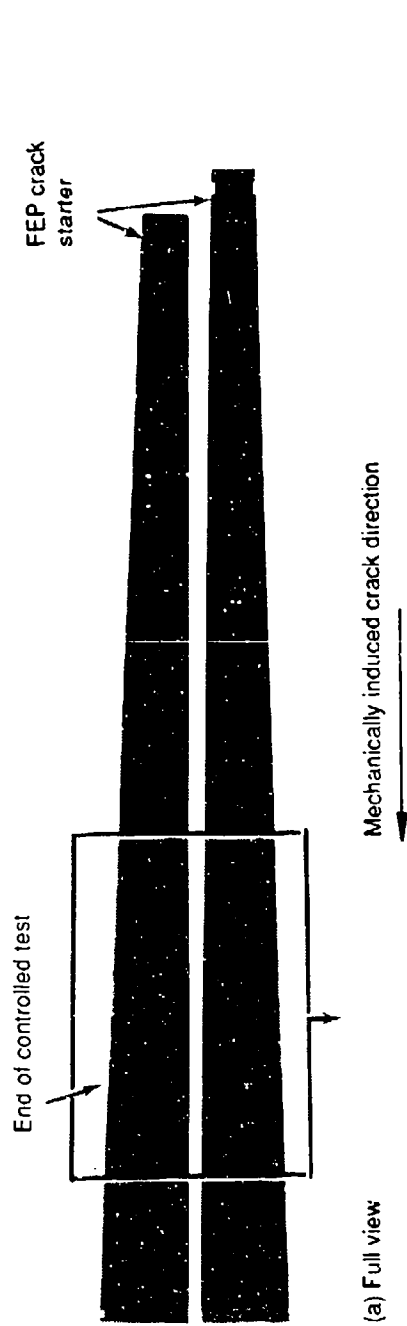


Legend:

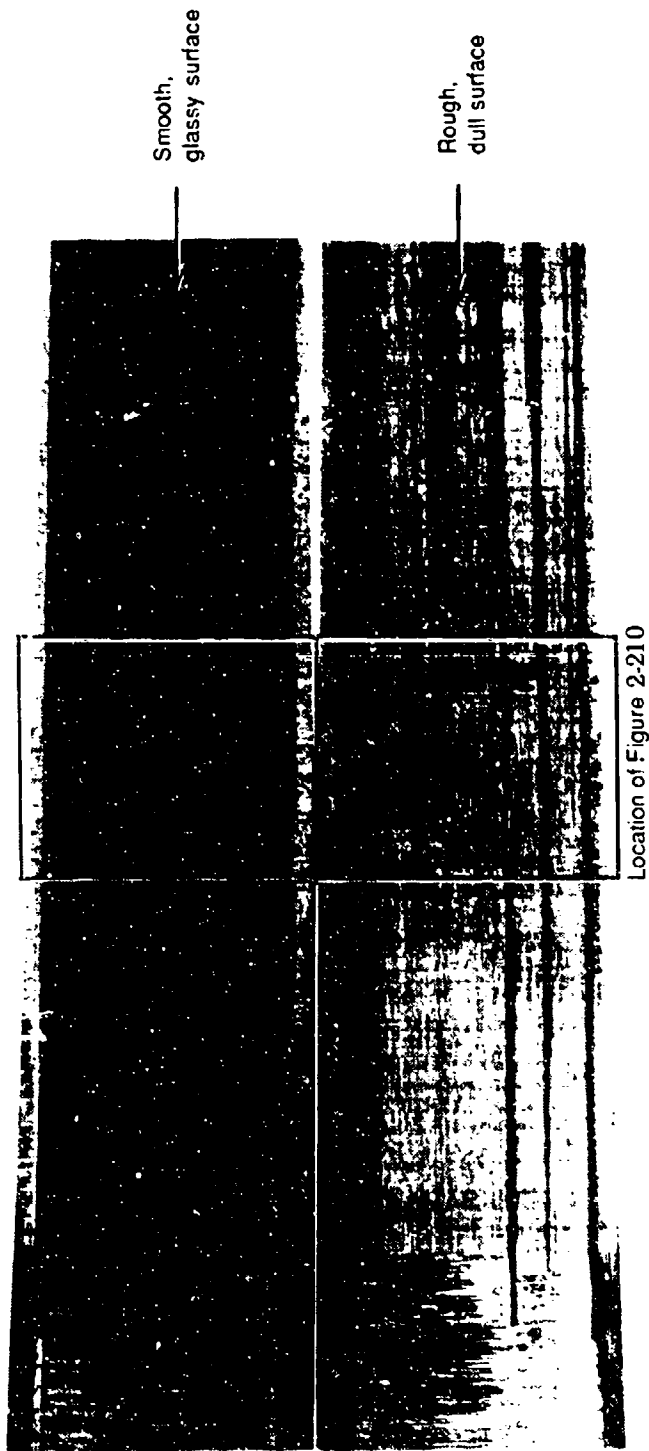
- H hackles
- F fiber/matrix separation
- S scallops
- Mechanically induced crack direction



Figure 2-207. SEM Fractographs of Interlaminar Mode II Shear, RT/Dry Creep, 0/90 Fracture Showing Glassy Surface
(Area Shown in Figure 2-205b)



Location of Figure 2-209



Location of Figure 2-210

Fracture 2-208. Photomicrographs of Interlaminar Mode II Shear, 270 F/Dry Creep, 0/90 Fracture

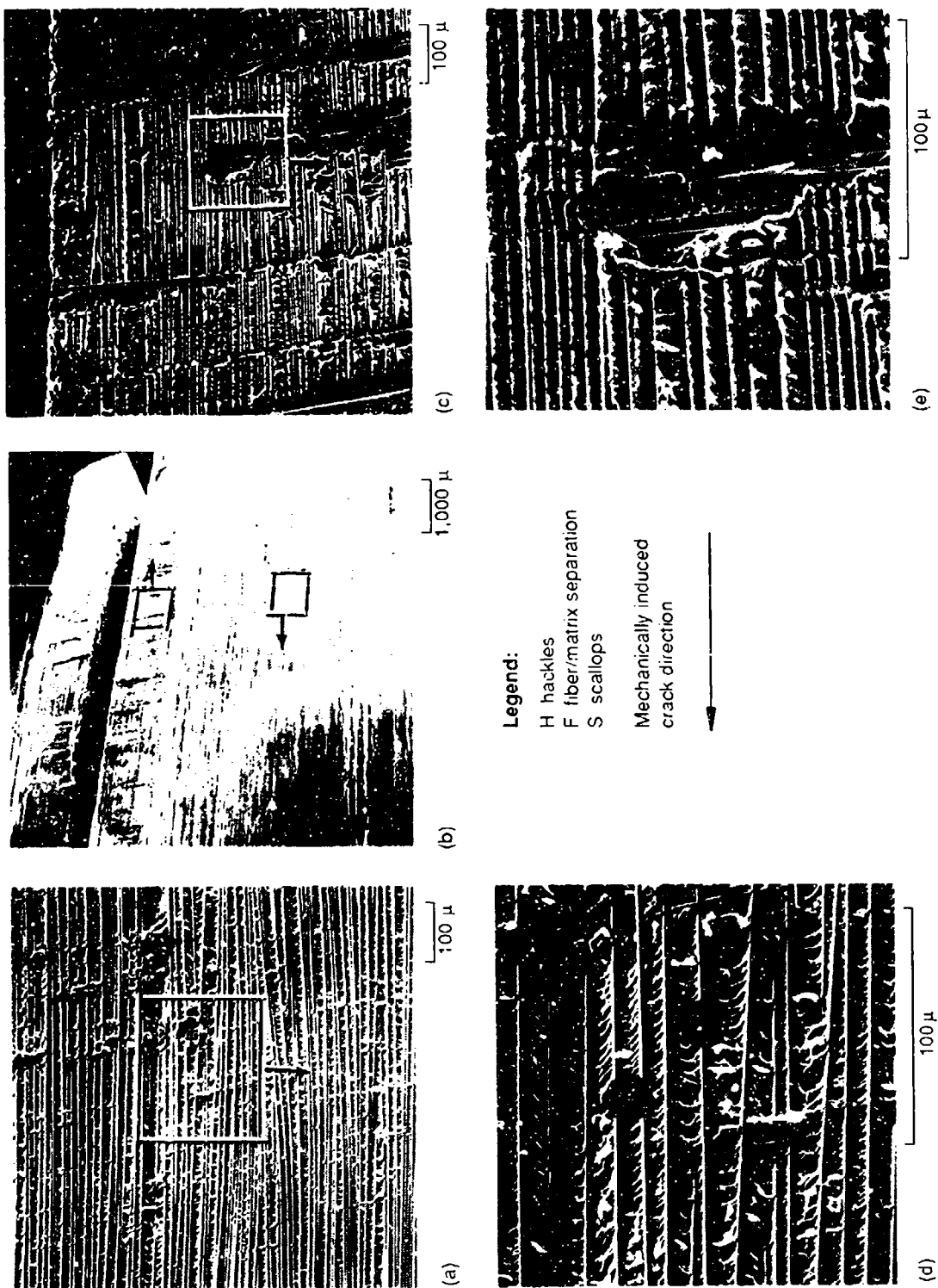


Figure 2-209. SEM Fractographs of Interlaminar Mode II Shear, 270 F/Dry Creep, 0/90 Fracture Showing Glassy Surface
(Area Shown in Figure 2-208b)

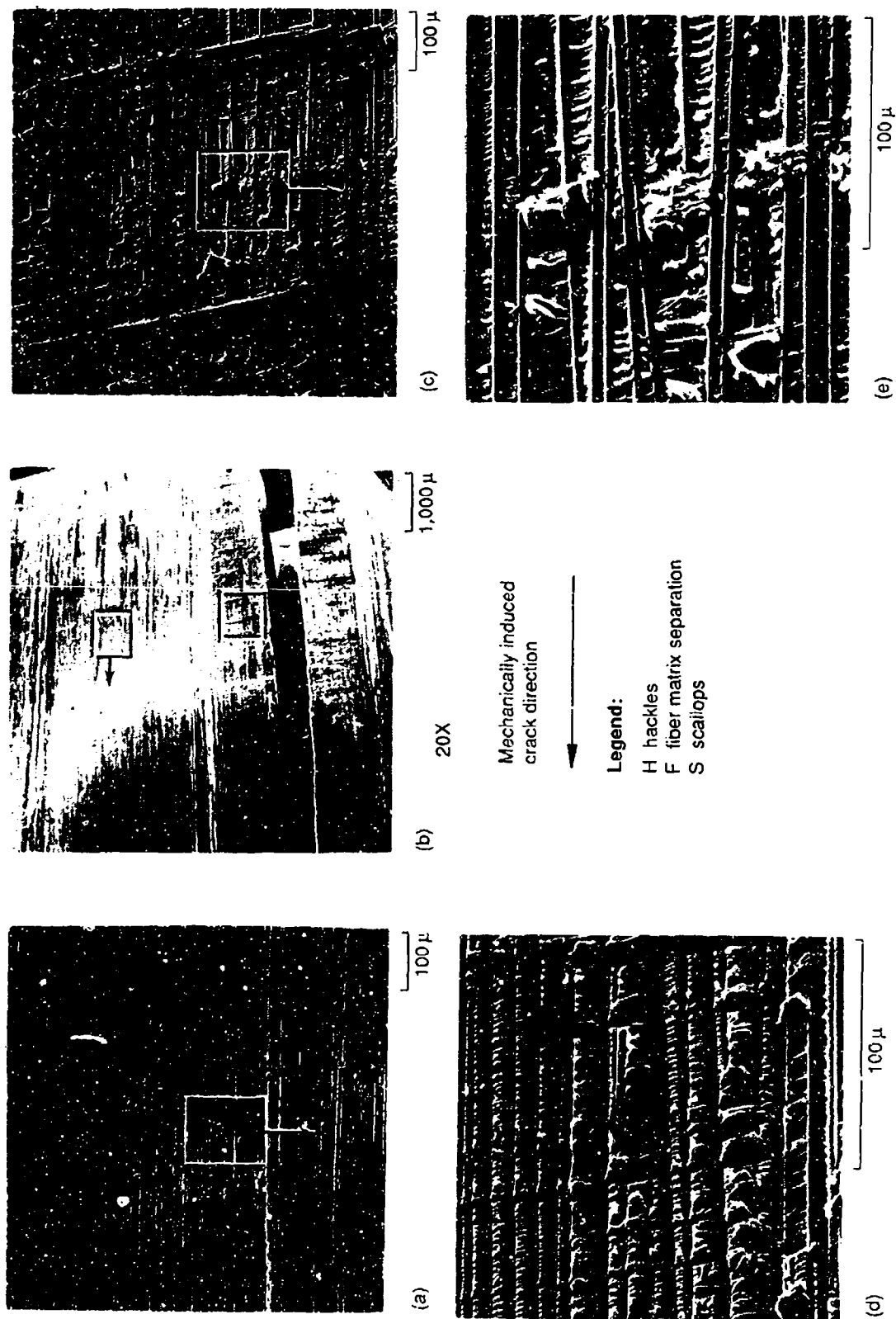


Figure 2-210. SEM Fractographs of Interlaminar Mode II Shear, 270 F/Dry Creep, 0/90 Fracture Showing Rough Surface
 (Area Shown in Figure 2-208b)

2.11 HIGH RATE

To create high-rate Mode I tension and Mode II shear fractures, projectiles were shot into a 1-inch by 10-inch specimen of 0/90 laminate protected by an aluminum plate at the location of penetration. For DCB specimens, a 1/2-inch thick aluminum plate was double-back taped to a cutout. A vise was used to hold one end of the specimen. The aluminum plate served as a shooting target deflecting the back half of the laminate away from the front half. This created a Mode I tension fracture. The interlaminar Mode II shear fracture was created by shooting a projectile at an aluminum target plate attached to the forward face of the ENF specimen. The force of the impact deflected both halves of the laminate. FEP crack starter initiated crack propagation by the sliding of the two halves of the laminate, creating a Mode II shear fracture. This contribution was made by Boeing.

2.11.1 Mode I Tension, RT/Dry

Visual observation of the DCB Mode I tension specimen, tested under conditions resulting in a high rate of fracture, revealed fractures somewhat different from those in a DCB/RT interlaminar Mode I tension specimen tested at constant rate. Due to the very rapid crack propagation, the fracture surface did not exhibit the clear macroscopic crack arrest marks which are characteristic of slow crack growth. In some locations, fiber splinters were peeled away from the matrix. Under the optical microscope, a cleavage fracture was observed with numerous rivermarks showing an overall crack direction (Figure 2-211).

To illustrate the different rates of fracture, two regions on the specimen were documented and analyzed. Region I was created by the initial projectile, and Region II was created by a second projectile penetration. SEM analysis showed that Region I experienced a lower energy fracture than Region II, as evidenced by its rougher surface and more mixed mode fracture (Figure 2-212). This may be a result of the initially delaminated portion driving the crack at a higher rate. There were also many fiber splinters and many areas of 90 degree intralaminar fracture in Region II (Figure 2-213).

2.11.2 Mode II Shear, RT/Dry

Visual observation of the high rate Mode II shear specimen revealed a fracture surface similar to a typical interlaminar Mode II shear specimen tested at constant rate; the only noticeable difference was the fiber splinters seen on the high load rate specimen.

Optical microscopy of the fracture surface showed a difference between the high rate specimen and the typical ENF specimen tested at constant rate (Figure 2-214). Due to the very rapid fracture, hackles were formed in various tilts and shapes; at slower crack growth rates, the hackles tend to form parallel to one another. Regions created by initial and secondary projectile penetration (resulting in different crack growth rates) exhibited no distinctly different features (Figures 2-215 and 2-216).

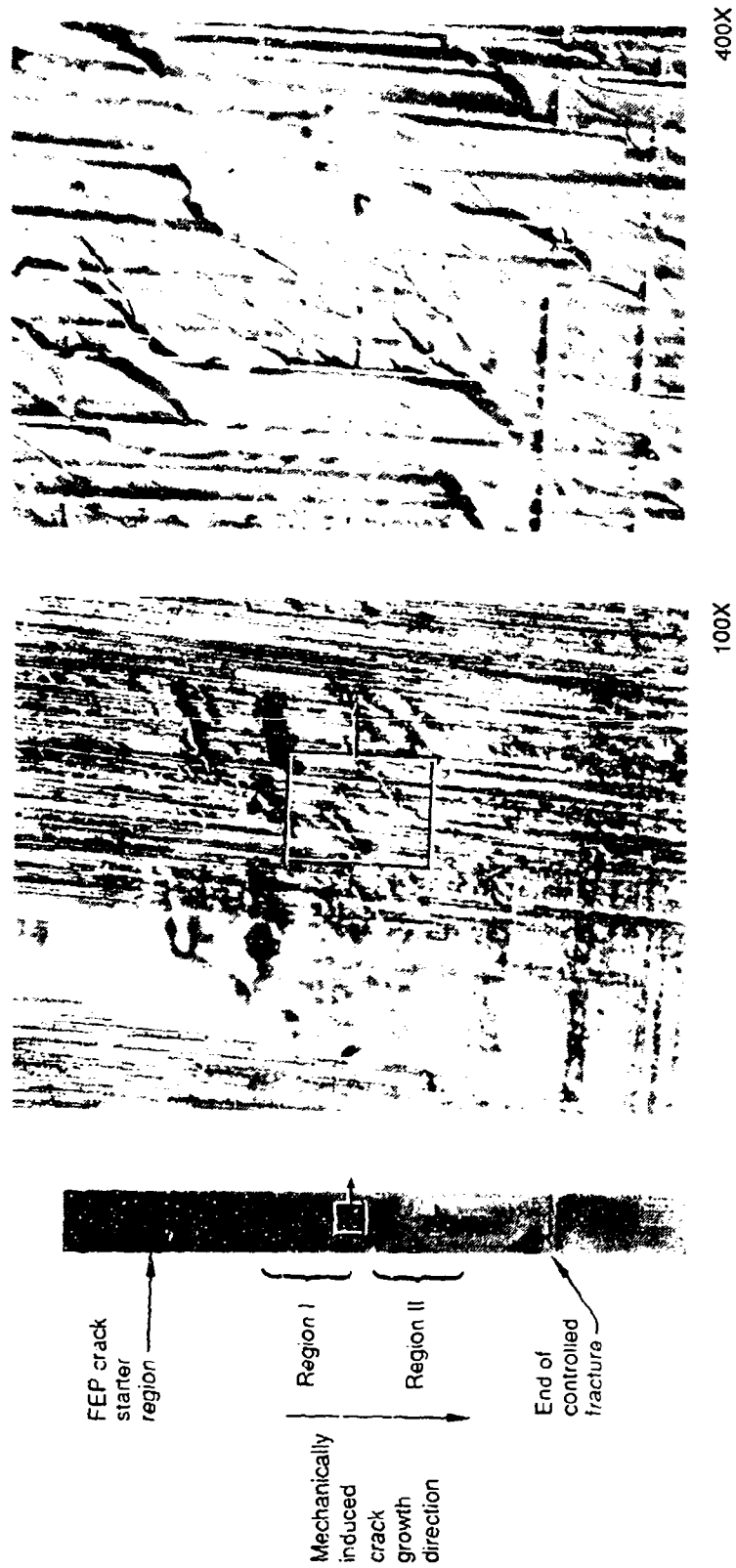
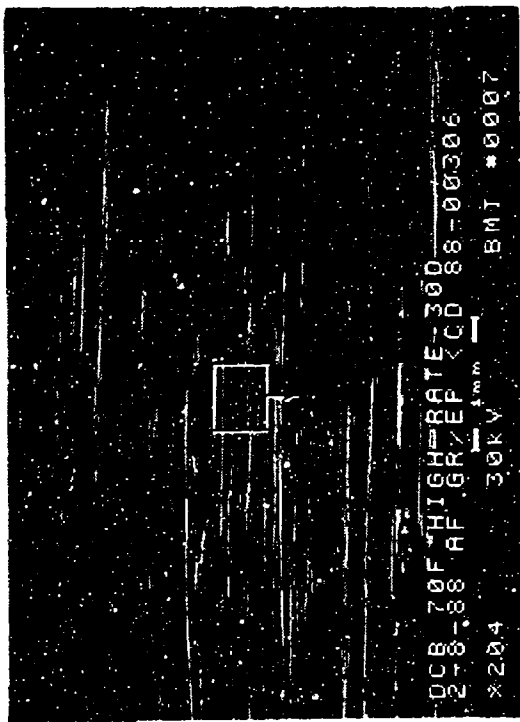


Figure 2-211. Optical Photomicrographs of Interlaminar Mode I Tension, High Rate, Room Temperature Fracture Between the 0/90 Plies

Legend:

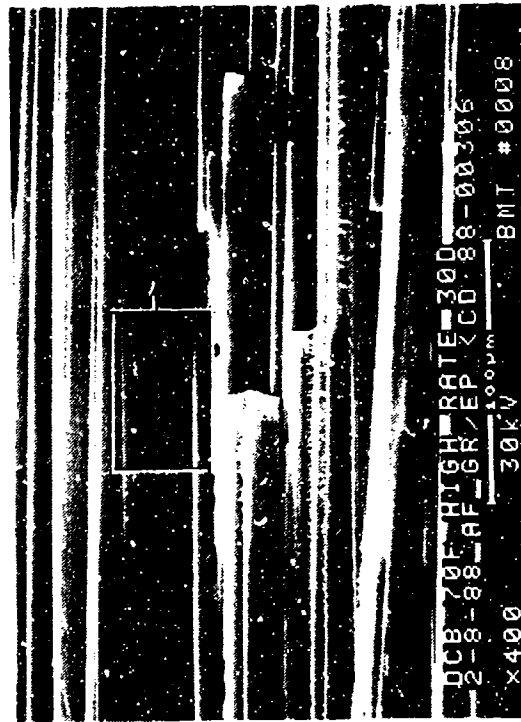
F fiber matrix
R rivermark
M matrix fracture

Mechanically induced
crack direction



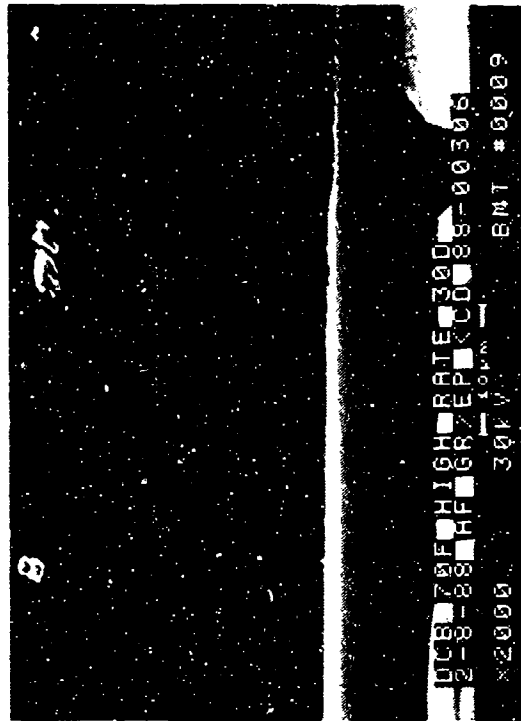
20X

30 degree tilt



400X

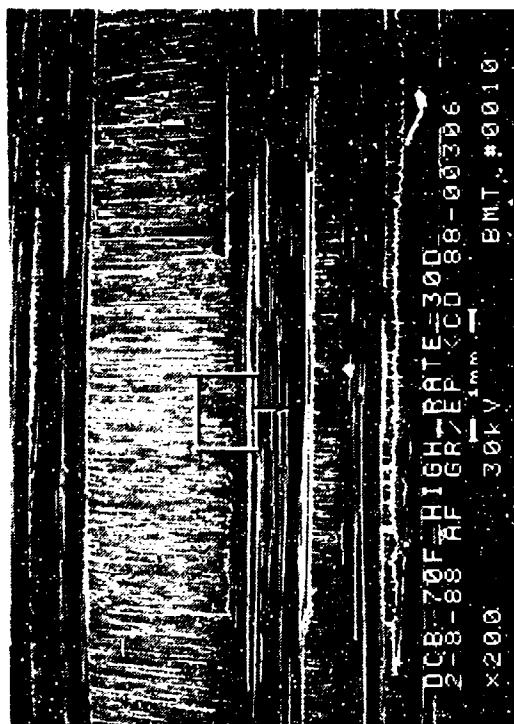
30 degree tilt



30 degree tilt

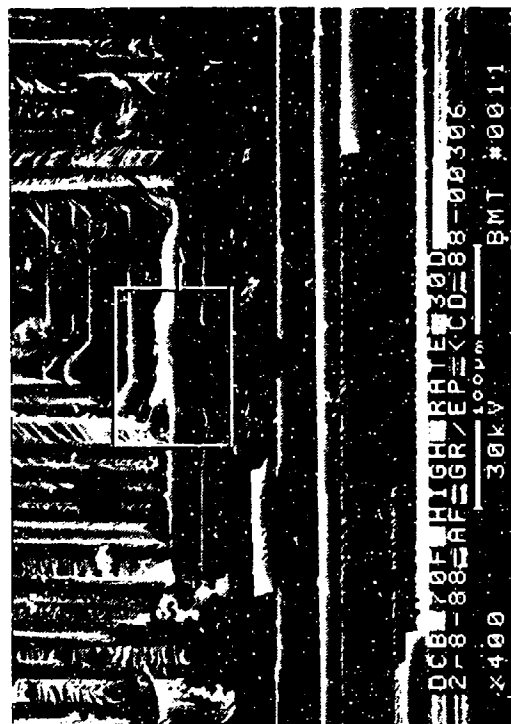
2,000X

Figure 2-212. SEM Fractographs of Interlaminar Mode I Tension, High Rate, Room Temperature Fracture (Region I of Figure 2-211)



30 degree tilt

20X



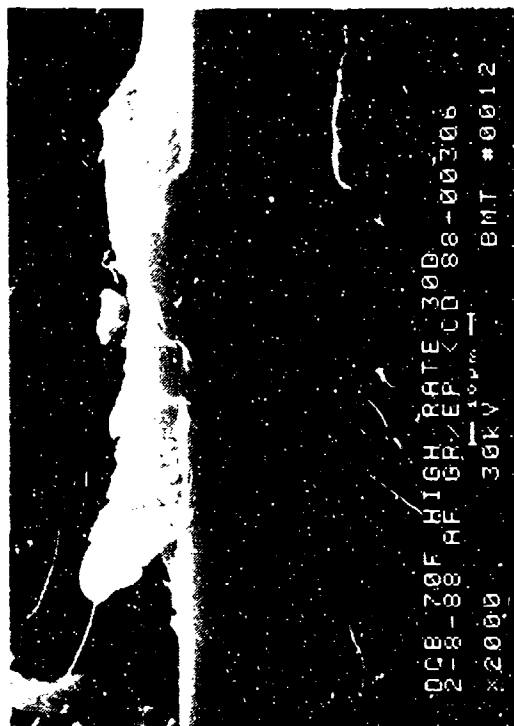
30 degree tilt

400X

Legend:

- R rivermark
- H hackle
- F fiber matrix separation
- M matrix fracture

Mechanically induced
crack direction



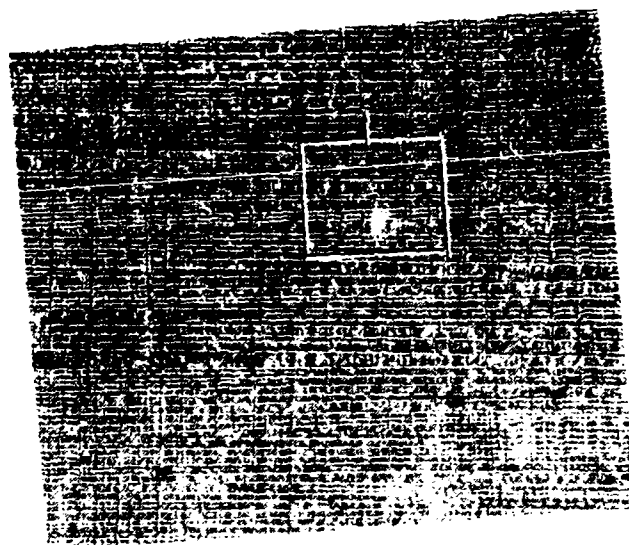
30 degree tilt

2,000X

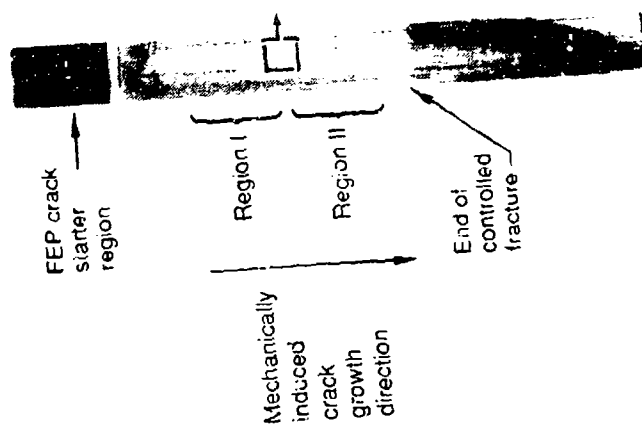
Figure 2-213. SEM Fractographs of Interlaminar Mode I Tension, High Rate, Room Temperature Fracture (Region II of Figure 2-211)



400X

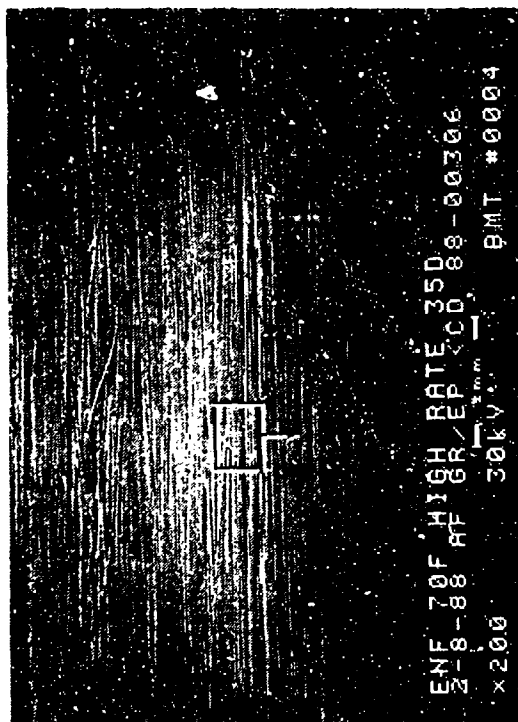


100X



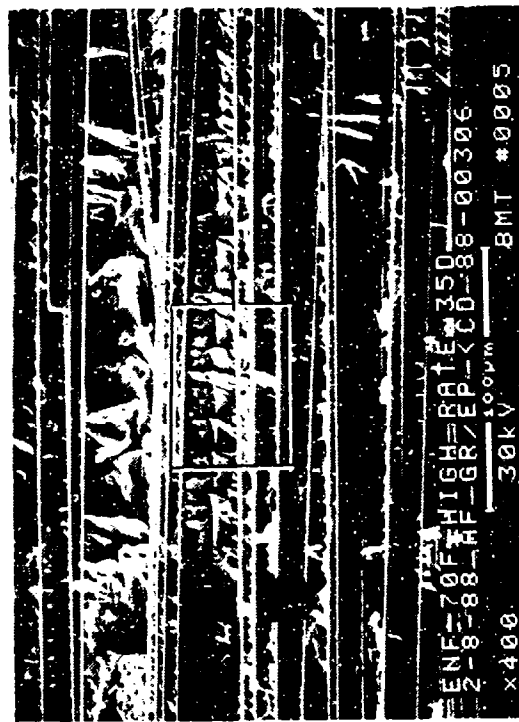
2-263

Figure 2-214. Optical Photomicrographs of Interlaminar Mode II Shear, High Rate, Room Temperature Fracture Between the 0/90 Plies



20X

35 degree tilt



400X

35 degree tilt

Legend:

F fiber matrix separation

H hackle

S scallop

M matrix fracture

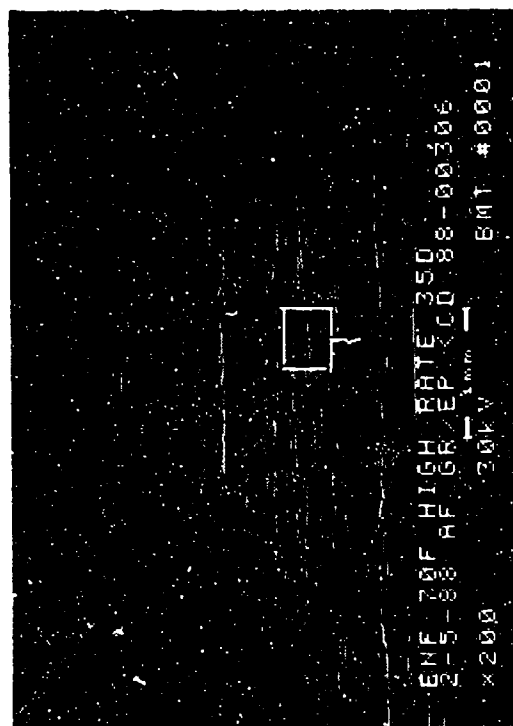
Mechanically induced
crack direction



35 degree tilt

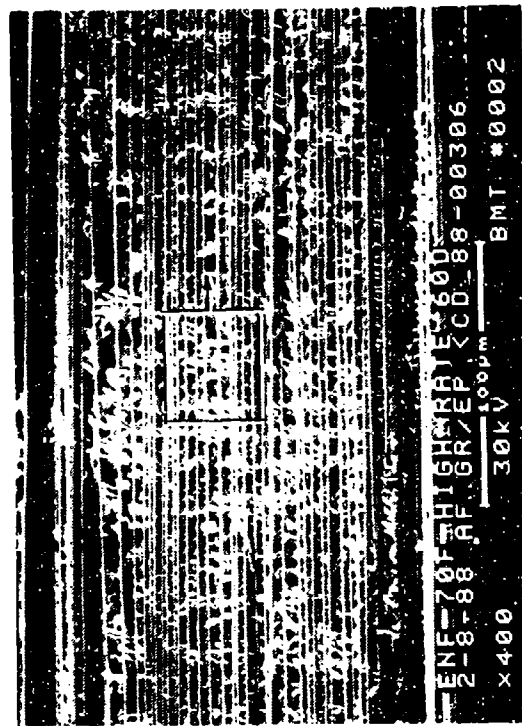
2,000X

Figure 2-215. SEM Fractographs of Interlaminar Mode II Shear, Room Temperature, High Rate Fracture (Region I of Figure 2-214)



35 degree tilt

20X



60 degree tilt

400X

Legend:

- F fiber matrix separation
- H hackle
- S scallop
- M matrix fracture

Mechanically induced
crack direction



60 degree tilt

2,000X

Figure 2-216. SEM Fractographs of Interlaminar Mode II Shear, Room Temperature, High Rate Fracture (Region II of Figure 2-214)

2.12 COMPRESSION-AFTER-IMPACT

The compression-after-impact (CAI) testing was performed on a 4-inch by 6-inch [0/+45/90/-45]_{4s} Gr/Ep laminate. The specimen was first centrally mounted on an impact support fixture and impacted on the tool side by an indenter with a 0.62 inch hemispherical tip at 1200 inch-lbs/inch. After impact, the specimen was examined using through transmission ultrasonic (TTU) techniques. The specimen was then placed on a 50 kip servohydraulic machine with a deflectometer and loaded to failure with a displacement of 0.05 inch/min. This contribution was made by Boeing.

The primary features associated with fractures produced with a CAI specimen are as follows:

1. Compression buckling of the laminate through the impact site (with extensive delamination)
2. Shear dominated interlaminar fracture features at the impact region (origin)
3. Tension dominated interlaminar fracture features at the specimen outer edges
4. Crack mapping of the river marks and resin microflow to identify crack-growth direction (and thus the origin).

Visual inspection revealed extensive buckling damage around the point of impact. Failure of the panel occurred in a band approximately 1.0 to 1.5 inches wide across the full width of the panel (Figure 2-217). TTU indicated a delamination which was exposed for further examination to determine the mode of failure in the vicinity of the impacted area. An examination was conducted under the optical microscope. In the region immediately surrounding the impact site (0.3 inch in diameter), the features were predominantly hackle formations indicating Mode II shear failure. The outer perimeter of the impact site was predominantly covered with rivermarks and resin microflow indicating Mode I tension failure (Figure 2-218). The crack initiated at the impact site and propagated radially through the specimen from the tool side in both interlaminar and translaminar fracture modes (Figure 2-219). Figure 2-220 shows CAI fractography performed by Boeing on a [0/45/90]_{8s} laminate. Additional CAI test fractography of a [0/45/90]_{8s} Gr/Ep laminate is shown in Figure 2-170.

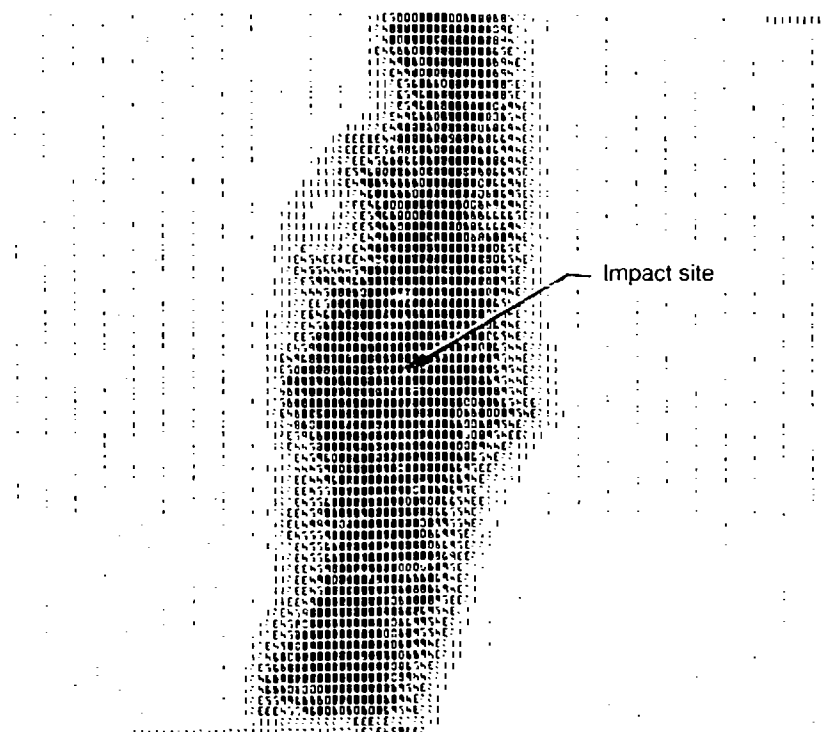
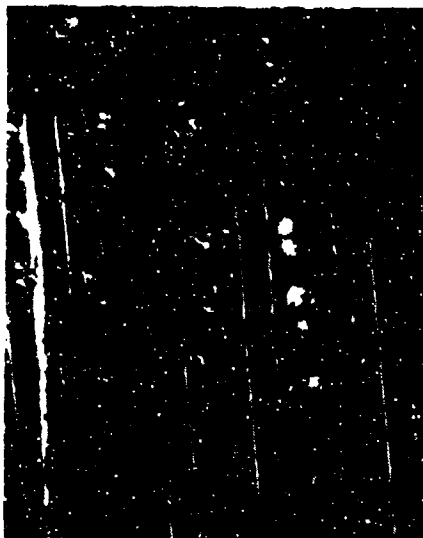


Figure 2-217. Extent of Impact Damage Identified by Through Transmission Ultrasonic (TTU) Scan of Impact Specimen



(a) Crack propagation direction 400X



(c) Crack propagation direction 400X



(b) Crack propagation direction 400X

Key to crack growth
direction arrows:
→ Mode I tension
↗ ↘ Mode II shear

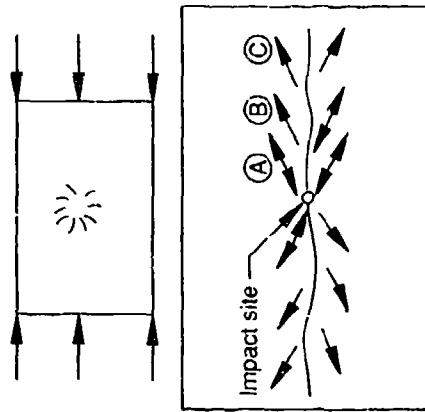
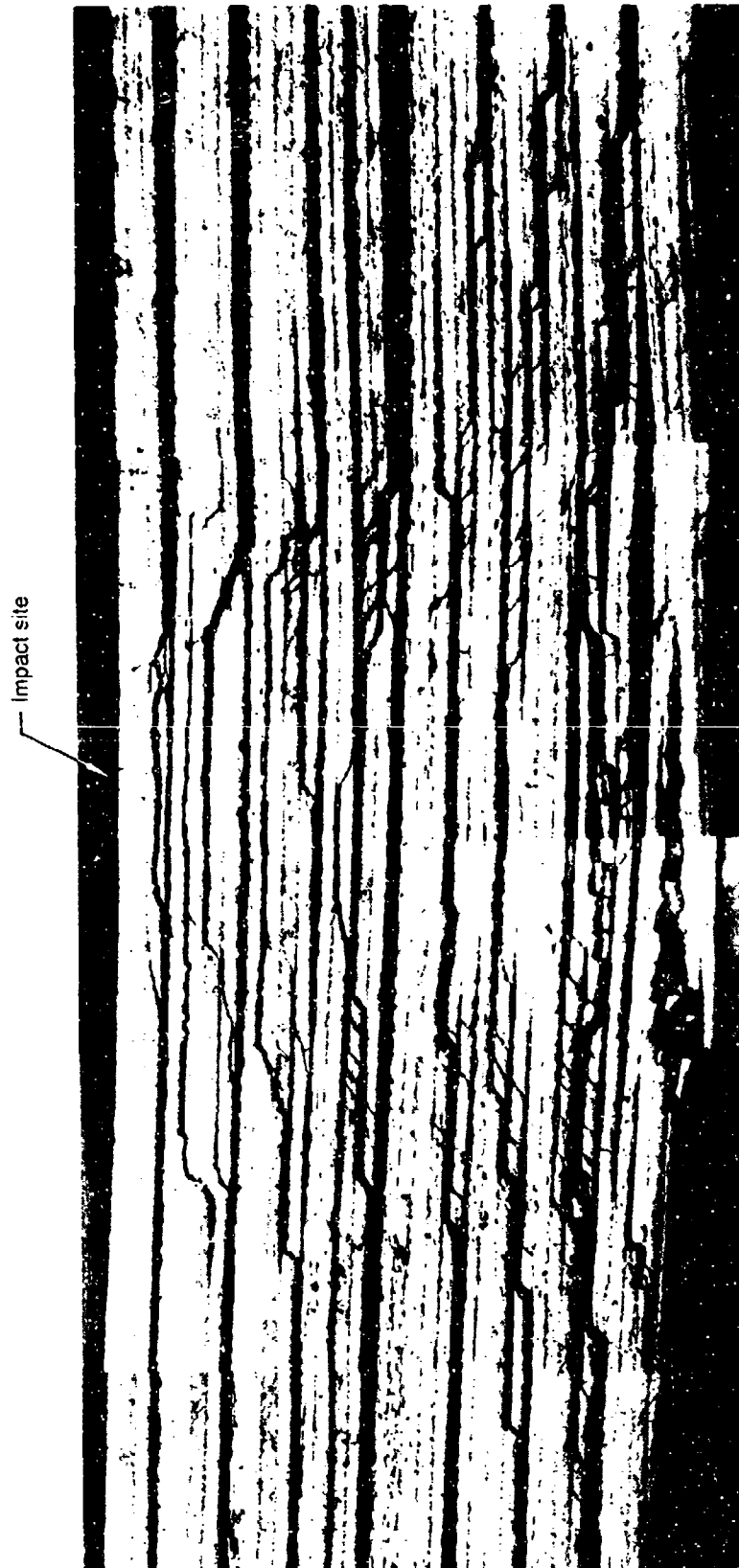


Figure 2-218. Optical Photomicrographs of Interlaminar Fracture of Compression-After-Impact, RT/Dry, [0/45/90/-45]_{4s} Specimen

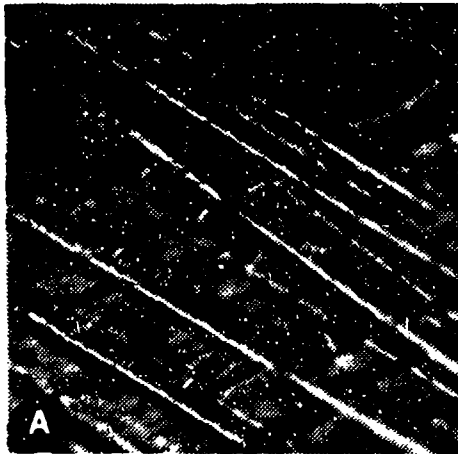


16X

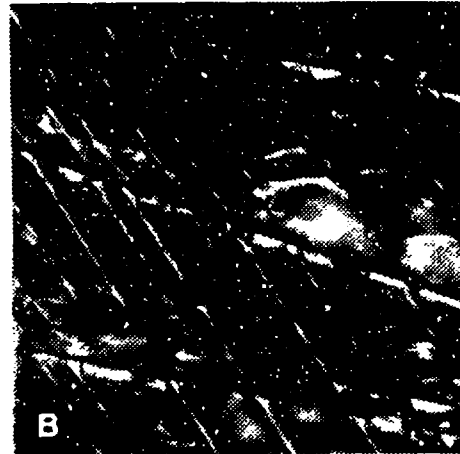
Figure 2-219. Cross-Sectional View of Compression-After-Impact, RT/Dry, [0/+45/90/-45]_s Specimen

Optical photomicrographs

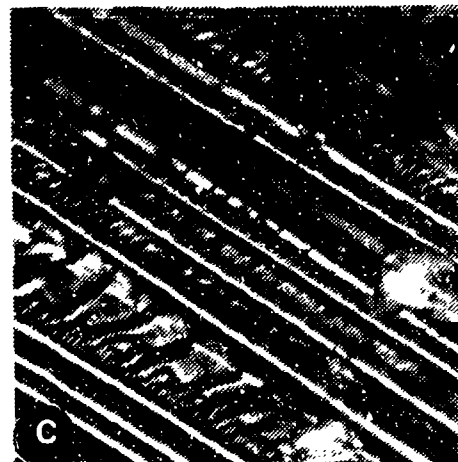
Fracture type	Interlaminar/translaminar
Ply layup	[0, 45, 90] _{8S}
Test type	Compression after impact
• Test conditions	Dry
• Fracture between	0/45/90 plies
Material	Hercules 3501-6/177°C cure AS4 fibers



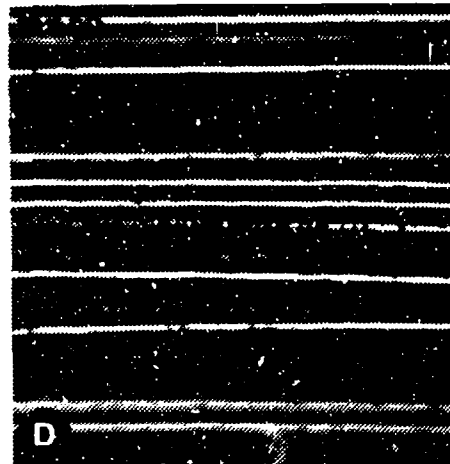
400X



400X



400X



400X

Key to crack growth
direction arrows:
— Mode I tension
— Mode II shear

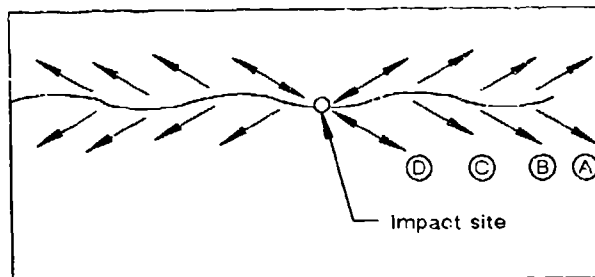


Figure 2-220. SEM Photographs of Interlaminar/Translaminar Compression After Impact, 0/45/90 Fracture

2.13 DEFECTS

2.13.1 Contaminants

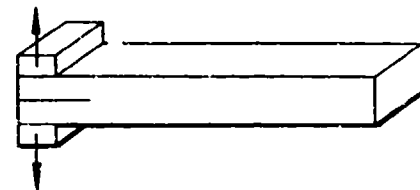
The key features observed on the contaminated specimens failed under either interlaminar Mode I tension or Mode II shear loading were as follows:

1. Teflon Contamination
 - a. Interconnected and fibrous appearing contamination regions
 - b. Matrix region fracture surfaces surrounding Teflon regions exhibit morphologies typical of the induced loading mode
2. Frekote Contamination
 - a. Interconnected and very smooth contaminated regions
 - b. Areas without resin fracture features (indicative of adhesive type separation)
 - c. Matrix resin fracture surfaces surrounding Frekote regions exhibit morphologies typical of the induced loading mode.

Figures 2-221 and 2-222 show photomicrographs of contaminants, Teflon and Frekote. When photomicrographs exhibit fractured resin particulate in the regions of contamination, it becomes more difficult to identify smooth adhesive separation. This contribution was made by Boeing.

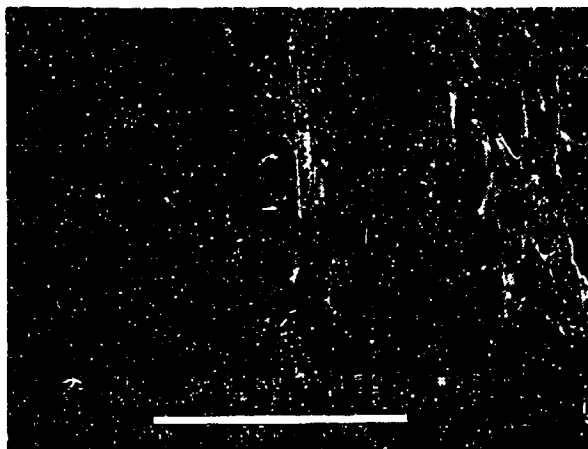
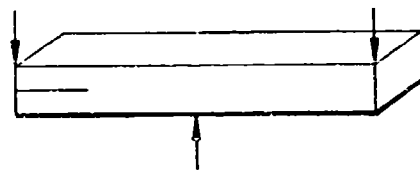
SEM photomicrographs

Fracture type	Interlaminar mode I tension
Ply layup	[0, 90] ₁₂ S
Test type	DCB with Teflon contamination
• Test conditions	21°C, dry
• Fracture between	0/90 plies
Material	Hercules 3501-6/177°C cure AS4 fibers



SEM photomicrographs

Fracture type	Interlaminar mode II shear
Ply layup	[0, 90] ₁₂ S
Test type	ENF with Teflon contamination
• Test conditions	21°C, dry
• Fracture between	0/90 plies
Material	Hercules 3501-6/177°C cure AS4 fibers



50X
Mode I tension

Mechanically induced crack direction

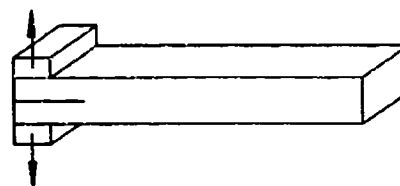


2000X
Mode II shear

Figure 2-221. SEM Photographs of Interlaminar Mode I Tension and Mode II Shear, 0/90 Fracture, Teflon Contamination, 70 F/Dry

SEM photomicrographs

Fracture type	Interlaminar mode I tension
Ply layup	[0, 45] 12S
Test type	DCB with Frekote contamination
• Test conditions	21°C, dry
• Fracture between	0, 45 plies
Material	Hercules 3501-6/177°C cure AS4 fibers

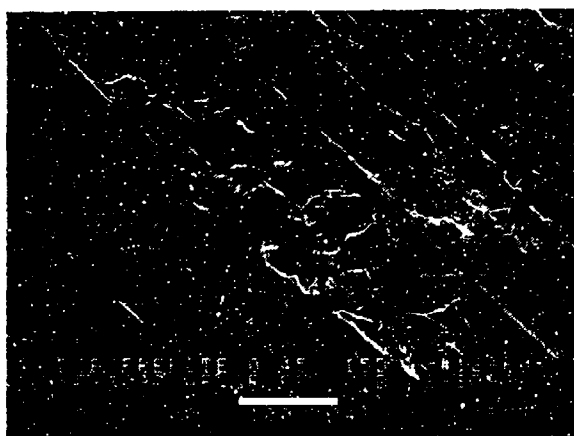


SEM photomicrographs

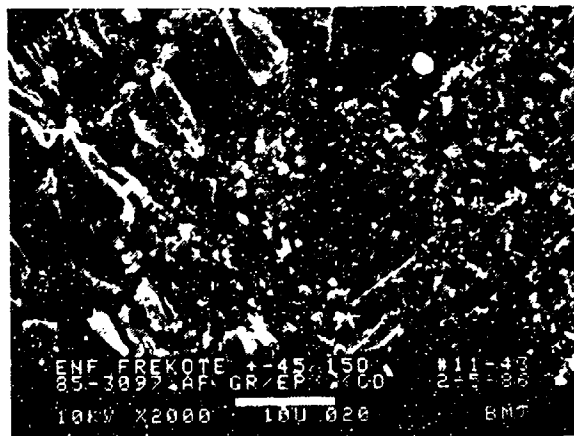
Fracture type	Interlaminar mode II shear
Ply layup	[+ 45, -45] 12S
Test type	ENF with Frekote contamination
• Test conditions	21°C, dry
• Fracture between	+45/-45 plies
Material	Hercules 3501-6/177°C cure AS4 fibers



Mechanically induced crack direction



200X
Mode I tension



2000X
Mode II shear

Figure 2-222. SEM Photographs of Interlaminar Mode I Tension and Mode II Shear, 0/45 and 45/45 Fractures, Frekote Contamination, 70 F/Dry

2.13.2 Voids

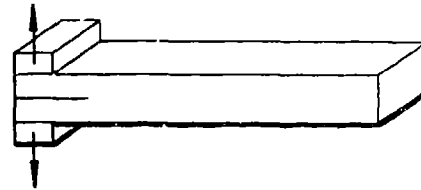
The primary features observed in the void containing specimens were as follows:

1. Smooth, featureless, rounded edged surfaces
2. Underlying fibers can be seen below voids
3. Fracture surface surrounding void region, exhibiting a matrix fracture morphology typical of the induced loading mode (allows determination of crack-growth and mode).

Figure 2-223 shows microphotographs of two test types of voids, DCB and ENF. This contribution was made by Boeing.

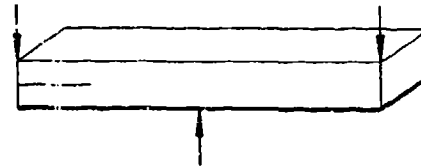
SEM photomicrographs

Fracture type	Interlaminar mode I tension
Ply layup	[0, 90] 12S
Test type	DCB—high void content
• Test conditions	21°C, dry
• Fracture between	0/90 plies
Material	Hercules 3501-6/177°C cure AS4 fibers



SEM photomicrographs

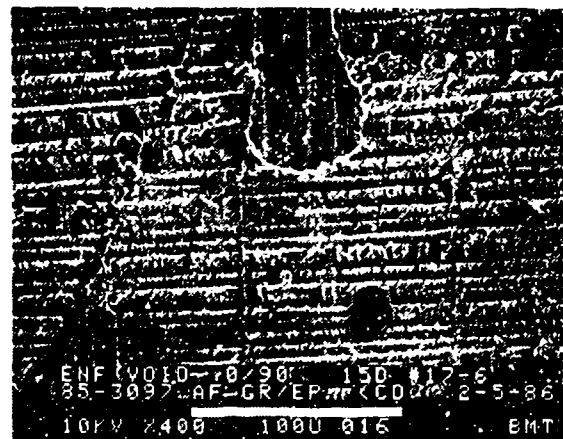
Fracture type	Interlaminar mode II shear
Ply layup	[0, 90] 12S
Test type	ENF—high void content
• Test conditions	21°C, dry
• Fracture between	0/90 plies
Material	Hercules 3501-6/177°C cure AS4 fibers



← Mechanically induced crack direction



200X



400X

Figure 2-223. SEM Photographs of Interlaminar Mode I Tension and Mode II Shear, 0/90 Fractures, With Voids, 70 F/Dry

SECTION 3
KEVLAR/EPOXY
49/3501-6

This section presents the results of fractography performed on Kevlar 49/3501-6 Kevlar/epoxy (K/Ep) test coupons. Testing was performed on interlaminar and translaminar fracture test coupons (DCB, ENF, MMF, and bend specimens). The test matrices are shown in Tables 3-1 and 3-2. The results reported include information on the baseline system and a few variable conditions.

On a macroscopic scale, the fracture surfaces consist of dense tangles of fibrils with no clear indicators of crack propagation direction. SEM examination of interlaminar fractures reveals stray rivers in peel failure modes that can be used to map crack-direction. Shear fractures are associated with stray hackles interspersed between the fibril tangles.

Translaminar tension and compression fractures do not exhibit features such as DAF radials or chop marks. Careful examination of plies parallel to the applied load may reveal stray interlaminar fracture features such as hackles or rivers; however, these are not present in sufficient quantity to map the crack-growth direction unequivocally .

Fractographs of 49/3501-6 Kevlar/epoxy are provided for interlaminar testing in Figures 3-1 through 3-9 and for translaminar testing in Figures 3-10 through 3-15. This contribution was made by Northrop.

Table 3-1. Kevlar 49/3501-6 Epoxy Interlaminar Fracture Test Matrix

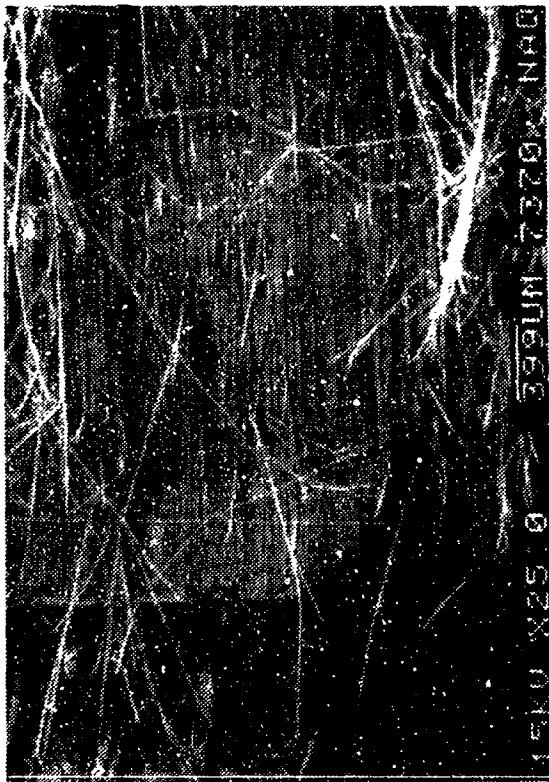
SPECIMEN, LOADING	VARIABLE CONDITION	LAYUP	LAMINATE DIMENSIONS	NO. OF LAMINATES
Mode I DCB, Tension	RTA	24/0	22 X 11	1
Mode II ENF, Shear	RTA			
Mode I + II MMF, Tension + Shear	RTA			
Mode I DCB, Tension	Cond. 180 F 2 weeks before test	24/0	13 X 13	1
Mode II ENF, Shear				
Mode I DCB, Tension	RTA	24/0,45	22 X 11	1
Mode II ENF, Shear	RTA			
Mode I DCB, Tension	Water immer. before test			

RTA = Room Temperature Ambient
Laminate dimensions in inches

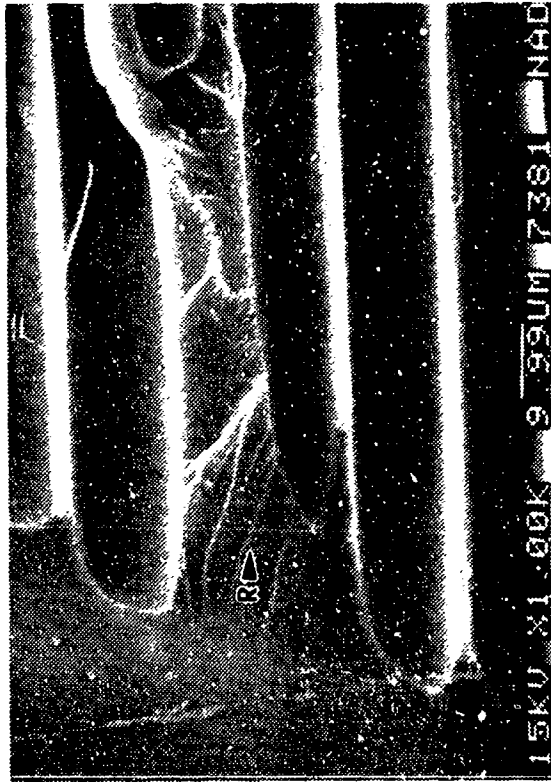
Table 3-2. Kevlar 49/3501-6 Epoxy Translaminar Fracture Test Matrix

SPECIMEN, LOADING	VARIABLE CONDITION	LAMINATE LAYUP	DIMENSIONS	NO. OF LAMINATES
Mode I Tension, 4 pt. load	RTA	32/90,0	14 x 7	1
Mode I Compression, 4 pt. load	Water Immer. before test			
Mode I Compression, 4 pt. load	RTA			
Mode I Compression, 4 pt. load	RTA	32/quasi	14 X 7	1
Mode I Compression, 4 pt. load	Water Immer. before test			
Mode I Compression, 4 pt. load	Cond. 180 F 2 weeks before test			

RTA = Room Temperature Ambient
Laminate dimensions in inches



(b)



(c)



(a)

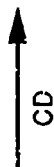
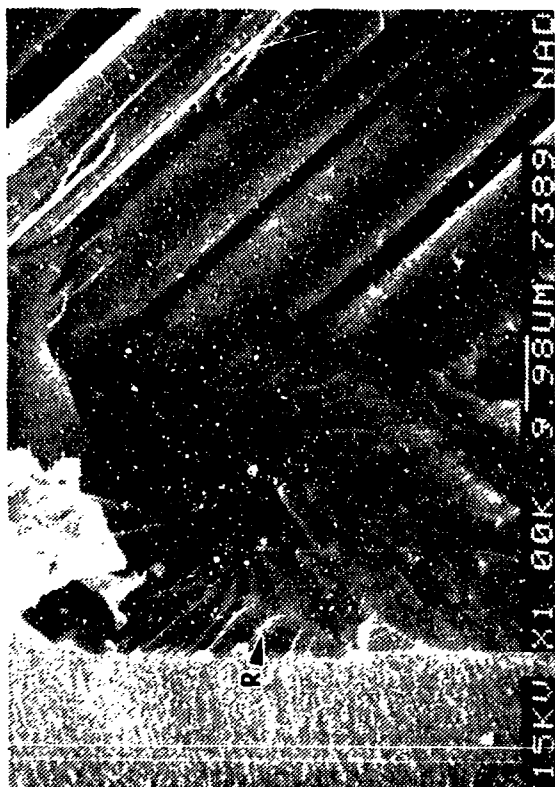
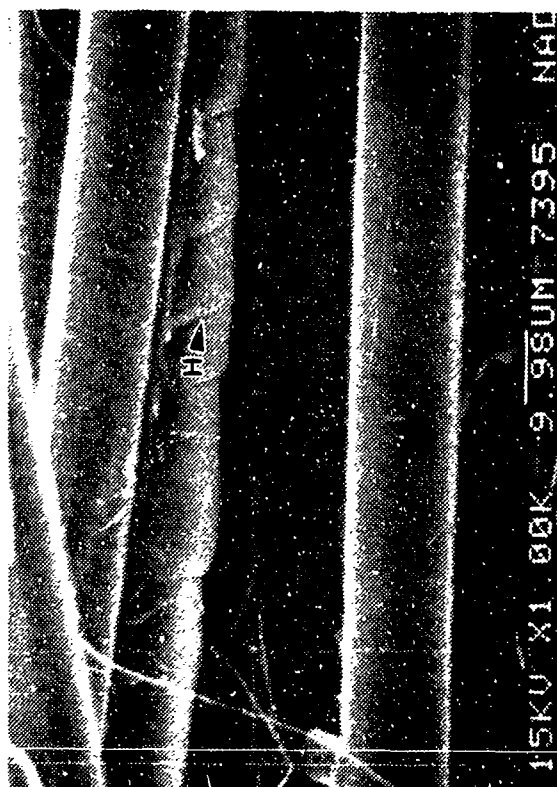


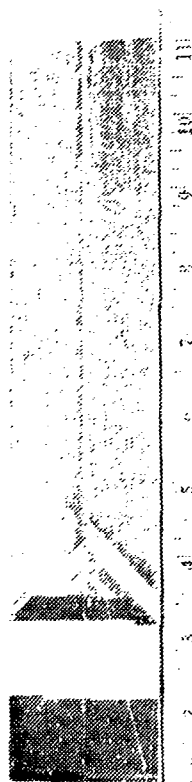
Figure 3-1. Optical and SEM Photographs of Mode I DCB Interlaminar Tension Fracture in 49/3501-6 Kevlar/Ep - [0]_{24T}, Room Temperature Ambient
 (a) Macro photograph of Fracture
 (b) Fiber Pull-Out
 (c) River Patterns (R) in Fractured Resin
 CD = Crack-propagation direction



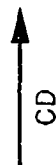
(a)



(b)



(c)



CD

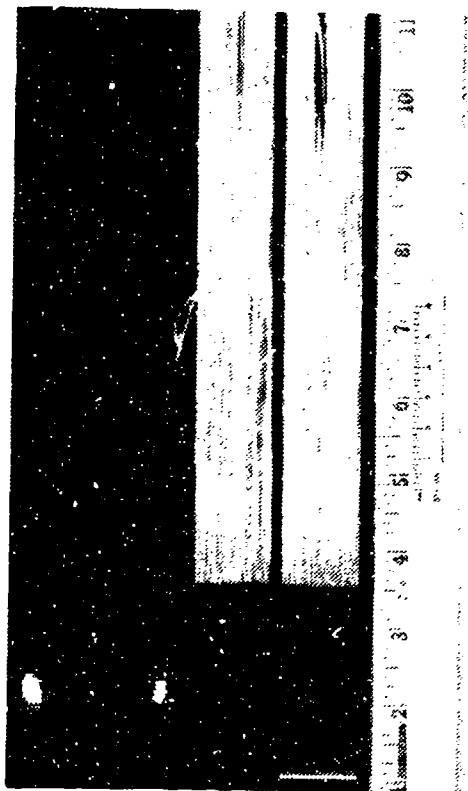
Figure 3-2. Optical and SEM Photographs of Mode I DCB Interlaminar Tension Fracture in 49/3501-6 Kevlar/Ep - [+45/0/-45]_s, Room Temperature Ambient

(a) Macro photograph of Fracture

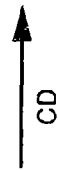
(b) River Patterns (R) at Initiation Site

(c) Hackles (H) in Fractured Resin

CD = Crack-propagation direction



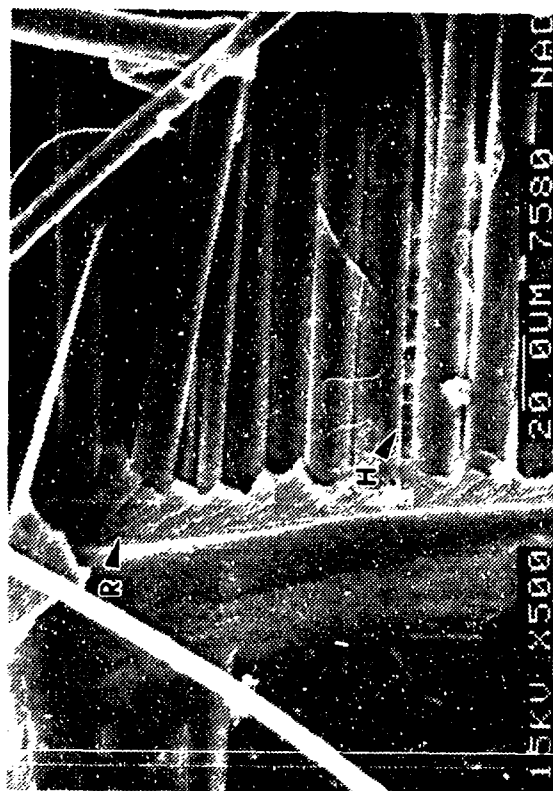
(a)



CD



(b)



(c)

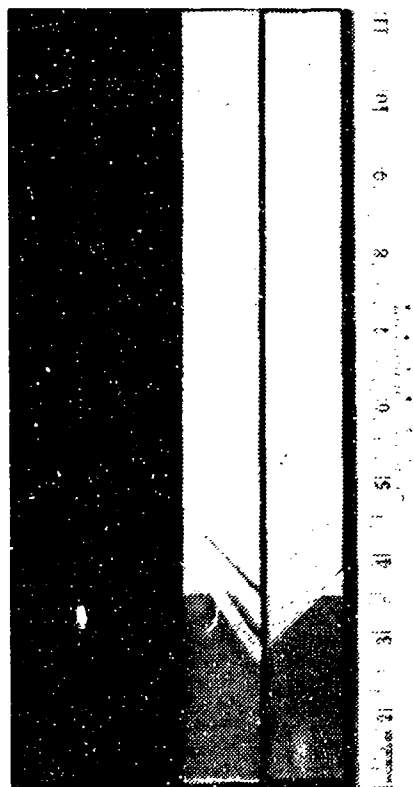
Figure 3-3. Optical and SEM Photographs of Mode I DCB Interlaminar Tension Fracture in 49/3501-6 Kevlar/Ep - [0]_{24T}, Conditioned 180 F Dry, ~ Weeks Before Test

(a) Macro photograph of Fracture

(b) Fiber Pull-Out

(c) River Patterns (R) and Hackles (H) in Precrack Region

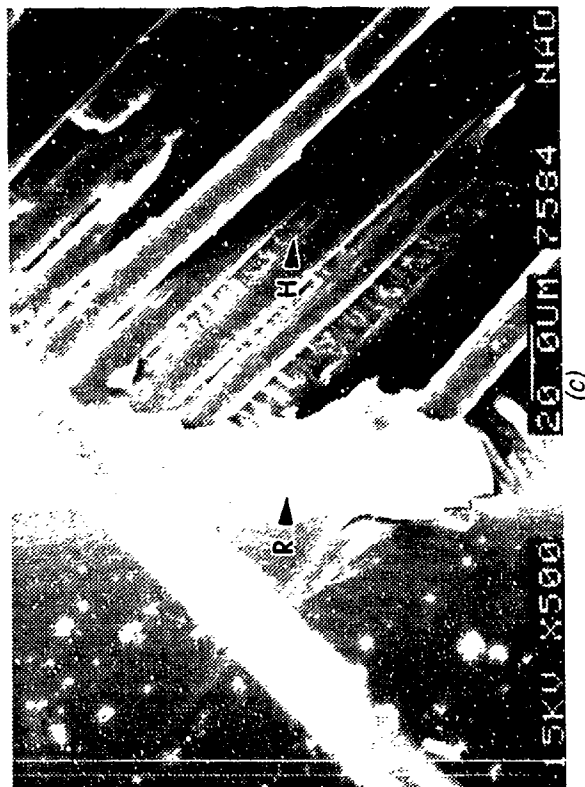
CD = Crack-propagation direction



(a)



(b)



(c)

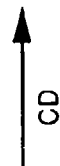
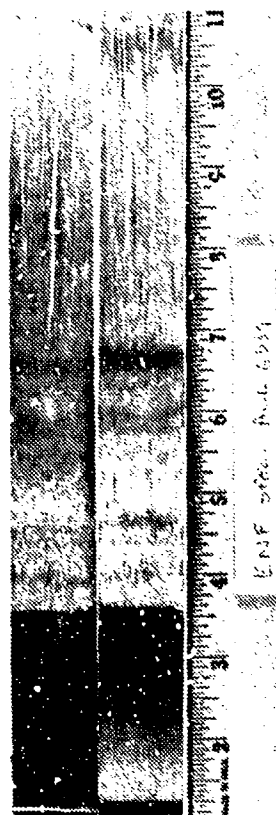


Figure 3-4. Optical and SEM Photographs of Mode I DCB Interlaminar Tension Fracture in 49/3501-6 Kevlar/Ep - [$+45/0/-45$]_{4s}, Water Immersed Before Test
 (a) Macrofracture of Fracture
 (b) Fiber Pull-Out
 (c) Rivers (R) and Hackles (H) in Fractured Resin
 CD = Crack propagation direction

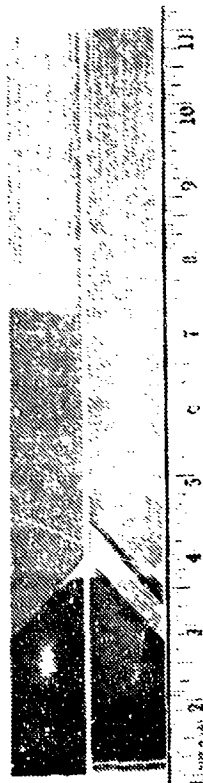


(a)

CD
↑

Figure 3-5. Optical and SEM Photographs of Mode II ENF Interlaminar Shear Fracture in 49/3501-6 Kevlar/Ep - [0]_{24T}, Room Temperature Ambient
(a) Macroscopic Photograph of Fracture
(b) Precrack Region Showing Fibrils
(c) River Patterns in Precrack Region (Arrow)

CD = Crack-propagation direction



(a)

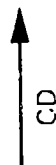


Figure 3-6. Optical and SEM Photographs of Mode II ENF Interlaminar Shear Fracture in 49/3501-6 Kevlar/Ep - [+45/0/-45]_s, Room Temperature Ambient

(a) Macrograph of Fracture

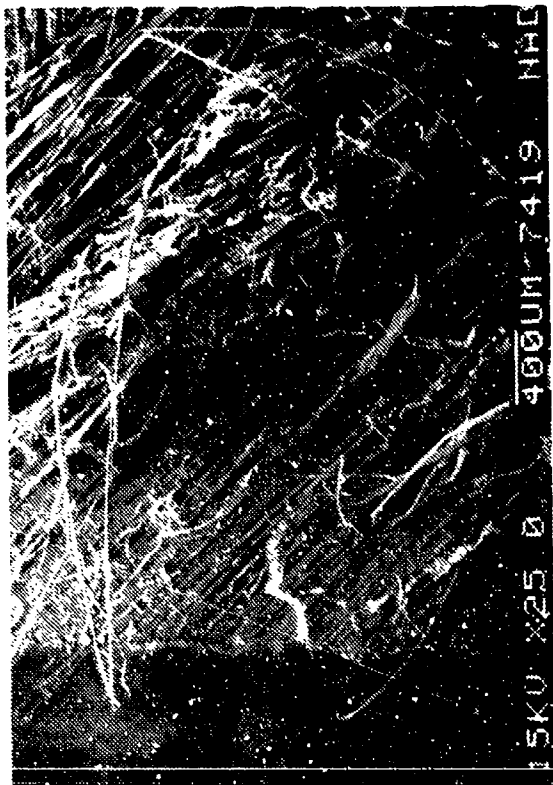
(b) Precrack Showing Fibrils

(c) Peeli (Hackles and Rivers) in Precrack Region

H = Hackles

R = Rivers

C/D = Crack propagation direction



(b)



(c)

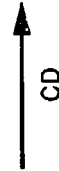
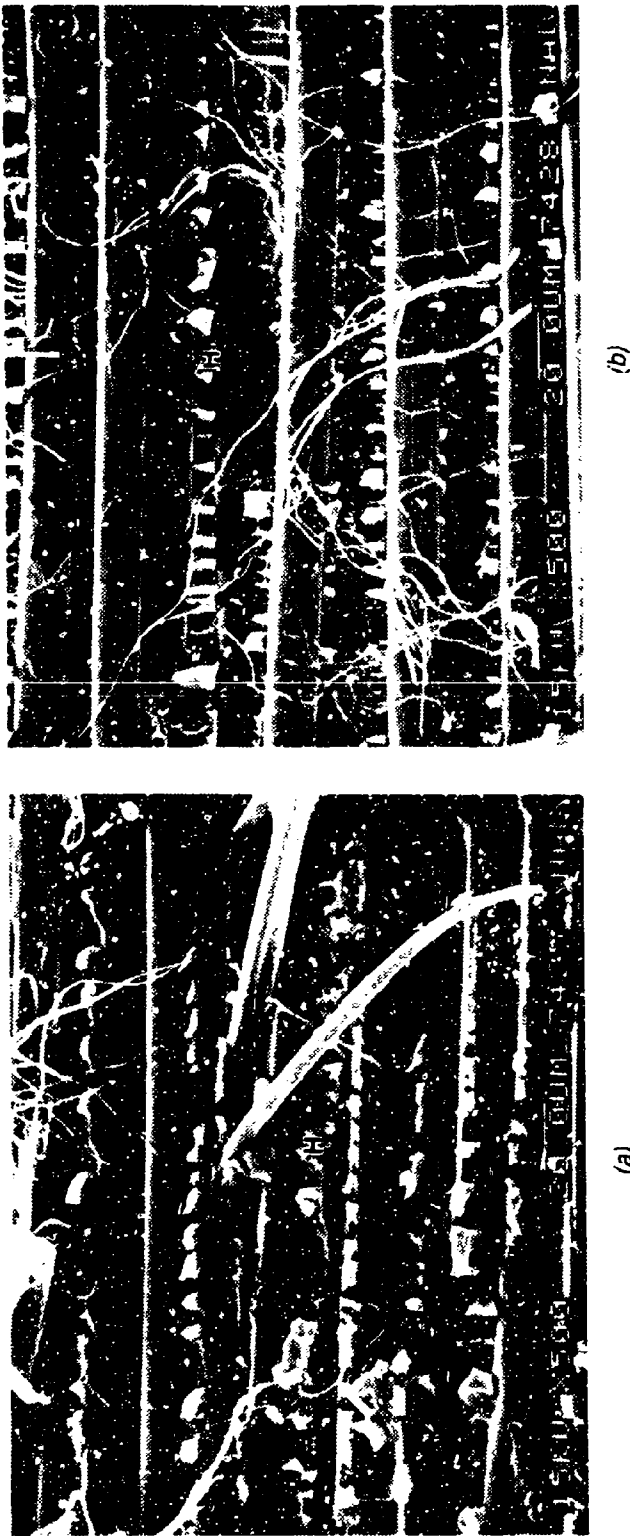


Figure 3-7. SEM Photographs of Mode II ENF Shear Crack-Growth Regions in 49/3501-6 Kevlar/Ep, Room Temperature Ambient
 (a) $[0]_{24T}$ Specimen
 (b) $[-45/0/-45]_{4S}$ Specimen
 CD = Crack-propagation direction
 H = Hackles

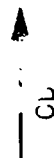


Figure 3-8. Optical and SEM Photographs of Mode II ENF Interlaminar Shear Fracture in 49/3501-6 Kevlar/Ep - [0]_{24T}. Conditioned 180 F Dry
 (a) Macrophotograph of Fracture
 (b) Precrack Region Showing Fibrils
 (c) Crack Growth Region Showing Hackles (H)

CL = Crack propagation direction

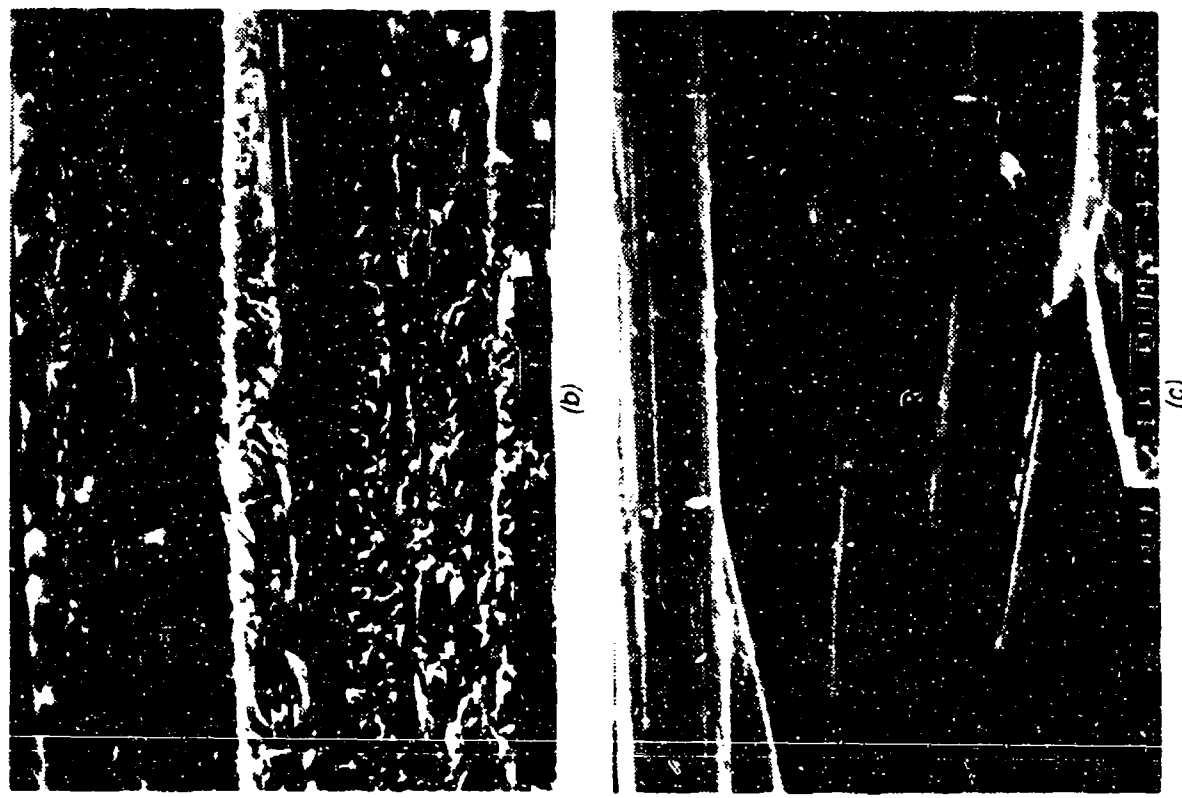


Figure 3-9. Optical and SEM Photographs of Mode I and Mode II MMF Interlaminar Fracture in 49/3501-6 Kevlar/Ep - $[0]_{24T}$. Room Temperature Ambient
 (a) Macro photograph of Fracture
 (b) Fibril Formation in Crack-Growth Region
 (c) River Patterns (R) in Crack-Growth Region Oriented Toward CD
 CD = Crack propagation direction

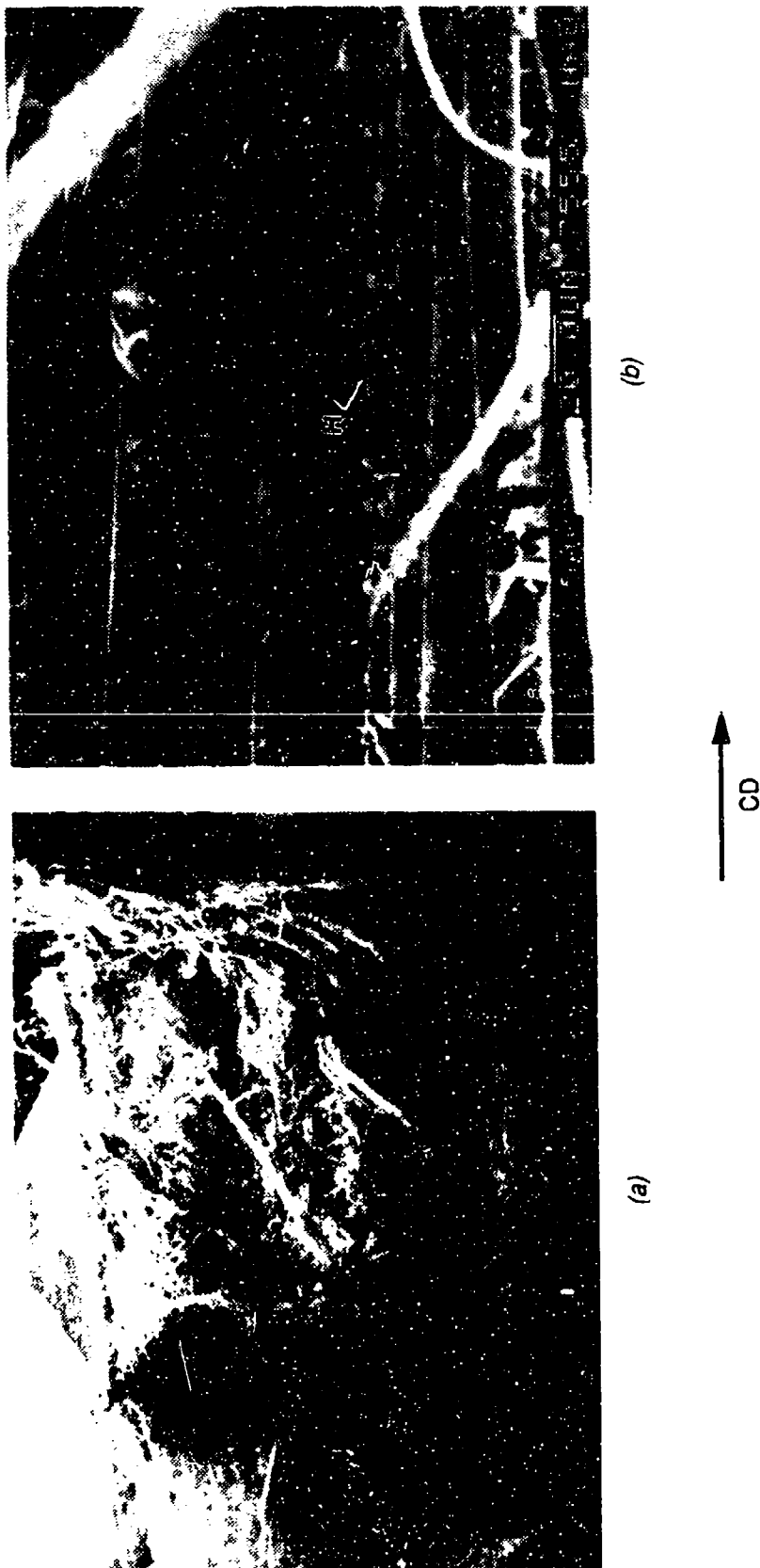


Figure 3-10. SEM Photographs of Mode I Translaminar Tension Fracture in 49/3501-6 Kevlar/Ep - [90/0]₉₀ , Room Temperature Ambient
 (a) Macro photograph Showing Dense Tangles of Fibrils
 (b) High Magnification Photograph Showing Hackles (H)
 CD = Crack propagation direction



(a)

(b)

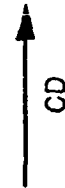


Figure 3-11. SEM Photographs of Mode I Translaminar Tension Fracture in 49/3501-6 Kevlar/Ep - [90/0]_{6s}, Conditioned 180 F Dry
(a) Dense Tangles of Fibrils
(b) Buckling or Piles

CD = Crack-propagation direction



(a)



(b)



(c)

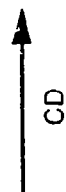


Figure 3-12. SEM Photographs of Mode I Translaminar Compression Fracture in 49/3501-6 Kevlar/Ep [90/0] as, Room Temperature Ambient

(a) Macrophotograph

C = Compression region

T = Tension region

(b) Fiber Ends in Compression Region

(c) Tension Fracture Region

CD = Crack propagation direction

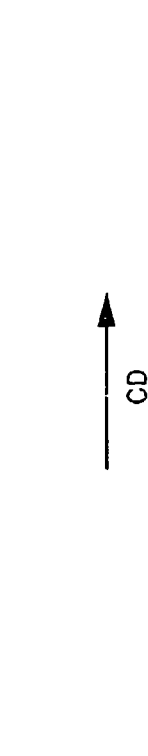


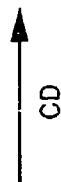
Figure 3-13. SEM Photographs of Mode I Translaminar Compression Fracture in 49/3501-6 Kevlar/Ep - 32 Ply/Quasi-Isotropic, Room Temperature Ambient

(a) Macro photograph
C = Compression region
T = Tension region

(b) Fiber Ends in Compression Region

(c) Hackles (H) in Tension Fracture Region

CD = Crack-propagation direction

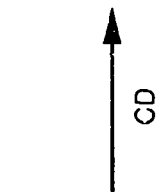




(a)

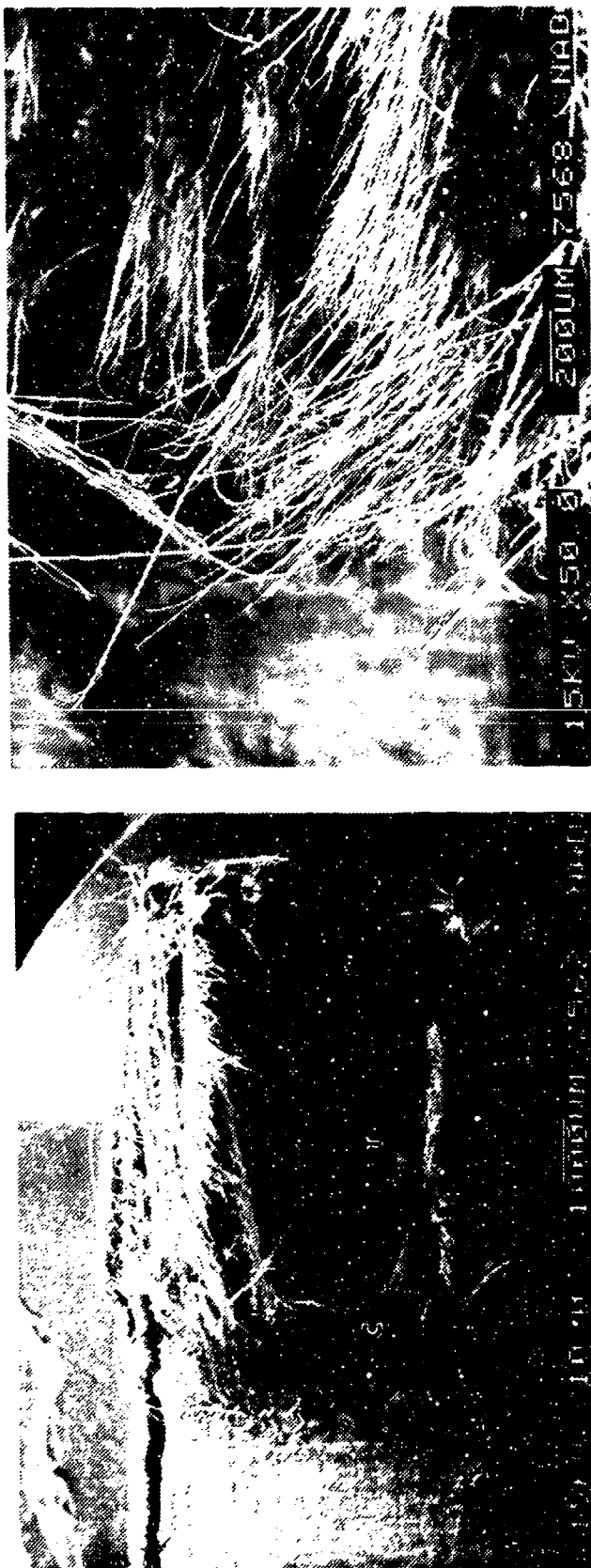


(b)



(c)

Figure 3-14. SEM Photographs of Mode I Translaminar Compression Fracture in 49/3501-6 Kevlar/Ep-[90/0]_{as}. Water Immersed Before Test
 (a) Macro photograph
 C = Compression region
 T = Tension region
 (b) Fiber Ends in Compression Region
 (c) Tension Fracture Region
 CD = Crack-propagation direction



(a)

(b)

CD

Figure 3-15. SEM Photographs of Mode I Translaminar Compression Fracture in 49/3501-6 Kevlar/Ep - 32 Ply/Quasi-Isotropic, Water Immersed Before Test

(a) Macro photograph

C = Compression Region

T = Tension Region

(b) Fiber Ends in Compression Region

CD = Crack propagation direction

SECTION 4
BORON/EPOXY
AVCO 5505/4

Interlaminar Mode I tension and Mode II shear and translaminar tension and compression tests were performed to produce fractures under RT/dry and 270°F/wet conditions. This contribution was made by Boeing.

4.1 INTERLAMINAR MODE I TENSION, RT/DRY

Visual observation of the fracture surface revealed five distinguishable planes of fracture leading to failure at the outer ply. The overall fracture surface span was only 2.5 inches from the crack initiation site. The boron/epoxy laminate exhibited a more complex crack path than those in carbon and glass fiber-reinforced epoxy laminates, mainly due to the resistance of the boron filaments to the crack front.

The fracture feature most frequently observed under the optical microscope was a resin flow line indicating the overall crack growth direction. This feature was similar to a river mark (Figure 4-1). The reflection of light from the boron-tungsten filament made it difficult to see some of the fine details of the critical fracture features.

SEM analysis showed both river marks and resin microflow lines on the fracture surface (Figure 4-2). This indicated that the crack direction could be identified from these microscopic features.

4.2 INTERLAMINAR MODE I TENSION, 270°F/WET

Visual examination revealed a fracture surface on only one or two stepped planes. This was in contrast to the RT specimen, which fractured over many stepped planes. The 270°F/wet condition made the resin ductile and prevented a multiple-plane fracture. The optical photomicrograph showed resin microflow lines similar to those observed in the RT/dry specimen (Figure 4-3).

Figure 4-4 shows the SEM fractographs of the interlaminar Mode I tension specimen exposed to humidity and tested at 270°F. The fracture surface showed river marks in some regions. The major difference between the RT/dry and 270°F/wet specimens was the latter's very poor adhesion at the fiber/matrix interface.

4.3 INTERLAMINAR MODE II SHEAR, RT/DRY

Under visual examination, the fracture surface was dull and milky due to the formation of hackles. This appearance was similar to that observed in previous work on the carbon-fiber reinforced epoxy system. Due to difficulties in creating a large area of interlaminar Mode II shear fracture surface for this material system, we were unable to provide a macrophotograph of the specimen. However, SEM analysis was performed on the available specimen. The fracture feature revealed resembled the hackles typically observed in the model material system, AS4/3501-6 (Figure 4-5).

4.4 INTERLAMINAR MODE II SHEAR, 270°F/WET

Visual examination revealed a fracture surface delaminated at various plies. Hackle formations were observed under the optical microscope (Figure 4-6).

Figure 4-7 illustrates the SEM fractograph of the interlaminar Mode II shear specimen exposed to humidity and tested at 270°F. The fracture surface showed hackles throughout the specimen. Poor fiber/matrix adhesion was observed, which is typical for shear fractures.

4.5 TRANSLAMINAR TENSION, RT/DRY

Visual inspection revealed a region of numerous protruding fibers. The protruding fibers exhibited a white, powder-like texture, and the fibers perpendicular to them were silvery.

The SEM analysis showed that the adhesion at the interface between the boron fibers and the epoxy matrix was poor at the time of the fracture. This was also evidenced by the fiber pullouts (Figure 4-8).

Unlike those in glass and carbon fibers, the radial patterns on the boron fiber ends initiated at the tungsten core/boron interface (Figure 4-9). This phenomenon may be due to the lower interfacial shear strength of the tungsten core/boron interface in comparison with the boron fiber/epoxy interface. The fracture features radiating from the center of the boron-tungsten fiber could not be used to determine the crack surface and propagate from one fiber to another, and the average of the individual crack directions indicated the overall crack direction.

4.6 TRANSLAMINAR TENSION, 270°F/WET

Visual examination revealed a fracture surface with numerous protruding fibers. Under the wide-field macroscope, it was evident that the fracture was fiber-dominated. The fracture surface exhibited many holes in the matrix, indicative of extensive fiber pullout (poor fiber/matrix adhesion). Additionally, the fibers pulled away from the matrix were much longer than those in the RT/dry specimen. This also indicated poor fiber/matrix adhesion (Figure 4-10).

The resin around the boron filaments exhibited such features as river marks that could be used for crack mapping. The fracture features on the fiber ends appeared similar to the features observed on the translaminar tension RT/dry specimen. The radial pattern could not be used to

determine the overall crack direction. The fiber surfaces were smooth and there were no traces of residual resin.

Further studies may need to be conducted to determine whether radial patterns on the boron fiber ends or the resin fracture features around the boron filament are usable for crack direction indication or crack mapping.

4.7 TRANSLAMINAR COMPRESSION, RT/DRY

Visual observation revealed numerous protruded boron-tungsten filaments. SEM analysis shown in Figures 4-11 and 4-12 confirmed the visual result. Unlike the glass and carbon fibers, the boron-tungsten fibers exhibited similar fracture features in both tension and compression specimens. This may be due to the higher ductility of the boron-tungsten fibers in comparison with the glass and carbon fibers. This eliminates the microbuckling effects (from compression) typically exhibited in fibers with higher stiffness. The neutral axes observed on the glass and carbon fiber ends were not present on the boron-tungsten translaminar compression specimen tested under RT/dry condition.

4.8 TRANSLAMINAR COMPRESSION, 270°F/WET

Visual examination revealed a fracture surface with numerous protruding fibers, similar to the fracture surface of the tension specimen. The ends of the boron filaments exhibited radial patterns similar to those of the translaminar compression RT/dry specimen (Figure 4-13). Boron fiber pullouts exhibited little residual resin on the fiber due to weak fiber/matrix adhesion; also, the boron fiber surface was not as smooth as is typical of carbon fiber (Figure 4-14). This is due to the chemical deposition process of boron onto the tungsten core. The neutral axes typically observed on glass and carbon fiber ends, a result of microbuckling, were not present on the boron-tungsten translaminar compression specimen tested under 270°F/wet conditions.

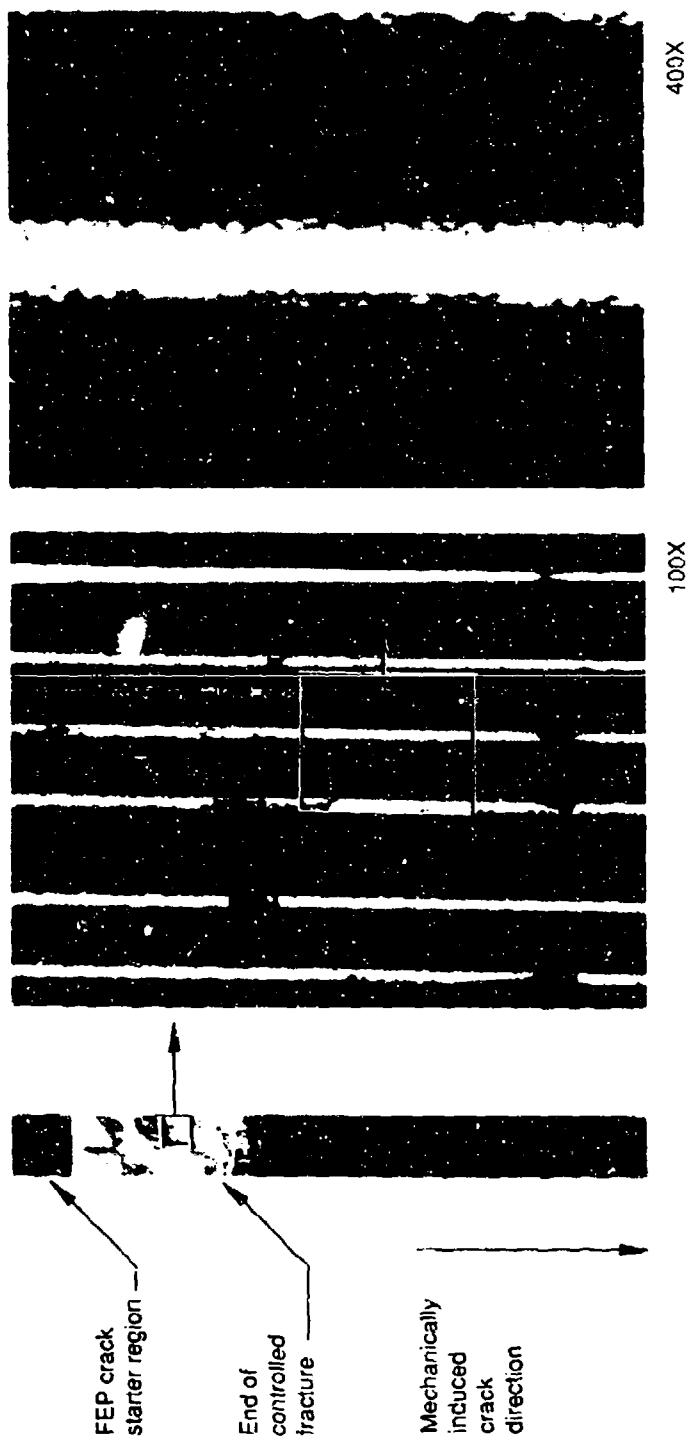
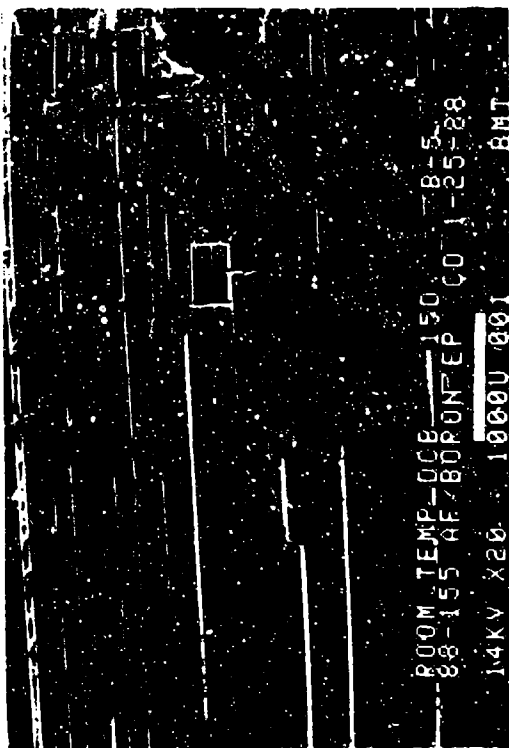
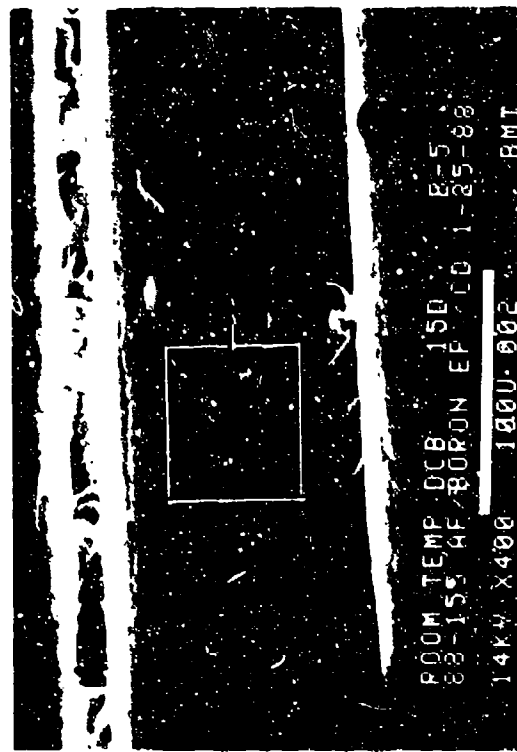


Figure 4-1. Optical Photomicrographs of Room Temperature/Dry, Interlaminar Mode I Tension, 0/90 Fracture in Boron/Epoxy



15 degree tilt

20X



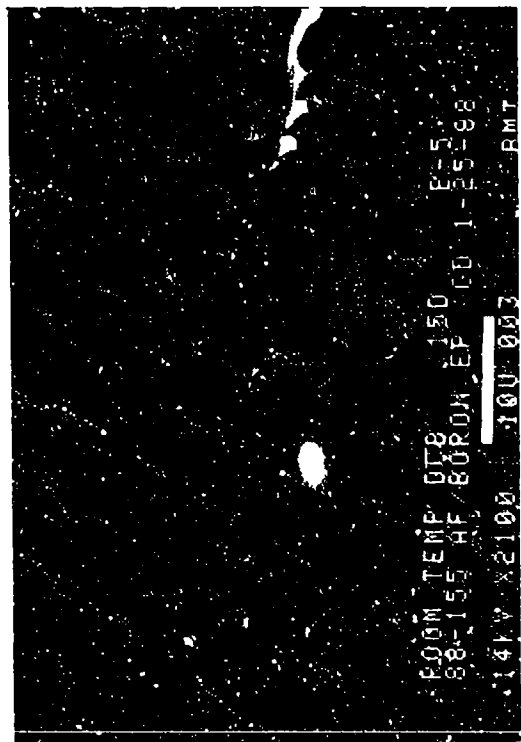
15 degree tilt

400X

Legend:

B boron-tungsten filament
R rivermark

Mechanically induced
crack direction



15 degree tilt

2,000X

Figure 4.2. SEM Fractographs of Room Temperature/Dry, Interlaminar Mode I Tension, 090 Fracture in Boron/Epoxy

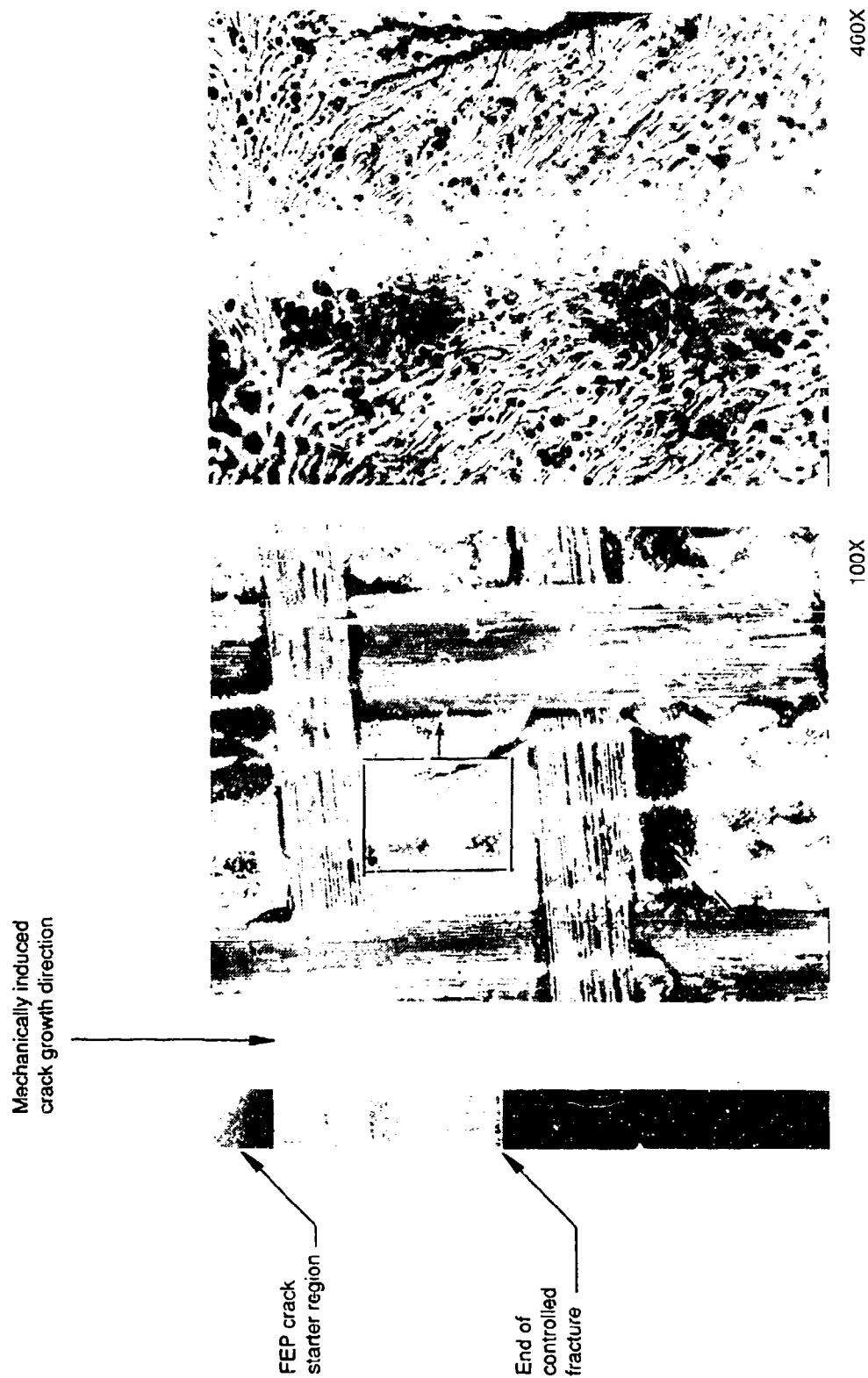
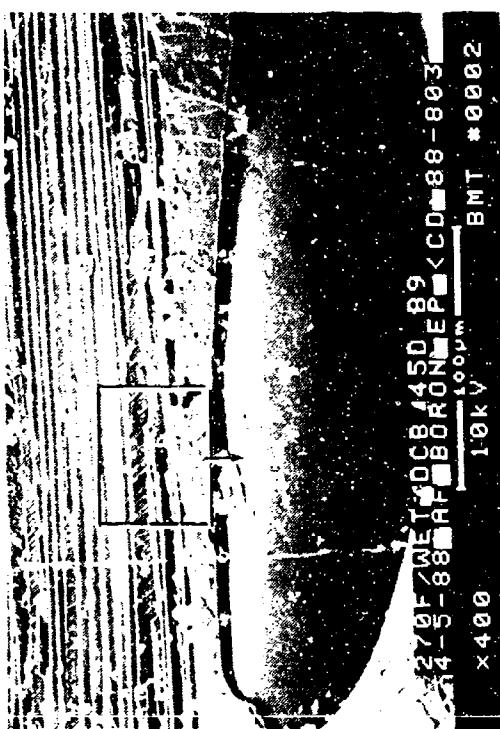


Figure 4-3. Optical Photomicrographs of 270 F/Wet, Interlaminar Mode I Tension, 0/90 Fracture in Boron/Epoxy



45 degree tilt (a) 20X



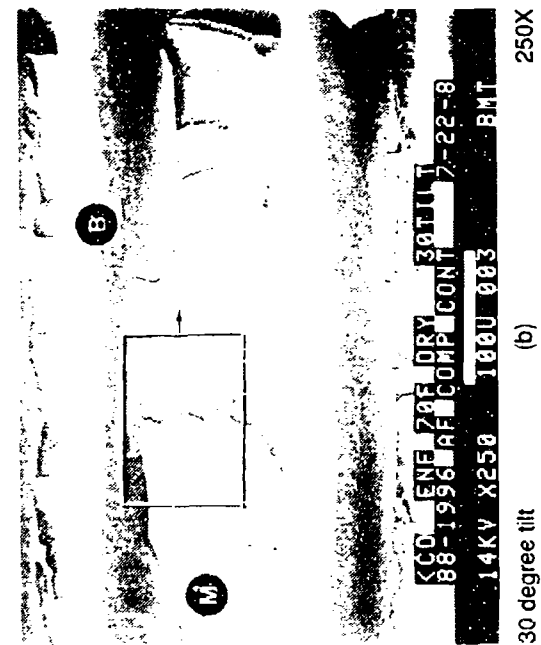
45 degree tilt (b) 400X

45 degree tilt (c) 200X

45 degree tilt (d) 2,000X

Mechanically induced crack direction

Figure 4-4. SEM Fractographs of 270 F/Wet, Interlaminar Mode I Tension, 0/90 Fracture in Boron/Epoxy



Legend:

- B boron filament
- M matrix fracture

Mechanically induced crack direction

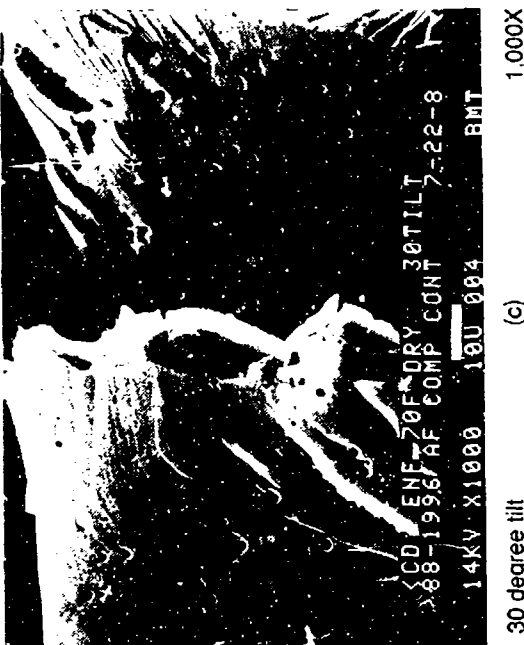


Figure 4-5. SEM Fractographs of Room Temperature/Dry, Interlaminar Mode II Shear, 0/90 Fracture in Boron/Epoxy

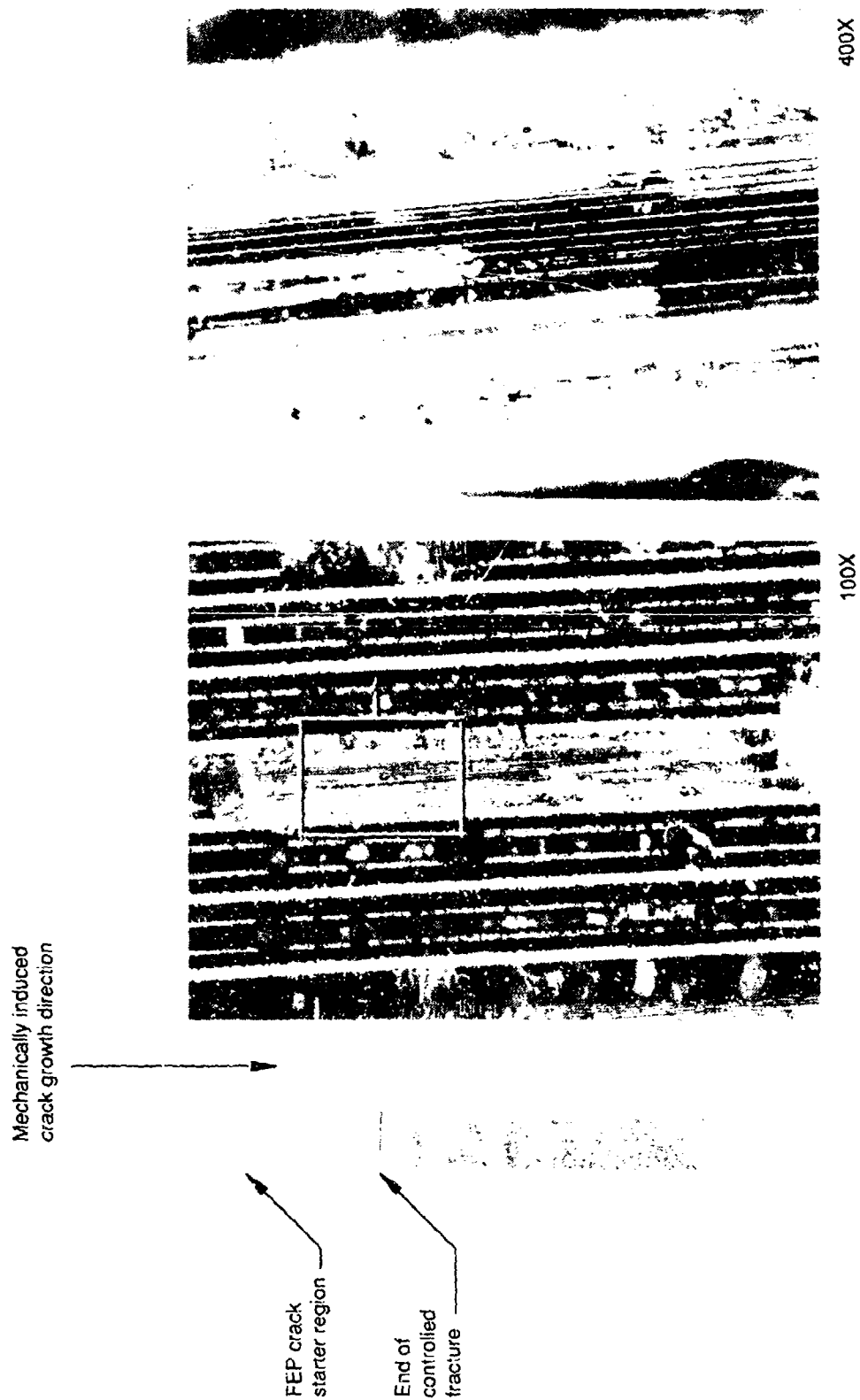
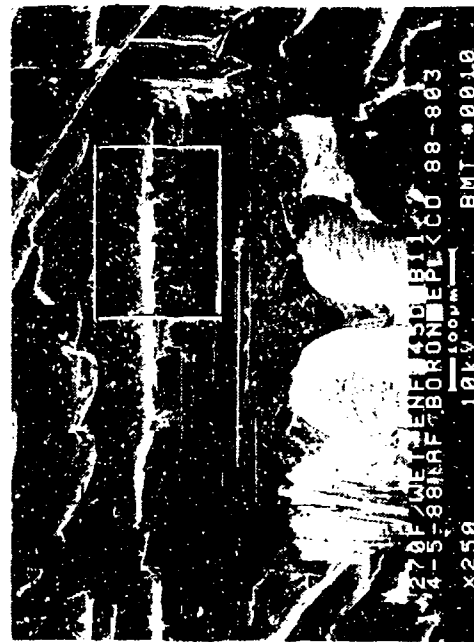


Figure 4-6. Optical Photomicrographs of 270 F/Wet, Interlaminar Mode II Shear, 0/90 Fracture in Boron/Epoxy



45 degree tilt (b) 50X



45 degree tilt (b) 250X

Mechanically induced
crack direction



45 degree tilt (c) 1,000X

Figure 4-7. SEM Fractographs of 270 F/Wet, Interlaminar Mode II Shear, 0/90 Fracture in Boron/Epoxy



40 degree tilt

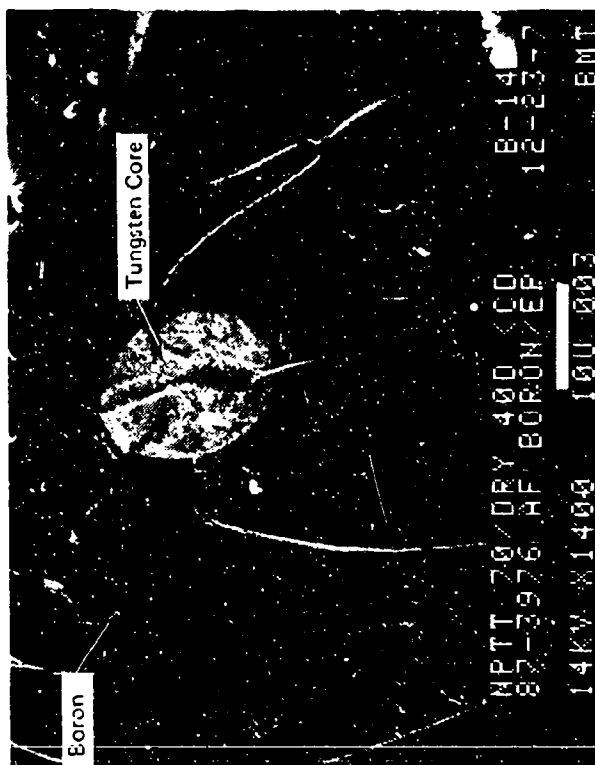
21X

Mechanically induced
crack direction



40 degree tilt

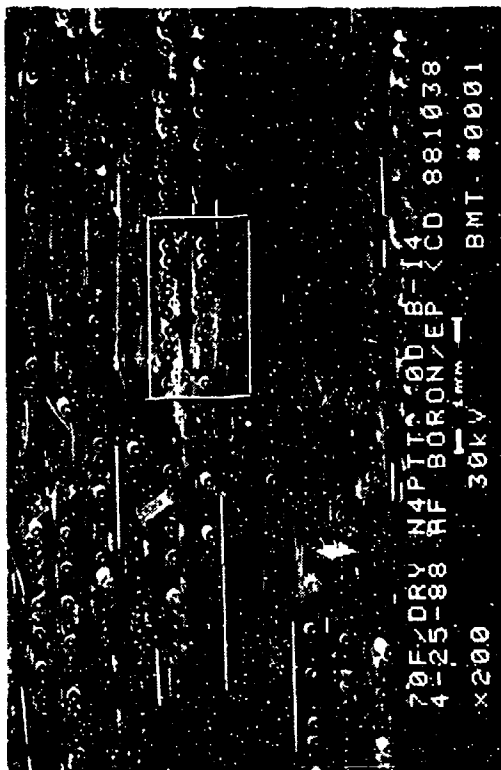
400X



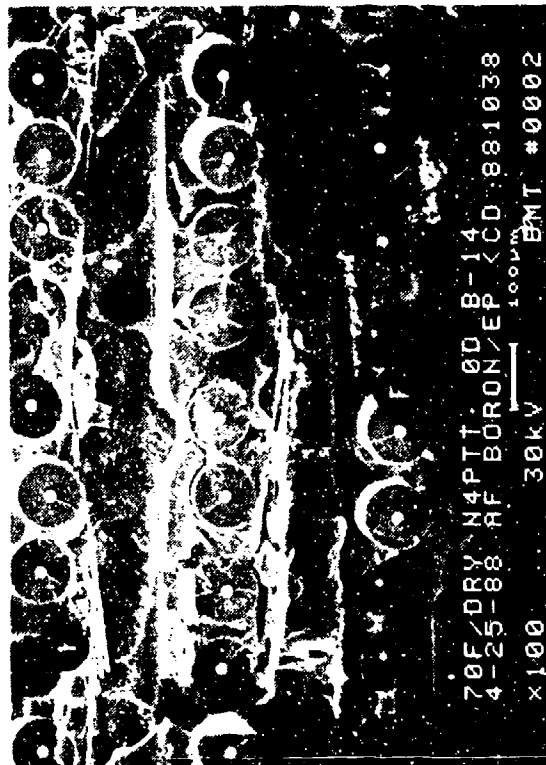
40 degree tilt

1,400X

Figure 4-8. SEM Fractographs of Room Temperature/Dry, Translaminar Tension, 0/90 Fracture in Boron/Epoxy



0 degree tilt (a) 20X

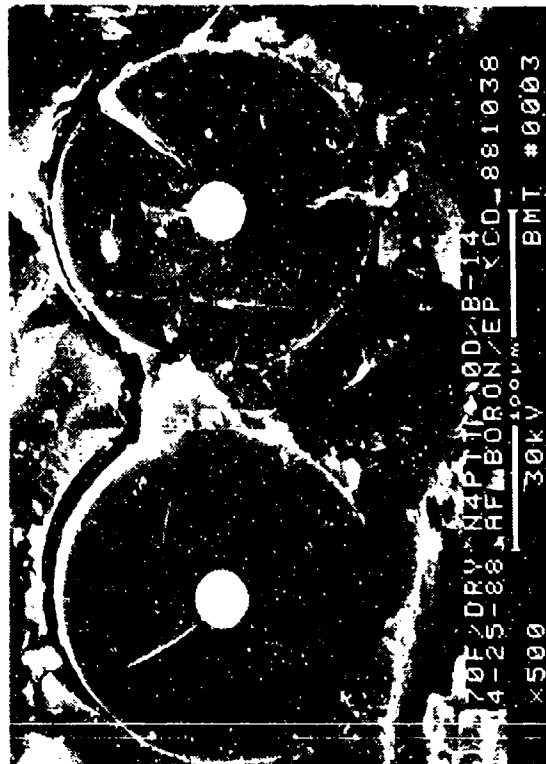


0 degree tilt (b) 100X

Legend:

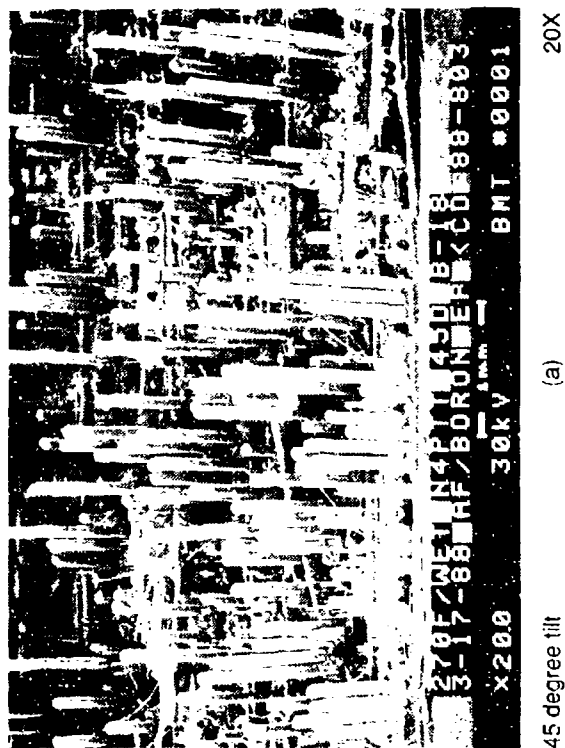
- P fiber pullout
- F fiber end fracture
- M matrix fracture

Mechanically induced
crack direction

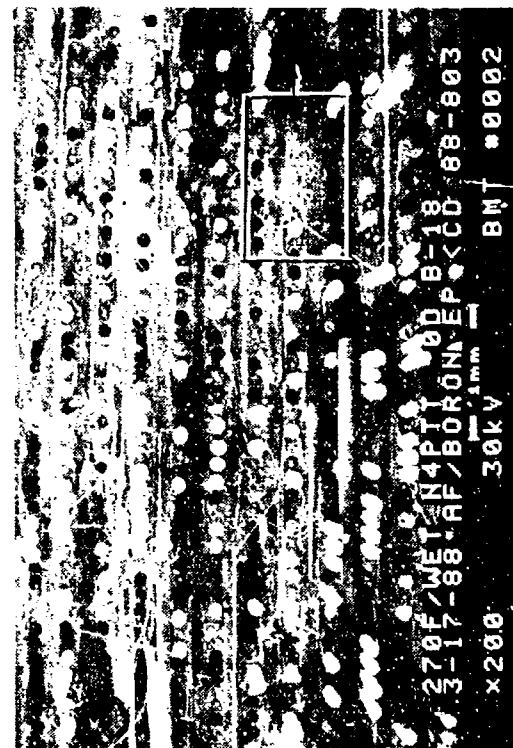


0 degree tilt (c) 500X

Figure 4-9. SEM Fractographs of Room Temperature/Dry, Translaminar Tension, 0/90 Fracture in Boron/Epoxy (0 Degree Tilt)



(a)



(b)

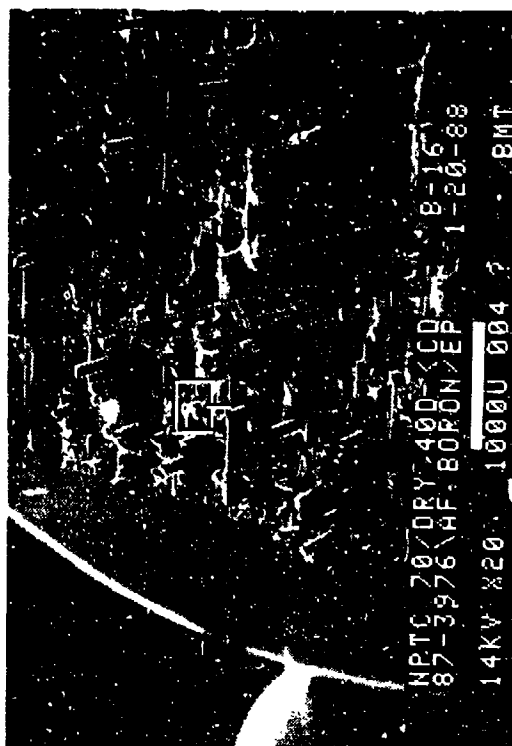
Mechanically induced
crack direction

Interlaminar resin fracture
(i.e. rivermarks)



(c)


Figure 4-10. SEM Fractographs of 270 F/Wet, Translaminar Tension, 0/90 Fracture in Boron/Epoxy (45 and 0 Degree Tilts)



40 degree tilt

20X

Mechanically induced
crack direction




40 degree tilt

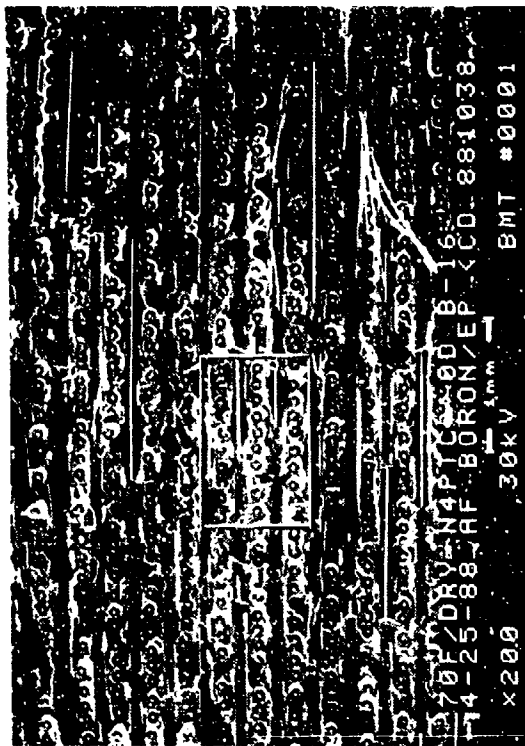
400X



40 degree tilt

1,000X

Figure 4-11. SEM Fractographs of Room Temperature/Dry, Translaminar Compression, n/90 Fracture in Boron/Epoxy (40 Degree Tilt)

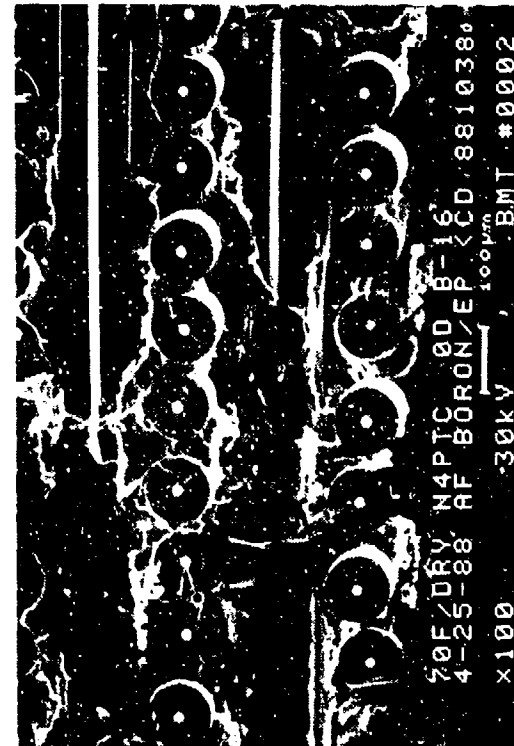


0 degree tilt

(a)

20X

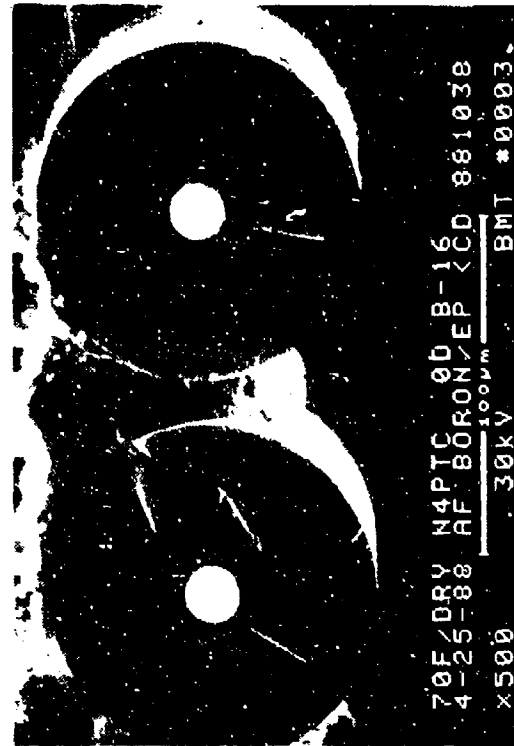
Mechanically induced
crack direction



0 degree tilt

(b)

100X

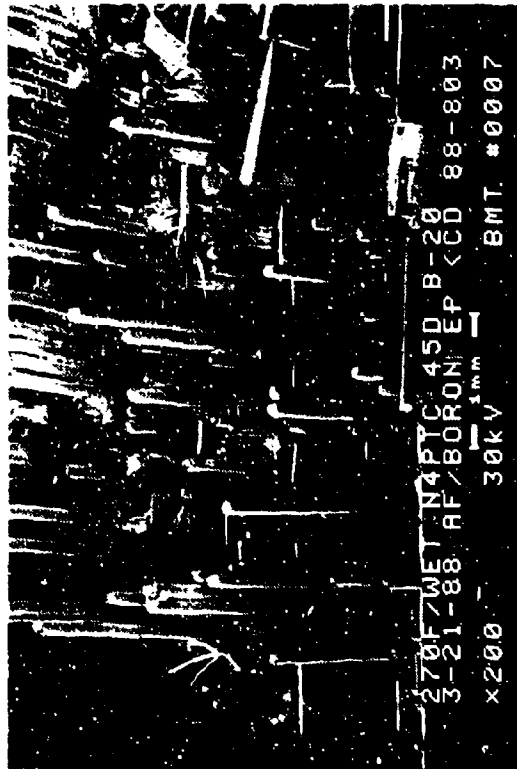


0 degree tilt

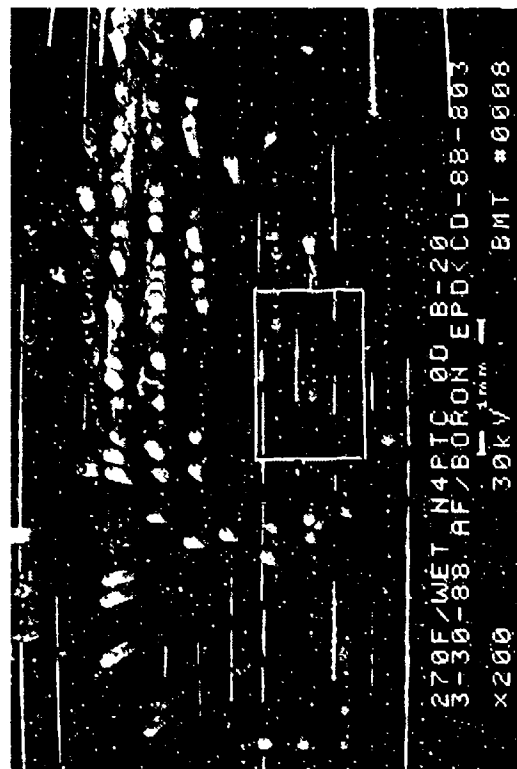
(c)

500X

Figure 4-12. SEM Fractographs of Room Temperature/Dry, Translaminar Compression, 0/9C Fracture in Boron/Epoxy (0 Degree Tilt)



45 degree tilt (a) 20X



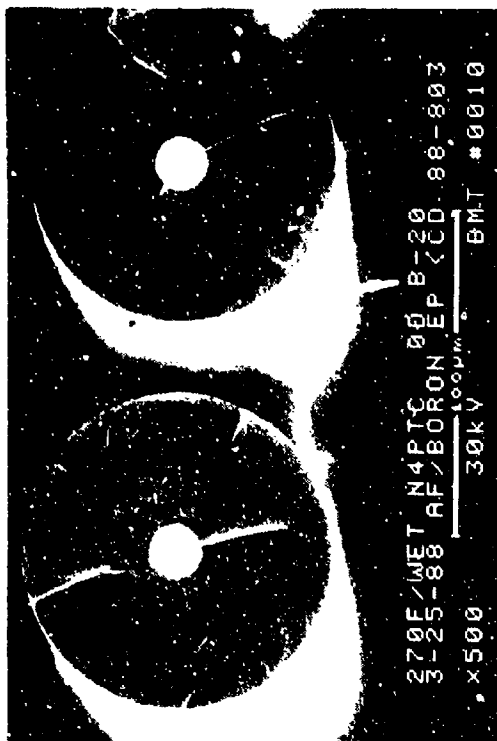
0 degree tilt (b) 20X

Mechanically induced
crack direction



0 degree tilt (c) 100X

Figure 4-13. SEM Fractographs of 270 FWet, Translaminar Compression, 0/90 Fracture in Boron/Epoxy

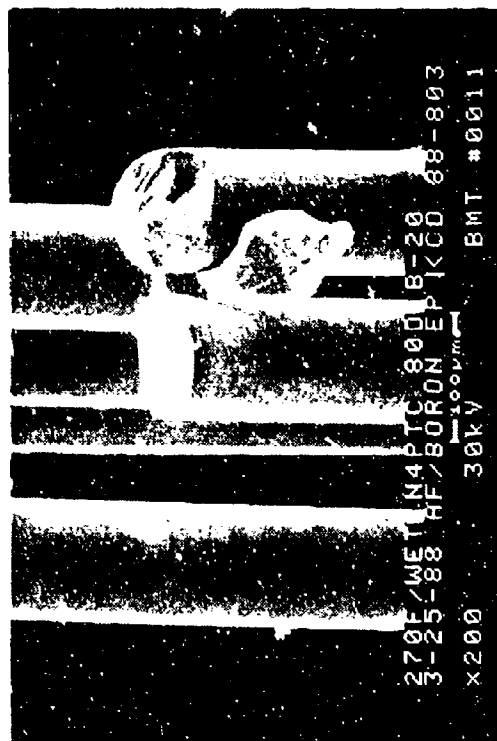


0 degree tilt

(a)

500X

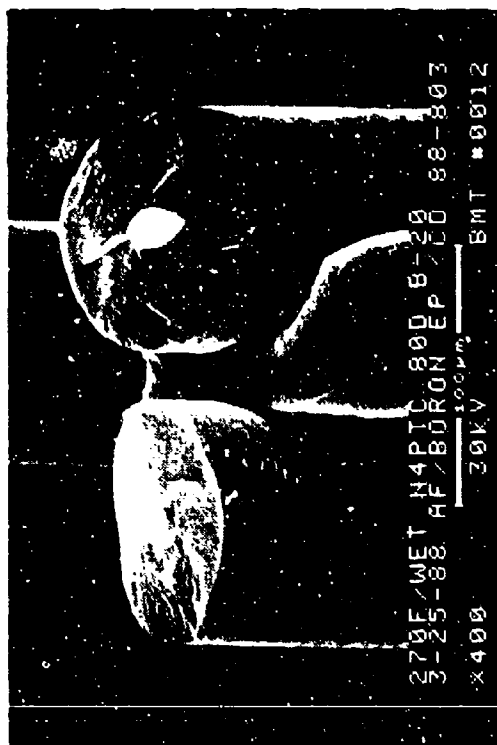
Mechanically induced
crack direction



80 degree tilt

(b)

200X



80 degree tilt

(c)

400X

Figure 4-14. SEM Fractographs of 270 F/Wet, Translaminar Compression, 0/90 Fracture in Boron/Epoxy (High Magnification)

SECTION 5
FIBERGLASS/EPOXY
HEXCEL E-GLASS/F155

Interlaminar Mode I tension and Mode II shear and translaminar tension and compression tests were performed to produce fractures under RT/dry and 200°F/wet conditions. This contribution was made by Boeing.

5.1 INTERLAMINAR MODE I TENSION, RT/DRY

Visual observation of the fracture revealed a smooth, glassy surface. Optical photomicrographs were not taken because of the transparency of the fiberglass/epoxy. Cleavage markings (river marks), typically seen in Mode I tension fractures of carbon fiber reinforced epoxies were observed under the SEM (Figure 5-1). These features were usually observed at the nodes where the weaves overlap one another. The fiber/matrix adhesion appeared to be poor at some locations. This is due to the low inherent interfacial shear strength at the fiberglass/epoxy interface.

5.2 INTERLAMINAR MODE I TENSION, 200°F/WET

Visual inspection of the 200°F/wet fracture revealed a much rougher surface than was observed in the RT/dry specimen. The specimen exhibited more resistance to breakage than the RT/dry specimen, as evidenced by specimen end deflection and incomplete fracture into two halves. The resistance of the 200°F/wet specimen to fracture may be due to the increased toughness of the resin matrix due to moisture exposure.

Figure 5-2 shows the SEM fractographs of the interlaminar Mode I tension, 200°F/wet specimen. Fiber/matrix adhesion was poor as evidenced by the smoothness of the fiber surface. Unlike the RT/dry specimen, this specimen, did not exhibit well-defined river marks indicating the crack direction. Instead, the surface showed taffy-pull hackles commonly seen in ductile resin matrices such as thermoplastics.

5.3 INTERLAMINAR MODE II SHEAR, RT/DRY

Visual observations of the fracture revealed a rough, . . . surface. There was evidence of surface ripples, running parallel to the direction of the crack growth, which could be used to identify shear mode fracture during macroscopic evaluation. This feature was not seen in any

other material system evaluated in this program. The surface ripples were observed only under oblique lighting.

SEM analysis (Figure 5-3) revealed a rough fracture surface consisting of large numbers of hackles, which appear similar to the platelets seen in Mode II shear fractures of carbon fiber reinforced epoxies. There was poor adhesion of the fiber/matrix interface at some locations, which was due to the low inherent interfacial shear strength.

Under SEM, the fracture surface appeared very rough and hackles were observed throughout the specimen. Although the Mode I tension fracture showed a cohesive type fiber/matrix fracture in the Mode II shear fracture, there was little resin debris on the fiber/matrix interface.

5.4 INTERLAMINAR MODE II SHEAR, 200°F/WET

Visual examination of the fracture revealed a rough, dull surface. The surface exhibited more of the white powder-like texture feature than the RT/dry specimen. The macroscopic ripples seen in the RT/dry specimen were also seen in the 200°F/wet specimen.

Figure 5-4 shows the SEM fractograph of the fracture surface which appeared rough and showed hackles as observed in the RT/dry specimen. These hackles were much larger, but fewer in number than those seen in the RT specimens.

5.5 TRANSLAMINAR TENSION, RT/DRY

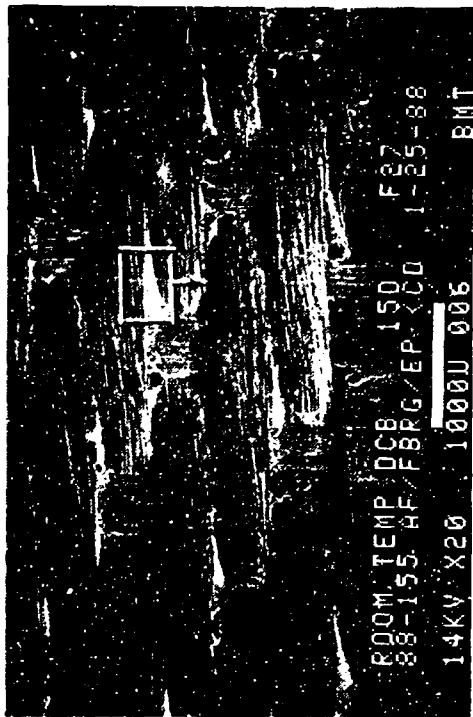
Visual and optical observation revealed a rough topography with protruding fibers of different lengths and directions (Figure 5-5). The surface of the fiber/matrix interface was smooth due to the fibers being pulled away from the matrix. There was evidence of fiber dominated fracture in the large percentage of fiber pullouts. Similar to the carbon fibers, the radial patterns were observed on the glass fiber ends and can be used to determine crack growth direction.

5.6 TRANSLAMINAR COMPRESSION, RT/DRY

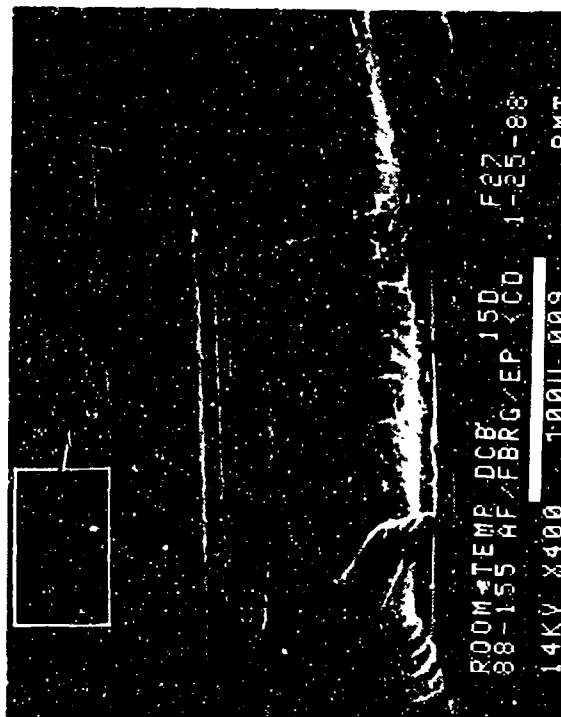
Visual and optical observations revealed a surface with uniform protruding fibers. The fiber/matrix interface showed good adhesion. Figures 5-6 and 5-7 show the SEM fractographs. A neutral axis line dividing the tension and compression regions on the fiber ends was observed.

5.7 TRANSLAMINAR COMPRESSION, 200°F/WET

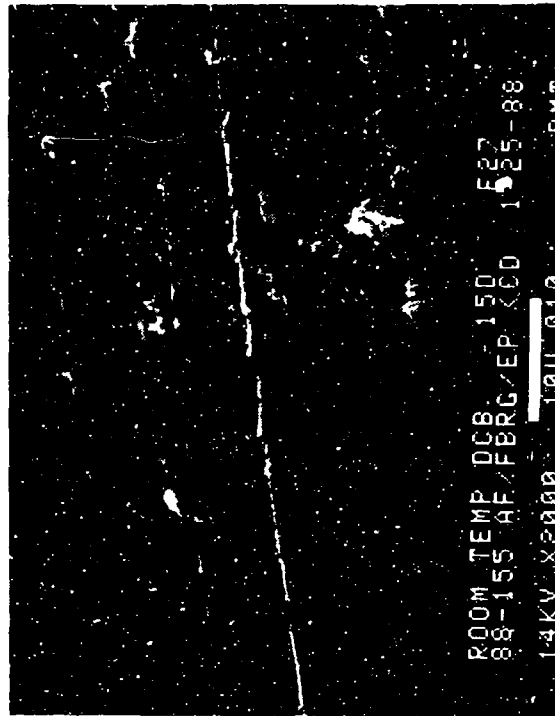
Optical observation of the 200°F/wet specimen revealed a fracture surface like that typically seen in RT/dry translaminar compression specimens. The compression damage occurred in the region just outside of the notch. The typical fracture of a translaminar compression specimen exhibited a flat surface with "chop" marks on the fiber ends (Figure 5-8). Compressively fractured fiber ends show two distinct regions separated by a neutral axis line. This line does not represent any kind of crack direction (Figure 5-9).



15 degree tilt 20X



15 degree tilt 400X



15 degree tilt 2,000X

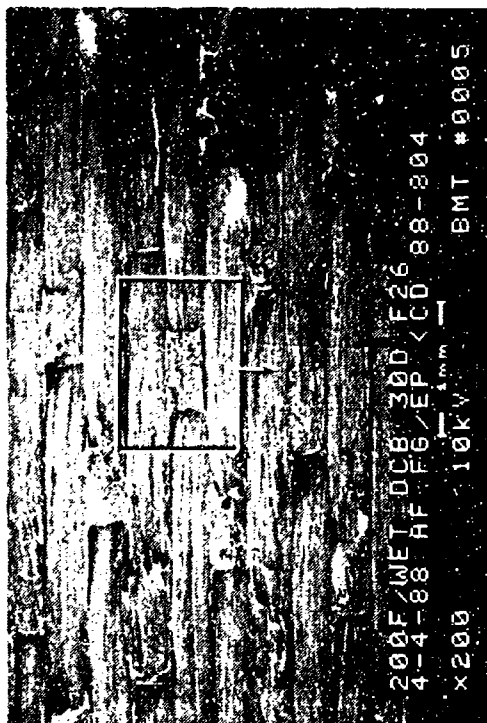
Legend:

F fiber matrix separation
R rivermark

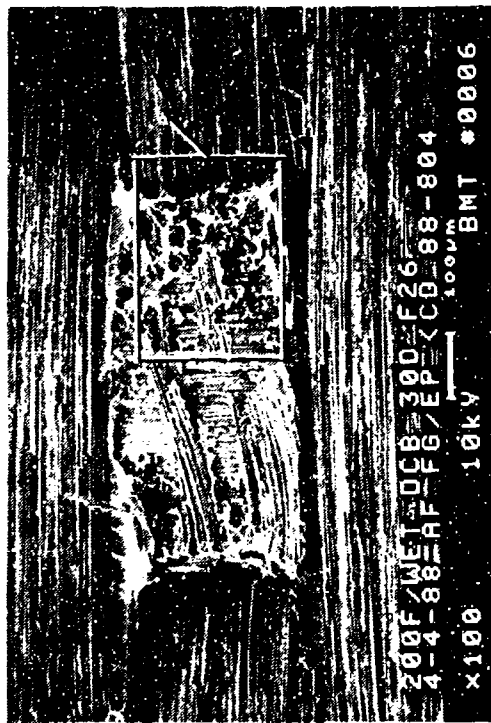
Mechanically induced
crack direction



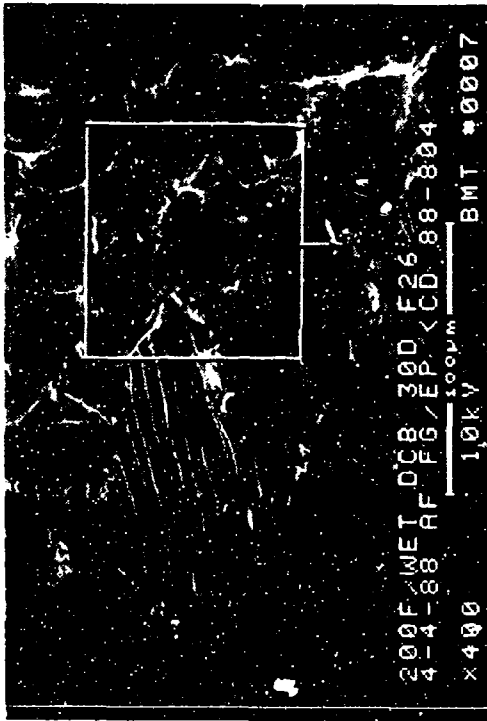
Figure 5-1. SEM Fractographs of Room Temperature/Dry, Interlaminar Mode I Tension, 0/90 Fracture in Fiberglass/Epoxy



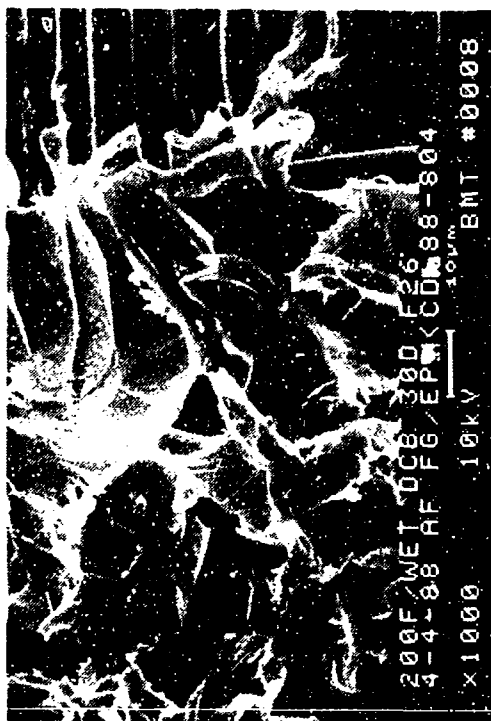
30 degree tilt (a) 20X



30 degree tilt (c) 100X



30 degree tilt (b) 400X



30 degree tilt (d) 1,000X

→ Mechanically induced crack direction

Figure 5-2. SEM Fractographs of 200 F/Wet, Interlaminar Mode I Tension, 0/90 Fracture in Fiberglass/Epoxy



Legend:
F fiber/matrix separation
H hackle

Mechanically induced
crack direction

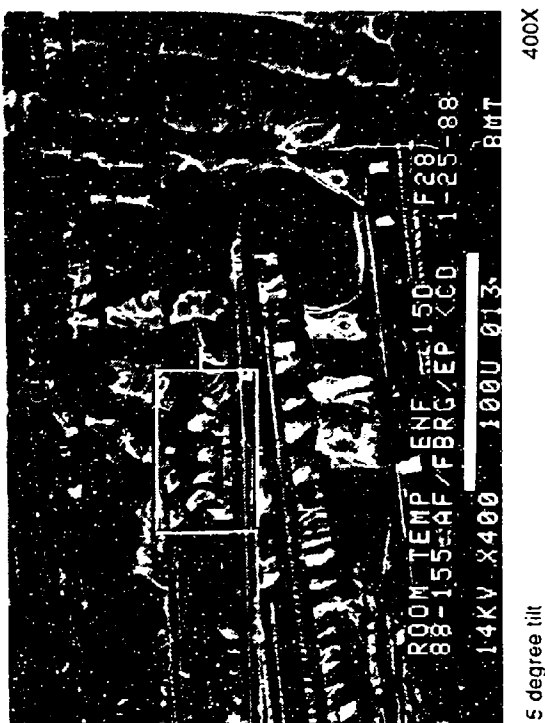
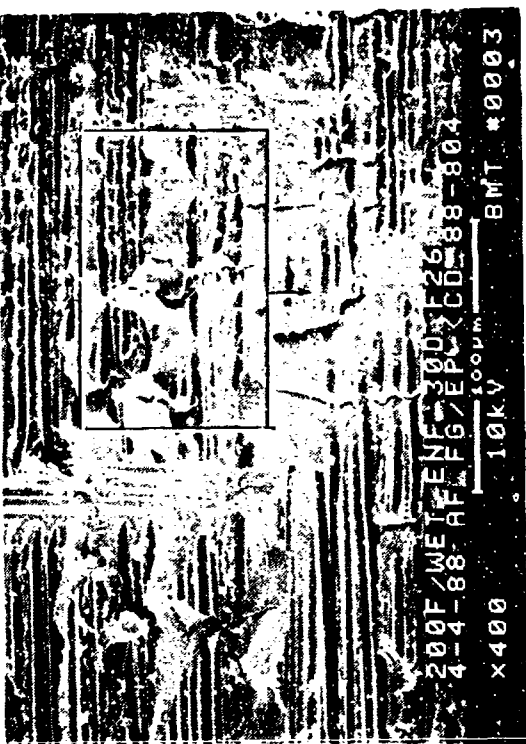


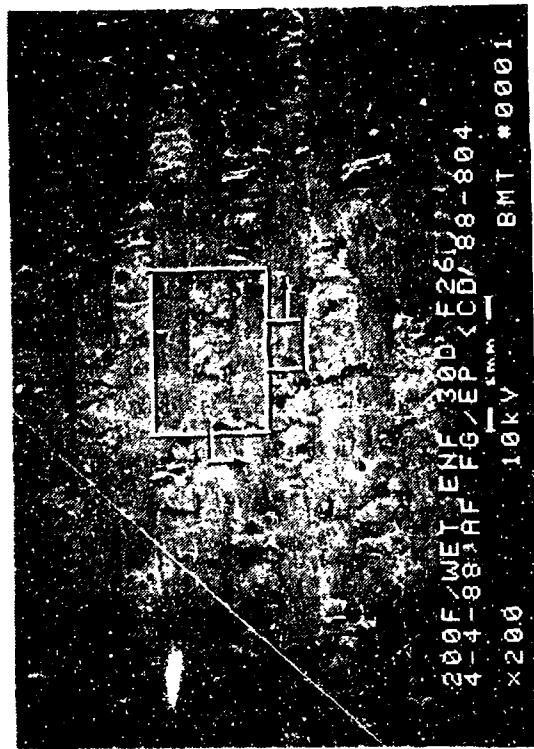
Figure 5-3. SEM Fractographs of Room Temperature/Dry, Interlaminar Mode II Shear, 0/90 Fracture in Fiberglass/Epoxy



(a) 20X 30 degree tilt



(b) 400X 30 degree tilt



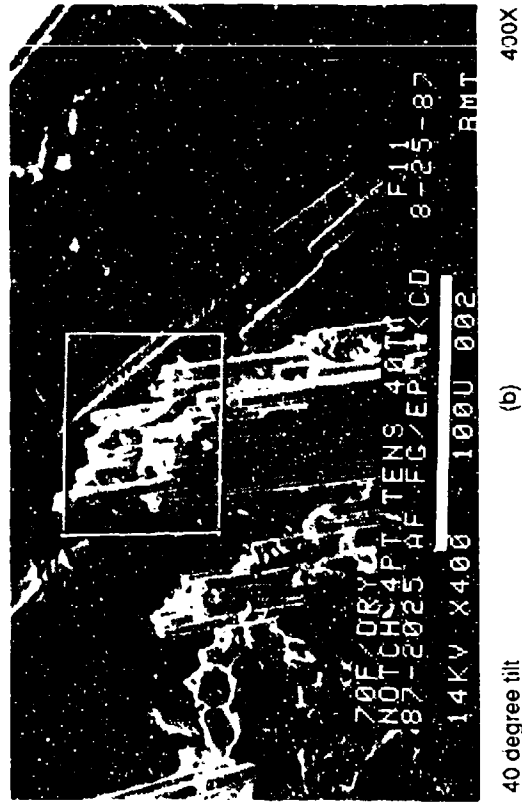
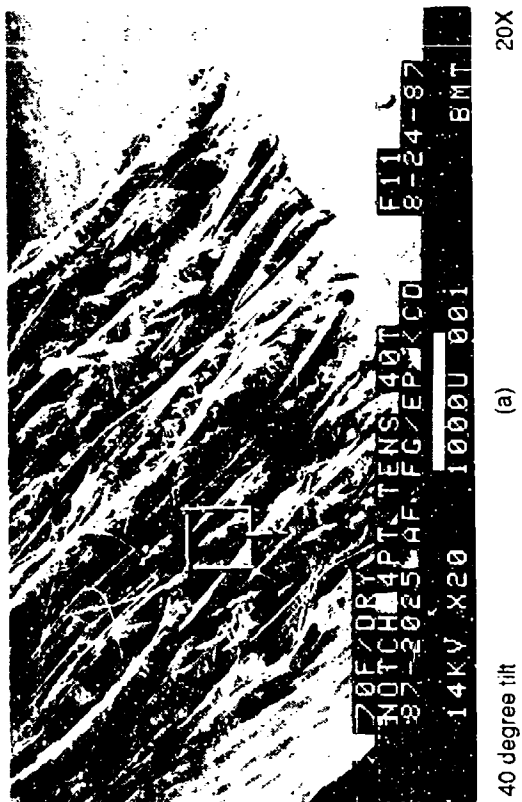
(c) 100X 30 degree tilt



(d) 1,000X 30 degree tilt

————— Mechanically induced crack direction

Figure 5-4. SEM Fractographs of 200 F/Wet, Interlaminar Mode II Shear, 0:90 Fracture in Fiberglass/Epoxy



Note: Higher magnifications of the boxed regions are shown in (c) and (d)

Mechanically induced
crack direction


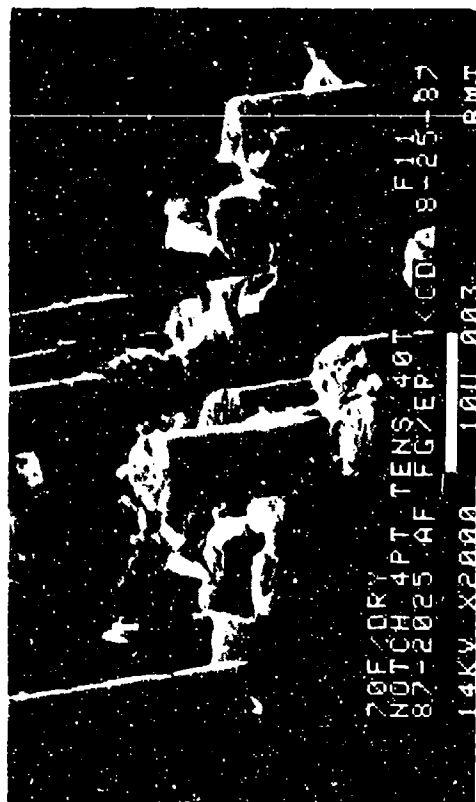


Figure 5-5. SEM Fractographs of 70 F/Dry, Translaminar Tension, 0/90 Fracture in Fiberglass/Epoxy



40 degree tilt (c) 2,000X



15 degree tilt (d) 2,000X

Mechanically induced
crack direction

Figure 5-5. SEM Fractographs of 70 F/Dry, Translaminar Tension, 0/90 Fracture in Fiberglass/Epoxy (Concluded)



0 degree tilt

(a)

250X



0 degree tilt

(b)

2,500X

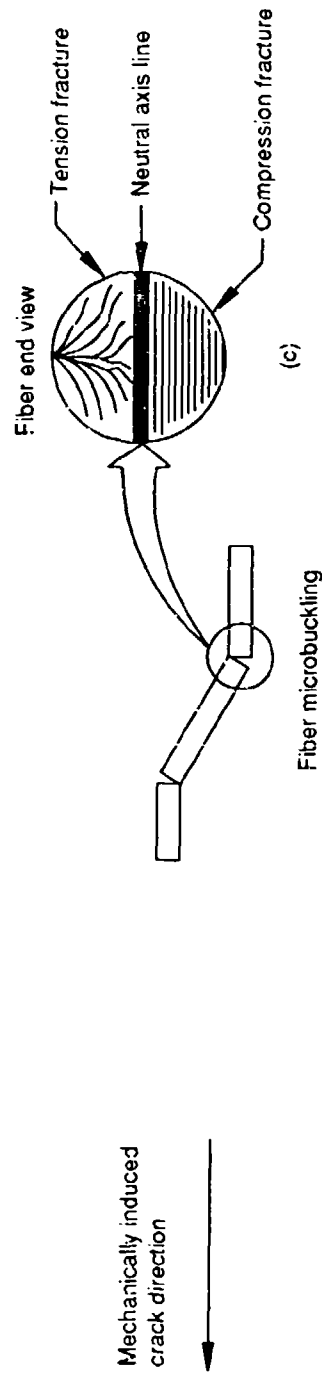
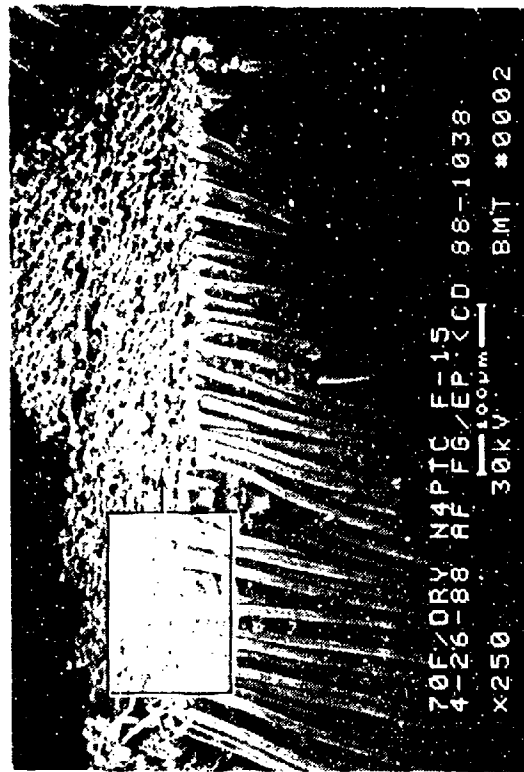


Figure 5-6. SEM Fractographs and Diagram of 70 F/Dry, Translaminar Compression, 0/90 Fracture in Fiberglass/Epoxy (0 Degree Tilt)

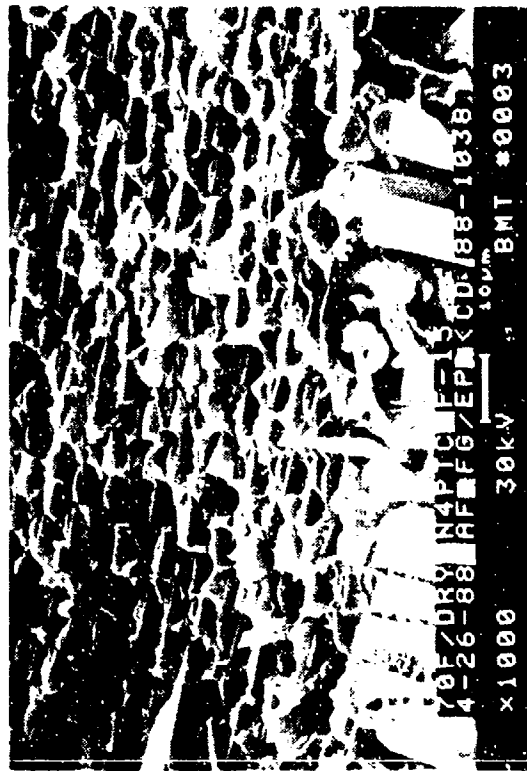


45 degree tilt (a) 20X



45 degree tilt (b) 250X

Mechanically induced
crack direction



45 degree tilt (c) 1,000X

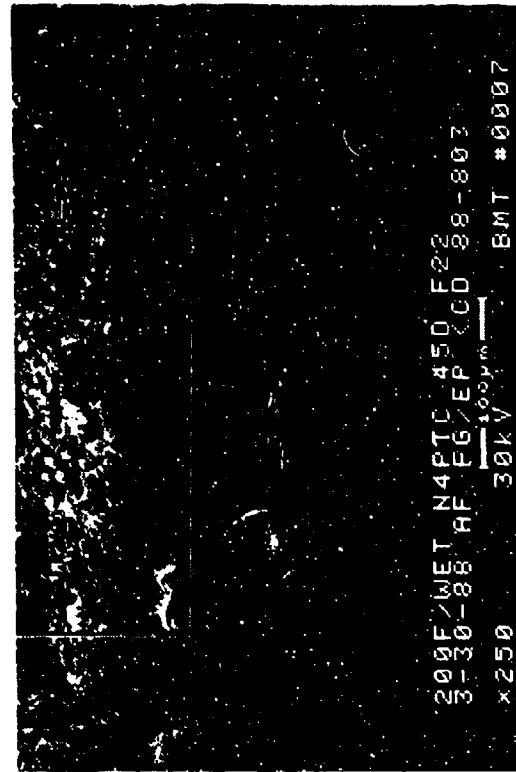
Figure 5-7. SEM Fractographs of 70 F/Dry, Translaminar Compression, 0/90 Fracture in Fiberglass/Epoxy (45 Degree Tilt)

Region representing the
compression damage

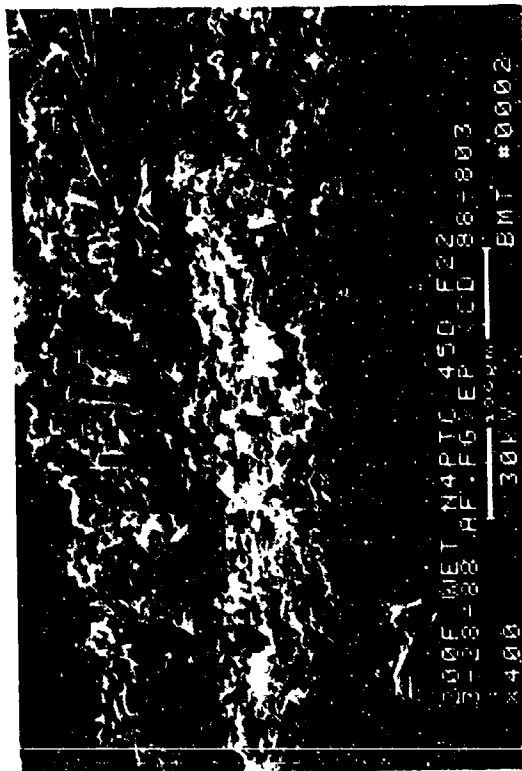


45 degree tilt (a) 20X

Mechanically induced
crack direction

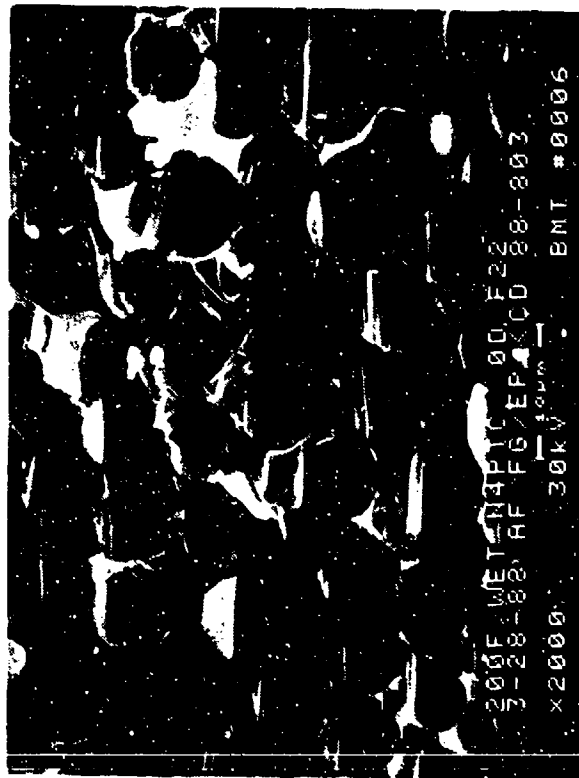


45 degree tilt (b) 250X



(c) 400X

Figure 5-8. SEM Fractographs of 200 F/Wet, Translaminar Compression, 0/90 Fracture in Fiberglass/Epoxy (45 Degree Tilt)



45 degree tilt

(a)

400X

(a)

2,000X

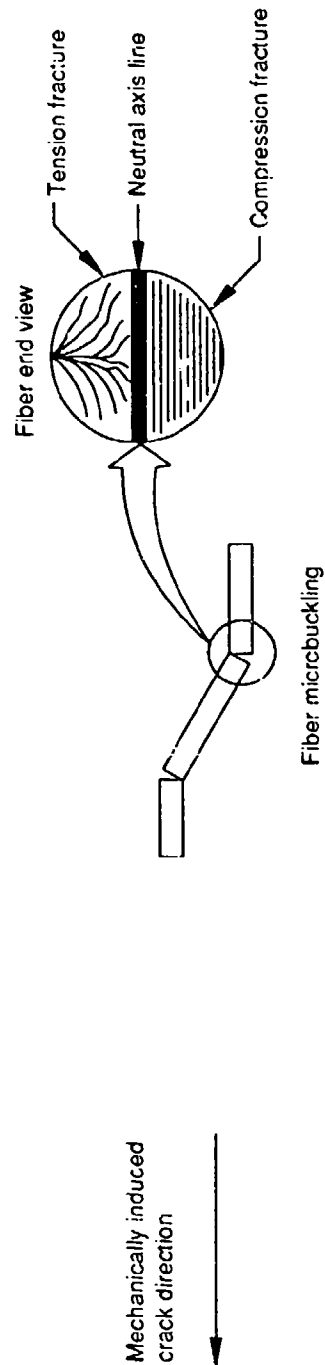


Figure 5-9. SEM Fractographs of 200 F/Wet, Translaminar Compression, 0/90 Fracture in Fiberglass/Epoxy (Higher Magnification)

SECTION 6
GRAPHITE/BISMALEIMIDE
AS4/5250-3

This section presents the results of fractography performed on AS4/5250-3 graphite/bismaleimide (Gr/BMI) test coupons. Gr/BMI systems are being used in several near-term military aircraft that will form part of the Air Force fleet. The tests performed consisted of testing of interlaminar and translaminar fracture test coupons (DCB, ENF, MMF, and bend specimens). The test matrices are shown in Tables 6-1 and 6-2. The results reported include information on the baseline system and processing variable conditions.

Applied load is the principal parameter that affects the fracture surface characteristics in Gr/BMI. Processing variables and water immersion before testing do not significantly alter the fracture characteristics. On a macroscopic scale, interlaminar fracture is characterized by fibers being "pulled out" from the matrix and bare fibers. Interlaminar Mode I tension and Mixed Mode Flexural fractures can be mapped by stray river patterns present in resin-rich areas. Mode II shear is characterized by hackle formation similar to Gr/Ep.

The translaminar fracture features of Gr/BMI are very similar to Gr/Ep. Translaminar tension failures can be mapped by DAF radials on fractured fiber ends, as in Gr/Ep. There are no significant fracture characteristics that can be used to map crack directions in compression failures.

Figures 6-1 through 6-4 provide interlaminar fractographs and Figures 6-5, 6-6 and 6-7 provide translaminar fractographs. This contribution was made by Northrop.

Table 6-1. AS4/5250-3 Gr/BMI Interlaminar Fracture Test Matrix

SPECIMEN, LOADING	VARIABLE CONDITION	LAYUP	LAMINATE DIMENSIONS	NO. OF LAMINATES
Mode I DCB, Tension	RTA	24/0	22 X 16.5	1
Mode I DCB, Tension	Water immer. before test			
Mode II ENF, Shear	RTA			
Mode II ENF, Shear	Water immer. before test			
Mode I + II MMF, Tension + Shear	RTA			

RTA = Room Temperature Ambient
Laminate dimensions in inches

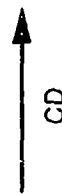
Table 6-2. AS4/5250-3 Gr/BMI Translaminar Fracture Test Matrix

SPECIMEN, LOADING	VARIABLE CONDITION	LAYUP	LAMINATE DIMENSIONS	NO. OF LAMINATES
Mode I Tension, 4 pt. load	RTA	32/90.0	14 X 7	1
Mode I Compression, 4 pt. load	RTA			
Mode I Compression, 4 pt. load	Water immer. before test			
Mode I Tension, 4 pt. load	RTA	32/quasi	8 X 6	1

RTA = Room Temperature Ambient
Laminate dimensions in inches



(a)



CD

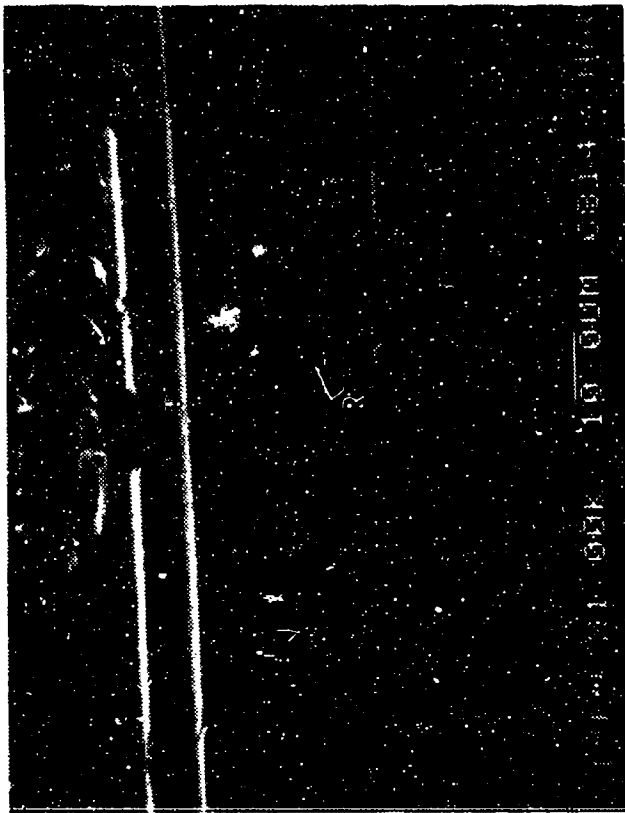
Figure 6-1. Optical and SEM Photographs of Mode I DCB Interlaminar Tension Fracture in AS4/5250-3 Gr/BMI - [0]_{24T}, Room Temperature Ambient
(a) Macro photograph of Fracture
R = River patterns
CD = Crack-propagation direction



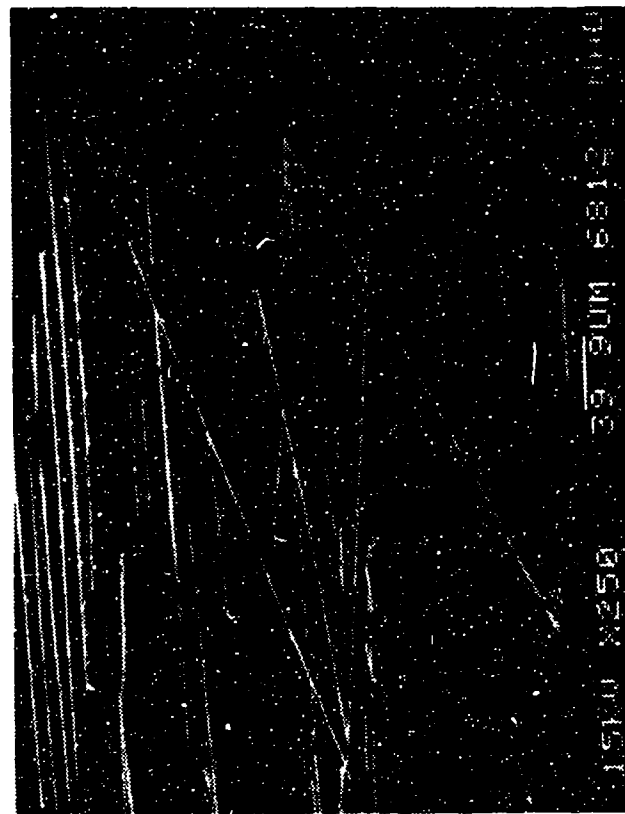
(b)



(c)



(d)



(e)

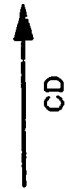


Figure 6-1. (Continued)
 (d) Clean Fibers in Crack-Growth Region
 (e) Stray River Patterns (R) Oriented at an Angle to CD
 CD = Crack-propagation direction



(a)

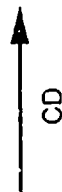
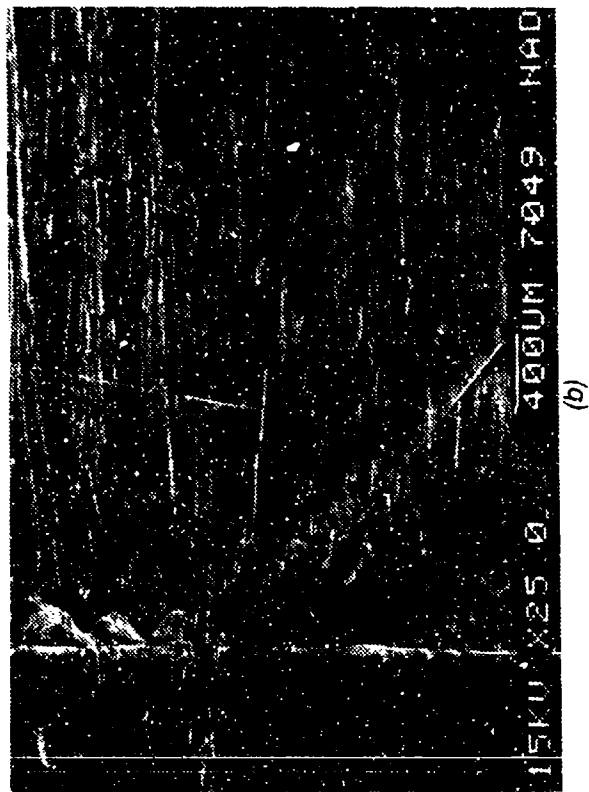
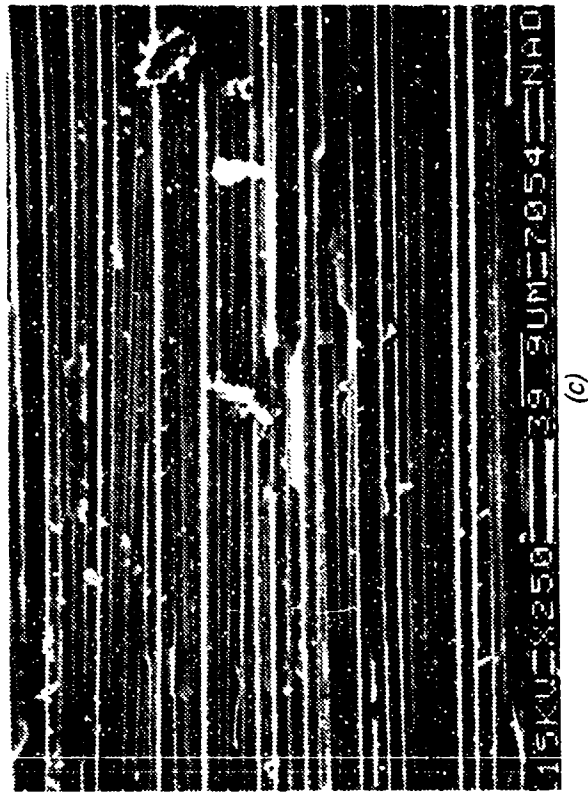


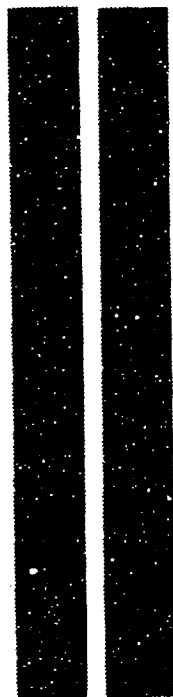
Figure 6-2. Optical and SEM Photographs of Mode I DCB Interlaminar Tension Fracture in AS4/5250-3 Gr/BMI - [0]_{24T}, Water Immersed Before Test
 (a) Macrofracture of Fracture
 (b) Precrack Region
 (c) Crack-Growth Region
 CD = Crack-propagation direction



(b)



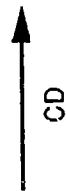
(c)



I II III

AS4/5250-3 Gr/BMI

(a)

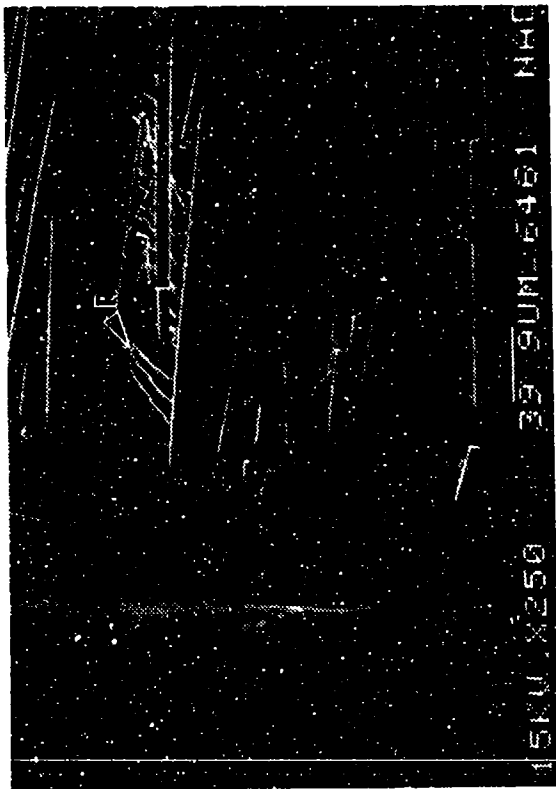


CD

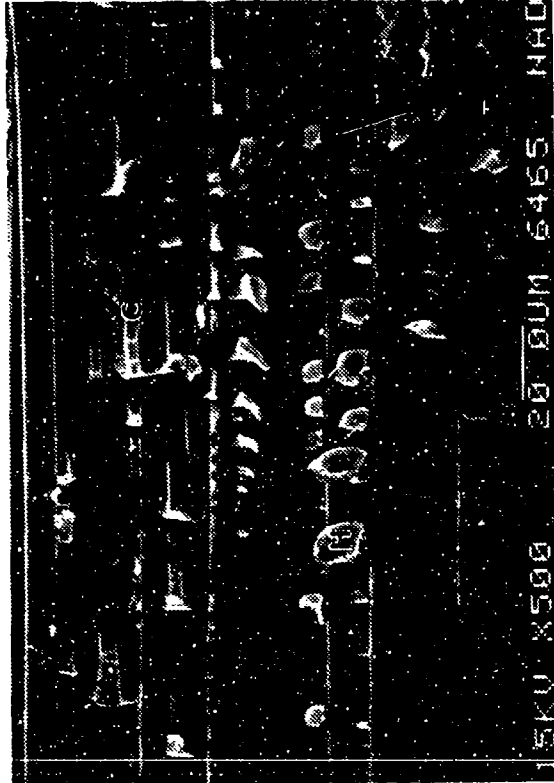
Figure 6-3. Optical and SEM Photographs of Mode II ENF Interlaminar Shear Fracture in AS4/5250-3 Gr/BMI - [0]_{24T}, Room Temperature Ambient

- (a) Macro photograph Showing Regions I, II, and III (Pre-crack, Crack-Growth, and Laboratory Overload)
- (b) River Patterns (R) in Initiation Region in Pre-crack
- (c) Hackles (H) and Cusps (C) in Crack-Growth Region

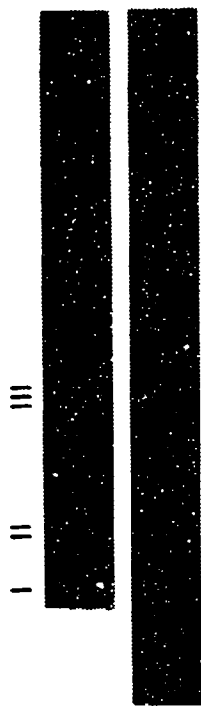
CD = Crack propagation direction



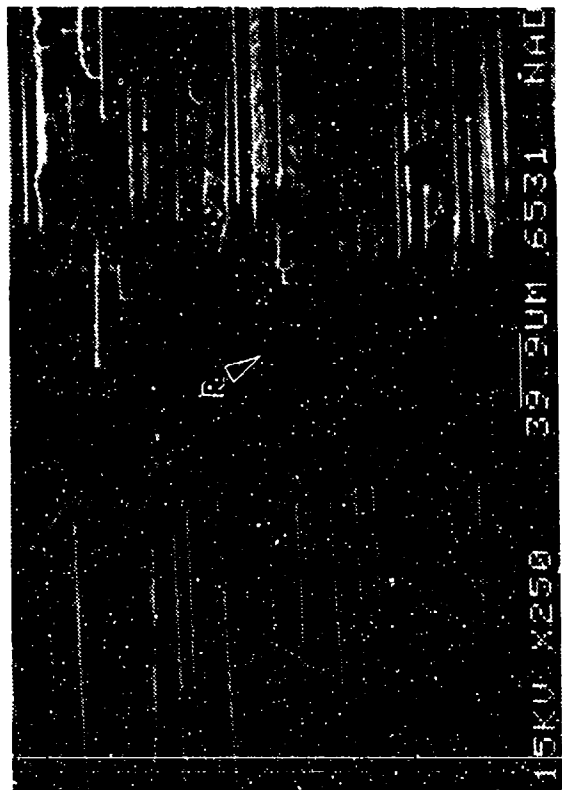
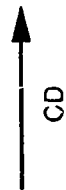
(b)



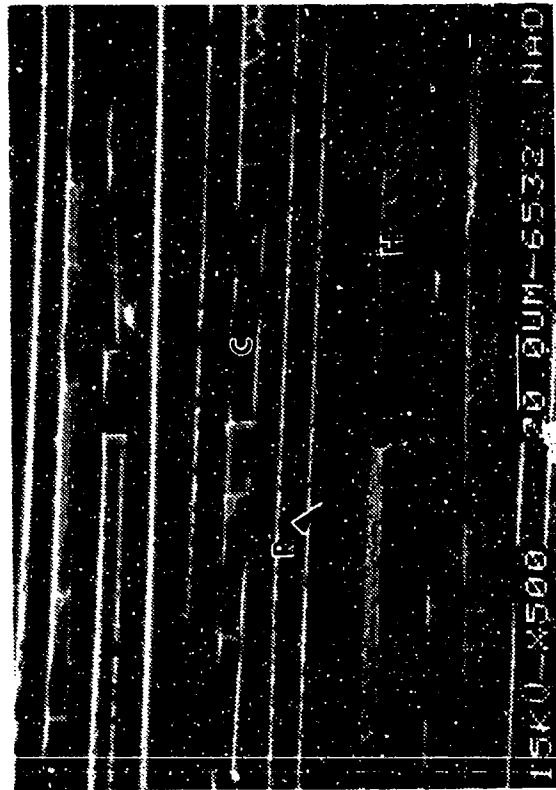
(c)



(a)



(b)



(c)

Figure 6-4. Optical and SEM Photographs of Mode I and Mode II MMF Interlaminar Fracture in AS4/5250-3 Gr/BMI - [0]₂₄. Room Temperature Ambient
(a) Macrophotograph Showing Regions I, II, and III (Precrack, Crack-Growth, and Laboratory Overload)
(b) River Patterns (R) in Initiation Region in Precrack
(c) Rivers (R), Hackles (H) and Cusps (C) in Crack-Growth Region

CD = Crack-propagation direction

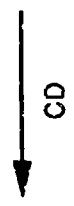
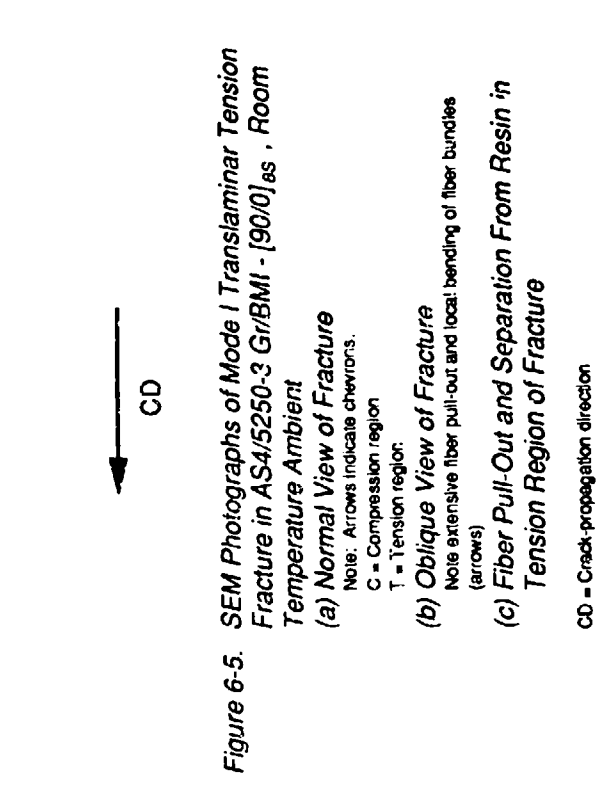
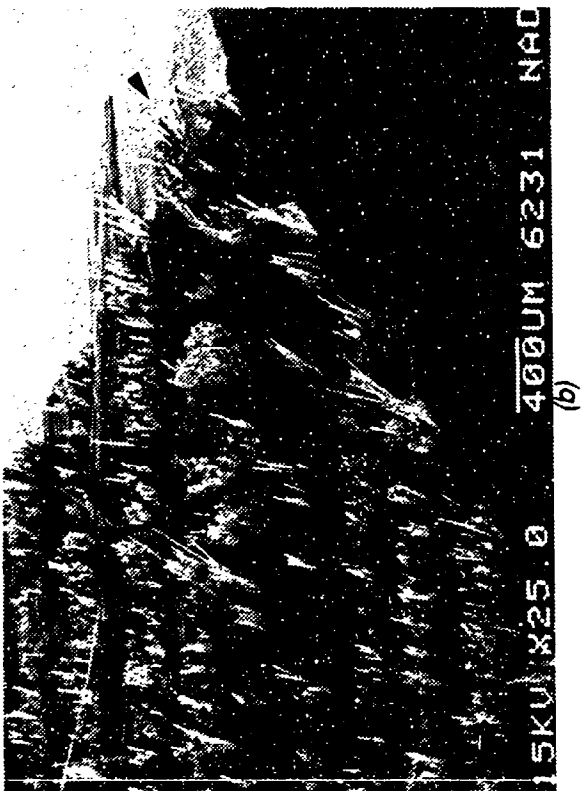
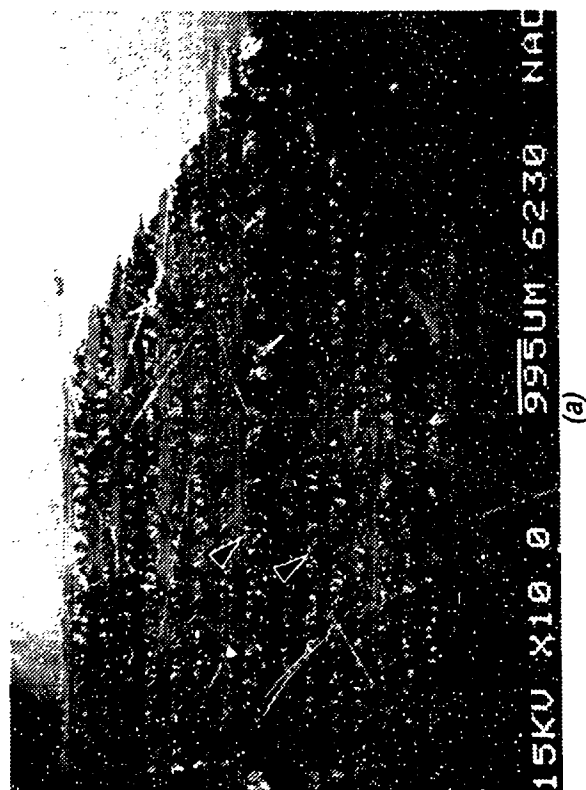


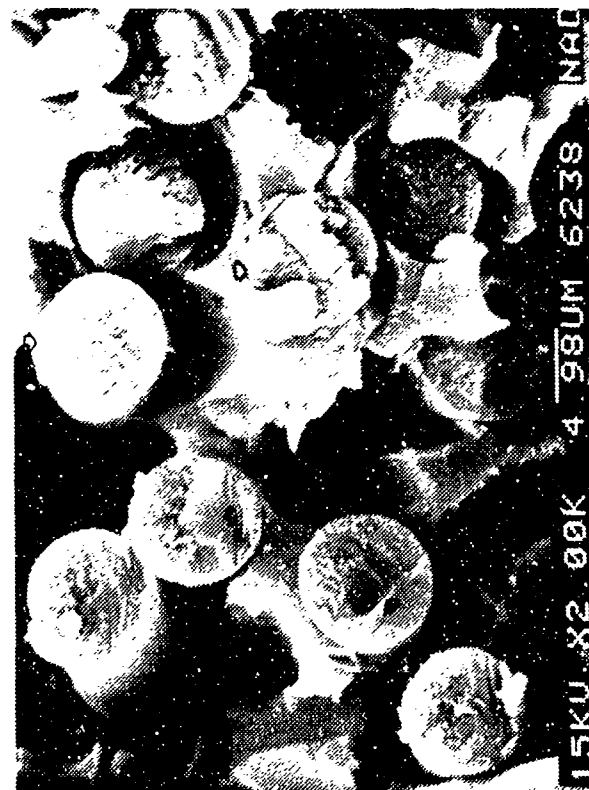
Figure 6-5. SEM Photographs of Mode I Translaminar Tension Fracture in AS4/5250-3 Gr/BMI - [90/0]_{as}, Room Temperature Ambient

(a) Normal View of Fracture
Note: Arrows indicate chevrons.
C = Compression region
T = Tension region

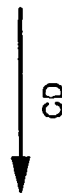
(b) Oblique View of Fracture
Note extensive fiber pull-out and local bending of fiber bundles (arrows)

(c) Fiber Pull-Out and Separation From Resin in Tension Region of Fracture

CD = Crack-propagation direction



(d)



CD

Figure 6-5. (Continued)

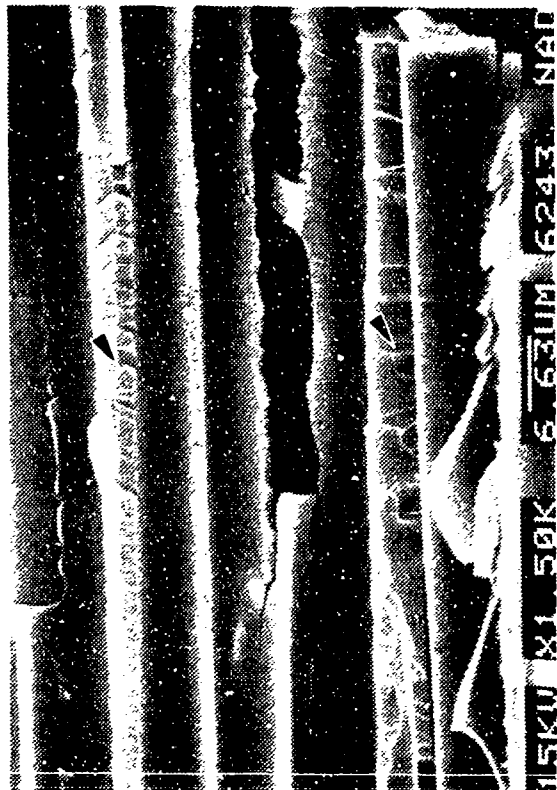
(d) Chop Marks (Solid Arrows) and DAF Radials
(Hollow Arrows) on Fiber Ends

(e) Resin Fracture in 90 Degree Ply (Tension Region)

Note river patterns (arrow)

(f) Chop Marks on Fiber Ends in Compression Region

CD = Crack propagation direction



(e)



(f)

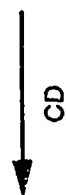
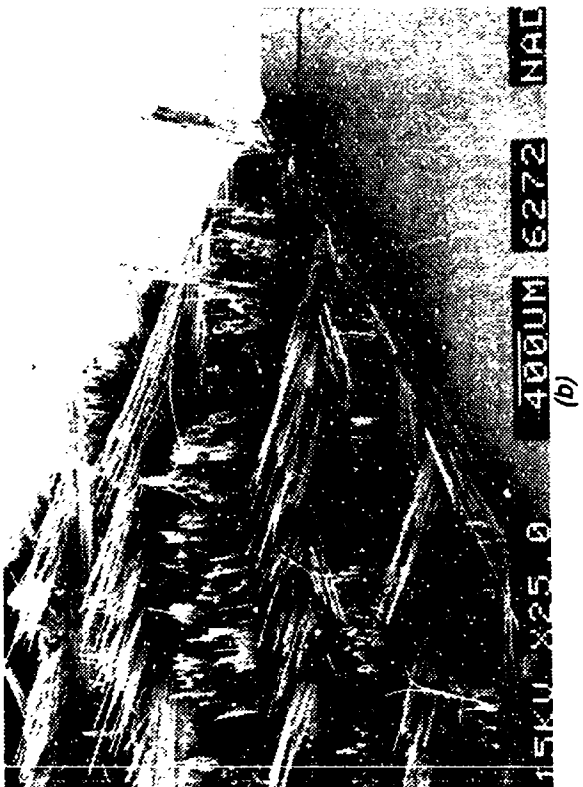
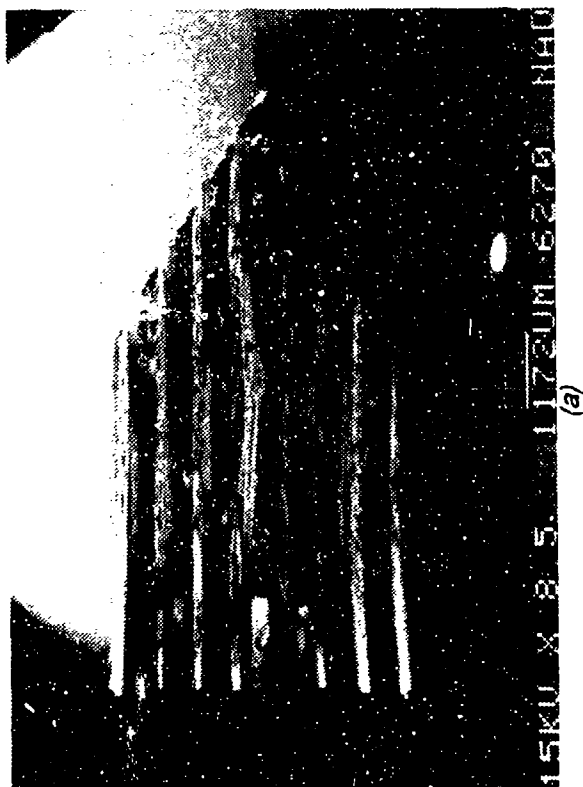


Figure 6-6. SEM Photographs of Mode I Translaminar Tension Fracture in AS4/5250-3 Gr/BMI - 32 Ply Quasi-Isotropic, Room Temperature Ambient

(a), (b) Normal and Oblique Views of Fracture

C = Compression region
T = Tension region

(c) DAF Radials (Arrows) on Fractured Fiber Ends (0 Degree Ply, Tension Region)

CD = Crack-propagation direction



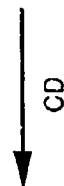
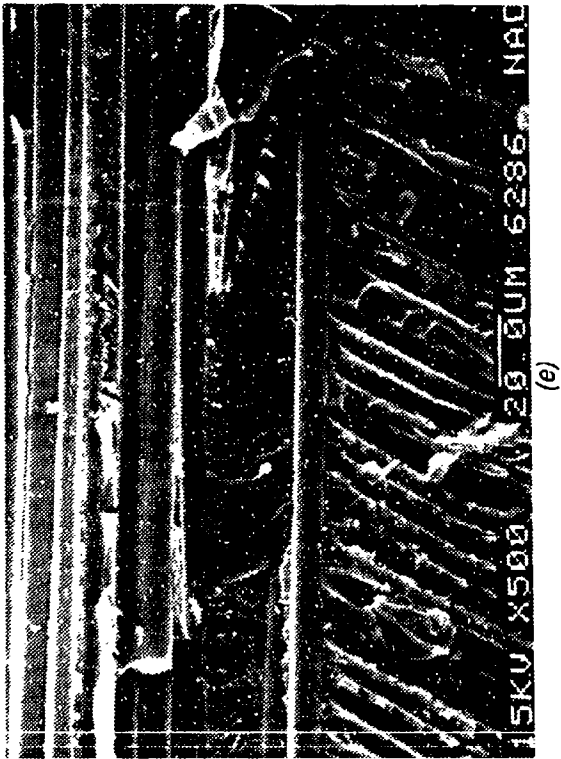
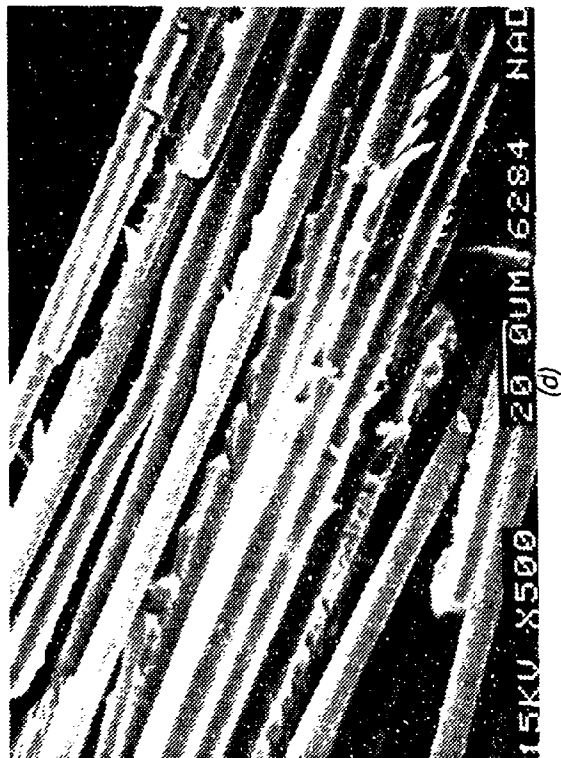
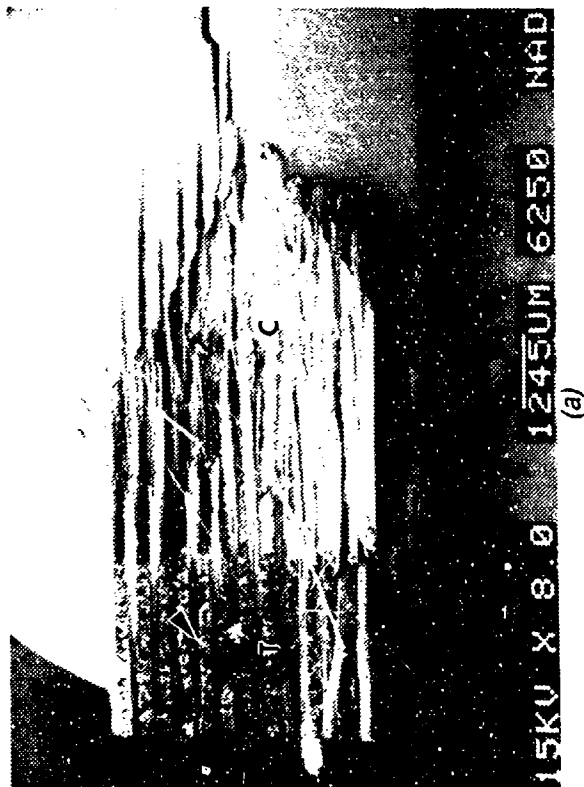


Figure 6-6. (Continued)
 (a), (e) Peel Fracture in 45 and 90 Degree Plies
 (f) Chop Marks (Arrows) on Fiber Ends in
 Compression Region

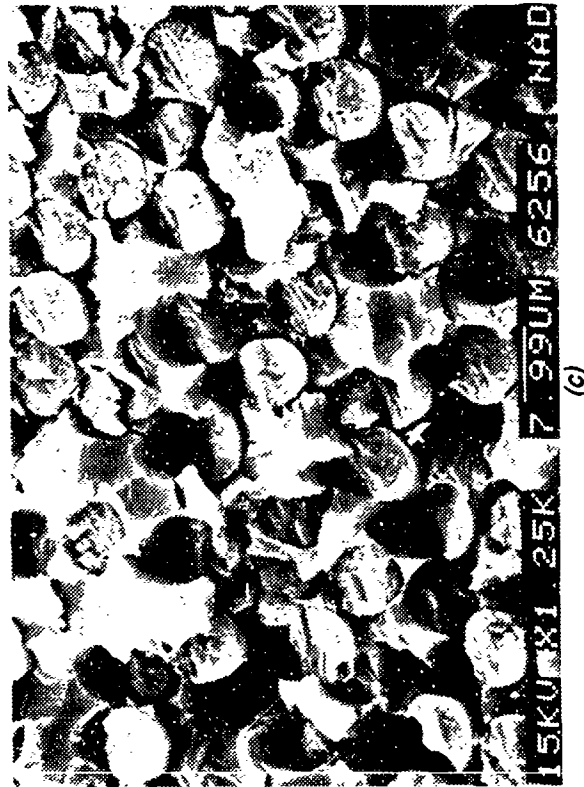
CD = Crack-propagation direction





(a)

(b)



(c)

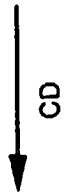


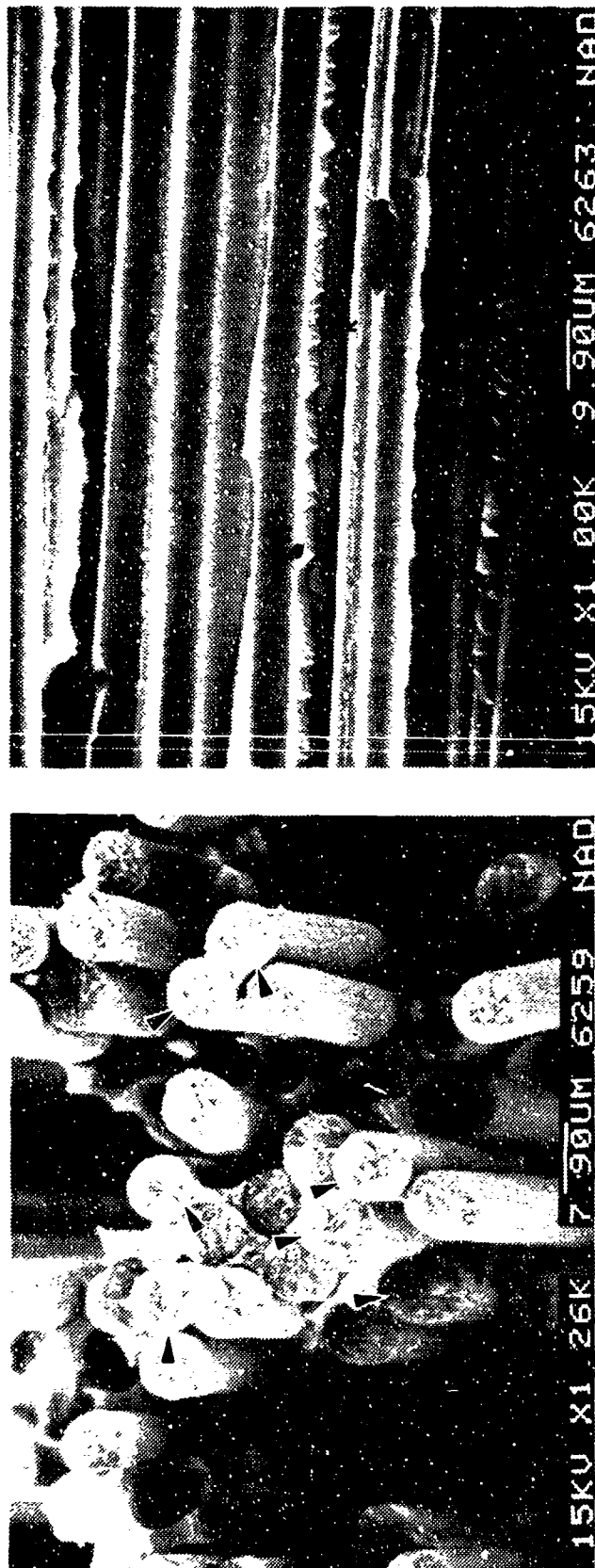
Figure 6-7. SEM Photographs of Mode I Translaminar Compression Fracture in AS4/5250-3 Gr/BMI - [90/0] _{gs}, Room Temperature Ambient

(a) Normal View of Fracture
 Note: Arrow indicates chevrons.
 C = Compression region
 T = Tension region

(b) Oblique View of Fracture
 Note: longitudinal splits close to apex of notch (arrow)

(c) Chop Marks on 0 Degree Fiber Ends in Compression Region

CD = Crack-propagation direction



(d)

(e)

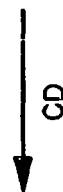


Figure 6-7. (Continued)
 (d) DAF Radials (Arrows) on Fractured Fiber Ends in Tension Region
 (e) Fracture Features Present in 90 Degree Ply Oriented Parallel to Fracture
 H = Hackles
 R = River patterns
 CD = Crack-propagation direction

SECTION 7

GRAPHITE/THERMOPLASTIC

AS4/APC-2

This section presents the results of fractography performed on AS4/APC-2 graphite/polyetheretherketone (Gr/PEEK) test coupons. The tests performed consisted of testing of interlaminar and translaminar fracture test coupons (DCB, ENF, MMR, and bend specimens). The test matrices performed by Northrop are shown in Tables 7-1 and 7-2. The results reported include fractography showing the significant surface features of each failure mode tested by Northrop as well as 270°F interlaminar and translaminar fractography contributed by Boeing. The variable conditions tested by Northrop that are not reported in this section showed no significant differences with the baseline conditions.

Work on Gr/PEEK indicates that the resin plays a strong role in controlling the resulting fracture surface characteristics. The fracture surface morphology includes features not observed in baseline Gr/Ep or Gr/BMI.

On a macroscopic scale, interlaminar peel (Mode I tension and Mixed Mode Flexural) fractures can be distinguished from shear through differences in specular reflectance. Pure interlaminar shear fractures are dull and whitish, whereas peel fractures appear darker and reflect more light. Peel failures can be confirmed through additional examination of broken fibers in the fractured areas. Fiber ends will exhibit no evidence of compression in this failure mode.

In pure shear, cusps (hackles) form oriented normal to the plane of shear. These cannot be used to predict crack-growth direction. However, in real-world situations, pure shear is often associated with local interlaminar tension, giving rise to local rivers, which can then be used to establish fracture direction.

In Gr/PEEK, the fracture surface morphology is a function of crack-growth rate. In peel fractures, transverse tensile forces cause "slow-ductile", "intermediate-brittle", and "fast-brittle" fractures. Slow-ductile peel is characterized by drawing of matrix craze filaments (fibrils), extremely similar to those observed in shear. In peel, the filaments will be oriented in the same direction on mating halves; whereas in shear, these will be oriented in opposite directions. Intermediate-brittle and fast-brittle peel fractures are characterized by the formation of cusps and rivers. The rivers can then be used to distinguish from pure shear through examination of mating fracture surfaces. Additionally, peel fractures are characterized by the formation of "ribs", that do not form in shear.

Interlaminar fracture mode fractographs are provided in Figures 7-1 through 7-9 and translaminar fracture mode fractographs are provided in Figures 7-10 through 7-13.

Table 7-1. AS4/APC-2 Gr/PEEK Interlaminar Fracture Test Matrix

SPECIMEN, LOADING	VARIABLE CONDITION	LAYUP	LAMINATE DIMENSIONS	NO. OF LAMINATES
Mode I DCB, Tension	RTA	24/0	22 X 16.5	1
Mode II ENF, Shear	RTA			
Mode I DCB, Tension	Cond. 180 F 2 weeks before test			
Mode I DCB, Tension	Water immer. before test			
Mode I + II MMF, Tension + Shear	RTA	24/0,45	13 X 13	1
Mode I DCB, Tension	RTA			
Mode I DCB, Tension	Cond. 180 F 2 weeks before test			
Mode I DCB, Tension	Cond. 180 F 2 weeks before test	24/90,0	13 X 8	1

RTA = Room Temperature Ambient
Laminate dimensions in inches

Table 7-2. AS4/APC-2 Gr/PEEK Translaminar Fracture Test Matrix

SPECIMEN, LOADING	VARIABLE CONDITION	LAYUP	LAMINATE DIMENSIONS	NO. OF LAMINATES
Mode I Tension, 4 pt. load	RTA	32/90,0	15 X 8	1
Mode I Compression, 4 pt. load	RTA			
Mode I Compression, 4 pt. load	Water Immer. before test			
Mode I Compression, 4 pt. load	Impact damage before test			
Mode I Tension, 4 pt. load	Cond. 180 F 2 weeks before	32/quasi	8 X 6	1

RTA = Room Temperature Ambient

Laminate dimensions in inches

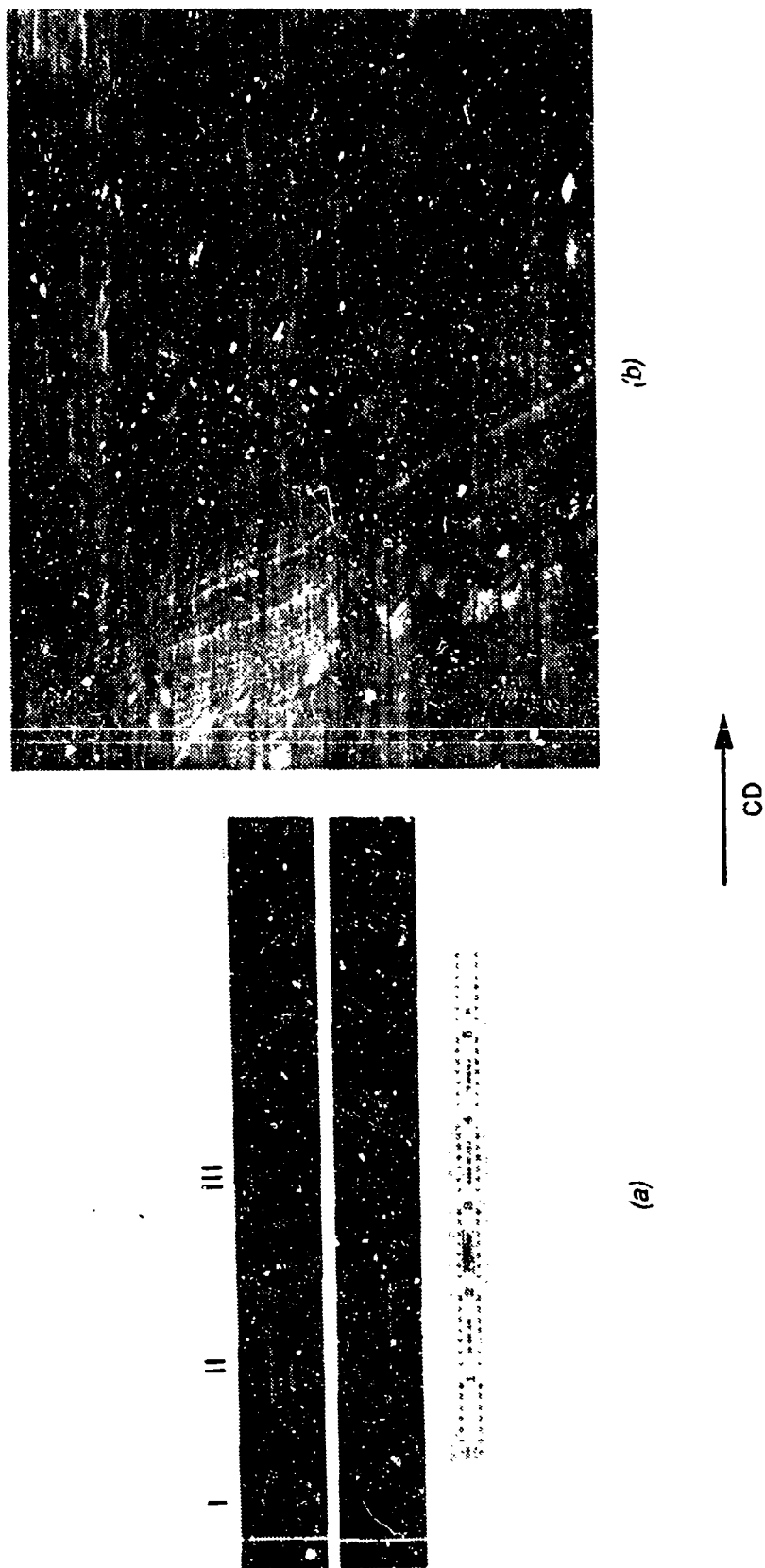
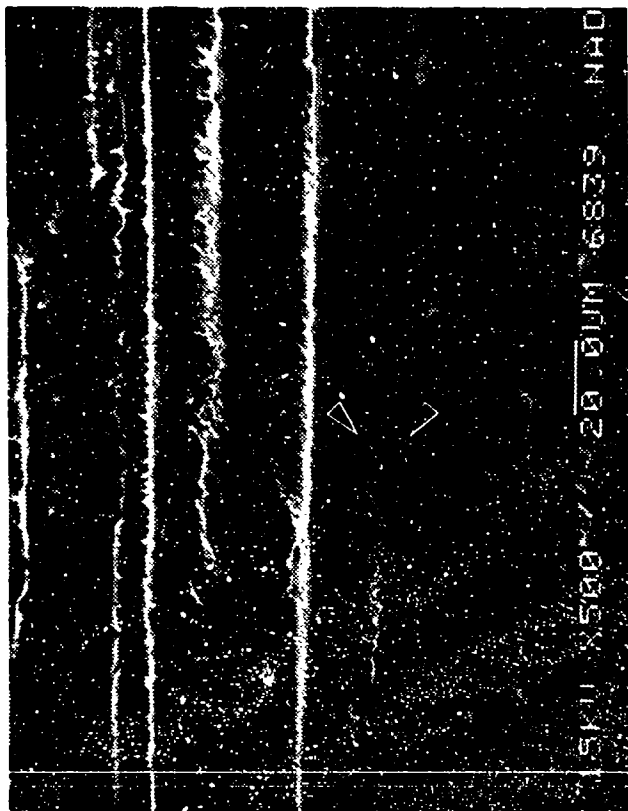
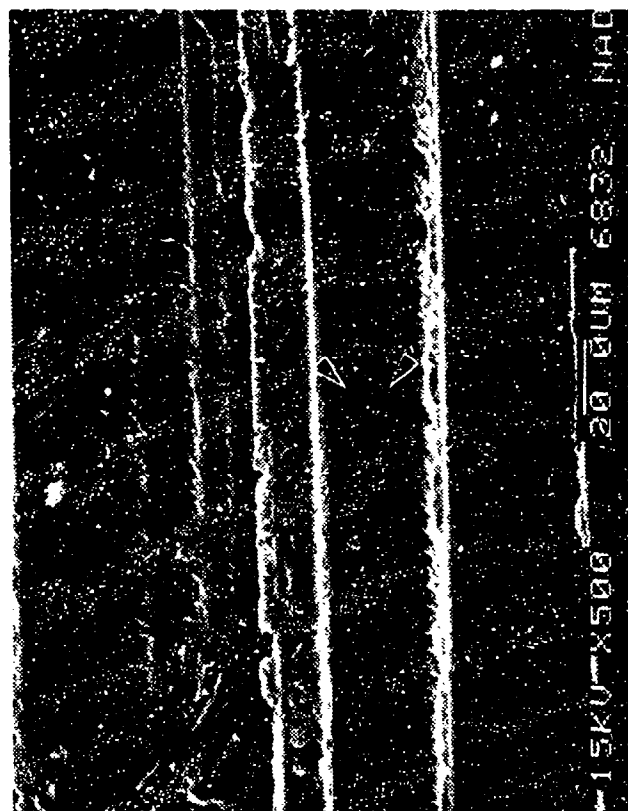


Figure 7-1. Optical and SEM Photographs of Mode I DCB Interlaminar Tension Fracture in AS4/APC-2 Gr/PEEK - $[0]_{24T}$, Room Temperature Ambient
 (a) Macro photograph Showing Regions I, II, III (Pre-crack, Crack-Growth, and Laboratory Overload)
 (b) Ribs (Arrows) Oriented Toward CD
 CD = Crack-propagation direction



(c)



(d)

Figure 7-1. (Continued)
(c), (d) Mating Fracture Surfaces Showing Fractured Fibrils (Arrows)

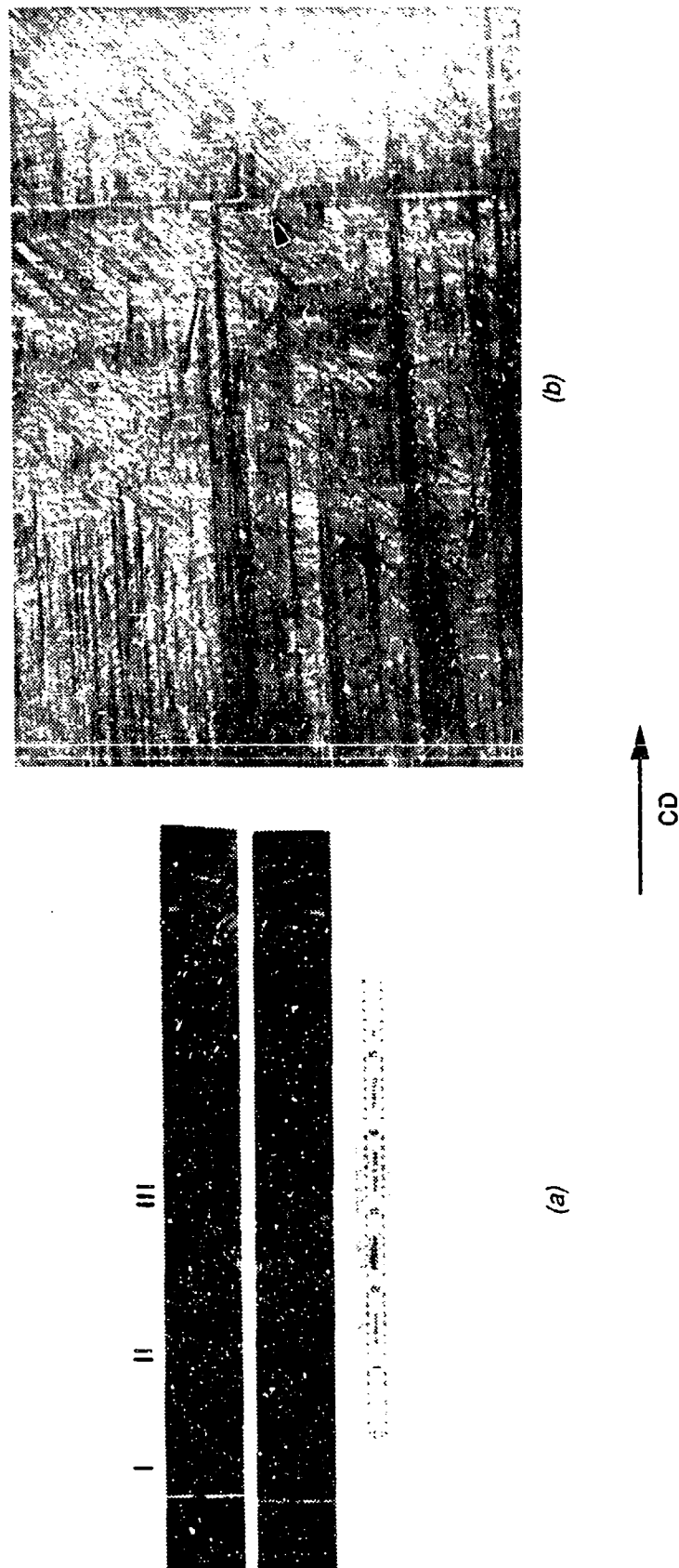
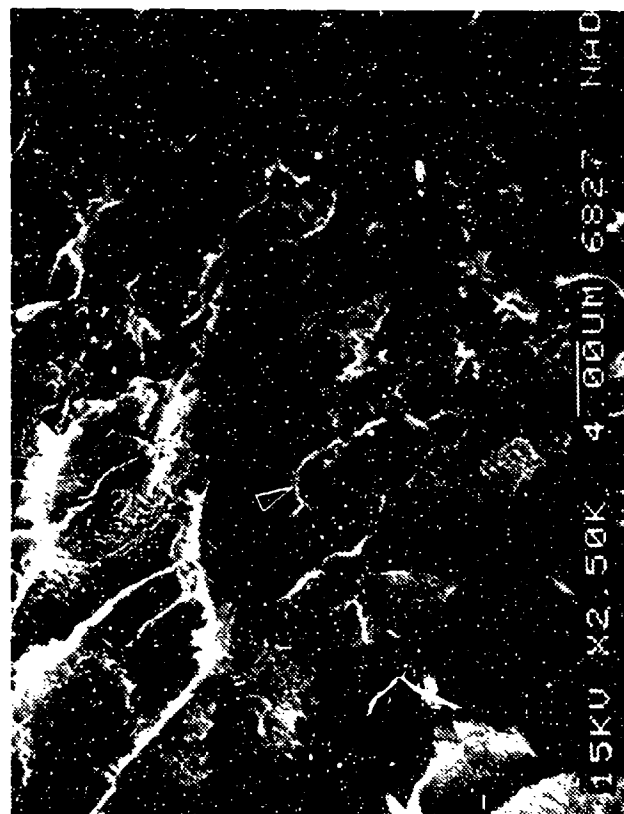
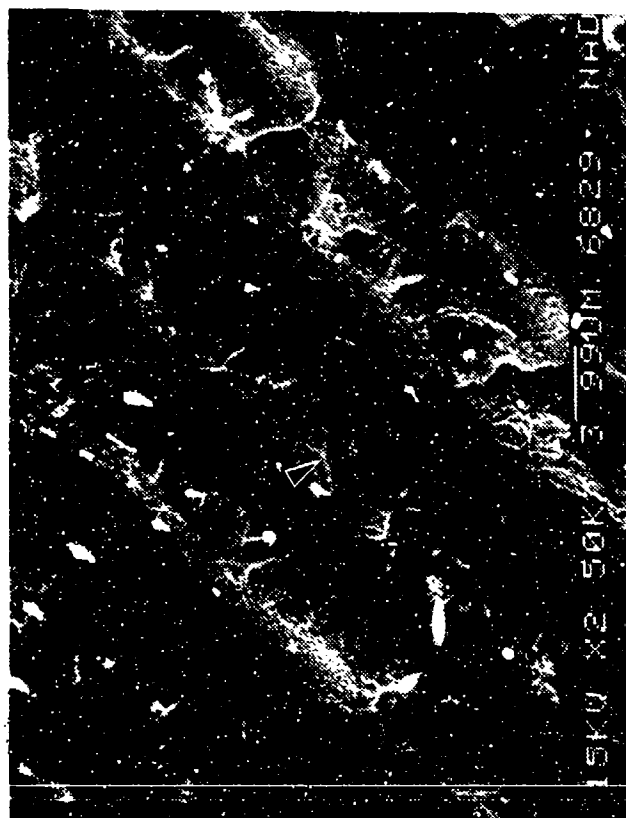


Figure 7-2. Optical and SEM Photographs of Mode I DCB Interlaminar Fracture in AS4/APC-2 Gr/PEEK - [+45/0/-45]_{4s}, Mode I DCB, Room Temperature Ambient
(a) Macrograph Showing Regions I, II, and III
(b) Ribbs (Arrows) Oriented Toward CD

CD = Crack-propagation direction



(c)



(d)

Figure 7-2. (Continued)
(c), (d) Mating Fracture Surfaces Showing Fractured Fibrils (Arrows)



60 degree tilt

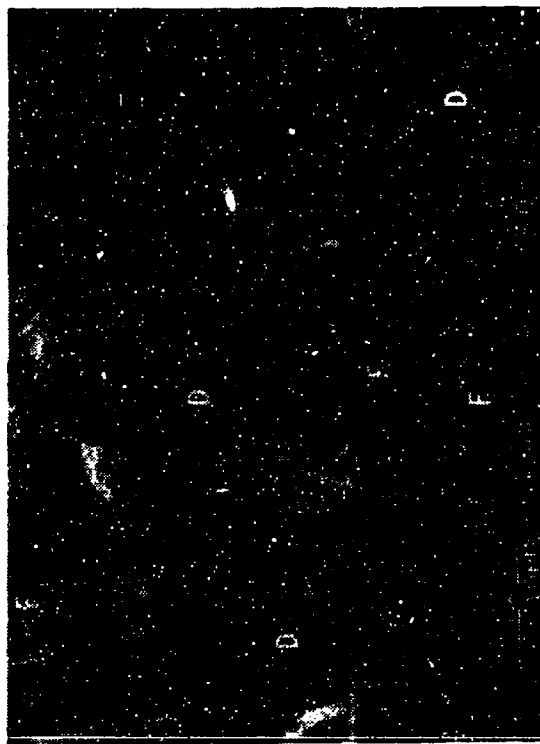
400X



60 degree tilt

400X

Legend:
 D ductile matrix fracture
 F fiber
 Mechanically induced crack direction



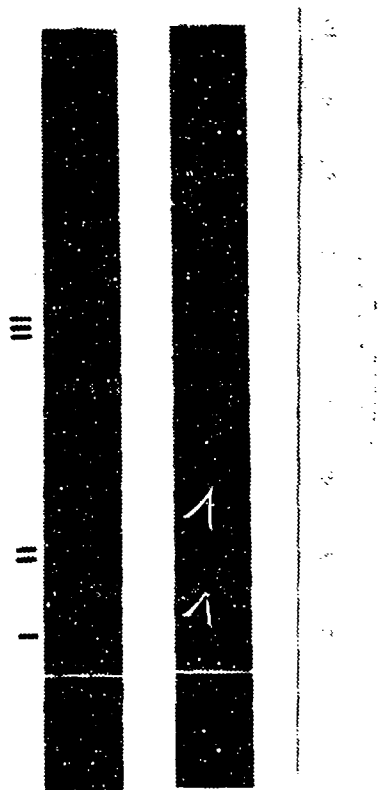
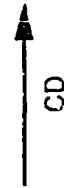
60 degree tilt

2,000X

Figure 7-3. SEM Fractographs of 270/F Wet, Interlaminar Mode I Tension, 0/90 Fracture in AS4/APC-2



(b)



(a)

Figure 7-4. Optical and SEM Photographs of Mode I DCB Interlaminar Tension Fracture in AS4/APC-2 Gr/PEEK - [0]_{24T}, Conditioned 180 F/Dry
(a) Macro photograph of Fracture Showing Regions I, II, and III
(Precrack, Crack-Growth, and Laboratory Overload)
Note: Arrows indicate ribs oriented toward CD.

(b) Ribs (Arrows)

CD = Crack propagation direction

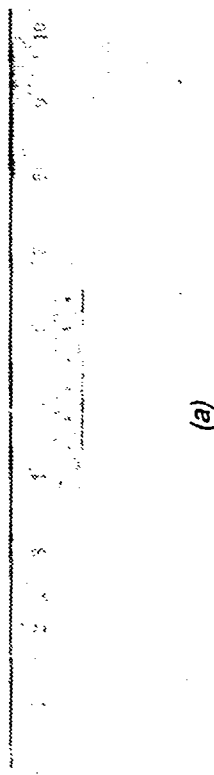
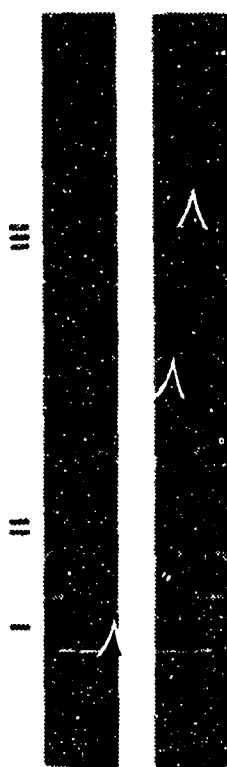
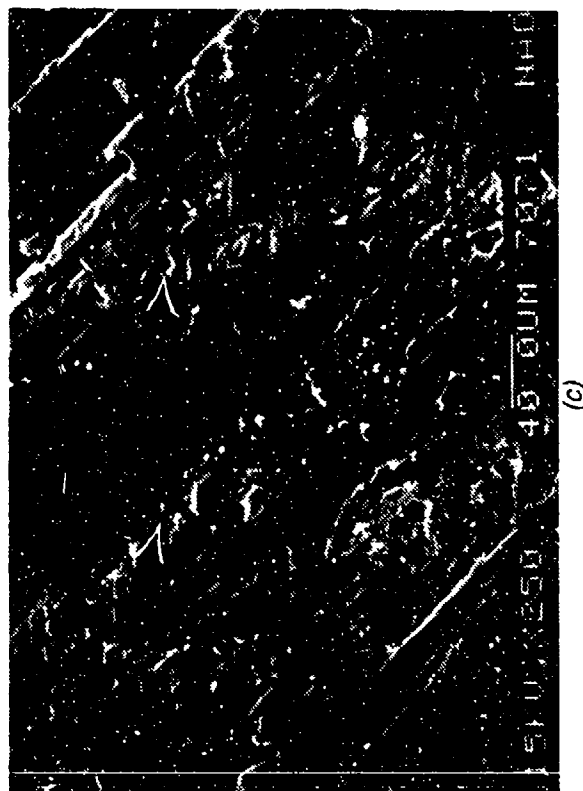
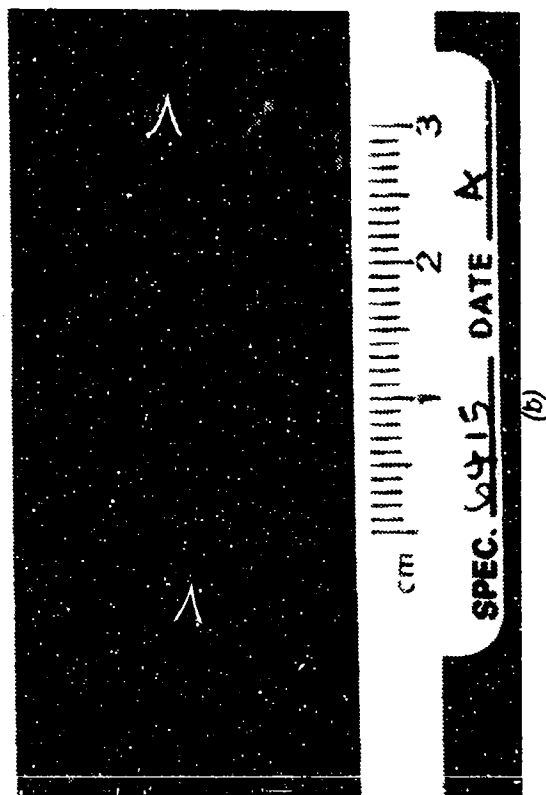


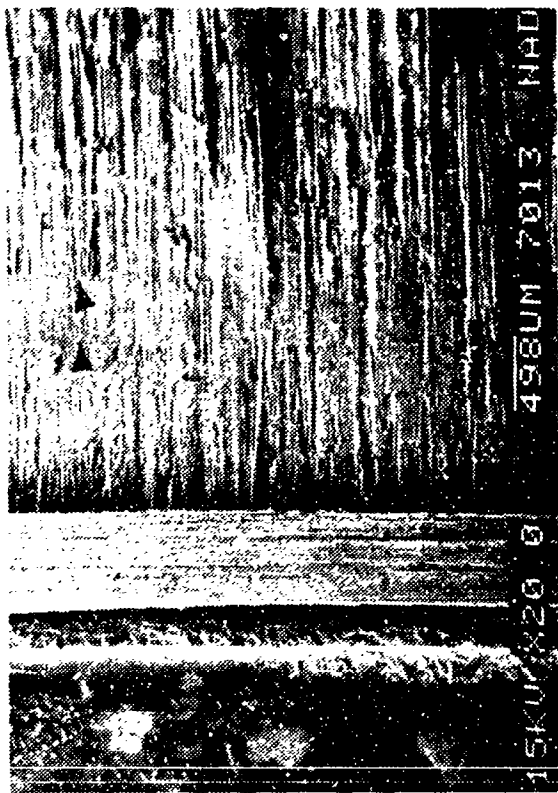
Figure 7-5. Optical and SEM Photographs of Mode I DCB Interlaminar Tension Fracture in AS4/APC-2 Gr/PEEK - [+45/0/-45]_{4s}, Conditioned 180 F/Dry

(a) Macro photograph of Fracture Showing Regions I, II, and III (Precrack, Crack-Growth, and Laboratory Overload)

Note: Arrows indicate ribs oriented toward CD.

(b), (c) Ribs (Arrows)

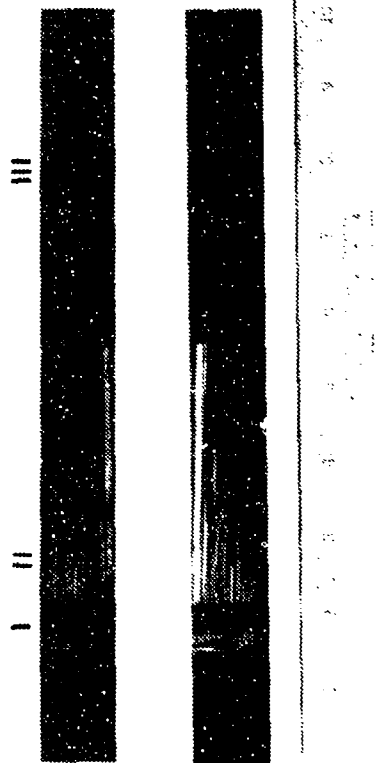
CD = Crack-propagation direction



(b)



(c)



(a)

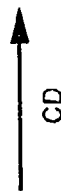


Figure 7-6. Optical and SEM Photographs of Mode I DCB Interlaminar Tension Fracture in AS4/APC-2 Gr/PEEK - [90/0]_{6s}, Conditioned 180 F/Dry

(a) Macro photograph of Fracture Showing Regions I, II, and III (Pre-crack, Crack-Growth, Laboratory Overload)

(b), (c) Ribs (Arrows) Oriented Toward CD

CD = Crack propagation direction



(a)

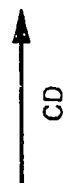
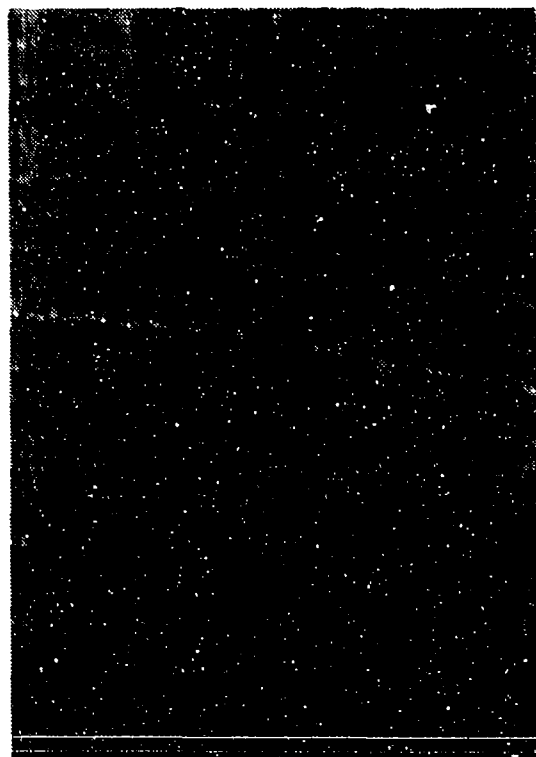
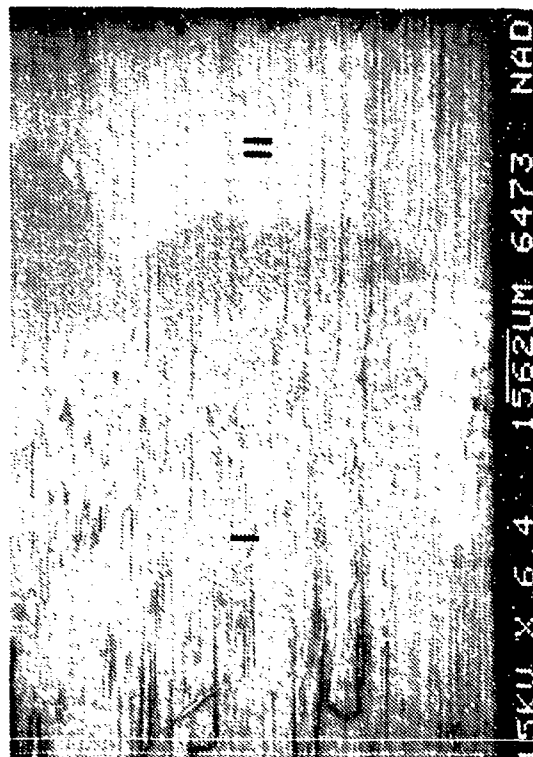


Figure 7-7. Optical and SEM Photographs of Mode II ENF Interlaminar Shear Fracture in AS4/APC-2 Gr/PEEK - [0]_{24T} , Room Temperature Ambient
 (a) Macro photograph of Fracture Showing Regions I, II, and III (Precrack, Crack-Growth, Laboratory Overload)
 Note banded appearance in Region III
 (b) Fibs in Region I Oriented Toward CD
 (c) Region I/II Transition
 Note absence of ribs in Region II

CD = Crack-propagation direction



(b)



(c)

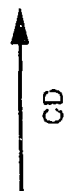
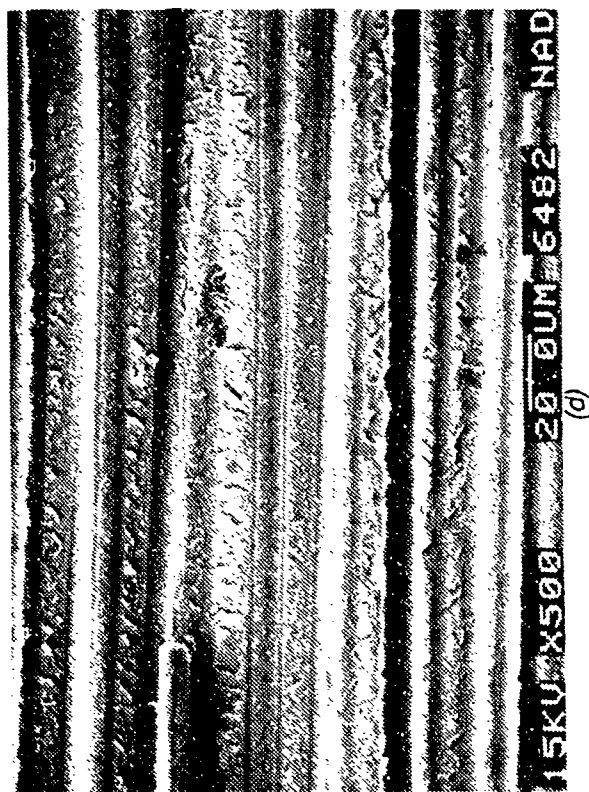
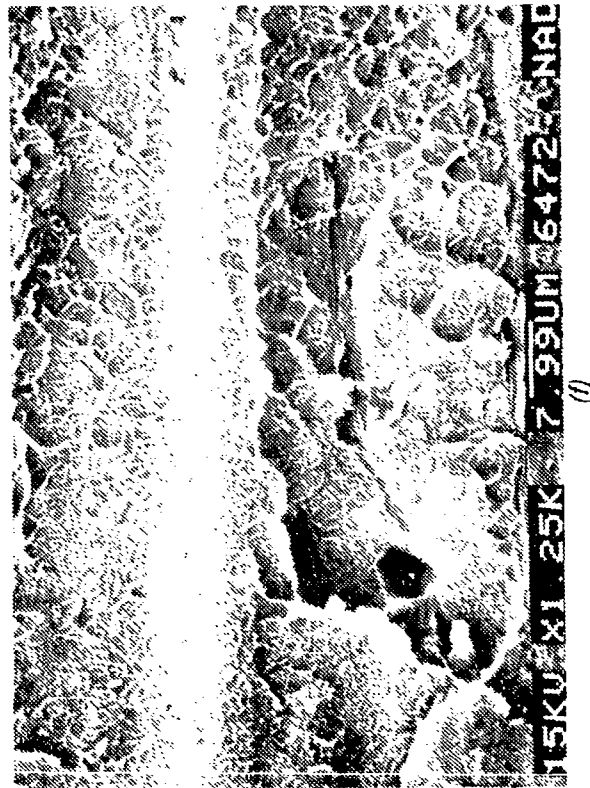
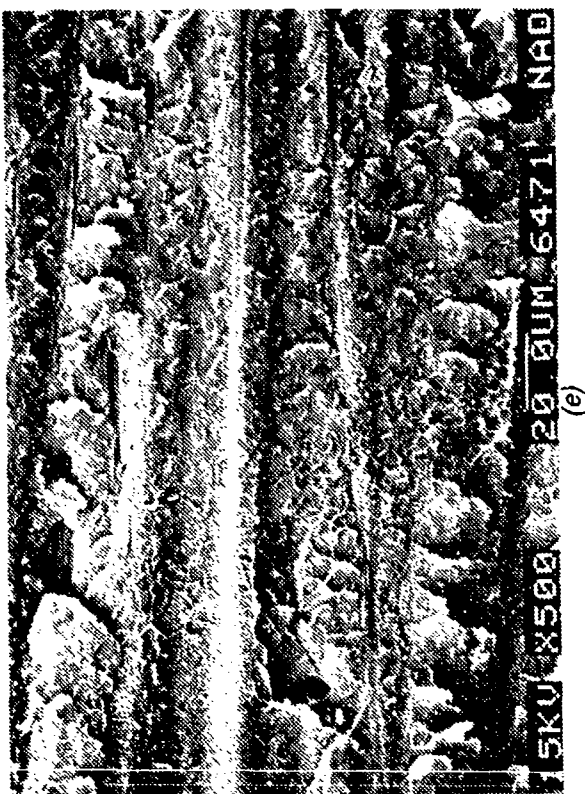
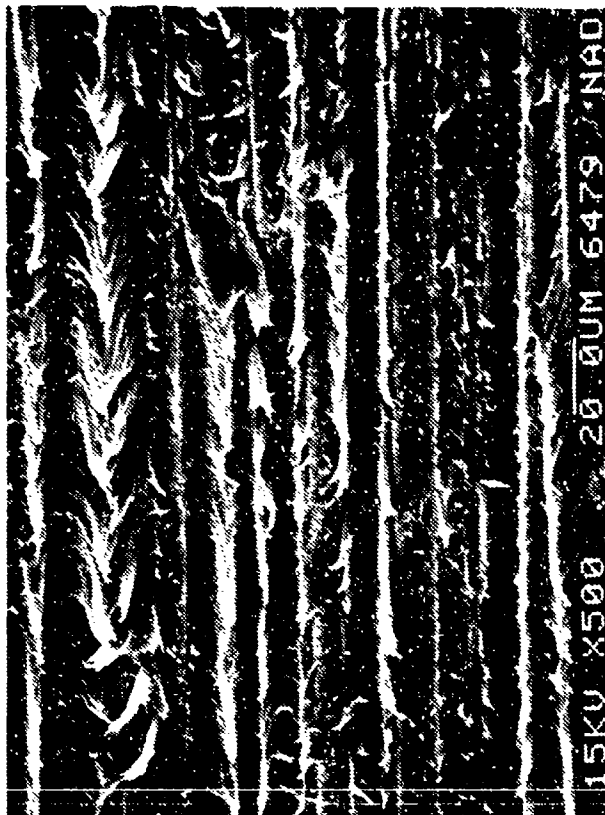
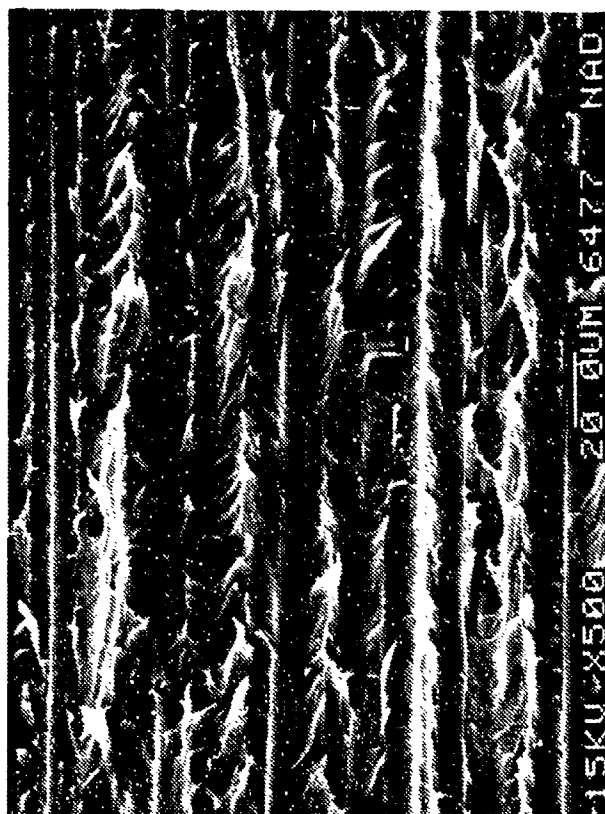


Figure 7-7. (Continued)
 (d), (e) Region I Fracture
 (f) Peel Fracture in Region I
 CD = Crack-propagation direction



(g)



(h)

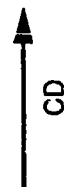
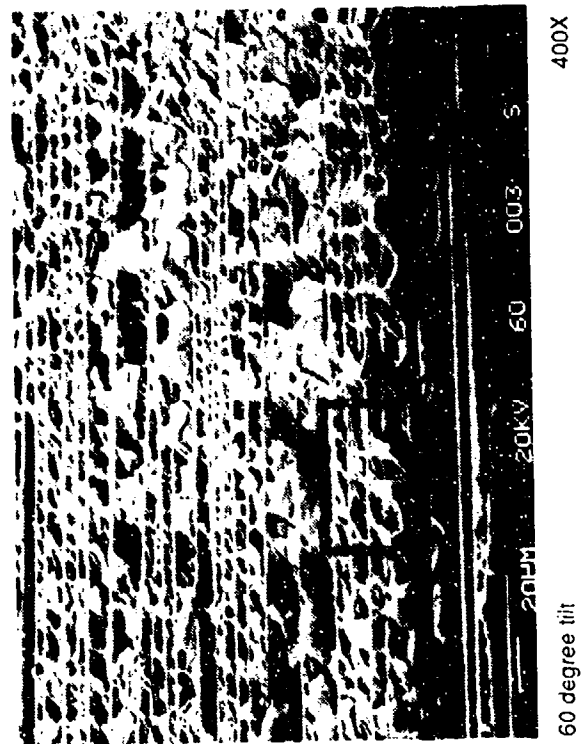
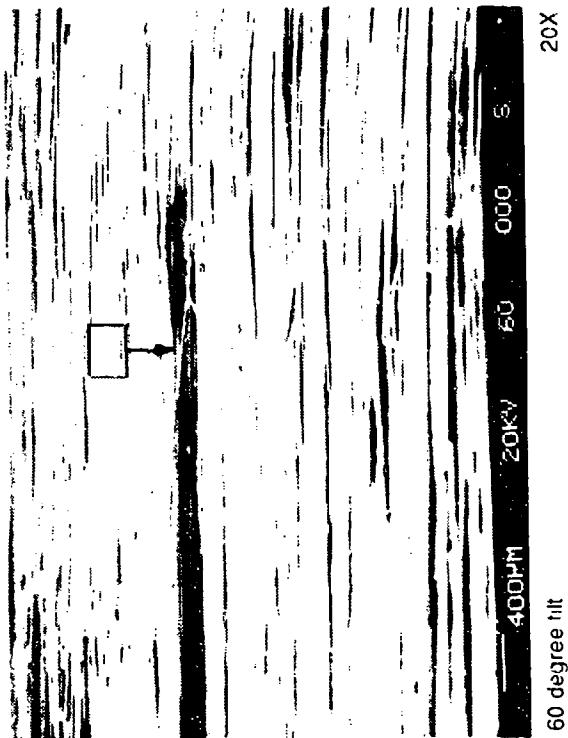


Figure 7-7. (Continued)
(g), (h) Shear Fracture Region in Mating Halves
Note orientation of drawn fibrils (arrows)

CD = Crack-propagation direction



Legend:

- D ductile overload
- H hackle
- S ductile shear

Mechanically induced
crack direction

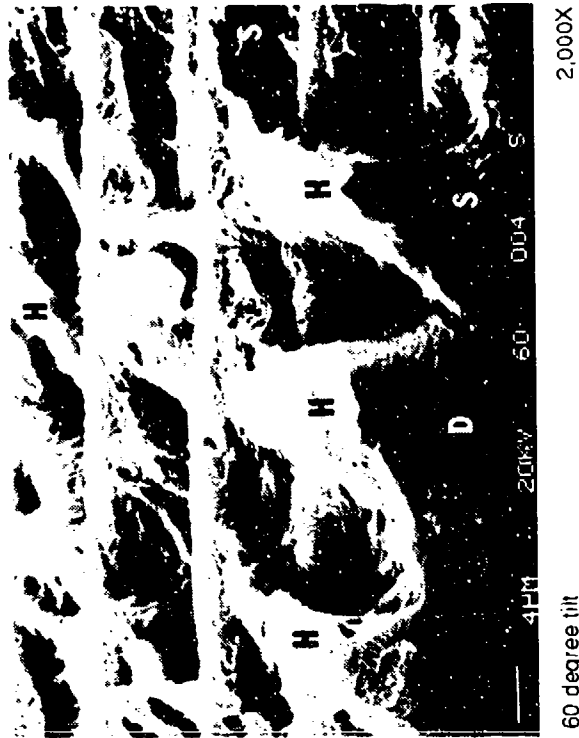


Figure 7-8. SEM Fractographs of 270/F Wet, Interlaminar Mode II Shear, 0/90 Fracture in AS4/APC-2

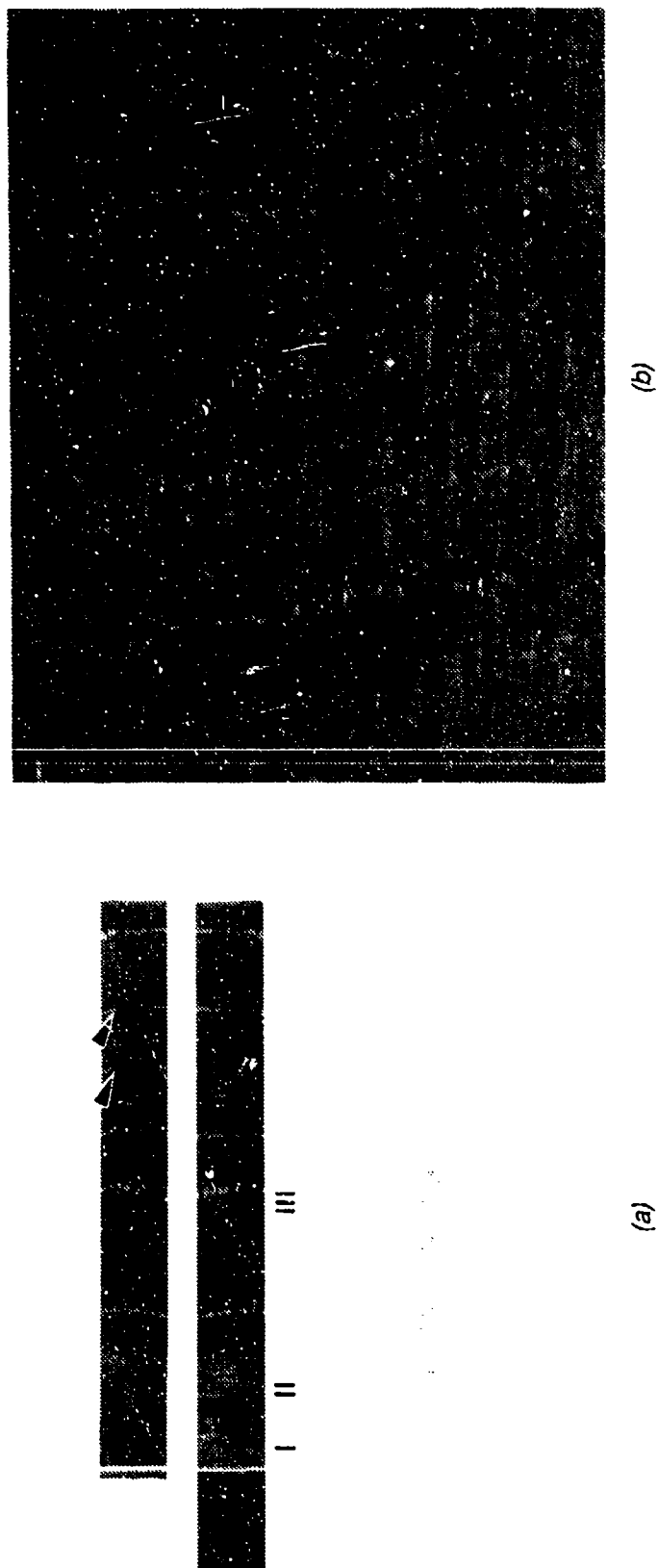
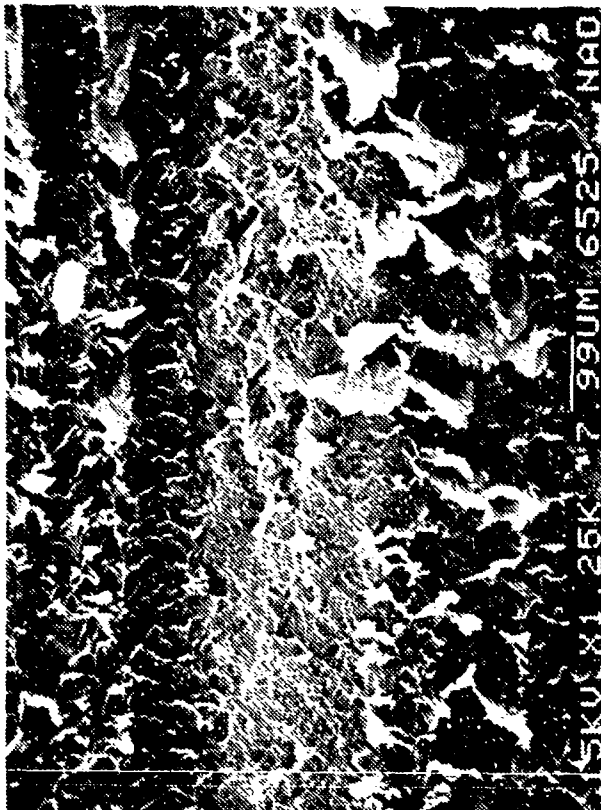
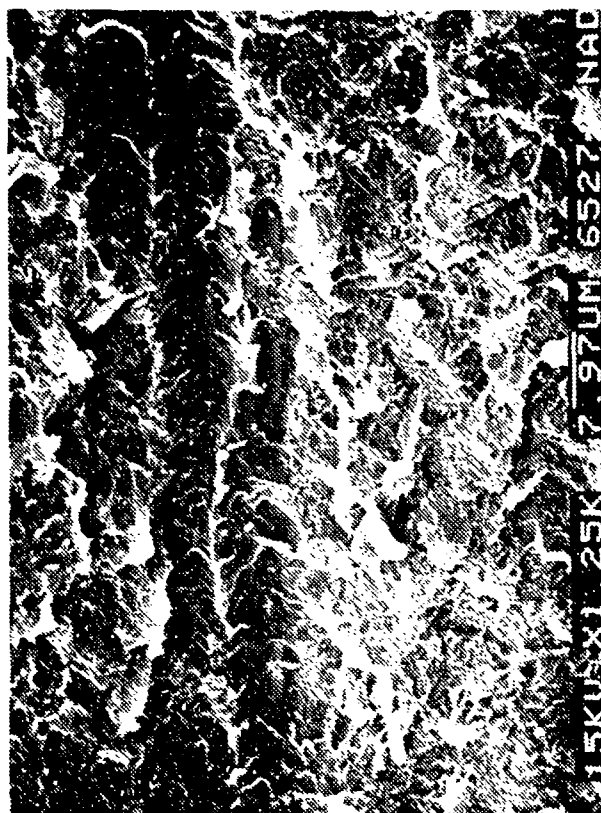


Figure 7-9. Optical and SEM Photographs of Mode I and II MMF Fracture in AS4/APC-2 Gr/PEEK - [0]_{24T}, Room Temperature Ambient
 (a) Macro photograph of Regions I, II, and III (Precrack, Crack-Growth, and Laboratory Overload)
 Note coarse ribs (arrows) in Region III
 (b) Ribs in Region II
 CD = Crack-propagation direction



(c)



(d)

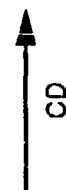


Figure 7-9. (Continued)
(c), (d) Shear Fracture Region in Mating Fracture Halves
Note orientation of drawn fibrils (arrows)

CD = Crack propagation direction

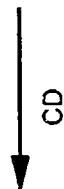
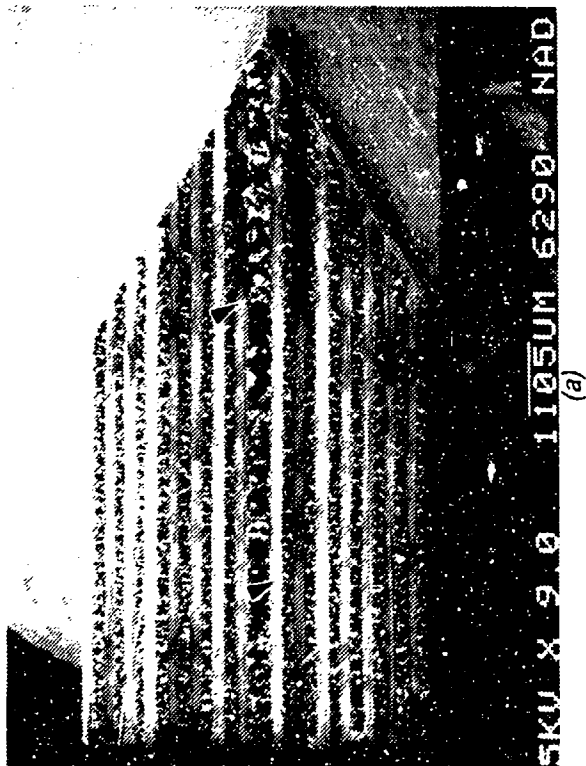


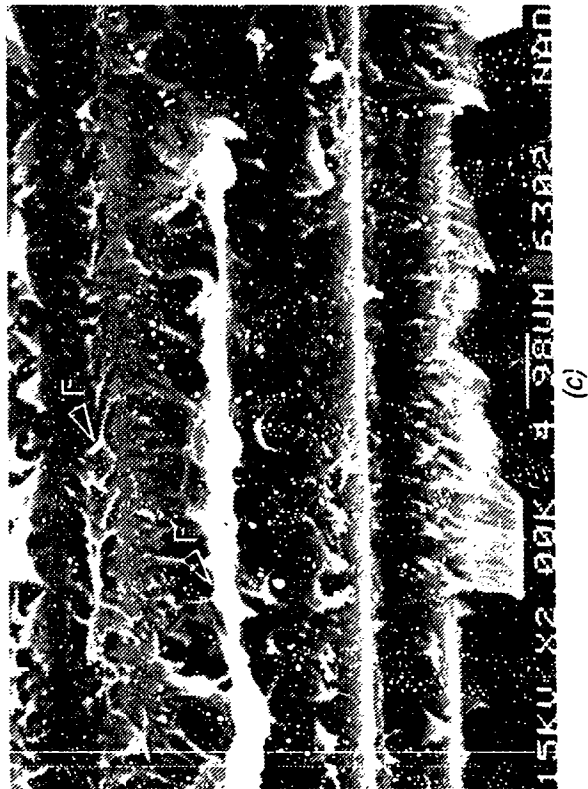
Figure 7-10. Optical and SEM Photographs of Mode I Translaminar Tension Fracture in AS4/APC-2 Gr/PEEK - [90/0] as

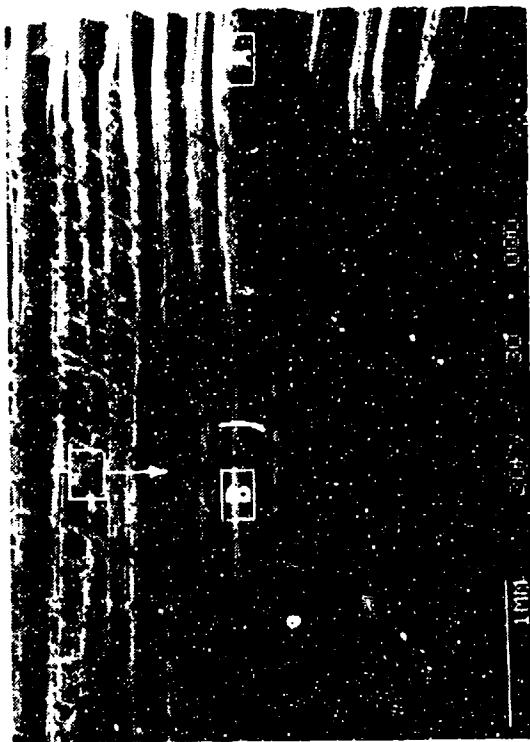
(a) Macrophotograph
Note: Arrows indicate chevrons.

(b) Fracture in 0 Degree Fibers (Tension Region)
Note: Arrows indicate DAF radials.

(c) Resin Fracture in 90 Degree Plies
Note: Fractured fibrils oriented along CD

CD = Crack propagation direction
F = Fibrils



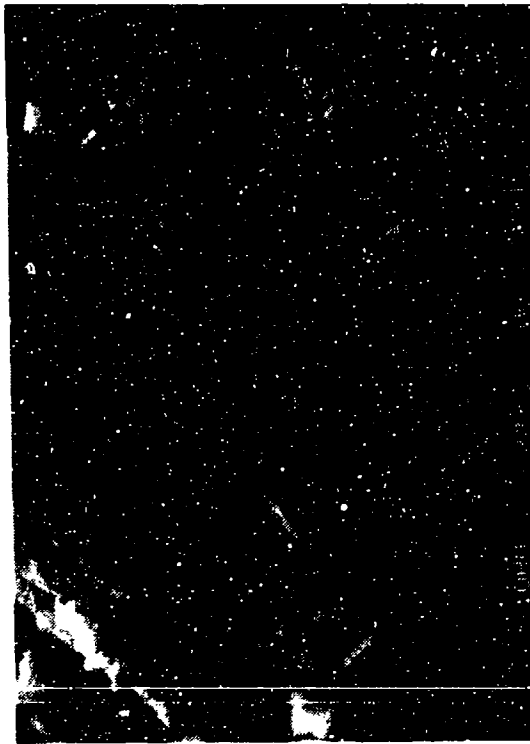


30 degree tilt 20X

Mechanically induced
crack direction



0 degree tilt 400X



0 degree tilt 2,000X

Figure 7-11. SEM Fractographs of 270/F Wet, Translaminar Tension, 0/90 Fracture in AS4/APC-2

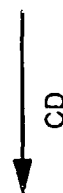
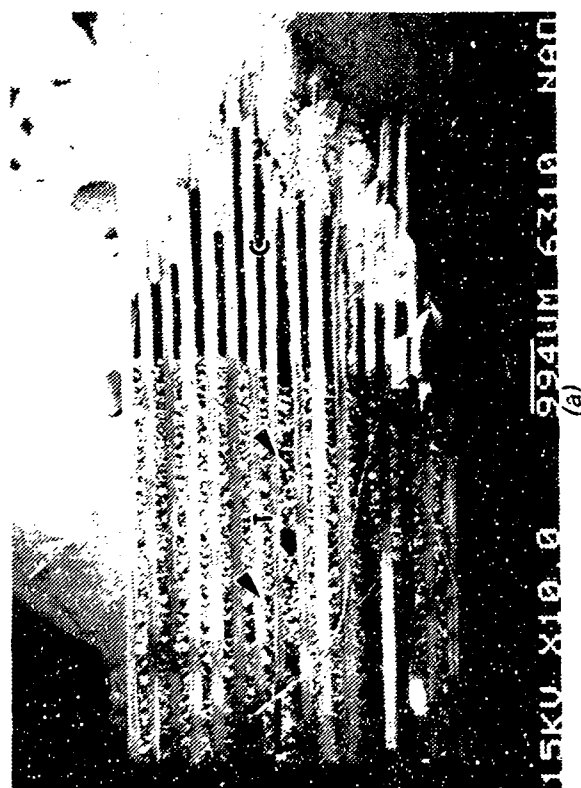
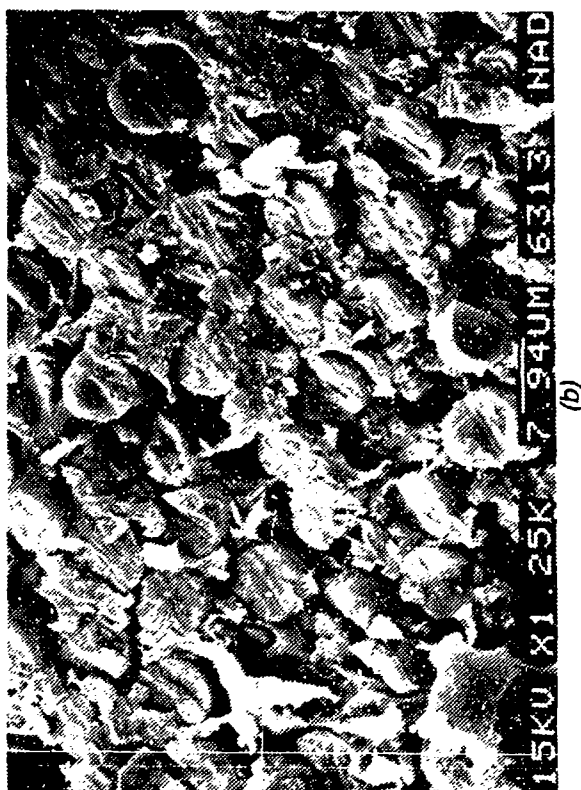


Figure 7-12. Optical and SEM Photographs of Mode I Translaminar Compression Fracture in AS4/APC-2 Gr/PEEK - [90/0]_{as}, Room Temperature Ambient

(a) Macro photograph
C = Compression region
T = Tension region

Note: Arrows indicate chevrons.

(b) Chop Marks on Fractured 0 Degree Fibers (Compression Region)

(c) DAF Radials on Fractured 0 Degree Fibers (Tension Region)

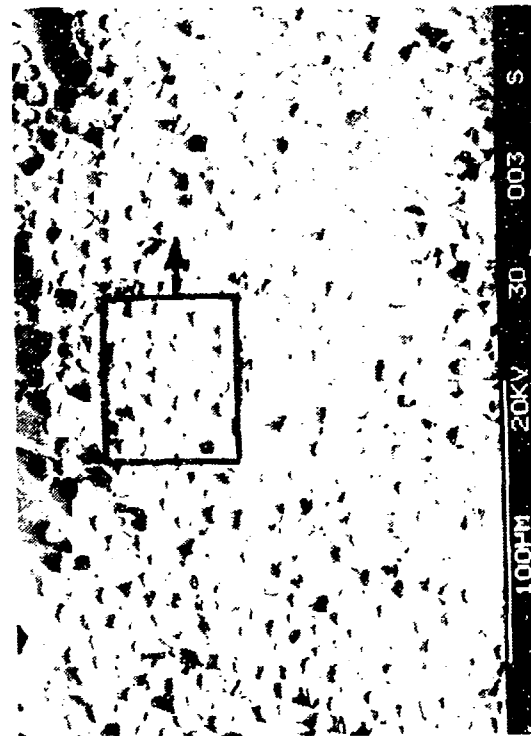
CD = Crack-propagation direction



30 degree tilt

20X

Mechanically induced
crack direction



30 degree tilt

400X



30 degree tilt

2,000X

Figure 7-13. SEM Fractographs of 270/F Wet, Translaminar Compression, 0/90 Fracture in AS4/APC-2

SECTION 8

CARBON/POLYIMIDE

C3K 8-HS/PMR-15 (CELION 3000 8H SATIN)

8.1 INTERLAMINAR FRACTURE

The specimens used for interlaminar fracture were produced from 0/90 ply laminates. Tests were conducted under RT/dry and 500°F/dry conditions. This contribution was made by Boeing.

8.1.1 Mode I DCB Tension

Specimens tested at room temperature (RT) exhibited a reflective interlaminar surface when examined optically. SEM fractography of tows oriented perpendicular to the mechanically induced crack propagation direction revealed river marks indicating a crack growth direction consistent with the mechanically induced crack direction (Figure 8-1). Fractures at tows oriented parallel to the mechanically induced crack propagation direction were characterized by a mixed-mode morphology with poorly formed hackles in the matrix indicating shear propagation due to the influence of fabric reinforcement. Resin-rich regions between tows exhibited river marks indicating crack propagation from one tow toward the center of the adjacent tow, regardless of the mechanically induced crack propagation direction. Fiber/matrix adhesion was poor, as most fibers were bare.

Specimens tested at 500°F exhibited a slightly reflective interlaminar surface when examined optically. SEM fractography of tows oriented perpendicular to the mechanically induced crack propagation direction revealed river marks which indicated propagation in directions both consistent with and opposite to the overall propagation direction (Figure 8-2). Fractures at tows oriented parallel to the mechanically induced crack propagation direction were characterized by featureless matrix fracture having the appearance of shear failure. Fiber/matrix adhesion was good.

8.1.2 Mode II ENF Shear

Specimens tested at RT exhibited a matte surface regularly associated with shear fracture when examined optically. SEM fractography of tows oriented parallel to the mechanically induced crack propagation direction revealed hackles and scallops, indicative of shear fracture (Figure 8-3). Fractures at tows oriented perpendicular to the mechanically induced crack

propagation direction were characterized by mixed-mode morphology. The cleavage features associated with the observed hackles did not indicate crack propagation in the mechanically induced direction. The fiber matrix adhesion was poor.

Specimens tested at 500°F did not exhibit the dull, matte or milky white appearance associated with Mode II shear fractures when examined optically. SEM fractography revealed hackles and scallops on both the parallel and perpendicular (relative to the crack propagation direction) tows (Figure 8-4). Crack propagation direction could not be determined from the fracture surface features. Fiber/matrix adhesion was good.

8.2 TRANSLAMINAR FRACTURE

The specimens used for translaminar fracture were produced from quasi-isotropic laminates. Tests were conducted under RT/dry and 500°F/dry conditions. This contribution was made by Boeing.

8.2.1 Tension

Specimens tested at RT appeared predominantly rough and jagged due to protruding ± 45 degree fibers when examined optically, and this appearance is typical of translaminar tensile fracture. SEM fractography of the tensile portion of the fracture surface revealed fiber end features with fan patterns showing an overall propagation direction consistent with the mechanically induced crack growth direction (Figure 8-5). River marks and resin microflow in the resin-rich areas of the tensile zone also indicated a crack growth direction consistent with the mechanically induced crack growth direction.

Specimens tested at 500°F exhibited rough translaminar tensile characteristics over a quarter of the surface when examined optically, and the remainder of the surface appeared compressive. SEM fractography of the tensile region revealed small bundles of fibers on the fracture plane, due to fiber pullout (Figure 8-6). Radial patterns found on fiber end fractures indicated a crack growth direction consistent with the mechanically induced crack growth direction. Microbuckling and typical compressive fiber end fractures were observed on the compressive portion of the fracture surface. Fiber/matrix adhesion was fair.

8.2.2 Compression

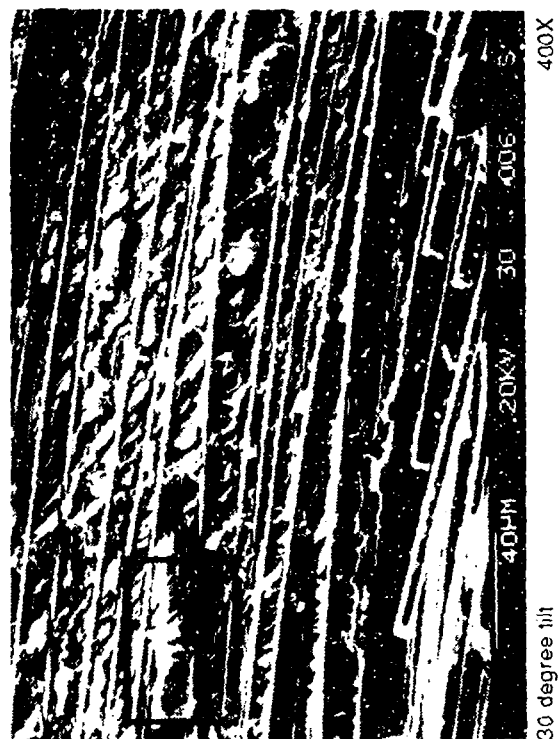
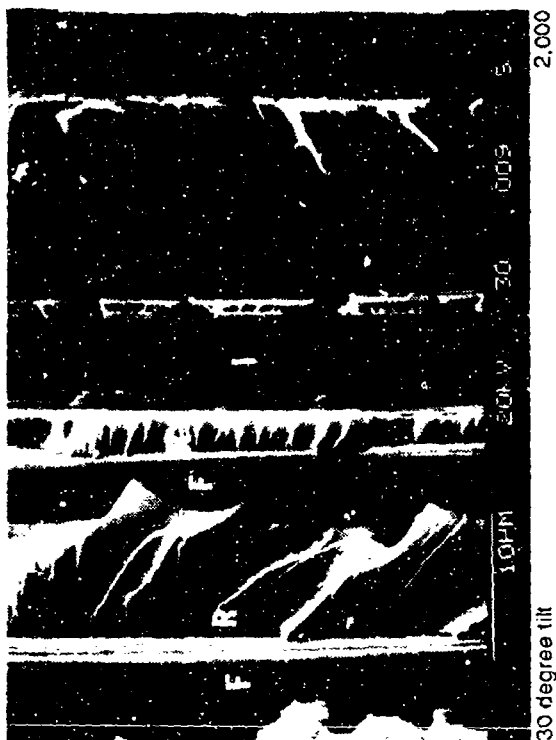
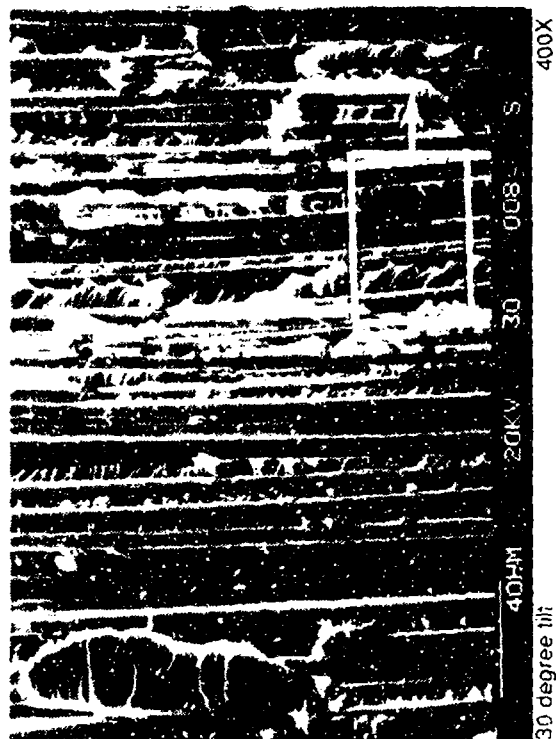
Optical examination of specimens tested at RT revealed both tensile and compressive regions, as was found on the translaminar tension specimens (Figure 8-7). The compressive zone in this specimen was approximately a third of the fracture surface with the remainder being tensile. The compressive loading appeared to have initiated a tensile crack on the opposite edge surface which propagated toward the notch and intersected the compressive damage. SEM examination of the tensile portion revealed fiber end fractures that indicated propagation toward the compressive zone. The compressive region revealed a debris-covered surface with fiber end fractures containing both tensile and compressive zones. Resin-rich fractures in the tensile zone

revealed river marks, indicating propagation opposite to the mechanically induced crack direction, as expected.

As in the translaminar tension specimens, plies oriented at 45 degree were observed protruding from the fracture surface. However, plies oriented at both +45 and -45 were observed on each fracture surface, with the +45 degree plies dominating. Delaminations were observed in these protruding plies.

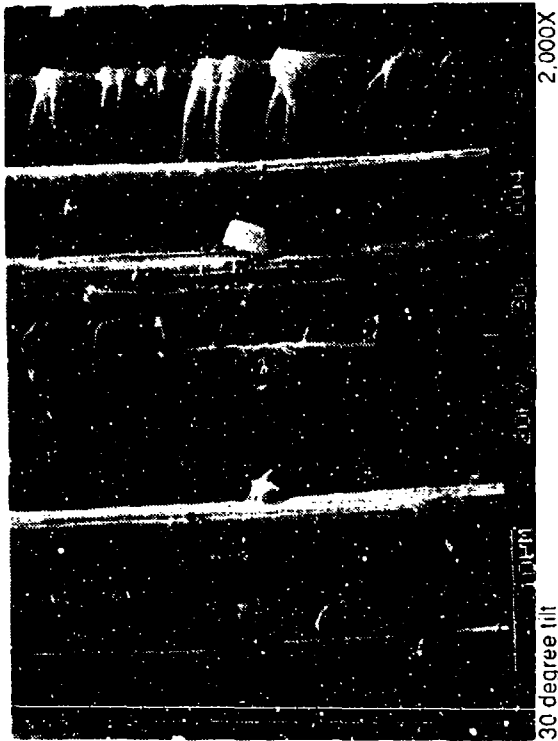
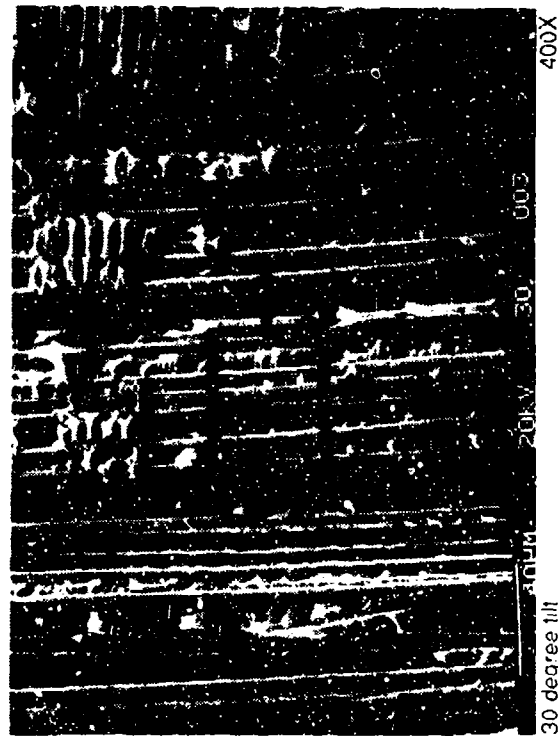
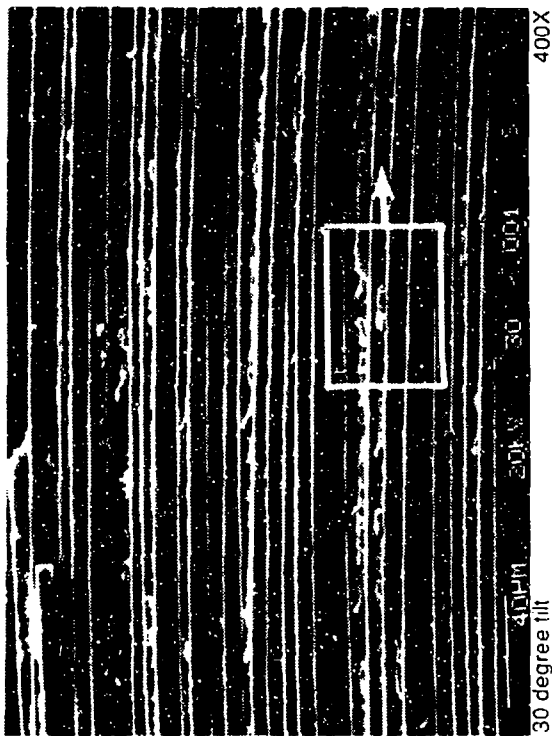
Macroscopically, the fractures were jagged due to protruding plies. The most outstanding features were the delaminated 45 degree plies which gave the appearance of strips of material. Fiber/matrix adhesion was poor, but fiber pullout was less pronounced than in the translaminar tension specimens.

Optical examination of specimens tested at 500°F revealed a rough, partly compressive and partly shear fracture. Compressive failure was found on approximately half of the fracture and was located on the notched portion (as intended). Compressive fracture occurred predominantly on the 0 and 90 degree plies, while the shear portion of the fracture occurred on the 45 degree plies. SEM examination of the compression portion of the fracture revealed fiber end fractures which had been obliterated by fracture debris (Figure 8-8). Microbuckling was observed. Hackles were found on the shear portion of the fracture. Fiber/matrix adhesion was poor.



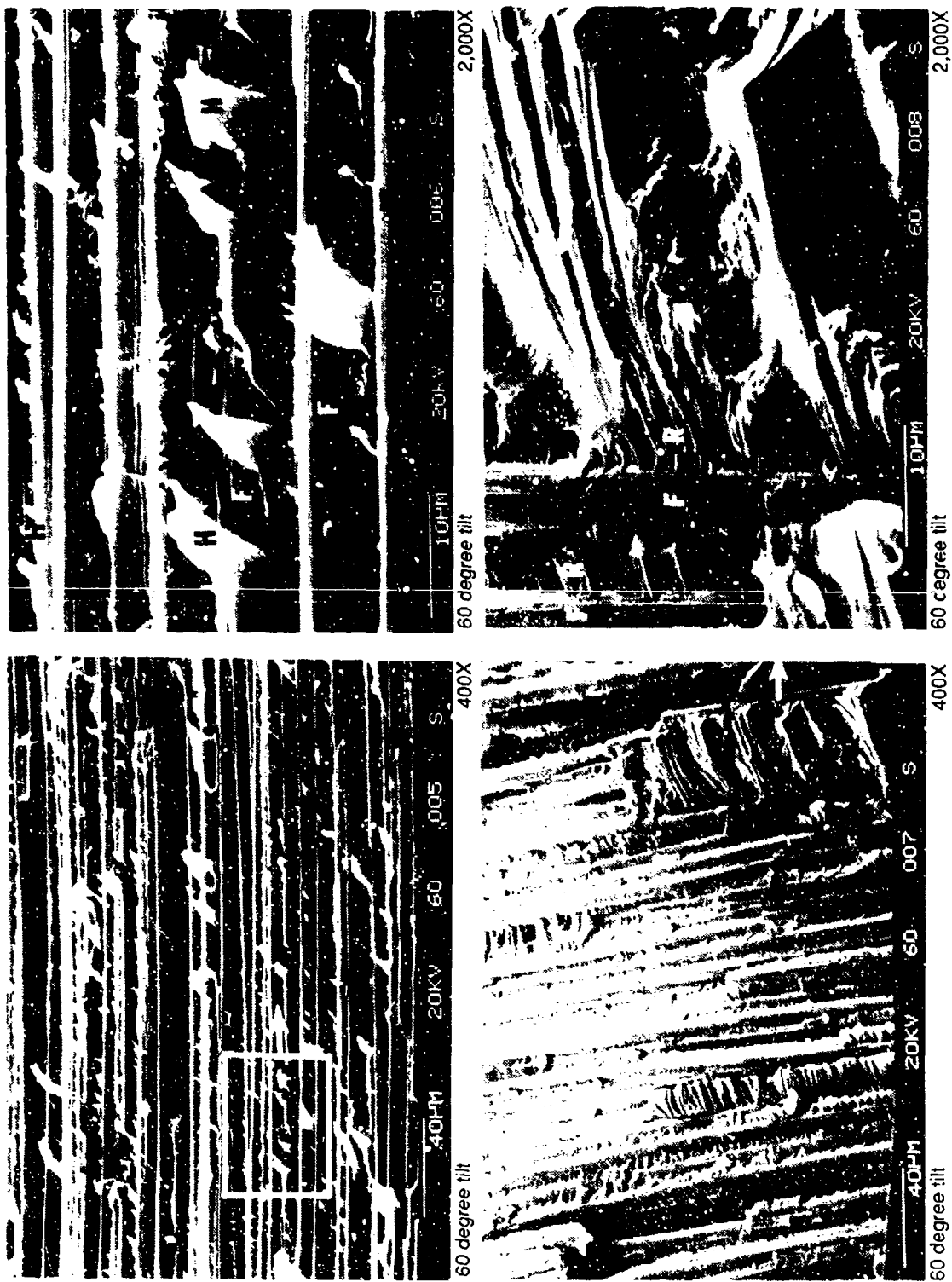
Mechanically induced crack direction

Legend: F fiber; H hackle; I fiber imprint; R rivermarks
 Figure 8-1. SEM Fractographs of Room Temperature, Mode I Interlaminar Tension Fracture in C3K 8-HS/PMR-15



↑
Mechanically induced crack direction

Legend: F fiber; M matrix failure; R rivermarks
Figure 8-2. SEM Fractographs of 500 F/Dry, Mode I Interlaminar Tension Fracture in C3K 8-HS/PMR-15





20X

60 degree tilt



400X

60 degree tilt



2,000X

60 degree tilt

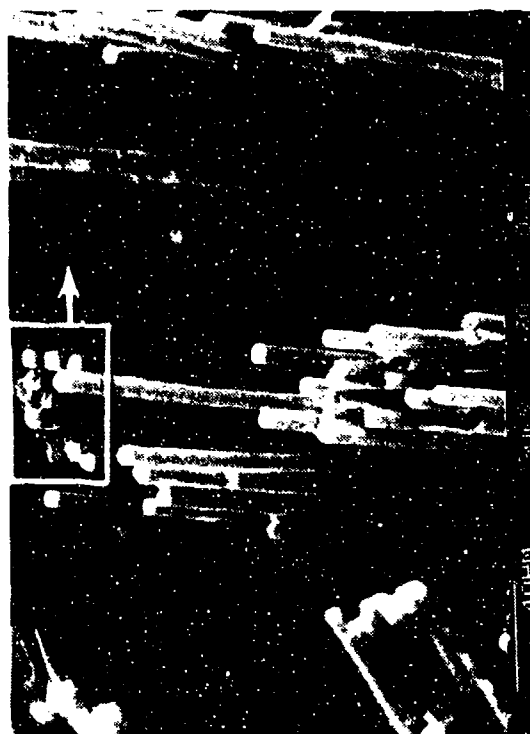
Legend:
F fiber matrix separation
H hackle
Mechanically induced crack direction



Figure 8-4. SEM Fractographs of 500 F/Dry, Mode II Interlaminar Shear Fracture in C3K 8-HS/PMR-15



30 degree tilt 20X



30 degree tilt 400X

Legend:

- F fiber fracture
- M matrix fracture

Mechanically induced
crack direction



30 degree tilt 2,000X

Figure 8-5. SEM Fractographs of Room Temperature/Dry, Translaminar Tension Fracture in C3K 8-HS/PMR-15



30 degree tilt 20X



30 degree tilt 400X

Mechanically induced
crack direction



30 degree tilt 2,000X

Figure 8-6. SEM Fractographs of 500 F/Dry, Translaminar Tension Fracture in C3K 8-HS/PMR-15



20 degree tilt 20X



20 degree tilt 400X

Legend:

C compression
N neutral axis
T tension

Mechanically induced
crack direction



20 degree tilt 2,000X

Figure 8-7. SEM Fractographs of Room Temperature/Dry, Translaminar Compression Fracture in C3K 8-HS/PMR-15

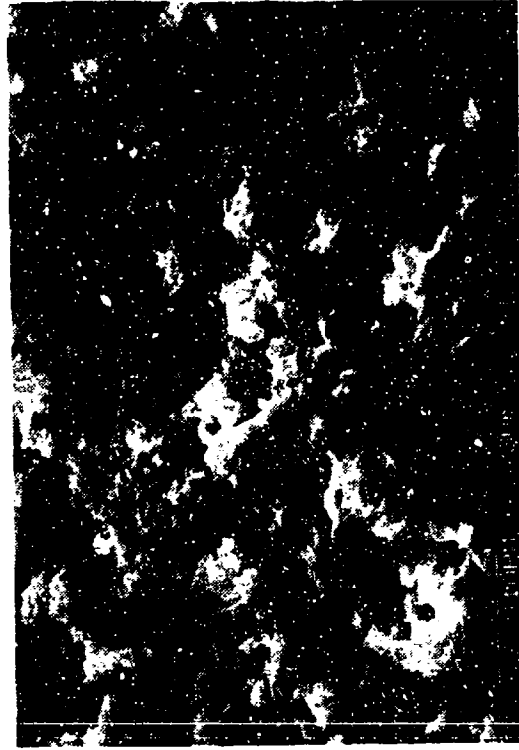


20X 30 degree tilt

Mechanically induced
crack direction



400X 30 degree tilt



2,000X 20 degree tilt

Figure 8-8. SEM Fractographs of 500 F/Dry, Translaminar Compression Fracture in C3K 8-HS/PMR-15

SECTION 9

BOLTED JOINTS

This section presents the results of fractographic characterizations of fractured Gr/Ep adherends joined using mechanical fasteners. Northrop ran the SAMCJ (Strength Analysis of Multifastened Composite Joints) computer program to develop the specimen test matrix for characterizing the six different failure modes in mechanically joined composite structures. This computer code, developed by Northrop for the USAF, enabled prediction of the failure mode(s) in single and multi-fastened bolted composite joints. Predictions were made through summation of the critical stresses at stress concentration points in the laminates, using known constitutive equations. The program also took into account the effects of the specimen geometries and bolt positions in prediction(s) of the failure mode(s).

A test matrix (Table 9-1) was developed for quasi-isotropic AS4/3501-6 Gr/Ep joined with titanium 'Hi-Lok' tension or shear-type flush head fasteners, using single lap-shear test specimens. Different failure modes are achieved through variations in the composite thicknesses (8 ply, 32 ply, 56 ply), specimen widths (w), and fastener-to-edge distances (e). In all cases, except for bolt pull through failure, a tension head type fastener was used with fastener diameter (d) being 0.25 in. The SAMCJ code also enabled the determination of the w/d and e/d ratios needed to create the required failure modes in the single-lap shear specimens, and these are shown in Table 9-2.

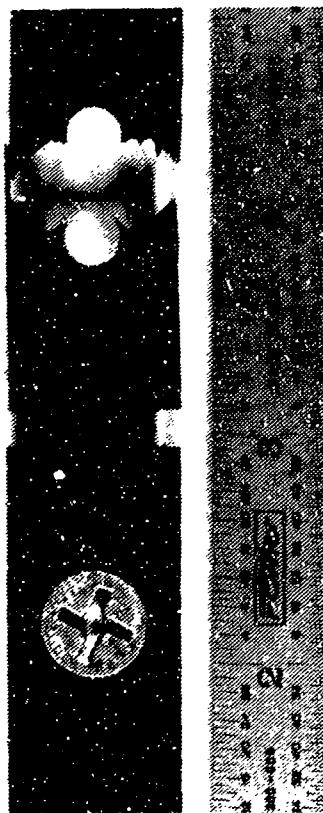
Table 9-1. Test Matrix for Mechanically Joined Composites

Failure Mode	No. of Specimens		
	32/Quasi	56/Quasi	8/Quasi
Tension	3	—	—
Tension Cleavage	3	—	—
Shear-Out	3	—	—
Bearing	3	—	—
Bolt Failure	—	3	—
Bolt Pull Through	—	—	3

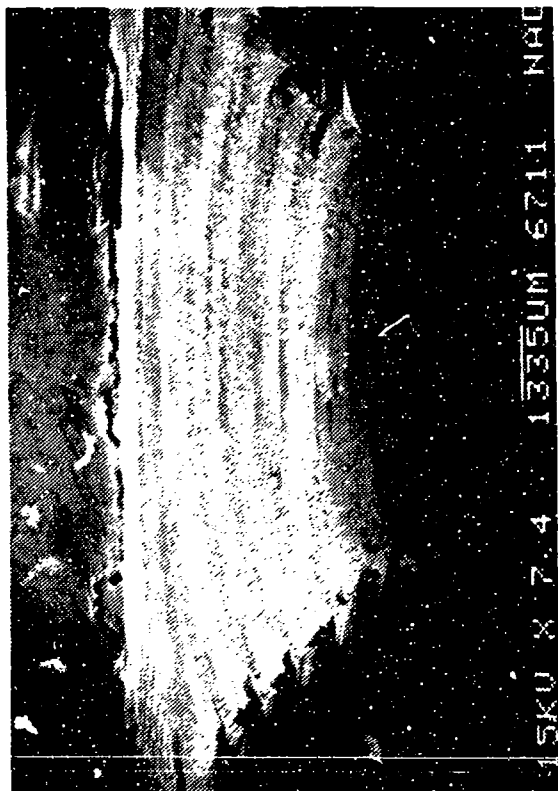
Table 9-2. Specimen Width/Fastener Diameter (w/d) and Fastener-Edge-Distance/Fastener Diameter (e/d) Ratios

Failure Mode	w/d	e/d
Tension	3	3
Tension Cleavage	3	1.5
Shear-Out	3	1
Bearing	5	3
Bolt Failure	6	3
Bolt Pull Through	6	3

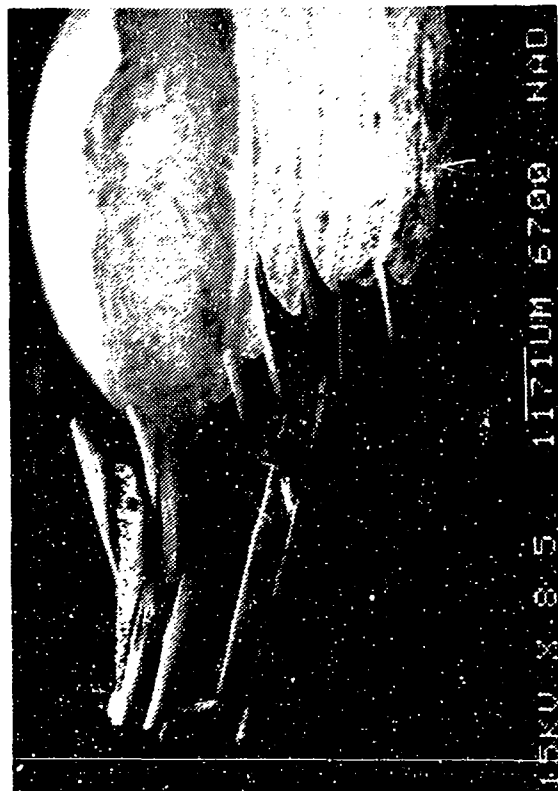
Fractographic evaluation of the bolted Gr/Ep joints indicates that varying failure modes occur in these specimens, and examination of individual plies can be used to establish the failure trends in these joined structures. The fractographs relating to bolted joints are provided in Figures 9-1 through 9-6. This contribution was made by Northrop.



(a)



(b)



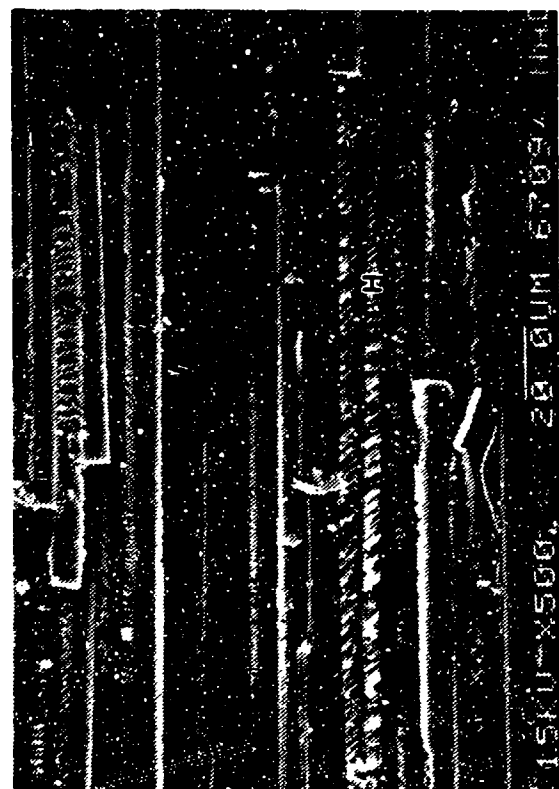
(c)

Figure 9-1. Optical and SEM Photographs of Tension Failure in a AS4/3501-6 Gr/Ep Bolted Joint

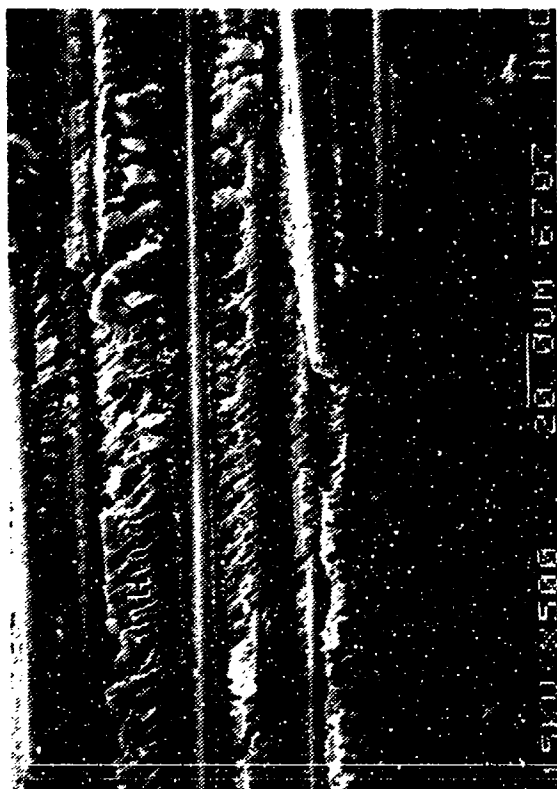
(a) Macro photograph of Failed Joint

(b), (c) Macro photographs of Failed Adherends

Note compression damage (arrows)



(d)



(e)



(f)

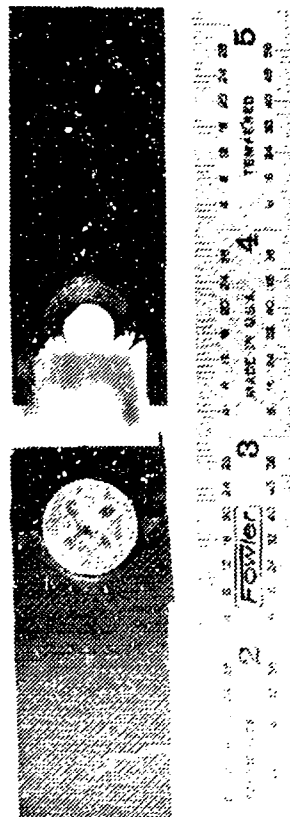
Figure 9-1. (Continued)
(d), (e) Hackles (H) in 90 and 45 Degree Plies
(f) DAF Radials on 0 Degree Fibers



(b)



(c)



(a)

Figure 9-2. Optical and SEM Photographs of Tension-Cleavage Failure in a AS4/3501-6 Gr/Ep Bolted Joint
(a) Macro photograph of Joint
(b), (c) Macro photographs of Peripheral Regions of Bolt-Hole in Mating Halves

C = Compression failure
T = Tension failure

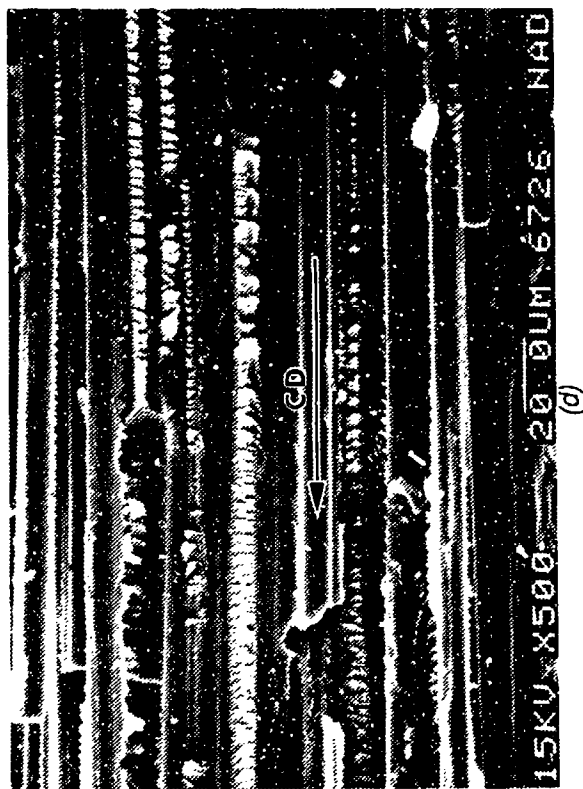


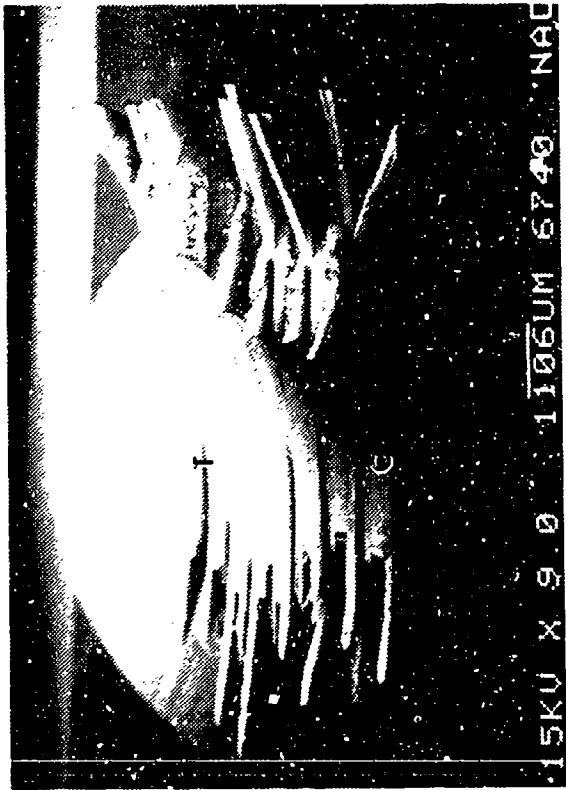
Figure 9-2. (Continued)
(d) Transaminar Fracture in 90 Degree Ply in Tensile Fracture Region

(e) Fracture in 45 Degree Ply

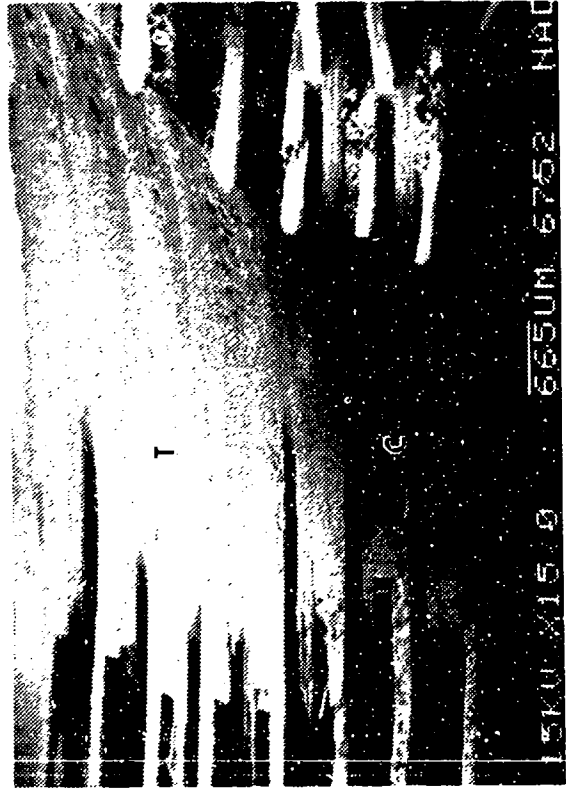
(f) Tensile Fracture in 0 Degree Ply
Note DAF radials (arrows)

CD = Crack propagation direction





(b)



(c)



(a)

Figure 9-3. Optical and SEM Photographs of Shear-Out Failure in a AS4/3501-6 Gr/Ep Bolted Joint

(a) Macro photograph of Failed Joint
(b), (c) Macro photographs of Failed Adherends

Note compression (C) and tension (T) regions

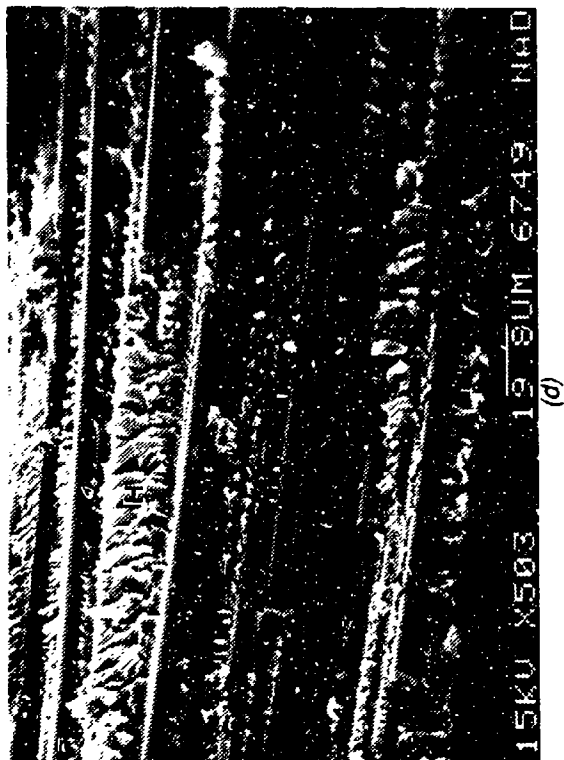
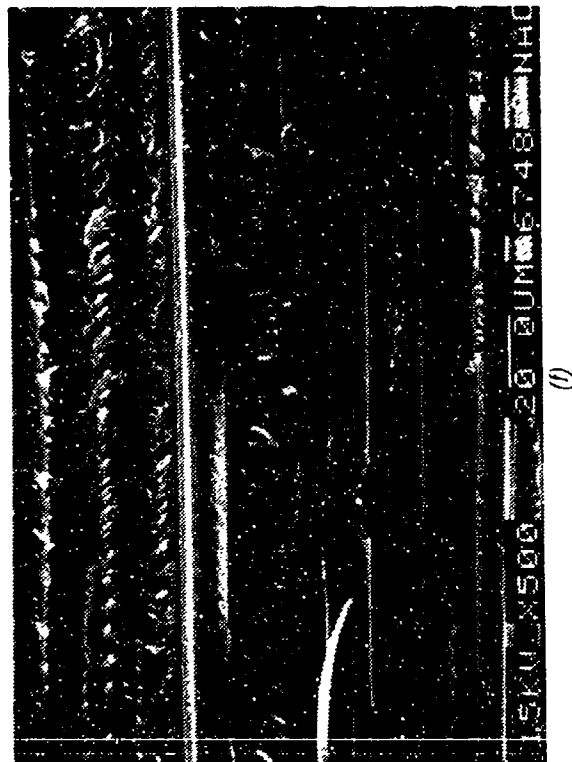
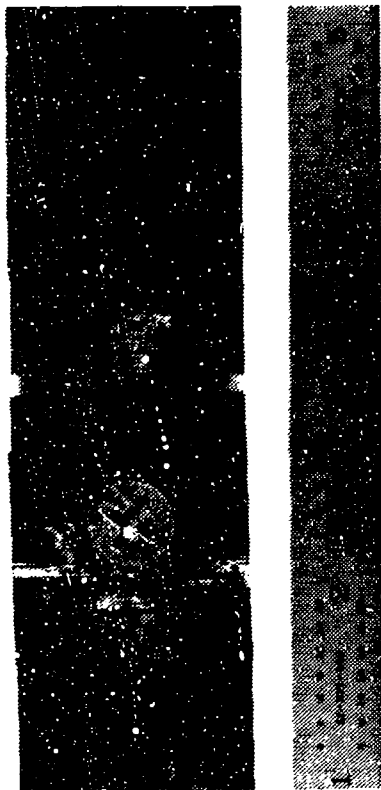


Figure 9-3. (Continued)
 (d) Hackles (H) in 45 Degree Plies
 (e) DAF Radials (Arrows) and Hackles (H) in
 0 Degree Plies
 (f) Peel Characteristics in 90 Degree Plies





(a)



(b)



(c)

Figure 9-4. Optical and SEM Photographs of Bearing Failure
in a AS4/3501-6 Gr/Ep Bolted Joint
(a) Macro photograph of Failed Joint
(b) Detail Near Bolt-Hole
(c) Fractured Adherends

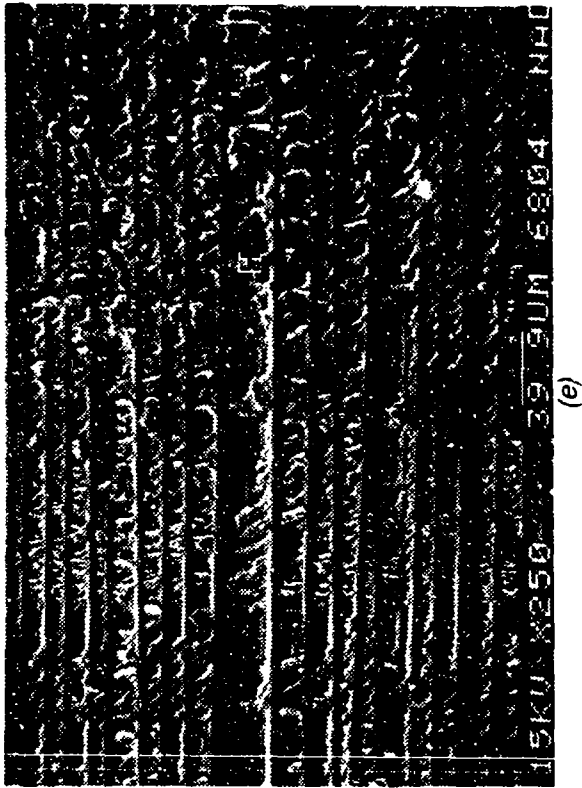
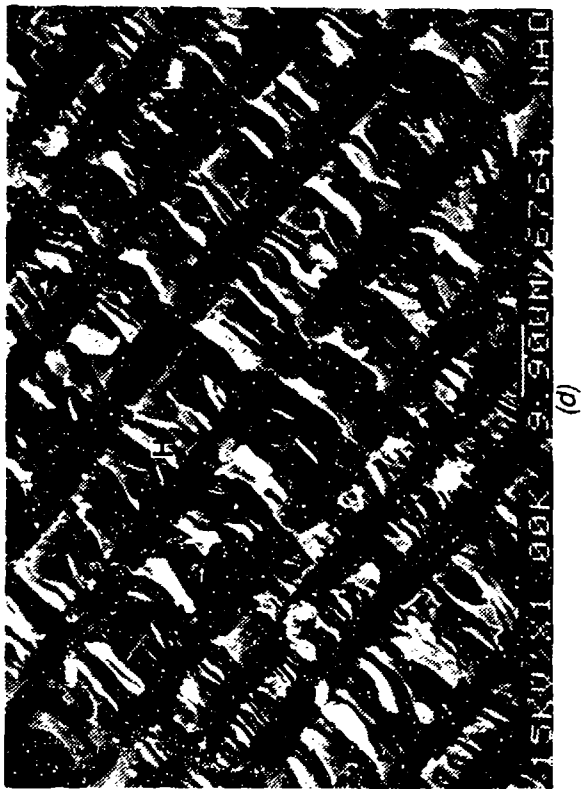
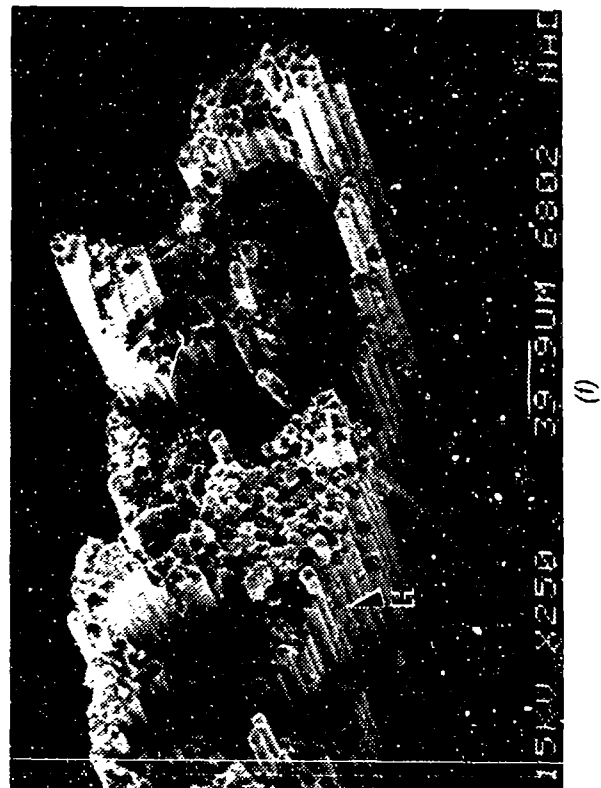


Figure 9-4. (Continued)
(d), (e), (f) Hackles (H) in 45, 90, and 0 Degree Plies





(a)

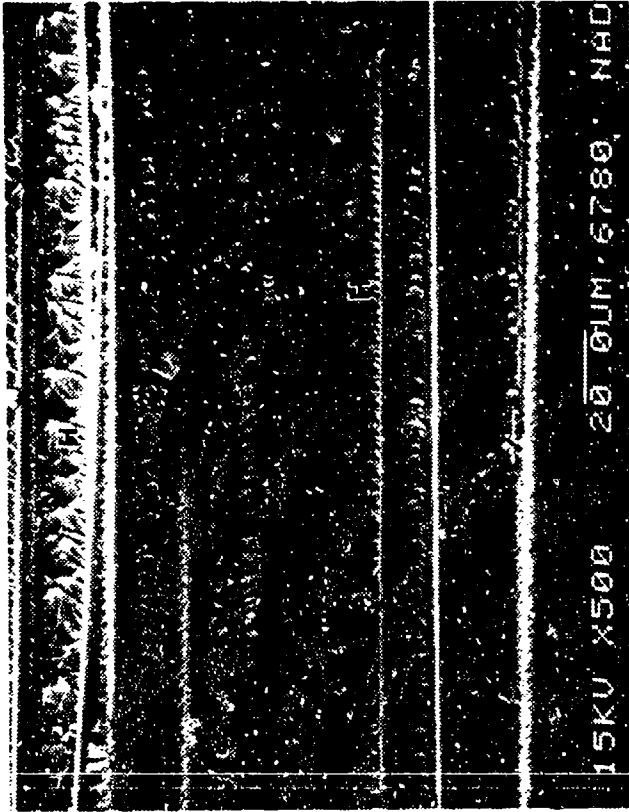


(b)

Figure 9-5. Optical and SEM Photographs of Bolt Failure in a AS4/3501-6 Gr/Ep Bolted Joint
(a), (b) Macro photographs of Fracture
Note fiber crush (F) and delamination (D)



(c)



(d)

Figure 9-5. (Continued)
 (c) Fracture Detail in Fiber Crush Region
 (d) Shear Fracture in Delamination Region
 Note hackles (H)



(a)



(b)

Figure 9-6. Optical and SEM Photographs of Bolt Failure in a AS4/3501-6 Gr/Ep Bolted Joint
 (a) Macro photograph Showing Delamination in Adherend (Arrow)
 (b) Peel Fracture in Surface Delamination (Low Magnification)



(c)



(d)

Figure 9-6. (Continued)
 (c) Peel Fracture in Surface Delamination (Intermediate Magnification)
 (d) Peel Fracture in an Internal Delamination

Note arrays of rivers (R) oriented along CD
 CD = Crack propagation direction

SECTION 10

ADHESIVELY BONDED COMPOSITES

This section presents the failure modes associated with fractures in Gr/Ep or Gr/BMI adherends joined with adhesive. The test matrices and tests performed are shown in Table 10-1. Tests were performed to develop cohesive failures, adhesive failures, and mixed failure modes, using variations in lap/strap ratios, ply layups, and overlap distances.

Fracture evaluation of the Gr/Ep and Gr/BMI bonded structures indicates that specimen geometry, lap/strap ratios and test load play roles in controlling fracture surface characteristics. Fractures can be mapped following adhesive or mixed failure modes through evaluation of features on the fractured adherends. Under these failure modes, rivers on the adherend fracture surfaces can be used to map fracture direction. Crack-direction cannot be easily mapped in pure cohesive joint failures, since no clear cut features are observed on the fractured adhesives.

Fractographs relating to adhesively bonded Gr/Ep are provided in Figures 10-1 through 10-8 and those relating to adhesively bonded Gr/BMI are provided in Figures 10-9 through 10-12. This contribution was made by Northrop.

Table 10-1. Test Matrix for Adhesively Bonded Composite Fractography

MATERIAL: AS4/3501-6 GR/EP

ADHESIVE: FM-300

LOADING/SPECIMEN	LAP/STRAP PLY ORIENTATIONS	
	0°/0°	0°/32 QUASI
MODE I TENSION, DCB	3	3
MODE II SHEAR, CONSTRAINED CLS		
OVERLAP 1	3	3
OVERLAP 2		—
MODE I TENSION + MODE II SHEAR, UNCONSTRAINED CLS		
OVERLAP 1	3	—
OVERLAP 2	3	3

MATERIAL: AS4/5250-3 GR/BMI

ADHESIVE: EA 9673

LOADING/SPECIMEN	LAP/STRAP PLY ORIENTATIONS	
	0°/0°	0°/32 QUASI
MODE I TENSION, DCB	3	3
MODE I TENSION + MODE II SHEAR, UNCONSTRAINED CLS		
OVERLAP 1	3	3

DCB = DOUBLE CANTILEVER BEAM

CLS = CRACKED-LAP SHEAR

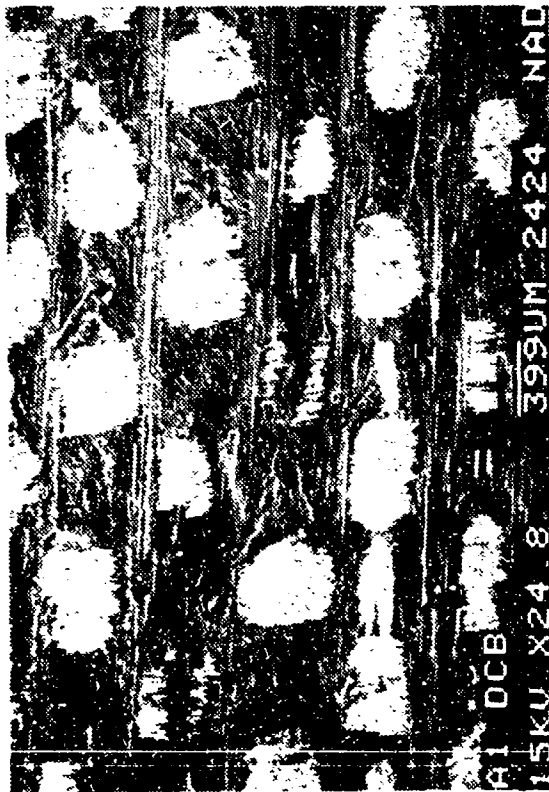
OVERLAP 1 = 7 INCHES

OVERLAP 2 = 5 INCHES

532 15



(b)



(c)



Failure in unidirectional AS4/3501-6 GFR/Ep adherends bonded with FM 300 adhesive and tested under interlaminar Mode I tension. The image shows a dark, textured surface with a bright, irregularly shaped region labeled 'A' indicating adhesive failure. A label 'C' is also visible near the bottom center.

(a)

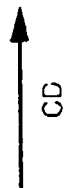
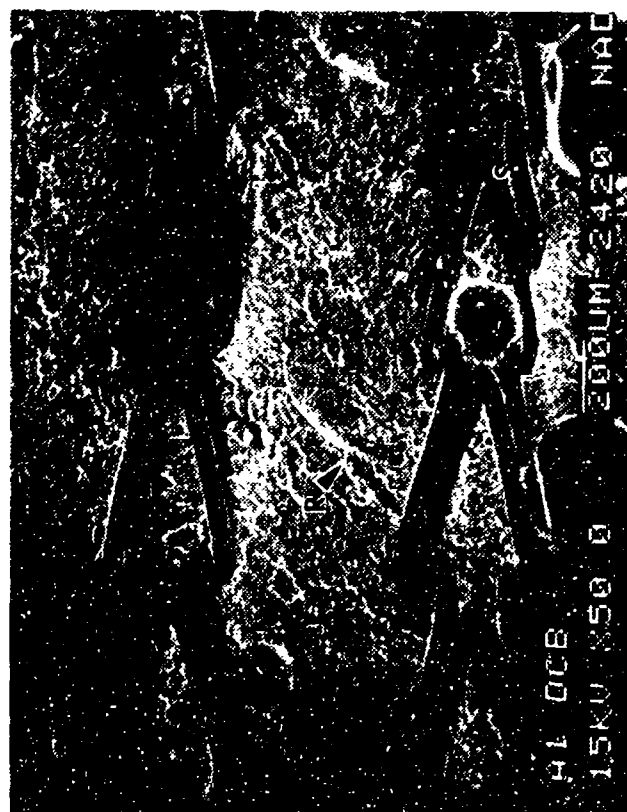


Figure 10-1. Optical and SEM Photographs of Failure in Unidirectional AS4/3501-6 GFR/Ep Adherends Bonded With FM 300 Adhesive and Tested Under Interlaminar Mode I Tension
(a) Macro photograph
(b) Low Magnification (4X) Photograph Showing Failure Detail
(c) Adhesive Failure Region

A = Adhesive failure
C = Cohesive failure
CD = Crack propagation direction



(e)



(d)

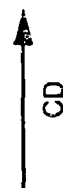
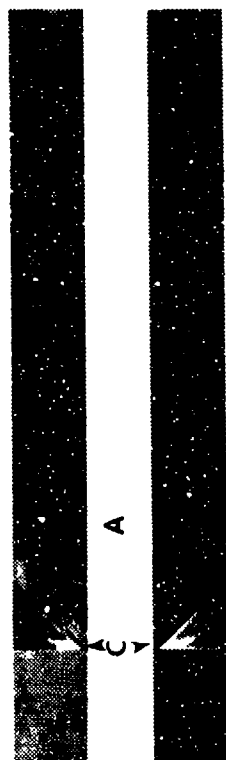
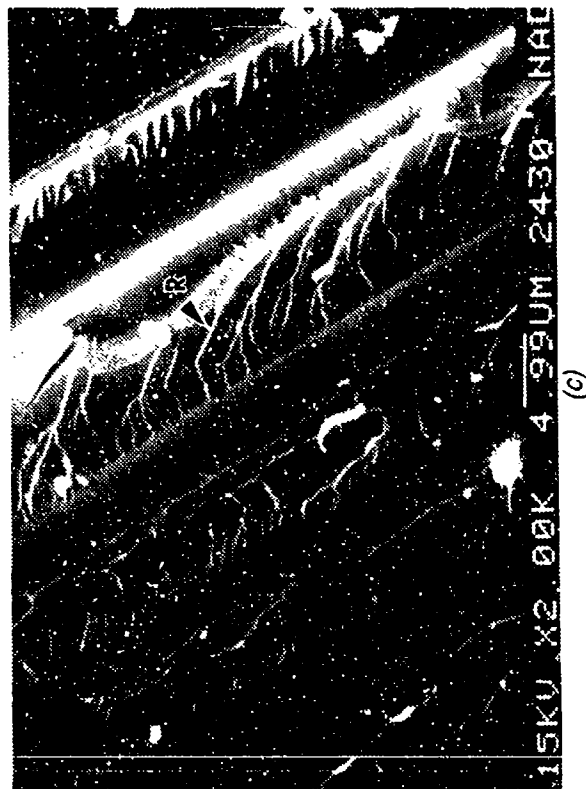


Figure 10-1. (Continued)
 (d) River Patterns (R) in Fractured Adhesive in Cohesive Failure Area
 (e) River Patterns (R) in Fractured Epoxy in Adhesive Failure Region

CD = Crack propagation direction
 S = Scrim



15KV X49.1K 203UM 2428 NAD

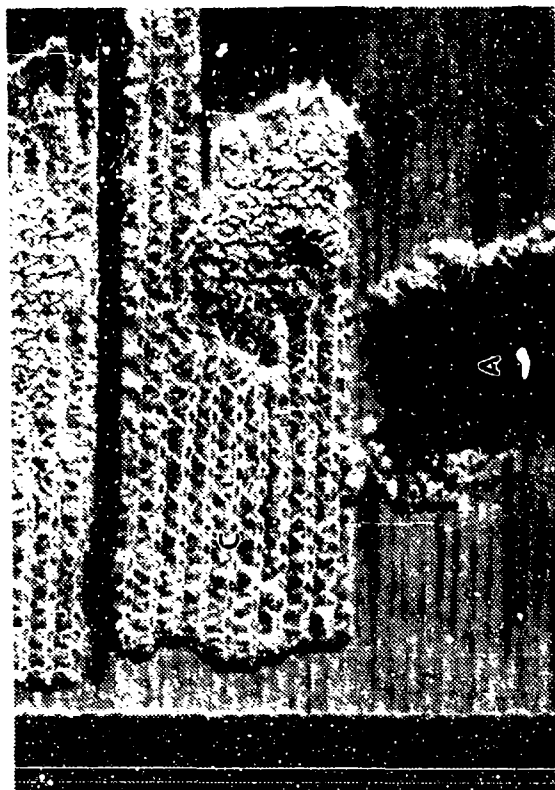
(a)

CD

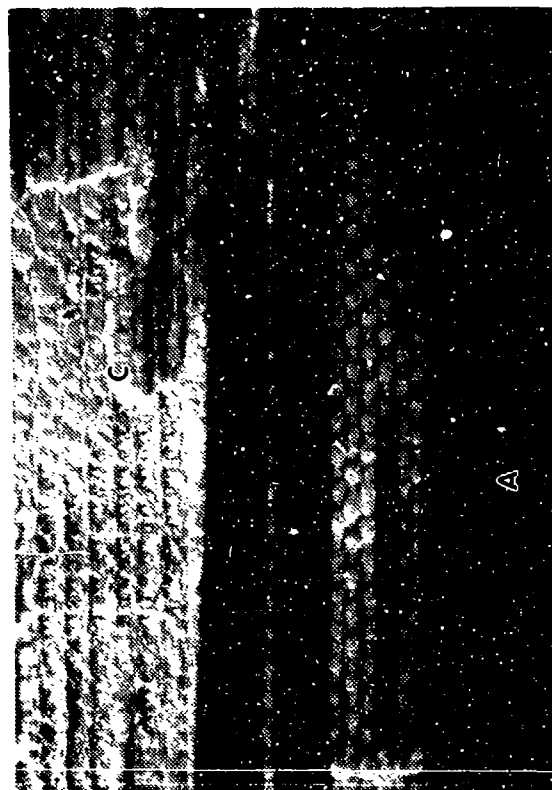
Figure 10-2. Optical and SEM Photographs of Failure in Unidirectional Gr/Ep Bonded to Quasi-Isotropic Gr/Ep With FM 300 Adhesive and Tested Under Mode I Tension

(a) Macro photograph
(b), (c) Adhesive Failure Region

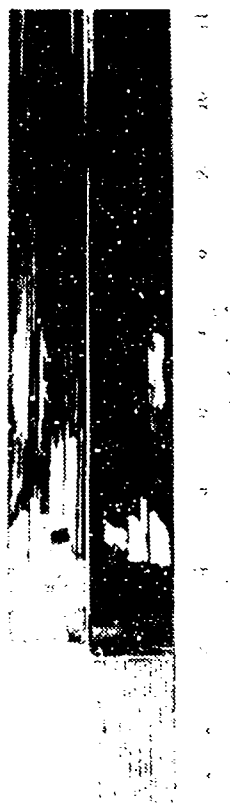
A = Adhesive failure
C = Cohesive failure
CD = Crack propagation direction
R = River patterns
S = Scum



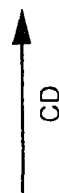
(a)



(b)



(c)



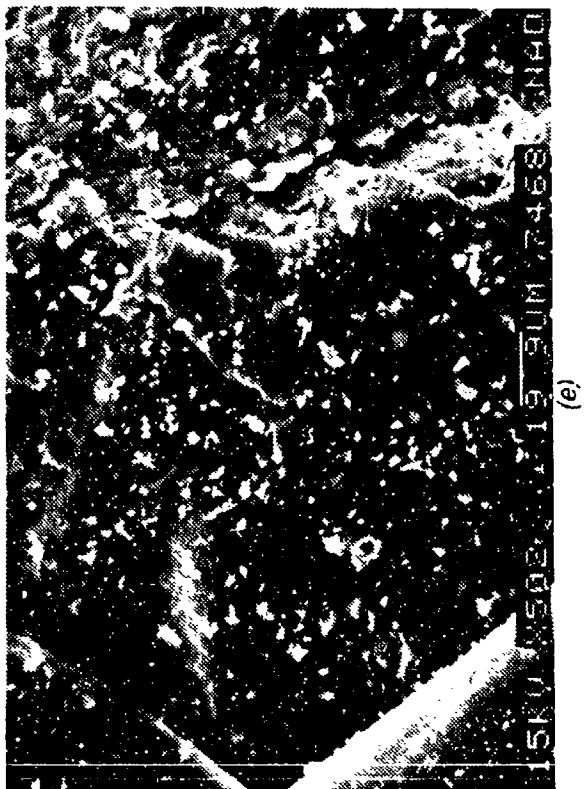
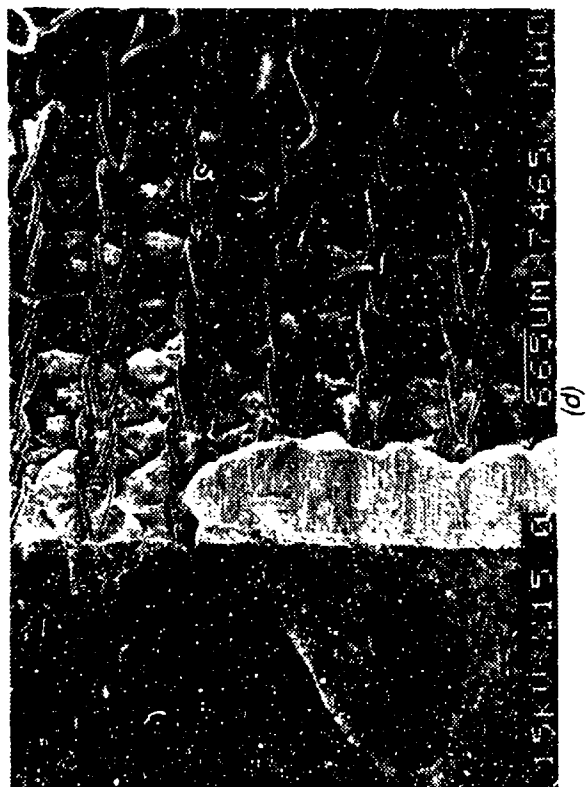
CD

Figure 10-3. Optical and SEM Photographs of Failure in Unidirectional AS4/3501-6 Gr/Ep Adherends Bonded With FM 300 Adhesive and Tested Under Mode II Interlaminar Shear

(a) Macro photograph

(b), (c) Low Magnification (4X) Photographs Showing Cohesive (C) and Adhesive (A) Failure Characteristics

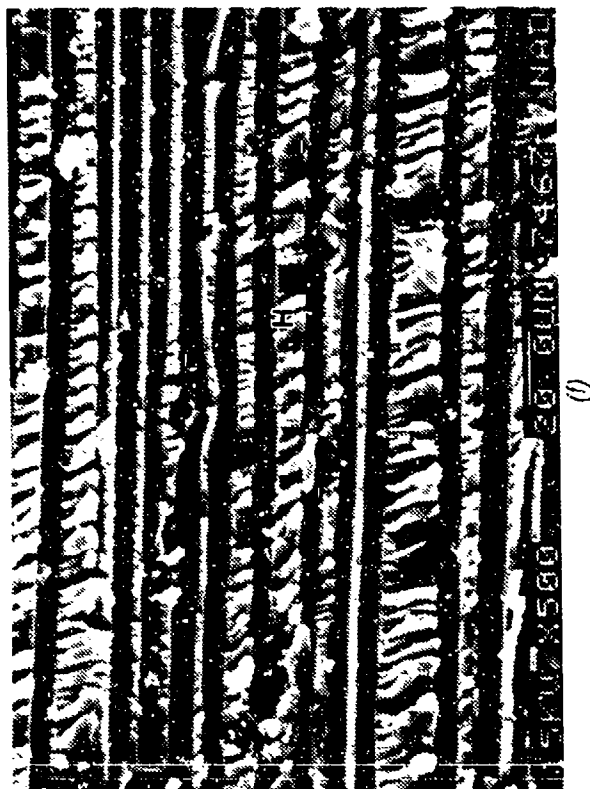
CD = Crack-propagation direction



CD
↑

Figure 10-3. (Continued)
(d), (e) Cohesive Failure in FM 300 Adhesive
(f) Hackles (H) in Fractured Adherends in Adhesive Failure Region

CD - Crack propagation direction
S = Scram



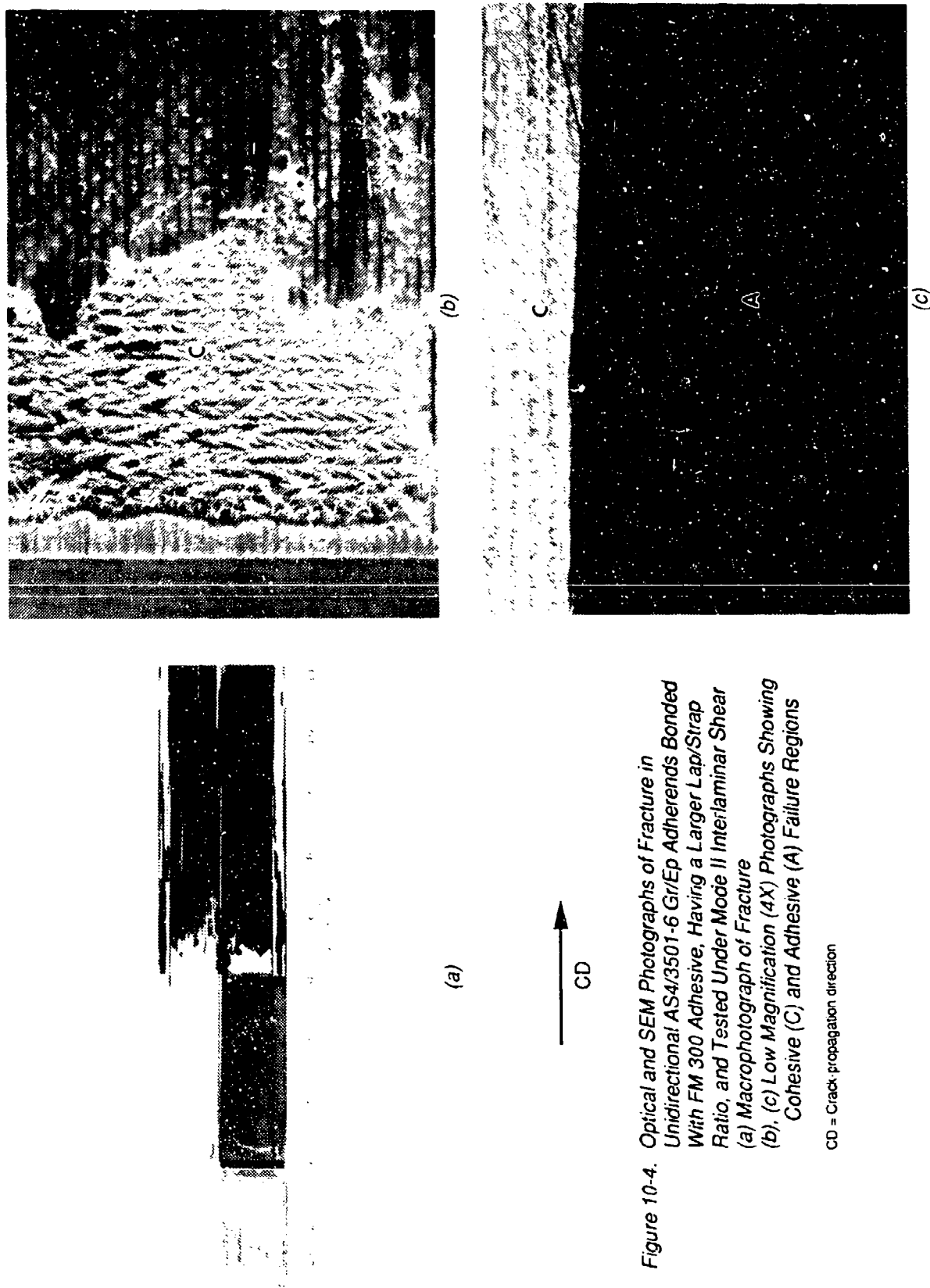


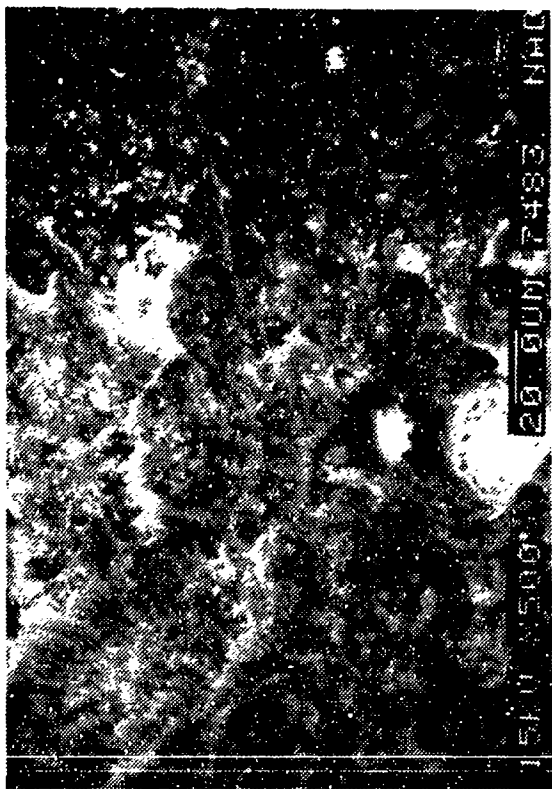
Figure 10-4. Optical and SEM Photographs of Fracture in Unidirectional AS4/3501-6 GrlEp Adherends Bonded With FM 300 Adhesive, Having a Larger Lap/Strap Ratio, and Tested Under Mode II Interlaminar Shear

(a) Macro photograph of Fracture
 (b), (c) Low Magnification (4X) Photographs Showing Cohesive (C) and Adhesive (A) Failure Regions

CD = Crack propagation direction



(d)



(e)



(f)

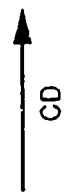
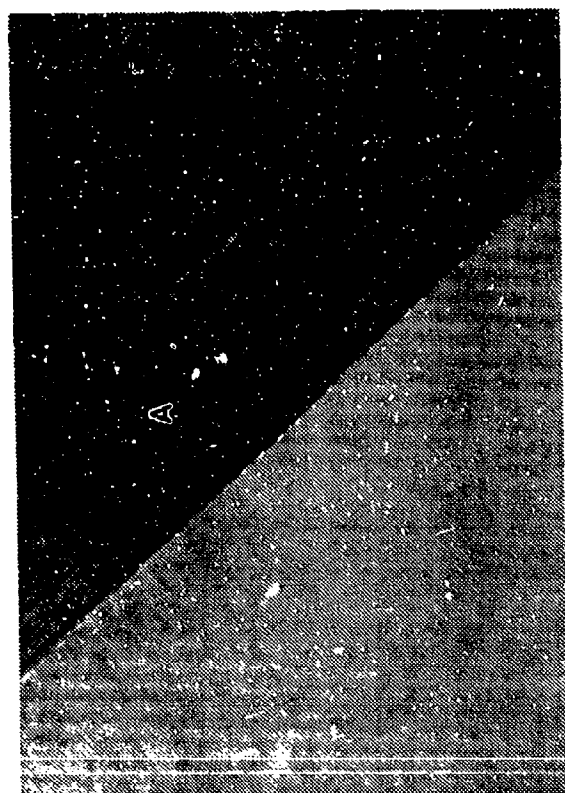
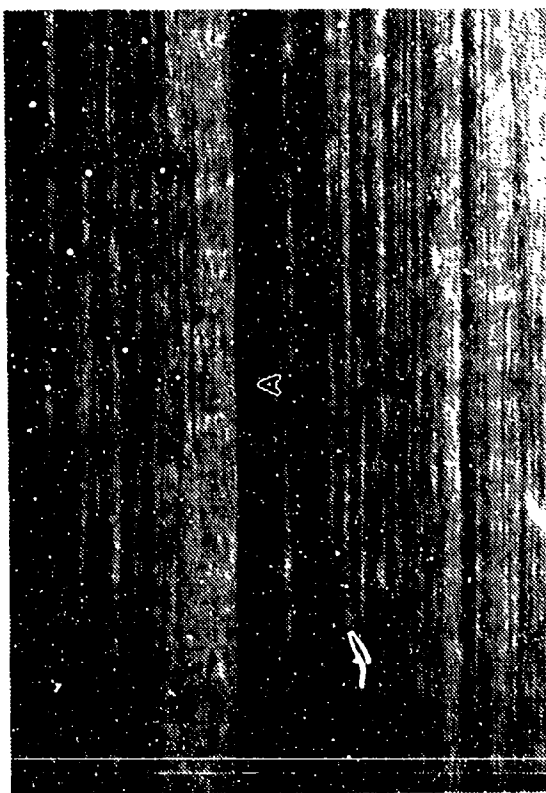


Figure 10-4. (Continued)
 (d). (e) Cohesive Failure in FM 300 Adhesive
 (f) Hackles (H) in Fractured Adherends in Adhesive Failure Region

CD = Crack-propagation direction



(b)



(c)



(a)

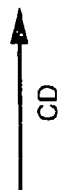


Figure 10-5. Optical and SEM Photographs of Fracture in Unidirectional Gr/Ep Bonded to Quasi-Isotropic Gr/Ep With FM 300 Adhesive and Tested Under Mode II Interlaminar Shear
(a) Macro photograph of Fracture
(b), (c) Low Magnification (4X) Photographs Showing Predominantly Adhesive (A) Failure Characteristics
CD = Crack propagation direction



(d)



(e)

CD →

Figure 10-5. (Continued)
 (d) Hackles in 45 Degree Ply
 (e) Hackles and Rivers in 0 Degree Ply
 H = Hackles
 R = Rivers
 CD = Crack-propagation direction

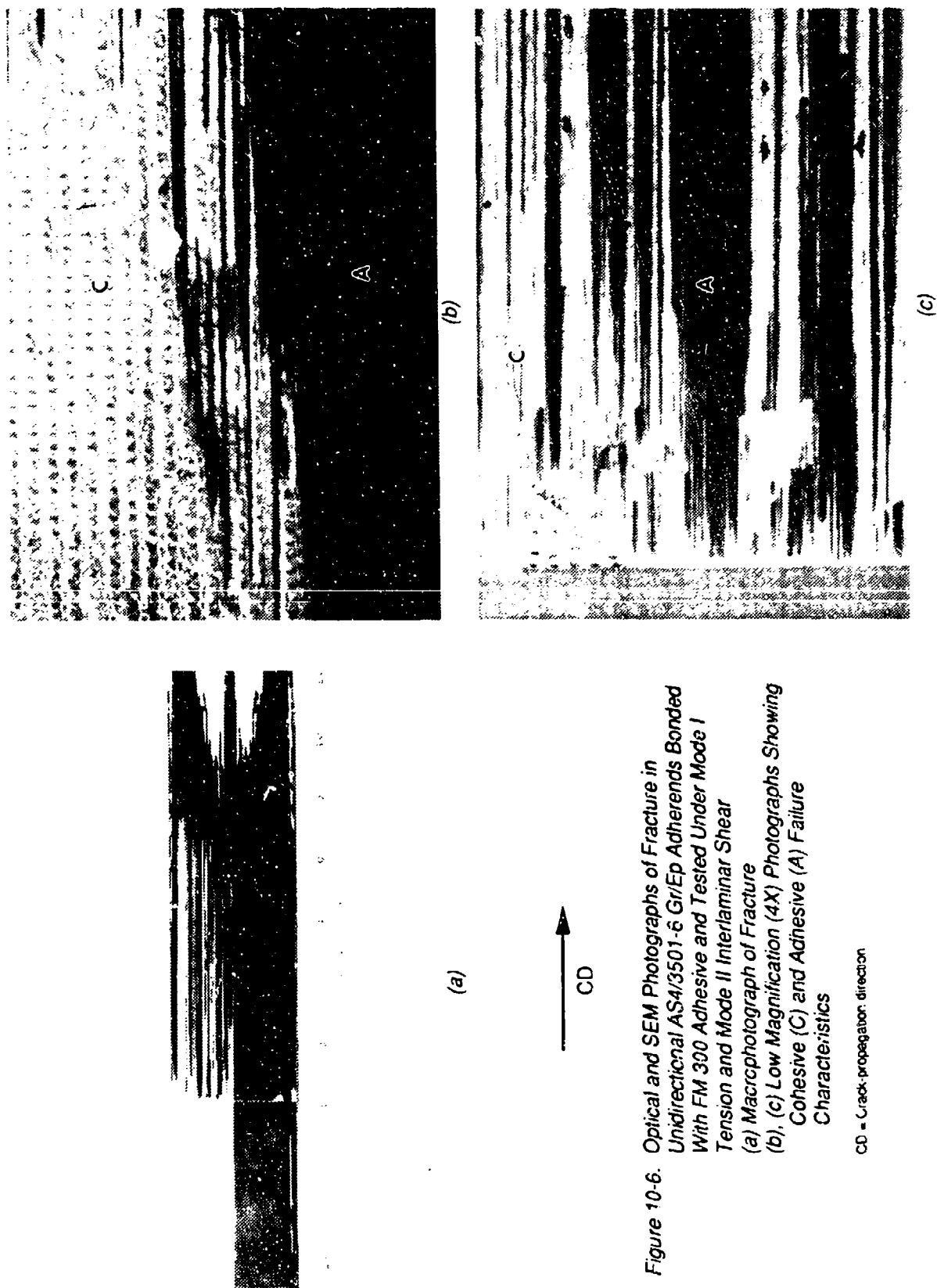



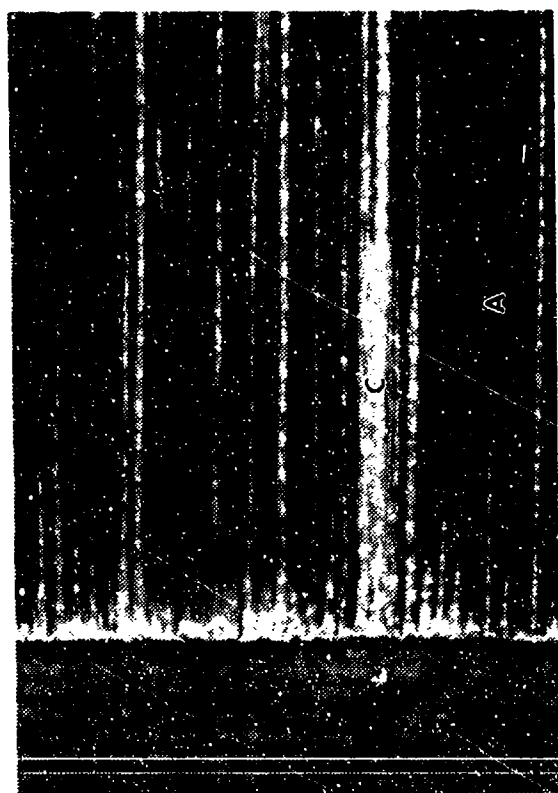
Figure 10-6. Optical and SEM Photographs of Fracture in Unidirectional AS4/3501-6 Gr/Ep Adherends Bonded With FM 300 Adhesive and Tested Under Mode I Tension and Mode II Interlaminar Shear
 (a) Macro photograph of Fracture
 (b), (c) Low Magnification (4X) Photographs Showing Cohesive (C) and Adhesive (A) Failure Characteristics
 CD = Crack-propagation direction



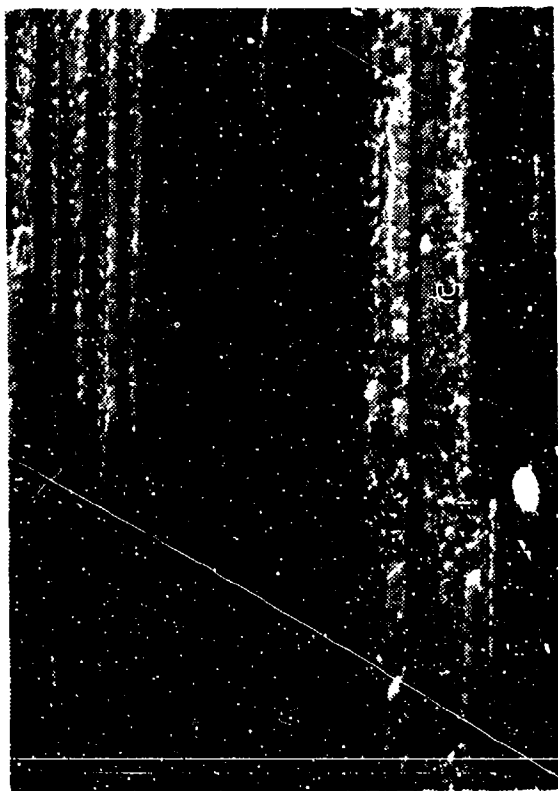


 CD

Figure 10-6. (Continued)
 (d), (e) Cohesive Failure in FM 300 Adhesive
 (f) Peel Characteristics in Fractured Adherends
 CD = Crack-propagation direction



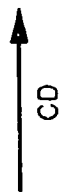
(b)



(c)



(a)



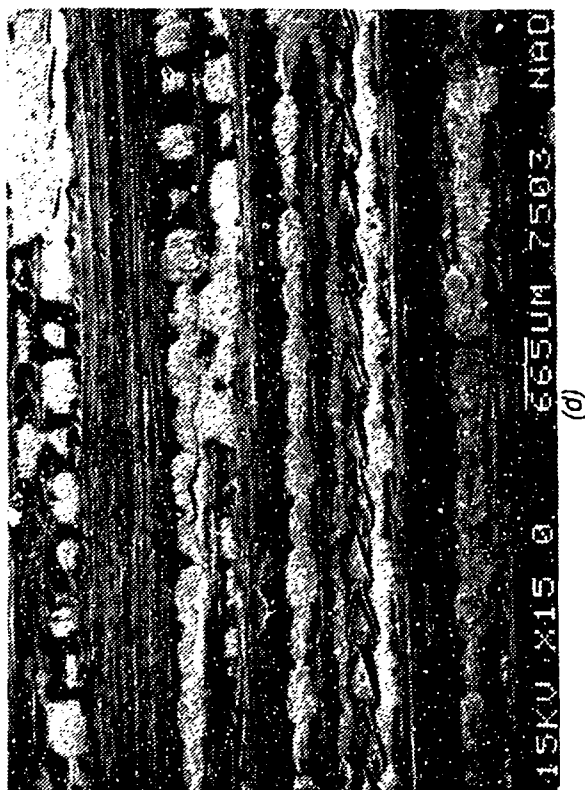
CD

Figure 10-7. Optical and SEM Photographs of Fracture in Unidirectional AS4/3501-6 Gr/Ep Adherends Bonded With FM 300 Adhesive, Larger Lap/Strap Ratio and Tested Under Mode I Tension and Mode II Interlaminar Shear

(a) Macro photograph of Fracture

(b), (c) Low Magnification (4X) Photographs Showing Cohesive (C) and Adhesive (A) Failure Characteristics

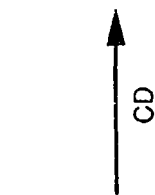
CD = Crack propagation direction



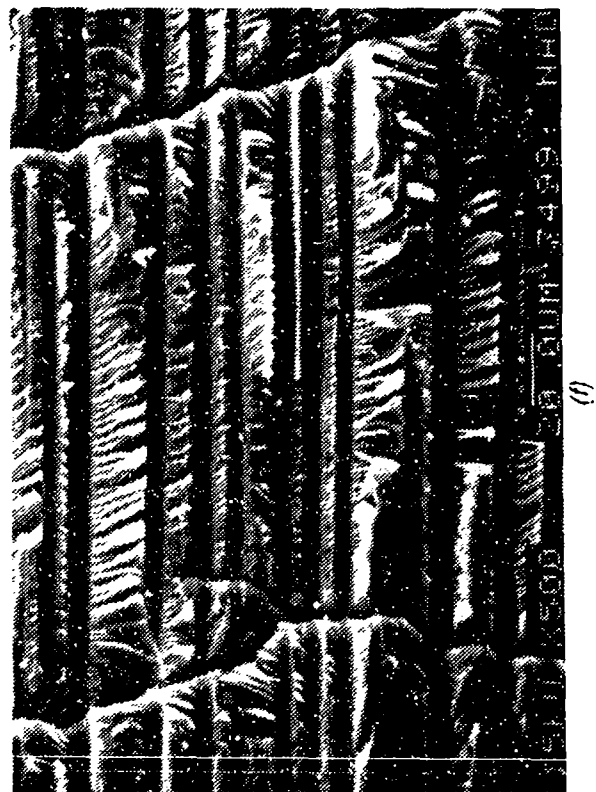
(d)



(e)

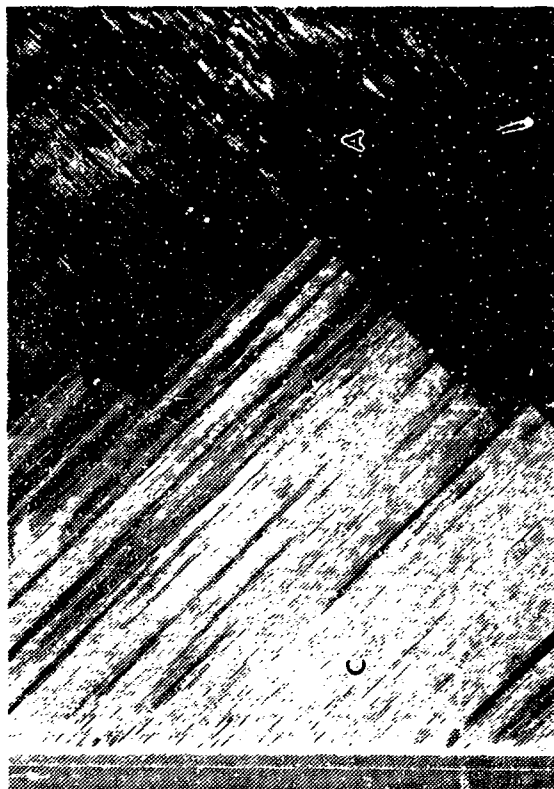


CD



(f)

Figure 10-7. (Continued)
 (d), (e) Cohesive Failure in FM 300 Adhesive
 (f) Peel Characteristics in Fractured Adherend
 CD = Crack-propagation direction



(b)



(c)



(a)

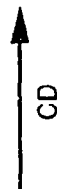
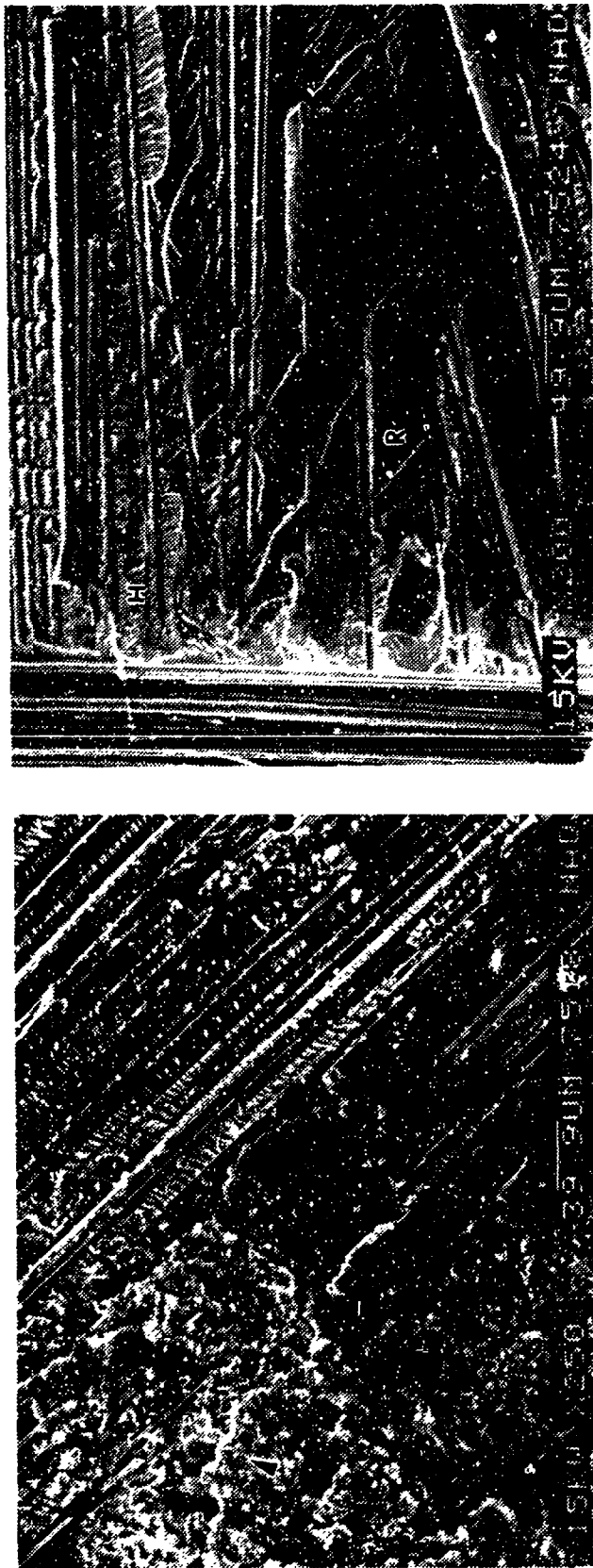


Figure 10-8. Optical and SEM Photographs of Fracture in Unidirectional Gr/Ep Bonded to Quasi-isotropic Gr/Ep Using FM 300 Adhesive, Large Lap/Strap Ratio and Tested Under Mode I Tension and Mode II Interlaminar Shear
(a) Macro photograph of Fracture
(b), (c) Low Magnification (4X) Photographs Showing Cohesive (C) and Adhesive (A) Failure Characteristics

CD = Crack-propagation direction



(d)

(e)

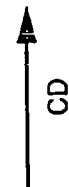


Figure 10-8. (Continued)
 (d) Cohesive Failure of Adhesive (Arrow) in Mixed Mode Failure Region
 (e) Hackles (H) and Rivers (R) in Adhesive Failure Region

CD = Crack-propagation direction

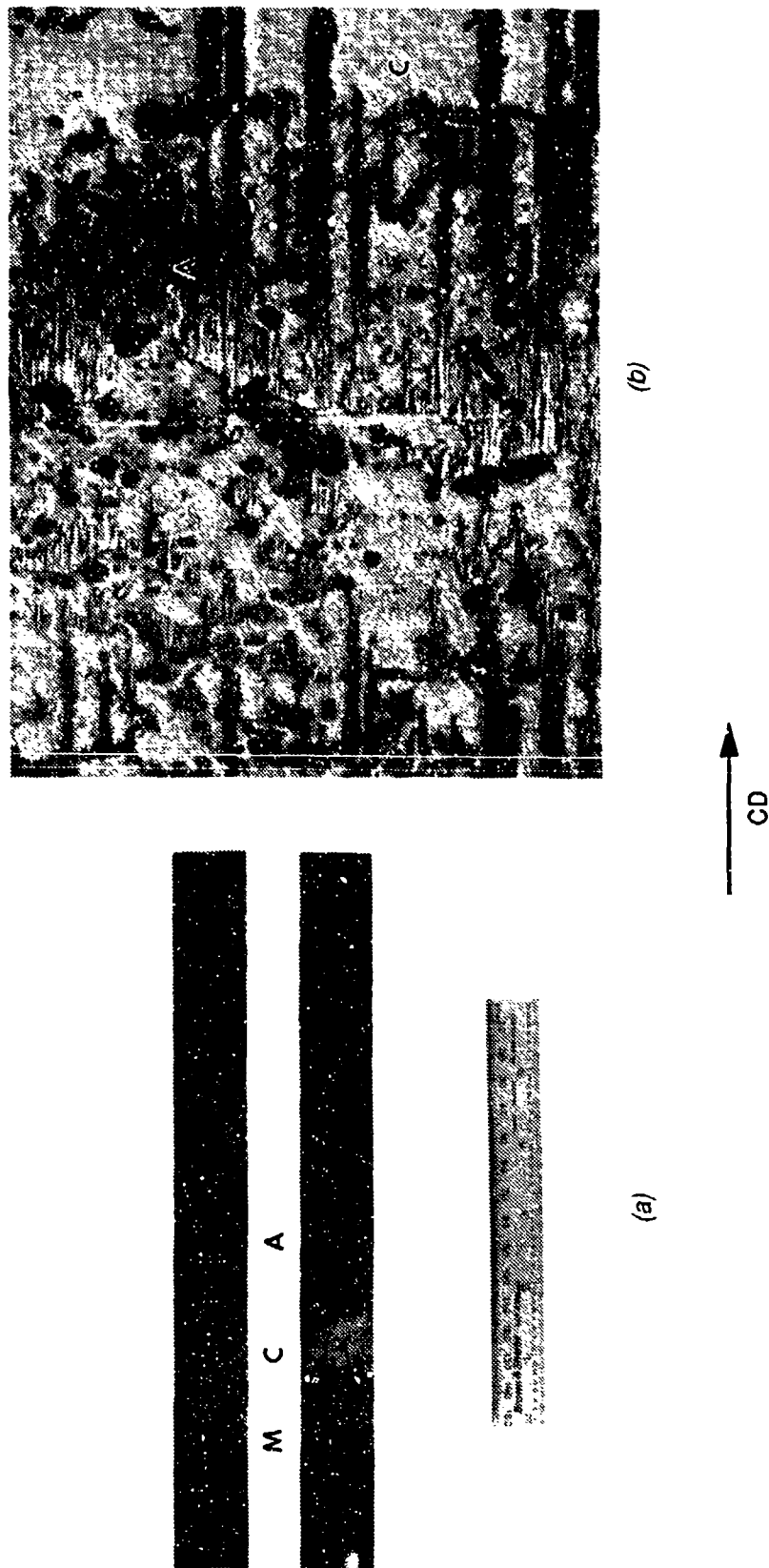
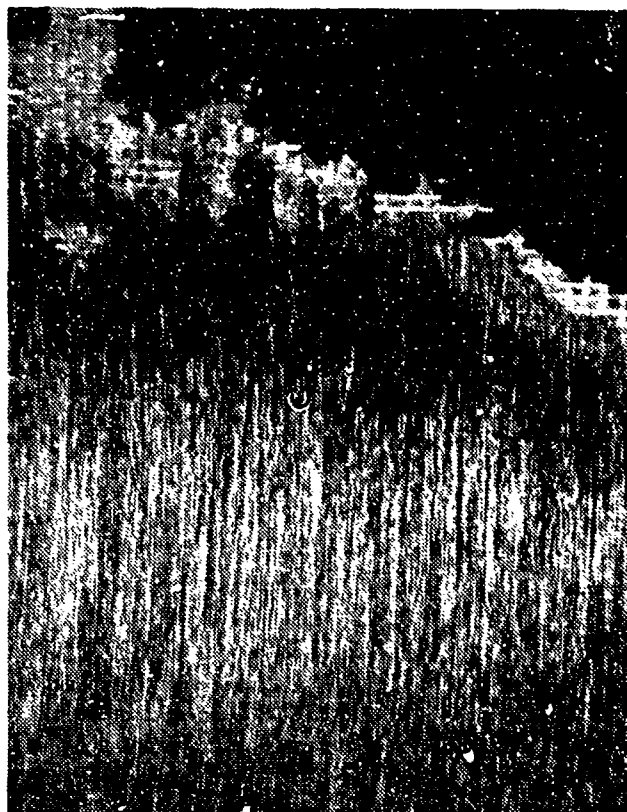


Figure 10-9. Optical and SEM Photographs of Failure in Unidirectional AS4/5250-3 Gr/BMI Bonded With EA 9673 Adhesive and Tested Under Interlaminar Mode I Tension
 (a) Macro photograph
 (b) Low Magnification (4X) Photograph Showing Details in Mixed Adhesive and Cohesive Failure Region

A = Adhesive failure
 C = Cohesive failure
 CD = Crack-propagation direction
 M = Mixed cohesive and adhesive failure



(c)



(d)

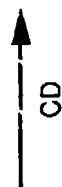


Figure 10-9. (Continued)
 (c) Low Magnification (4X) Photograph Showing Details in Cohesive Failure Region
 (d) River Patterns (R) in Adhesive Failure Region

C = Cohesive failure
 CD = Crack-propagation direction

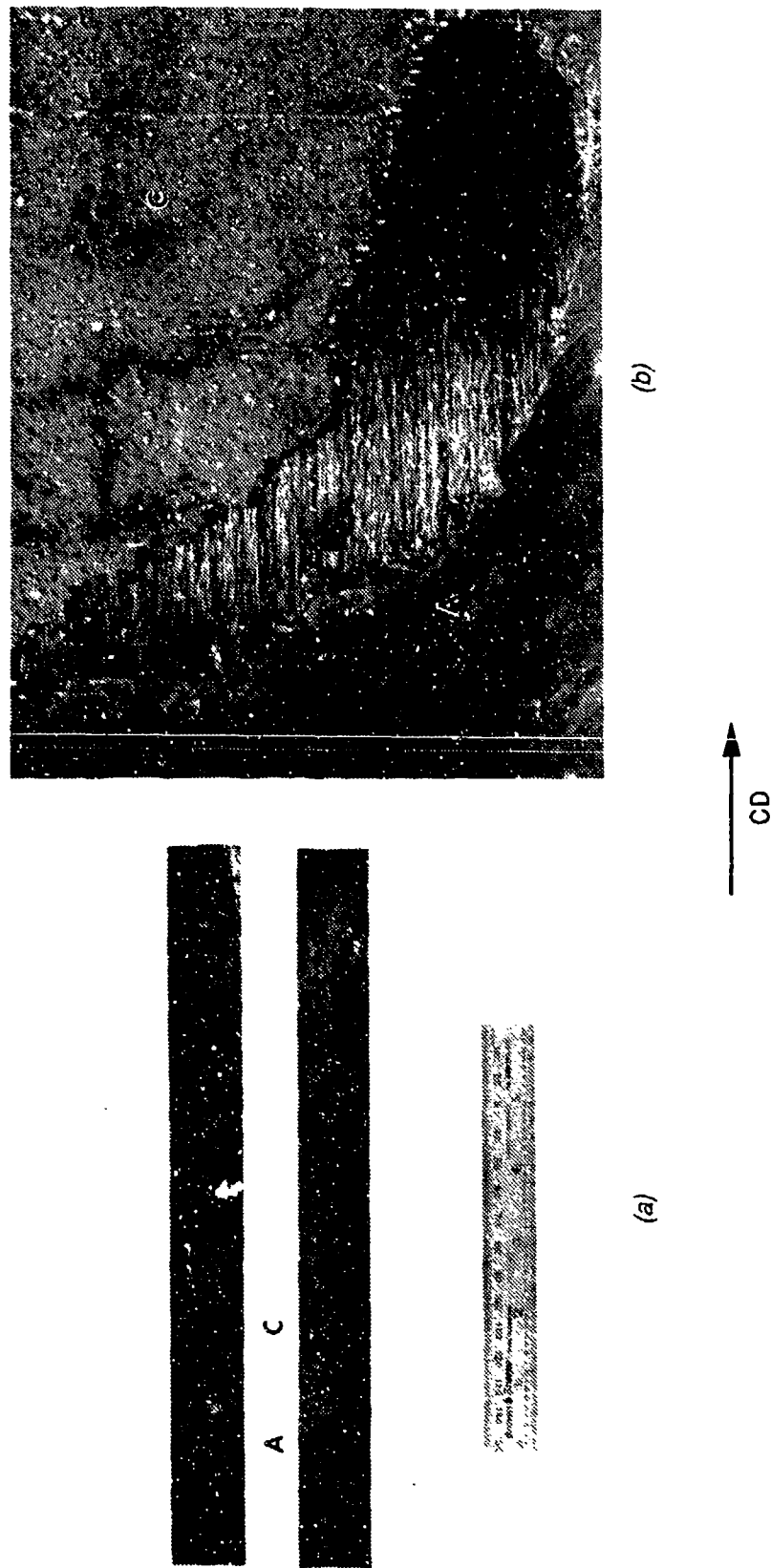
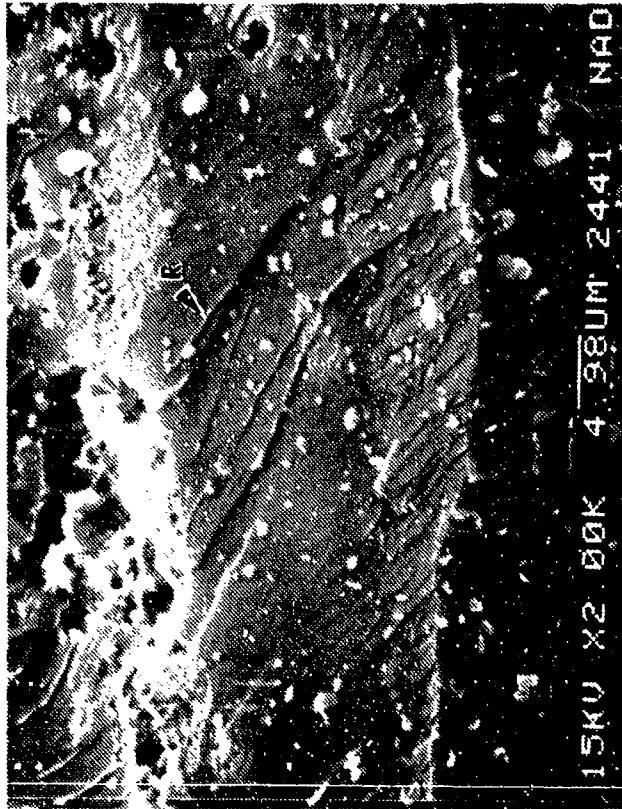


Figure 10-10. Optical and SEM Photographs of Failure in Unidirectional Gr/BMI Bonded to Quasi-Isotropic Gr/BMI With EA 9673 Adhesive and Tested Under Mode I Tension
 (a) Macro photograph
 (b) Low Magnification Photograph (4X) Showing Transition From Adhesive to Cohesive Failure

A = Adhesive failure
 C = Cohesive failure
 CD = Crack-propagation direction



(c)



(d)

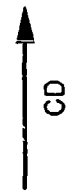


Figure 10-10. (Continued)
 (c) Adhesive Failure Area
 (d) Cohesive Failure Area

CD = Crack-propagation direction
 R = River patterns



(a)



(b)

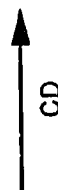
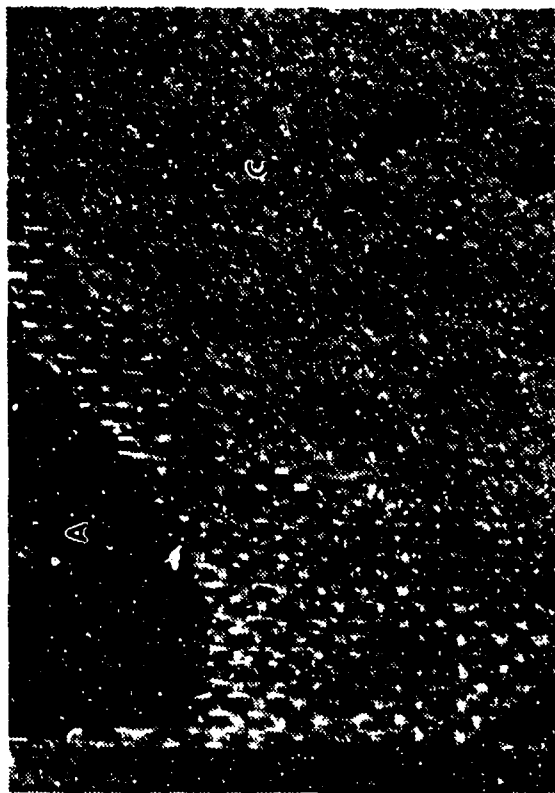


Figure 10-11. Photographs of Fracture in Unidirectional AS4/5250-3 Gr/BMI Adhrends Bonded With EA 9673 Adhesive, and Tested Under Mode I Tension and Mode II Interlaminar Shear
(a) Macro photograph of Fracture
(b) Low Magnification (4X) Photograph Showing Cohesive Failure Characteristics

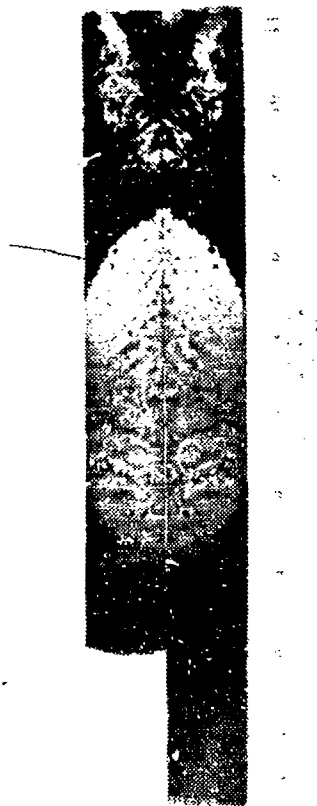
CD = Crack-propagation direction



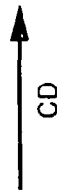
(b)



(c)



(a)



CD

Figure 10-12. Optical and SEM Photographs of Fracture in Unidirectional Gr/BMI Bonded to Quasi-Isotropic Gr/BMI Using EA 9673 Adhesive, Large Lap/Strap Ratio, Tested Under Mode I Tension and Mode II Interlaminar Shear

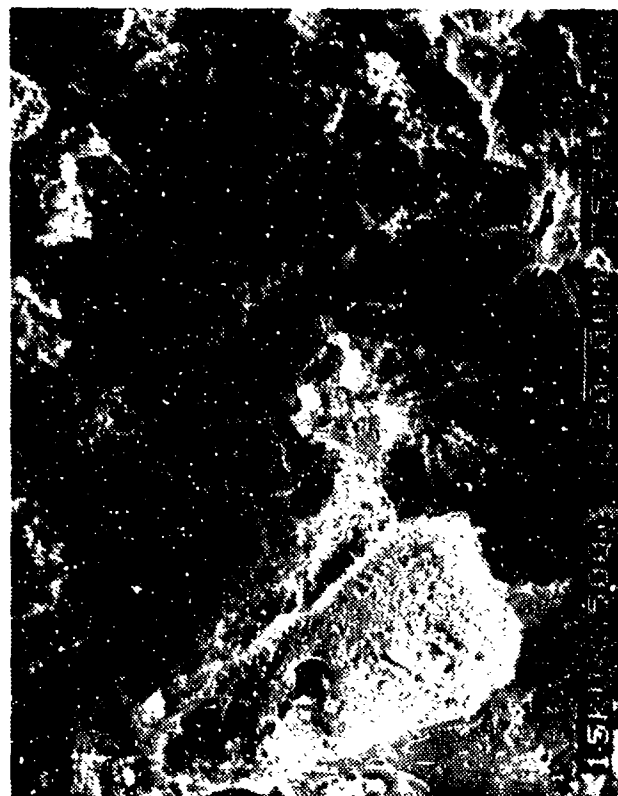
(a) Macro photograph of Fracture

(b), (c) Low Magnification (4X) Photographs Showing Cohesive (C) and Adhesive (A) Failure Characteristics

CD = Crack propagation direction



(e)



(d)

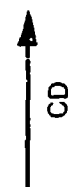


Figure 10-12. (Continued)
 (d) Cohesive Failure of Adhesive
 (e) Hackles (H) and Rivers (R) in Fractured Adherend
 CD = Crack-propagation direction